SYNAPTIC ASSEMBLY AND NEURAL CIRCUIT DEVELOPMENT

EDITED BY: Jaewon Ko and Chen Zhang
PUBLISHED IN: Frontiers in Molecular Neuroscience, Frontiers in Synaptic Neuroscience, Frontiers in Cellular Neuroscience and Frontiers in Neuroscience

frontiers Research Topics

ISSN 1664-8714
ISBN 978-2-88945-630-7
DOI 10.3389/978-2-88945-630-7

About Frontiers

Frontiers is more than just an open-access publisher of scholarly articles: it is a pioneering approach to the world of academia, radically improving the way scholarly research is managed. The grand vision of Frontiers is a world where all people have an equal opportunity to seek, share and generate knowledge. Frontiers provides immediate and permanent online open access to all its publications, but this alone is not enough to realize our grand goals.

Frontiers Journal Series

The Frontiers Journal Series is a multi-tier and interdisciplinary set of open-access, online journals, promising a paradigm shift from the current review, selection and dissemination processes in academic publishing. All Frontiers journals are driven by researchers for researchers; therefore, they constitute a service to the scholarly community. At the same time, the Frontiers Journal Series operates on a revolutionary invention, the tiered publishing system, initially addressing specific communities of scholars, and gradually climbing up to broader public understanding, thus serving the interests of the lay society, too.

Dedication to Quality

Each Frontiers article is a landmark of the highest quality, thanks to genuinely collaborative interactions between authors and review editors, who include some of the world's best academicians. Research must be certified by peers before entering a stream of knowledge that may eventually reach the public - and shape society; therefore, Frontiers only applies the most rigorous and unbiased reviews.
Frontiers revolutionizes research publishing by freely delivering the most outstanding research, evaluated with no bias from both the academic and social point of view. By applying the most advanced information technologies, Frontiers is catapulting scholarly publishing into a new generation.

What are Frontiers Research Topics?

Frontiers Research Topics are very popular trademarks of the Frontiers Journals Series: they are collections of at least ten articles, all centered on a particular subject. With their unique mix of varied contributions from Original Research to Review Articles, Frontiers Research Topics unify the most influential researchers, the latest key findings and historical advances in a hot research area! Find out more on how to host your own Frontiers Research Topic or contribute to one as an author by contacting the Frontiers Editorial Office: researchtopics@frontiersin.org

SYNAPTIC ASSEMBLY AND NEURAL CIRCUIT DEVELOPMENT

Topic Editors:
Jaewon Ko, Daegu Gyeongbuk Institute of Science and Technology (DGIST), South Korea
Chen Zhang, Peking University, China

Citation: Ko, J., Zhang, C., eds (2018). Synaptic Assembly and Neural Circuit Development. Lausanne: Frontiers Media. doi: 10.3389/978-2-88945-630-7

Table of Contents

frontiers in Synaptic Neuroscience

EDITORIAL
published: 18 September 2018
doi: 10.3389/fnsyn.2018.00030

Editorial: Synaptic Assembly and Neural Circuit Development

Chen Zhang[1,2] *and Jaewon Ko*[3]*

[1] School of Basic Medical Sciences, Capital Medical University, Beijing, China, [2] PKU-IDG/McGovern Institute for Brain Research, Peking University, Beijing, China, [3] Department of Brain and Cognitive Sciences, Daegu Gyeongbuk Institute of Science and Technology, Daegu, South Korea

Keywords: synapse, neural circuit assembly, synaptic adhesion molecule, recognition, neuron

Editorial on the Research Topic

Synaptic Assembly and Neural Circuit Development

Neurons transfer and process neural information via specialized junctional structures called synapses. All synapses in the brain operate by identical molecular and cellular principles, but they differ in their specific properties, depending on brain regions and types of neurons to which synapses are connected. Neural circuits are defined as collections of various types of synapses that form networks to perform specific functions. These circuits receive inputs and yield outputs through the operation of various synapse properties. Despite the attention paid to synapses and neural circuits in neuroscience over the past century, less is understood about synaptic assembly and neural circuit development at the molecular level. Recent increases in understanding are due, at least in part, to significant progress in the functional investigation of *trans*-synaptic adhesion molecules. Synaptic adhesion molecules are regarded as playing fundamental and universal roles in the initiation, assembly, refinement, and elimination of synapses and neural circuits. These molecules are thought to mediate physical and chemical recognition by and among neural cells, and to orchestrate various signaling pathways by interacting with other synaptic proteins. Fowler et al. [SynCAMs], Tan et al. [GPI-anchored IGSFs], Terauchi et al. [FGF22], and Lie et al. [SALMs] discussed their recent progress on the designated vertebrate synaptic adhesion molecules, particularly focusing on their functions in promoting synapse formation. Meanwhile, two papers from Victor Cilleros' group (Tomàs et al.) revealed that presynaptic muscarinic acetylcholine autoreceptors, adenosine autoreceptors, and trophic factor receptors have combined actions with intracellular protein kinases during the neuromuscular junction development and synapse elimination.

Won et al. proposed an intriguing competitive mechanism between protein ligands and heparan sulfates, the latter of which critically mediate synaptic specificity, as extensively discussed by Condomitti and de Wit. Um highlighted the putative roles of these synapse organizers in various glial cell types (astrocytes, microglia, and oligodendrocytes) in the context of shaping GABAergic inhibitory synapses and related neural circuits. Encouragingly, their roles have been recently tested in the context of various neural circuits using transgenic animals, suggesting a bridge between molecular and system neurosciences.

In addition to the synaptic cell-adhesion molecules that function at cellular membranes, various intracellular signaling proteins, scaffolds, and cytoskeletal proteins are critical for synapse assembly and neural circuit architecture. In particular, transcription factors have recently emerged as critical

Edited and reviewed by:
Per Jesper Sjöström, McGill University, Canada

***Correspondence:**
Jaewon Ko
jaewonko@dgist.ac.kr

Received: *21 July 2018*
Accepted: *15 August 2018*
Published: *18 September 2018*

Citation:
Zhang C and Ko J (2018) Editorial: Synaptic Assembly and Neural Circuit Development. Front. Synaptic Neurosci. 10:30. doi: 10.3389/fnsyn.2018.00030

players. Gong et al. showed that the transcription factor, Insm1a, contributes to governing motor neuron development. Meanwhile, Oswald et al. employed various functional approaches to reveal that a network driven by the transcription repressor, FOXP2, is involved in brain disorders, and Tian et al. characterized the role of the FMRP1 protein in long-term synaptic plasticity and spatial learning in rats.

The advances in a variety of neuroscience fields, particularly systems and computational neuroscience, have transformed neuroscience, leading to innovative new insights into our understanding on synaptic assembly and neural circuit development. However, our molecular understanding is still incomplete, and more detailed and sophisticated molecular and cellular approaches should be rigorously applied in the coming years.

AUTHOR CONTRIBUTIONS

All authors listed have made a substantial, direct and intellectual contribution to the work, and approved it for publication.

FUNDING

This work was supported by grants from the National Research Foundation of Korea (NRF) funded by the Ministry of Science and ICT (2016R1A2B200682 to JK).

ACKNOWLEDGMENTS

We are grateful to all authors who contributed to this Research Topic and to the reviewers who helped us choose a set of high quality articles in this field.

Conflict of Interest Statement: The authors declare that the research was conducted in the absence of any commercial or financial relationships that could be construed as a potential conflict of interest.

frontiers in Molecular Neuroscience

REVIEW
published: 05 April 2018
doi: 10.3389/fnmol.2018.00105

SALM/Lrfn Family Synaptic Adhesion Molecules

Eunkyung Lie[1†], Yan Li[1†], Ryunhee Kim[2†] and Eunjoon Kim[1,2]*

[1]*Center for Synaptic Brain Dysfunctions, Institute for Basic Science (IBS), Daejeon, South Korea,* [2]*Department of Biological Sciences, Korea Advanced Institute of Science and Technology (KAIST), Daejeon, South Korea*

Synaptic adhesion-like molecules (SALMs) are a family of cell adhesion molecules involved in regulating neuronal and synapse development that have also been implicated in diverse brain dysfunctions, including autism spectrum disorders (ASDs). SALMs, also known as leucine-rich repeat (LRR) and fibronectin III domain-containing (LRFN) proteins, were originally identified as a group of novel adhesion-like molecules that contain LRRs in the extracellular region as well as a PDZ domain-binding tail that couples to PSD-95, an abundant excitatory postsynaptic scaffolding protein. While studies over the last decade have steadily explored the basic properties and synaptic and neuronal functions of SALMs, a number of recent studies have provided novel insights into molecular, structural, functional and clinical aspects of SALMs. Here we summarize these findings and discuss how SALMs act in concert with other synaptic proteins to regulate synapse development and function.

Keywords: adhesion molecules, synaptic, SALM, Lrfn, PSD-95

OPEN ACCESS

Edited by:
Jaewon Ko,
Daegu Gyeongbuk Institute of Science and Technology (DGIST), South Korea

Reviewed by:
Joris De Wit,
VIB & KU Leuven Center for Brain & Disease Research, Belgium
Hideto Takahashi,
Institut de Recherches Cliniques de Montreal, Canada

****Correspondence:***
Eunjoon Kim
kime@kaist.ac.kr

†These authors have contributed equally to this work.

Received: *06 February 2018*
Accepted: *19 March 2018*
Published: *05 April 2018*

Citation:
Lie E, Li Y, Kim R and Kim E (2018) SALM/Lrfn Family Synaptic Adhesion Molecules. Front. Mol. Neurosci. 11:105. doi: 10.3389/fnmol.2018.00105

INTRODUCTION

Synaptic adhesion molecules play important roles in the regulation of various processes involved in synapse development and function, including early axo-dendritic contacts, maturation of early synapses, synaptic transmission and plasticity, and synapse maintenance and elimination (Dalva et al., 2007; Biederer and Stagi, 2008; Han and Kim, 2008; Sanes and Yamagata, 2009; Woo et al., 2009b; Shen and Scheiffele, 2010; Siddiqui and Craig, 2011; Krueger et al., 2012; Missler et al., 2012; Valnegri et al., 2012; Takahashi and Craig, 2013; Um and Ko, 2013, 2017; Bemben et al., 2015; Ko J. et al., 2015; de Wit and Ghosh, 2016; Cao and Tabuchi, 2017; Jang et al., 2017; Krueger-Burg et al., 2017; Sudhof, 2017; Yuzaki, 2018). Prototypical examples of such molecules are neuroligins and neurexins (Sudhof, 2017). Subsequent studies have identified a large number of other synaptic molecules, suggesting that diverse synaptic adhesion molecules may act in concert to regulate synapse specificity, maturation and plasticity.

Synaptic adhesion-like molecules (SALMs), also known as leucine-rich repeat (LRR) and fibronectin III domain-containing (LRFN) proteins, are a family of synaptic adhesion molecules originally identified independently by three groups as novel cell adhesion-like molecules that bind through their C-terminal tails to the PDZ domains of PSD-95 (Ko et al., 2006; Morimura et al., 2006; Wang et al., 2006; Nam et al., 2011), an abundant excitatory postsynaptic scaffolding protein (Sheng and Kim, 2011). A total of five members of the SALM family have been identified: SALM1/Lrfn2, SALM2/Lrfn1, SALM3/Lrfn4, SALM4/Lrfn3 and SALM5/Lrfn5 (Ko et al., 2006; Morimura et al., 2006; Wang et al., 2006; Nam et al., 2011).

These molecules share a similar domain structure, containing six LRRs, an immunoglobulin (Ig) domain, and a fibronectin type III (FNIII) domain in the extracellular side, followed by a transmembrane domain and a cytoplasmic region that ends with PDZ domain-binding motif (**Figure 1A**). The PDZ domain-binding motif is present in SALMs 1–3, but not SALM4 or SALM5. In contrast to the extracellular domains of SALMs, which share high amino acid sequence identities, especially in adhesion domains, the cytoplasmic regions lack shared domains and substantially differ in length as well as amino acid sequence, suggesting that they may have distinct functions.

Our previous review of SALMs summarized basic and functional characteristics of SALMs, including chromosomal locations of the corresponding genes and exon-intron structures, mRNA and protein expression patterns, protein–protein interactions, and involvement in regulating neuronal and synapse development (Nam et al., 2011). One prominent function of SALMs is to regulate neurite outgrowth and branching through mechanisms including lipid raft-associated flotillin proteins (Wang et al., 2006, 2008; Swanwick et al., 2009, 2010; Seabold et al., 2012). SALMs also regulate synapse development and function through mechanisms involving interactions with PSD-95 and glutamate receptors (Ko et al., 2006; Wang et al., 2006; Mah et al., 2010).

Notably, these functional features of SALMs have been identified mainly through *in vitro* studies. Recently, however, additional studies on SALMs using *in vivo* approaches, such as genetic mouse models, have provided intriguing insights into the physiological functions of SALMs (Li et al., 2015; Lie et al., 2016; Morimura et al., 2017). In addition, SALM3 and SALM5, which unlike other SALMs possess synaptogenic activities (Mah et al., 2010), have been found to interact trans-synaptically with presynaptic LAR family receptor tyrosine phosphatases (LAR-RPTPs; Li et al., 2015; Choi et al., 2016), a group of adhesion molecules with cytoplasmic phosphatase activity that are critically involved in various aspects of neuro- and synapse development across many species (Johnson and Van Vactor, 2003; Takahashi and Craig, 2013; Um and Ko, 2013; **Figure 1B**). Moreover, two independent X-ray crystallography studies have determined the stoichiometry and molecular details of the interaction of SALM5 with LAR-RPTPs (Goto-Ito et al., 2018; Lin et al., 2018). Lastly, recent clinical studies have additionally identified associations of SALMs with diverse neurodevelopmental disorders (Nho et al., 2015; Rautiainen et al., 2016; Thevenon et al., 2016; Farwell Hagman et al., 2017; Morimura et al., 2017; Bereczki et al., 2018). This review article will summarize these new findings and discuss how SALMs regulate synapse development and function.

SYNAPTIC LOCALIZATION OF SALMs

As implied by the name "synaptic adhesion-like molecule", it was initially unclear whether SALMs are indeed localized at neuronal synapses and regulate synapse development and function through cis/trans-synaptic adhesion. The first, albeit indirect, evidence came from the fact that some SALMs directly interact with well-known excitatory synaptic proteins, such as PSD-95, N-methyl-D-aspartate receptors (NMDARs), and α-amino-3-hydroxy-5-methylisoxazole-4-propionic acid receptors (AMPARs; Ko et al., 2006; Morimura et al., 2006; Wang et al., 2006). Functionally, SALM2, artificially clustered on neuronal dendrites by antibody-coated beads, was shown to be able to recruit PSD-95 and NMDARs/AMPARs (Ko et al., 2006). In addition, SALM3 and SALM5 expressed in heterologous cells was shown to induce presynaptic differentiation in contacting axons of cocultured neurons in mixed culture assays (Mah et al., 2010), in which synaptogenic activity is tested by coculturing neurons with heterologous cells exogenously expressing synaptic adhesion molecules (Scheiffele et al., 2000; Biederer and Scheiffele, 2007).

More direct evidence for synaptic localization of SALMs has come from electron microscopy, immunocytochemistry, biochemical and proteomic analyses. One early study using immunocytochemistry detected endogenous SALM2 signals at excitatory, but not inhibitory, synapses in cultured rat hippocampal neurons (Ko et al., 2006). A subsequent electron microscopy study detected endogenous SALM4 signals at various subcellular locations in rat brain hippocampal neurons, including synaptic and extra-synaptic sites, pre- and postsynaptic sites, and dendrites and axons (Seabold et al., 2008). Biochemical experiments further demonstrated that SALMs are enriched in the postsynaptic density (PSD)—electron-dense multiprotein complexes at excitatory postsynaptic sites that contain neurotransmitter receptors, adaptor/scaffolding proteins and signaling molecules (Sheng and Sala, 2001; Sheng and Hoogenraad, 2007); SALM1 (Wang et al., 2006), SALM2 (Ko et al., 2006), SALM3 (Mah et al., 2010), SALM4 (Lie et al., 2016) and SALM5 (Mah et al., 2010).

More recently, an elegant study using proximity biotinylation, a method combining an engineered enzyme and proteomic mapping of biotinylated proteins within 10–50 nm of a particular bait protein in a subcellular environment (Han et al., 2017), identified SALMs among a large number of synaptic cleft proteins (Loh et al., 2016). Specifically, SALM1/Lrfn2 and SALM3/Lrfn4 were found to be present in the vicinity of LRRTM2 and LRRTM3, the reference excitatory synaptic adhesion molecules used in this study. Another study also using proximity biotinylation detected SALM1/Lrfn2 in close proximity to PSD-95 (Uezu et al., 2016). However, SALMs were not found to be close neighbors of the inhibitory adhesion molecules, neuroligin-2 and Slitrk3, or gephyrin (Loh et al., 2016; Uezu et al., 2016), a major inhibitory synaptic scaffolding protein (Tyagarajan and Fritschy, 2014; Choii and Ko, 2015; Krueger-Burg et al., 2017). These results suggest that some SALMs are important components of excitatory synapses; however, they do not preclude their possible presence at inhibitory synapses, since the biotinylation approach used is likely biased toward identification of more abundant proteins.

Collectively, these previous observations suggest that SALMs are present or enriched at synaptic sites, but also highlight important details that still remain to be determined, including excitatory vs. inhibitory synaptic localization of SALMs, pre- vs. postsynaptic localization, and changes in synaptic localization

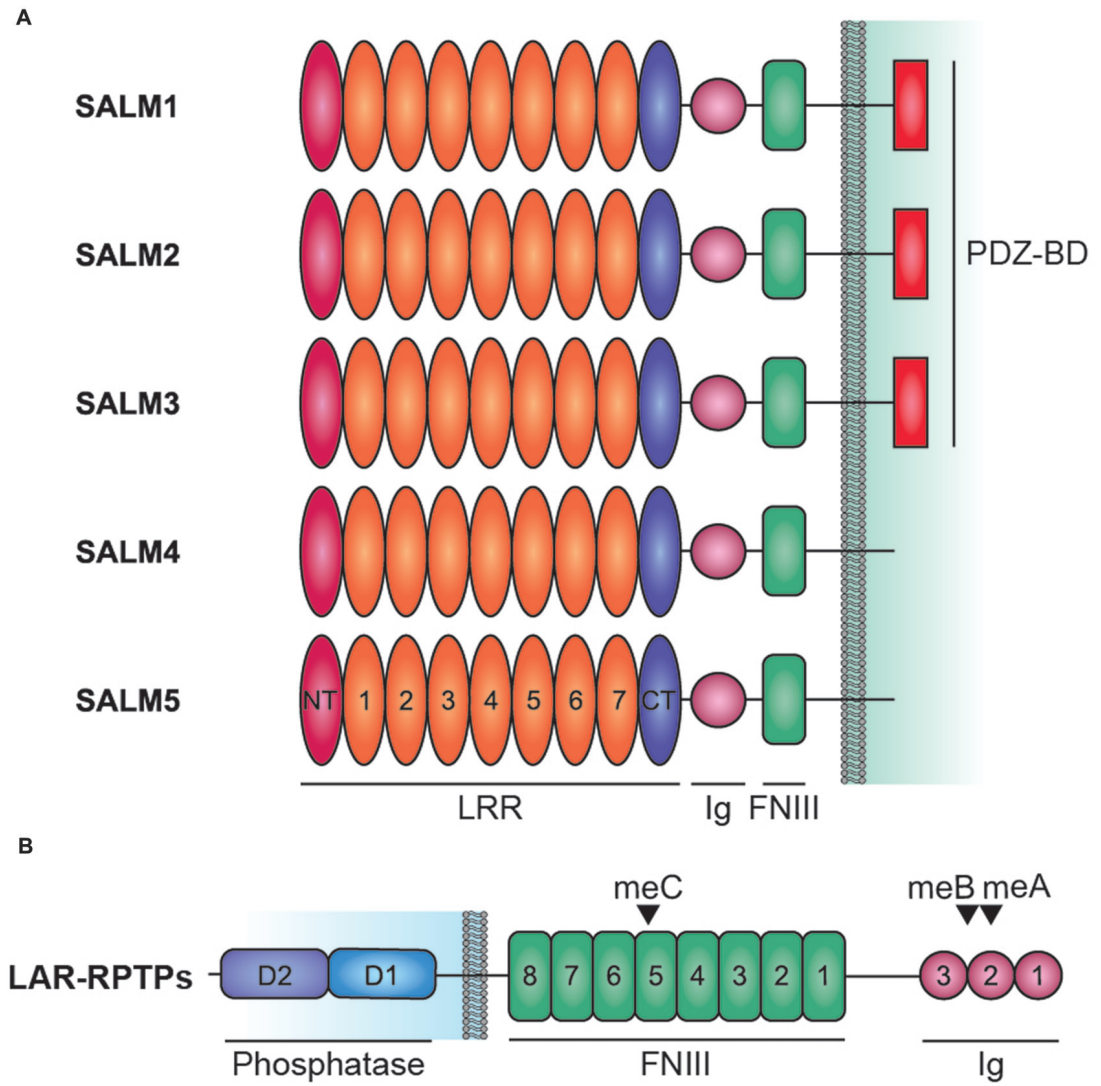

FIGURE 1 | Domain structure of Synaptic adhesion-like molecules (SALMs) and LAR-RPTPs. **(A)** Domain structure of SALMs 1–5. Note that the PDZ domain-binding motif (PDZ-BD) is present in SALMs 1–3 but not in SALM4 or SALM5. FNIII, fibronectin III domain; Ig, immunoglobulin domain; LRR, leucine-rich repeats; NT and CT, N-terminal and C-terminal LRR. Note that the number of LRRs in this diagram is seven, although it was suggested to be six in early studies based on amino acid sequence analyses (Ko et al., 2006; Morimura et al., 2006; Wang et al., 2006; Nam et al., 2011). Recent X-ray crystallographic studies have identified seven LRRs in SALM5 (Lin et al., 2018) and eight LRRs in SALM2 and SALM5 (Goto-Ito et al., 2018), which may reflect different ways of defining LRRs. **(B)** Domain structure of LAR-RPTPs (LAR, PTPσ and PTPδ). D1 and D2, membrane-proximal and -distal tyrosine phosphatase domains of LAR-RPTPs; meA/B/C; mini-exon A/B/C.

during development and activity. Addressing these additional questions could be aided by knockout (KO) animals combined with high-quality antibodies, as well as advanced methodologies, such as proximity biotinylation and endogenous protein tagging using CRISPR/Cas9-mediated homology-independent targeted integration (Suzuki et al., 2016).

TRANS-SYNAPTIC ADHESIONS OF SALMs

An early study reported that SALM3 and SALM5, but not other SALMs, expressed in heterologous cells induce presynaptic differentiation in contacting axons of cocultured neurons (Mah et al., 2010). However, it has remained unclear which presynaptic adhesion molecules mediate SALM3/5-dependent presynaptic differentiation.

A recent study found that SALM3 interacts with presynaptic LAR-RPTPs to promote presynaptic differentiation (Li et al., 2015; **Figure 2**). This conclusion is supported by several lines of evidence, including protein binding, cell aggregation, and coculture assays. All three known member of the LAR-RPTP family (LAR, PTPσ and PTPδ) can interact with SALM3. Importantly, these interactions are regulated by alternative splicing of LAR-RPTPs. Specifically, the splice B insert (termed mini-exon B or meB), but not the splice A insert (meA), both of

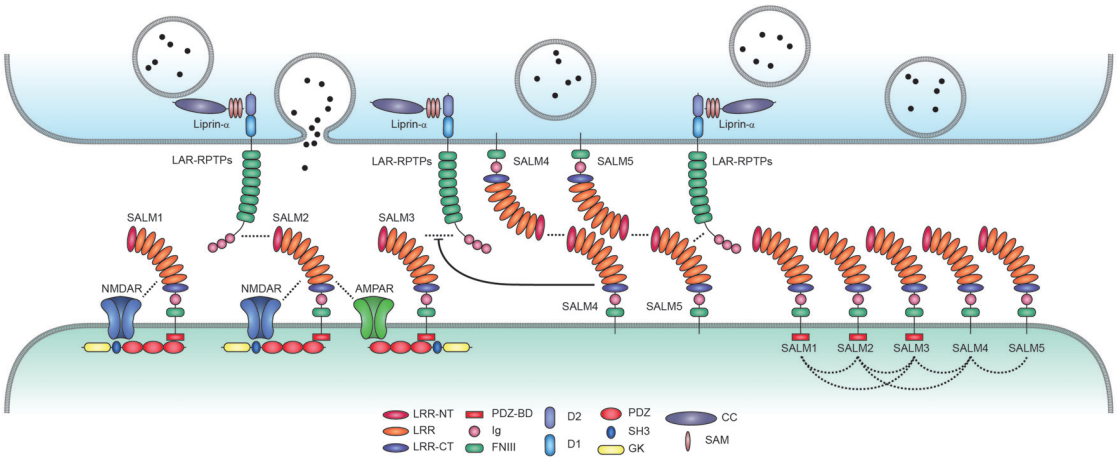

FIGURE 2 | Trans-synaptic, cis-, and cytoplasmic interactions of SALMs. SALMs interact trans-synaptically with presynaptic LAR-RPTPs (LAR, PTPσ and PTPδ), in cis with AMPA/NMDA receptors and other SALM proteins, and cytoplasmically with the postsynaptic scaffolding protein PSD-95 (in the case of SALMs 1–3 but not SALM4 or SALM5). Protein interactions are indicated by the close proximity of the indicated proteins/domains or by dotted lines. Whether SALMs directly interact with NMDA/AMPA receptors remains to be determined. The trans-synaptic interactions between postsynaptic SALM3/5 and presynaptic LAR-RPTPs are known to promote presynaptic differentiation, although the function of the newly identified SALM2–LAR-RPTP (PTPδ) interaction is unclear. SALM4 interacts in cis with SALM3 to suppress the binding of SALM3 to presynaptic LAR-RPTPs and SALM3-dependent presynaptic differentiation. Postsynaptic SALM5 can also interacts with presynaptic SALM5 in a homophilic manner, which may interfere with the trans-synaptic interaction between presynaptic LAR-RPTPs and postsynaptic SALM5. The cis-interactions between different postsynaptic SALMs are based on both *in vitro* and *in vivo* results, and may be mediated by the SALM–SALM dimerization revealed by X-ray crystallographic studies. Although not shown here, some LAR-RPTPs are thought to be present and function at postsynaptic sites, in addition to presynaptic sites.

TABLE 1 | Influences of meA/B splice inserts in LAR-RPTPs on the interaction between LAR-RPTPs and SALMs.

Mini-exon	Interaction and change	Method	Reference
MeA	SALM3-LAR/PTPδ/PTPσ–	Purified protein binding to cells	Li et al. (2015)
	SALM5-LAR –SALM5-PTPδ/PTPσ ↓	Cell aggregation	Choi et al. (2016)
	SALM5-PTPδ –	Surface plasmon resonance	Lin et al. (2018)
	SALM5-PTPδ –	Surface plasmon resonance	Goto-Ito et al. (2018)
MeB	SALM3-LAR/PTPδ/PTPσ ↑	Protein-binding assay	Li et al. (2015)
	SALM5-LAR/PTPδ/PTPσ ↓	Cell aggregation	Choi et al. (2016)
	SALM5-PTPδ ↑	Surface plasmon resonance	Lin et al. (2018)
	SALM5-PTPδ ↑	Surface plasmon resonance	Goto-Ito et al. (2018)

No changes, increases and decreases are indicated as horizontal bars, up arrows and down arrows, respectively.

which are located in the N-terminal three Ig domains of LAR-RPTPs, is required for the interaction with SALM3 (**Table 1**).

Like SALM3, SALM5 also interacts with LAR-RPTPs (Choi et al., 2016; **Figure 2**). In this case, the meB splice insert in LAR-RPTPs suppresses SALM5–LAR-RPTP interactions, an effect opposite that of meB on SALM3–LAR-RPTP interactions. Therefore, both SALM3 and SALM5 interact with LAR-RPTPs in a splicing-dependent manner, although the polarity of the modulatory effect of the insert appears to differ (but see below for conflicting results and related structural and biochemical data).

Presynaptic LAR-RPTPs are known to interact with several other postsynaptic adhesion molecules in addition to SALM3/5, including NGL-3, Slitrks, TrkC, IL1RAPL1 and IL-1RAcP (Woo et al., 2009a,b; Kwon et al., 2010; Takahashi et al., 2011, 2012; Valnegri et al., 2011; Yoshida et al., 2011, 2012; Yim et al., 2013; Li et al., 2015); also see reviews by Craig, Ko and colleagues (Takahashi and Craig, 2013; Um and Ko, 2013) for further details. These results give rise to a number of obvious questions: Why are there multiple LAR-RPTP-binding postsynaptic adhesion molecules? Does a single synapse contain all, or a majority, of the postsynaptic LAR-RPTP ligands? If so, do they compete with each other for mutually exclusive LAR-RPTP binding, or do they act in concert to fine-tune synapse regulation? These questions can also be applied to the three presynaptic LAR-RPTPs, LAR, PTPσ and PTPδ.

First, it seems unlikely that all three LAR-RPTPs are present in the same synapses, in part because LAR, PTPσ and PTPδ are differentially expressed in distinct brain regions (Kwon et al., 2010). In addition, evidence suggests that LAR, PTPσ and PTPδ differentially localize to and regulate excitatory and inhibitory synapses, with PTPσ and PTPδ being more important at excitatory and inhibitory synapses, respectively (Takahashi et al., 2011, 2012; Takahashi and Craig, 2013; Um and Ko, 2013); however, additional details remain to be determined. Splice variants of LAR-RPTPs are tightly regulated in a spatiotemporal manner (O'Grady et al., 1994;

Pulido et al., 1995a,b; Zhang and Longo, 1995). In particular, each LAR-RPTP protein's mini-exon profile, which strongly influences interactions with their postsynaptic partners (Takahashi and Craig, 2013; Um and Ko, 2013), appears to be distinct in specific brain regions. For instance, the meB splice insert in the rat hippocampus is almost always present in PTPδ, but is rarely found in LAR and is only present in about half of PTPσ molecules (Li et al., 2015), suggesting that hippocampal SALM3 is likely to interact with LAR-RPTPs in the rank order, PTPδ > PTPσ ≫ LAR (Li et al., 2015). Similarly, the majority of PTPδ splice variants in the mouse hippocampus contain the meB splice insert (Yoshida et al., 2011). Therefore, LAR-RPTPs are likely to interact with their postsynaptic partners in a spatiotemporally and molecularly regulated manner.

It can also be expected that postsynaptic LAR-RPTP ligands would be differentially expressed in specific brain regions and cell types. In addition, each postsynaptic LAR-RPTP ligand apparently has a unique preference for particular splice variants of LAR-RPTPs. For instance, meB is required for (or positively regulates) LAR-RPTP binding to SALM3, Slitrks, IL1RAPL1 and IL-1RAcP (Yoshida et al., 2011, 2012; Takahashi et al., 2012; Yim et al., 2013; Li et al., 2015), but inhibits LAR-RPTP binding to TrkC (Takahashi et al., 2011). Notably, NGL-3 differs from other postsynaptic LAR-RPTP-binding proteins in that it binds to the first two FNIII domains of LAR-RPTPs (Woo et al., 2009a), whereas all other such proteins bind to the N-terminal Ig domains of LAR-RPTPs (Takahashi et al., 2011, 2012; Yoshida et al., 2011, 2012; Yim et al., 2013; Li et al., 2015; Choi et al., 2016). This suggests the intriguing possibility that LAR-RPTPs form ternary protein complexes with NGL-3 and other postsynaptic LAR-RPTP binders, and hints at the potential interplay among these complex components. Therefore, interactions of trans-synaptic LAR-RPTPs with their postsynaptic partners likely occur in a precisely regulated manner.

It is thought that LAR-RPTPs are present mainly at presynaptic sites, because LAR proteins expressed in heterologous cells do not induce presynaptic protein clustering at contacting axons of cocultured neurons, but do induce postsynaptic protein clustering in contacting dendrites (Woo et al., 2009a). However, although some light microscopy-level immunostaining has been performed (Takahashi et al., 2011; Farhy-Tselnicker et al., 2017), clear pre- vs. postsynaptic localization of endogenous LAR-RPTPs has not been determined at the electron microscopy level. In addition, postsynaptic LAR-RPTPs have been shown to regulate dendritic spines and AMPAR-mediated synaptic transmission (Dunah et al., 2005). More recently, PTPδ coexpressed with IL1RAPL1 in cultured hippocampal neurons was found to inhibit IL1RAPL1-dependent suppression of dendritic branching, suggesting that postsynaptic PTPδ interacts in *cis* with, and inhibits, IL1RAP1 (Montani et al., 2017). Therefore, it is possible that SALM3/5-LAR-RPTP interactions also occur at postsynaptic sites in a *cis* manner.

Experiments using heterologous cells and cultured neurons have shown that SALM5 can engage in both transcellular and homophilic adhesions (Seabold et al., 2008). This suggests that presynaptic SALM5 may compete with presynaptic LAR-RPTPs for binding to postsynaptic SALM5. Alternatively, these two interactions may occur in a spatiotemporally distinct manner.

Lastly, heparan sulfate proteoglycans interact with LAR-RPTPs in the presynaptic membrane to regulate their interactions and functions (Aricescu et al., 2002; Johnson et al., 2006; Song and Kim, 2013; Coles et al., 2014; Ko J. S. et al., 2015; Farhy-Tselnicker et al., 2017; Won et al., 2017), and thus may regulate SALM–LAR-RPTP interactions and functions. In addition, LAR proteins associate with netrin-G1, a glycosylphosphatidylinositol-anchored presynaptic adhesion molecule (Nakashiba et al., 2000), at the presynaptic side when netrin-G1 is coupled with its cognate postsynaptic ligand NGL-1 (Song et al., 2013), suggesting the possibility that trans-synaptic SALM3/5–LAR-RPTP interactions is regulated by a neighboring trans-synaptic netrin-G1-NGL-1 interaction.

STRUCTURES OF SALMs IN COMPLEX WITH LAR-RPTPs

Although previous studies have identified interactions between SALM3/5 and LAR-RPTPs, the molecular stoichiometry and mechanistic details of these interactions have remained unclear. Two recent X-ray crystallography studies have been instrumental in resolving many of these uncertainties.

The first revealed that SALM5 can form a dimeric structure, in which dimerization is mediated mainly by the N-terminal LRR domain, and that this dimer forms a complex with two PTPδ monomers (Lin et al., 2018; **Figures 3A,B**). In this 2:2 stoichiometry, a SALM5 dimer bridges two PTPδ monomers, which are positioned at opposite sides of the SALM5 dimer. The overall shape of the complex has two components: a central platform-like structure formed by two antiparallel LRR domains of SALM5 with a concave core in its center, and four leg-like structures formed by two Ig domains of SALM5 and two Ig3 domains of PTPδ.

It was found that the specific molecular interfaces that mediate the SALM5–PTPδ interaction are the LRR domain of SALM5, which interacts with the second Ig domain of PTPδ, and the Ig domain of SALM5, which interacts with both the second and third Ig domains of PTPδ. Importantly, mutations in the LRR domain of SALM5 that disrupt dimerization were shown to abolish SALM5–LAR-RPTPs interactions and SALM5-dependent presynaptic differentiation. Therefore, SALM5 dimerization is critical for both the trans-synaptic adhesion and synaptogenic activity of SALM5.

These conclusions are further confirmed by a second study, which reported a SALM5 dimer in complex with two PTPδ monomers (Goto-Ito et al., 2018). This study identified eight LRRs whereas the other study identified seven LRRs; notably, both values differ from the number predicted in previous studies (six) based on amino acid sequence analyses (Ko et al., 2006; Morimura et al., 2006; Wang et al., 2006; Nam et al., 2011). These differences appear to reflect the specific criteria authors used to define LRRs in the different studies.

Intriguingly, this second study also solved the 2:2 structure of PTPδ in complex with SALM2 (Goto-Ito et al., 2018), a member of the SALM family that, unlike SALM3 and SALM5,

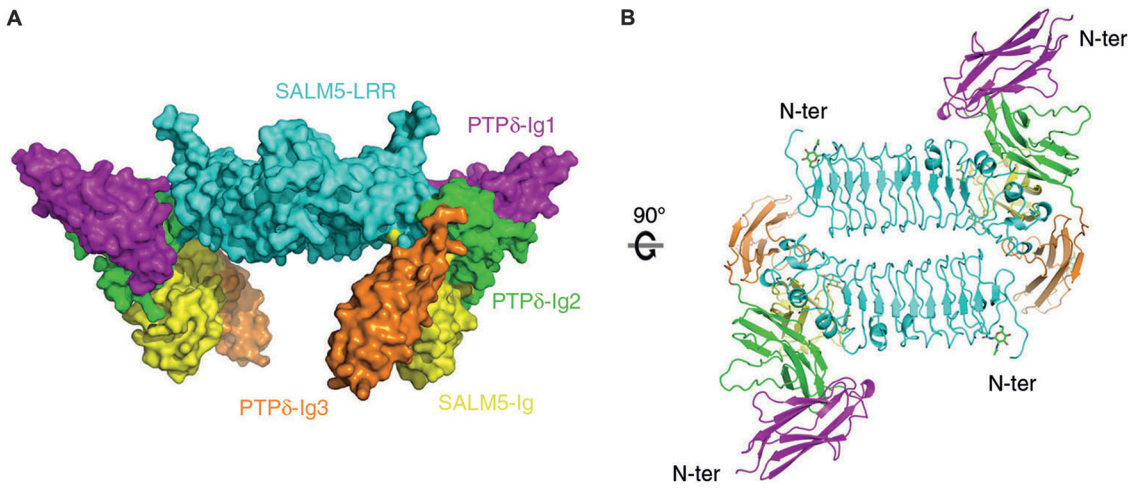

FIGURE 3 | X-ray crystal structure of SALM5 in complex with PTPδ in a 2:2 heterotetrameric format. **(A)** Side view of the structure (surface representation). **(B)** Top-down view of the structure (ribbon diagram). These images were borrowed without modification from Figures 1B,C of a recent report on the crystal structure of SALM5 in complex with PTPδ (Lin et al., 2018), which are under a Creative Commons Attribution 4.0 International License (http://creativecommons.org/licenses/by/4.0/).

has little or no synaptogenic activity (Mah et al., 2010). It is possible that SALM2 actually has synaptogenic activity that has gone unidentified in previous studies employing coculture assays and neuronal overexpression (Ko et al., 2006). Alternatively, SALM2 may interact with PTPδ to regulate other aspects of neuronal synapses. For instance, SALM2 is capable of associating with PSD-95 and NMDA/AMPARs (Ko et al., 2006). Therefore, the PTPδ–SALM2 interaction may promote postsynaptic protein clustering rather than presynaptic differentiation.

These two studies have also provided significant molecular insights into how alternative splicing regulates SALM-LAR-RPTP interactions. Specifically, they show that the meB, but not meA, splice insert is located in the junctional region between Ig2 and Ig3 domains of PTPδ, both of which are engaged in SALM5 interactions. The meB splice insert, although not directly interacting with SALM5, appears to function as a flexible linker that optimizes the position of the PTPδ-Ig3 domain for its high-affinity interaction with the SALM5-Ig domain (Goto-Ito et al., 2018; Lin et al., 2018). This conclusion is further supported by surface plasmon resonance assays that used purified PTPδ proteins, with or without meB, and demonstrated that the presence of meB increases the affinities between SALM5 and PTPδ by ∼7–30 fold (Goto-Ito et al., 2018; Lin et al., 2018; **Table 1**).

Overall, these results are in apparent contrast with an earlier report that meB suppresses the interaction between LAR-RPTPs and SALM5 (Choi et al., 2016). A possible reason for this discrepancy is differences in the method used to assess binding—cell aggregation assays in this earlier report (Choi et al., 2016) and binding assays using purified proteins in the more recent studies (Goto-Ito et al., 2018; Lin et al., 2018). Indeed, the effects of meB on SALM3–LAR-RPTP interactions were substantially weakened in cell aggregation assays relative to protein binding assays (Li et al., 2015).

The findings of these two X-ray crystallography studies are largely similar to those investigating other LAR-RPTP interactions, which showed that meB is required for (or promotes) interactions between Slitrk1 and PTPσ (Um et al., 2014), Sltrk2 and PTPδ (Yamagata et al., 2015a), and IL1RAPL1/IL-1RAcP and PTPδ (Yamagata et al., 2015b). Therefore, these interactions, if present in the same synapse together with the SALM4–LAR-RPTP complex, are likely to be simultaneously regulated by meB.

The 2:2 stoichiometry of SALM5–LAR-RPTP interactions that involves an antiparallel LRR dimerization, something that is not observed in other LAR-RPTP-related crystal structures (Coles et al., 2014; Um et al., 2014; Yamagata et al., 2015a,b; Won et al., 2017), carries multiple potential functional implications. One possibility is that this stoichiometry could increase the affinity of the trans-synaptic SALM5–LAR-RPTP interaction. Indeed, the K_d values for the SALM5–PTPδ interaction determined in two independent studies ranged from 0.07 μM to 14.4 μM, indicating weaker interactions than those for LAR-RPTPs with Slitrk1, Slitrk2, IL1RAPL1, IL-1RAcP or TrkC, which are in the sub-micromolar range (0.15–0.55 μM). However, it remains unclear whether the SALM5–PTPδ interactions measured under the surface plasmon resonance condition involves the 2:2 stoichiometry.

What advantages might accrue to SALMs because they are able to achieve an appropriate trans-synaptic affinity through dimerization—a property lacking in other LAR-RPTP ligands? It is possible that a SALM5 dimer brings two PTPδ molecules close to each other to more efficiently promote presynaptic differentiation through liprin-α. Liprin-α belongs to a family of LAR-RPTP-binding scaffolding/adaptor proteins whose members are known to form homodimers and bridge LAR-RPTPs with their phospho-tyrosine protein substrates, such as β-catenin (Serra-Pagès et al., 1995, 1998;

Dunah et al., 2005; Stryker and Johnson, 2007; de Curtis, 2011).

On the postsynaptic side, SALM2 dimers, which are clearly revealed in crystal structures (Goto-Ito et al., 2018), may efficiently interact with PSD-95 and PSD-95–associated proteins known to form dimeric/multimeric structures, such as Shank and Homer (Kim et al., 1996; Hsueh et al., 1997; Xiao et al., 1998; Naisbitt et al., 1999; Hayashi et al., 2009). These multimeric interactions may facilitate the formation of platform-like multi-protein structures in the PSD.

CIS INTERACTIONS OF SALMs

Cis-interactions of diverse synaptic adhesion molecules have received increasing attention because they often regulate trans-synaptic interactions as well as receptor-mediated synaptic transmission (Jang et al., 2017). For example, neuroligin-1 interacts in *cis* with the GluN1 subunit of NMDARs through extracellular domains to increase the synaptic abundance of NMDARs (Budreck et al., 2013). In addition, postsynaptic neurexin-1β interacts in *cis* with neuroligin-1 to suppress the trans-synaptic interaction of neuroligin-1 with presynaptic neurexins (Taniguchi et al., 2007). More recently, MDGAs (MAM domain-containing glycosylphosphatidylinositol anchors) have been found to interact in *cis* with neuroligins to modulate trans-synaptic neuroligin–neurexin interactions (Lee et al., 2013; Pettem et al., 2013; Elegheert et al., 2017; Gangwar et al., 2017; Kim et al., 2017; Thoumine and Marchot, 2017).

SALMs are involved in *cis*-interactions in addition to *trans*-interactions. The first clue came from the original study on SALMs, which reported that SALM1 associates with and promotes surface expression and clustering of NMDARs (Wang et al., 2006; **Figure 2**). This required the C-terminal tail of SALM1, which interacts with PSD-95 and subsequently with GluN2B subunits of NMDARs, suggesting that SALM1 indirectly interacts with and clusters NMDARs through PSD-95. However, SALM1 can also associate with GluN1, a subunit of NMDARs that lacks the cytoplasmic region, suggesting that SALM1 can directly interact with NMDARs. Additional clues for *cis*-interactions of SALMs came from the finding that bead-mediated direct clustering of SALM2 on the dendritic surface of cultured neurons induces secondary clustering of PSD-95 as well as AMPA/NMDARs (Ko et al., 2006), although whether this is mediated by direct interactions remains unclear.

A careful examination of *cis*-interactions between different SALM family members showed that all SALM members coimmunoprecipitate with each other in both a homomeric and heteromeric manner in heterologous cells (Seabold et al., 2008; **Figure 2**). The extracellular domains of SALMs are important for these *cis*-interactions, as evidenced by the fact that a SALM1 mutant lacking the entire cytoplasmic domain can form homo- and heteromultimers. In the brain, however, heteromeric SALM complexes are formed between SALMs 1–3, but not SALM4 or SALM5. The ability of SALM4 and SALM5, but not other SALMs, to mediate homophilic trans-synaptic adhesion suggests that postsynaptic SALMs can be segregated into three subgroups: (1) SALMs 1–3; (2) SALM4; and (3) SALM5.

However, a recent study has complicated this picture, reporting that SALM4 can coimmunoprecipitate with SALM2 in the mouse brain (Lie et al., 2016). This study further showed that SALM4 can also form complexes with SALM3 and SALM5 in heterologous cells. Additional domain-mapping experiments revealed that the LRR domain of SALM4 is important for its interactions with SALM2/5, whereas the transmembrane domain is important for its interaction with SALM3. Thus, *cis*-interactions between SALMs may be more complex than previously thought.

What might be the molecular mechanisms underlying the *cis*-interactions of SALMs? Perhaps, the aforementioned dimeric nature of SALMs revealed by X-ray crystallography may explain some of these interactions. The fact that the LRR domain of SALM4 is important for its *cis*-complex formation with SALM2/5 is consistent with the critical role of LRR domains in SALM dimerization. However, the SALM4–SALM3 *cis*-interaction, which requires the transmembrane domain, is unlikely to involve LRR dimerization.

What could be the possible functions of *cis*-interactions in SALMs? If heteromeric dimerization occurs, these interactions may increase the diversity of the subunit composition of SALM dimers. For instance, a SALM2–SALM5 dimer might bring SALM5 into proximity with the SALM2–PSD-95 complex and promote SALM5-dependent presynaptic differentiation at excitatory synapses, thereby shifting the balance of excitatory and inhibitory synapses towards excitation. In addition, these interactions may increase the diversity of non-SALM proteins, including trans-synaptic adhesion proteins, *cis*-neighboring membrane proteins, and cytoplasmic adaptor/signaling proteins around SALM complexes. This, in turn, could influence the synaptic trafficking and synapse-modulatory actions of SALMs.

IN VIVO FUNCTIONS OF SALM1/Lrfn2

As noted above, SALM1 was previously shown to be involved in surface expression and dendritic clustering of NMDARs (Wang et al., 2006). More recently, immunogold electron microscopy has revealed strong colocalization of SALM1 with the GluN1 subunit of NMDARs (Thevenon et al., 2016). These results suggest that SALM1 promotes synaptic clustering of NMDARs, although *in vivo* support for these findings has been lacking.

A recent study reported a mouse line that lacks exon 2 of the *Lrfn2* gene encoding SALM1 (*Lrfn2*$^{-/-}$ mice; Morimura et al., 2017; **Table 2**). Contrary to the expectation that *Lrfn2* KO would suppress synaptic NMDAR function, *Lrfn2*$^{-/-}$ mice displayed normal NMDAR-mediated synaptic transmission in the hippocampus. Instead, many SALM1-lacking synapses also lacked AMPARs, as evidenced by the slightly reduced number of dendritic spines, but markedly reduced frequency of miniature excitatory postsynaptic currents (mEPSCs), as well as altered failure rates with minimal stimulation of NMDA/AMPA-evoked postsynaptic currents (EPSCs). This suggests that many *Lrfn2*$^{-/-}$ excitatory synapses are silent synapses, an immature form of excitatory synapse that harbors NMDARs, but not AMPARs (Isaac et al., 1995; Liao et al., 1995). Therefore, *Lrfn2* KO appears

TABLE 2 | Main phenotypes of SALM/Lrfn-mutant mice.

Protein/gene name	Main synaptic phenotypes	Main behavioral phenotypes	Reference
SALM1/Lrfn2	Spine head size ↓ Spine length ↑ Silent synapse number ↑ LTP ↑	Social interaction ↓ Repetitive behavior ↑ Acoustic startle ↑ Prepulse inhibition ↓	Morimura et al. (2017)
SALM3/Lrfn4	Excitatory synapse number ↓ LTP and LTD –	Locomotor activity ↓	Li et al. (2015)
SALM4/Lrfn3	Excitatory and inhibitory synapse number ↑ Excitatory synapse number normalized by SALM4/SALM3 double KO		Lie et al. (2016)

to suppress synaptic delivery of AMPARs to NMDAR-only synapses during developmental synapse maturation, rather than acting at the previous step to suppress synaptic levels of NMDARs. In line with this change, *Lrfn2* KO causes an increase in NMDAR-dependent long-term potentiation (LTP), likely because silent synapses have more room to accommodate incoming AMPARs. In addition to these functional changes at excitatory synapses, *Lrfn2*$^{-/-}$ mice show morphological changes, including reduced spine head size and increased spine length (Morimura et al., 2017), suggesting that *Lrfn2* KO suppresses normal development of dendritic spines. Collectively, these findings suggest that *Lrfn2* KO suppresses both morphological and functional maturation of excitatory synapses.

Behaviorally, *Lrfn2*$^{-/-}$ mice display autistic-like behavioral abnormalities, including suppressed social interaction and enhanced repetitive behaviors. They also show enhanced acoustic startle and suppressed prepulse inhibition, suggestive of impaired sensory-motor gating. Furthermore, using targeted gene sequencing, this study identified point mutations of the *LRFN2* gene in individuals with autism spectrum disorders (ASDs), and demonstrated that a missense mutation inhibits the association of SALM1 with PSD-95. Interestingly, *Lrfn2*$^{-/-}$ mice show enhanced spatial learning and fear memory, consistent with the enhanced LTP observed in these mice and a report that some individuals with *LRFN2* mutations show enhanced memory together with delayed speech development (Thevenon et al., 2016).

IN VIVO FUNCTIONS OF SALM3/Lrfn4

Mice carrying a null mutation of the *Lrfn4* gene (*Lrfn4*$^{-/-}$ mice) have been used to investigate *in vivo* functions of SALM3 (Li et al., 2015). These mice show reduced excitatory synapse number, as supported by spontaneous excitatory synaptic transmission and electron microscopic data, but their inhibitory synapses are minimally affected. However, NMDAR-mediated synaptic transmission and NMDAR-dependent synaptic plasticity—both LTP and LTD (long-term depression)—were unaffected in *Lrfn4*$^{-/-}$ mice.

The strong influence of *Lrfn4* KO on excitatory synapse development relative to synaptic function or plasticity is in line with the role of SALM3 as a synapse organizer that regulates presynaptic differentiation by interacting with LAR-RPTPs. SALM3/Lrfn4 was found to associate with 14-3-3 and NCK signaling adaptors to regulate actin-rich lamellipodial structures in monocytes through mechanisms involving the Rac1 small GTPase (Konakahara et al., 2011, 2012). Given that dendritic spines are actin-rich structures (Cingolani and Goda, 2008), LAR-RPTP–induced SALM3 clustering at postsynaptic sites might promote 14-3-3/NCK- and Rac1-dependent actin polymerization to promote synapse development.

Behaviorally, *Lrfn4*$^{-/-}$ mice show reduced locomotor activity in both novel and familiar environments, but exhibit normal anxiety-like behaviors. These mice also perform normally in learning and memory tests, including Morris water maze, novel object recognition, contextual fear conditioning, and T-maze spontaneous/reward alternations. The minimal effect of *Lrfn4* KO on learning and memory behaviors is in keeping with the largely normal LTP in these mice. However, it remains unclear how *Lrfn4* KO leads to behavioral hypoactivity.

SALM3 has recently been implicated in the regulation of epilepsy (Li et al., 2017). This study showed that SALM3/Lrfn4 expression is significantly increased in two distinct animal models of epilepsy, and further found that suppression of SALM3 expression by virus-mediated SALM3 knockdown ameliorates seizure activity as well as neuronal hyperexcitability. These results suggest that SALM3 promotes epileptogenesis and that its suppression has therapeutic potential.

IN VIVO FUNCTIONS OF SALM4/Lrfn3

Whether SALM4 regulates synapse development or function has remained unclear, partly because SALM4 does not have synaptogenic activity (unlike SALM3 and SALM5) or a PSD-95-binding C-terminal tail (unlike SALMs1–3). However, it should be noted that SALM4 is immunodetected in neuronal synapses in addition to dendrites and axons (Seabold et al., 2008). A recent study using mice lacking SALM4 (*Lrfn3*$^{-/-}$ mice) demonstrated that SALM4 has unexpected negative effects on the density of excitatory and inhibitory synapses (Lie et al., 2016). Specifically, *Lrfn3*$^{-/-}$ mice display increases in the number of excitatory and inhibitory synapses in the hippocampus, as supported by the density of PSDs and frequency of mE/IPSCs.

This study further addressed the mechanisms underlying the SALM4-dependent negative regulation of synapse density, reporting that postsynaptic SALM4 interacts in *cis* with SALM3,

which possesses synaptogenic activity and exhibits a highly overlapping distribution pattern in the brain (Mah et al., 2010; Lie et al., 2016). This *cis*-interaction, in turn, inhibits the trans-synaptic interaction of SALM3 with presynaptic LAR-RPTPs and suppresses SALM3-dependent presynaptic differentiation (Lie et al., 2016). In support of these conclusions, coexpression of SALM4 with SALM3 in heterologous cells blocks binding of purified soluble LAR to SALM3 and inhibits SALM3-dependent presynaptic differentiation in contacting axons of cocultured neurons. Given that the transmembrane domain of SALM4 is required for *cis*-interactions with and inhibition of SALM3, it is unlikely that LRR-mediated SALM4–SALM3 heterodimerization, if it occurs, underlies the *cis*-inhibition.

Importantly, genetic support for these conclusions is provided by SALM3/SALM4 double-KO mice, in which the increased excitatory synapse density observed in SALM4 single-KO mice is normalized, as supported by both electron microscopy and mEPSC recordings (Lie et al., 2016). In contrast, double KO does not normalize the increased density of inhibitory synapses, suggesting that SALM4 negatively regulates inhibitory synapses through mechanisms independent of SALM3. Because SALM4 can also interact in *cis* with SALM5, which possesses synaptogenic activity (Mah et al., 2010), SALM5 might also play a role in SALM4-dependent regulation of inhibitory synapses. In support of this possibility, expression of SALM3 and SALM5 in heterologous cells and cultured neurons induces both excitatory and inhibitory presynaptic contacts, and SALM5 knockdown in cultured neurons suppresses both excitatory and inhibitory synapses (Mah et al., 2010). However, whereas SALM3, artificially aggregated on dendritic surfaces of cultured neurons, induces secondary clustering of PSD-95, aggregated SALM5 does not induce gephyrin clustering (Mah et al., 2010).

SALMs IN NEURODEVELOPMENTAL DISORDERS

SALMs have been implicated in diverse neurodevelopmental and psychiatric disorders (**Table 3**). *LRFN2*, encoding SALM1, has recently been implicated in learning disabilities, as supported by impaired working memory and executive function in three individuals in a family with a 6p21 autosomal dominant microdeletion (∼870 kb) encompassing three genes, including *LRFN2* (Thevenon et al., 2016). Similarly, levels of SALM1/LRFN2 proteins were found to be substantially decreased in postmortem brains of patients with neurodegenerative disorders associated with cognitive declines such as Alzheimer's disease and Parkinson's disease with dementia (Bereczki et al., 2018). In addition, single nucleotide polymorphism (SNP) analyses have linked *LRFN2* with the risk of antisocial personality disorder (Rautiainen et al., 2016). More recently, a targeted gene sequencing strategy identified missense mutations of *LRFN2* in individuals with ASD (Morimura et al., 2017), as noted above.

LRFN5, encoding SALM5, has been frequently associated with ASDs. SNP analyses have linked a chromosomal locus on 14q21.1 between *FBXO33* and *LRFN5* to a risk for ASD (Wang et al., 2009). A balanced de novo t(14;21)(q21.1;p11.2) translocation that leads to a ∼10-fold reduction in the expression of *LRFN5*, located ∼2 Mb from the translocation breakpoint, was identified in a 19-year-old girl with autism and intellectual disability (de Bruijn et al., 2010). In addition, a genome-wide association study showed that *LRFN5* is associated with a risk for ASDs (Connolly et al., 2013). Similar results were reported in a whole-exome sequencing study, although the association score was not high (De Rubeis et al., 2014). More recently, family-based diagnostic exome sequencing identified a point mutation (p.V572X) in *LRFN5* in an individual with ASD (Farwell Hagman et al., 2017).

LRFN5 has also been implicated in other neurodevelopmental and psychiatric disorders. For example, an ∼890-kb deletion encompassing *LRFN5* exons was identified in a girl with developmental delay, learning disability, seizures, microcephaly and receding forehead by high-resolution array comparative genomic hybridization (Mikhail et al., 2011). In addition, a high-resolution linkage analysis identified *LRFN5* among schizophrenia-related copy number variations (Xu et al., 2009). Lastly, a recent genome-wide gene- and pathway-based analysis identified *LRFN5* as one of four depression-associated genes (Nho et al., 2015). It is unclear why *LRFN5* is frequently associated with brain disorders. Although its synaptogenic activity might be a contributor, the fact that SALM3, another synaptogenic SALM, is not closely associated with brain disorders suggests against this possibility. Studies using transgenic mice lacking *Lrfn5* may provide insight into this question.

TABLE 3 | Associations of SALMs/LRFNs with neurodevelopmental and psychiatric disorders.

Gene/protein name	Disorders	Reference
LRFN2/SALM1	Learning disability	Thevenon et al. (2016)
	Antisocial personality disorder	Rautiainen et al. (2016)
	ASD	Morimura et al. (2017)
	Schizophrenia	Morimura et al. (2017)
LRFN5/SALM5	ASD	Wang et al. (2009)
	ASD and intellectual disability	de Bruijn et al. (2010)
	ASD	Connolly et al. (2013)
	ASD	De Rubeis et al. (2014)
	ASD	Farwell Hagman et al. (2017)
	Schizophrenia	Xu et al. (2009)
	Developmental delay and seizure	Mikhail et al. (2011)
	Depression	Nho et al. (2015)

PERSPECTIVES

Since the discovery of the SALM/Lrfn family about a decade ago, a large number of studies have elucidated basic characteristics and functional features of SALMs. Recent reports have shed additional light on the properties and functions of SALMs, identifying novel presynaptic ligands (LAR-RPTPs) of SALM3/5, resolving the crystal structures of SALMs in complex with LAR-RPTPs, elucidating the *in vivo* functions of SALMs, and revealing clinical implications of SALMs, collectively helping to better

understand the functions of this protein family. However, our understanding of SALMs remains at a relatively early stage, leaving a number of questions to be explored.

For example, although SALMs can form heterodimers, and SALM dimers can explain the reported heteromeric *cis*-interactions between SALMs in the brain, it remains unclear whether SALM family members other than SALM5 and SALM2 form dimeric structures. It is also unclear whether SALMs directly interact with NMDA/AMPARs and, if so, whether these interactions regulate receptor functions or synaptic adhesions in a reciprocal manner. Because SALM3 and -5 are part of many LAR-RPTP–interacting postsynaptic adhesion molecules, whether SALM3/5 has its own unique roles, or redundant functions, remains to be determined.

In vivo functions of SALMs also require further exploration. It will be interesting to determine whether SALMs have distinct functions in different brain regions and cell types. Because individual SALMs have largely unique cytoplasmic regions, SALM-associated synaptic signaling pathways are likely to be quite diverse. Circuit mechanisms underlying various behavioral phenotypes of *Salm*-KO mice, in particular those associated with SALM-related developmental and psychiatric disorders, also need to be investigated. Given the rapid increase in information on the biology and pathophysiology of SALMs, the next 10 years are likely to witness a dramatic increase in our understanding of this interesting family of synaptic adhesion molecules.

AUTHOR CONTRIBUTIONS

EL, YL, RK and EK wrote the manuscript.

ACKNOWLEDGMENTS

We would like thank Haram Park for help with figure design and drawing, and Yeonsoo Choi and Dr. Doyoun Kim for helpful comments on the manuscript. This study was supported by the Institute for Basic Science (IBS-R002-D1 to EK).

REFERENCES

Aricescu, A. R., McKinnell, I. W., Halfter, W., and Stoker, A. W. (2002). Heparan sulfate proteoglycans are ligands for receptor protein tyrosine phosphatase sigma. *Mol. Cell. Biol.* 22, 1881–1892. doi: 10.1128/mcb.22.6.1881-1892.2002

Bemben, M. A., Shipman, S. L., Nicoll, R. A., and Roche, K. W. (2015). The cellular and molecular landscape of neuroligins. *Trends Neurosci.* 38, 496–505. doi: 10.1016/j.tins.2015.06.004

Bereczki, E., Branca, R. M., Francis, P. T., Pereira, J. B., Baek, J. H., Hortobágyi, T., et al. (2018). Synaptic markers of cognitive decline in neurodegenerative diseases: a proteomic approach. *Brain* 141, 582–595. doi: 10.1093/brain/awx352

Biederer, T., and Scheiffele, P. (2007). Mixed-culture assays for analyzing neuronal synapse formation. *Nat. Protoc.* 2, 670–676. doi: 10.1038/nprot.2007.92

Biederer, T., and Stagi, M. (2008). Signaling by synaptogenic molecules. *Curr. Opin. Neurobiol.* 18, 261–269. doi: 10.1016/j.conb.2008.07.014

Budreck, E. C., Kwon, O. B., Jung, J. H., Baudouin, S., Thommen, A., Kim, H. S., et al. (2013). Neuroligin-1 controls synaptic abundance of NMDA-type glutamate receptors through extracellular coupling. *Proc. Natl. Acad. Sci. U S A* 110, 725–730. doi: 10.1073/pnas.1214718110

Cao, X., and Tabuchi, K. (2017). Functions of synapse adhesion molecules neurexin/neuroligins and neurodevelopmental disorders. *Neurosci. Res.* 116, 3–9. doi: 10.1016/j.neures.2016.09.005

Choi, Y., Nam, J., Whitcomb, D. J., Song, Y. S., Kim, D., Jeon, S., et al. (2016). SALM5 trans-synaptically interacts with LAR-RPTPs in a splicing-dependent manner to regulate synapse development. *Sci. Rep.* 6:26676. doi: 10.1038/srep26676

Choii, G., and Ko, J. (2015). Gephyrin: a central GABAergic synapse organizer. *Exp. Mol. Med.* 47:e158. doi: 10.1038/emm.2015.5

Cingolani, L. A., and Goda, Y. (2008). Actin in action: the interplay between the actin cytoskeleton and synaptic efficacy. *Nat. Rev. Neurosci.* 9, 344–356. doi: 10.1038/nrn2373

Coles, C. H., Mitakidis, N., Zhang, P., Elegheert, J., Lu, W., Stoker, A. W., et al. (2014). Structural basis for extracellular cis and trans RPTPsigma signal competition in synaptogenesis. *Nat. Commun.* 5:5209. doi: 10.1038/ncomms6209

Connolly, J. J., Glessner, J. T., and Hakonarson, H. (2013). A genome-wide association study of autism incorporating autism diagnostic interview-revised, autism diagnostic observation schedule, and social responsiveness scale. *Child Dev.* 84, 17–33. doi: 10.1111/j.1467-8624.2012.01838.x

Dalva, M. B., McClelland, A. C., and Kayser, M. S. (2007). Cell adhesion molecules: signalling functions at the synapse. *Nat. Rev. Neurosci.* 8, 206–220. doi: 10.1038/nrn2075

de Bruijn, D. R., van Dijk, A. H., Pfundt, R., Hoischen, A., Merkx, G. F., Gradek, G. A., et al. (2010). Severe progressive autism associated with two de novo changes: a 2.6-Mb 2q31.1 deletion and a balanced t(14;21)(q21.1;p11.2) translocation with long-range epigenetic silencing of LRFN5 expression. *Mol. Syndromol.* 1, 46–57. doi: 10.1159/000280290

de Curtis, I. (2011). Function of liprins in cell motility. *Exp. Cell Res.* 317, 1–8. doi: 10.1016/j.yexcr.2010.09.014

De Rubeis, S., He, X., Goldberg, A. P., Poultney, C. S., Samocha, K., Cicek, A. E., et al. (2014). Synaptic, transcriptional and chromatin genes disrupted in autism. *Nature* 515, 209–215. doi: 10.1038/nature13772

de Wit, J., and Ghosh, A. (2016). Specification of synaptic connectivity by cell surface interactions. *Nat. Rev. Neurosci.* 17, 22–35. doi: 10.1038/nrn.2015.3

Dunah, A. W., Hueske, E., Wyszynski, M., Hoogenraad, C. C., Jaworski, J., Pak, D. T., et al. (2005). LAR receptor protein tyrosine phosphatases in the development and maintenance of excitatory synapses. *Nat. Neurosci.* 8, 458–467. doi: 10.1038/nn1416

Elegheert, J., Cvetkovska, V., Clayton, A. J., Heroven, C., Vennekens, K. M., Smukowski, S. N., et al. (2017). Structural mechanism for modulation of synaptic neuroligin-neurexin signaling by MDGA proteins. *Neuron* 95, 896.e10–913.e10. doi: 10.1016/j.neuron.2017.07.040

Farhy-Tselnicker, I., van Casteren, A. C. M., Lee, A., Chang, V. T., Aricescu, A. R., and Allen, N. J. (2017). Astrocyte-secreted glypican 4 regulates release of neuronal pentraxin 1 from axons to induce functional synapse formation. *Neuron* 96, 428.e13–445.e13. doi: 10.1016/j.neuron.2017.09.053

Farwell Hagman, K. D., Shinde, D. N., Mroske, C., Smith, E., Radtke, K., Shahmirzadi, L., et al. (2017). Candidate-gene criteria for clinical reporting: diagnostic exome sequencing identifies altered candidate genes among 8% of patients with undiagnosed diseases. *Genet. Med.* 19, 224–235. doi: 10.1038/gim.2016.95

Gangwar, S. P., Zhong, X., Seshadrinathan, S., Chen, H., Machius, M., and Rudenko, G. (2017). Molecular mechanism of MDGA1: regulation of neuroligin 2: neurexin trans-synaptic bridges. *Neuron* 94, 1132.e4–1141.e4. doi: 10.1016/j.neuron.2017.06.009

Goto-Ito, S., Yamagata, A., Sato, Y., Uemura, T., Shiroshima, T., Maeda, A., et al. (2018). Structural basis of trans-synaptic interactions between PTPδ and SALMs for inducing synapse formation. *Nat. Commun.* 9:269. doi: 10.1038/s41467-017-02417-z

Han, K., and Kim, E. (2008). Synaptic adhesion molecules and PSD-95. *Prog. Neurobiol.* 84, 263–283. doi: 10.1016/j.pneurobio.2007.10.011

Han, S., Li, J., and Ting, A. Y. (2017). Proximity labeling: spatially resolved proteomic mapping for neurobiology. *Curr. Opin. Neurobiol.* 50, 17–23. doi: 10.1016/j.conb.2017.10.015

Hayashi, M. K., Tang, C., Verpelli, C., Narayanan, R., Stearns, M. H., Xu, R. M., et al. (2009). The postsynaptic density proteins Homer and Shank form

a polymeric network structure. *Cell* 137, 159–171. doi: 10.1016/j.cell.2009.01.050

Hsueh, Y. P., Kim, E., and Sheng, M. (1997). Disulfide-linked head-to-head multimerization in the mechanism of ion channel clustering by PSD-95. *Neuron* 18, 803–814. doi: 10.1016/s0896-6273(00)80319-0

Isaac, J. T., Nicoll, R. A., and Malenka, R. C. (1995). Evidence for silent synapses: implications for the expression of LTP. *Neuron* 15, 427–434. doi: 10.1016/0896-6273(95)90046-2

Jang, S., Lee, H., and Kim, E. (2017). Synaptic adhesion molecules and excitatory synaptic transmission. *Curr. Opin. Neurobiol.* 45, 45–50. doi: 10.1016/j.conb.2017.03.005

Johnson, K. G., Tenney, A. P., Ghose, A., Duckworth, A. M., Higashi, M. E., Parfitt, K., et al. (2006). The HSPGs syndecan and dallylike bind the receptor phosphatase LAR and exert distinct effects on synaptic development. *Neuron* 49, 517–531. doi: 10.1016/j.neuron.2006.01.026

Johnson, K. G., and Van Vactor, D. (2003). Receptor protein tyrosine phosphatases in nervous system development. *Physiol. Rev.* 83, 1–24. doi: 10.1152/physrev.00016.2002

Kim, E., Cho, K. O., Rothschild, A., and Sheng, M. (1996). Heteromultimerization and NMDA receptor-clustering activity of Chapsyn-110, a member of the PSD-95 family of proteins. *Neuron* 17, 103–113. doi: 10.1016/s0896-6273(00)80284-6

Kim, J. A., Kim, D., Won, S. Y., Han, K. A., Park, D., Cho, E., et al. (2017). Structural insights into modulation of neurexin-neuroligin trans-synaptic adhesion by MDGA1/neuroligin-2 complex. *Neuron* 94, 1121.e6–1131.e6. doi: 10.1016/j.neuron.2017.05.034

Ko, J., Choii, G., and Um, J. W. (2015). The balancing act of GABAergic synapse organizers. *Trends Mol. Med.* 21, 256–268. doi: 10.1016/j.molmed.2015.01.004

Ko, J., Kim, S., Chung, H. S., Kim, K., Han, K., Kim, H., et al. (2006). SALM synaptic cell adhesion-like molecules regulate the differentiation of excitatory synapses. *Neuron* 50, 233–245. doi: 10.1016/j.neuron.2006.04.005

Ko, J. S., Pramanik, G., Um, J. W., Shim, J. S., Lee, D., Kim, K. H., et al. (2015). PTPσ functions as a presynaptic receptor for the glypican-4/LRRTM4 complex and is essential for excitatory synaptic transmission. *Proc. Natl. Acad. Sci. U S A* 112, 1874–1879. doi: 10.1073/pnas.1410138112

Konakahara, S., Saitou, M., Hori, S., Nakane, T., Murai, K., Itoh, R., et al. (2011). A neuronal transmembrane protein LRFN4 induces monocyte/macrophage migration via actin cytoskeleton reorganization. *FEBS Lett.* 585, 2377–2384. doi: 10.1016/j.febslet.2011.06.011

Konakahara, S., Suzuki, Y., Kawakami, T., Saitou, M., Kajikawa, M., Masuho, Y., et al. (2012). A neuronal transmembrane protein LRFN4 complexes with 14–3-3s and NCK1 to induce morphological change in monocytic cells via Rac1-mediated actin cytoskeleton reorganization. *FEBS Lett.* 586, 2251–2259. doi: 10.1016/j.febslet.2012.05.053

Krueger, D. D., Tuffy, L. P., Papadopoulos, T., and Brose, N. (2012). The role of neurexins and neuroligins in the formation, maturation, and function of vertebrate synapses. *Curr. Opin. Neurobiol.* 22, 412–422. doi: 10.1016/j.conb.2012.02.012

Krueger-Burg, D., Papadopoulos, T., and Brose, N. (2017). Organizers of inhibitory synapses come of age. *Curr. Opin. Neurobiol.* 45, 66–77. doi: 10.1016/j.conb.2017.04.003

Kwon, S. K., Woo, J., Kim, S. Y., Kim, H., and Kim, E. (2010). Trans-synaptic adhesions between netrin-G ligand-3 (NGL-3) and receptor tyrosine phosphatases LAR, protein-tyrosine phosphatase δ (PTPδ), and PTPσ via specific domains regulate excitatory synapse formation. *J. Biol. Chem.* 285, 13966–13978. doi: 10.1074/jbc.M109.061127

Lee, K., Kim, Y., Lee, S. J., Qiang, Y., Lee, D., Lee, H. W., et al. (2013). MDGAs interact selectively with neuroligin-2 but not other neuroligins to regulate inhibitory synapse development. *Proc. Natl. Acad. Sci. U S A* 110, 336–341. doi: 10.1073/pnas.1219987110

Li, J., Chen, L., Wang, N., Jiang, G., Wu, Y., and Zhang, Y. (2017). Effect of synaptic adhesion-like molecule 3 on epileptic seizures: evidence from animal models. *Epilepsy Behav.* 69, 18–23. doi: 10.1016/j.yebeh.2016.11.023

Li, Y., Zhang, P., Choi, T. Y., Park, S. K., Park, H., Lee, E. J., et al. (2015). Splicing-dependent trans-synaptic SALM3-LAR-RPTP interactions regulate excitatory synapse development and locomotion. *Cell Rep.* 12, 1618–1630. doi: 10.1016/j.celrep.2015.08.002

Liao, D., Hessler, N. A., and Malinow, R. (1995). Activation of postsynaptically silent synapses during pairing-induced LTP in CA1 region of hippocampal slice. *Nature* 375, 400–404. doi: 10.1038/375400a0

Lie, E., Ko, J. S., Choi, S. Y., Roh, J. D., Cho, Y. S., Noh, R., et al. (2016). SALM4 suppresses excitatory synapse development by cis-inhibiting trans-synaptic SALM3-LAR adhesion. *Nat. Commun.* 7:12328. doi: 10.1038/ncomms12328

Lin, Z., Liu, J., Ding, H., Xu, F., and Liu, H. (2018). Structural basis of SALM5-induced PTPδ dimerization for synaptic differentiation. *Nat. Commun.* 9:268. doi: 10.1038/s41467-017-02414-2

Loh, K. H., Stawski, P. S., Draycott, A. S., Udeshi, N. D., Lehrman, E. K., Wilton, D. K., et al. (2016). Proteomic analysis of unbounded cellular compartments: synaptic clefts. *Cell* 166, 1295.e21–1307.e21. doi: 10.1016/j.cell.2016.07.041

Mah, W., Ko, J., Nam, J., Han, K., Chung, W. S., and Kim, E. (2010). Selected SALM (synaptic adhesion-like molecule) family proteins regulate synapse formation. *J. Neurosci.* 30, 5559–5568. doi: 10.1523/JNEUROSCI.4839-09.2010

Mikhail, F. M., Lose, E. J., Robin, N. H., Descartes, M. D., Rutledge, K. D., Rutledge, S. L., et al. (2011). Clinically relevant single gene or intragenic deletions encompassing critical neurodevelopmental genes in patients with developmental delay, mental retardation, and/or autism spectrum disorders. *Am. J. Med. Genet. A* 155A, 2386–2396. doi: 10.1002/ajmg.a.34177

Missler, M., Sudhof, T. C., and Biederer, T. (2012). Synaptic cell adhesion. *Cold Spring Harb. Perspect. Biol.* 4:a005694. doi: 10.1101/cshperspect.a005694

Montani, C., Ramos-Brossier, M., Ponzoni, L., Gritti, L., Cwetsch, A. W., Braida, D., et al. (2017). The X-linked intellectual disability protein IL1RAPL1 regulates dendrite complexity. *J. Neurosci.* 37, 6606–6627. doi: 10.1523/JNEUROSCI.3775-16.2017

Morimura, N., Inoue, T., Katayama, K., and Aruga, J. (2006). Comparative analysis of structure, expression and PSD95-binding capacity of Lrfn, a novel family of neuronal transmembrane proteins. *Gene* 380, 72–83. doi: 10.1016/j.gene.2006.05.014

Morimura, N., Yasuda, H., Yamaguchi, K., Katayama, K. I., Hatayama, M., Tomioka, N. H., et al. (2017). Autism-like behaviours and enhanced memory formation and synaptic plasticity in Lrfn2/SALM1-deficient mice. *Nat. Commun.* 8:15800. doi: 10.1038/ncomms15800

Naisbitt, S., Kim, E., Tu, J. C., Xiao, B., Sala, C., Valtschanoff, J., et al. (1999). Shank, a novel family of postsynaptic density proteins that binds to the NMDA receptor/PSD-95/GKAP complex and cortactin. *Neuron* 23, 569–582. doi: 10.1016/s0896-6273(00)80809-0

Nakashiba, T., Ikeda, T., Nishimura, S., Tashiro, K., Honjo, T., Culotti, J. G., et al. (2000). Netrin-G1: a novel glycosyl phosphatidylinositol-linked mammalian netrin that is functionally divergent from classical netrins. *J. Neurosci.* 20, 6540–6550.

Nam, J., Mah, W., and Kim, E. (2011). The SALM/Lrfn family of leucine-rich repeat-containing cell adhesion molecules. *Semin Cell Dev. Biol.* 22, 492–498. doi: 10.1016/j.semcdb.2011.06.005

Nho, K., Ramanan, V. K., Horgusluoglu, E., Kim, S., Inlow, M. H., Risacher, S. L., et al. (2015). Comprehensive gene- and pathway-based analysis of depressive symptoms in older adults. *J. Alzheimers Dis.* 45, 1197–1206. doi: 10.3233/JAD-148009

O'Grady, P., Krueger, N. X., Streuli, M., and Saito, H. (1994). Genomic organization of the human LAR protein tyrosine phosphatase gene and alternative splicing in the extracellular fibronectin type-III domains. *J. Biol. Chem.* 269, 25193–25199.

Pettem, K. L., Yokomaku, D., Takahashi, H., Ge, Y., and Craig, A. M. (2013). Interaction between autism-linked MDGAs and neuroligins suppresses inhibitory synapse development. *J. Cell Biol.* 200, 321–336. doi: 10.1083/jcb.201206028

Pulido, R., Krueger, N. X., Serra-Pagès, C., Saito, H., and Streuli, M. (1995a). Molecular characterization of the human transmembrane protein-tyrosine phosphatase δ. Evidence for tissue-specific expression of alternative human transmembrane protein-tyrosine phosphatase δ isoforms. *J. Biol. Chem.* 270, 6722–6728. doi: 10.1074/jbc.270.12.6722

Pulido, R., Serra-Pagès, C., Tang, M., and Streuli, M. (1995b). The LAR/PTP δ/PTP σ subfamily of transmembrane protein-tyrosine- phosphatases: multiple human LAR, PTP δ and PTP σ isoforms are expressed in a tissue-specific

manner and associate with the LAR- interacting protein LIP.1. *Proc. Natl. Acad. Sci. U S A* 92, 11686–11690. doi: 10.1073/pnas.92.25.11686

Rautiainen, M. R., Paunio, T., Repo-Tiihonen, E., Virkkunen, M., Ollila, H. M., Sulkava, S., et al. (2016). Genome-wide association study of antisocial personality disorder. *Transl. Psychiatry* 6:e883. doi: 10.1038/tp.2016.155

Sanes, J. R., and Yamagata, M. (2009). Many paths to synaptic specificity. *Annu. Rev. Cell Dev. Biol.* 25, 161–195. doi: 10.1146/annurev.cellbio.24.110707.175402

Scheiffele, P., Fan, J., Choih, J., Fetter, R., and Serafini, T. (2000). Neuroligin expressed in nonneuronal cells triggers presynaptic development in contacting axons. *Cell* 101, 657–669. doi: 10.1016/s0092-8674(00)80877-6

Seabold, G. K., Wang, P. Y., Chang, K., Wang, C. Y., Wang, Y. X., Petralia, R. S., et al. (2008). The SALM family of adhesion-like molecules forms heteromeric and homomeric complexes. *J. Biol. Chem.* 283, 8395–8405. doi: 10.1074/jbc.M709456200

Seabold, G. K., Wang, P. Y., Petralia, R. S., Chang, K., Zhou, A., Mcdermott, M. I., et al. (2012). Dileucine and PDZ-binding motifs mediate synaptic adhesion-like molecule 1 (SALM1) trafficking in hippocampal neurons. *J. Biol. Chem.* 287, 4470–4484. doi: 10.1074/jbc.M111.279661

Serra-Pagès, C., Kedersha, N. L., Fazikas, L., Medley, Q., Debant, A., and Streuli, M. (1995). The LAR transmembrane protein tyrosine phosphatase and a coiled-coil LAR-interacting protein co-localize at focal adhesions. *EMBO J.* 14, 2827–2838.

Serra-Pagès, C., Medley, Q. G., Tang, M., Hart, A., and Streuli, M. (1998). Liprins, a family of LAR transmembrane protein-tyrosine phosphatase- interacting proteins. *J. Biol. Chem.* 273, 15611–15620. doi: 10.1074/jbc.273.25.15611

Shen, K., and Scheiffele, P. (2010). Genetics and cell biology of building specific synapse connectivity. *Annu. Rev. Neurosci.* 33, 473–507. doi: 10.1146/annurev.neuro.051508.135302

Sheng, M., and Hoogenraad, C. C. (2007). The postsynaptic architecture of excitatory synapses: a more quantitative view. *Annu. Rev. Biochem.* 76, 823–847. doi: 10.1146/annurev.biochem.76.060805.160029

Sheng, M., and Kim, E. (2011). The postsynaptic organization of synapses. *Cold Spring Harb. Perspect. Biol.* 3:a005678. doi: 10.1101/cshperspect.a005678

Sheng, M., and Sala, C. (2001). PDZ domains and the organization of supramolecular complexes. *Annu. Rev. Neurosci.* 24, 1–29. doi: 10.1146/annurev.neuro.24.1.1

Siddiqui, T. J., and Craig, A. M. (2011). Synaptic organizing complexes. *Curr. Opin. Neurobiol.* 21, 132–143. doi: 10.1016/j.conb.2010.08.016

Song, Y. S., and Kim, E. (2013). Presynaptic proteoglycans: sweet organizers of synapse development. *Neuron* 79, 609–611. doi: 10.1016/j.neuron.2013.07.048

Song, Y. S., Lee, H. J., Prosselkov, P., Itohara, S., and Kim, E. (2013). Trans-induced cis interaction in the tripartite NGL-1, netrin-G1 and LAR adhesion complex promotes development of excitatory synapses. *J. Cell Sci.* 126, 4926–4938. doi: 10.1242/jcs.129718

Stryker, E., and Johnson, K. G. (2007). LAR, liprin α and the regulation of active zone morphogenesis. *J. Cell Sci.* 120, 3723–3728. doi: 10.1242/jcs.03491

Sudhof, T. C. (2017). Synaptic neurexin complexes: a molecular code for the logic of neural circuits. *Cell* 171, 745–769. doi: 10.1016/j.cell.2017.10.024

Suzuki, K., Tsunekawa, Y., Hernandez-Benitez, R., Wu, J., Zhu, J., Kim, E. J., et al. (2016). *in vivo* genome editing via CRISPR/Cas9 mediated homology-independent targeted integration. *Nature* 540, 144–149. doi: 10.1038/nature20565

Swanwick, C. C., Shapiro, M. E., Vicini, S., and Wenthold, R. J. (2010). Flotillin-1 mediates neurite branching induced by synaptic adhesion-like molecule 4 in hippocampal neurons. *Mol. Cell. Neurosci.* 45, 213–225. doi: 10.1016/j.mcn.2010.06.012

Swanwick, C. C., Shapiro, M. E., Yi, Z., Chang, K., and Wenthold, R. J. (2009). NMDA receptors interact with flotillin-1 and -2, lipid raft-associated proteins. *FEBS Lett.* 583, 1226–1230. doi: 10.1016/j.febslet.2009.03.017

Takahashi, H., Arstikaitis, P., Prasad, T., Bartlett, T. E., Wang, Y. T., Murphy, T. H., et al. (2011). Postsynaptic TrkC and presynaptic PTPsigma function as a bidirectional excitatory synaptic organizing complex. *Neuron* 69, 287–303. doi: 10.1016/j.neuron.2010.12.024

Takahashi, H., and Craig, A. (2013). Protein tyrosine phosphatases PTPδ, PTPσ, and LAR: presynaptic hubs for synapse organization. *Trends Neurosci.* 36, 522–534. doi: 10.1016/j.tins.2013.06.002

Takahashi, H., Katayama, K., Sohya, K., Miyamoto, H., Prasad, T., Matsumoto, Y., et al. (2012). Selective control of inhibitory synapse development by Slitrk3-PTPδ trans-synaptic interaction. *Nat. Neurosci.* 15, 389–398. doi: 10.1038/nn.3040

Taniguchi, H., Gollan, L., Scholl, F. G., Mahadomrongkul, V., Dobler, E., Limthong, N., et al. (2007). Silencing of neuroligin function by postsynaptic neurexins. *J. Neurosci.* 27, 2815–2824. doi: 10.1523/JNEUROSCI.0032-07.2007

Thevenon, J., Souchay, C., Seabold, G. K., Dygai-Cochet, I., Callier, P., Gay, S., et al. (2016). Heterozygous deletion of the LRFN2 gene is associated with working memory deficits. *Eur. J. Hum. Genet.* 24, 911–918. doi: 10.1038/ejhg.2015.221

Thoumine, O., and Marchot, P. (2017). A triad of crystals sheds light on MDGA interference with neuroligation. *Neuron* 95, 729–732. doi: 10.1016/j.neuron.2017.08.001

Tyagarajan, S. K., and Fritschy, J. M. (2014). Gephyrin: a master regulator of neuronal function? *Nat. Rev. Neurosci.* 15, 141–156. doi: 10.1038/nrn3670

Uezu, A., Kanak, D. J., Bradshaw, T. W., Soderblom, E. J., Catavero, C. M., Burette, A. C., et al. (2016). Identification of an elaborate complex mediating postsynaptic inhibition. *Science* 353, 1123–1129. doi: 10.1126/science.aag0821

Um, J. W., Kim, K. H., Park, B. S., Choi, Y., Kim, D., Kim, C. Y., et al. (2014). Structural basis for LAR-RPTP/Slitrk complex-mediated synaptic adhesion. *Nat. Commun.* 5:5423. doi: 10.1038/ncomms6423

Um, J. W., and Ko, J. (2013). LAR-RPTPs: synaptic adhesion molecules that shape synapse development. *Trends Cell Biol.* 23, 465–475. doi: 10.1016/j.tcb.2013.07.004

Um, J. W., and Ko, J. (2017). Neural glycosylphosphatidylinositol-anchored proteins in synaptic specification. *Trends Cell Biol.* 27, 931–945. doi: 10.1016/j.tcb.2017.06.007

Valnegri, P., Montrasio, C., Brambilla, D., Ko, J., Passafaro, M., and Sala, C. (2011). The X-linked intellectual disability protein IL1RAPL1 regulates excitatory synapse formation by binding PTPδ and RhoGAP2. *Hum. Mol. Genet.* 20, 4797–4809. doi: 10.1093/hmg/ddr418

Valnegri, P., Sala, C., and Passafaro, M. (2012). Synaptic dysfunction and intellectual disability. *Adv. Exp. Med. Biol.* 970, 433–449. doi: 10.1007/978-3-7091-0932-8_19

Wang, C. Y., Chang, K., Petralia, R. S., Wang, Y. X., Seabold, G. K., and Wenthold, R. J. (2006). A novel family of adhesion-like molecules that interacts with the NMDA receptor. *J. Neurosci.* 26, 2174–2183. doi: 10.1523/JNEUROSCI.3799-05.2006

Wang, K., Zhang, H., Ma, D., Bucan, M., Glessner, J. T., Abrahams, B. S., et al. (2009). Common genetic variants on 5p14.1 associate with autism spectrum disorders. *Nature* 459, 528–533. doi: 10.1038/nature07999

Wang, P. Y., Seabold, G. K., and Wenthold, R. J. (2008). Synaptic adhesion-like molecules (SALMs) promote neurite outgrowth. *Mol. Cell. Neurosci.* 39, 83–94. doi: 10.1016/j.mcn.2008.05.019

Won, S. Y., Kim, C. Y., Kim, D., Ko, J., Um, J. W., Lee, S. B., et al. (2017). LAR-RPTP clustering is modulated by competitive binding between synaptic adhesion partners and heparan sulfate. *Front. Mol. Neurosci.* 10:327. doi: 10.3389/fnmol.2017.00327

Woo, J., Kwon, S. K., Choi, S., Kim, S., Lee, J., Dunah, A. W., et al. (2009a). Trans-synaptic adhesion between NGL-3 and LAR regulates the formation of excitatory synapses. *Nat. Neurosci.* 12, 428–437. doi: 10.1038/nn.2279

Woo, J., Kwon, S. K., and Kim, E. (2009b). The NGL family of leucine-rich repeat-containing synaptic adhesion molecules. *Mol. Cell. Neurosci.* 42, 1–10. doi: 10.1016/j.mcn.2009.05.008

Xiao, B., Tu, J. C., Petralia, R. S., Yuan, J. P., Doan, A., Breder, C. D., et al. (1998). Homer regulates the association of group 1 metabotropic glutamate receptors with multivalent complexes of homer-related, synaptic proteins. *Neuron* 21, 707–716. doi: 10.1016/s0896-6273(00)80588-7

Xu, B., Woodroffe, A., Rodriguez-Murillo, L., Roos, J. L., van Rensburg, E. J., Abecasis, G. R., et al. (2009). Elucidating the genetic architecture of familial schizophrenia using rare copy number variant and linkage scans. *Proc. Natl. Acad. Sci. U S A* 106, 16746–16751. doi: 10.1073/pnas.0908584106

Yamagata, A., Sato, Y., Goto-Ito, S., Uemura, T., Maeda, A., Shiroshima, T., et al. (2015a). Structure of Slitrk2-PTPδ complex reveals mechanisms for splicing-dependent trans-synaptic adhesion. *Sci. Rep.* 5:9686. doi: 10.1038/srep09686

Yamagata, A., Yoshida, T., Sato, Y., Goto-Ito, S., Uemura, T., Maeda, A., et al. (2015b). Mechanisms of splicing-dependent trans-synaptic adhesion by PTPδ-IL1RAPL1/IL-1RAcP for synaptic differentiation. *Nat. Commun.* 6:6926. doi: 10.1038/ncomms7926

Yim, Y. S., Kwon, Y., Nam, J., Yoon, H. I., Lee, K., Kim, D. G., et al. (2013). Slitrks control excitatory and inhibitory synapse formation with LAR receptor protein tyrosine phosphatases. *Proc. Natl. Acad. Sci. U S A* 110, 4057–4062. doi: 10.1073/pnas.1209881110

Yoshida, T., Shiroshima, T., Lee, S. J., Yasumura, M., Uemura, T., Chen, X., et al. (2012). Interleukin-1 receptor accessory protein organizes neuronal synaptogenesis as a cell adhesion molecule. *J. Neurosci.* 32, 2588–2600. doi: 10.1523/JNEUROSCI.4637-11.2012

Yoshida, T., Yasumura, M., Uemura, T., Lee, S. J., Ra, M., Taguchi, R., et al. (2011). IL-1 receptor accessory protein-like 1 associated with mental retardation and autism mediates synapse formation by trans-synaptic interaction with protein tyrosine phosphatase δ. *J. Neurosci.* 31, 13485–13499. doi: 10.1523/JNEUROSCI.2136-11.2011

Yuzaki, M. (2018). Two classes of secreted synaptic organizers in the central nervous system. *Annu. Rev. Physiol.* 80, 243–262. doi: 10.1146/annurev-physiol-021317-121322

Zhang, J. S., and Longo, F. M. (1995). LAR tyrosine phosphatase receptor: alternative splicing is preferential to the nervous system, coordinated with cell growth and generates novel isoforms containing extensive CAG repeats. *J. Cell Biol.* 128, 415–431. doi: 10.1083/jcb.128.3.415

Conflict of Interest Statement: The authors declare that the research was conducted in the absence of any commercial or financial relationships that could be construed as a potential conflict of interest.

frontiers in Molecular Neuroscience

REVIEW
published: 26 January 2018
doi: 10.3389/fnmol.2018.00014

Heparan Sulfate Proteoglycans as Emerging Players in Synaptic Specificity

Giuseppe Condomitti[1,2] *and Joris de Wit*[1,2]*

[1]VIB Center for Brain & Disease Research, Leuven, Belgium, [2]Department of Neurosciences, KU Leuven, Leuven, Belgium

Neural circuits consist of distinct neuronal cell types connected in specific patterns. The specificity of these connections is achieved in a series of sequential developmental steps that involve the targeting of neurites, the identification of synaptic partners, and the formation of specific types of synapses. Cell-surface proteins play a critical role in each of these steps. The heparan sulfate proteoglycan (HSPG) family of cell-surface proteins is emerging as a key regulator of connectivity. HSPGs are expressed throughout brain development and play important roles in axon guidance, synapse development and synapse function. New insights indicate that neuronal cell types express unique combinations of HSPGs and HS-modifying enzymes. Furthermore, HSPGs interact with cell type-specific binding partners to mediate synapse development. This suggests that cell type-specific repertoires of HSPGs and specific patterns of HS modifications on the cell surface are required for the development of specific synaptic connections. Genome-wide association studies have linked these proteins to neurodevelopmental and neuropsychiatric diseases. Thus, HSPGs play an important role in the development of specific synaptic connectivity patterns important for neural circuit function, and their dysfunction may be involved in the development of brain disorders.

Keywords: heparan sulfate proteoglycans, synapse, circuit assembly, cell surface receptor, connectivity, synapse development, wiring logic, receptor ligand interaction

OPEN ACCESS

Edited by:
Jaewon Ko,
Daegu Gyeongbuk Institute of Science and Technology (DGIST), South Korea

Reviewed by:
Eunjoon Kim,
Institute for Basic Science (IBS), South Korea
Hisashi Umemori,
Boston Children's Hospital, Harvard University, United States

***Correspondence:**
Joris de Wit
joris.dewit@kuleuven.vib.be

Received: *30 November 2017*
Accepted: *10 January 2018*
Published: *26 January 2018*

Citation:
Condomitti G and de Wit J (2018) Heparan Sulfate Proteoglycans as Emerging Players in Synaptic Specificity. Front. Mol. Neurosci. 11:14. doi: 10.3389/fnmol.2018.00014

INTRODUCTION

The brain harbors a large variety of neuronal cell types connected by specific patterns of synaptic connectivity. Establishing precisely connected, functional neural circuits requires the guidance of neuronal processes to target areas, the identification of postsynaptic target cells, and the formation of specific types of synapses on defined subcellular compartments of those cells (Sanes and Yamagata, 2009; Shen and Scheiffele, 2010; Williams et al., 2010; Yogev and Shen, 2014). The molecular mechanisms orchestrating this extraordinary synaptic specificity are now starting to be unraveled. Rapid advances in experimental methodologies, such as cell-type specific transcriptome analysis, proteomics, interactome studies and genetics have identified a key role for cell-surface proteins in synaptic specificity (Kolodkin and Tessier-Lavigne, 2011; de Wit and Ghosh, 2016). In this review article, we focus on an ancient class of cell-surface molecules that is emerging as a novel regulator of synaptic specificity: the heparan sulfate proteoglycans (HSPGs). We will first discuss the role of these molecules in different aspects of synapse formation and function, in invertebrate and vertebrate species. We will then consider emerging evidence that supports a role for HSPGs as novel regulators

of synaptic specificity in developing neural circuits. Finally, we discuss the implications of perturbations in HSPG expression and biology in neurodevelopmental disorders for the function of neural circuits.

HSPG BIOLOGY

HSPGs are cell-surface and secreted proteins consisting of a core domain to which long linear HS glycosaminoglycan chains are covalently attached (Sarrazin et al., 2011). HSPGs function in a wide range of cellular processes by direct interactions with different binding partners. Most of these interactions occur in an HS-dependent and specific manner, with interacting proteins binding to defined structural motifs in the HS chains (Xu and Esko, 2014). Based on their subcellular localization, HSPGs can be grouped into three main subfamilies. The first subfamily consists of the four syndecans (SDC1-4 in vertebrates), which are localized at the cell surface via their transmembrane domain. The second subfamily is represented by the glypicans (GPC1-6 in vertebrates), which are localized at the cell membrane via a glycosylphosphatidylinositol (GPI) anchor (**Figure 1A**). In addition to syndecans and glypicans, other membrane-associated HSPGs have been identified, such as epican and betaglycan, which also localize to the cell membrane through a transmembrane domain. The third main HSPG subfamily is comprised of the secreted HSPGs agrin, perlecan and collagen type XVIII (**Figure 1B**). Lastly, a fourth subtype of HSPG has been described: serglycin, which specifically localizes to the luminal side of intracellular vesicles of mast cells and hematopoietic cells (Sarrazin et al., 2011).

These HSPG subfamilies are conserved throughout evolution, from the nematode *Caenorhabditis elegans* and the arthropod *Drosophila melanogaster* to *Homo sapiens*. Vertebrates express multiple members of each HSPG subfamily, whereas invertebrate organisms express fewer members. For instance, the *Drosophila* genome encodes only one copy of syndecan and two copies of glypicans, Dally and Dally-like protein (Dlp; Selleck, 2001). Phylogenetic analysis of HSPG sequences has shown that HSPGs were already present five hundred million years ago in metazoan organisms such as Cnidaria, indicating that HSPGs are ancient molecules (Medeiros et al., 2000; Van Vactor et al., 2006).

Each type of HSPG contains a defined number of HS chains linked to the core protein domain, with syndecans carrying up to five HS chains, while glypicans and secreted HSPGs comprise up to three HS chains. These polysaccharide chains consist of repeated disaccharide units, glucuronic acid and N-acetylglucosamine, which are synthesized in the Golgi apparatus and polymerized onto the core protein through a multistep process that requires the coordinate action of different enzymes (Esko and Selleck, 2002). Following the polymerization steps, the newly synthesized chains undergo a sequential modification process catalyzed by various enzymes. N-deacetylase/N-sulfotransferase (NDST); 2-O-, 3-O- and 6-O-Sulfotransferases (HS2ST1, HS3ST1 and HS6ST1); and C5-Epimerase (GLCE) catalyze deacetylation, sulfation and epimerization reactions, respectively, at the level of specific disaccharide residues (**Figure 1C**). The combined action of these enzymes differentially affects the composition and properties of the HS chain. NDST activity causes the simultaneous formation of highly sulfated and acetylated subdomains, which form important components of ligand-binding motifs. In addition, the 2-O-, 3-O- and 6-O-sulfotransferase enzymes mediate the addition of sulfate groups only to specific glucosamine residues. Furthermore, two endosulfatases, SULF1 and 2, localize to the plasma membrane and selectively catalyze the removal of 6-O sulfate groups from a subset of trisulfate disaccharide residues in the HS chain (Ai et al., 2006). GLCE-mediated epimerization regulates the conversion of glucuronic acid to iduronic acid (IdoA). As IdoA residues are subsequently sulfated by HS2ST, epimerization is necessary to instruct the positioning of sulfation on the HS chains (Kreuger and Kjellén, 2012).

Importantly, these enzymatic modifications occur in clusters along the HS chain, with short stretches of modified subregions interspersed with long unmodified regions. This heterogeneity of the HS chain is thought to provide specific binding regions that allow the interaction of HS with different protein ligands (Xu and Esko, 2014). HS chain composition is highly regulated, as HS-modifying enzymes show tissue-specific, as well as cell type-specific expression patterns. Furthermore, HS-modifying enzyme expression patterns vary during development (Allen and Rapraeger, 2003; Paul et al., 2017). Within a given cell type, different types of HSPGs contain HS chains with indistinguishable modification patterns and highly similar structural properties (Kato et al., 1994; Tumova et al., 2000; Zako et al., 2003). As the brain is a highly heterogeneous tissue harboring many different cell types, there is an enormous potential for HS diversity. This has led to the hypothesis of a "HS code", which poses that tissue- and cell type-specific HS modifications control the interaction with particular binding partners in a localized fashion to regulate wiring specificity (Bülow and Hobert, 2004; Holt and Dickson, 2005; Bülow et al., 2008).

REGULATION OF CELLULAR FUNCTION BY HSPGs

HSPGs were initially described as a component of the extracellular matrix (ECM). Perlecan, agrin and collagen XVIII are indeed found in the extracellular environment of various tissues, where they are important for providing mechanical resistance and for allowing diffusion of molecules throughout the ECM (Bishop et al., 2007). In addition to this structural role, it has become clear that HSPGs are major, and multi-faceted, regulators of developmental signaling, by binding to and modulating the activity of key molecules, such as fibroblast growth factor (FGF), WNT, transforming growth factor (TGFβ) and hedgehog (Hh). One way by which HSPGs regulate these signaling molecules, is by promoting the formation and the maintenance of morphogen gradients. Ablation of HSPGs or of HSPG-biosynthetic enzymes alters

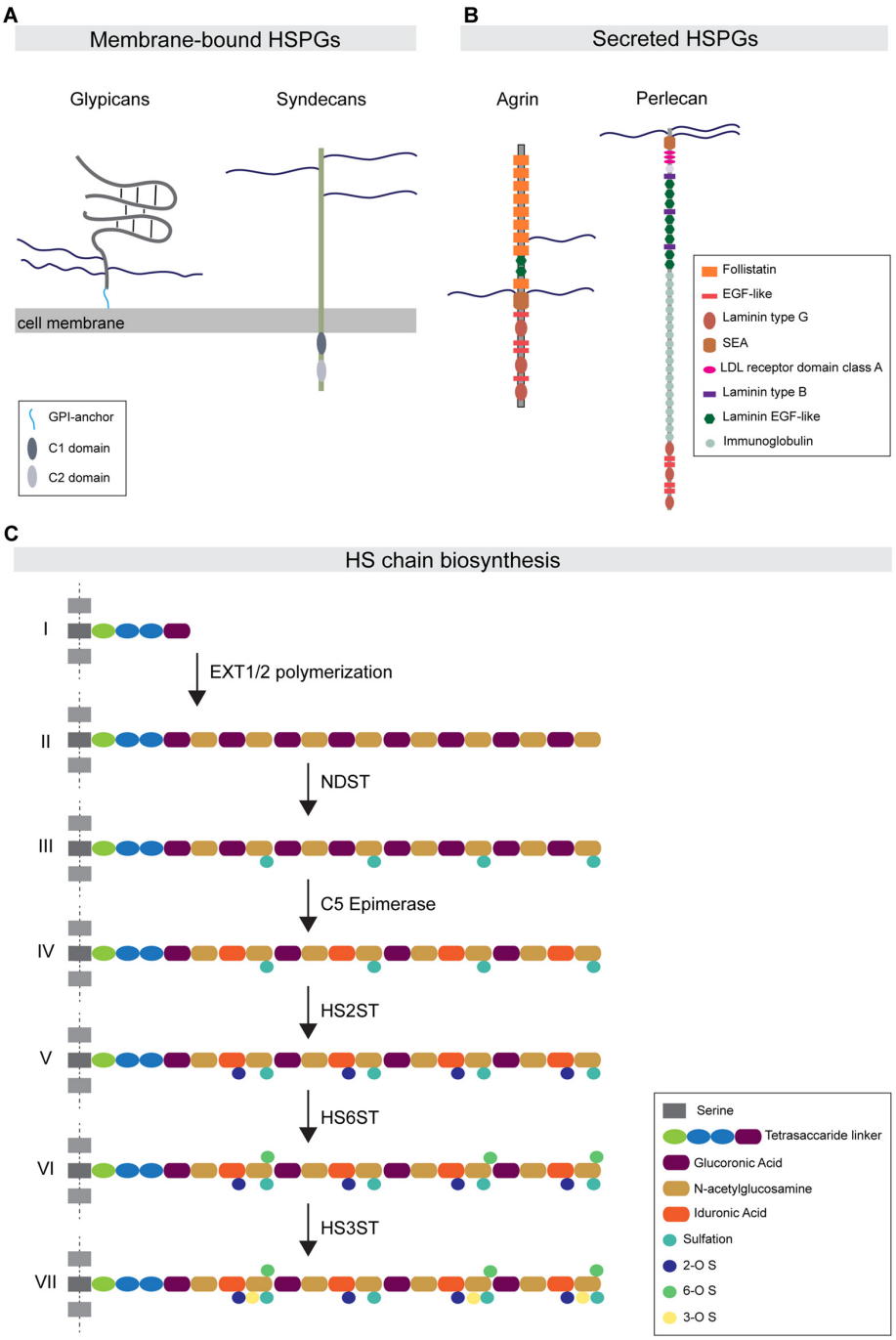

FIGURE 1 | Heparan sulfate proteoglycan (HSPG) protein family organization and HS biosynthesis. **(A)** Major HSPG protein families. Membrane-bound HSPGs can be distinguished in glypicans and syndecans. Glypicans are characterized by a globular protein domain (gray) and a stalk-like domain that contains three attachment sites for HS chains (blue). These molecules are attached to the external leaflet of the cell membrane through a glycosylphosphatidylinositol (GPI)-anchor (light blue). The transmembrane syndecans are characterized by the presence of three HS chains at the N-terminal portion of the protein. The syndecan intracellular tail contains two conserved regions: the C1 domain (dark gray) and C2 (light gray). **(B)** The major secreted HSPGs are Agrin and Perlecan. Agrin carries its HS chains in a central domain and is characterized by the presence of several follistatin domains. Perlecan presents HS chains only at the N-terminal portion of the protein. Its core protein organization is characterized by the presence of multiple conserved domains, such as the immunoglobulin domain. **(C)** The HS chain biosynthetic pathway: (I) HS biosynthesis starts with the attachment of a tetrasaccharide linker to specific serine residues. (II) The EXT family of co-polymerases mediates the elongation of the HS chain by adding disaccharide units composed of glucuronic acid (purple) and N-acetylglucosamine (ocher). (III) Subsequently, the enzyme NDST mediates the simultaneous sulfation and de-acetylation of specific N-acetylglucosamine residues. (IV) The C5-epimerase induces the epimerization of glucuronic acid to iduronic acid (IdoA). (V–VII) The subsequent action of the enzymes HS2ST, HS6ST and HS3ST mediates the attachment of sulfate groups to specific saccharide residues.

the development of these morphogen patterns (Häcker et al., 2005). In addition to this cellular function, HSPGs can also directly act as signaling molecules. Some HSPGs can be enzymatically cleaved and secreted in the extracellular space, where they act as biological effectors. For example, the transmembrane HSPGs SDC1 and SDC4 are cleaved by different types of matrix metalloproteinases in response to several stimuli (Fitzgerald et al., 2000; Park et al., 2000). The released SDC1 ectodomain plays an important role during inflammatory processes (Kainulainen et al., 1998; Li Q. et al., 2002). During acute lung injury, released SDC1 interacts in an HS-dependent manner with the chemokine Cxcl1. The shed SDC1/Cxcl1 complex establishes a chemotactic gradient that guides invading neutrophils to the inflammation site (Li Q. et al., 2002). In addition to a role as signaling molecules, HSPGs can also act in a cell-autonomous way, by functioning on the cell surface as co-receptors for growth factors and their receptors. This is exemplified by the role of HSPGs in the interaction of the growth factor FGF with its receptor (FGFR). HS chains mediate the high affinity binding between FGF and FGFR, and control FGF-mediated signaling during *Drosophila* development (Ornitz, 2000; Schlessinger et al., 2000; Yan and Lin, 2007). In *Drosophila* tracheal morphogenesis, the HSPG Dally-like specifically mediates the interaction between FGF and its receptor Breathless (BTL), and is required to induce a FGF-BTL-mediated signaling cascade (Yan and Lin, 2007). Finally, HSPGs can recruit and cluster cell-surface molecules in membrane domains and regulate their function by promoting their secretion or endocytosis. SDC1 has been shown to be internalized from the cell surface membrane through an endocytic process that is clathrin- and caveolin-independent, but requires actin microfilament polymerization and occurs at the level of lipid rafts (Fuki et al., 2000; Zimmermann et al., 2005). Internalization of SDC1 causes the uptake of the SDC1 binding partners FGFR and β1-integrins, leading to an impairment in cell spreading. SDC1 and its binding partners can be recycled to the cell surface membrane through Arf6-positive vesicles, which restores cell motility (Zimmermann et al., 2005). Thus, endocytosis and recycling of SDC1 and its binding partners regulates their cell surface availability important for normal cell function.

The above examples illustrate the various ways by which HSPGs regulate cellular processes, in an HS-dependent manner. Enzymatic modifications of the HS chains generate HS-specific binding motifs that are important for HSPG–protein interactions and consequently for cellular processes. In cerebellar granule cell precursors for example, the morphogen Sonic Hedgehog (Shh) interacts in an HS-dependent manner with GPC5 to promote precursor cell proliferation. This interaction specifically requires 2-O sulfation modifications on IdoA residues of GPC5's HS chains, which are then recognized and bound to the Cardin-Weintraub structural motif of Shh. Downregulation of GPC5 expression levels, or enzymatic removal of GPC5's 2-O sulfation patterns, severely affects Shh-mediated signaling (Witt et al., 2013).

Lastly, in addition to HS-dependent binding to proteins, which form the majority of HSPG interactions, direct binding of signaling molecules to the HSPG protein core has also been described, such as the interaction of the morphogen Hh with the core domain of GPC3 (Capurro et al., 2008). The GPC3-Hh complex is internalized in the cell and directed for degradation in the lysosomal compartment, indicating that GPC3 controls developmental signaling processes by acting as a negative regulator of Hh-mediated signaling (Capurro et al., 2008). Altogether, these examples demonstrate how HSPGs represent a highly diverse and versatile protein family important for regulating a broad range of cellular functions. In the next sections, we will discuss how HSPGs play an important role during brain development as regulators of the various steps leading to synaptic specificity.

HSPGs AS REGULATORS OF AXON GUIDANCE

HSPGs and HS-specific modifications play an important role in the formation of neural connectivity. HSPGs are important regulators of axon guidance, a first key step in the assembly of specific synaptic connections. Here, we provide a brief summary of the roles of HSPGs in this process, as the cellular and molecular mechanisms by which HSPGs regulate axon guidance and targeting have been extensively reviewed elsewhere (Lee and Chien, 2004; de Wit and Verhaagen, 2007). Pioneering studies in cultured cockroach embryos and in *Xenopus laevis* retinal ganglion cells (RGCs) demonstrated that treatment with exogenous HS or enzymatic degradation of HS chains impaired axonal growth and guidance (Wang and Denburg, 1992; Walz et al., 1997). These initial observations were subsequently confirmed in a mouse model in which HS was removed through the conditional deletion of the enzyme Exostosin 1 (EXT1), the key enzyme in HS chain biosynthesis. Loss of EXT1 causes severe axon guidance errors of the major commissural axon tracts (Inatani et al., 2003), indicating that HSPGs are important regulators of axon guidance. Subsequent studies demonstrated that HSPGs control axon guidance through the binding and regulation of different axon guidance cues. For example, HSPGs interact with members of the Slit protein family and promote the binding to their receptor Robo in order to induce Slit-mediated repulsive function (Hu, 2001; Steigemann et al., 2004; Hussain et al., 2006). Furthermore, HSPGs positively regulate the attractive function of the transmembrane guidance molecule Semaphorin 5 (Kantor et al., 2004). Finally, binding of the membrane-anchored guidance molecule Ephrin A3 to HS chains is required for mediating Ephrin A3-induced axon repulsion (Irie et al., 2008). In addition to the general role for HS chains in axon guidance, experimental evidence from different model organisms has also shown the involvement of specific HS enzymatic modifications in this process. Multiple studies in which specific HS-modifying enzymes were deleted in a cell type-specific manner, found different, yet specific axonal targeting defects (Bülow and Hobert, 2004; Bülow et al., 2008; Tillo et al., 2016). In *C. elegans*, ventral D-type motorneuron axons initially grow and fasciculate along the right ventral

cord, then cross the midline and on the contralateral side project to the dorsal side of the animal. Bülow and Hobert (2004) demonstrated that each of these steps is differentially affected by the removal of the *C. elegans* homologs of 6-O sulfotransferase (hst-6), 2-O sulfotransferase (hst-2) and the C5-epimerase (hse-5). In particular loss of hse-5 and hst-2 severely impairs axonal fasciculation and dorsal projection (Bülow and Hobert, 2004). However, the loss of hst-6 only affects midline crossing, suggesting that the different steps of D-type motorneuron axon growth require specific HS modification patterns. Strikingly, when the same enzymes were ablated in a distinct type of motorneurons, the DA motorneurons that make similar axon guidance choices, no major defects were observed (Bülow and Hobert, 2004), indicating that cell-type specific HS modification patterns control axon guidance. Altogether, these studies demonstrate that HSPGs and cell type-specific HS chain modification patterns are important regulators of axonal growth and targeting.

HSPGs AS REGULATORS OF SYNAPSE DEVELOPMENT

Studies in different model organisms, from *C. elegans* to mouse, have demonstrated that different HSPGs and HS-modifying enzymes regulate multiple aspects of synapse development. In the following section, we highlight the roles of the HSPG protein family in controlling general synapse formation, composition and function, before turning to emerging evidence for a role of HSPGs in synaptic specificity.

Modulating Localization of Synaptic Signaling Molecules

Secreted synaptogenic molecules, such as WNT and FGFs, are important regulators of synapse formation and maturation (Siddiqui and Craig, 2011). These molecules can be released from the pre-or postsynaptic compartment, or from neighboring astrocytes, and promote synaptic differentiation through binding to their receptors on the neuronal membrane. Recent studies have started to shed light on the role of HSPGs in controlling the synaptic localization of specific secreted synaptogenic molecules. Terribly reduced optic lobe (trol), the *Drosophila* ortholog of perlecan, is secreted by the postsynaptic muscle cells and accumulates in the synaptic cleft (Kamimura et al., 2013). *Trol* mutants show an overproduction of boutons, as well as a reduction in the subsynaptic reticulum area and in glutamate receptor content (Kamimura et al., 2013). Presynaptic organization and composition were unaffected however. The structural defects observed in *trol* mutants are similar to the effects observed in *Wg* mutants, a *Drosophila* homolog of WNT. Indeed, loss of trol causes a reduction in the extracellular levels of Wg, and in particular in its localization in proximity to the postsynaptic compartment. This suggests that the secreted HSPG trol regulates the distribution and localization of Wg at the fly neuromuscular junction (NMJ), thus mediating structural and ultrastructural maturation of the postsynaptic compartment (Kamimura et al., 2013; **Figure 2A**). In vertebrates, postsynaptic SDC2 interacts with the secreted protein FGF22 in an HS-dependent manner to present FGF22 to the presynaptic FGF receptor, driving bidirectional synaptic maturation (Hu et al., 2016; **Figure 2B**).

Organizing the Synaptic ECM

Synapses are enwrapped by a layer of ECM (Frischknecht and Gundelfinger, 2012), which is important for shaping and maintaining synaptic morphology and function. Important components of the ECM are the secreted HSPGs collagen type XVIII, perlecan and agrin (Barros et al., 2011). However, whether and how these secreted molecules contribute to the structural organization of the ECM and synapse development is largely uncharacterized. Evidence for a role of secreted HSPGs in controlling ECM organization and synapse development comes from studies on the *C. elegans* NMJ. Mutant worms for *emb-9* and *cle-1*, the orthologs of collagen type IV and XVIII, have ectopic presynaptic terminals, suggesting that these two molecules are required to restrict the growth of presynaptic boutons (Qin et al., 2014). The growth of ectopic boutons upon loss of Emb-9 and Cle-1 is partially explained by a fragmentation of the basal membrane surrounding the presynaptic bouton, which may favor the formation of ectopic presynaptic terminals (Qin et al., 2014). Interestingly, the ectopic presynaptic terminal growth and ECM defects observed in *emb-9* mutants are reverted by the simultaneous ablation of *unc-52*, the *C. elegans* ortholog of Perlecan, indicating that secreted perlecan promotes bouton growth (Qin et al., 2014). These observations suggest that collagens and perlecan differentially regulate synapse development, by acting either as synapse growth-restricting or -promoting factors, respectively. Thus, different secreted HSPGs act simultaneously to control ECM organization and synapse growth. The molecular mechanisms underlying this differential capacity are currently unknown, but it has been previously demonstrated that secreted HSPGs differently control the biomechanical properties of the ECM during *Drosophila* development (Pastor-Pareja and Xu, 2011). The accumulation of collagen type IV causes a more rigid ECM, while perlecan antagonizes collagen IV's effect, leading to a more elastic extracellular environment (Pastor-Pareja and Xu, 2011). Thus, it seems plausible that at the worm NMJ, the loss of collagen type IV may create a more elastic environment permissive for ectopic bouton growth. In addition to changes in biomechanical properties however, the different ECM composition might also affect the distribution of secreted molecules that regulate synapse development. Whether in addition to secreted HSPGs, other types of HSPGs contribute to organizing the synaptic ECM, and whether HS-specific modification patterns regulate this process is still unknown.

HSPGs as Synaptic Organizing Molecules

Important regulators of synapse assembly and maturation are the synaptic organizing proteins (Takahashi and Craig, 2013; Ko J. et al., 2015; Jang et al., 2017). These proteins

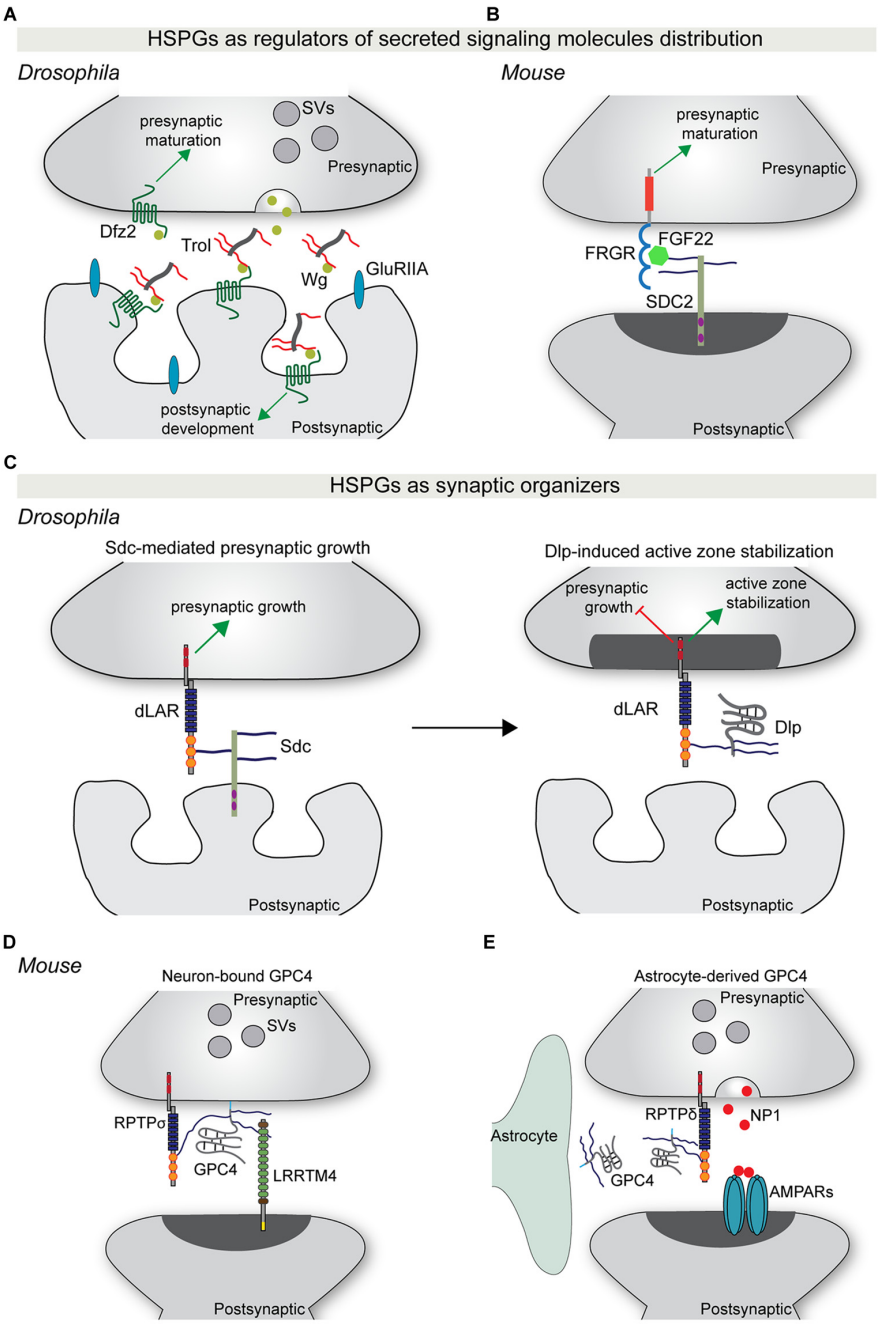

FIGURE 2 | HSPGs as regulators of synapse development. **(A)** The secreted HSPG trol regulates Wg-mediated synaptic differentiation at the *Drosophila* neuromuscular junction (NMJ). Trol is released in the synaptic cleft from the postsynaptic muscle cell. Here, trol binds and sequesters Wg to the surface of the postsynaptic compartment, allowing the interaction with its postsynaptic receptor Dfz2 and the induction of postsynaptic structural and functional maturation. At the same time, Wg also acts presynaptically in a trol-independent manner to instruct presynaptic maturation. **(B)** During vertebrate synapse development, postsynaptic SDC2 binds FGF22 in an HS-dependent manner and facilitates its presentation to the presynaptic receptor FGFR. This interaction promotes presynaptic differentiation. **(C)** HSPGs act as synaptic organizers. During *Drosophila* NMJ development, postsynaptic Sdc promotes presynaptic growth through binding to the presynaptic RPTP dLAR. Subsequently, Dlp, which has a higher affinity for dLAR, competes with Sdc-dLAR binding to inhibit presynaptic growth and promote active zone stabilization. **(D)** GPC4 acts as a presynaptic binding partner for the postsynaptic adhesion protein LRRTM4. GPC4-LRRTM4 interaction occurs in an HS-dependent manner and forms a *trans*-synaptic complex that regulates the development of excitatory synapses. This complex requires RPTPσ, which acts as a presynaptic GPC4 *cis*-receptor to mediate presynaptic development and function. **(E)** During early postnatal mouse visual system development, astrocytes release GPC4. GPC4 binds presynaptic RPTPδ, most probably in an HS-dependent manner, and instructs presynaptic release of NP1, which clusters AMPARs and promotes the formation of active synapses. Abbreviations: SV, synaptic vesicles; SDC2, syndecan 2; Dlp, Dally-like protein; NP1, neuronal pentraxin 1; GPC4, glypican 4.

localize to the pre- and postsynaptic membrane, or are secreted in the synaptic cleft, and induce the differentiation of the pre-and postsynaptic element by recruiting components of the synaptic machinery. Synaptic organizing proteins include neurexins (Graf et al., 2004), neuroligins (Scheiffele et al., 2000), leucine-rich repeat transmembrane neuronal proteins (LRRTMs; de Wit et al., 2009; Ko et al., 2009; Linhoff et al., 2009), FGFs (Fox et al., 2007; Terauchi et al., 2010) and thrombospondins (Christopherson et al., 2005; Eroglu et al., 2009). Many additional synaptic organizing proteins have been identified (Siddiqui and Craig, 2011; Um and Ko, 2013; Ko J. et al., 2015; Jang et al., 2017). The first neural synaptic organizer identified was the secreted HSPG agrin (Godfrey et al., 1984; Gautam et al., 1996; Glass et al., 1996). Agrin is secreted by the presynaptic compartment of motorneurons and localizes to the synaptic cleft, where it instructs NMJ postsynaptic differentiation. Loss of agrin causes a reduction in acetylcholine receptor content, a decrease in postsynaptic membrane size and fragmentation of the basal lamina of the synaptic cleft (Gautam et al., 1996). Agrin-mediated postsynaptic organization occurs through the ability of agrin to bind, cluster and activate the postsynaptic tyrosine kinase receptor MuSK (Glass et al., 1996).

More recently, syndecans and glypicans have been identified as synaptic organizers. At the *Drosophila* NMJ, Sdc is expressed by muscle cells and postsynaptically localized, while Dally-like (Dlp) localizes to the perisynaptic space. Both HSPGs regulate different aspects of NMJ synapse formation and function (Johnson et al., 2006; Nguyen et al., 2016). Sdc promotes presynaptic bouton growth, whereas Dlp restricts presynaptic active zone morphogenesis (Johnson et al., 2006). The differential regulation of synaptic architecture by Sdc and Dlp is reflected at the functional level, with loss of *Dlp*, but not of *Sdc*, causing an increase in neurotransmitter release (Johnson et al., 2006). Remarkably, Sdc and Dlp interact with the same presynaptic receptor, the protein tyrosine phosphatase receptor (RPTP) Dlar. Sdc and Dlp bind Dlar at overlapping sites and in an HS-dependent manner. Dlp has a greater affinity for Dlar and effectively competes with Sdc for Dlar binding (Johnson et al., 2006; **Figure 2C**). Furthermore, Dlp inhibits Dlar signaling, but how Dlar can discriminate between the two HSPGs to instruct differential effects on presynaptic bouton morphology and function remains unclear.

Although these experiments at the fly NMJ indicate that Sdc and Dlp mainly act presynaptically, the cellular source of Dlp is not entirely clear. Experiments in vertebrates have shown that neuron-, as well as glial-derived glypicans play an important role in synapse development. Two independent studies identified HSPGs, and in particular glypican 4 (GPC4), as presynaptic binding partners for the postsynaptic adhesion protein LRRTM4 (de Wit et al., 2013; Siddiqui et al., 2013). GPC4 binds LRRTM4 via its HS sugar chains to form a *trans*-synaptic complex that organizes excitatory synapse development through the clustering of pre- and postsynaptic components (de Wit et al., 2013; Siddiqui et al., 2013). The LRRTM4-GPC4 complex requires presynaptic RPTPσ, which acts as an HS-dependent *cis*-receptor for GPC4 on the presynaptic membrane, to instruct presynaptic development and function (Ko J. S. et al., 2015; **Figure 2D**).

In addition to a role in the presynaptic neuron, *Gpc4* and *Gpc6* are also expressed and secreted by astrocytes in the early stages of postnatal development. Soluble GPC4 and GPC6 induce excitatory synapse formation in cultured retinal ganglion cells (RGCs) and GluA1-containing glutamate receptor clustering (Allen et al., 2012). Astrocyte-derived GPC4 binds to presynaptic RPTPδ and RPTPσ and induces release of the glycoprotein neuronal pentraxin 1 (NP1) from the presynaptic compartment, which subsequently clusters postsynaptic GluA1-containing glutamate receptors (Farhy-Tselnicker et al., 2017). Interfering with RPTPδ or RPTPσ-mediated signaling blocks GPC4-induced NP1 release and synapse formation. *In vivo*, astrocyte-specific *Gpc4* deletion in the RGC target region, the superior colliculus and *Rptpδ* ablation in both RGCs and the superior colliculus, caused a reduction in synapse formation (Farhy-Tselnicker et al., 2017; **Figure 2E**).

The studies described above in fly and vertebrate systems demonstrate that presynaptic RPTPs form a central hub to mediate HSPG-induced synaptic development. Whether RPTPs can distinguish GPC4 derived from neurons or glia, and whether GPC4 from different cellular sources would have differential functional effects, is currently unknown. Furthermore, whether glial cells can act as source of GPC4 during later developmental stages and in adulthood is an intriguing possibility that remains to be addressed.

The ability of HSPGs to control synapse development requires an interaction with specific co-receptors in the case of glypicans, which lack a cytoplasmic domain, but can also be accomplished by direct activation of specific intracellular signaling cascades in the case of transmembrane syndecans. In cultured hippocampal neurons, postsynaptic SDC2 clusters in dendritic spines concomitantly with dendritic spine maturation. Overexpression of SDC2 in immature neurons accelerates the development of mature dendritic spines (Ethell and Yamaguchi, 1999). SDC2's capacity to trigger spine morphogenesis is dependent on its intracellular region. The tyrosine kinase receptor EphB2 phosphorylates SDC2 at tyrosine residues Y281 and Y189 and these two modifications are necessary for SDC2 spine clustering and for triggering spine morphogenesis (Ethell et al., 2001). SDC2 interacts with additional intracellular binding partners, such as syntenin, calcium/CaM-dependent serine protein kinase (CASK), synbindin and synectin (Hsueh et al., 1998; Chen et al., 2011), and the negative regulator of the Ras signaling pathway neurofibromin (Lin et al., 2007). This suggests that SDC2's interaction with specific scaffolding and signaling proteins regulates dendritic spine maturation.

HSPGs IN SYNAPTIC SPECIFICITY

Recent technological advances are accelerating the discovery of the molecular principles underlying synaptic specificity.

Genomic, proteomic and interactomic analyses, even at the level of single neurons, are enabling the identification and characterization of classes of cell-surface molecules that might be required for synaptic specificity. To be able to instruct the development of specific synaptic connectivity patterns, these molecules should have several characteristics: they should be expressed in a brain region- and cell type-specific manner; they should be able to interact with distinct and region-specific binding partners; and they should have enough molecular diversity in order to confer cell type- and possibly even synapse type-specific identities (de Wit and Ghosh, 2016). Recent work has started to reveal that, in addition to their role as synaptic organizers, HSPGs show highly specific expression patterns; interact with diverse, region-specific interactors; and also carry synapse-specific modification patterns, suggesting that HSPGs can act as regulators of synapse specificity.

Cell Type-Specific Expression Patterns of HSPGs and HS-modifying Enzymes

An important property for molecules involved in synaptic specificity is region- and cell type-specific expression. Recent advances in single-cell sequencing demonstrate that several synaptic molecules that play an important role in synapse formation are expressed in the brain in a cell type-specific manner (Tan et al., 2015; Földy et al., 2016; Shekhar et al., 2016; Li et al., 2017; Paul et al., 2017). Syndecans and glypicans also show discrete expression patterns in the mouse hippocampus (**Figure 3A**). Initial *in situ* hybridization studies revealed that syndecans have different, moderately overlapping expression patterns in adult rat brains. *Sdc1* is mainly expressed in the cerebellum, while *Sdc2* and *Sdc4* are enriched in the granule cells of the dentate gyrus (DG) and glial cells, respectively (Hsueh and Sheng, 1999). Glypicans show highly specific expression patterns. *Gpc1*, *2* and *4* are expressed in the hippocampus. *Gpc1* is highly enriched in CA3 pyramidal neurons, while *Gpc2* and *4* are abundant in DG granule cells (with an enrichment of *Gpc4* also in CA1 pyramidal neurons; de Wit et al., 2013; Ko J. S. et al., 2015). Interestingly, the expression pattern of some glypicans changes during development (Ko J. S. et al., 2015). These cell type-specific expression profiles are supported by gene expression profile analysis of the principal hippocampal neuron populations by RNA sequencing (Cembrowski et al., 2016). In addition, recent single-cell RNA sequencing studies have further characterized cell type-specific expression patterns for HSPGs. Li et al. (2017) demonstrated that in the *Drosophila* olfactory bulb, the VM2 projection neurons (VM2-PN) are specifically characterized by the expression of the HSPG *trol*. Furthermore, single-cell transcriptomic analysis of different GABAergic populations in the mouse primary visual cortex has identified a vasoactive intestinal peptide (VIP)-positive interneuron subpopulation that localizes to deep cortical layers and is characterized by the expression of *Gpc3* (Tasic et al., 2016). Altogether, these results indicate that HSPGs have brain region- and cell type-specific expression patterns, supporting a possible involvement in synaptic specificity.

Interestingly, the brain region- and cell type-specificity is not restricted to HSPGs; different HS-modifying enzymes show discrete expression patterns in the brain as well. In the adult mouse brain, the extracellular 6-O-endosulfatases SULF1 and 2 show different expression profiles, with *Sulf2* being broadly expressed, while *Sulf1* is restricted to defined cell layers, such as cortical layer V and the Purkinje cell layer of the cerebellum (Kalus et al., 2009; **Figure 3A**, hippocampal expression analysis). Single-cell RNA sequencing of six different populations of genetically labeled and phenotypically characterized GABAergic neurons demonstrated cell type-specific expression patterns of sulfotransferases and a layer-specific distribution in adult mouse cortex (Paul et al., 2017; **Figure 3B**). In addition, by generating a panel of different HS-specific single chain variable fragment antibodies, Attreed et al. (2012, 2016) have shown that in the *C. elegans* central nervous system, distinct cell types present unique HS epitopes on their surface. Furthermore, their results hint at synapse-specific HS modification patterns (Attreed et al., 2016). Together, these findings suggest that different cell types, and possibly different synapse types, display a distinct composition of HSPGs and a specific pattern of HS modifications on their surface, which may be required for the development of precise synaptic connectivity.

Cell Type-Specific HSPG Binding Partners

In addition to cell type-specific expression patterns, molecules involved in the development of precise synaptic connectivity patterns may interact with region- and cell type-specific binding partners. HSPGs have been shown to interact with synaptic binding partners that are highly restricted to specific brain regions or cell types. As previously described, GPC4 regulates excitatory synapse formation through a *trans*-synaptic interaction with the postsynaptic protein LRRTM4 (de Wit et al., 2013; Siddiqui et al., 2013). In the hippocampus, *Lrrtm4* is only expressed in DG granule cells, while *Gpc4* is broadly expressed in hippocampus and cortex (de Wit et al., 2013; Ko J. S. et al., 2015). Loss of LRRTM4 specifically affects synapse number, function and composition in granule cells, while CA1 pyramidal neurons are unaffected (Siddiqui et al., 2013). As *Gpc4*, and other glypicans, are expressed in different brain regions, these observations suggest that glypicans might interact with different binding partners in other parts of the brain. The extracellular interactomes for glypicans and syndecans have not yet been elucidated.

HS Modification in Synapse Development

Recent studies have started to explore whether HS chain modifications play a role in synapse development. Using an RNAi-based screen in *Drosophila*, Dani et al. (2012) found that Sulf1 and Hs6st differentially affect synapse composition and function at the NMJ. Loss of *Sulf1* or *Hs6st* causes an increased number of synaptic boutons, but has differential effects on synaptic transmission. *Sulf1* mutants show an increased strength of synaptic transmission, while *Hs6st* mutants have weaker neurotransmission (Dani et al., 2012). Loss of these

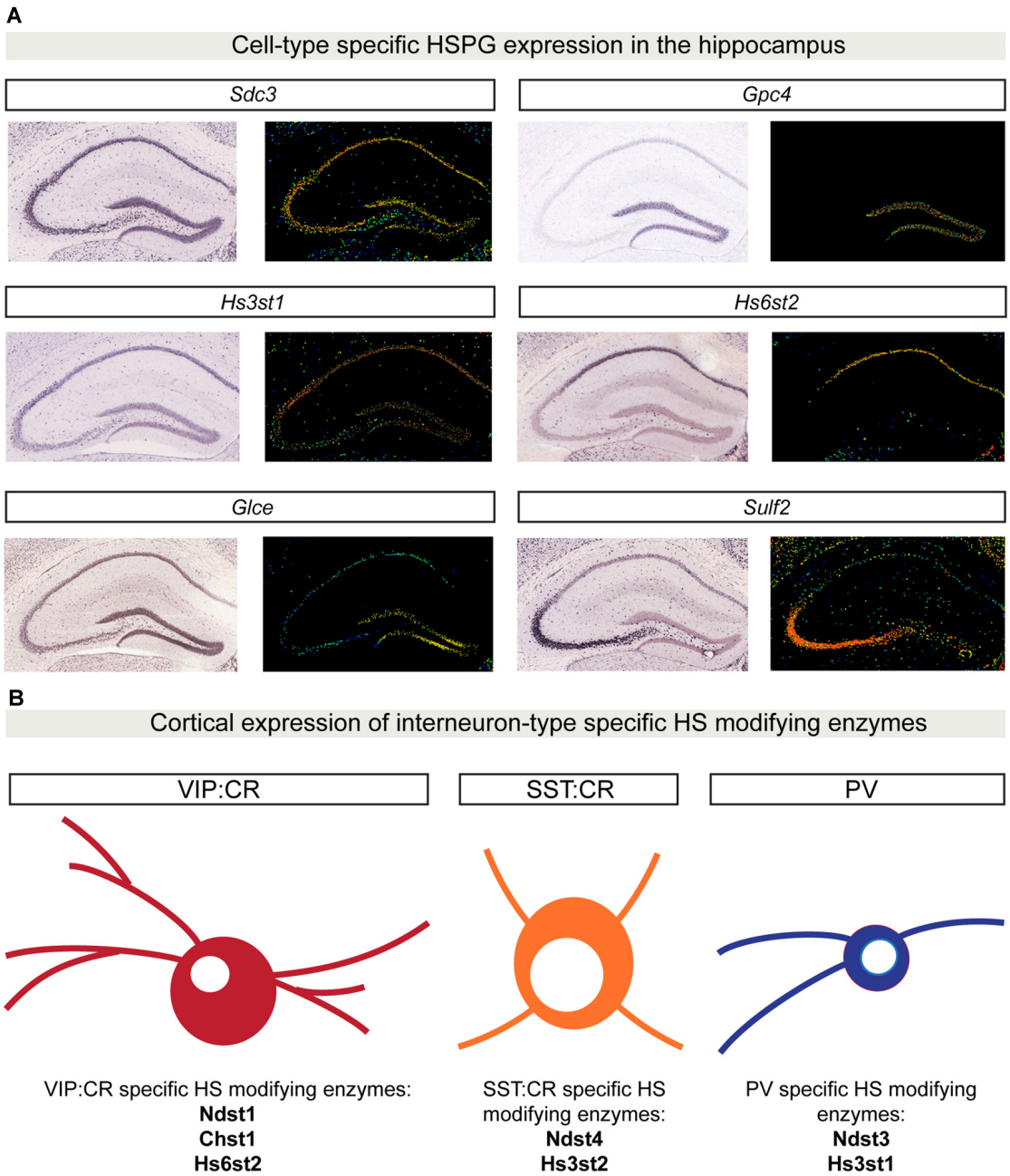

FIGURE 3 | Cell type-specific HSPG and HS-modifying enzyme expression patterns. **(A)** *In situ* hybridization showing gene expression patterns in P56 mouse coronal hippocampal sections for a limited set of HSPGs and HS-modifying enzymes. *Sdc3* (http://mouse.brain-map.org/gene/show/20731) is broadly expressed in the hippocampus, whereas *Gpc4* (http://mouse.brain-map.org/gene/show/14511) is highly enriched in the dentate gyrus (DG) region. The 3-O sulfotransferase *Hs3st1* (http://mouse.brain-map.org/experiment/show/2305) is mainly expressed in CA1 and DG, while *Hs6st2* (http://mouse.brain-map.org/experiment/show/72129255) is specifically expressed only in CA1. *Glce* (http://mouse.brain-map.org/experiment/show/74641306) is specifically expressed in DG, while *Sulf2* (http://mouse.brain-map.org/experiment/show/72007935) expression is highly enriched in CA3. All images in **(A)** are obtained from the Allen Brain Atlas (http://www.brain-map.org/). For each gene, left panel shows the original *in situ* hybridization signal; right panel shows a heat map color scale to indicate intensity of expression. **(B)** Cell type-specific expression patterns for HS-modifying enzymes in distinct cortical interneuron populations. Using single-cell RNA sequencing in six different populations of genetically labeled and phenotypically characterized GABAergic neurons, Paul and colleagues showed a cell type-specific expression pattern of different HS-modifying enzymes. In **(B)**, examples of three different GABAergic isolated populations are shown: vasoactive intestinal peptide (VIP) CR positive GABAergic cells are characterized by the expression of *Ndst1, Chst1* and *Hs6st2*. SST:CR GABAergic cells are characterized by the expression of *Hs3st2* and *Ndst4*. PV positive cells specifically express the enzymes *Hs3st1* and *Ndst3*. Abbreviations: SDC3, syndecan 3; GPC4, glypican 4; Hs3st1, 3-O sulfotransferase type 1; Hs6st2, 6-O sulfotransferase type 2; Glce, C5-epimerase; Sulf2, sulfotransferase 2; Chst1, sulfotransferase 1; Ndst1, N-deacetylase and N-sulfotransferase 1; Hs3st2, 3-O sulfotransferase type 2; Ndst4, N-deacetylase and N-sulfotransferase 4.

HS-modifying enzymes affects the synaptic levels of Dlp and Sdc, but do not simply phenocopy the effects of Dlp and Sdc loss (Johnson et al., 2006). *Hs6st* loss reduces Dlp levels, while *Sulf1* removal increases the levels of both Sdc and Dlp. Altered synaptic levels of Dlp and Sdc impair anterograde Wg and retrograde Gbb *trans*-synaptic signaling, important to instruct pre- and postsynaptic maturation (Dani et al., 2012). These findings suggest that a combinatorial function of HSPGs and HS chain modifications mediate synapse formation, function and composition.

Lastly, it is emerging that also in vertebrates, specific HS modification patterns can instruct synapse formation and function. In the CA1 region of the hippocampus, loss of SULF1 specifically causes a reduction in dendritic spine density and impairment in synaptic plasticity, while SULF2 removal does not cause any synaptic structural and functional effects (Kalus et al., 2009). These findings suggest that patterns of HS modification are also required to specify structural and functional synaptic properties in the vertebrate system.

HSPGs AND DISEASE

The importance of synaptic organizing proteins in normal synaptic function, and therefore proper brain activity, is highlighted by the fact that several recent large-scale genomic analyses have revealed a correlation between genes encoding synaptic proteins and brain disorders (Parikshak et al., 2013; De Rubeis et al., 2014). Recent work has started to shed light on the contribution of HSPGs and of HS-modifying enzymes in neurodevelopmental and neuropsychiatric disorders. A need for HSPGs in proper brain function has initially been demonstrated by Irie et al. (2012). Taking advantage of a conditional knockout mouse for the HS-polymerizing enzyme EXT1, the authors abolished HSPG expression in postnatal excitatory neurons. Postnatal loss of EXT1 did not cause any brain morphological defects, but resulted in autism-like behavioral phenotypes (Irie et al., 2012). The behavioral defects were accompanied by impaired glutamatergic transmission (Irie et al., 2012). Genetic analysis on patients affected by hereditary multiple exostosis and autism-associated mental retardation has identified deletion mutations in the gene encoding EXT1 (Li H. et al., 2002). These observations indicate that neuron-specific HSPG loss recapitulates important aspects of autism pathogenesis, further underscoring the importance of these molecules in normal brain function.

Among all the HSPGs, alterations in glypicans expression have been frequently found in different neuropathological conditions, such as autism spectrum disorders (ASDs), schizophrenia and neuroticism (Potkin et al., 2009; Calboli et al., 2010; Pinto et al., 2010; Doan et al., 2016). For instance, in a genome-wide study in autism patients to identify novel copy number variations (CNVs), four independent CNVs in the *GPC5*/*GPC6* gene cluster were identified (Pinto et al., 2010). Furthermore, Doan et al. (2016) have recently characterized novel human accelerated regions (HARs) in the *GPC4* genomic locus. HARs are human genomic sequences that are conserved in vertebrate evolution, but that are highly divergent in humans. Interestingly, HARs are particularly enriched in genes expressed in the central nervous system (Kamm et al., 2013), and based on their high frequency of mutation, HARs are considered as important genomic elements in the development of human-specific traits (Franchini and Pollard, 2017). Novel HARs have been identified within the *GPC4* genomic locus. In addition, two cases of ASD and intellectual disability (ID) present point mutations in HARs within the *GPC4* locus leading to decreased *GPC4* expression (Doan et al., 2016). These data indicate that regulated *GPC4* expression in the human brain is important for normal central nervous system development. Lastly, in another genome-wide association study to identify common genetic risks that underlie ASDs, a single nucleotide polymorphism that associated with the disease has been identified in the gene encoding the HS 3-O sulfotransferase *HS3ST5* (Wang et al., 2009). Although the molecular mechanisms that link alterations in HSPG and HS-modifying enzyme expression to disease development are still unknown, these findings further strengthen the requirement of HSPGs and HS-modifying enzymes in normal brain development and function.

CONCLUSIONS AND FUTURE DIRECTIONS

The formation of specific synaptic connectivity patterns is a key step in the assembly of functional neural circuits. This process depends on diverse molecules that are expressed in a cell type-specific manner, interact with distinct region- and cell type-specific binding partners, and instruct synapse-specific properties. The HSPG protein family is emerging as an important regulator of synaptic specificity. HSPGs are synaptic organizers and are expressed in a brain region- and cell type-specific manner. HSPGs interact with binding partners expressed in discrete cell types, and through particular HS chain modification patterns exert differential effects on synaptic function. However, many challenges remain in order to elucidate the role of HSPGs in the development of specific synaptic connectivity patterns.

Evidence in support of cell type-specific HSPGs expression patterns comes from recent single-cell transcriptomic analysis of different projection neuron types in the *Drosophila* olfactory bulb and distinct GABAergic populations in the adult mouse cortex that revealed a cell type-specific expression patterns of distinct HSPGs and HS-modifying enzymes (Tasic et al., 2016; Li et al., 2017; Paul et al., 2017). It will be important to determine whether cell type-specific combinations of HSPGs and HS-modifying enzymes broadly exist throughout the brain, and to experimentally address whether these combinations can mediate the formation of specific synaptic contacts and the development of their particular structural and functional properties.

The extent to which different HSPGs interact with region-specific binding partners is also not fully understood. Large-scale interactome screening efforts may accelerate the characterization

of the extracellular interactome of different HSPGs and can determine whether these interactions are mediated by the HS chains or the core proteins (Özkan et al., 2013). A greater challenge will be to determine to what extent such interactions are modulated by HS modifications. In combination with expression and protein distribution analysis, region-specific HSPG-ligand interactions can then be tested for a role in instructing the assembly of specific synaptic connections.

In addition to elucidating the HSPG extracellular interactome, a major challenge will be to determine whether, at the level of specific synaptic connections, differential HS modifications occur and are required for synapse development. By individual or simultaneous, cell type-specific, ablation of HS-modifying genes, it will be possible to explore whether HS modifications regulate different aspects of synapse-specific assembly and function. Altogether, these approaches will allow us to establish whether combinatorial codes of different HSPGs and specific HS modification exist, and whether such codes contribute to the specification of synaptic connectivity.

Finally, some members of the HSPG protein family, like GPC4, GPC5 and GPC6 have been linked to neurodevelopmental diseases such as autism, schizophrenia (Potkin et al., 2009; Doan et al., 2016). The link of glypicans to disease strengthens the importance of HSPGs in proper brain development and function. Therefore, elucidating the role of HSPGs and HS-modifying enzymes in the development of specific synaptic connectivity patterns will not only increase our understanding of the molecular logic underlying neural circuit assembly, but also provide new insight into the molecular basis of brain disorders.

AUTHOR CONTRIBUTIONS

GC and JW wrote the manuscript.

ACKNOWLEDGMENTS

This work in the authors' lab on the role of HSPGs in synaptic connectivity is supported by a European Research Council Starting Grant (#311083), an FWO Odysseus grant, FWO Project grant G094016N, ERANET NEURON 2015 and KU Leuven Methusalem grant.

REFERENCES

Ai, X., Do, A. T., Kusche-Gullberg, M., Lindahl, U., Lu, K., and Emerson, C. P. Jr. (2006). Substrate specificity and domain functions of extracellular heparan sulfate 6-*O*-endosulfatases, QSulf1 and QSulf2. *J. Biol. Chem.* 281, 4969–4976. doi: 10.1074/jbc.M511902200

Allen, N. J., Bennett, M. L., Foo, L. C., Wang, G. X., Chakraborty, C., Smith, S. J., et al. (2012). Astrocyte glypicans 4 and 6 promote formation of excitatory synapses via GluA1 AMPA receptors. *Nature* 486, 410–414. doi: 10.1038/nature11059

Allen, B. L., and Rapraeger, A. C. (2003). Spatial and temporal expression of heparan sulfate in mouse development regulates FGF and FGF receptor assembly. *J. Cell Biol.* 163, 637–648. doi: 10.1083/jcb.200307053

Attreed, M., Desbois, M., van Kuppevelt, T. H., and Bülow, H. E. (2012). Direct visualization of specifically modified extracellular glycans in living animals. *Nat. Methods* 9, 477–479. doi: 10.1038/nmeth.1945

Attreed, M., Saied-Santiago, K., and Bülow, H. E. (2016). Conservation of anatomically restricted glycosaminoglycan structures in divergent nematode species. *Glycobiology* 26, 862–870. doi: 10.1093/glycob/cww037

Barros, C. S., Franco, S. J., and Müller, U. (2011). Extracellular matrix: functions in the nervous system. *Cold Spring Harb. Perspect. Biol.* 3:a005108. doi: 10.1101/cshperspect.a005108

Bishop, J. R., Schuksz, M., and Esko, J. D. (2007). Heparan sulphate proteoglycans fine-tune mammalian physiology. *Nature* 446, 1030–1037. doi: 10.1038/nature05817

Bülow, H. E., and Hobert, O. (2004). Differential sulfations and epimerization define heparan sulfate specificity in nervous system development. *Neuron* 41, 723–736. doi: 10.1016/s0896-6273(04)00084-4

Bülow, H. E., Tjoe, N., Townley, R. A., Didiano, D., van Kuppevelt, T. H., and Hobert, O. (2008). Extracellular sugar modifications provide instructive and cell-specific information for axon-guidance choices. *Curr. Biol.* 18, 1978–1985. doi: 10.1016/j.cub.2008.11.023

Calboli, F. C. F., Tozzi, F., Galwey, N. W., Antoniades, A., Mooser, V., Preisig, M., et al. (2010). A genome-wide association study of neuroticism in a population-based sample. *PLoS One* 5:e11504. doi: 10.1371/journal.pone.0011504

Capurro, M. I., Xu, P., Shi, W., Li, F., Jia, A., and Filmus, J. (2008). Glypican-3 inhibits hedgehog signaling during development by competing with patched for hedgehog binding. *Dev. Cell* 14, 700–711. doi: 10.1016/j.devcel.2008.03.006

Cembrowski, M. S., Wang, L., Sugino, K., Shields, B. C., and Spruston, N. (2016). Hipposeq: a comprehensive RNA-seq database of gene expression in hippocampal principal neurons. *Elife* 5:e14997. doi: 10.7554/eLife.14997

Chen, C. Y., Lin, C. W., Chang, C. Y., Jian, S. T., and Hsueh, Y. P. (2011). Sarm1, a negative regulator of innate immunity, interacts with syndecan-2 and regulates neuronal morphology. *J. Cell Biol.* 193, 769–784. doi: 10.1083/jcb.201008050

Christopherson, K. S., Ullian, E. M., Stokes, C. C. A., Mullowney, C. E., Hell, J. W., Agah, A., et al. (2005). Thrombospondins are astrocyte-secreted proteins that promote CNS synaptogenesis. *Cell* 120, 421–433. doi: 10.1016/j.cell.2004.12.020

Dani, N., Nahm, M., Lee, S., and Broadie, K. (2012). A targeted glycan-related gene screen reveals heparan sulfate proteoglycan sulfation regulates WNT and BMP trans-synaptic signaling. *PLoS Genet.* 8:e1003031. doi: 10.1371/journal.pgen.1003031

De Rubeis, S., He, X., Goldberg, A. P., Poultney, C. S., Samocha, K., Cicek, A. E., et al. (2014). Synaptic, transcriptional and chromatin genes disrupted in autism. *Nature* 515, 209–215. doi: 10.1038/nature13772

de Wit, J., and Ghosh, A. (2016). Specification of synaptic connectivity by cell surface interactions. *Nat. Rev. Neurosci.* 17, 22–35. doi: 10.1038/nrn.2015.3

de Wit, J., O'Sullivan, M. L., Savas, J. N., Condomitti, G., Caccese, M. C., Vennekens, K. M., et al. (2013). Unbiased discovery of glypican as a receptor for LRRTM4 in regulating excitatory synapse development. *Neuron* 79, 696–711. doi: 10.1016/j.neuron.2013.06.049

de Wit, J., Sylwestrak, E., O'Sullivan, M. L., Otto, S., Tiglio, K., Savas, J. N., et al. (2009). LRRTM2 interacts with Neurexin1 and regulates excitatory synapse formation. *Neuron* 64, 799–806. doi: 10.1016/j.neuron.2009.12.019

de Wit, J., and Verhaagen, J. (2007). Proteoglycans as modulators of axon guidance cue function. *Adv. Exp. Med. Biol.* 600, 73–89. doi: 10.1007/978-0-387-70956-7_7

Doan, R. N., Bae, B.-I., Cubelos, B., Chang, C., Hossain, A. A., Al-Saad, S., et al. (2016). Mutations in human accelerated regions disrupt cognition and social behavior. *Cell* 167, 341.e12–354.e12. doi: 10.1016/j.cell.2016.08.071

Eroglu, Ç., Allen, N. J., Susman, M. W., O'Rourke, N. A., Park, C. Y., Özkan, E., et al. (2009). Gabapentin receptor α2δ-1 is a neuronal thrombospondin receptor responsible for excitatory CNS synaptogenesis. *Cell* 139, 380–392. doi: 10.1016/j.cell.2009.09.025

Esko, J. D., and Selleck, S. B. (2002). Order out of chaos: assembly of ligand binding sites in heparan sulfate. *Annu. Rev. Biochem.* 71, 435–471. doi: 10.1146/annurev.biochem.71.110601.135458

Ethell, I. M., Irie, F., Kalo, M. S., Couchman, J. R., Pasquale, E. B., and Yamaguchi, Y. (2001). EphB/syndecan-2 signaling in dendritic spine morphogenesis. *Neuron* 31, 1001–1013. doi: 10.1016/s0896-6273(01)00440-8

Ethell, I. M., and Yamaguchi, Y. (1999). Cell surface heparan sulfate proteoglycan syndecan-2 induces the maturation of dendritic spines in rat hippocampal neurons. *J. Cell Biol.* 144, 575–586. doi: 10.1083/jcb.144.3.575

Farhy-Tselnicker, I., van Casteren, A. C. M., Lee, A., Chang, V. T., Aricescu, A. R., and Allen, N. J. (2017). Astrocyte-secreted glypican 4 regulates release of neuronal pentraxin 1 from axons to induce functional synapse formation. *Neuron* 96, 428.e13–445.e13. doi: 10.1016/j.neuron.2017.09.053

Fitzgerald, M. L., Wang, Z., Park, P. W., Murphy, G., and Bernfield, M. (2000). Shedding of syndecan-1 and -4 ectodomains is regulated by multiple signaling pathways and mediated by a TIMP-3-sensitive metalloproteinase. *J. Cell Biol.* 148, 811–824. doi: 10.1083/jcb.148.4.811

Földy, C., Darmanis, S., Aoto, J., Malenka, R. C., Quake, S. R., and Südhof, T. C. (2016). Single-cell RNAseq reveals cell adhesion molecule profiles in electrophysiologically defined neurons. *Proc. Natl. Acad. Sci. U S A* 113, E5222–E5231. doi: 10.1073/pnas.1610155113

Fox, M. A., Sanes, J. R., Borza, D. B., Eswarakumar, V. P., Fässler, R., Hudson, B. G., et al. (2007). Distinct target-derived signals organize formation, maturation, and maintenance of motor nerve terminals. *Cell* 129, 179–193. doi: 10.1016/j.cell.2007.02.035

Franchini, L. F., and Pollard, K. S. (2017). Human evolution: the non-coding revolution. *BMC Biol.* 15:89. doi: 10.1186/s12915-017-0428-9

Frischknecht, R., and Gundelfinger, E. D. (2012). The brain's extracellular matrix and its role in synaptic plasticity. *Adv. Exp. Med. Biol.* 970, 153–171. doi: 10.1007/978-3-7091-0932-8_7

Fuki, I. V., Meyer, M. E., and Williams, K. J. (2000). Transmembrane and cytoplasmic domains of syndecan mediate a multi-step endocytic pathway involving detergent-insoluble membrane rafts. *Biochem. J.* 351, 607–612. doi: 10.1042/0264-6021:3510607

Gautam, M., Noakes, P. G., Moscoso, L., Rupp, F., Scheller, R. H., Merlie, J. P., et al. (1996). Defective neuromuscular synaptogenesis in agrin-deficient mutant mice. *Cell* 85, 525–535. doi: 10.1016/s0092-8674(00)81253-2

Glass, D. J., Bowen, D. C., Stitt, T. N., Radziejewski, C., Bruno, J. A., Ryan, T. E., et al. (1996). Agrin acts via a MuSK receptor complex. *Cell* 85, 513–523. doi: 10.1016/s0092-8674(00)81252-0

Godfrey, E. W., Nitkin, R. M., Wallace, B. G., Rubin, L. L., and McMahan, U. J. (1984). Components of Torpedo electric organ and muscle that cause aggregation of acetylcholine receptors on cultured muscle cells. *J. Cell Biol.* 99, 615–627. doi: 10.1083/jcb.99.2.615

Graf, E. R., Zhang, X., Jin, S. X., Linhoff, M. W., and Craig, A. M. (2004). Neurexins induce differentiation of GABA and glutamate postsynaptic specializations via neuroligins. *Cell* 119, 1013–1026. doi: 10.1016/j.cell.2004.11.035

Häcker, U., Nybakken, K., and Perrimon, N. (2005). Heparan sulphate proteoglycans: the sweet side of development. *Nat. Rev. Mol. Cell Biol.* 6, 530–541. doi: 10.1038/nrm1681

Holt, C. E., and Dickson, B. J. (2005). Sugar codes for axons? *Neuron* 46, 169–172. doi: 10.1016/j.neuron.2005.03.021

Hsueh, Y. P., and Sheng, M. (1999). Regulated expression and subcellular localization of syndecan heparan sulfate proteoglycans and the syndecan-binding protein CASK/LIN-2 during rat brain development. *J. Neurosci.* 19, 7415–7425.

Hsueh, Y. P., Yang, F. C., Kharazia, V., Naisbitt, S., Cohen, A. R., Weinberg, R. J., et al. (1998). Direct interaction of CASK/LIN-2 and syndecan heparan sulfate proteoglycan and their overlapping distribution in neuronal synapses. *J. Cell Biol.* 142, 139–151. doi: 10.1083/jcb.142.1.139

Hu, H. (2001). Cell-surface heparan sulfate is involved in the repulsive guidance activities of Slit2 protein. *Nat. Neurosci.* 4, 695–701. doi: 10.1038/89482

Hu, H.-T., Umemori, H., and Hsueh, Y.-P. (2016). Postsynaptic SDC2 induces transsynaptic signaling via FGF22 for bidirectional synaptic formation. *Sci. Rep.* 6:33592. doi: 10.1038/srep33592

Hussain, S. A., Piper, M., Fukuhara, N., Strochlic, L., Cho, G., Howitt, J. A., et al. (2006). A molecular mechanism for the heparan sulfate dependence of slit-robo signaling. *J. Biol. Chem.* 281, 39693–39698. doi: 10.1074/jbc.M609384200

Inatani, M., Irie, F., Plump, A. S., Tessier-Lavigne, M., and Yamaguchi, Y. (2003). Mammalian brain morphogenesis and midline axon guidance require heparan sulfate. *Science* 302, 1044–1046. doi: 10.1126/science.1090497

Irie, F., Badie-Mahdavi, H., and Yamaguchi, Y. (2012). Autism-like socio-communicative deficits and stereotypies in mice lacking heparan sulfate. *Proc. Natl. Acad. Sci. U S A* 109, 5052–5056. doi: 10.1073/pnas.1117881109

Irie, F., Okuno, M., Matsumoto, K., Pasquale, E. B., and Yamaguchi, Y. (2008). Heparan sulfate regulates ephrin-A3/EphA receptor signaling. *Proc. Natl. Acad. Sci. U S A* 105, 12307–12312. doi: 10.1073/pnas.0801302105

Jang, S., Lee, H., and Kim, E. (2017). Synaptic adhesion molecules and excitatory synaptic transmission. *Curr. Opin. Neurobiol.* 45, 45–50. doi: 10.1016/j.conb.2017.03.005

Johnson, K. G., Tenney, A. P., Ghose, A., Duckworth, A. M., Higashi, M. E., Parfitt, K., et al. (2006). The HSPGs Syndecan and dallylike bind the receptor phosphatase LAR and exert distinct effects on synaptic development. *Neuron* 49, 517–531. doi: 10.1016/j.neuron.2006.01.026

Kainulainen, V., Wang, H., Schick, C., and Bernfield, M. (1998). Syndecans, heparan sulfate proteoglycans, maintain the proteolytic balance of acute wound fluids. *J. Biol. Chem.* 273, 11563–11569. doi: 10.1074/jbc.273.19.11563

Kalus, I., Salmen, B., Viebahn, C., von Figura, K., Schmitz, D., D'Hooge, R., et al. (2009). Differential involvement of the extracellular 6-O-endosulfatases Sulf1 and Sulf2 in brain development and neuronal and behavioural plasticity. *J. Cell. Mol. Med.* 13, 4505–4521. doi: 10.1111/j.1582-4934.2008.00558.x

Kamimura, K., Ueno, K., Nakagawa, J., Hamada, R., Saitoe, M., and Maeda, N. (2013). Perlecan regulates bidirectional Wnt signaling at the *Drosophila* neuromuscular junction. *J. Cell Biol.* 200, 219–233. doi: 10.1083/jcb.201207036

Kamm, G. B., Pisciottano, F., Kliger, R., and Franchini, L. F. (2013). The developmental brain gene NPAS3 contains the largest number of accelerated regulatory sequences in the human genome. *Mol. Biol. Evol.* 30, 1088–1102. doi: 10.1093/molbev/mst023

Kantor, D. B., Chivatakarn, O., Peer, K. L., Oster, S. F., Inatani, M., Hansen, M. J., et al. (2004). Semaphorin 5A is a bifunctional axon guidance cue regulated by heparan and chondroitin sulfate proteoglycans. *Neuron* 44, 961–975. doi: 10.1016/j.neuron.2004.12.002

Kato, M., Wang, H., Bernfield, M., Gallagher, J. T., and Turnbull, J. E. (1994). Cell surface syndecan-1 on distinct cell types differs in fine structure and ligand binding of its heparan sulfate chains. *J. Biol. Chem.* 269, 18881–18890.

Ko, J., Choii, G., and Um, J. W. (2015). The balancing act of GABAergic synapse organizers. *Trends Mol. Med.* 21, 256–268. doi: 10.1016/j.molmed.2015.01.004

Ko, J., Fuccillo, M. V., Malenka, R. C., and Südhof, T. C. (2009). LRRTM2 functions as a neurexin ligand in promoting excitatory synapse formation. *Neuron* 64, 791–798. doi: 10.1016/j.neuron.2009.12.012

Ko, J. S., Pramanik, G., Um, J. W., Shim, J. S., Lee, D., Kim, K. H., et al. (2015). PTPσ functions as a presynaptic receptor for the glypican-4/LRRTM4 complex and is essential for excitatory synaptic transmission. *Proc. Natl. Acad. Sci. U S A* 112, 1874–1879. doi: 10.1073/pnas.1410138112

Kolodkin, A. L., and Tessier-Lavigne, M. (2011). Mechanisms and molecules of neuronal wiring: a primer. *Cold Spring Harb. Perspect. Biol.* 3:a001727. doi: 10.1101/cshperspect.a001727

Kreuger, J., and Kjellén, L. (2012). Heparan sulfate biosynthesis. *J. Histochem. Cytochem.* 60, 898–907. doi: 10.1369/0022155412464972

Lee, J., and Chien, C. (2004). When sugars guide axons: insights from heparan sulphate proteoglycan mutants. *Nat. Rev. Genet.* 5, 923–935. doi: 10.1038/nrg1490

Li, H., Horns, F., Xie, Q., Xie, Q., Li, T., Luginbuhl, D. J., et al. (2017). Classifying *Drosophila* olfactory projection neuron subtypes by single-cell RNA sequencing. *Cell* 171, 1206.e22–1207.e22. doi: 10.1016/j.cell.2017.10.019

Li, Q., Park, P. W., Wilson, C. L., and Parks, W. C. (2002). Matrilysin shedding of syndecan-1 regulates chemokine mobilization and transepithelial efflux of neutrophils in acute lung injury. *Cell* 111, 635–646. doi: 10.1016/s0092-8674(02)01079-6

Li, H., Yamagata, T., Mori, M., and Momoi, M. Y. (2002). Association of autism in two patients with hereditary multiple exostoses caused by novel deletion mutations of EXT1. *J. Hum. Genet.* 47, 262–265. doi: 10.1007/s10038020036

Lin, Y.-L., Lei, Y.-T., Hong, C.-J., and Hsueh, Y.-P. (2007). Syndecan-2 induces filopodia and dendritic spine formation via the neurofibromin-PKA-Ena/VASP pathway. *J. Cell Biol.* 177, 829–841. doi: 10.1083/jcb.200608121

Linhoff, M. W., Laurén, J., Cassidy, R. M., Dobie, F. A., Takahashi, H., Nygaard, H. B., et al. (2009). An unbiased expression screen for synaptogenic proteins identifies the LRRTM protein family as synaptic organizers. *Neuron* 61, 734–749. doi: 10.1016/j.neuron.2009.01.017

Medeiros, G. F., Mendes, A., Castro, R. A. B., Baú, E. C., Nader, H. B., and Dietrich, C. P. (2000). Distribution of sulfated glycosaminoglycans in the animal kingdom: widespread occurrence of heparin-like compounds in invertebrates. *Biochim. Biophys. Acta* 1475, 287–294. doi: 10.1016/s0304-4165(00)00079-9

Nguyen, M. U., Kwong, J., Chang, J., Gillet, V. G., Lee, R. M., and Johnson, K. G. (2016). The extracellular and cytoplasmic domains of syndecan cooperate postsynaptically to promote synapse growth at the *Drosophila* neuromuscular junction. *PLoS One* 11:e0151621. doi: 10.1371/journal.pone.0151621

Ornitz, D. M. (2000). FGFs, heparan sulfate and FGFRs: complex interactions essential for development. *Bioessays* 22, 108–112. doi: 10.1002/(sici)1521-1878(200002)22:2<108::aid-bies2>3.0.co;2-m

Özkan, E., Carrillo, R. A., Eastman, C. L., Weiszmann, R., Waghray, D., Johnson, K. G., et al. (2013). An extracellular interactome of immunoglobulin and LRR proteins reveals receptor-ligand networks. *Cell* 154, 228–239. doi: 10.1016/j.cell.2013.06.006

Parikshak, N. N., Luo, R., Zhang, A., Won, H., Lowe, J. K., Chandran, V., et al. (2013). Integrative functional genomic analyses implicate specific molecular pathways and circuits in autism. *Cell* 155, 1008–1021. doi: 10.1016/j.cell.2013.10.031

Park, P. W., Reizes, O., and Bernfield, M. (2000). Cell surface heparan sulfate proteoglycans: selective regulators of ligand-receptor encounters. *J. Biol. Chem.* 275, 29923–29926. doi: 10.1074/jbc.R000008200

Pastor-Pareja, J. C., and Xu, T. (2011). Shaping cells and organs in *Drosophila* by opposing roles of fat body-secreted collagen IV and perlecan. *Dev. Cell* 21, 245–256. doi: 10.1016/j.devcel.2011.06.026

Paul, A., Crow, M., Raudales, R., He, M., Gillis, J., and Huang, Z. J. (2017). Transcriptional architecture of synaptic communication delineates GABAergic neuron identity. *Cell* 171, 522.e20–539.e20. doi: 10.1016/j.cell.2017.08.032

Pinto, D., Pagnamenta, A. T., Klei, L., Anney, R., Merico, D., Regan, R., et al. (2010). Functional impact of global rare copy number variation in autism spectrum disorders. *Nature* 466, 368–372. doi: 10.1038/nature09146

Potkin, S. G., Turner, J. A., Fallon, J. A., Lakatos, A., Keator, D. B., Guffanti, G., et al. (2009). Gene discovery through imaging genetics: identification of two novel genes associated with schizophrenia. *Mol. Psychiatry* 14, 416–428. doi: 10.1038/mp.2008.127

Qin, J., Liang, J., and Ding, M. (2014). Perlecan antagonizes collagen IV and ADAMTS9/GON-1 in restricting the growth of presynaptic boutons. *J. Neurosci.* 34, 10311–10324. doi: 10.1523/JNEUROSCI.5128-13.2014

Sanes, J. R., and Yamagata, M. (2009). Many paths to synaptic specificity. *Annu. Rev. Cell Dev. Biol.* 25, 161–195. doi: 10.1146/annurev.cellbio.24.110707.175402

Sarrazin, S., Lamanna, W. C., and Esko, J. D. (2011). Heparan sulfate proteoglycans. *Cold Spring Harb. Perspect. Biol.* 3:a004952. doi: 10.1101/cshperspect.a004952

Scheiffele, P., Fan, J., Choih, J., Fetter, R., and Serafini, T. (2000). Neuroligin expressed in nonneuronal cells triggers presynaptic development in contacting axons. *Cell* 101, 657–669. doi: 10.1016/s0092-8674(00)80877-6

Schlessinger, J., Plotnikov, A. N., Ibrahimi, O. A., Eliseenkova, A. V., Yeh, B. K., Yayon, A., et al. (2000). Crystal structure of a ternary FGF-FGFR-heparin complex reveals a dual role for heparin in FGFR binding and dimerization. *Mol. Cell* 6, 743–750. doi: 10.1016/s1097-2765(00)00073-3

Selleck, S. B. (2001). Genetic dissection of proteoglycan function in *Drosophila* and *C. elegans*. *Semin. Cell Dev. Biol.* 12, 127–134. doi: 10.1006/scdb.2000.0242

Shekhar, K., Lapan, S. W., Whitney, I. E., Tran, N. M., Macosko, E. Z., Kowalczyk, M., et al. (2016). Comprehensive classification of retinal bipolar neurons by single-cell transcriptomics. *Cell* 166, 1308.e30–1323.e30. doi: 10.1016/j.cell.2016.07.054

Shen, K., and Scheiffele, P. (2010). Genetics and cell biology of building specific synaptic connectivity. *Annu. Rev. Neurosci.* 33, 473–507. doi: 10.1146/annurev.neuro.051508.135302

Siddiqui, T. J., and Craig, A. M. (2011). Synaptic organizing complexes. *Curr. Opin. Neurobiol.* 21, 132–143. doi: 10.1016/j.conb.2010.08.016

Siddiqui, T. J., Tari, P., Connor, S. A., Zhang, P., Dobie, F. A., She, K., et al. (2013). An LRRTM4-HSPG complex mediates excitatory synapse development on dentate gyrus granule cells. *Neuron* 79, 680–695. doi: 10.1016/j.neuron.2013.06.029

Steigemann, P., Molitor, A., Fellert, S., Jäckle, H., and Vorbrüggen, G. (2004). Heparan sulfate proteoglycan syndecan promotes axonal and myotube guidance by slit/robo signaling. *Curr. Biol.* 14, 225–230. doi: 10.1016/j.cub.2004.01.006

Takahashi, H., and Craig, A. M. (2013). Protein tyrosine phosphatases PTPδ, PTPσ and, LAR: presynaptic hubs for synapse organization. *Trends Neurosci.* 36, 522–534. doi: 10.1016/j.tins.2013.06.002

Tan, L., Zhang, K. X., Pecot, M. Y., Nagarkar-Jaiswal, S., Lee, P. T., Takemura, S. Y., et al. (2015). Ig superfamily ligand receptor pairs expressed in synaptic partners in *Drosophila*. *Cell* 163, 1756–1769. doi: 10.1016/j.cell.2015.11.021

Tasic, B., Menon, V., Nguyen, T. N., Kim, T. K., Jarsky, T., Yao, Z., et al. (2016). Adult mouse cortical cell taxonomy revealed by single cell transcriptomics. *Nat. Neurosci.* 19, 335–346. doi: 10.1038/nn.4216

Terauchi, A., Johnson-Venkatesh, E. M., Toth, A. B., Javed, D., Sutton, M. A., and Umemori, H. (2010). Distinct FGFs promote differentiation of excitatory and inhibitory synapses. *Nature* 465, 783–787. doi: 10.1038/nature09041

Tillo, M., Charoy, C., Schwarz, Q., Maden, C. H., Davidson, K., Fantin, A., et al. (2016). 2- and 6- O -sulfated proteoglycans have distinct and complementary roles in cranial axon guidance and motor neuron migration. *Development* 143, 1907–1913. doi: 10.1242/dev.126854

Tumova, S., Woods, A., and Couchman, J. R. (2000). Heparan sulfate chains from glypican and syndecans bind the Hep II domain of fibronectin similarly despite minor structural differences. *J. Biol. Chem.* 275, 9410–9417. doi: 10.1074/jbc.275.13.9410

Um, J. W., and Ko, J. (2013). LAR-RPTPs: synaptic adhesion molecules that shape synapse development. *Trends Cell Biol.* 23, 465–475. doi: 10.1016/j.tcb.2013.07.004

Van Vactor, D., Wall, D. P., and Johnson, K. G. (2006). Heparan sulfate proteoglycans and the emergence of neuronal connectivity. *Curr. Opin. Neurobiol.* 16, 40–51. doi: 10.1016/j.conb.2006.01.011

Walz, A., McFarlane, S., Brickman, Y. G., Nurcombe, V., Bartlett, P. F., and Holt, C. E. (1997). Essential role of heparan sulfates in axon navigation and targeting in the developing visual system. *Development* 124, 2421–2430.

Wang, L., and Denburg, J. L. (1992). A role for proteoglycans in the guidance of a subset of pioneer axons in cultured embryos of the cockroach. *Neuron* 8, 701–714. doi: 10.1016/0896-6273(92)90091-q

Wang, K., Zhang, H., Ma, D., Bucan, M., Glessner, J. T., Abrahams, B. S., et al. (2009). Common genetic variants on 5p14.1 associate with autism spectrum disorders. *Nature* 459, 528–533. doi: 10.1038/nature07999

Williams, M. E., de Wit, J., and Ghosh, A. (2010). Molecular mechanisms of synaptic specificity in developing neural circuits. *Neuron* 68, 9–18. doi: 10.1016/j.neuron.2010.09.007

Witt, R. M., Hecht, M. L., Pazyra-Murphy, M. F., Cohen, S. M., Noti, C., Van Kuppevelt, T. H., et al. (2013). Heparan sulfate proteoglycans containing a glypican 5 core and 2-*O*-sulfo-iduronic acid function as sonic hedgehog co-receptors to promote proliferation. *J. Biol. Chem.* 288, 26275–26288. doi: 10.1074/jbc.p112.438937

Xu, D., and Esko, J. D. (2014). Demystifying heparan sulfate-protein interactions. *Annu. Rev. Biochem.* 83, 129–157. doi: 10.1146/annurev-biochem-060713-035314

Yan, D., and Lin, X. (2007). *Drosophila* glypican Dally-like acts in FGF-receiving cells to modulate FGF signaling during tracheal morphogenesis. *Dev. Biol.* 312, 203–216. doi: 10.1016/j.ydbio.2007.09.015

Yogev, S., and Shen, K. (2014). Cellular and molecular mechanisms of synaptic specificity. *Annu. Rev. Cell Dev. Biol.* 30, 417–437. doi: 10.1146/annurev-cellbio-100913-012953

Zako, M., Dong, J., Goldberger, O., Bernfield, M., Gallagher, J. T., and Deakins, J. A. (2003). Syndecan-1 and -4 synthesized simultaneously by mouse mammary gland epithelial cells bear heparan sulfate chains that are apparently structurally indistinguishable. *J. Biol. Chem.* 278, 13561–13569. doi: 10.1074/jbc.m209658200

Zimmermann, P., Zhang, Z., Degeest, G., Mortier, E., Leenaerts, I., Coomans, C., et al. (2005). Syndecan recyling is controlled by syntenin-PIP2 interaction and Arf6. *Dev. Cell* 9, 377–388. doi: 10.1016/j.devcel.2005.07.011

Conflict of Interest Statement: The authors declare that the research was conducted in the absence of any commercial or financial relationships that could be construed as a potential conflict of interest.

frontiers in Synaptic Neuroscience

ORIGINAL RESEARCH
published: 19 December 2017
doi: 10.3389/fnsyn.2017.00017

Selective Inactivation of Fibroblast Growth Factor 22 (FGF22) in CA3 Pyramidal Neurons Impairs Local Synaptogenesis and Affective Behavior Without Affecting Dentate Neurogenesis

*Akiko Terauchi, Elizabeth Gavin, Julia Wilson and Hisashi Umemori**

F.M. Kirby Neurobiology Center, Department of Neurology, Boston Children's Hospital, Harvard Medical School, Harvard University, Boston, MA, United States

OPEN ACCESS

Edited by:
Jaewon Ko, Daegu Gyeongbuk Institute of Science and Technology (DGIST), South Korea

Reviewed by:
Michael Fox, Virginia Tech Carilion Research Institute, United States
Eunjoon Kim, Institute for Basic Science (IBS), South Korea
Yutaka Yoshida, Cincinnati Children's Hospital Medical Center, United States

***Correspondence:**
Hisashi Umemori
hisashi.umemori@childrens.harvard.edu

Received: *03 October 2017*
Accepted: *05 December 2017*
Published: *19 December 2017*

Citation:
Terauchi A, Gavin E, Wilson J and Umemori H (2017) Selective Inactivation of Fibroblast Growth Factor 22 (FGF22) in CA3 Pyramidal Neurons Impairs Local Synaptogenesis and Affective Behavior Without Affecting Dentate Neurogenesis. Front. Synaptic Neurosci. 9:17. doi: 10.3389/fnsyn.2017.00017

Various growth factors regulate synapse development and neurogenesis, and are essential for brain function. Changes in growth factor signaling are implicated in many neuropsychiatric disorders such as depression, autism and epilepsy. We have previously identified that fibroblast growth factor 22 (FGF22) is critical for excitatory synapse formation in several brain regions including the hippocampus. Mice with a genetic deletion of FGF22 (FGF22 null mice) have fewer excitatory synapses in the hippocampus. We have further found that as a behavioral consequence, FGF22 null mice show a depression-like behavior phenotype such as increased passive stress-coping behavior and anhedonia, without any changes in motor, anxiety, or social cognitive tests, suggesting that FGF22 is specifically important for affective behavior. Thus, addressing the precise roles of FGF22 in the brain will help understand how synaptogenic growth factors regulate affective behavior. In the hippocampus, FGF22 is expressed mainly by CA3 pyramidal neurons, but also by a subset of dentate granule cells. We find that in addition to synapse formation, FGF22 also contributes to neurogenesis in the dentate gyrus: FGF22 null mice show decreased dentate neurogenesis. To understand the cell type-specific roles of FGF22, we generated and analyzed CA3-specific FGF22 knockout mice (FGF22-CA3KO). We show that FGF22-CA3KO mice have reduced excitatory synapses on CA3 pyramidal neurons, but do not show changes in dentate neurogenesis. Behaviorally, FGF22-CA3KO mice still show increased immobility and decreased latency to float in the forced swim test and decreased preference for sucrose in the sucrose preference test, which are suggestive of a depressive-like phenotype similar to FGF22 null mice. These results demonstrate that: (i) CA3-derived FGF22 serves as a target-derived excitatory synaptic organizer in CA3 *in vivo*; (ii) FGF22 plays important roles in dentate neurogenesis, but CA3-derived FGF22 is not involved in neurogenesis; and

(iii) a depression-like phenotype can result from FGF22 inactivation selectively in CA3 pyramidal neurons. Our results link the role of CA3-derived FGF22 in synapse development, and not in neurogenesis, to affective behavior.

Keywords: hippocampus, synaptogenesis, neurogenesis, fibroblast growth factor, conditional knockout mice, CA3, depression

INTRODUCTION

Growth factor signaling is implicated in many aspects of brain development and function. Fibroblast growth factors (FGFs) regulate a variety of events during brain development such as neuronal proliferation and differentiation, synaptic development and neurogenesis (Ornitz and Itoh, 2001; Thisse and Thisse, 2005; Umemori, 2009; Turner and Grose, 2010; Turner et al., 2012). Alteration in the FGF and FGF receptor signaling has been found in many neuropsychiatric diseases, including depression (Evans et al., 2004), altered social behavior (Scearce-Levie et al., 2008), seizures (Terauchi et al., 2010; Williams and Umemori, 2014), and intellectual disability (Williams and Umemori, 2014). Thus, understanding the precise roles of FGF signaling in brain development will shed light on the pathophysiology of such disorders and may provide clues for designing novel treatment strategies.

We have previously found that a subfamily of FGFs, Fibroblast Growth Factor 22 (FGF22), 7 and 10, acts as synaptic organizing molecules (Umemori et al., 2004). FGF22 is critical for the establishment of excitatory synapses in the developing brain, including the cerebellum, hippocampus and lateral geniculate nucleus (Umemori et al., 2004; Terauchi et al., 2010; Singh et al., 2012). Mice genetically lacking FGF22 (FGF22 null mice) show impaired excitatory synapse formation in the brain during development. The defects persist into adulthood: FGF22 null mice have fewer excitatory synapses later in life (Terauchi et al., 2010). Mechanistically, we proposed that FGF22 serves as a target (postsynaptic neuron)-derived presynaptic organizer in the hippocampus, because, using cultured neurons, we found: (i) FGF22 overexpression induced excitatory synapses on the FGF22 expressing neurons; and (ii) postsynaptic expression of FGF22 rescued impaired excitatory synapse formation in cultures prepared from FGF22 null mice (Terauchi et al., 2010). However, this idea has not been tested *in vivo*. Therefore, in this article, we ask whether FGF22 acts as a target-derived presynaptic organizer *in vivo* using mice in which FGF22 is selectively inactivated in CA3 pyramidal neurons, where FGF22 is highly expressed during development.

In addition to synapse development, FGF22 appears to be involved in the regulation of activity-dependent neurogenesis in the dentate gyrus, where neurogenesis continues throughout life. In wild-type mice, dentate neurogenesis has been shown to increase in response to seizure activity (Parent, 2007; Song et al., 2012; Lee and Umemori, 2013; Cho et al., 2015). In contrast, we found that FGF22 null mice do not show increased neurogenesis after seizure (Lee and Umemori, 2013). However, whether FGF22 is important for normal neurogenesis is not known. In this article, we ask whether FGF22 is involved in neurogenesis using FGF22 null mice. As CA3-derived FGF22 acts on the axons of dentate granule cells (DGCs), we also ask whether CA3-derived FGF22 plays a role in regulating neurogenesis using CA3-specific FGF22 knockout mice.

Finally, as a behavioral consequence of FGF22 inactivation, FGF22 null mice display depression-like behaviors such as increased passive stress-coping behavior and anhedonia (Williams et al., 2016). FGF22 null mice do not show any changes in anxiety-like behaviors, social cognition and motor phenotypes (Williams et al., 2016). These results suggest that FGF22 plays a unique role in affective behaviors, and FGF22 is a potential target for the development of novel antidepressant agents. In order to provide further insights into the molecular mechanisms underlying depression-like behaviors, in this article, we ask cell-type specific roles of FGF22 in the regulation of affective behavior using CA3-specific FGF22 knockout mice.

FGF22 is expressed by various neurons in the brain. In the hippocampus, FGF22 is highly expressed by CA3 pyramidal neurons as well as a subset of DGCs (Terauchi et al., 2010). In order to address the questions listed above, we utilized a conditional, cell-type specific FGF22 knockout mice. We generated CA3-specific FGF22 knockout (FGF22-CA3KO) mice and analyzed their synapse development, dentate neurogenesis, and affective behaviors. Here we show: (i) FGF22-CA3KO mice have reduced excitatory synapses formed onto CA3 pyramidal neurons; (ii) FGF22 null mice show decreased dentate neurogenesis throughout life; (iii) In contrast, FGF22-CA3KO mice does not show any changes in dentate neurogenesis; and (iv) FGF22-CA3KO mice exhibit increased passive stress coping behaviors and anhedonia, similarly to FGF22 null mice. These results suggest that CA3-derived FGF22 serves as a target-derived excitatory presynaptic organizer *in vivo* and contributes to the establishment of synaptic circuits involved in affective behavior.

MATERIALS AND METHODS

Animals

Fgf22$^{-/-}$ mice (FGF22 null mice) were described previously (Terauchi et al., 2010). *Fgf22*$^{-/-}$ mice were backcrossed with C57/BL6J (Jackson Laboratories, Bar Harbor, ME, USA) for more than 15 generations. *Fgf22*$^{flox/flox}$ mice (*Fgf22*$^{tm1a(EUCOMM)Hmgu}$) were from EUCOMM (Terauchi et al., 2016). Grik4-Cre mice were from Jackson (Nakazawa et al., 2002). *Fgf22*$^{flox/flox}$ mice were mated with Grik4-Cre mice to generate CA3-specific FGF22 knockout mice (FGF22-CA3KO mice; see **Figure 1A**). Both males and females were used in our study. The numbers of animals used in the behavioral studies are shown in **Table 1** and figure legends. The numbers of animals used in the histological

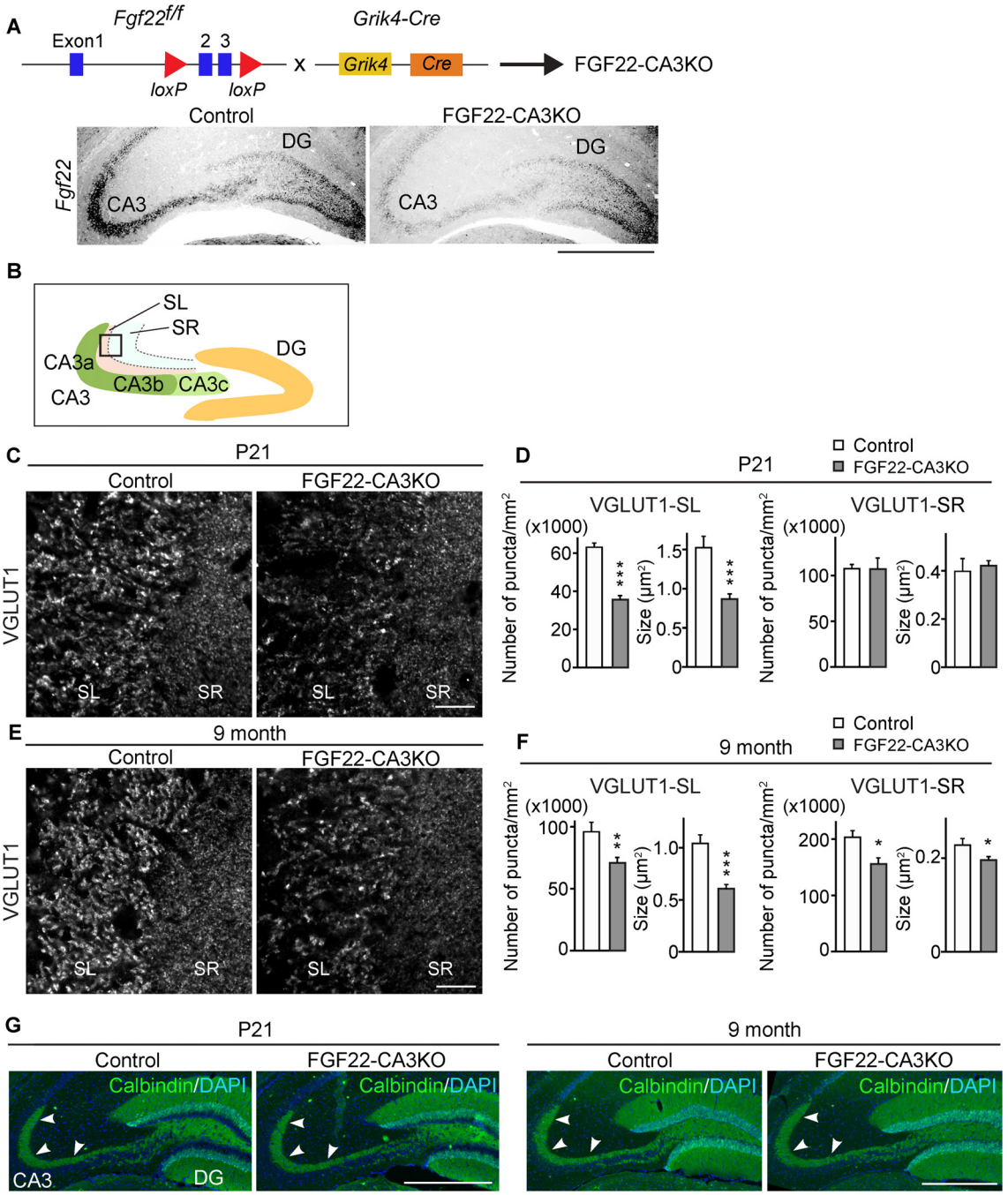

FIGURE 1 | CA3-derived Fibroblast Growth Factor 22 (FGF22) is required for excitatory synapse formation in the hippocampal CA3 region. **(A)** (Top) Schematic diagram of the strategy to generate CA3-specific *Fgf22* knockout mice (FGF22-CA3KO mice). *Fgf22*$^{flox/flox}$ (*Fgf22*$^{f/f}$) mice were crossed with mice carrying *Grik4*-promoter-driven Cre (*Grik4-Cre*). (Bottom) *In situ* hybridization for *Fgf22* mRNA with hippocampal sections from P9 wild-type littermates (Control) and FGF22-CA3KO mice (*Fgf22*$^{f/f}$::*Grik4-Cre*). *Fgf22* expression is specifically eliminated from CA3 pyramidal neurons in FGF22-CA3KO mice. **(B)** Images in **(C,E)** were taken from the boxed area. Analysis was performed from images taken in CA3a and CA3b. **(C,D)** Hippocampal sections from Control and FGF22-CA3KO mice at P21 were immunostained for vesicular glutamate transporter 1 (VGLUT1). **(C)** Representative pictures from the CA3 region. SL, stratum lucidum; SR, stratum radiatum. Density (number/mm^2) and size (μm^2) of VGLUT1 puncta were quantified and shown in **(D)**. **(E,F)** Hippocampal sections from adult Control and FGF22-CA3KO mice (9 months of age) were immunostained for VGLUT1. **(E)** Representative pictures from the CA3 region. Density and size of VGLUT1 puncta were quantified and shown in **(F)**. FGF22-CA3KO mice show decreased VGLUT1 puncta in the CA3 SL layer at P21 and in SL and SR layers in adults. Bars indicate mean ± SEM. **(G)** DGC axon targeting is not impaired in FGF22-CA3KO mice. Hippocampal sections were immunostained for calbindin to visualize DGC axons (arrowheads). Data are from **(C)** 10–17 sections from five mice and **(E)** 13–22 fields in 5–7 sections from three mice. Significant difference from wild-type mice at $^*p < 0.05$, $^{**}p < 0.01$, and $^{***}p < 0.001$ by Student's *t*-test. Scale bars, **(A,G)** 500 μm, **(C,E)** 20 μm.

analysis are shown in figure legends. All animal care and use was in accordance with the institutional guidelines and approved by the Institutional Animal Care and Use Committees at Boston Children's Hospital.

Immunostaining and Antibodies

Mice were transcardially perfused with PBS followed by 4% paraformaldehyde (PFA; Electron Microscopy Sciences, Hatfield, PA, USA) in PBS. Brains were dissected, further fixed in 4% PFA in PBS for overnight, transferred in 30% sucrose in PBS, and frozen in Neg-50 Frozen Section Medium (Richard Alan Scientific, Kalamazoo, MI, USA). Coronal sections were prepared on a cryostat (16 μm thick), and processed for staining. The sections were blocked in 2% BSA (Fraction V, Sigma-Aldrich, St. Louis, MO, USA), 2% normal goat serum (Sigma-Aldrich), and 0.1% TritonX-100 (Sigma-Aldrich) for 30 min at room temperature followed by incubation with primary antibodies for overnight at 4°C or for 2 h at room temperature. The sections were washed with PBS three times, and secondary antibodies were applied for 1 h at room temperature. The sections were washed with PBS three times again, and the slides were mounted in glycerol with 0.5% p-phenylenediamine (Sigma-Aldrich). Dilutions and sources of primary antibodies used are: anti-doublecortin (DCX; 1:500, ab18723, Abcam, Cambridge, MA, USA), anti-Prox1 (1:500, MAB5652, EMD Millipore, Burlington, MA, USA), anti-vesicular glutamate transporter 1 (anti-VGLUT1; 1:5000, AB5905, EMD Millipore), anti-vesicular GABA transporter (anti-VGAT; 1:1500, 131003, Synaptic Systems, Goettingen, Germany), anti-calbindin (1:500, Calbindin-Go-Af1040, Frontier Institute, Hokkaido, Japan). Secondary antibodies used are (1:500 dilutions): Alexa 488-conjugated goat anti-guinea pig IgG (A-11073, Invitrogen, Carlsbad, CA, USA), Alexa 568-conjugated goat anti-guinea pig IgG (A-11075, Invitrogen), Alexa 488-conjugated goat anti-rabbit IgG (A-11034, Invitrogen), Alexa 568-conjugated goat anti-rabbit IgG (A-11036, Invitrogen), Alexa 488-conjugated goat anti-mouse IgG1 (A-21121, Invitrogen), and Alexa 594-conjugated donkey anti-goat IgG (705–585–147, Jackson ImmunoResearch, West Grove, PA, USA). DAPI (Sigma-Aldrich) was added to each section as a nuclear stain.

In Situ Hybridization

In situ hybridization was performed as described (Schaeren-Wiemers and Gerfin-Moser, 1993; Terauchi et al., 2010). Digoxigenin-labeled cRNA probes were generated by *in vitro* transcription using DIG RNA labeling mix (Roche, Basel, Switzerland). The probe for *Fgf22* was generated from the cording region of the mouse *Fgf22* cDNA. *In situ* images were taken with a digital camera (Alpha 5100, Sony, Tokyo, Japan) attached to an Olympus BX63 upright microscope (Olympus, Tokyo, Japan) under bright-field optics with 10× objective lenses.

Imaging and Analysis

Fluorescent images were taken on epi-fluorescence microscopes (Olympus BX61 and BX63). Twelve-bit images were acquired using 20× objective lenses with an F-View II CCD camera (Olympus Soft Imaging Solutions, Muenster, Germany) or an XM10 Monochrome camera (Olympus) at 1376 × 1032 (Olympus BX61) or 1376 × 1038 (Olympus BX63) pixel resolution. Images were taken at the best-focus position, where the staining signals were brightest in the section.

Synapse formation in the CA3 region was assessed using immunostaining for VGLUT1 and VGAT. Images were taken from the CA3a and CA3b regions of CA3 (see **Figure 1B**). The size and density of stained puncta were quantified and analyzed using MetaMorph software (Molecular Devices, Sunnyvale, CA, USA). The staining intensity in the fimbria, a myelinated tract of axons located in the medial region of CA3, was calculated and used for background subtraction from each image. Neurogenesis within the DGC layer was assessed using immunostaining for DCX, a marker for immature neurons, and Prox1, a marker for DGCs. The number of DCX-positive cells was divided by the number of Prox1-positive DGCs or that of DAPI-positive DGCs. Quantification was done from both the upper and lower blades of the DGC layer.

Behavioral Tests

Forced Swim Test

Mice were allowed to adapt to the testing room environment at least for 30 min before the test. Each animal was then placed into a 4 L beaker with 2.75 L of tepid water (21–23°C) for 6 min, and their behavior was recorded using a video camera (HDC-SD60, Panasonic, Osaka, Japan) mounted on the same level as the base of the beaker. Video recordings were reviewed and scored by a trained observer blinded to genotype. Animals were assessed for the total duration of floating during the last 4 min and the latency

TABLE 1 | List of the numbers and ages of animals used in the behavioral tests.

	Forced swim		Sucrose preference	
	N	Age (month)	*N*	Age (month)
Control				
Total	38	5.77 ± 0.38	25	7.87 ± 0.57
Females	21	5.85 ± 0.51	14	8.61 ± 0.79
Males	17	5.33 ± 0.55	11	6.93 ± 0.76
FGF22-CA3KO				
Total	29	5.26 ± 0.36	21	6.86 ± 0.54
Females	16	5.41 ± 0.55	11	7.55 ± 0.79
Males	13	5.02 ± 0.43	10	6.09 ± 0.70

to start floating for more than 3 s in the water. Mice were judged to be floating when making only the movements necessary to keep their heads above water.

Sucrose Preference Test

Sucrose preference was assessed using a two-bottle choice experiment: one bottle containing water and the other containing 2% (v/v) sucrose for 5 days. One day before the test, mice were singly housed in their housing room and given a bottle filled with 2% sucrose to experience sweet taste. On the morning of day 1, a sucrose bottle and a water bottle were weighed and placed in the cage. Twenty-four hours later, the bottles were weighed and the bottle positions were switched, to control for any side position preferences in the mice. The bottle positions were switched every 24 h during the 5-days test, weighing the bottles each day before switching. Data are presented as the amount of sucrose consumed as a percentage of total liquid consumed over the testing period.

Statistical Analysis

Data were prepared and analyzed using Excel or GraphPad Prism 7. The statistical tests performed were two-tailed Student's *t*-test as indicated in the figure legend. No data points were excluded from any experiments. The results were considered significant when $p < 0.05$ (denoted in all graphs as follows: $^{*}p < 0.05$; $^{**}p < 0.01$, $^{***}p < 0.001$).

RESULTS

CA3-derived FGF22 Is Critical for Excitatory Presynaptic Differentiation in the Hippocampal CA3 Region

FGF22 plays important roles for excitatory synapse formation in the mammalian brain, including the hippocampus, cerebellum and lateral geniculate nucleus (Umemori et al., 2004; Terauchi et al., 2010; Singh et al., 2012). Mice genetically lacking FGF22 (FGF22 null mice) have decreased excitatory presynaptic terminals in the brain. In the hippocampus, FGF22 is highly expressed by hippocampal CA3 pyramidal neurons but also expressed by a subset of dentate granule cells (DGCs; Terauchi et al., 2010). Aiming at understanding the cell type-specific role of FGF22, we generated CA3-specific FGF22 knockout mice (FGF22-CA3KO mice) using $Fgf22^{flox/flox}$ mice ($Fgf22^{f/f}$; EUCOMM) crossed with *Grik4-Cre* mice (**Figure 1A**). *Grik4-Cre* mice express Cre in nearly 100% of CA3 pyramidal neurons (Nakazawa et al., 2002). In other regions in the brain, Cre is only expressed in a very small subset (less than 10%) of neurons, if any (Nakazawa et al., 2002). We first confirmed the CA3-specific inactivation of *Fgf22* in FGF22-CA3KO mice by performing *in situ* hybridization at P9, during synapse formation (**Figure 1A**). In wild-type control mice, *Fgf22* was highly expressed in CA3 pyramidal neurons and at a lower level, in some of DGCs. In $Fgf22^{f/f}$::*Grik4-Cre* mice, *Fgf22* expression in CA3 pyramidal neurons was almost completely eliminated, while it was maintained in DGCs. These results demonstrate that $Fgf22^{f/f}$::*Grik4-Cre* mice are indeed CA3-specific FGF22 knockout mice. Since *Fgf22* expression in control mice was highest in the CA3a and CA3b subregions (**Figures 1A,B**), we focused on these subregions for the analysis of synapses. In order to investigate whether CA3-derived FGF22 is necessary for excitatory presynaptic differentiation in CA3, we evaluated the clustering of excitatory synaptic vesicles by staining for VGLUT1, which is on the excitatory synaptic vesicles. We found that at P21, FGF22-CA3 KO mice showed a significant decrease in the number and size of VGLUT1 puncta in the CA3 stratum lucidum (SL) region, where the axons of DGCs form excitatory synapses with CA3 pyramidal neurons (**Figures 1C,D**), without apparently affecting the DGC axon targeting (assessed by calbindin staining; **Figure 1G**). In adult FGF22-CA3KO mice (9 months of age), clustering of VGLUT1 was reduced in the SL as well as the stratum radiatum (SR) region, where CA3 axons form excitatory synapses onto CA3 pyramidal neurons (**Figures 1E,F**). These results indicate that FGF22, derived from CA3 pyramidal neurons, is critical for the development of excitatory presynaptic terminals formed onto CA3 pyramidal neurons. Our results demonstrate that FGF22 is a target-derived presynaptic organizer in the mammalian hippocampus *in vivo*.

CA3-derived FGF22 Does Not Regulate Inhibitory Presynaptic Differentiation in the Hippocampal CA3 Region

We next asked whether CA3-derived FGF22 is necessary for inhibitory presynaptic differentiation in CA3. For this, we evaluated the clustering of inhibitory synaptic vesicles by staining for VGAT. Inhibitory presynaptic differentiation was not impaired in the stratum pyramidale (SP), SL and SR layers of the CA3 region of FGF22-CA3KO mice at P21 (**Figures 2A,B**) and in adults (9 months of age, **Figures 2C,D**). Thus, CA3-derived FGF22 is an excitatory synapse-specific presynaptic organizer in the hippocampus.

FGF22 Is Involved in Neurogenesis in the Dentate Gyrus Throughout Life

In the hippocampus, the dentate gyrus undergoes continuous neurogenesis throughout life, and the newly born DGCs are integrated into pre-existing neuronal circuits. Because various growth factors control both developmental and adult neurogenesis in the brain (Zhao et al., 2007; Haan et al., 2013; Oliveira et al., 2013; Vivar et al., 2013; Woodbury and Ikezu, 2014; Kang and Hebert, 2015), we next asked whether FGF22 plays a role in dentate neurogenesis in the hippocampus. We first examined neurogenesis in FGF22 null mice. We assessed neurogenesis in the DGC layer by staining hippocampal sections for DCX, a marker of immature neurons (Francis et al., 1999; Gleeson et al., 1999; Abrous et al., 2005). FGF22 null mice had a significantly lower number of DCX-positive cells in the DGC layer relative to wild-type mice at P21 (**Figures 3A,B**), suggesting that neurogenesis is

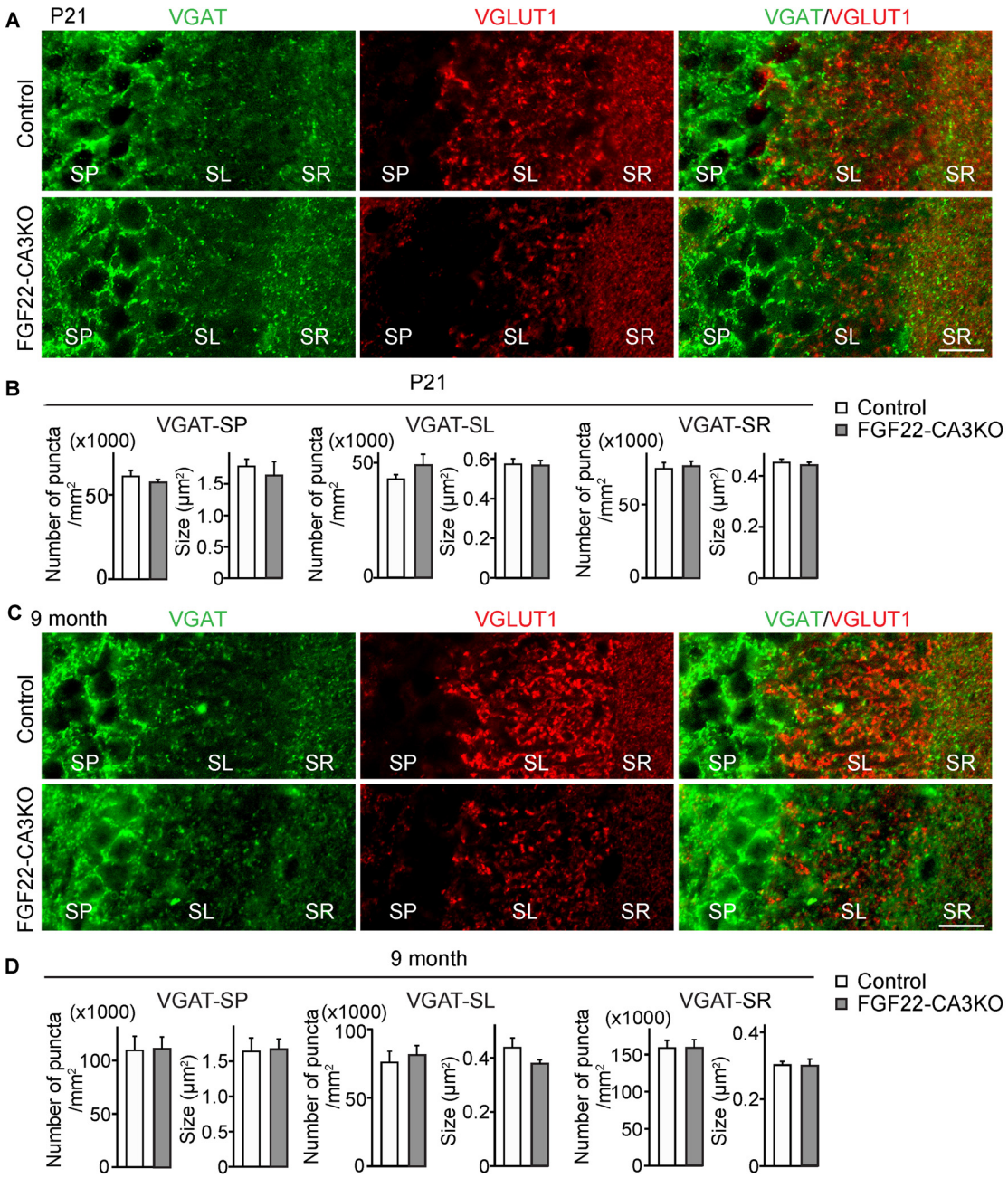

FIGURE 2 | CA3-specific FGF22 deletion does not alter inhibitory synapse formation in CA3. Hippocampal sections from Control and FGF22-CA3KO mice were immunostained for vesicular GABA transporter (VGAT) and VGLUT1. **(A)** Representative pictures from CA3 at P21. SP, stratum pyramidale; SL, stratum lucidum; SR, stratum radiatum. **(B)** Quantification of the density and size of VGAT puncta in CA3 at P21. **(C)** Representative pictures from CA3 in adults (9 months of age). **(D)** Quantification of the density and size of VGAT puncta in CA3 in adults. There is no significant difference in inhibitory synapse formation, assessed by VGAT accumulation, between Control and FGF22-CA3KO mice at P21 and in adults. Bars indicate mean ± SEM. Data are from **(B)** 24 fields in eight sections from three mice and **(D)** 18 fields in six sections from three mice. Scale bars, 20 μm.

decreased in the developing hippocampus in the absence of FGF22. Decreased neurogenesis was also detected in FGF22 null mice at older ages (2 and 5 months of age; **Figures 3A,B**). These results indicate that FGF22 contributes to dentate neurogenesis throughout life.

CA3-derived FGF22 Does Not Contribute to Neurogenesis in the Dentate Gyrus

How does FGF22 regulate dentate neurogenesis? One possibility is that CA3-derived FGF22 sends retrograde signals to DGCs and influences dentate neurogenesis. We have previously

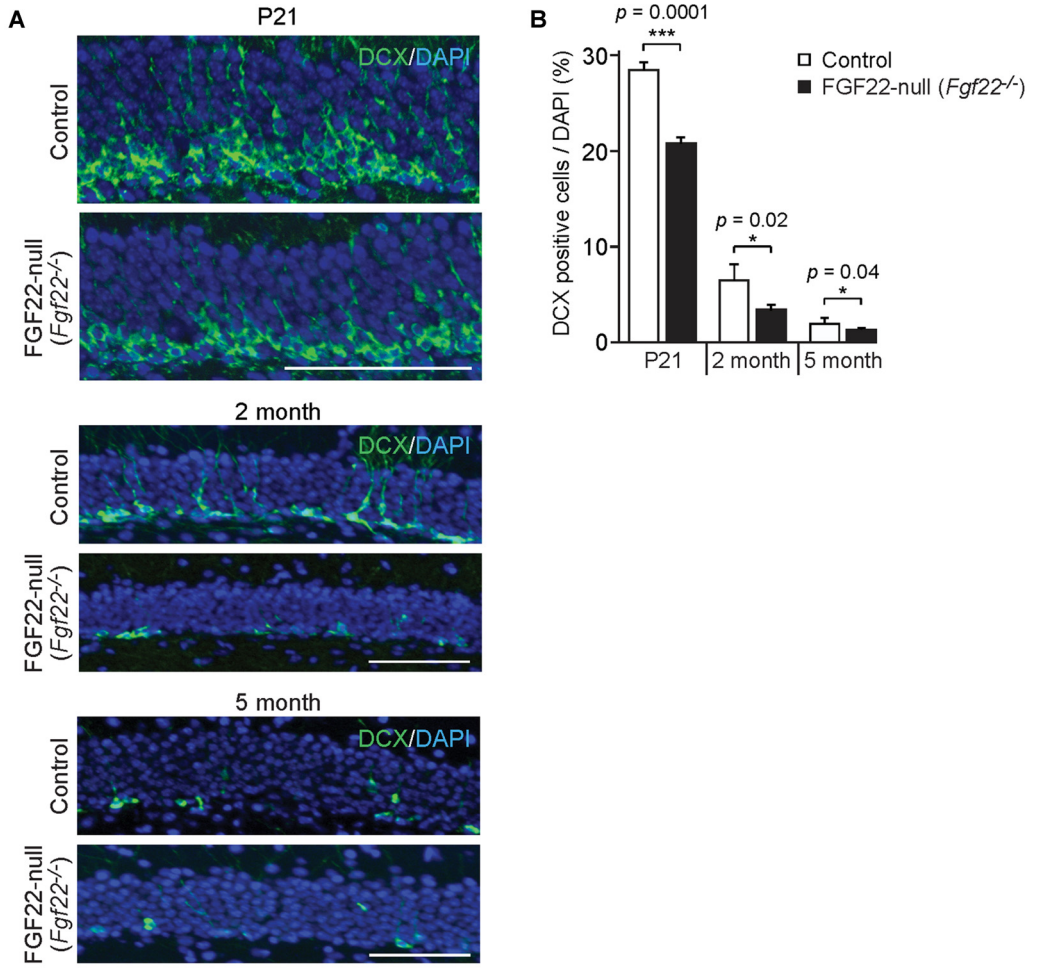

FIGURE 3 | FGF22 null mice (*Fgf22*$^{-/-}$) show reduced dentate neurogenesis throughout life. Region-matched hippocampal sections from wild-type littermates (Control) and FGF22 null mice (*Fgf22*$^{-/-}$) at P21, 2 months of age and 5 months of age were immunostained for doublecortin (DCX), a marker for immature neurons. **(A)** Representative pictures of DCX-positive cells (green) with DAPI (blue) in the dentate granule cell (DGC) layer of Control and FGF22 null mice. **(B)** Quantification of the percentage of DCX-positive cells in the DGC layer. Dentate neurogenesis, assessed by the number of DCX-positive cells in DGCs, was significantly decreased in FGF22 null mice compared to wild-type mice at all the age points examined. Bars indicate mean ± SEM. Data are from nine sections from three mice (P21) and 4–6 sections from three mice (2 and 5 months of age). Scale bars, 100 μm.

shown that, using microfluidic chambers, application of FGF22 to the axons of DGCs induces insulin-like growth factor 2 (IGF2) in the cell body of DGCs (Terauchi et al., 2016). Hence, one hypothesis is that CA3-derived FGF22 regulates gene expression in DGCs, which may influence dentate neurogenesis. On the other hand, FGF22 is also expressed by a subset of DGCs (18.5% ± 1.24%) as well as CA3 pyramidal neurons, so it is possible that DGC-derived FGF22 has a main role on dentate neurogenesis. Using FGF22-CA3KO mice, we investigated whether CA3-derived FGF22 is involved in dentate neurogenesis. Dentate neurogenesis, assessed by the number of DCX-positive cells in DGCs, is unchanged in FGF22-CA3KO mice at P21 (**Figures 4A,C**) and in adults (3 months of age, **Figures 4B,C**). The number of Prox1-positive DGCs was also not changed in FGF22-CA3KO mice (P21: Control 13281.56 ± 263.61 cells/mm^2, FGF22-CA3KO 13094.29 ± 259.32 cells/mm^2; 9-month-old: Control 11901.01 ± 180.17 cells/mm^2, FGF22-CA3KO 11940.50 ± 164.63 cells/mm^2). These results suggest that CA3-derived FGF22 does not regulate dentate neurogenesis.

FGF22-CA3KO Mice Show Depression-Like Behaviors

The hippocampus is implicated in mood, anxiety, and learning and memory (Femenia et al., 2012; Bannerman et al., 2014; Tovote et al., 2015). FGF22 null mice show reduced excitatory synapse formation (Terauchi et al., 2010) and dentate neurogenesis (**Figure 3**) in the hippocampus. As a behavioral consequence, FGF22 null mice show depression-like behaviors such as increased passive stress-coping behavior

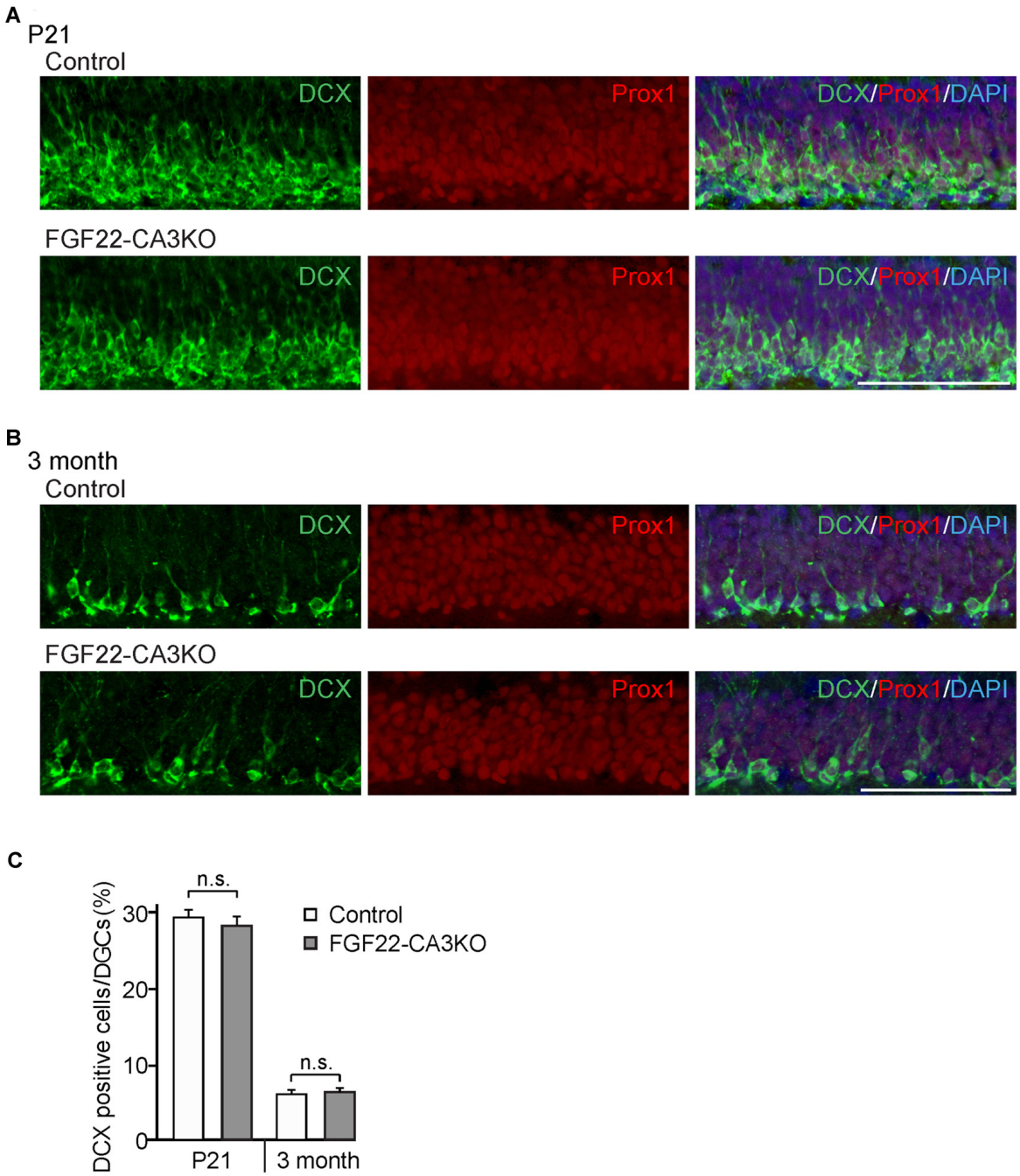

FIGURE 4 | Dentate neurogenesis is not affected in CA3-specific FGF22 knockout mice. Region-matched coronal brain sections from Control and FGF22-CA3KO mice were immunostained for DCX and Prox1, a marker for DGCs. **(A,B)** Representative pictures of DCX-positive cells (green) and Prox1-positive cells (red) in the DGC layer of Control and FGF22-CA3KO mice at P21 **(A)** and in adults (3 months of age; **B**). **(C)** Quantification of the percentages of DCX-positive cells in Prox1-positive DGCs. Dentate neurogenesis, assessed by the number of DCX-positive cells, did not differ between Control and FGF22-CA3KO mice. Bars indicate mean ± SEM. Data are from eight sections from three mice (both P21 and 3 months of age). Scale bars, 100 μm.

and anhedonia (Williams et al., 2016). FGF22 null mice display normal motor, anxiety and social cognitive tests, indicating a role of FGF22 specifically in affective behaviors. Using FGF22-CA3KO mice, we asked whether CA3-derived FGF22 plays a role in regulating affective behavior. The forced swim test is one of the commonly used rodent behavioral tests to measure coping strategy to an acute inescapable stress (Kitada et al., 1981). It is often used as a behavioral

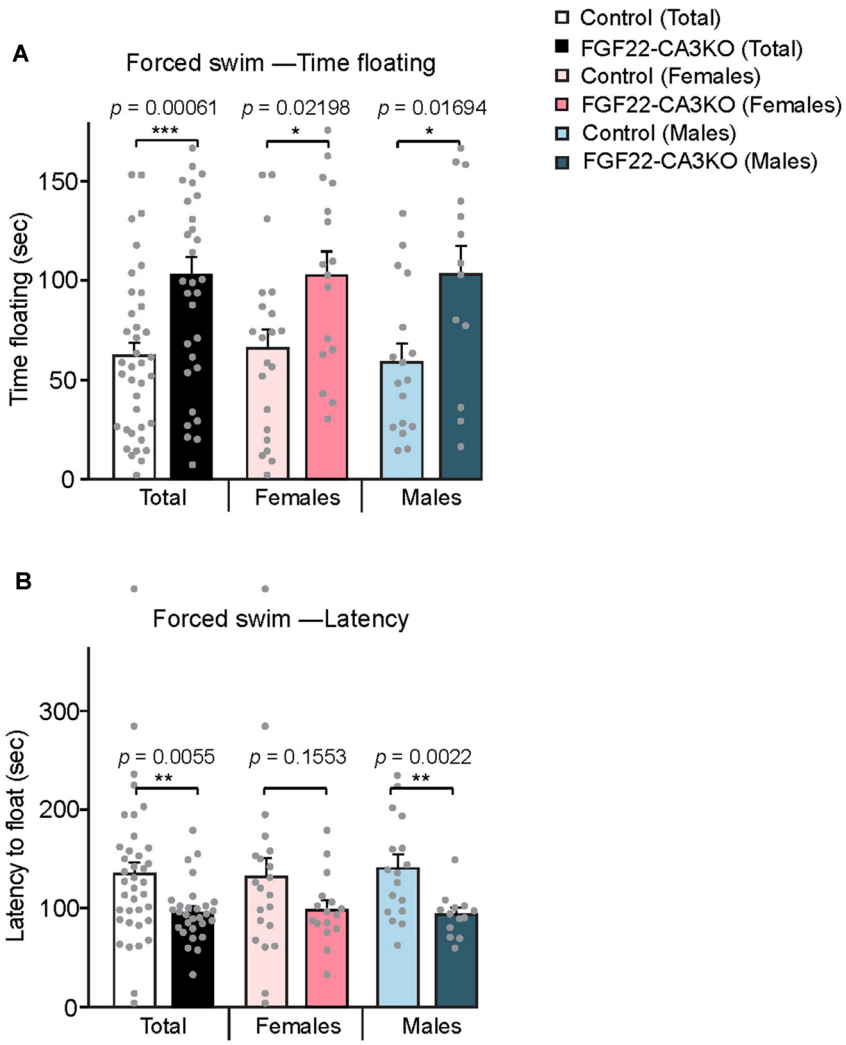

FIGURE 5 | CA3-specific FGF22 knockout mice display increased passive stress-coping responses in the forced swim test. **(A)** Time floating during the 4-min forced swim test for Control littermates and FGF22-CA3KO mice. Data separated by the gender are also shown. FGF22-CA3KO mice, both females and males, spent significantly more time floating than control mice. **(B)** Latency to float for Control littermates and FGF22-CA3KO mice. FGF22-CA3KO mice start floating more quickly. Bars indicate mean ± SEM. The numbers of mice used were: 21 females and 17 males for Control, and 16 females and 13 males for FGF22-CA3KO. Significant difference from controls at $^{*}p < 0.05$, $^{**}p < 0.01$ and $^{***}p < 0.001$ by Student's *t*-test.

screen for antidepressant drugs and evaluating the efficacy of the drugs. In the forced swim test, we found that both female and male FGF22-CA3KO mice spent significantly more time floating than control littermates (**Figure 5A**). In addition, FGF22-CA3KO mice displayed a shorter latency to float than control littermates (**Figure 5B**; when females and males were separately analyzed, males showed more significant differences). These results show that FGF22-CA3KO mice display increased passive stress-coping phenotypes, suggesting that CA3-derived FGF22 plays important roles in regulating stress-coping behavior.

We next tested whether FGF22-CA3KO mice display anhedonia, the failure to engage in pleasurable activity, which is a hallmark of depression. The sucrose preference test is a reward-based behavioral test to assess preference for sucrose-sweetened water over regular water and used as an indicator of anhedonia (Powell et al., 2012). Typically, mice prefer to drink sucrose with a high ratio, but mice that display anhedonia show less preference to sucrose. We found that FGF22-CA3 KO mice demonstrated a significantly less preference to sucrose over water than control littermates (**Figure 6**), consistent with anhedonia. When females and males were separately analyzed, females showed more significant changes.

Taken together, these behavioral tests suggest that FGF22-CA3KO mice exhibit behavioral changes consistent with depression-like behaviors and that there are some sex differences in their phenotype.

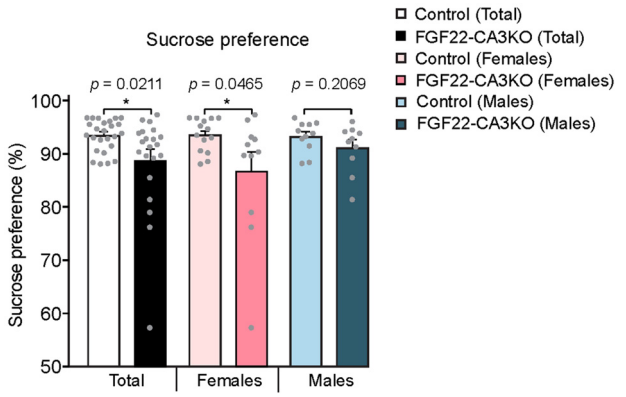

FIGURE 6 | CA3-specific FGF22 knockout mice display anhedonia. Sucrose preference test with Control littermates and FGF22-CA3KO mice. Data shown are the percentage of sucrose consumed relative to total liquid consumed. FGF22-CA3KO mice drink less sucrose than Control littermates. Bars indicate mean ± SEM. The numbers of mice used were: 14 females and 11 males for Control, and 11 females and 10 males for FGF22-CA3KO. Significant difference from controls at $^*p < 0.05$ by Student's *t*-test.

DISCUSSION

FGF22 plays important roles in brain development and function (Umemori et al., 2004; Terauchi et al., 2010; Singh et al., 2012; Williams et al., 2016). In this article, we investigated the cell type-specific roles of FGF22 in the hippocampus. Using CA3-specific FGF22 knockout mice (FGF22-CA3KO mice) and FGF22 null mice, we showed: (i) CA3-derived FGF22 acts as a target-derived presynaptic organizer at excitatory synapses *in vivo*; (ii) FGF22 regulates dentate neurogenesis, but CA3-derived FGF22 does not play such a role; and (iii) Inactivation of FGF22 selectively in CA3 pyramidal neurons is sufficient for the mice (FGF22-CA3KO) to display increased stress coping behaviors and anhedonia, similarly to FGF22 null mice. These results indicate that CA3-derived FGF22 plays critical roles in local synapse formation and the regulation of affective behavior. Our results reveal cell-type specific roles of FGF signaling in brain development and function.

FGF22 as a Target-derived Presynaptic Organizer *in Vivo*

In cultured neurons, FGF22 promotes synaptic vesicle accumulation at the excitatory nerve terminals (Umemori et al., 2004; Terauchi et al., 2010). In FGF22 null mice, synaptic vesicles fail to cluster at excitatory synapses in the CA3 region of the hippocampus (Terauchi et al., 2010). These results indicate that FGF22 organizes excitatory presynaptic terminals. Using cultured neurons, we had proposed that FGF22 acts as a target-derived presynaptic organizer, because: (i) overexpression of FGF22 in cultured neurons increased excitatory synapses formed onto FGF22-transfected neurons; and (ii) postsynaptic expression of FGF22 rescued the presynaptic defects in FGF22-deficient neurons (Terauchi et al., 2010). However, since cultured neurons lack precise spatial information, it is important to test whether FGF22 really acts as a local, target-derived factor *in vivo*. Here, utilizing CA3-specific FGF22 knockout (FGF22-CA3KO) mice, we showed that FGF22 indeed acts as a target-derived excitatory presynaptic organizer *in vivo*: FGF22-CA3KO mice showed excitatory, and not inhibitory, presynaptic defects in CA3 (**Figures 1**, **2**). There was one difference between FGF22-CA3KO and FGF22 null mice: the synaptic defect in the CA3 SR layer of FGF22 null mice was apparent at P21, but it was not apparent until adults in FGF22KO-CA3KO mice. This may be due to a delayed onset of Cre expression in *Grik4-Cre* mice (Cre starts to express from P4 and gradually increases during development; Nakazawa et al., 2002; Allen Mouse Brain Atlas found at http://mouse.brain-map.org/).

The Role of FGF22 in Dentate Neurogenesis

We found that FGF22 is involved in dentate neurogenesis throughout life (**Figure 3**). Since FGF22 is expressed by CA3 pyramidal neurons as well as a subset of DGCs (Terauchi et al., 2010; **Figure 1A**), FGF22 from either cell could contribute to dentate neurogenesis. FGF22 from DGCs may directly regulate dentate neurogenesis. Indeed, deletion or activation of FGF receptors in neural precursor cells modifies maintenance of SGZ stem cells and induction of neurogenesis (Kang and Hebert, 2015). In addition, FGF22 from CA3 neurons may induce gene expression in the presynaptic DGCs, and induced genes may influence neurogenesis. As for the latter possibility, we have previously shown that FGF22 signaling induces IGF2 in DGCs (Terauchi et al., 2016). IGF2 is known to regulate neurogenesis, so it is possible that CA3-derived FGF22 may regulate dentate neurogenesis through the expression of IGF2. Here we tested this possibility using FGF22-CA3KO mice. We found that FGF22-CA3KO mice did not show changes in dentate neurogenesis (**Figure 4**), indicating that CA3-derived FGF22 is not necessary for dentate neurogenesis. This suggests that FGF22 from other cells, possibly DGCs, contributes to dentate neurogenesis.

Neurogenesis is also dependent on neuronal activity. For example, enriched environment enhances the survival of newborn neurons (Leuner et al., 2006; Drapeau et al., 2007; Sisti et al., 2007); physical exercises, such as wheel running and forced treadmill, increase the proliferation of precursor neurons (van Praag et al., 1999) and LTP induction in the hippocampus increases proliferation of dentate progenitor cells and helps survival of new born DGCs (Bruel-Jungerman et al., 2006). Interestingly, we have previously found that FGF22 is important for seizure-induced dentate neurogenesis: FGF22 null mice do not display increased neurogenesis in response to seizures (Lee and Umemori, 2013). How FGF22 regulates normal and activity-dependent dentate neurogenesis is an important future question to address.

Implication of CA3-derived FGF22 in Affective Behavior

FGF22 null mice display a depression-like phenotype: increased passive stress coping behavior and anhedonia (Williams et al.,

2016). FGF22 null mice do not display defects in motor and exploratory behaviors, anxiety-like behaviors and social behaviors or memory. These results suggest that FGF22 has a unique role in affective behaviors. Here, using FGF22-CA3KO mice, we showed that loss of FGF22 in CA3 pyramidal neurons was enough to affect affective behaviors: FGF22-CA3KO mice showed increased floating time and decreased latency to float in the forced swim test, and decreased preference for sucrose in the sucrose preference test (**Figures 5**, **6**). Our results also suggest that there are some differences between females and males in the behavioral tests. It would be interesting to further examine whether and how FGF22 acts differently in females and males.

In summary, these results show a cell-type specific role of FGF22 in affective behavior. Our results suggest that FGF22-dependent synapse development in CA3, and not dentate neurogenesis, may be regulating affective behavior. Adult dentate neurogenesis is proposed to contribute to a depression-like behavior (Lee et al., 2013; Anacker and Hen, 2017), while some studies showed that mice lacking adult neurogenesis did not display abnormal stress-coping behaviors (Iascone et al., 2013; Jedynak et al., 2014). It is likely that there are various molecular and pathophysiological changes that contribute to depression-like behaviors, and we propose that synapse development mediated by CA3-derived FGF22 is one such underlying mechanism. Our study raises a possibility to target FGF22 in CA3 as a possible treatment of certain aspects of depression.

AUTHOR CONTRIBUTIONS

AT and HU designed the experiments and wrote the manuscript. AT, EG and JW performed the experiments. HU secured funding and supervised the project. All authors commented on the manuscript.

FUNDING

This work was supported by March of Dimes Research Foundation Grant, Bipolar Disorder Fund for Neuroscience Research at Harvard University supported by Kent and Liz Dauten, and National Institute of Neurological Disorders and Stroke (NINDS; NIH) grant R01-NS070005 (HU).

ACKNOWLEDGMENTS

We thank Erin Johnson-Venkatesh for critical reading of the manuscript.

REFERENCES

Abrous, D. N., Koehl, M., and Le Moal, M. (2005). Adult neurogenesis: from precursors to network and physiology. *Physiol. Rev.* 85, 523–569. doi: 10.1152/physrev.00055.2003

Anacker, C., and Hen, R. (2017). Adult hippocampal neurogenesis and cognitive flexibility—linking memory and mood. *Nat. Rev. Neurosci.* 18, 335–346. doi: 10.1038/nrn.2017.45

Bannerman, D. M., Sprengel, R., Sanderson, D. J., McHugh, S. B., Rawlins, J. N., Monyer, H., et al. (2014). Hippocampal synaptic plasticity, spatial memory and anxiety. *Nat. Rev. Neurosci.* 15, 181–192. doi: 10.1038/nrn3677

Bruel-Jungerman, E., Davis, S., Rampon, C., and Laroche, S. (2006). Long-term potentiation enhances neurogenesis in the adult dentate gyrus. *J. Neurosci.* 26, 5888–5893. doi: 10.1523/JNEUROSCI.0782-06.2006

Cho, K. O., Lybrand, Z. R., Ito, N., Brulet, R., Tafacory, F., Zhang, L., et al. (2015). Aberrant hippocampal neurogenesis contributes to epilepsy and associated cognitive decline. *Nat. Commun.* 6:6606. doi: 10.1038/ncomms7606

Drapeau, E., Montaron, M. F., Aguerre, S., and Abrous, D. N. (2007). Learning-induced survival of new neurons depends on the cognitive status of aged rats. *J. Neurosci.* 27, 6037–6044. doi: 10.1523/JNEUROSCI.1031-07.2007

Evans, S. J., Choudary, P. V., Neal, C. R., Li, J. Z., Vawter, M. P., Tomita, H., et al. (2004). Dysregulation of the fibroblast growth factor system in major depression. *Proc. Natl. Acad. Sci. U S A* 101, 15506–15511. doi: 10.1073/pnas.0406788101

Femenia, T., Gómez-Galán, M., Lindskog, M., and Magara, S. (2012). Dysfunctional hippocampal activity affects emotion and cognition in mood disorders. *Brain Res.* 1476, 58–70. doi: 10.1016/j.brainres.2012.03.053

Francis, F., Koulakoff, A., Boucher, D., Chafey, P., Schaar, B., Vinet, M. C., et al. (1999). Doublecortin is a developmentally regulated, microtubule-associated protein expressed in migrating and differentiating neurons. *Neuron* 23, 247–256. doi: 10.1016/s0896-6273(00)80777-1

Gleeson, J. G., Lin, P. T., Flanagan, L. A., and Walsh, C. A. (1999). Doublecortin is a microtubule-associated protein and is expressed widely by migrating neurons. *Neuron* 23, 257–271. doi: 10.1016/s0896-6273(00)80778-3

Haan, N., Goodman, T., Najdi-Samiei, A., Stratford, C. M., Rice, R., El Agha, E., et al. (2013). Fgf10-expressing tanycytes add new neurons to the appetite/energy-balance regulating centers of the postnatal and adult hypothalamus. *J. Neurosci.* 33, 6170–6180. doi: 10.1523/JNEUROSCI.2437-12.2013

Iascone, D. M., Padidam, S., Pyfer, M. S., Zhang, X., Zhao, L., and Chin, J. (2013). Impairments in neurogenesis are not tightly linked to depressive behavior in a transgenic mouse model of Alzheimer's disease. *PLoS One* 8:e79651. doi: 10.1371/journal.pone.0079651

Jedynak, P., Kos, T., Sandi, C., Kaczmarek, L., and Filipkowski, R. K. (2014). Mice with ablated adult brain neurogenesis are not impaired in antidepressant response to chronic fluoxetine. *J. Psychiatr. Res.* 56, 106–111. doi: 10.1016/j.jpsychires.2014.05.009

Kang, W., and Hebert, J. M. (2015). FGF signaling is necessary for neurogenesis in young mice and sufficient to reverse its decline in old mice. *J. Neurosci.* 35, 10217–10223. doi: 10.1523/JNEUROSCI.1469-15.2015

Kitada, Y., Miyauchi, T., Satoh, A., and Satoh, S. (1981). Effects of antidepressants in the rat forced swimming test. *Eur. J. Pharmacol.* 72, 145–152. doi: 10.1016/0014-2999(81)90269-7

Lee, M. M., Reif, A., and Schmitt, A. G. (2013). Major depression: a role for hippocampal neurogenesis? *Curr. Top. Behav. Neurosci.* 14, 153–179. doi: 10.1007/7854_2012_226

Lee, C. H., and Umemori, H. (2013). Suppression of epileptogenesis-associated changes in response to seizures in FGF22-deficient mice. *Front. Cell. Neurosci.* 7:43. doi: 10.3389/fncel.2013.00043

Leuner, B., Gould, E., and Shors, T. J. (2006). Is there a link between adult neurogenesis and learning? *Hippocampus* 16, 216–224. doi: 10.1002/hipo.20153

Nakazawa, K., Quirk, M. C., Chitwood, R. A., Watanabe, M., Yeckel, M. F., Sun, L. D., et al. (2002). Requirement for hippocampal CA3 NMDA receptors in associative memory recall. *Science* 297, 211–218. doi: 10.1126/science.1071795

Oliveira, S. L., Pillat, M. M., Cheffer, A., Lameu, C., Schwindt, T. T., and Ulrich, H. (2013). Functions of neurotrophins and growth factors in neurogenesis and brain repair. *Cytometry A* 83, 76–89. doi: 10.1002/cyto.a.22161

Ornitz, D. M., and Itoh, N. (2001). Fibroblast growth factors. *Genome Biol.* 2:reviews3005.1. doi: 10.1186/gb-2001-2-3-reviews3005

Parent, J. M. (2007). Adult neurogenesis in the intact and epileptic dentate gyrus. *Prog. Brain Res.* 163, 529–540. doi: 10.1016/s0079-6123(07)63028-3

Powell, T. R., Fernandes, C., and Schalkwyk, L. C. (2012). Depression-related behavioral tests. *Curr. Protoc. Mouse Biol.* 2, 119–127. doi: 10.1002/9780470942390.mo110176

Scearce-Levie, K., Roberson, E. D., Gerstein, H., Cholfin, J. A., Mandiyan, V. S., Shah, N. M., et al. (2008). Abnormal social behaviors in mice lacking Fgf17. *Genes Brain Behav.* 7, 344–354. doi: 10.1111/j.1601-183x.2007.00357.x

Schaeren-Wiemers, N., and Gerfin-Moser, A. (1993). A single protocol to detect transcripts of various types and expression levels in neural tissue and cultured cells: *in situ* hybridization using digoxigenin-labelled cRNA probes. *Histochemistry* 100, 431–440. doi: 10.1007/bf00267823

Singh, R., Su, J., Brooks, J., Terauchi, A., Umemori, H., and Fox, M. A. (2012). Fibroblast growth factor 22 contributes to the development of retinal nerve terminals in the dorsal lateral geniculate nucleus. *Front. Mol. Neurosci.* 4:61. doi: 10.3389/fnmol.2011.00061

Sisti, H. M., Glass, A. L., and Shors, T. J. (2007). Neurogenesis and the spacing effect: learning over time enhances memory and the survival of new neurons. *Learn. Mem.* 14, 368–375. doi: 10.1101/lm.488707

Song, J., Christian, K. M., Ming, G. L., and Song, H. (2012). Modification of hippocampal circuitry by adult neurogenesis. *Dev. Neurobiol.* 72, 1032–1043. doi: 10.1002/dneu.22014

Terauchi, A., Johnson-Venkatesh, E. M., Bullock, B., Lehtinen, M. K., and Umemori, H. (2016). Retrograde fibroblast growth factor 22 (FGF22) signaling regulates insulin-like growth factor 2 (IGF2) expression for activity-dependent synapse stabilization in the mammalian brain. *Elife* 5:e12151. doi: 10.7554/eLife.12151

Terauchi, A., Johnson-Venkatesh, E. M., Toth, A. B., Javed, D., Sutton, M. A., and Umemori, H. (2010). Distinct FGFs promote differentiation of excitatory and inhibitory synapses. *Nature* 465, 783–787. doi: 10.1038/nature09041

Thisse, B., and Thisse, C. (2005). Functions and regulations of fibroblast growth factor signaling during embryonic development. *Dev. Biol.* 287, 390–402. doi: 10.1016/j.ydbio.2005.09.011

Tovote, P., Fadok, J. P., and Lüthi, A. (2015). Neuronal circuits for fear and anxiety. *Nat. Rev. Neurosci.* 16, 317–331. doi: 10.1038/nrn3945

Turner, C. A., Watson, S. J., and Akil, H. (2012). The fibroblast growth factor family: neuromodulation of affective behavior. *Neuron* 76, 160–174. doi: 10.1016/j.neuron.2012.08.037

Turner, N., and Grose, R. (2010). Fibroblast growth factor signalling: from development to cancer. *Nat. Rev. Cancer* 10, 116–129. doi: 10.1038/nrc2780

Umemori, H. (2009). Weaving the neuronal net with target-derived fibroblast growth factors. *Dev. Growth Differ.* 51, 263–270. doi: 10.1111/j.1440-169x.2008.01079.x

Umemori, H., Linhoff, M. W., Ornitz, D. M., and Sanes, J. R. (2004). FGF22 and its close relatives are presynaptic organizing molecules in the mammalian brain. *Cell* 118, 257–270. doi: 10.1016/j.cell.2004.06.025

van Praag, H., Kempermann, G., and Gage, F. H. (1999). Running increases cell proliferation and neurogenesis in the adult mouse dentate gyrus. *Nat. Neurosci.* 2, 266–270. doi: 10.1038/6368

Vivar, C., Potter, M. C., and van Praag, H. (2013). All about running: synaptic plasticity, growth factors and adult hippocampal neurogenesis. *Curr. Top. Behav. Neurosci.* 15, 189–210. doi: 10.1007/7854_2012_220

Williams, A. J., and Umemori, H. (2014). The best-laid plans go oft awry: synaptogenic growth factor signaling in neuropsychiatric disease. *Front. Synaptic Neurosci.* 6:4. doi: 10.3389/fnsyn.2014.00004

Williams, A. J., Yee, P., Smith, M. C., Murphy, G. G., and Umemori, H. (2016). Deletion of fibroblast growth factor 22 (FGF22) causes a depression-like phenotype in adult mice. *Behav. Brain Res.* 307, 11–17. doi: 10.1016/j.bbr.2016.03.047

Woodbury, M. E., and Ikezu, T. (2014). Fibroblast growth factor-2 signaling in neurogenesis and neurodegeneration. *J. Neuroimmune Pharmacol.* 9, 92–101. doi: 10.1007/s11481-013-9501-5

Zhao, M., Li, D., Shimazu, K., Zhou, Y. X., Lu, B., and Deng, C. X. (2007). Fibroblast growth factor receptor-1 is required for long-term potentiation, memory consolidation, and neurogenesis. *Biol. Psychiatry* 62, 381–390. doi: 10.1016/j.biopsych.2006.10.019

Conflict of Interest Statement: The authors declare that the research was conducted in the absence of any commercial or financial relationships that could be construed as a potential conflict of interest.

frontiers in Molecular Neuroscience

REVIEW
published: 15 November 2017
doi: 10.3389/fnmol.2017.00378

Glycosylphosphatidylinositol-Anchored Immunoglobulin Superfamily Cell Adhesion Molecules and Their Role in Neuronal Development and Synapse Regulation

*Rui P. A. Tan, Iryna Leshchyns'ka and Vladimir Sytnyk**

School of Biotechnology and Biomolecular Sciences, The University of New South Wales, Sydney, NSW, Australia

Immunoglobulin superfamily (IgSF) cell adhesion molecules (CAMs) are cell surface glycoproteins that not only mediate interactions between neurons but also between neurons and other cells in the nervous system. While typical IgSF CAMs are transmembrane molecules, this superfamily also includes CAMs, which do not possess transmembrane and intracellular domains and are instead attached to the plasma membrane via a glycosylphosphatidylinositol (GPI) anchor. In this review, we focus on the role GPI-anchored IgSF CAMs have as signal transducers and ligands in neurons, and discuss their functions in regulation of neuronal development, synapse formation, synaptic plasticity, learning, and behavior. We also review the links between GPI-anchored IgSF CAMs and brain disorders.

Keywords: cell adhesion molecules, neuronal, GPI anchor, synapses, neurite outgrowth, synaptic plasticity (LTP/LTD), learning and memory

OPEN ACCESS

Edited by:
Jaewon Ko,
Daegu Gyeongbuk Institute of Science and Technology (DGIST), South Korea

Reviewed by:
Davide Comoletti,
Rutgers University, The State University of New Jersey, United States
Valentin Stein,
University of Bonn, Germany

***Correspondence:**
Vladimir Sytnyk
v.sytnyk@unsw.edu.au

Received: *14 September 2017*
Accepted: *30 October 2017*
Published: *15 November 2017*

Citation:
Tan RPA, Leshchyns'ka I and Sytnyk V (2017) Glycosylphosphatidylinositol-Anchored Immunoglobulin Superfamily Cell Adhesion Molecules and Their Role in Neuronal Development and Synapse Regulation. Front. Mol. Neurosci. 10:378. doi: 10.3389/fnmol.2017.00378

INTRODUCTION

Cell adhesion molecules (CAMs) are expressed across all cell types. In the nervous system, multiple families of CAMs are expressed in neurons, including integrins, cadherins, selectins, neuroligins, neurexins, and the immunoglobulin superfamily (IgSF) of CAMs (Brümmendorf and Rathjen, 1993; Chothia and Jones, 1997; Buckley et al., 1998; Südhof, 2008; Sytnyk et al., 2017). These molecules play numerous roles in the developing and mature nervous system by regulating growth and branching of neurites, navigating growing axons and dendrites to the appropriate targets, regulating formation and maturation of synaptic contacts, and maintaining synapse function and plasticity during learning and memory formation.

Typically, and for some families exclusively, CAMs are transmembrane proteins. While the extracellular domains of these molecules mediate interactions not only between neurons but also between neurons and other cells by interacting with the same molecules or other types of molecules either on the membranes of other cells or in the extracellular matrix, the intracellular domains are involved in interactions with the cytoskeleton and signal transduction (Leshchyns'ka and Sytnyk, 2016). However, CAMs can also be anchored to the plasma membranes via a glycosylphosphatidylinositol (GPI) anchor, with the highest number of the GPI-anchored CAMs within the IgSF (**Figure 1** and **Table 1**). Although these proteins do not possess intracellular

domains, their functions are not limited to mediating cell adhesion only. In this review, we summarize the role GPI-anchored IgSF CAMs have as signal transducers, ligands, synapse formation regulators, as well as their role in synaptic plasticity and brain disorders.

GPI-Anchored IgSF CAMs and Their Homophilic and Heterophilic Interactions

Immunoglobulin superfamily CAMs are identified by the presence of immunoglobulin (Ig)-like domains in their ectodomains. There are several types of Ig domains present in IgSF CAMs including C2-, V-, and I-type (Williams and Barclay, 1988; Harpaz and Chothia, 1994). The V-type is similar to the variable V-domain in Igs, whereas the C2 type is similar to C1-domains in Igs (Barclay, 2003). The I-type (I for intermediate) shares similarities with C1- and V-type domains and was initially identified in Telokin, an intracellular smooth muscle protein (Harpaz and Chothia, 1994). GPI-anchored IgSF CAMs differ in the numbers of V-, C2-, or I-type Ig domains present in their ectodomains. For example, only one V-type Ig domain is present in Thy-1, while there are three C2-type Ig domains present in neuronal growth regulator 1 (NEGR1), and six C2-type domains present in contactin-1, -2, -3 (Ranscht, 1988; Williams and Barclay, 1988; Brümmendorf et al., 1989; Zuellig et al., 1992; **Figure 1**). The first four Ig domains of contactin-2 have also been classified as I-type Ig domains in some studies (Harpaz and Chothia, 1994; Freigang et al., 2000). All Ig domains of the IgSF CAMs have a core of two β-sheets facing each other and stabilized by an intra-chain disulfide bridge (Chothia et al., 1998; **Figure 2**). Ectodomains of IgSF CAMs may also contain fibronectin type III repeats, which are also present in ectodomains of some GPI-anchored IgSF CAMs, such as contactin-1, -2, -3 (**Figures 1**, **2**).

In the human and murine genomes, genes coding for GPI-anchored IgSF CAMs include *NEGR1*, *opioid-binding cell adhesion molecule* (*OBCAM*), *neurotrimin* (*Ntm*), *limbic system-associated membrane protein* (*LAMP*), *IgLON5*, *contactin-1, -2, -3, -4, -5, -6*, *Thy-1*, and *carcinoembryonic antigen-related cell adhesion molecule* (*CEACAM*)*-5, -6, -7*, and *-8* (Williams and Gagnon, 1982; Oikawa et al., 1987; Yoshihara et al., 1994, 1995; Hachisuka et al., 1996; Ogawa et al., 1996; Funatsu et al., 1999; Itoh et al., 2008; Sabater et al., 2016) (**Table 1** and **Figure 1**). OBCAM, Ntm, LAMP, NEGR1, and IgLON5 constitute the IgLON family (Yamada et al., 2007; Hashimoto et al., 2009; Sanz et al., 2015). In addition, short isoforms of some transmembrane IgSF CAMs, such as the shortest isoform of the neural cell adhesion molecule (NCAM) with the molecular weight 120 kDa (NCAM120), are also GPI-anchored (Hemperly et al., 1986).

Glycosylphosphatidylinositol-anchoring of proteins to the plasma membranes is a highly conserved post-translational modification across all eukaryotes (Fujita and Kinoshita, 2012). The GPI anchor is a complex structure consisting of a phosphoethanolamine linker, glycan core, and phospholipid tail. Structural variations of the anchor are possible by the modification of phosphoinositol, glucosamine, and mannose residues within the glycan core (Paulick and Bertozzi, 2008; Fujita and Kinoshita, 2012). Application of phosphatidylinositol-specific phospholipase C (PI-PLC), an enzyme capable of cleaving the GPI anchor, induces removal of GPI-anchored IgSF CAMs

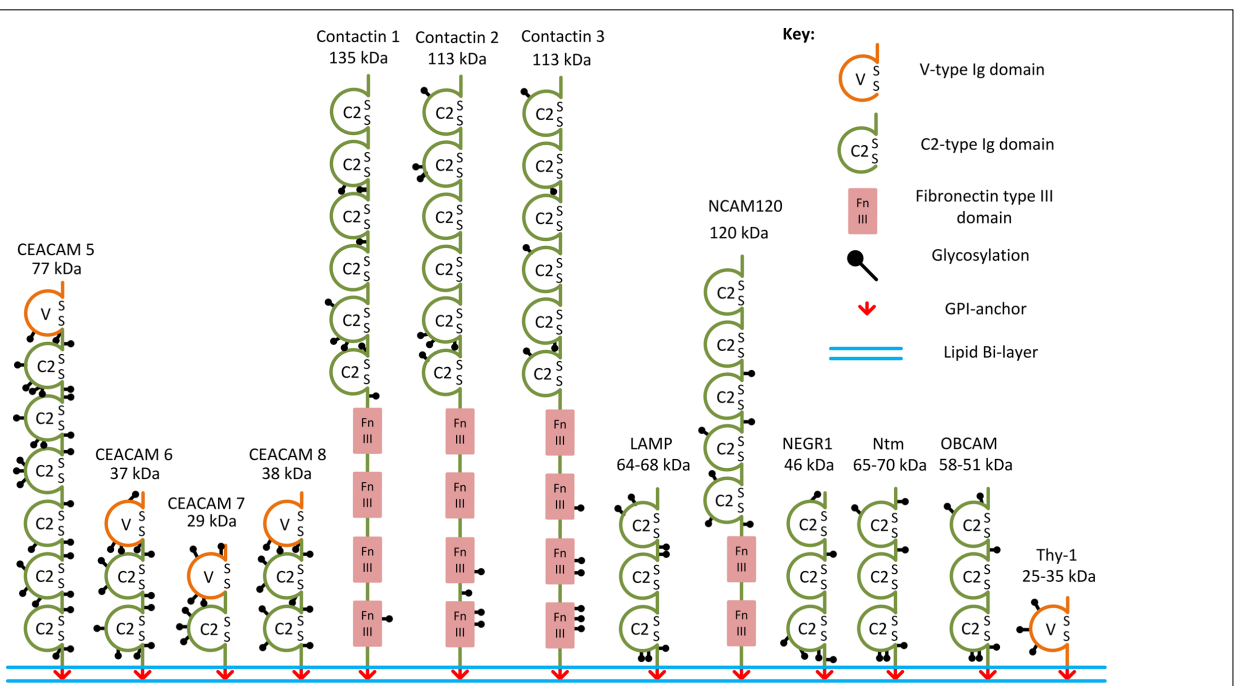

FIGURE 1 | Examples of the GPI-anchored IgSF CAMs. Structural domains and putative glycosylation sites in the GPI-anchored IgSF CAMs are represented according to the Uniprot database. SS, disulfide bridges present in Ig domains.

from the cell surface, indicating that the GPI anchor is critical for the attachment of these proteins to the cellular membranes (Sanz et al., 2015). The complexity of the GPI anchor, however, suggests that it also plays a role in other multiple functions aside from membrane anchorage, including signal transduction, protein sorting, as well as the structure and function regulation of the GPI-anchored IgSF CAMs. In particular, the GPI anchor links these molecules to membrane microdomains that are insoluble in cold non-ionic detergents (Varma and Mayor, 1998; Fujita and Kinoshita, 2012). Such specialized membrane microdomains are referred to as lipid rafts and render GPI-anchored proteins resistant to cold non-ionic detergent extraction (Schroeder et al., 1994; Simons and Ikonen, 1997).

The ectodomains of GPI-anchored IgSF CAMs contain multiple glycosylation sites. For example, IgLON protein family members with three Ig domains contain six or seven *N*-glycosylation sites in their ectodomains (**Figure 1**; Pimenta et al., 1996; Itoh et al., 2008). NCAM120 is a prominent example of a glycosylated GPI-anchored IgSF CAM (Yoshihara et al., 1991), because similarly to transmembrane NCAM isoforms it can carry polysialic acid (PSA) (Dityatev et al., 2004).

Multiple subdomains in the extracellular domains of IgSF CAMs have been suggested to contain binding sites for interactions with other Ig domain-containing proteins (Brümmendorf and Rathjen, 1993). Indeed, Ig domains have been shown to play a key role in homophilic and heterophilic *trans*-interactions between IgSF CAMs, i.e., the interaction between two identical IgSF CAMs on membranes of adjacent cells, and the interaction of IgSF CAMs with other proteins in the extracellular environment (Reed et al., 2004; Walmod et al., 2004; Kulahin et al., 2011). In addition to mediating *trans*-interactions, IgSF CAMs bind in *cis*, i.e., laterally, to surface proteins present in the same cell surface plasma membrane (Held and Mariuzza, 2011). *Cis*-interactions can enhance the *trans*-interactions of IgSF CAMs and are also involved in signal transduction across the membrane (Soroka et al., 2003; Kiselyov et al., 2005). Similarly to transmembrane IgSF CAMs, GPI-anchored IgSF CAMs mediate homo- and heterophilic interactions. For example, LAMP, OBCAM, Ntm, Thy-1, CEACAM5, contactin-2, and NCAM120 bind homophilically *in trans* while CEACAM6 binds heterophilically *in trans* to CEACAM8 (Oikawa et al., 1991; Mahanthappa and Patterson, 1992; Rader et al., 1993; Zhou et al., 1993; Zhukareva and Levitt, 1995; Lodge et al., 2000; Taheri et al., 2000; Gil et al., 2002). Neurotractin (a chick homolog of human NEGR1) appears to be unique in the IgLON family in that it does not bind homophilically, but heterophilically binds to Ntm and LAMP (Marg et al., 1999), although a later study reported that mammalian NEGR1 was able to interact homophilically (Miyata et al., 2003a). GPI-anchored IgSF CAMs also interact in *cis*. For example, LAMP and OBCAM heterophilically interact in *cis* to create dimeric IgLONS (diglons) and formation of this complex changes the ability of both proteins to regulate neuronal development (Horstkorte et al., 1993; Ranheim et al., 1996; Reed et al., 2004; Held and Mariuzza, 2011).

GPI-Anchored IgSF CAMs As Functional Receptors

The role for IgSF CAMs as functional receptors has been suggested by studies analyzing effects of antibodies against these molecules on neurite outgrowth. Early studies using antibodies against Thy-1 as a growth substrate showed that Thy-1 antibodies enhance regeneration of neurites in rat retinal ganglion neurons and promote survival of mouse cerebellar Purkinje cells (Leifer et al., 1984; Messer et al., 1984). Similarly, antibodies against Thy-1 promote neurite outgrowth in rat dorsal root ganglion (DRG) neurons when applied in the culture medium (Chen et al., 2005). Later, natural ligands of GPI-anchored IgSF CAMs have also been shown to induce neurite outgrowth changes. Retinal ganglion cells from Thy-1 knock-out mice show impaired neurite outgrowth over different substrates made of the proteins of the extracellular matrix, including fibronectin and collagen, and Thy-1 knock-out mice demonstrate abnormal retinal formation with thinner retinae (Simon et al., 1999). Thy-1 has also been identified as a receptor for αVβ3 integrin. Binding of integrins to Thy-1 at the neuronal cell surface induces signal transduction across the cell membrane resulting in inactivation of the c-Src protein tyrosine kinase, reduced neurite outgrowth, as well as neurite retraction (Herrera-Molina et al., 2012). In this study, neuron-derived Cath-a-differentiated (CAD) cells grown on a monolayer of DITNC1 astrocyte cells, which expressed αVβ3 and β3 integrins, had inhibited neurite outgrowth compared to CAD cells grown over a monolayer of DITNC1 cells treated with Thy-1-Fc protein, anti-β3 integrin antibodies, or transfected with siRNA against the β3 chain of the integrin. Neurite outgrowth inhibition in CAD cells on a substrate of αVβ3-Fc was abolished by silencing Thy-1 expression by shRNA. Furthermore, while αVβ3-Fc reduced dendritic length in primary cortical neurons, application of PI-PLC to cleave Thy-1 prior to the addition of αVβ3-Fc prevented the inhibition of dendrite outgrowth (Herrera-Molina et al., 2012).

Chondroitin sulfate E has been shown to activate contactin-1 to stimulate neurite outgrowth in primary mouse hippocampal neurons (Mikami et al., 2009). In addition to being a receptor to chondroitin sulfate E, contactin-1 binds to the second and third fibronectin type III (FNIII)-like domains of tenascin-R. Binding of tenascin-R to contactin-1 promotes neurite outgrowth (Norenberg et al., 1995), and induces formation of filopodia and lamellipodia along neurites (Zacharias, 2002). Contactin-1 is also a receptor for the receptor-type protein tyrosine phosphatase zeta (PTPRZ) (Peles et al., 1995; Bouyain and Watkins, 2010), and induces neurite outgrowth in chick tectal neurons in response to binding to PTPRZ (Peles et al., 1995). Recent work also showed that contactin-1 at the cell surface of hippocampal neurons binds in *trans* to contactin-associated transmembrane receptor 2 (CASPR2) (Rubio-Marrero et al., 2016). The physiological role of this interaction remains to be analyzed. The role for contactin-1 as a functional receptor in regulation of neuronal development is also supported by *in vivo* observations in contactin-1 knock-out mice. Granule cells are the major neuron population expressing contactin-1 in axons in the cerebellum. In wild-type mice, the parallel fibers of granule cells extend perpendicular to the

TABLE 1 | List of the GPI-anchored IgSF CAMs and their functions in neurite outgrowth and synapse formation and plasticity.

IgSF member	Number and type of Ig domains	Homophilic interaction	Examples of heterophilic binding partners	Function in neurite outgrowth as a receptor	Function in neurite outgrowth as a ligand	Role in synapse formation	Changes in LTP/LTD in knock-out (KO) or transgenic (TG) mice
CEACAM5/ CD66e/CEA	One V-type and six C2-type domains (Oikawa et al., 1987).	In *trans* (Zhou et al., 1993; Taheri et al., 2000).	*Trans* – NA; *Cis* – NA; *ECM* – NA.	NA	NA	NA	NA
CEACAM6/ CD66c/NCA	One V-type and two C2-type domains (Oikawa et al., 1987).	NA	*Trans* – CEACAM8 (Oikawa et al., 1991); *Cis* – NA; *ECM* – NA.	NA	NA	NA	NA
CEACAM7/ CGM2	One V-type and one C2-type domains (Oikawa et al., 1987).	NA	*Trans* – NA; *Cis* – NA; *ECM* – NA.	NA	NA	NA	NA
CEACAM8/ CD66b/CGM6	One V-type and two C2-type domains (Oikawa et al., 1987).	NA	*Trans* – CEACAM6 (Oikawa et al., 1991); *Cis* – NA; *ECM* – NA.	NA	NA	NA	NA
Contactin1 / F3/F11/ Contactin	Six C2-type domains (Ranscht, 1988; Brümmendorf et al., 1989).	NA	*Trans* – NrCAM, NgCAM (Morales et al., 1993); – PTPRZ (Peles et al., 1995; Bouyain and Watkins, 2010); – CASPR2 (Rubio-Marrero et al., 2016); – Notch (Hu et al., 2003). *Cis* – CASPR (Peles et al., 1997); – L1 (Olive et al., 2002). *ECM* – Chondroitin sulfate E (Mikami et al., 2009); – Tenascin-R (Norenberg et al., 1995).	– Promotes (Mikami et al., 2009); – Promotes filopodia and lamellipodia (Zacharias, 2002).	– Promotes (Treubert and Brümmendorf, 1998).	NA	KO: – LTP in CA1 is normal, – LTD in CA1 is impaired (Murai et al., 2002); TG (overexpressing): – LTP in CA1 is normal at 5 months, increased at 12 months of age (Puzzo et al., 2013).
Contactin2/ Tag1/axonin1	Six C2-type domains (but see text) (Zuellig et al., 1992; Freigang et al., 2000).	in *trans* (Rader et al., 1993; Felsenfeld et al., 1994; Malhotra et al., 1998; Lustig et al., 1999; Traka et al., 2003).	*Trans* –NrCAM (Lustig et al., 1999); – NgCAM (Fitzli et al., 2000); – L1 (Kuhn et al., 1991; Stoeckli et al., 1991; Felsenfeld et al., 1994; Wang et al., 2011); – β1 integrin (Felsenfeld et al., 1994); – APP (Ma et al., 2008). *Cis* – L1 (Malhotra et al., 1998); – NgCAM (Buchstaller et al., 1996); – CASPR2 (Traka et al., 2003). *ECM* – NA.	– Promotes (Buchstaller et al., 1996; Lustig et al., 1999).	– Promotes (Kuhn et al., 1991; Stoeckli et al., 1991; Kasahara et al., 2002).	NA	NA

(Continued)

TABLE 1 | Continued

IgSF member	Number and type of Ig domains	Homophilic interaction	Examples of heterophilic binding partners	Function in neurite outgrowth as a receptor	Function in neurite outgrowth as a ligand	Role in synapse formation	Changes in LTP/LTD in knock-out (KO) or transgenic (TG) mice
Contactin3/ BIG-1	Six C2-type domains (Yoshihara et al., 1994).	NA	*Trans* – PTPRG (Bouyain and Watkins, 2010). *Cis* – PTPRG (Bouyain and Watkins, 2010; Nikolaienko et al., 2016). *ECM* – NA.	NA	– Promotes (Yoshihara et al., 1994).	NA	NA
Contactin4/ BIG-2	Six C2-type domains (Yoshihara et al., 1995).	NA	*Trans* – PTPRG (Bouyain and Watkins, 2010). *Cis* – PTPRG (Bouyain and Watkins, 2010). *Soluble* – NA.	NA	– Promotes (Yoshihara et al., 1995)	NA	NA
Contactin5/ NB-2	Six C2-type domains (Ogawa et al., 1996)	NA	*Trans* – PTPRG (Bouyain and Watkins, 2010). *Cis* – PTPRG (Bouyain and Watkins, 2010); – APLP1 (Shimoda et al., 2012). *ECM* – NA.	NA	– Promotes (Bouyain and Watkins, 2010; Mercati et al., 2013).	NA	NA
Contactin6/ NB-3	Six C2-type domains (Ogawa et al., 1996).	NA	*Trans* – PTPRG (Bouyain and Watkins, 2010). *Cis* – PTPRG (Bouyain and Watkins, 2010); – CHL1 (Ye et al., 2008). *ECM* – NA.	NA	– Promotes (Bouyain and Watkins, 2010; Mercati et al., 2013).	NA	NA
IgLON5	NA	NA	*Trans* – NA; *Cis* – NA; *ECM* – NA.	NA	NA	NA	NA
LAMP/ LSAMP/IGLON3	Three C2-type domains (Pimenta et al., 1996).	in *trans* (Zhukareva and Levitt, 1995; Lodge et al., 2000; Gil et al., 2002).	*Trans* – Ntm (Gil et al., 2002). *Cis* – OBCAM (Reed et al., 2004). *ECM* – NA.	– Promotes (Eagleson et al., 2003).	– Promotes via the first Ig-like domain (Eagleson et al., 2003; Sanz et al., 2015); – Inhibits via the second Ig-like domain (Eagleson et al., 2003).	– Promotes (Hashimoto et al., 2009).	KO: – LTP in CA1 is decreased (Qiu et al., 2010).
NEGR1/ Klion/IGLON4	Three C2-type domains (Funatsu et al., 1999).	in *trans* (Miyata et al., 2003a) But see, (Marg et al., 1999).	*Trans* – Ntm, LAMP (Marg et al., 1999); – FGFR2 (Pischedda and Piccoli, 2015); – ObCAM (Miyata et al., 2003a). *Cis* – NA; *ECM* – NA.	NA	– Promotes (Pischedda and Piccoli, 2015; Sanz et al., 2015).	– Inhibits (Hashimoto et al., 2009).	NA
Ntm/ NT/IGLON2	Three C2-type domains (Struyk et al., 1995).	in *trans* (Lodge et al., 2000).	Trans – LAMP (Gil et al., 2002) *Cis* – NA; *ECM* – NA.	– Promotes (Gil et al., 1998, 2002).	– Promotes (Sanz et al., 2015).	NA	NA
OBCAM/ OPCML/IGLON1	Three C2-type domains (Hachisuka et al., 1996).	in *trans* (Lodge et al., 2000).	*Trans* – NEGR1 (Miyata et al., 2003a). *Cis* – LAMP (Lodge et al., 2000). *ECM* – NA.	NA	– Promotes (Sanz et al., 2015).	– Promotes (Li et al., 2006; Yamada et al., 2007; Hashimoto et al., 2009).	NA

(Continued)

TABLE 1 | Continued

IgSF member	Number and type of Ig domains	Homophilic interaction	Examples of heterophilic binding partners	Function in neurite outgrowth as a receptor	Function in neurite outgrowth as a ligand	Role in synapse formation	Changes in LTP/LTD in knock-out (KO) or transgenic (TG) mice
Thy1/ CD90/CDw90	One V-type domain (Williams and Gagnon, 1982).	In *trans* (Mahanthappa and Patterson, 1992).	*Trans* – β3 integrin (Leyton et al., 2001). *Cis* – Integrins (Kuroiwa et al., 2012). *ECM* – NA.	– Promotes when binds to antibodies (Leifer et al., 1984; Messer et al., 1984; Chen et al., 2005); – Inhibits when binds to αVβ3 integrins (Herrera-Molina et al., 2012).	NA	NA	KO: – LTP in CA1 is normal; – LTP in dentate gyrus is impaired (Zacco et al., 1990).

The table lists GPI-anchored IgSF CAMs expressed in humans and rodents. Recommended names (in bold) used throughout the text and alternative names are listed. The table describes whether the GPI-anchored IgSF CAM has been shown to interact homophilically, provides examples of heterophilic binding partners of GPI-anchored IgSF CAMs expressed on membranes of other cells (Trans), the same cells as the IgSF CAM is expressed (Cis), or in the extracellular matrix (ECM), describes the functions of the GPI-anchored IgSF CAMs in neurite outgrowth (as receptors or ligands), in synapse formation, and long-term potentiation (LTP) or long-term depression (LTD). NA, not analyzed.

dendritic arborizations of Purkinje cells. In contrast, the parallel fibers extend parallel to the plane of Purkinje cell dendritic branches in contactin-1 knock-out mice indicating misguidance of granule cell axon subpopulations (Berglund et al., 1999).

Contactin-2 has been shown to function as a receptor for neuronal cell adhesion molecule (NrCAM) but not for the neuron–glia cell adhesion molecule (NgCAM) in DRG and sympathetic ganglion neurons (Lustig et al., 1999). In these neurons, substrate-coated NgCAM and NrCAM, two L1 family CAMs, promote neurite outgrowth. Anti-contactin-2 Fab fragments do not affect the neurite outgrowth induced by NgCAM, but inhibit the NrCAM-dependent neurite outgrowth (Lustig et al., 1999). Substrate-coated NrCAM and NgCAM interact heterophilically in *trans* with contactin-2 at the cell surface of chick commissural axons and both molecules cooperate in the axonal guidance. However, this interaction is not involved in regulation of the axonal outgrowth (Fitzli et al., 2000). Knock down of contactin-2 with ex-ovo RNAi in the chick embryo affects guidance but not growth of axons of granule cells in the cerebellum (Baeriswyl and Stoeckli, 2008). Knock down of contactin-2 results in the failure of granule cells to extend their axons parallel to the pial surface of the cerebellum, creating an uneven molecular layer with decreased parallel fiber density. Since known binding partners of contactin-2, including NgCAM and NrCAM, are not expressed during granule cell axon extension, homophilic interactions of contactin-2 were proposed to be involved in axon guidance in these neurons (Baeriswyl and Stoeckli, 2008). Loss of contactin-2 in chick retinal neurons also impairs the ability of retinal neurons to contain their arbors within appropriate sublaminae (Yamagata and Sanes, 2012).

Glycosylphosphatidylinositol-anchored IgSF CAMs can also function as receptors when they are involved in homophilic binding. Cortical neurons grown on a substrate of recombinant OBCAM or LAMP demonstrate a dose-dependent increase in neurite outgrowth (Sanz et al., 2015). This neurite outgrowth-promoting activity of LAMP has been attributed to the first Ig domain within LAMP mediating homophilic interactions (Eagleson et al., 2003). Homophilic binding of Ntm also induces neurite growth in hippocampal neurons (Gil et al., 1998, 2002).

GPI-Anchored IgSF CAMs As Signal Transducers and Membrane Domain Organizers

While GPI-anchored IgSF CAMs do not possess intracellular domains, they induce intracellular signaling and regulate formation of the functional membrane domains by interacting in *cis* with other transmembrane proteins. For example, activation of the intracellular signaling by Thy-1 antibodies is likely to be induced by cross-linking Thy-1 molecules and associated proteins, such as integrins (Kuroiwa et al., 2012).

Contactin-1 interacts in *cis* with CASPR (Peles et al., 1997). The CASPR/contactin-1 complex accumulates in paranodal junctions in myelinated axons during myelination of peripheral nerves (Rios et al., 2000). Contactin-1 is necessary to target CASPR to the synaptic membrane, because CASPR is synthesized but not targeted to the cell surface plasma membrane in the

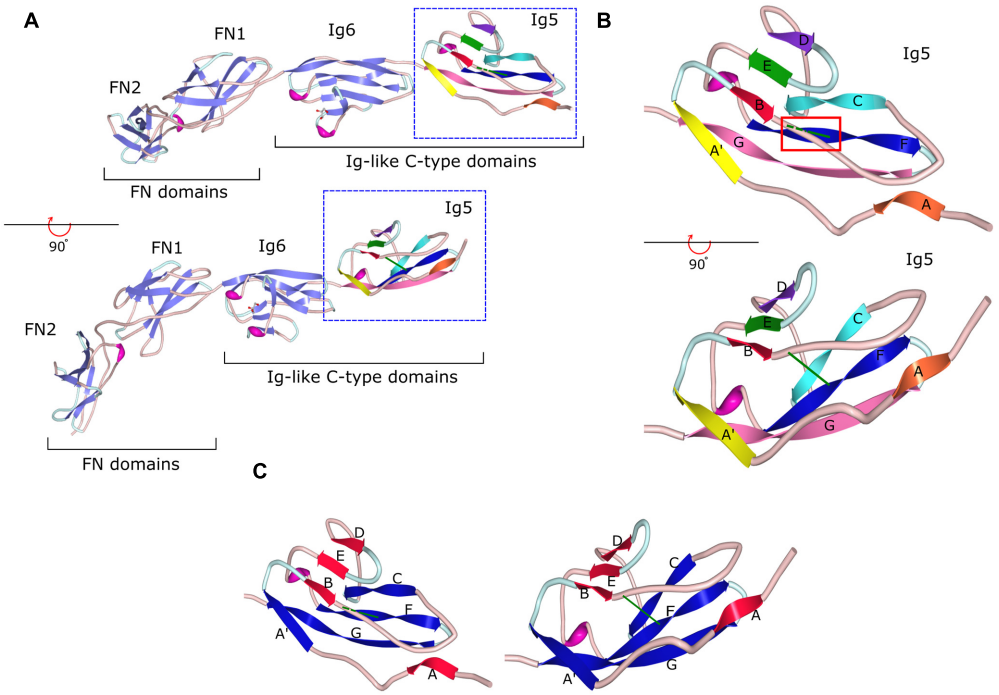

FIGURE 2 | Crystal structure of the fragment of contactin-3 containing Ig-like domains 5 and 6 and fibronectin type III domains 1 and 2. **(A)** fibronectin type III (FN) and immunoglobulin-like (Ig) C2-type domains of contactin-3 are shown as a ribbon diagram in two views flipped 90° to demonstrate the β-sheet orientation and disulfide bonds in Ig domains (green lines). β-Sheet strands are shown as light purple arrows in Ig6, FN2, and FN1 and multicolored arrows in Ig5. Coils are in light pink and turns are in light blue. **(B)** A ribbon diagram of the Ig5 domain with one β-sheet represented by strands A (orange), B (red), E (green), and D (purple) and the second sheet represented by strands A′ (yellow), C (cyan), F (blue), and G (pink). Strands E and F are connected by a short helix (in magenta). Two views flipped 90° are shown to demonstrate the β-sheet orientation and the disulfide bond represented as a green line in both views and highlighted by a red box in the upper view. Dashed green line represents the disulfide bond behind the B–C coil. **(C)** A ribbon diagram of the Ig5 domain with β-sheet strands re-colored to demonstrate the two sheets, one comprised of strands A, B, E, and D (red) and another comprised of strands A′, C, F, and G (blue) with the disulfide bond (green) holding the two sheets together. Image of PDB ID 5I99 (Nikolaienko et al., 2016) created with Protein Workshop (Moreland et al., 2005).

hippocampus of contactin-1-deficient mice (Rios et al., 2000; Murai et al., 2002). Contactin-1 also forms a complex with L1 and Fyn kinase in the mouse cerebellum, suggestive of the capability to transduce signals to intracellular proteins via L1 (Olive et al., 2002).

Contactin-2 binds in *cis* to L1. This interaction can be induced by homophilic *trans* interactions of contactin-2 resulting in the *cis* binding to L1 and L1-mediated ankyrin recruitment to the complex (Malhotra et al., 1998). Contactin-2 also binds in *cis* to NgCAM. This heterophilic *cis* interaction promotes neurite outgrowth, whereas heterophilic *trans* interaction between NgCAM and contactin-2 has no effect on neurite outgrowth (Buchstaller et al., 1996). Contactin-2 binds directly to the ectodomain of CASPR2 (Lu et al., 2016), and both proteins form a *cis* complex but are unable to form a *trans* complex. Despite this, contactin-2 is able to bind homophilically in *trans* to contactin-2 that has formed a *cis* complex with CASPR2 (Traka et al., 2003). The physiological significance of this interaction is illustrated by observations in contactin-2 and CASPR2 knock-out mice showing that contactin-2 is necessary for CASPR2 localization at juxtaparanodes in myelinated axons (Traka et al., 2003), whereas targeting of contactin-2 to juxtaparanodes depends on CASPR2 and both contactin-2 and CASPR2 are required for accumulation of voltage-gated potassium channels at the juxtaparanodes (Poliak et al., 2003).

Other contactins also associate in *cis* with various cell surface receptors. For example, contactin-5 forms a *cis* complex with amyloid precursor-like protein 1 (APLP1) on the presynaptic membrane (Shimoda et al., 2012). The second and third Ig domains of contactin-3, -4, -5, and -6 bind to receptor-type protein tyrosine phosphatase G (PTPRG) (Bouyain and Watkins, 2010) and contactin-3 and -6 associate in *cis* with PTPRG at the surface of mouse rod photoreceptor cells (Nikolaienko et al., 2016). Contactin-6 also interacts *in cis* with the Close Homolog of L1 (CHL1) and binds to and regulates the activity of the receptor-type protein tyrosine phosphatase α (PTPRα) (Ye et al., 2008).

Glycosylphosphatidylinositol-anchored IgSF CAMs also interact with the intracellular enzymes and cytoskeleton via lipids. NCAM120 co-localizes and associates with the membrane-cytoskeleton linker protein spectrin in transfected CHO cells and mouse hippocampal neurons, and this association is lost after disruption of the lipid rafts (Leshchyns'ka et al., 2003). Overexpression of NCAM120 in cultured hippocampal neurons from NCAM knock-out mice, however, is not sufficient to induce neurite outgrowth in response to recombinant extracellular

domain of NCAM (Niethammer et al., 2002). The interaction with spectrin may, however, be important in glial cells where NCAM120 is enriched. Contactin-2 associates with ganglioside GD3 in cerebellar neurons, and clustering of this complex induces activation of the Src family kinase Lyn (Kasahara et al., 2000, 2002). A recent study showing that NEGR1 interacts with Niemann-Pick disease Type C2 (NPC2) protein and functions in cholesterol transport (Kim et al., 2017) suggests that GPI-anchored IgSF CAMs may also be involved in regulation of the lipid composition of the plasma membrane.

GPI-Anchored IgSF CAMs As Functional Ligands

Glycosylphosphatidylinositol-anchored IgSF CAMs also function as ligands for other cell surface receptors in neurons and other cells. Early work on contactin-1 has demonstrated that neurite outgrowth in DRG neurons grown on CHO cells transfected with contactin-1 is increased (Gennarini et al., 1989, 1991). Further work showed that contactin-1 exerts dual cell-specific effects on neurite outgrowth by inhibiting neurite outgrowth in cerebellar granule cells and stimulating neurite outgrowth in sensory neurons, whereas it does not affect hippocampal neurons (Gennarini et al., 1991; Buttiglione et al., 1996), suggesting that contactin-1 activates different receptors expressed by these cells (Buttiglione et al., 1996). Among neuronal receptors for contactin-1 are members of the L1 family. NrCAM and NgCAM have been shown to interact heterophilically with contactin-1 (Morales et al., 1993). However, despite having shown that contactin-1 interacts with NrCAM and NgCAM, only NrCAM was found to enhance the outgrowth of chick retinal neurons (Treubert and Brümmendorf, 1998). Tectal cells adhere to and extend neurites on a substrate of contactin-1 and this effect is blocked by the application of Fab fragments against NrCAM but not NgCAM (Morales et al., 1993). While these experiments indicate that the interaction between contactin-1 and NrCAM induces neurite outgrowth, receptors mediating the inhibitory effects of contactin-1 on neurite outgrowth and the role that the interaction between contactin-1 and NgCAM plays remain to be determined. Contactin-1 was also identified to be a ligand of Notch in oligodendrocytes being involved in the signaling pathway of oligodendrocyte maturation (Hu et al., 2003). The role for contactin-1 as a functional ligand is also supported by *in vivo* observations. Contactin-1 is not detected in dendrites of granule cells (Faivre-Sarrailh et al., 1992). However, development of the dendrites is affected in contactin-1 knock-out mice resulting in a significant reduction of granule cell postsynaptic area (Berglund et al., 1999), suggesting that contactin-1 expressed on other cells acts as a functional ligand to regulate dendrite formation.

Contactin-2 used as a substrate induces neurite outgrowth in rat and chick DRG neurons (Furley et al., 1990; Stoeckli et al., 1991) and in rat and mouse cerebellar neurons (Kasahara et al., 2002; Wang et al., 2011). Removal of contactin-2 by PI-PLC from DRG neurons cultured on a substrate of contactin-2 does not affect the effect of contactin-2 substrate on neurite outgrowth (Felsenfeld et al., 1994) indicating that homophilic interactions of contactin-2 are not involved. Contactin-2-dependent neurite outgrowth is blocked by Fab fragments against L1 (Kuhn et al., 1991; Stoeckli et al., 1991; Felsenfeld et al., 1994; Wang et al., 2011) and β1 integrin (Felsenfeld et al., 1994), indicating that L1 and integrins are contactin-2 receptors, which promote neurite outgrowth. Contactin-2 was also shown to be a ligand of amyloid precursor protein (APP). Binding of contactin-2 to APP triggers cleavage of APP resulting in the release of its intracellular domain, which negatively modulates neurogenesis (Ma et al., 2008).

Neurite outgrowth in rat hippocampal neurons is enhanced when they are grown on substrate-coated recombinant contactin-3 and -4 (Yoshihara et al., 1994, 1995), or on HEK293 cells transfected with contactin-4, -5, and -6 (Bouyain and Watkins, 2010; Mercati et al., 2013), indicating that other CAMs of the contactin family can also function as *trans* ligands. Contactin-3 and -6 associate with PTPRG not only in *cis* but also in *trans* when expressed on the surfaces of apposing cells (Nikolaienko et al., 2016). Hence, PTPRG is likely to be a neuronal receptor for these CAMs of the contactin family. However, contactin-4, -5, and -6 display identical binding to PTPRG but differentially promote neurite outgrowth and branching at distinct developmental stages (Mercati et al., 2013), suggesting that other receptors are also involved. These receptors remain to be identified in future work.

Trans-interactions have also been reported for Thy-1 presented as a ligand. Thy-1 was identified in a neurite outgrowth-promoting complex containing also laminin and a heparin sulfate proteoglycan (Greenspan and O'brien, 1989). Thy-1 expressed at the neuronal cell surface functions as a ligand for αVβ3 integrin at the cell surface of astrocytes (Hermosilla et al., 2008). This interaction leads to integrin clustering, tyrosine phosphorylation of focal adhesion kinase (FAK) and p130Cas, activation of RhoA and p160ROCK, recruitment of paxillin, vinculin, and FAK to focal contacts resulting in formation of focal adhesion and stress fibers in rat astrocytes (Leyton et al., 2001; Avalos et al., 2002, 2004).

Cell adhesion molecules of the IgLON family NEGR1 and Ntm are constitutively shed from the cell surface and create a growth permissive substrate. Inhibition of their shedding by a pan-metalloproteinase inhibitor (BB-94) inhibits neurite outgrowth in cortical neurons and IgLON CAMs accumulate at the cell surface, whereas an increase in shedding by PI-PLC promotes neurite outgrowth (Sanz et al., 2015). A recent report showing that soluble NEGR1 promotes neuronal arborization in FGFR2- and ERK1/2-dependent manner (Pischedda and Piccoli, 2015) suggests that FGFR2 is one of the receptors for NEGR1 at the neuronal cell surface. The shedding of IgLON CAMs not only provides a growth permissive substrate but also renders cortical neurons grown on the IgLON substrate insensitive to the growth inhibitory effects of BB-94 suggesting that shed IgLON CAMs mitigate inhibitory signals transduced by a NEGR1- or Ntm-containing complex at the neuronal cell surface (Sanz et al., 2015).

Another member of IgLON family, LAMP, inhibits the neurite outgrowth in DRG neurons by heterophilically binding to Ntm expressed in these neurons (Gil et al., 2002). The second Ig domain of LAMP, which is not involved in homophilic interactions, harbors the outgrowth inhibiting activity (Eagleson

et al., 2003). Soluble recombinant Ntm induces neurite outgrowth in DRG neurons. This effect is also observed after removal of Ntm from the cell surface of these neurons by PI-PLC indicating that it is mediated by heterophilic interactions of Ntm. In contrast, Ntm inhibits neurite outgrowth in SCG neurons. These neurons do not express Ntm, and therefore Ntm's effects are also mediated by heterophilic interactions (Gil et al., 1998, 2002).

GPI-Anchored IgSF CAMs Are Present in Synapses in Neurons

The presence of multiple GPI-anchored IgSF CAMs in synapses was first suggested by biochemical analysis of synaptic terminals, synaptosomes, isolated from the brain tissue. Early work with Thy-1 antigen showed that Thy-1 was present in synaptosomes isolated from the mouse brain with later work showing that Thy-1 is a component of large dense core and small clear vesicles of PC12 cells which are similar to neuronal synaptic vesicles (Stohl and Gonatas, 1977; Jeng et al., 1998). Later studies showed the presence of different GPI-anchored IgSF CAMs in synaptosomes, including contactin-1 and contactin-2 (Murai et al., 2002; Bakkaloglu et al., 2008).

Immunoelectron microscopic analysis of contactin-1 localization revealed that depending on the type of synapse, contactin-1 is localized to either the pre- or post-synaptic membranes (Faivre-Sarrailh et al., 1992). For example, in the mouse cerebellum contactin-1 is localized pre-synaptically in synapses between parallel fibers of granule cells and dendritic spines of Purkinje cells and in synapses between mossy fiber terminals and granule cell dendrites, and is localized post-synaptically in synapses formed on Golgi cell dendrites (Faivre-Sarrailh et al., 1992). In the hippocampal CA1 region, contactin-1 is distributed at the surface of pyramidal cell dendrites, dendritic spine heads, and post-synaptic densities, and is also present in biochemically isolated post-synaptic density fractions (Murai et al., 2002). Contactin-2 has also been shown to localize to synaptic plasma membranes isolated from rat forebrain (Bakkaloglu et al., 2008).

In contrast to contactin-1, Ntm has been shown to accumulate both pre- and post-synaptically in synapses between parallel fibers of granule cells and dendritic spines of Purkinje cells and in synapses between mossy fiber terminals and granule cell dendrites but was not present in inhibitory synapses made by stellate or basket cells (Chen et al., 2001). LAMP is expressed pre- and post-synaptically in synapses in the developing lateral septum, but is detected only post-synaptically in synapses formed on granule cells of the dentate gyrus in adult hippocampus (Zacco et al., 1990).

Electron microscopic immunohistochemistry has demonstrated that NEGR1 is present at high levels in post-synaptic densities and at lower levels pre-synaptically in synapses along dendrites and on somata of neurons in the cerebral cortex and hippocampal CA3 region of adult rats (Miyata et al., 2003a). OBCAM shows similar ultrastructural distribution as NEGR1 with OBCAM immunoreactivity limited to postsynaptic densities of dendritic and somatic synapses in the cerebral cortex and hippocampal CA3 region of adult rats (Miyata et al., 2003a).

Several studies indicate that GPI-anchored IgSF CAMs are also present in synaptic organelles. Biochemical analysis of Thy-1 in the rat brain showed that it is targeted to small synaptic vesicles (SSVs) and large dense core vesicles (LDCVs) (Jeng et al., 1998). OBCAM is present in neurosecretory granules in neurites of hypothalamic magnocellular neurons (Miyata et al., 2003b). Mass spectrometry analysis of synaptic vesicles also identified NEGR1, OBCAM, Ntm, Thy-1, LAMP, and contactin-1 as components of synaptic vesicles (Takamori et al., 2006).

Role of the GPI-Anchored IgSF CAMs in Synapse Formation Regulation

Protein expression and localization of the GPI-anchored IgSF CAMs is developmentally regulated. Levels of Thy-1 strongly increase from postnatal day 14, whereas levels of NEGR1, OBCAM, and contactin-1 gradually increase during development and reach the highest level at 4 weeks after birth in the cerebral cortex, diencephalon, hippocampus, and cerebellum (Miyata et al., 2003a). Ntm levels gradually increase in the forebrain during development reaching the plateau at postnatal day 7 and then decline in adults (Struyk et al., 1995). Ntm levels are also increased in the molecular layer and the internal granular layer of the cerebellum during the period of synaptogenesis and reduce shortly after the active period of synaptogenesis ends, but remain high at synaptic contacts (Chen et al., 2001). Levels of NCAM and particularly NCAM120 increase in chick cornea and corneal nerves during corneal innervation (Mao et al., 2012). High expression of the GPI-anchored IgSF CAMs at the time of active synaptogenesis and their synaptic localization suggests that they play a role in synapse formation.

The role of the GPI-anchored IgSF CAMs in synapse formation is further indicated by studies showing that disruption of their functions or increase in their levels in neurons affect synaptogenesis. Overexpression of OBCAM in hippocampal neurons increases numbers of synapses along dendrites of transfected neurons (Hashimoto et al., 2009), whereas disruption of OBCAM functions using antibodies or by suppressing its expression using the antisense oligodeoxynucleotide results in impaired formation of synapses on dendrites of hippocampal neurons indicating that OBCAM promotes synapse formation (Yamada et al., 2007). OBCAM expression has been observed to be higher during early postnatal development and it decreases over time suggesting that OBCAM is active in the regulation of synapse formation (Li et al., 2006; Yamada et al., 2007). An increase in synapse formation has also been observed in cultured hippocampal neurons overexpressing LAMP (Hashimoto et al., 2009) and NCAM120 (Dityatev et al., 2004). Interestingly, overexpression of NEGR1 decreases numbers of synapses formed on dendrites of hippocampal neurons (Hashimoto et al., 2009). Thus, different GPI-anchored IgSF CAMs not only promote, but can also reduce synaptogenesis.

The molecular mechanisms of synaptogenesis regulation by the GPI-anchored IgSF CAMs remain poorly understood. Interestingly, ablation of NCAM expression in GABAergic basket interneurons in the postnatal mouse cortex results in impaired maturation of perisomatic synapses formed by these neurons,

and this phenotype is rescued by NCAM120 (Chattopadhyaya et al., 2013). The NCAM120-dependent maturation of synapses is inhibited by a dominant-negative form of Fyn kinase (Chattopadhyaya et al., 2013) indicating that GPI-anchored IgSF CAMs regulate synapse formation not only via changes in cell adhesion but also by activating intracellular signaling.

GPI-Anchored IgSF CAMs in Regulation of Synaptic Plasticity

Recent reports indicate that GPI-anchored IgSF CAMs also play a role in synaptic plasticity. Constitutively contactin-1-deficient mice show decreased paired pulse facilitation (PPF). Long-term potentiation (LTP) in the CA1 region of the hippocampus of these mice is normal, whereas long-term depression (LTD) is impaired (Murai et al., 2002). In contactin-1 transgenic mice generated to induce overexpression of full-length contactin-1 under control of the human contactin-2 promoter, PPF is not changed at 5 and 12 months of age indicating that the short-term plasticity is not altered by contactin-1 overexpression. However, LTP in the CA1 region of the hippocampus is increased in contactin-1-overexpressing mice at 12 months of age despite no change in LTP in contactin-1 transgenic mice at 5 months of age (Puzzo et al., 2013). Further analysis of LTP in the CA1 region of the hippocampus in older animals showed that LTP is impaired in 24-month-old wild-type mice when compared to 3–5-month-old wild-type animals. However, the age-dependent decline in LTP was slower in mice overexpressing contactin-1. Hence, contactin-1 is likely to play a role in maintaining synaptic plasticity in the adult brain during aging (Puzzo et al., 2013, 2015). Synaptic transmission is impaired in LAMP knock-out mice with a reduction in LTP in the CA1 region of the hippocampus (Qiu et al., 2010). LTP in the CA1 region of the hippocampus in Thy-1 knock-out mice was normal although LTP was absent in the dentate gyrus of these mice (Nosten-Bertrand et al., 1996). These observations indicate that GPI-anchored IgSF CAMs are involved in regulation of the different forms of synaptic plasticity in brain region-dependent manner.

GPI-Anchored IgSF CAMs in Regulation of Learning and Behavior

Glycosylphosphatidylinositol-anchored IgSF CAMs are also involved in regulation of learning and behavior. Thy-1 knock-out mice have been found to fail in observing social cues to select food that had been socially cued (Mayeux-Portas et al., 2000). It was therefore proposed that the loss of Thy-1 while not fatal is still under evolutionary pressure as the inability to select cued (and therefore safe) food would quickly push for the conservation of Thy-1. Spatial learning as assessed by the Morris water maze test was not affected in Thy-1 knock-out mice (Nosten-Bertrand et al., 1996).

Mice deficient for LAMP exhibit heightened reactivity to novelty, lower anxiety, and lower sensitivity to stressful environment (Catania et al., 2008; Innos et al., 2011, 2012). LAMP deficiency in mice also results in impaired spatial learning as indicated by increased time LAMP-deficient mice need to locate the underwater platform in the Morris water maze (Qiu et al., 2010). The role for LAMP in regulation of behavior is further suggested by observations showing that LAMP expression levels are increased in the hippocampus of mice exposed to the enriched environment (Heinla et al., 2015).

The link between changes in contactin-1 expression and age-dependent learning impairments has been demonstrated in studies showing that the age-dependent decline in contactin-1 levels in wild-type mice correlates with a higher latency in finding the hidden platform in the Morris water maze (Palmeri et al., 2013; Puzzo et al., 2015). The age-dependent increase in the time required to find the hidden platform in the Morris water maze is reduced in transgenic contactin-1-overexpressing mice (Puzzo et al., 2015). Furthermore, while old wild-type mice spend equal amounts of time exploring the novel and familiar objects in the novel object recognition test analyzing recognition memory, the old contactin-1-overexpressing mice spend more time exploring the novel object (Puzzo et al., 2015).

GPI-Anchored IgSF CAMs in Brain Disorders

Several observations indicate that contactin-2 may play a role in the onset of epilepsy. A homozygous single base pair deletion (c.503_503delG) of contactin-2 was identified to be present in individuals affected with autosomal recessive cortical myoclonic tremor and epilepsy in a consanguineous Egyptian family (Stogmann et al., 2013). The role of contactin-2 in epilepsy is further suggested by studies in mice showing that while gross brain morphology of contactin-2 null mice appears to be indistinguishable from their wild-type littermates, contactin-2 null mice display spontaneous episodes of seizures despite demonstrating normal behavior and are more sensitive to convulsant stimuli than their wild-type littermates (Fukamauchi et al., 2001).

Genome-wide analysis of copy number variations in autism spectrum disorder (ASD) patients identified a trend for the contactin gene family (*contactin-4*, *-5*, *-6*) to be associated with ASD (Van Daalen et al., 2011; Nava et al., 2014; Poot, 2014). The identification of multiple contactin CAMs in ASD has led to the suggestion that genetic interactions between contactins are involved in different degrees of ASD (Poot, 2014).

Autoantibodies against contactin-1 were shown to be present in a subset of patients suffering from chronic inflammatory demyelinating polyneuropathy (CIDP) (Querol et al., 2013), suggesting that contactin-1 is involved in neuromyopathies. Chronic passive transfer of anti-contactin-1 IgG4 in Lewis rats results in progressive motor deterioration (Manso et al., 2016), indicating that antibodies against contactin-1 are pathogenic in CIDP. A study on a consanguineous family with a homozygous contactin-1 mutation presenting with lethal congenital myopathy also supports the role contactin-1 may have in peripheral neuromyopathies (Compton et al., 2008).

Increased levels of NCAM120 were found in the cerebrospinal fluid (CSF) of patients suffering from bipolar disorder and depression suggesting that NCAM120 may be involved in mood disorders (Poltorak et al., 1996).

Patient case studies found that deletions of 1p31.1 to 1p31.3 containing the *NEGR1* gene present with developmental co-ordination disorder, attention deficit/hyperactivity disorder, learning disability, as well as delayed speech and language development (Gillberg and FitzPatrick, 2010; Tassano et al., 2015). A genome-wide copy number scan identified *NEGR1* to be one of five new candidate genes involved in dyslexia (Veerappa et al., 2013). A case study on two siblings with interstitial microdeletion of 1p31.1 involving only *NEGR1* presented with learning and behavioral problems, hypotonia, hypermobility, scoliosis, and aortic root dilation (Genovese et al., 2015). Further suggestive of the role NEGR1 has in brain disorders, NEGR1 is also elevated in the CSF of bipolar and depressed patients (Maccarrone et al., 2013). In Dark Agouti rats, NEGR1 is upregulated in response to venlafaxine (VLX), a serotonin and noradrenaline reuptake inhibitor used to treat major depressive disorder (MDD), suggesting that NEGR1 contributes to the VLX effect in MDD possibly by contributing to the establishment of new neuronal connections and changes in synaptic plasticity (Tamási et al., 2014).

A study on male contemplated suicide identified LAMP SNPs to be associated with suicide (Must et al., 2008). However, it is important to note that after multiple correction tests the association did not maintain statistical significance leading the authors to suggest that LAMP may play a role in suicidal behavior but more work is required to confirm their initial findings. Genotyping showed that four SNPs (rs1461131, rs4831089, rs16824691, and rs9874470) of LAMP were significantly associated with MDD (Koido et al., 2012). In addition, LAMP expression was significantly increased in the dorsolateral prefrontal cortex of schizophrenic and bipolar disorder patients (Behan et al., 2009).

In a study on late-onset Alzheimer's disease, four SNPs (rs1629316, rs1547897, rs11222931, and rs11222932) in intron 1 of the Ntm gene (11q25) and one SNP (rs11223225) in intron 1 of the OBCAM gene (located on the same chromosome as Ntm < 80 kb apart) have been found to be associated with late-onset Alzheimer's disease (Liu et al., 2007). Genome-linkage studies in two independent Dutch populations indicate that depression is also associated with a locus on chromosome 11q25 suggesting a link to OBCAM (Schol-Gelok et al., 2010). In a study of schizophrenia in Thai populations, four SNPs (rs3016384, rs1784519, rs1894193, and rs1939498) of OBCAM have been identified to be linked to schizophrenia (Panichareon et al., 2012). An earlier study also identified OBCAM to be implicated in schizophrenia; however, the association was nominally significant (O'Donovan et al., 2008). Genome-wide analysis of aggressiveness in attention deficit hyperactivity disorder (ADHD) found that one of two significant loci associated with aggressiveness in ADHD was within the Ntm gene (Brevik et al., 2016). Additionally, Ntm has also been identified to be associated with intelligence as demonstrated by a family-based association study (Pan et al., 2011).

Conclusion and Future Directions

Glycosylphosphatidylinositol-anchored IgSF CAMs play important roles in regulation of neuronal development, synapse formation and function, learning, and behavior. Previous research indicates that in addition to mediating adhesive interactions, these molecules induce intracellular signaling by binding to other cell surface receptors, regulating their levels and functions, and assembling membrane microdomains.

Further research is, however, needed to characterize the whole repertoire of the interactions of GPI-anchored IgSF CAMs in developing and mature neurons, and in synapses to fully understand the role these molecules play in the developing and mature nervous system and molecular mechanisms involved. While several neurite outgrowth-promoting receptors for GPI-anchored IgSF CAMs have been described, observations showing that even relatively well-characterized contactin-1 not only promotes but also inhibits neurite outgrowth in a neuron-specific manner suggest that there are still other receptors that remain to be identified. How the repertoire of molecular interactions involving GPI-anchored IgSF CAMs changes during neuronal development remains also poorly understood. The roles that these interactions play in regulating synapse formation and function are mostly unknown. It is possible that GPI-anchored IgSF CAMs promote synapse formation by forming homophilic adhesive bonds connecting pre- and post-synaptic membranes. However, these molecules are often asymmetrically expressed in synapses and are found either pre- or post-synaptically. This observation suggests that GPI-anchored IgSF CAMs regulate synapse formation by heterophilically interacting with other receptors or CAMs in synaptic membranes. Further characterization of the synaptic interactions of GPI-anchored IgSF CAMs is necessary to understand molecular mechanisms activated by these molecules during synapse formation. It may also help to understand the role that GPI-anchored IgSF CAMs play in synaptic plasticity suggested by abnormalities in mice with altered expression of these molecules, and to characterize the signaling pathways regulated by GPI-anchored IgSF CAMs in synapses.

Further analysis of the post-translational modifications of GPI-anchored IgSF CAMs is necessary to understand mechanisms of the regulation of the functions of these molecules. Shedding of the IgLON family members was shown to play an important role during neuronal development. The role that proteolysis of GPI-anchored IgSF CAMs plays in regulation of synapse numbers and remodeling during synaptic plasticity remains to be investigated. Regulation of the homophilic and heterophilic interactions of GPI-anchored IgSF CAMs by glycosylation of the multiple sites within their ectodomains is also an intriguing possibility, which remains to be analyzed. Whether GPI anchor-mediated interactions with lipids play a role in the transport of GPI-anchored IgSF CAMs, their sorting to lipid rafts, microdomain assembly, and signal transduction also remains to be investigated.

Genetic association studies in humans have started to illuminate the role of GPI-anchored IgSF CAMs in brain

disorders. Biochemical analyses of the changes in levels and synaptic targeting of GPI-anchored IgSF CAMs in postmortem human brain tissue and in animal models are necessary to corroborate these findings and may reveal yet unknown roles of these molecules in brain disorders. Future research analyzing molecular mechanisms of GPI-anchored IgSF CAM function and regulation will help to understand the molecular mechanisms of brain disorders linked to abnormal expression or function of these molecules, and may pave the way for development of new treatments of these disorders.

AUTHOR CONTRIBUTIONS

RT, IL, and VS were involved in analyzing the literature and writing the manuscript.

FUNDING

This work was supported by the National Health and Medical Research Council grant (APP1129869).

REFERENCES

Avalos, A. M., Arthur, W. T., Schneider, P., Quest, A. F. G., Burridge, K., and Leyton, L. (2004). Aggregation of integrins and RhoA activation are required for Thy-1-induced morphological changes in astrocytes. *J. Biol. Chem.* 279, 39139–39145. doi: 10.1074/jbc.M403439200

Avalos, A. M., Labra, C. V., Quest, A. F. G., and Leyton, L. (2002). Signaling triggered by Thy-1 interaction with β3 integrin on astrocytes is an essential step towards unraveling neuronal Thy-1 function. *Biol. Res.* 35, 231–238. doi: 10.4067/S0716-97602002000200015

Baeriswyl, T., and Stoeckli, E. T. (2008). Axonin-1/TAG-1 is required for pathfinding of granule cell axons in the developing cerebellum. *Neural Dev.* 3:7. doi: 10.1186/1749-8104-3-7

Bakkaloglu, B., O'Roak, B. J., Louvi, A., Gupta, A. R., Abelson, J. F., Morgan, T. M., et al. (2008). Molecular cytogenetic analysis and resequencing of contactin associated protein-like 2 in autism spectrum disorders. *Am. J. Hum. Genet.* 82, 165–173. doi: 10.1016/j.ajhg.2007.09.017

Barclay, A. N. (2003). Membrane proteins with immunoglobulin-like domains - A master superfamily of interaction molecules. *Semin. Immunol.* 15, 215–223. doi: 10.1016/S1044-5323(03)00047-2

Behan, Á., Byrne, C., Dunn, M. J., Cagney, G., and Cotter, D. R. (2009). Proteomic analysis of membrane microdomain-associated proteins in the dorsolateral prefrontal cortex in schizophrenia and bipolar disorder reveals alterations in LAMP, STXBP1 and BASP1 protein expression. *Mol. Psychiatry* 14, 601–613. doi: 10.1038/mp.2008.7

Berglund, E. O., Murai, K. K., Fredette, B., Sekerková, G., Marturano, B., Weber, L., et al. (1999). Ataxia and abnormal cerebellar microorganization in mice with ablated contactin gene expression. *Neuron* 24, 739–750. doi: 10.1016/S0896-6273(00)81126-5

Bouyain, S., and Watkins, D. J. (2010). The protein tyrosine phosphatases PTPRZ and PTPRG bind to distinct members of the contactin family of neural recognition molecules. *Proc. Natl. Acad. Sci. U.S.A.* 107, 2443–2448. doi: 10.1073/pnas.0911235107

Brevik, E. J., van Donkelaar, M. M. J., Weber, H., Sánchez-Mora, C., Jacob, C., Rivero, O., et al. (2016). Genome-wide analyses of aggressiveness in attention-deficit hyperactivity disorder. *Am. J. Med. Genet. Part B Neuropsychiatr. Genet.* 171, 733–747. doi: 10.1002/ajmg.b.32434

Brümmendorf, T., Michael Wolff, J., Frank, R., and Rathjen, F. G. (1989). Neural cell recognition molecule F11: homology with fibronectin type III and immunoglobulin type C domains. *Neuron* 2, 1351–1361. doi: 10.1016/0896-6273(89)90073-1

Brümmendorf, T., and Rathjen, F. G. (1993). Axonal glycoproteins with immunoglobulin- and fibronectin type III-related domains in vertebrates: structural features, binding activities, and signal transduction. *J. Neurochem.* 61, 1207–1219. doi: 10.1111/j.1471-4159.1993.tb13611.x

Buchstaller, A., Kunz, S., Berger, P., Kunz, B., Ziegler, U., Rader, C., et al. (1996). Cell adhesion molecules NgCAM and axonin-1 form heterodimers in the neuronal membrane and cooperate in neurite outgrowth promotion. *J. Cell Biol.* 135, 1593–1607. doi: 10.1083/jcb.135.6.1593

Buckley, C. D., Rainger, G. E., Bradfield, P. F., Nash, G. B., and Simmons, D. L. (1998). Cell adhesion: more than just glue (Review). *Mol. Membr. Biol.* 15, 167–176. doi: 10.3109/09687689709044318

Buttiglione, M., Revest, J. M., Rougon, G., and Faivre-Sarrailh, C. (1996). F3 neuronal adhesion molecule controls outgrowth and fasciculation of cerebellar granule cell neurites: a cell-type-specific effect mediated by the Ig-like domains. *Mol. Cell. Neurosci.* 8, 53–69. doi: 10.1006/mcne.1996.0043

Catania, E. H., Pimenta, A., and Levitt, P. (2008). Genetic deletion of *Lsamp* causes exaggerated behavioral activation in novel environments. *Behav. Brain Res.* 188, 380–390. doi: 10.1016/j.bbr.2007.11.022

Chattopadhyaya, B., Baho, E., Huang, Z. J., Schachner, M., and Di Cristo, G. (2013). Neural cell adhesion molecule-mediated Fyn activation promotes GABAergic synapse maturation in postnatal mouse cortex. *J. Neurosci.* 33, 5957–5968. doi: 10.1523/JNEUROSCI.1306-12.2013

Chen, C. H., Wang, S. M., Yang, S. H., and Jeng, C. J. (2005). Role of Thy-1 in in vivo and in vitro neural development and regeneration of dorsal root ganglionic neurons. *J. Cell. Biochem.* 94, 684–694. doi: 10.1002/jcb.20341

Chen, S., Gil, O., Ren, Y. Q., Zanazzi, G., Salzer, J. L., and Hillman, D. E. (2001). Neurotrimin expression during cerebellar development suggests roles in axon fasciculation and synaptogenesis. *J. Neurocytol.* 30, 927–937. doi: 10.1023/A:1020673318536

Chothia, C., Gelfand, I., and Kister, A. (1998). Structural determinants in the sequences of immunoglobulin variable domain. *J. Mol. Biol.* 278, 457–479. doi: 10.1006/jmbi.1998.1653

Chothia, C., and Jones, E. Y. (1997). The molecular structure of cell adhesion molecules. *Annu. Rev. Biochem.* 66, 823–862. doi: 10.1146/annurev.biochem.66.1.823

Compton, A. G., Albrecht, D. E., Seto, J. T., Cooper, S. T., Ilkovski, B., Jones, K. J., et al. (2008). Mutations in contactin-1, a neural adhesion and neuromuscular junction protein, cause a familial form of lethal congenital myopathy. *Am. J. Hum. Genet.* 83, 714–724. doi: 10.1016/j.ajhg.2008.10.022

Dityatev, A., Dityateva, G., Sytnyk, V., Delling, M., Toni, N., Nikonenko, I., et al. (2004). Polysialylated neural cell adhesion molecule promotes remodeling and formation of hippocampal synapses. *J. Neurosci.* 24, 9372–9382. doi: 10.1523/JNEUROSCI.1702-04.2004

Eagleson, K. L., Pimenta, A. F., Burns, M. M., Fairfull, L. D., Cornuet, P. K., Zhang, L., et al. (2003). Distinct domains of the limbic system-associated membrane protein (LAMP) mediate discrete effects on neurite outgrowth. *Mol. Cell. Neurosci.* 24, 725–740. doi: 10.1016/S1044-7431(03)00237-9

Faivre-Sarrailh, C., Gennarini, G., Goridis, C., and Rougon, G. (1992). F3/F11 cell surface molecule expression in the developing mouse cerebellum is polarized at synaptic sites and within granule cells. *J. Neurosci.* 12, 257–267.

Felsenfeld, D. P., Hynes, M. A., Skoler, K. M., Furley, A. J., and Jessell, T. M. (1994). TAG-1 can mediate homophilic binding, but neurite outgrowth on TAG-1 requires an L1-like molecule and β1 integrins. *Neuron* 12, 675–690. doi: 10.1016/0896-6273(94)90222-4

Fitzli, D., Stoeckli, E. T., Kunz, S., Siribour, K., Rader, C., Kunz, B., et al. (2000). A direct interaction of axonin-1 with NgCAM-related cell adhesion molecule (NrCAM) results in guidance, but not growth of commissural axons. *J. Cell Biol.* 149, 951–968. doi: 10.1083/jcb.149.4.951

Freigang, J., Proba, K., Leder, L., Diederichs, K., Sonderegger, P., and Welte, W. (2000). The crystal structure of the ligand binding module of axonin-1/TAG-1 suggests a zipper mechanism for neural cell adhesion. *Cell* 101, 425–433. doi: 10.1016/S0092-8674(00)80852-1

Fujita, M., and Kinoshita, T. (2012). GPI-anchor remodeling: potential functions of GPI-anchors in intracellular trafficking and membrane dynamics. *Biochim. Biophys. Acta* 1821, 1050–1058. doi: 10.1016/j.bbalip.2012.01.004

Fukamauchi, F., Aihara, O., Wang, Y. J., Akasaka, K., Takeda, Y., Horie, M., et al. (2001). TAG-1-deficient mice have marked elevation of adenosine A1 receptors in the hippocampus. *Biochem. Biophys. Res. Commun.* 281, 220–226. doi: 10.1006/bbrc.2001.4334

Funatsu, N., Miyata, S., Kumanogoh, H., Shigeta, M., Hamada, K., Endo, Y., et al. (1999). Characterization of a novel rat brain glycosylphosphatidylinositol-anchored Protein (Kilon), a member of the IgLON Cell adhesion molecule family. *J. Biol. Chem.* 274, 8224–8230. doi: 10.1074/jbc.274.12.8224

Furley, A. J., Morton, S. B., Manalo, D., Karagogeos, D., Dodd, J., and Jessell, T. M. (1990). The axonal glycoprotein TAG-1 is an immunoglobulin superfamily member with neurite outgrowth-promoting activity. *Cell* 61, 157–170. doi: 10.1016/0092-8674(90)90223-2

Gennarini, G., Cibelli, G., Rougon, G., Mattei, M. G., and Goridis, C. (1989). The mouse neuronal cell surface protein F3: a phosphatidylinositol-anchored member of the immunoglobulin superfamily related to chicken contactin. *J. Cell Biol.* 109, 775–788. doi: 10.1083/jcb.109.2.775

Gennarini, G., Durbec, P., Boned, A., Rougon, G., and Goridis, C. (1991). Transfected F3/F11 neuronal cell surface protein mediates intercellular adhesion and promotes neurite outgrowth. *Neuron* 6, 595–606. doi: 10.1016/0896-6273(91)90062-5

Genovese, A., Cox, D. M., and Butler, M. G. (2015). Partial deletion of chromosome 1p31.1 including only the neuronal growth regulator 1 gene in two siblings. *J. Pediatr. Genet.* 4, 23–28. doi: 10.1055/s-0035-1554977

Gil, O. D., Zanazzi, G., Struyk, A. F., and Salzer, J. L. (1998). Neurotrimin mediates bifunctional effects on neurite outgrowth via homophilic and heterophilic interactions. *J. Neurosci.* 18, 9312–9325.

Gil, O. D., Zhang, L., Chen, S., Ren, Y. Q., Pimenta, A., Zanazzi, G., et al. (2002). Complementary expression and heterophilic interactions between IgLON family members neurotrimin and LAMP. *J. Neurobiol.* 51, 190–204. doi: 10.1002/neu.10050

Gillberg, C., and FitzPatrick, D. (2010). Case report: further evidence for a recognisable syndrome caused by deletion of 1p31. *Adv. Clin. Neurosci. Rehabil.* 10, 16–17.

Greenspan, R. J., and O'brien, M. C. (1989). Genetic evidence for the role of Thy-1 in neurite outgrowth in the mouse. *J. Neurogenet.* 5, 25–36. doi: 10.3109/01677068909167262

Hachisuka, A., Yamazaki, T., Sawada, J., and Terao, T. (1996). Characterization and tissue distribution of opioid-binding cell adhesion molecule (OBCAM) using monoclonal antibodies. *Neurochem. Int.* 28, 373–379. doi: 10.1016/0197-0186(95)00108-5

Harpaz, Y., and Chothia, C. (1994). Many of the immunoglobulin superfamily domains in cell adhesion molecules and surface receptors belong to a new structural set which is close to that containing variable domains. *J. Mol. Biol.* 238, 528–539. doi: 10.1006/jmbi.1994.1312

Hashimoto, T., Maekawa, S., and Miyata, S. (2009). IgLON cell adhesion molecules regulate synaptogenesis in hippocampal neurons. *Cell Biochem. Funct.* 27, 496–498. doi: 10.1002/cbf.1600

Heinla, I., Leidmaa, E., Kongi, K., Pennert, A., Innos, J., Nurk, K., et al. (2015). Gene expression patterns and environmental enrichment-induced effects in the hippocampi of mice suggest importance of Lsamp in plasticity. *Front. Neurosci.* 9:205. doi: 10.3389/fnins.2015.00205

Held, W., and Mariuzza, R. A. (2011). Cis–trans interactions of cell surface receptors: biological roles and structural basis. *Cell. Mol. Life Sci.* 68, 3469–3478. doi: 10.1007/s00018-011-0798-z

Hemperly, J. J., Edelman, G. M., and Cunningham, B. A. (1986). cDNA clones of the neural cell adhesion molecule (N-CAM) lacking a membrane-spanning region consistent with evidence for membrane attachment via a phosphatidylinositol intermediate. *Proc. Natl. Acad. Sci. U.S.A.* 83, 9822–9826. doi: 10.1073/pnas.83.24.9822

Hermosilla, T., Muñoz, D., Herrera-Molina, R., Valdivia, A., Muñoz, N., Nham, S., et al. (2008). Direct Thy-1/αVβ3 integrin interaction mediates neuron to astrocyte communication. *Biochim. Biophys. Acta* 1783, 1111–1120. doi: 10.1016/j.bbamcr.2008.01.034

Herrera-Molina, R., Frischknecht, R., Maldonado, H., Seidenbecher, C. I., Gundelfinger, E. D., Hetz, C., et al. (2012). Astrocytic αVβ3 integrin inhibits neurite outgrowth and promotes retraction of neuronal processes by clustering Thy-1. *PLOS ONE* 7:e34295. doi: 10.1371/journal.pone.0034295

Horstkorte, R., Schachner, M., Magyar, J. P., Vorherr, T., and Schmitz, B. (1993). The fourth immunoglobulin-like domain of NCAM contains a carbohydrate recognition domain for oligomannosidic glycans implicated in association with L1 and neurite outgrowth. *J. Cell Biol.* 121, 1409–1421. doi: 10.1083/jcb.121.6.1409

Hu, Q. D., Ang, B. T., Karsak, M., Hu, W. P., Cui, X. Y., Duka, T., et al. (2003). F3/contactin acts as a functional ligand for notch during oligodendrocyte maturation. *Cell* 115, 163–175. doi: 10.1016/S0092-8674(03)00810-9

Innos, J., Philips, M. A., Leidmaa, E., Heinla, I., Raud, S., Reemann, P., et al. (2011). Lower anxiety and a decrease in agonistic behaviour in Lsamp-deficient mice. *Behav. Brain Res.* 217, 21–31. doi: 10.1016/j.bbr.2010.09.019

Innos, J., Philips, M. A., Raud, S., Lilleväli, K., Kõks, S., and Vasar, E. (2012). Deletion of the Lsamp gene lowers sensitivity to stressful environmental manipulations in mice. *Behav. Brain Res.* 228, 74–81. doi: 10.1016/j.bbr.2011.11.033

Itoh, S., Hachisuka, A., Kawasaki, N., Hashii, N., Teshima, R., Hayakawa, T., et al. (2008). Glycosylation analysis of IgLON family proteins in rat brain by liquid chromatography and multiple-stage mass spectrometry. *Biochemistry* 47, 10132–10154. doi: 10.1021/bi8009778

Jeng, C.-J., McCarroll, S. A., Martin, T. F. J., Floor, E., Adams, J., Krantz, D., et al. (1998). Thy-1 is a component common to multiple populations of synaptic vesicles. *J. Cell Biol.* 140, 685–698. doi: 10.1083/jcb.140.3.685

Kasahara, K., Watanabe, K., Kozutsumi, Y., Oohira, A., Yamamoto, T., and Sanai, Y. (2002). Association of GPI-anchored protein TAG-1 with Src-family kinase Lyn in lipid rafts of cerebellar granule cells. *Neurochem. Res.* 27, 823–829. doi: 10.1023/A:1020265225916

Kasahara, K., Watanabe, K., Takeuchi, K., Kaneko, H., Oohira, A., Yamamoto, T., et al. (2000). Involvement of gangliosides in glycosylphosphatidylinositol-anchored neuronal cell adhesion molecule TAG-1 signaling in lipid rafts. *J. Biol. Chem.* 275, 34701–34709. doi: 10.1074/jbc.M003163200

Kim, H., Chun, Y., Che, L., Kim, J., Lee, S., and Lee, S. (2017). The new obesity-associated protein, neuronal growth regulator 1 (NEGR1), is implicated in Niemann-Pick disease Type C (NPC2)-mediated cholesterol trafficking. *Biochem. Biophys. Res. Commun.* 482, 1367–1374. doi: 10.1016/j.bbrc.2016.12.043

Kiselyov, V. V., Soroka, V., Berezin, V., and Bock, E. (2005). Structural biology of NCAM homophilic binding and activation of FGFR. *J. Neurochem.* 94, 1169–1179. doi: 10.1111/j.1471-4159.2005.03284.x

Koido, K., Traks, T., Balõtšev, R., Eller, T., Must, A., Koks, S., et al. (2012). Associations between LSAMP gene polymorphisms and major depressive disorder and panic disorder. *Transl. Psychiatry* 2, e152. doi: 10.1038/tp.2012.74

Kuhn, T. B., Stoeckli, E. T., Condrau, M. A., Rathjen, F. G., and Sonderegger, P. (1991). Neurite outgrowth on immobilized axonin-1 is mediated by a heterophilic interaction with L1(G4). *J. Cell Biol.* 115, 1113–1126. doi: 10.1083/jcb.115.4.1113

Kulahin, N., Kristensen, O., Rasmussen, K. K., Olsen, L., Rydberg, P., Vestergaard, B., et al. (2011). Structural model and trans-interaction of the entire ectodomain of the olfactory cell adhesion molecule. *Structure* 19, 203–211. doi: 10.1016/j.str.2010.12.014

Kuroiwa, K., Torikai, Y., Osawa, M., Nakashima, T., Nakashima, M., Endo, H., et al. (2012). Epitope determination of anti rat thy-1 monoclonal antibody that regulates neurite outgrowth. *Hybridoma* 31, 225–232. doi: 10.1089/hyb.2012.0002

Leifer, D., Lipton, S. A., Barnstable, C. J., and Masland, R. H. (1984). Monoclonal antibody to Thy-1 enhances regeneration of processes by rat retinal ganglion cells in culture. *Science* 224, 303–306. doi: 10.1126/science.6143400

Leshchyns'ka, I., and Sytnyk, V. (2016). Reciprocal interactions between cell adhesion molecules of the immunoglobulin superfamily and the cytoskeleton in neurons. *Front. Cell Dev. Biol.* 4:9. doi: 10.3389/fcell.2016.00009

Leshchyns'ka, I., Sytnyk, V., Morrow, J. S., and Schachner, M. (2003). Neural cell adhesion molecule (NCAM) association with PKCβ 2 via βI spectrin is implicated in NCAM-mediated neurite outgrowth. *J. Cell Biol.* 161, 625–639. doi: 10.1083/jcb.200303020

Leyton, L., Schneider, P., Labra, C. V., Rüegg, C., Hetz, C. A., Quest, A. F. G., et al. (2001). Thy-1 binds to integrin β3 on astrocytes and triggers formation of focal contact sites. *Curr. Biol.* 11, 1028–1038. doi: 10.1016/S0960-9822(01)00262-7

Li, P., Prasad, S. S., Mitchell, D. E., Hachisuka, A., Sawada, J. -Í, Al-Housseini, A. M., et al. (2006). Postnatal expression profile of OBCAM implies its involvement in visual cortex development and plasticity. *Cereb. Cortex* 16, 291–299. doi: 10.1093/cercor/bhi109

Liu, F., Arias-Vásquez, A., Sleegers, K., Aulchenko, Y. S., Kayser, M., Sanchez-Juan, P., et al. (2007). A genomewide screen for late-onset alzheimer disease in a genetically isolated dutch population. *Am. J. Hum. Genet.* 81, 17–31. doi: 10.1086/518720

Lodge, A. P., Howard, M. R., McNamee, C. J., and Moss, D. J. (2000). Co-localisation, heterophilic interactions and regulated expression of IgLON family proteins in the chick nervous system. *Mol. Brain Res.* 82, 84–94. doi: 10.1016/S0169-328X(00)00184-4

Lu, Z., Reddy, M. V., Liu, J., Kalichava, A., Liu, J., Zhang, L., et al. (2016). Molecular architecture of contactin-Associated protein-like 2 (CNTNAP2) and its interaction with contactin 2 (CNTN2). *J. Biol. Chem.* 291, 24133–24147. doi: 10.1074/jbc.M116.748236

Lustig, M., Sakurai, T., and Grumet, M. (1999). Nr-CAM promotes neurite outgrowth from peripheral ganglia by a mechanism involving axonin-1 as a neuronal receptor. *Dev. Biol.* 209, 340–351. doi: 10.1006/dbio.1999.9250

Ma, Q.-H., Futagawa, T., Yang, W.-L., Jiang, X.-D., Zeng, L., Takeda, Y., et al. (2008). A TAG1-APP signalling pathway through Fe65 negatively modulates neurogenesis. *Nat. Cell Biol.* 10, 283–294. doi: 10.1038/ncb1690

Maccarrone, G., Ditzen, C., Yassouridis, A., Rewerts, C., Uhr, M., Uhlen, M., et al. (2013). Psychiatric patient stratification using biosignatures based on cerebrospinal fluid protein expression clusters. *J. Psychiatr. Res.* 47, 1572–1580. doi: 10.1016/j.jpsychires.2013.07.021

Mahanthappa, N. K., and Patterson, P. H. (1992). Thy-1 involvement in neurite outgrowth: perturbation by antibodies, phospholipase C, and mutation. *Dev. Biol.* 150, 47–59. doi: 10.1016/0012-1606(92)90006-3

Malhotra, J. D., Tsiotra, P., Karagogeos, D., and Hortsch, M. (1998). Cis-activation of L1-mediated ankyrin recruitment by TAG-1 homophilic cell adhesion. *J. Biol. Chem.* 273, 33354–33359. doi: 10.1074/jbc.273.50.33354

Manso, C., Querol, L., Mekaouche, M., Illa, I., and Devaux, J. J. (2016). Contactin-1 IgG4 antibodies cause paranode dismantling and conduction defects. *Brain* 139, 1700–1712. doi: 10.1093/brain/aww062

Mao, X., Schwend, T., and Conrad, G. W. (2012). Expression and localization of neural cell adhesion molecule and polysialic acid during chick corneal development. *Investig. Ophthalmol. Vis. Sci.* 53, 1234–1243. doi: 10.1167/iovs.11-8834

Marg, A., Sirim, P., Spaltmann, F., Plagge, A., Kauselmann, G., Buck, F., et al. (1999). Neurotractin, a novel neurite outgrowth-promoting Ig-like protein that interacts with CEPU-1 and LAMP. *J. Cell Biol.* 145, 865–876. doi: 10.1083/jcb.145.4.865

Mayeux-Portas, V., File, S. E., Stewart, C. L., and Morris, R. J. (2000). Mice lacking the cell adhesion molecule Thy-1 fail to use socially transmitted cues to direct their choice of food. *Curr. Biol.* 10, 68–75. doi: 10.1016/S0960-9822(99)00278-X

Mercati, O., Danckaert, A., Andre-Leroux, G., Bellinzoni, M., Gouder, L., Watanabe, K., et al. (2013). Contactin 4, -5 and -6 differentially regulate neuritogenesis while they display identical PTPRG binding sites. *Biol. Open* 2, 324–334. doi: 10.1242/bio.20133343

Messer, A., Snodgrass, G. L., and Maskin, P. (1984). Enhanced survival of cultured cerebellar Purkinje cells by plating on antibody to Thy-1. *Cell. Mol. Neurobiol.* 4, 285–290. doi: 10.1007/BF00733591

Mikami, T., Yasunaga, D., and Kitagawa, H. (2009). Contactin-1 is a functional receptor for neuroregulatory chondroitin sulfate-E. *J. Biol. Chem.* 284, 4494–4499. doi: 10.1074/jbc.M809227200

Miyata, S., Matsumoto, N., Taguchi, K., Akagi, A., Iino, T., Funatsu, N., et al. (2003a). Biochemical and ultrastructural analyses of IgLON cell adhesion molecules, Kilon and OBCAM in the rat brain. *Neuroscience* 117, 645–658. doi: 10.1016/S0306-4522(02)00873-4

Miyata, S., Taguchi, K., and Maekawa, S. (2003b). Dendrite-associated opioid-binding cell adhesion molecule localizes at neurosecretory granules in the hypothalamic magnocellular neurons. *Neuroscience* 122, 169–181. doi: 10.1016/S0306-4522(03)00609-2

Morales, G., Hubert, M., Brümmendorf, T., Treubert, U., Tárnok, A., Schwarz, U., et al. (1993). Induction of axonal growth by heterophilic interactions between the cell surface recognition proteins Fll and Nr-CAM/Bravo. *Neuron* 11, 1113–1122. doi: 10.1016/0896-6273(93)90224-F

Moreland, J. L., Gramada, A., Buzko, O. V., Zhang, Q., and Bourne, P. E. (2005). The molecular biology toolkit (MBT): a modular platform for developing molecular visualization applications. *BMC Bioinformatics* 6:21. doi: 10.1186/1471-2105-6-21

Murai, K. K., Misner, D., and Ranscht, B. (2002). Contactin supports synaptic plasticity associated with hippocampal long-term depression but not potentiation. *Curr. Biol.* 12, 181–190. doi: 10.1016/S0960-9822(02)00680-2

Must, A., Tasa, G., Lang, A., Vasar, E., Kõks, S., Maron, E., et al. (2008). Association of limbic system-associated membrane protein (LSAMP) to male completed suicide. *BMC Med. Genet.* 9:34. doi: 10.1186/1471-2350-9-34

Nava, C., Keren, B., Mignot, C., Rastetter, A., Chantot-Bastaraud, S., Faudet, A., et al. (2014). Prospective diagnostic analysis of copy number variants using SNP microarrays in individuals with autism spectrum disorders. *Eur. J. Hum. Genet.* 22, 71–78. doi: 10.1038/ejhg.2013.88

Niethammer, P., Delling, M., Sytnyk, V., Dityatev, A., Fukami, K., and Schachner, M. (2002). Cosignaling of NCAM via lipid rafts and the FGF receptor is required for neuritogenesis. *J. Cell Biol.* 157, 521–532. doi: 10.1083/jcb.200109059

Nikolaienko, R. M., Hammel, M., Dubreuil, V., Zalmai, R., Hall, D. R., Mehzabeen, N., et al. (2016). Structural basis for interactions between contactin family members and protein-tyrosine phosphatase receptor type G in neural tissues. *J. Biol. Chem.* 291, 21335–21349. doi: 10.1074/jbc.M116.742163

Norenberg, U., Hubert, M., Brummendorf, T., Tarnok, A., and Rathjen, F. G. (1995). Characterization of functional domains of the tenascin-R (restrictin) polypeptide: cell attachment site, binding with F11, and enhancement of F11- mediated neurite outgrowth by tenascin-R. *J. Cell Biol.* 130, 473–484. doi: 10.1083/jcb.130.2.473

Nosten-Bertrand, M., Errington, M. L., Murphy, K. P. S. J., Tokugawa, Y., Barboni, E., Kozlova, E., et al. (1996). Normal spatial learning despite regional inhibition of LTP in mice lacking Thy-1. *Nature* 379, 826–829. doi: 10.1038/379826a0

O'Donovan, M. C., Craddock, N., Norton, N., Williams, H., Peirce, T., Moskvina, V., et al. (2008). Identification of loci associated with schizophrenia by genome-wide association and follow-up. *Nat. Genet.* 40, 1053–1055. doi: 10.1038/ng.201

Ogawa, J., Kaneko, H., Masuda, T., Nagata, S., Hosoya, H., and Watanabe, K. (1996). Novel neural adhesion molecules in the Contactin/F3 subgroup of the immunoglobulin superfamily: isolation and characterization of cDNAs from rat brain. *Neurosci. Lett.* 218, 173–176. doi: 10.1016/S0304-3940(96)13156-6

Oikawa, S., Imajo, S., Noguchi, T., Kosaki, G., and Nakazato, H. (1987). The carcinoembryonic antigen (CEA) contains multiple immunoglobulin-like domains. *Biochem. Biophys. Res. Commun.* 144, 634–642. doi: 10.1016/S0006-291X(87)80013-X

Oikawa, S., Inuzuka, C., Kuroki, M., Arakawa, F., Matsuoka, Y., Kosaki, G., et al. (1991). A specific heterotypic cell adhesion activity between members of carcinoembryonic antigen family, W272 and NCA, is mediated by N-domains. *J. Biol. Chem.* 266, 7995–8001.

Olive, S., Dubois, C., Schachner, M., and Rougon, G. (2002). The F3 neuronal glycosylphosphatidylinositol-linked molecule is localized to glycolipid-enriched membrane subdomains and interacts with L1 and fyn kinase in cerebellum. *J. Neurochem.* 65, 2307–2317. doi: 10.1046/j.1471-4159.1995.65052307.x

Palmeri, A., Privitera, L., Giunta, S., Loreto, C., and Puzzo, D. (2013). Inhibition of phosphodiesterase-5 rescues age-related impairment of synaptic plasticity and memory. *Behav. Brain Res.* 240, 11–20. doi: 10.1016/j.bbr.2012.10.060

Pan, Y., Wang, K. S., and Aragam, N. (2011). NTM and NR3C2 polymorphisms influencing intelligence: family-based association studies. *Prog. Neuropsychopharmacol. Biol. Psychiatry* 35, 154–160. doi: 10.1016/j.pnpbp.2010.10.016

Panichareon, B., Nakayama, K., Thurakitwannakarn, W., Iwamoto, S., and Sukhumsirichart, W. (2012). OPCML gene as a schizophrenia susceptibility locus in Thai population. *J. Mol. Neurosci.* 46, 373–377. doi: 10.1007/s12031-011-9595-2

Paulick, M. G., and Bertozzi, C. R. (2008). The glycosylphosphatidylinositol anchor: a complex membrane-anchoring structure for proteins. *Biochemistry* 47, 6991–7000. doi: 10.1021/bi8006324

Peles, E., Nativ, M., Campbell, P. L., Sakurai, T., Martinez, R., Levt, S., et al. (1995). The carbonic anhydrase domain of receptor tyrosine phosphatase β is a functional ligand for the axonal cell recognition molecule contactin. *Cell* 82, 251–260. doi: 10.1016/0092-8674(95)90312-7

Peles, E., Nativ, M., Lustig, M., Grumet, M., Schilling, J., Martinez, R., et al. (1997). Identification of a novel contactin-associated transmembrane receptor with multiple domains implicated in protein-protein interactions. *EMBO J.* 16, 978–988. doi: 10.1093/emboj/16.5.978

Pimenta, A. F., Fischer, I., and Levitt, P. (1996). cDNA cloning and structural analysis of the human limbic-system-associated membrane protein (LAMP). *Gene* 170, 189–195. doi: 10.1016/0378-1119(96)84698-1

Pischedda, F., and Piccoli, G. (2015). The IgLON family member NEGR1 promotes neuronal arborization acting as soluble factor via FGFR2. *Front. Mol. Neurosci.* 8:89. doi: 10.3389/fnmol.2015.00089

Poliak, S., Salomon, D., Elhanany, H., Sabanay, H., Kiernan, B., Pevny, L., et al. (2003). Juxtaparanodal clustering of Shaker-like K+ channels in myelinated axons depends on Caspr2 and TAG-1. *J. Cell Biol.* 162, 1149–1160. doi: 10.1083/jcb.200305018

Poltorak, M., Frye, M. A., Wright, R., Hemperly, J. J., George, M. S., Pazzaglia, P. J., et al. (1996). Increased neural cell adhesion molecule in the CSF of patients with mood disorder. *J. Neurochem.* 66, 1532–1538. doi: 10.1046/j.1471-4159.1996.66041532.x

Poot, M. (2014). A candidate gene association study further corroborates involvement of contactin genes in autism. *Mol. Syndromol.* 5, 229–235. doi: 10.1159/000362891

Puzzo, D., Bizzoca, A., Loreto, C., Guida, C. A., Gulisano, W., Frasca, G., et al. (2015). Role of F3/contactin expression profile in synaptic plasticity and memory in aged mice. *Neurobiol. Aging* 36, 1702–1715. doi: 10.1016/j.neurobiolaging.2015.01.004

Puzzo, D., Bizzoca, A., Privitera, L., Furnari, D., Giunta, S., Girolamo, F., et al. (2013). F3/Contactin promotes hippocampal neurogenesis, synaptic plasticity, and memory in adult mice. *Hippocampus* 23, 1367–1382. doi: 10.1002/hipo.22186

Qiu, S., Champagne, D. L., Peters, M., Catania, E. H., Weeber, E. J., Levitt, P., et al. (2010). Loss of limbic system-associated membrane protein leads to reduced hippocampal mineralocorticoid receptor expression, impaired synaptic plasticity, and spatial memory deficit. *Biol. Psychiatry* 68, 197–204. doi: 10.1016/j.biopsych.2010.02.013

Querol, L., Nogales-Gadea, G., Rojas-Garcia, R., Martinez-Hernandez, E., Diaz-Manera, J., Suárez-Calvet, X., et al. (2013). Antibodies to contactin-1 in chronic inflammatory demyelinating polyneuropathy. *Ann. Neurol.* 73, 370–380. doi: 10.1002/ana.23794

Rader, C., Stoeckli, E. T., Ziegler, U., Osterwalder, T., Kunz, B., and Sonderegger, P. (1993). Cell-cell adhesion by homophilic interaction of the neuronal recognition molecule axonin-1. *Eur. J. Biochem.* 215, 133–141. doi: 10.1111/j.1432-1033.1993.tb18015.x

Ranheim, T. S., Edelman, G. M., and Cunningham, B. A. (1996). Homophilic adhesion mediated by the neural cell adhesion molecule involves multiple immunoglobulin domains. *Proc. Natl. Acad. Sci. U.S.A.* 93, 4071–4075. doi: 10.1073/pnas.93.9.4071

Ranscht, B. (1988). Sequence of contactin, a 130-kD glycoprotein concentrated in areas of interneuronal contact, defines a new member of the immunoglobulin supergene family in the nervous system. *J. Cell Biol.* 107, 1561–1573. doi: 10.1083/jcb.107.4.1561

Reed, J., McNamee, C., Rackstraw, S., Jenkins, J., and Moss, D. (2004). Diglons are heterodimeric proteins composed of IgLON subunits, and Diglon-CO inhibits neurite outgrowth from cerebellar granule cells. *J. Cell Sci.* 117, 3961–3973. doi: 10.1242/jcs.01261

Rios, J. C., Melendez-Vasquez, C. V., Einheber, S., Lustig, M., Grumet, M., Hemperly, J., et al. (2000). Contactin-associated protein (Caspr) and contactin form a complex that is targeted to the paranodal junctions during myelination. *J. Neurosci.* 20, 8354–8364.

Rubio-Marrero, E. N., Vincelli, G., Jeffries, C. M., Shaikh, T. R., Pakos, I. S., Ranaivoson, F. M., et al. (2016). Structural characterization of the extracellular domain of CASPR2 and insights into its association with the novel ligand contactin1. *J. Biol. Chem.* 291, 5788–5802. doi: 10.1074/jbc.M115.705681

Sabater, L., Planagumà, J., Dalmau, J., and Graus, F. (2016). Cellular investigations with human antibodies associated with the anti-IgLON5 syndrome. *J. Neuroinflammation* 13, 226. doi: 10.1186/s12974-016-0689-1

Sanz, R., Ferraro, G. B., and Fournier, A. E. (2015). IgLON cell adhesion molecules are shed from the cell surface of cortical neurons to promote neuronal growth. *J. Biol. Chem.* 290, 4330–4342. doi: 10.1074/jbc.M114.628438

Schol-Gelok, S., Janssens, A. C. J. W., Tiemeier, H., Liu, F., Lopez-Leon, S., Zorkoltseva, I. V., et al. (2010). A genome-wide screen for depression in two independent dutch populations. *Biol. Psychiatry* 68, 187–196. doi: 10.1016/j.biopsych.2010.01.033

Schroeder, R., London, E., and Brown, D. (1994). Interactions between saturated acyl chains confer detergent resistance on lipids and glycosylphosphatidylinositol (GPI)-anchored proteins: GPI-anchored proteins in liposomes and cells show similar behavior. *Proc. Natl. Acad. Sci. U.S.A.* 91, 12130–12134. doi: 10.1073/pnas.91.25.12130

Shimoda, Y., Koseki, F., Itoh, M., Toyoshima, M., and Watanabe, K. (2012). A cis-complex of NB-2/contactin-5 with amyloid precursor-like protein 1 is localized on the presynaptic membrane. *Neurosci. Lett.* 510, 148–153. doi: 10.1016/j.neulet.2012.01.026

Simon, P. D., McConnell, J., Zurakowski, D., Vorwerk, C. K., Naskar, R., Grosskreutz, C. L., et al. (1999). Thy-1 is critical for normal retinal development. *Dev. Brain Res.* 117, 219–223. doi: 10.1016/S0165-3806(99)00123-6

Simons, K., and Ikonen, E. (1997). Functional rafts in cell membranes. *Nature* 387, 569–572. doi: 10.1038/42408

Soroka, V., Kolkova, K., Kastrup, J. S., Diederichs, K., Breed, J., Kiselyov, V. V., et al. (2003). Structure and interactions of NCAM Ig1-2-3 suggest a novel zipper mechanism for homophilic adhesion. *Structure* 11, 1291–1301. doi: 10.1016/j.str.2003.09.006

Stoeckli, E. T., Kuhn, T. B., Duc, C. O., Ruegg, M. A., and Sonderegger, P. (1991). The axonally secreted protein axonin-1 is a potent substratum for neurite growth. *J. Cell Biol.* 112, 449–455. doi: 10.1083/jcb.112.3.449

Stogmann, E., Reinthaler, E., Eltawil, S., El Etribi, M. A., Hemeda, M., El Nahhas, N., et al. (2013). Autosomal recessive cortical myoclonic tremor and epilepsy: association with a mutation in the potassium channel associated gene CNTN2. *Brain* 136, 1155–1160. doi: 10.1093/brain/awt068

Stohl, W., and Gonatas, N. K. (1977). Distribution of the thy-1 antigen in cellular and subcellular fractions of adult mouse brain. *J. Immunol.* 119, 422–427.

Struyk, A. F., Canoll, P. D., Wolfgang, M. J., Rosen, C. L., D'Eustachio, P., and Salzer, J. L. (1995). Cloning of neurotrimin defines a new subfamily of differentially expressed neural cell adhesion molecules. *J. Neurosci.* 15, 2141–2156.

Südhof, T. C. (2008). Neuroligins and neurexins link synaptic function to cognitive disease. *Nature* 455, 903–911. doi: 10.1038/nature07456

Sytnyk, V., Leshchyns'ka, I., and Schachner, M. (2017). Neural cell adhesion molecules of the immunoglobulin superfamily regulate synapse formation, maintenance, and function. *Trends Neurosci.* 40, 295–308. doi: 10.1016/j.tins.2017.03.003

Taheri, M., Saragovi, U., Fuks, A., Makkerh, J., Mort, J., and Stanners, C. P. (2000). Self recognition in the Ig superfamily: identification of precise subdomains in carcinoembryonic antigen required for intercellular adhesion. *J. Biol. Chem.* 275, 26935–26943. doi: 10.1074/jbc.M909242199

Takamori, S., Holt, M., Stenius, K., Lemke, E. A., Grønborg, M., Riedel, D., et al. (2006). Molecular anatomy of a trafficking organelle. *Cell* 127, 831–846. doi: 10.1016/j.cell.2006.10.030

Tamási, V., Petschner, P., Adori, C., Kirilly, E., Ando, R. D., Tothfalusi, L., et al. (2014). Transcriptional evidence for the role of chronic venlafaxine treatment in neurotrophic signaling and neuroplasticity including also glutatmatergic- and insulin-mediated neuronal processes. *PLOS ONE* 9:e113662. doi: 10.1371/journal.pone.0113662

Tassano, E., Gamucci, A., Celle, M. E., Ronchetto, P., Cuoco, C., and Gimelli, G. (2015). Clinical and molecular cytogenetic characterization of a de novo interstitial 1p31.1p31.3 deletion in a boy with moderate intellectual disability and severe language impairment. *Cytogenet. Genome Res.* 146, 39–43. doi: 10.1159/000431391

Traka, M., Goutebroze, L., Denisenko, N., Bessa, M., Nifli, A., Havaki, S., et al. (2003). Association of TAG-1 with Caspr2 is essential for the molecular

organization of juxtaparanodal regions of myelinated fibers. *J. Cell Biol.* 162, 1161–1172. doi: 10.1083/jcb.200305078

Treubert, U., and Brümmendorf, T. (1998). Functional cooperation of beta1-integrins and members of the Ig superfamily in neurite outgrowth induction. *J. Neurosci.* 18, 1795–1805.

Van Daalen, E., Kemner, C., Verbeek, N. E., Van Der Zwaag, B., Dijkhuizen, T., Rump, P., et al. (2011). Social responsiveness scale-aided analysis of the clinical impact of copy number variations in autism. *Neurogenetics* 12, 315–323. doi: 10.1007/s10048-011-0297-2

Varma, R., and Mayor, S. (1998). GPI-anchored proteins are organized in submicron domains at the cell surface. *Nature* 394, 798–801. doi: 10.1038/29563

Veerappa, A. M., Saldanha, M., Padakannaya, P., and Ramachandra, N. B. (2013). Genome-wide copy number scan identifies disruption of PCDH11X in developmental dyslexia. *Am. J. Med. Genet. Part B Neuropsychiatr. Genet.* 162, 889–897. doi: 10.1002/ajmg.b.32199

Walmod, P. S., Kolkova, K., Berezin, V., and Bock, E. (2004). Zippers make signals: NCAM-mediated molecular interactions and signal transduction. *Neurochem. Res.* 29, 2015–2035. doi: 10.1007/s11064-004-6875-z

Wang, W., Karagogeos, D., and Kilpatrick, D. L. (2011). The effects of Tag-1 on the maturation of mouse cerebellar granule neurons. *Cell. Mol. Neurobiol.* 31, 351–356. doi: 10.1007/s10571-010-9641-6

Williams, A. F., and Barclay, A. N. (1988). The immunoglobulin superfamily—domains for cell surface recognition. *Annu. Rev. Immunol.* 6, 381–405. doi: 10.1146/annurev.iy.06.040188.002121

Williams, A. F., and Gagnon, J. (1982). Neuronal cell Thy-1 glycoprotein: homology with immunoglobulin. *Science* 216, 696–703. doi: 10.1126/science.6177036

Yamada, M., Hashimoto, T., Hayashi, N., Higuchi, M., Murakami, A., Nakashima, T., et al. (2007). Synaptic adhesion molecule OBCAM; synaptogenesis and dynamic internalization. *Brain Res.* 1165, 5–14. doi: 10.1016/j.brainres.2007.04.062

Yamagata, M., and Sanes, J. R. (2012). Expanding the immunoglobulin superfamily code for laminar specificity in retina: expression and role of contactins. *J. Neurosci.* 32, 14402–14414. doi: 10.1523/JNEUROSCI.3193-12.2012

Ye, H., Tan, Y. L. J., Ponniah, S., Takeda, Y., Wang, S.-Q., Schachner, M., et al. (2008). Neural recognition molecules CHL1 and NB-3 regulate apical dendrite orientation in the neocortex via PTP alpha. *EMBO J.* 27, 188–200. doi: 10.1038/sj.emboj.7601939

Yoshihara, Y., Kawasaki, M., Tamada, A., Nagata, S., Kagamiyama, H., and Mori, K. (1995). Overlapping and differential expression of BIG-2, BIG-1, TAG-1, and F3: four members of an axon-associated cell adhesion molecule subgroup of the immunoglobulin superfamily. *J. Neurobiol.* 28, 51–69. doi: 10.1002/neu.480280106

Yoshihara, Y., Kawasaki, M., Tani, A., Tamada, A., Nagata, S., Kagamiyama, H., et al. (1994). BIG-1: a new TAG-1/F3-related member of the immunoglobulin superfamily with neurite outgrowth-promoting activity. *Neuron* 13, 415–426. doi: 10.1016/0896-6273(94)90357-3

Yoshihara, Y., Oka, S., Ikeda, J., and Mori, K. (1991). Immunoglobulin superfamily molecules in the nervous system. *Neurosci. Res.* 10, 83–105. doi: 10.1016/0168-0102(91)90033-U

Zacco, A., Cooper, V., Chantler, P. D., Fisher-Hyland, S., Horton, H. L., and Levitt, P. (1990). Isolation, biochemical characterization and ultrastructural analysis of the limbic system-associated membrane protein (LAMP), a protein expressed by neurons comprising functional neural circuits. *J. Neurosci.* 10, 73–90.

Zacharias, U. (2002). Tenascin-R induces actin-rich microprocesses and branches along neurite shafts. *Mol. Cell. Neurosci.* 21, 626–633. doi: 10.1006/mcne.2002.1203

Zhou, H., Fuks, A., Alcaraz, G., Bolling, T. J., and Stanners, C. P. (1993). Homophilic adhesion between Ig superfamily carcinoembryonic antigen molecules involves double reciprocal bonds. *J. Cell Biol.* 122, 951–960. doi: 10.1083/jcb.122.4.951

Zhukareva, V., and Levitt, P. (1995). The limbic system-associated membrane protein (LAMP) selectively mediates interactions with specific central neuron populations. *Development* 121, 1161–1172.

Zuellig, R. A., Rader, C., Schroeder, A., Kalousek, M. B., Von Bohlen und Halbach, F., Osterwalder, T., et al. (1992). The axonally secreted cell adhesion molecule, axonin-1. Primary structure, immunoglobulin-like and fibronectin-type-III-like domains and glycosyl-phosphatidylinositol anchorage. *Eur. J. Biochem.* 204, 453–463. doi: 10.1111/j.1432-1033.1992.tb16655.x

Conflict of Interest Statement: The authors declare that the research was conducted in the absence of any commercial or financial relationships that could be construed as a potential conflict of interest.

frontiers in Molecular Neuroscience

MINI REVIEW
published: 13 November 2017
doi: 10.3389/fnmol.2017.00381

Roles of Glial Cells in Sculpting Inhibitory Synapses and Neural Circuits

*Ji Won Um**

Department of Brain and Cognitive Sciences, Daegu Gyeongbuk Institute of Science and Technology (DGIST), Daegu, South Korea

Glial cells are essential for every aspect of normal neuronal development, synapse formation, and function in the central nervous system (CNS). Astrocytes secrete a variety of factors that regulate synaptic connectivity and circuit formation. Microglia also modulate synapse development through phagocytic activity. Most of the known actions of CNS glial cells are limited to roles at excitatory synapses. Nevertheless, studies have indicated that both astrocytes and microglia shape inhibitory synaptic connections through various mechanisms, including release of regulatory molecules, direct contact with synaptic terminals, and utilization of mediators in the extracellular matrix. This review summarizes recent investigations into the mechanisms underlying CNS glial cell-mediated inhibitory synapse development.

Keywords: astrocytes, glia, inhibitory synapse, neural circuits, neurons

INTRODUCTION

Synapses are the fundamental information-processing units underlying neuronal networks in the brain. It is across synapses that neurons receive excitatory synaptic inputs from neighboring glutamatergic neurons and inhibitory inputs from various γ-aminobutyric acid-expressing (GABAergic) interneurons. In particular, GABAergic interneurons play important roles in controlling the properties of pyramidal neurons, such as firing frequency, to shape the activity of neuronal networks, and contribute to the generation of cortical rhythms (Buzsáki and Draguhn, 2004; Bartos et al., 2007; Bonifazi et al., 2009; Jensen and Mazaheri, 2010; Kullmann, 2011). An imbalance in the ratio of excitatory to inhibitory (E/I) synaptic activity has emerged as a shared pathophysiological mechanism in several neuropsychiatric disorders, including autism spectrum disorder (ASD) and schizophrenia, and in neurological disorders such as epilepsy (Lee et al., 2017). Thus, investigations of the key molecular mechanisms underlying both excitatory and inhibitory synapse development collectively contribute to a comprehensive understanding of the pathophysiological mechanisms of brain disorders.

Over the past 20 years, numerous studies have shown that various types of glial cells actively and distinctively participate in the control of various neuronal processes in both the peripheral nervous system (PNS) and central nervous system (CNS; Pfrieger and Barres, 1996; Christopherson et al., 2005; Perea et al., 2009; Eroglu and Barres, 2010; Stipursky et al., 2011). Among these cell types, astrocytes have received the most attention because of their crucial roles in synapse formation, transmission and plasticity (Clarke and Barres, 2013; Baldwin and Eroglu, 2017). Astrocytes are not uniform throughout the CNS; rather, depending on the brain region, they exhibit differences in characteristics ranging from cell shape to protein composition (Chai et al., 2017). Thus, astrocytes may execute their differential functions in a brain region-specific manner.

OPEN ACCESS

Edited by:
Chen Zhang,
Peking University, China

Reviewed by:
Yan Gu,
Zhejiang University, China
Arturo Ortega,
Center for Research and Advanced Studies of the National Polytechnic Institute (CINVESTAV), Mexico

***Correspondence:**
Ji Won Um
jiwonum@dgist.ac.kr

Received: *26 September 2017*
Accepted: *01 November 2017*
Published: *13 November 2017*

Citation:
Um JW (2017) Roles of Glial Cells in Sculpting Inhibitory Synapses and Neural Circuits.
Front. Mol. Neurosci. 10:381.
doi: 10.3389/fnmol.2017.00381

In this context, it has been reported that astrocyte-conditioned media (ACM) from different brain regions possess different excitatory synaptogenic properties, reflecting distinct expression profiles of astrocyte-derived synaptogenic molecules, such as glypicans, SPARC (secreted protein acidic and cysteine rich) and hevin (also known as SPARC-like 1 [SPARCL1]) in astrocytes from different brain regions (Buosi et al., 2017). Similarly, the inhibitory synaptogenic potential of astrocytes may also differ in distinct brain regions owing to the unique expression profiles of various glial genes, a potential that warrants further investigation.

Microglia also impact synaptic functions through release of specific molecules that influence the phagocytic activities involved in synapse elimination (Wu et al., 2015). Although the various mechanisms underlying glia-mediated excitatory synapse development have been well established (Nagler et al., 2001; Ullian et al., 2001, 2004; Risher et al., 2014), the roles of glial cells in inhibitory synapse development have only recently been investigated. In the present review, I focus on the actions of glial cells in orchestrating inhibitory synapse development and relevant neural circuits. Additionally, where possible I highlight the implications of these mechanisms for various brain disorders. The roles of glial cells in excitatory synapse development have been the subject of excellent recent reviews (Perea et al., 2009; Chung et al., 2015) and will not be addressed here in detail.

The main role of oligodendrocytes is to generate myelin sheaths around axons (Barres, 2008), but a few studies have shown that a new class of glial cells—proteoglycan NG2-positive oligodendrocyte precursor cells (OPCs)—receive the input from glutamatergic or GABAergic neurons (Bergles et al., 2000; Lin and Bergles, 2004; Lin et al., 2005). However, the precise function of these direct contacts remains to be investigated; thus, the related topic is not covered in the current review.

ROLES OF ASTROCYTIC FACTORS IN REGULATING INHIBITORY SYNAPSE STRUCTURE AND FUNCTION

Astrocyte-Secreted Factors

Results from various studies have indicated that astrocytes regulate synaptic transmission and plasticity, partly via the release of gliotransmitters, such as glutamate, D-serine or ATP, in response to activity-dependent calcium influx (Zhang et al., 2003; Fellin et al., 2004; Volterra and Meldolesi, 2005; Haydon and Carmignoto, 2006; Jourdain et al., 2007; Perea et al., 2009; Araque et al., 2014). For example, it has been shown that astrocyte-derived DISC1 (disrupted in schizophrenia-1) is involved in dendritic arborization and maturation of excitatory, but not inhibitory, synapses by modulating D-serine production in a hippocampal neuron-astrocyte coculture system (Xia et al., 2016). Astrocyte-derived ATP was recently shown to regulate the excitability of cholecystokinin (CCK)-positive interneurons through activation of P2Y1 purinergic receptors (Tan et al., 2017). In addition to the above-mentioned gliotransmitters, astrocytes release a number of substances including thrombospondin, hevin, SPARC, transforming growth factor-β1 (TGF-β1), glypican 4/6, semaphorin 3A, γ-protocadherin (γ-Pcdh), ephrin-A3, cholesterol and brain-derived neurotrophic factor (BDNF), that are involved in directing the formation of synapses and ultimately building specific neural circuits (Baldwin and Eroglu, 2017).

In contrast, the impact of astrocytes on inhibitory synapse development has been largely unexplored. There are signaling pathways that link astrocytes with the GABA system, as suggested by earlier studies showing that astrocytes potentiate GABA-mediated currents in hippocampal cultured neurons (Liu et al., 1996, 1997). Moreover, astrocytes increase inhibitory synaptic transmission in hippocampal CA1 pyramidal neurons through astrocytic calcium signaling (Kang et al., 1998). Because the addition of ACM to neuronal cultures also induces GABAergic synapse-promoting effects similar to those observed in a neuron-astrocyte coculture system (Liu et al., 1996, 1997), it is possible that astrocytes secrete substances that are crucial for inhibitory synaptogenesis. In cultured hippocampal neurons, astrocyte-induced increases in the number of $GABA_A$ receptor clusters were shown to be compromised by scavenging BDNF, indicating that signaling pathways involving BDNF and its receptor, tropomyosin receptor kinase B (TrkB), are required for astrocyte-mediated facilitation of inhibitory synapse development (Elmariah et al., 2005; **Figure 1**). Strikingly, astrocytic BDNF is not required for modulation of $GABA_A$ receptor clustering, as evidenced by the fact that ACM from astrocytic-BDNF-deficient mice retains the ability to potentiate $GABA_A$ receptor clustering (Elmariah et al., 2005). This suggests that unknown factors from astrocytes govern neuronal BDNF-TrkB signaling to promote inhibitory synapse development. In addition to modulating $GABA_A$ receptor clustering, soluble astrocyte-derived factors selectively enhance axon length, branching, synapse number and function of GABAergic inhibitory neurons (Hughes et al., 2010). Intriguingly, thrombospondins, which positively regulate excitatory synapses, do not promote inhibitory synaptogenesis (Hughes et al., 2010).

Several astrocyte-secreted factors have recently been identified as inhibitory synapse regulators. For example, astrocyte-derived endozepines, endogenous ligands with benzodiazepine-like effects, potentiate synaptic inhibition in the thalamic reticular nucleus (Christian and Huguenard, 2013). In addition, TGF-β secreted by human and murine astrocytes induces inhibitory synapse formation in cortical cultured neurons (Diniz et al., 2014). In this latter study, disruption of calcium/calmodulin-dependent protein kinase II (CaMKII) function by either pharmacological inhibition or RNA interference (RNAi)-based knockdown abrogated ACM-triggered inhibitory synapse development, as assessed by clustering of inhibitory synaptic marker proteins (Diniz et al., 2014). Collectively, these results suggest that the TGF-β/CaMKII signaling pathway constitutes a key mechanism underlying astrocyte-mediated inhibitory synapse development (**Figure 1**), and that astrocytes regulate the synaptic E/I balance through a variety of molecular pathways.

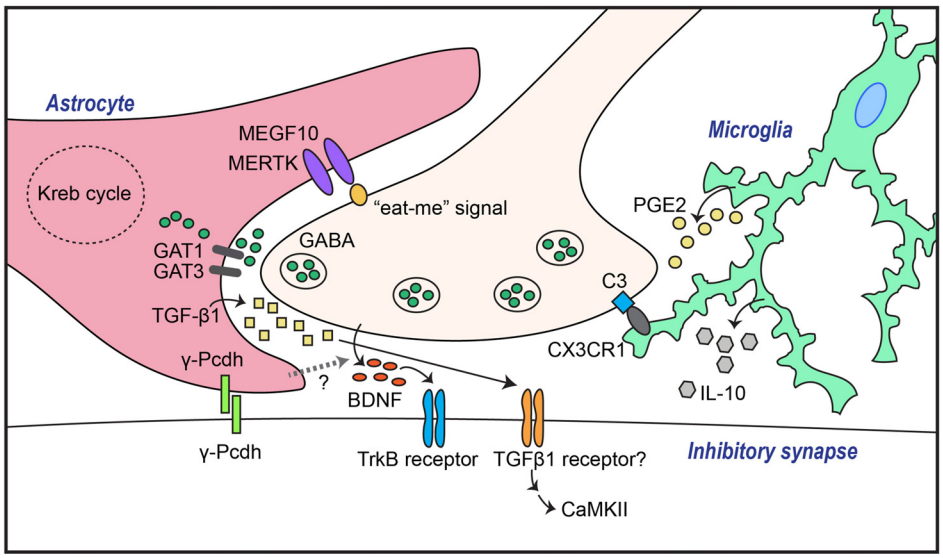

FIGURE 1 | Astrocytes and microglia mediate both GABAergic synapse formation and elimination through a variety of molecular mechanisms. Transforming growth factor-β1 (TGF-β1) secreted from astrocytes induces inhibitory synapse formation through activation of neuronal calcium/calmodulin-dependent protein kinase II (CaMKII). In addition, GABAergic inhibitory synapse formation is regulated by astrocytic γ-Pcdh-mediated adhesion events, astrocytic GABA transporters (GATs), and/or unidentified factors that control neuronal brain-derived neurotrophic factor (BDNF)-TrkB signaling. Synapse elimination is mediated by astrocytic recognition of the so-called "eat-me" signal on neuronal membranes through pathways involving MEGF10 and MERTK, or by microglial recognition of complement C3 expression through complement receptor 3 (CR3), followed by phagocytosis.

Extracellular Matrix Molecules

Astrocyte-derived ECM molecules are additional important factors that regulate key synaptic processes (Dityatev and Schachner, 2003; Christopherson et al., 2005; Faissner et al., 2010). Several studies have demonstrated that chondroitin sulfate proteoglycans (CSPGs) are involved in the regulation of synaptic plasticity (Pizzorusso et al., 2002; Frischknecht et al., 2009; Gogolla et al., 2009). Treatment with chondroitinase ABC (ChABC), an enzyme that eliminates CS chains, was shown to massively impair excitatory synaptic transmission in cultured hippocampal neurons (Pyka et al., 2011). However, inhibitory synaptic transmission was not affected (Pyka et al., 2011), indicating that the effects of CSPGs are restricted to excitatory synapses. Whether other ECMs are involved in specifically regulating inhibitory synapse development remains to be determined.

Perineuronal nets (PNNs)—specialized ECM structures surrounding neuronal soma and dendrites, particularly fast-spiking parvalbumin-positive (PV^+) interneurons—inhibit synapse formation and reorganization (Sorg et al., 2016). Various proteoglycans, including neurocan, aggrecan, tenascins and hyaluronan, are concentrated in PNNs, and induction of their degradation by enzymatic treatment or genetic ablation leads to increased excitability of PV^+ cells (Dityatev et al., 2007; Kim et al., 2016). PV^+-interneurons are involved in the generation of synchronous γ-oscillations, which coordinate the activation of principal pyramidal neurons to maintain appropriate information processing and E/I balance, suggesting that components of PNNs involving PV^+-interneurons may play an important role in fine-tuning the connectivity and/or activity of neural circuits. Disruption of this circuit formation manifest as pathophysiological correlates of discrete brain disorders, including epilepsy.

Cell-Surface Proteins

Direct adhesion between neurons and astrocytes is also critical for synapse development. One factor that mediates astrocyte-neuron adhesion is γ-Pcdh, which promotes synaptogenesis through homophilic interactions (Frank and Kemler, 2002). Astrocytic γ-Pcdh promotes both excitatory and inhibitory synapse development, as revealed by genetic ablation of γ-Pcdh in either neurons or astrocytes (Garrett and Weiner, 2009; **Figure 1**). More than 20 adhesion proteins identified to date in pre- and postsynaptic membranes have been shown to organize various aspects of neuronal development processes (Um and Ko, 2013). However, whether these proteins are exclusively expressed in either neurons or glial cells, or both, has not been systematically investigated. Thus, it is conceivable that additional, as yet undiscovered, membrane proteins are involved in astrocyte-neuron adhesion processes.

Synapse elimination is crucial for normal synapse development across the CNS and PNS (Eroglu and Barres, 2010; Neniskyte and Gross, 2017). Excess synapses that form initially are removed during brain development to enable functional neural circuit formation. Recent studies have shown that astrocytes are involved in eliminating both excess excitatory and inhibitory synapse structures, likely through interactions of astrocytic multiple epidermal growth

factor-like domains 10 (MEGF10) and MER proto-oncogene, tyrosine kinase (MERK) with unidentified neuronal membrane proteins (Chung et al., 2013, 2015). Phosphatidylserine, acting as an "eat-me" signal, drives remodeling of the synaptic architecture during brain development by binding to astrocytic MEGF10 and MERTK, which leads to phagocytosis (Chung et al., 2013; **Figure 1**). A recent study showed that astrocytes regulate synapse elimination through the release of ATP via a mechanism that is dependent on the type II inositol 1,4,5-triphosphate receptor (Yang et al., 2016). However, further studies are required to uncover the precise mechanisms underlying astrocyte-mediated synapse elimination. It further remains to be determined whether astrocytes are involved in eliminating both synapse types, and whether shared or distinct signaling pathways are involved in these processes. More importantly, how interactions of astrocytes, microglia, and neurons coordinate synapse elimination remains to be elucidated.

Miscellaneous Factors

In addition to the mechanisms highlighted above, the modulation of GABAergic synapse development depends on a series of astrocytic metabolic pathways of the Krebs cycle (Kaczor et al., 2015; Kaczor and Mozrzymas, 2017). For example, inhibitory synapse number and transmission are increased and plasticity is enhanced in neurons cocultured with astrocytes compared to those cultured alone (Kaczor et al., 2015; Kaczor and Mozrzymas, 2017). These effects of astrocyte coculture disappear following treatment with a subset of selective Krebs cycle inhibitors, such as fluoroacetate, indicating the involvement of key astrocyte-expressed metabolic enzymes in GABAergic plasticity.

Because GABA in the extrasynaptic space shapes inhibitory synaptic transmission, it is conceivable that inhibitory synaptic transmission is regulated by the activity and/or level of GABA transporters (GATs). Four types of GATs (GAT1–4) have been identified in humans and rats. GAT1 and GAT3, in particular, are strongly expressed in astrocytes (Vitellaro-Zuccarello et al., 2003). Indeed, changes in astrocytic GAT1 or -3 expression level or activity alter inhibitory synaptic transmission in hippocampal interneurons (Beenhakker and Huguenard, 2010; Shigetomi et al., 2012; Kersanté et al., 2013; Muthukumar et al., 2014), suggesting that astrocytic GATs control the excitability of neurons in a neural network through regulation of extracellular GABA levels (**Figure 1**). Thus, astrocytic GATs may be considered potential therapeutic targets for neurological and psychiatric disorders.

ROLES OF ASTROCYTES IN REGULATING THE FORMATION OF INHIBITORY INPUTS IN NEURAL CIRCUITS DURING EMBRYONIC DEVELOPMENT

Although the roles of glial cells in shaping neural circuits, particularly those that modulate GABAergic synaptic properties, remain largely unexplored, a few studies have implicated astrocytes in dictating the properties of discrete neural circuits. For example, in the auditory brainstem, inhibitory projections from the superior olivary nucleus (SON) to the nucleus laminaris (NL) are established during embryonic development (Burger et al., 2005). Treatment of organotypic slices from the avian auditory brainstem with ACM enhances the number of inhibitory synaptic inputs onto NL neurons, suggesting that soluble factors secreted by astrocytes promote inhibitory synaptogenesis during embryonic development (Korn et al., 2012; Cramer and Rubel, 2016). In the cerebellar cortex, Bergmann glial cells, a type of highly polarized astrocyte, guide stellate axons to form inhibitory synapses onto Purkinje neuronal dendrites during postnatal development (Ango et al., 2008), underscoring the importance of glial cells in shaping the cerebellar circuitry. Genetic deletion of specific developmental populations of astrocytes in the spinal cord was shown to increase inhibitory synapse numbers, but decrease excitatory synapse numbers (Tsai et al., 2012). These results indicate that astrocytes are crucial for maintaining the appropriate E/I ratio at synapses and neural circuits in the spinal cord. In the microcircuit connecting the thalamic reticular nucleus and ventrobasal nucleus, astrocytes regulate synaptic inhibition through endozepines and GATs (Khakh and Sofroniew, 2015). In addition, in the visual cortex, activation of astrocytes enhances the spontaneous firing rate of PV+ interneurons, contributing to shaping diverse sensory information-processing events in the primary visual cortical network (Perea et al., 2014; Ben Haim and Rowitch, 2017).

ROLES OF MICROGLIA IN INHIBITORY SYNAPSE FORMATION AND ELIMINATION

Microglia are the resident macrophages in the CNS. In line with their immune cell identity, microglia have been traditionally investigated as mediators of inflammatory responses and phagocytosis of pathogens and cell debris under pathological conditions (Shemer et al., 2015). However, roles of microglia under normal conditions have recently begun to emerge. During postnatal development, microglia contribute to the reconstruction of neuronal circuits through phagocytosis of excess neuronal synapses and newborn neurons (Stevens et al., 2007; Paolicelli et al., 2011; Tremblay et al., 2011). A variety of molecules are responsible for phagocytosis-mediated synaptic pruning. These include CX3C chemokine receptor 1 (CX3XR1), a receptor of the neuronal chemokine fractalkine, CX3XL1, that is expressed exclusively in microglia (Paolicelli et al., 2011), and complement receptor 3 (CR3), a receptor for complement component C3 located at neuronal synapses (Schafer et al., 2012; **Figure 1**). In addition to their phagocytic activity, microglia also influence synapse development through the release of various factors, such as BDNF (Parkhurst et al., 2013), interleukin (IL)-10 (Lim et al., 2013), ATP (Pascual et al., 2012) and tumor necrosis factor α (TNFα; Lewitus

et al., 2016). In terms of microglial regulation of inhibitory synapses, microglial IL-10 was found to promote both excitatory and inhibitory synapse development in cultured hippocampal neurons (Lim et al., 2013; **Figure 1**). In addition, a recent study demonstrated that activated microglia displace inhibitory GABAergic presynaptic terminals in adult mice, resulting in increased synchronized neuronal activity (Chen et al., 2014). Increased neuronal activity causes an elevation in intracellular calcium levels, leading to activation of CaMKII and increased expression of anti-apoptotic proteins (Chen et al., 2014). These data suggest a novel role of activated microglia in protecting the adult brain in addition to their phagocytic role (Chen et al., 2014). Further studies are required to establish the molecular factors involved in evoking protective microglia in brain disease states. In addition to GABAergic synapses, glycinergic inhibitory synapses are also regulated by microglia (Cantaut-Belarif et al., 2017). Stimulated microglia acutely regulate glycinergic synapse development in the spinal cord by modulating the activity of microglial prostaglandin E2 (PGE2; Cantaut-Belarif et al., 2017; **Figure 1**).

DISEASE RELEVANCE

Synaptic dysfunction has been considered a hallmark of various neurological diseases, including Alzheimer disease (AD), ASD and schizophrenia (Penzes et al., 2011; Zoghbi and Bear, 2012; Li et al., 2017). Both astrocytes and microglia influence synapse formation and elimination; thus, it is likely that impaired glial function contributes to the onset and progression of neurological disorders. Specifically, dysregulation of glial functions that disrupts the E/I balance at synapses and circuits may lead to disease states. Recently, a rare variant of a microglial gene encoding triggering receptor expressed on myeloid cell 2 (TREM2) has been identified as a risk factor for AD (Jonsson et al., 2013). In addition, microglial activation has been demonstrated in the brains of individuals with ASD or schizophrenia (van Berckel et al., 2008; Voineagu et al., 2011). However, it is not clear how microglial activation is related to synaptic deficits in these diseases. Also, because most published reports have focused on the roles of various glial cells in regulating excitatory synapse formation, function or elimination, the issue of whether glial cells also play critical roles in controlling inhibitory synapse development and function remains to be investigated.

Reactive astrocytes have been associated with many neurological diseases, including epilepsy, AD and stroke (Seifert et al., 2006). Mounting evidence has demonstrated multifaceted functions of reactive astrocytes in disease states, but little is known about the roles of these astrocytes from an inhibitory synapse or circuit perspective. One study showed that, in the astrocytotic region, neurons exhibit reduced inhibitory, but not excitatory, synaptic transmission through actions of the astrocytic glutamate-glutamine cycle, which triggered hyperexcitability in hippocampal circuits (Ortinski et al., 2010). Given the significance of GABAergic inhibition in neuronal circuits, these studies underscore the functional consequences of astrocytosis for neurological diseases as well as alterations of neuronal circuits, with attendant effects on cognition, learning and memory and epileptic seizures.

Extensive evidence has linked microglia to neuroinflammation, which in turn is associated with a variety of neurodegenerative diseases. However, impacts of microglia on the sculpting of synaptic connectivity have only recently been reported. Microglia in the healthy brain have been shown to function in the refinement of synapses in brain development, as described above. Disruption of microglial complement proteins or receptor proteins results in abnormal synaptic wiring (Paolicelli et al., 2011; Schafer et al., 2012), which may contribute to the synaptic abnormalities observed in several neurodevelopmental disorders.

CONCLUDING REMARKS

In this review, I have highlighted recent literature reports that collectively reveal the various roles of astrocytes and microglia in regulating inhibitory synapse development and neural circuits. Considered in light of the essential role of GABAergic synapses in shaping network activity through filtering of incoming neural information and dictating the activity of principal neurons, the cellular and molecular mechanisms underlying inhibitory synapse structure, transmission, and plasticity mediated by various glial cell types should be comprehensible. Although recent technological developments have accelerated advances in our understanding of the roles of glial cells in various aspects of synapse development, only a few studies have provided mechanistic insights into the contributions of various glial cell types to the development of GABAergic synapses and relevant neural circuits. Investigations of unidentified astrocyte- and microglia-based mechanisms that direct the development of GABAergic synapses and neural circuits will not only enhance our understanding of synapse development in health, but also guide the development of novel therapeutic strategies against various brain disorders.

AUTHOR CONTRIBUTIONS

JWU wrote the manuscript.

FUNDING

Work on this topic in my laboratory has been supported by grants from the DGIST R&D Program of the Ministry of Science, ICT and Future Planning (2017020004 to JWU) and from the Ministry for Health and Welfare Affairs, Republic of Korea (HI15C3026 to JWU).

ACKNOWLEDGMENTS

The author thanks Dr. Jaewon Ko (DGIST, South Korea) for valuable discussions and for critically reviewing the initial manuscript.

REFERENCES

Ango, F., Wu, C., Van der Want, J. J., Wu, P., Schachner, M., and Huang, Z. J. (2008). Bergmann glia and the recognition molecule CHL1 organize GABAergic axons and direct innervation of Purkinje cell dendrites. *PLoS Biol.* 6:e103. doi: 10.1371/journal.pbio.0060103

Araque, A., Carmignoto, G., Haydon, P. G., Oliet, S. H., Robitaille, R., and Volterra, A. (2014). Gliotransmitters travel in time and space. *Neuron* 81, 728–739. doi: 10.1016/j.neuron.2014.02.007

Baldwin, K. T., and Eroglu, C. (2017). Molecular mechanisms of astrocyte-induced synaptogenesis. *Curr. Opin. Neurobiol.* 45, 113–120. doi: 10.1016/j.conb.2017.05.006

Barres, B. A. (2008). The mystery and magic of glia: a perspective on their roles in health and disease. *Neuron* 60, 430–440. doi: 10.1016/j.neuron.2008.10.013

Bartos, M., Vida, I., and Jonas, P. (2007). Synaptic mechanisms of synchronized γ oscillations in inhibitory interneuron networks. *Nat. Rev. Neurosci.* 8, 45–56. doi: 10.1038/nrn2044

Beenhakker, M. P., and Huguenard, J. R. (2010). Astrocytes as gatekeepers of $GABA_B$ receptor function. *J. Neurosci.* 30, 15262–15276. doi: 10.1523/JNEUROSCI.3243-10.2010

Ben Haim, L., and Rowitch, D. H. (2017). Functional diversity of astrocytes in neural circuit regulation. *Nat. Rev. Neurosci.* 18, 31–41. doi: 10.1038/nrn.2016.159

Bergles, D. E., Roberts, J. D., Somogyi, P., and Jahr, C. E. (2000). Glutamatergic synapses on oligodendrocyte precursor cells in the hippocampus. *Nature* 405, 187–191. doi: 10.1038/35012083

Bonifazi, P., Goldin, M., Picardo, M. A., Jorquera, I., Cattani, A., Bianconi, G., et al. (2009). GABAergic hub neurons orchestrate synchrony in developing hippocampal networks. *Science* 326, 1419–1424. doi: 10.1126/science.1175509

Buosi, A. S., Matias, I., Araujo, A. P., Batista, C., and Gomes, F. C. (2017). Heterogeneity in synaptogenic profile of astrocytes from different brain regions. *Mol. Neurobiol.* doi: 10.1007/s12035-016-0343-z [Epub ahead of print].

Burger, R. M., Cramer, K. S., Pfeiffer, J. D., and Rubel, E. W. (2005). Avian superior olivary nucleus provides divergent inhibitory input to parallel auditory pathways. *J. Comp. Neurol.* 481, 6–18. doi: 10.1002/cne.20334

Buzsáki, G., and Draguhn, A. (2004). Neuronal oscillations in cortical networks. *Science* 304, 1926–1929. doi: 10.1126/science.1099745

Cantaut-Belarif, Y., Antri, M., Pizzarelli, R., Colasse, S., Vaccari, I., Soares, S., et al. (2017). Microglia control the glycinergic but not the GABAergic synapses via prostaglandin E2 in the spinal cord. *J. Cell Biol.* 216, 2979–2989. doi: 10.1083/jcb.201607048

Chai, H., Diaz-Castro, B., Shigetomi, E., Monte, E., Octeau, J. C., Yu, X., et al. (2017). Neural circuit-specialized astrocytes: transcriptomic, proteomic, morphological, and functional evidence. *Neuron* 95, 531.e9–549.e9. doi: 10.1016/j.neuron.2017.06.029

Chen, Z., Jalabi, W., Hu, W., Park, H. J., Gale, J. T., Kidd, G. J., et al. (2014). Microglial displacement of inhibitory synapses provides neuroprotection in the adult brain. *Nat. Commun.* 5:4486. doi: 10.1038/ncomms5486

Christian, C. A., and Huguenard, J. R. (2013). Astrocytes potentiate GABAergic transmission in the thalamic reticular nucleus via endozepine signaling. *Proc. Natl. Acad. Sci. U S A* 110, 20278–20283. doi: 10.1073/pnas.1318031110

Christopherson, K. S., Ullian, E. M., Stokes, C. C. A., Mullowney, C. E., Hell, J. W., Agah, A., et al. (2005). Thrombospondins are astrocyte-secreted proteins that promote CNS synaptogenesis. *Cell* 120, 421–433. doi: 10.1016/j.cell.2004.12.020

Chung, W. S., Allen, N. J., and Eroglu, C. (2015). Astrocytes control synapse formation, function and elimination. *Cold Spring Harb. Perspect. Biol.* 7:a020370. doi: 10.1101/cshperspect.a020370

Chung, W.-S., Clarke, L. E., Wang, G. X., Stafford, B. K., Sher, A., Chakraborty, C., et al. (2013). Astrocytes mediate synapse elimination through MEGF10 and MERTK pathways. *Nature* 504, 394–400. doi: 10.1038/nature12776

Clarke, L. E., and Barres, B. A. (2013). Emerging roles of astrocytes in neural circuit development. *Nat. Rev. Neurosci.* 14, 311–321. doi: 10.1038/nrn3484

Cramer, K. S., and Rubel, E. W. (2016). Glial cell contributions to auditory brainstem development. *Front. Neural Circuits* 10:83. doi: 10.3389/fncir.2016.00083

Diniz, L. P., Tortelli, V., Garcia, M. N., Araújo, A. P., Melo, H. M., Silva, G. S., et al. (2014). Astrocyte transforming growth factor β1 promotes inhibitory synapse formation via CaM kinase II signaling. *Glia* 62, 1917–1931. doi: 10.1002/glia.22713

Dityatev, A., Brückner, G., Dityateva, G., Grosche, J., Kleene, R., and Schachner, M. (2007). Activity-dependent formation and functions of chondroitin sulfate-rich extracellular matrix of perineuronal nets. *Dev. Neurobiol.* 67, 570–588. doi: 10.1002/dneu.20361

Dityatev, A., and Schachner, M. (2003). Extracellular matrix molecules and synaptic plasticity. *Nat. Rev. Neurosci.* 4, 456–468. doi: 10.1038/nrn1115

Elmariah, S. B., Oh, E. J., Hughes, E. G., and Balice-Gordon, R. J. (2005). Astrocytes regulate inhibitory synapse formation via Trk-mediated modulation of postsynaptic $GABA_A$ receptors. *J. Neurosci.* 25, 3638–3650. doi: 10.1523/JNEUROSCI.3980-04.2005

Eroglu, C., and Barres, B. A. (2010). Regulation of synaptic connectivity by glia. *Nature* 468, 223–231. doi: 10.1038/nature09612

Faissner, A., Pyka, M., Geissler, M., Sobik, T., Frischknecht, R., Gundelfinger, E. D., et al. (2010). Contributions of astrocytes to synapse formation and maturation—Potential functions of the perisynaptic extracellular matrix. *Brain Res. Rev.* 63, 26–38. doi: 10.1016/j.brainresrev.2010.01.001

Fellin, T., Pascual, O., Gobbo, S., Pozzan, T., Haydon, P. G., and Carmignoto, G. (2004). Neuronal synchrony mediated by astrocytic glutamate through activation of extrasynaptic NMDA receptors. *Neuron* 43, 729–743. doi: 10.1016/j.neuron.2004.08.011

Frank, M., and Kemler, R. (2002). Protocadherins. *Curr. Opin. Cell Biol.* 14, 557–562. doi: 10.1016/S0955-0674(02)00365-4

Frischknecht, R., Heine, M., Perrais, D., Seidenbecher, C. I., Choquet, D., and Gundelfinger, E. D. (2009). Brain extracellular matrix affects AMPA receptor lateral mobility and short-term synaptic plasticity. *Nat. Neurosci.* 12, 897–904. doi: 10.1038/nn.2338

Garrett, A. M., and Weiner, J. A. (2009). Control of CNS synapse development by γ-Protocadherin-mediated astrocyte-neuron contact. *J. Neurosci.* 29, 11723–11731. doi: 10.1523/jneurosci.2818-09.2009

Gogolla, N., Caroni, P., Lüthi, A., and Herry, C. (2009). Perineuronal nets protect fear memories from erasure. *Science* 325, 1258–1261. doi: 10.1126/science.1174146

Haydon, P. G., and Carmignoto, G. (2006). Astrocyte control of synaptic transmission and neurovascular coupling. *Physiol. Rev.* 86, 1009–1031. doi: 10.1152/physrev.00049.2005

Hughes, E. G., Elmariah, S. B., and Balice-Gordon, R. J. (2010). Astrocyte secreted proteins selectively increase hippocampal GABAergic axon length, branching, and synaptogenesis. *Mol. Cell. Neurosci.* 43, 136–145. doi: 10.1016/j.mcn.2009.10.004

Jensen, O., and Mazaheri, A. (2010). Shaping functional architecture by oscillatory α activity: gating by inhibition. *Front. Hum. Neurosci.* 4:186. doi: 10.3389/fnhum.2010.00186

Jonsson, T., Stefansson, H., Steinberg, S., Jonsdottir, I., Jonsson, P. V., Snaedal, J., et al. (2013). Variant of TREM2 associated with the risk of Alzheimer's disease. *N Engl J. Med.* 368, 107–116. doi: 10.1056/NEJMoa1211103

Jourdain, P., Bergersen, L. H., Bhaukaurally, K., Bezzi, P., Santello, M., Domercq, M., et al. (2007). Glutamate exocytosis from astrocytes controls synaptic strength. *Nat. Neurosci.* 10, 331–339. doi: 10.1038/nn1849

Kaczor, P. T., and Mozrzymas, J. W. (2017). Key metabolic enzymes underlying astrocytic upregulation of GABAergic plasticity. *Front. Cell. Neurosci.* 11:144. doi: 10.3389/fncel.2017.00144

Kaczor, P., Rakus, D., and Mozrzymas, J. W. (2015). Neuron-astrocyte interaction enhance GABAergic synaptic transmission in a manner dependent on key metabolic enzymes. *Front. Cell. Neurosci.* 9:120. doi: 10.3389/fncel.2015.00120

Kang, J., Jiang, L., Goldman, S. A., and Nedergaard, M. (1998). Astrocyte-mediated potentiation of inhibitory synaptic transmission. *Nat. Neurosci.* 1, 683–692. doi: 10.1038/3684

Kersanté, F., Rowley, S. C. S., Pavlov, I., Gutièrrez-Mecinas, M., Semyanov, A., Reul, J. M. H. M., et al. (2013). A functional role for both γ-aminobutyric acid (GABA) transporter-1 and GABA transporter-3 in the modulation of extracellular GABA and GABAergic tonic conductances in the rat hippocampus. *J. Physiol.* 591, 2429–2441. doi: 10.1113/jphysiol.2012.246298

Khakh, B. S., and Sofroniew, M. V. (2015). Diversity of astrocyte functions and phenotypes in neural circuits. *Nat. Neurosci.* 18, 942–952. doi: 10.1038/nn.4043

Kim, S. Y., Porter, B. E., Friedman, A., and Kaufer, D. (2016). A potential role for glia-derived extracellular matrix remodeling in postinjury epilepsy. *J. Neurosci. Res.* 94, 794–803. doi: 10.1002/jnr.23758

Korn, M. J., Koppel, S. J., Li, L. H., Mehta, D., Mehta, S. B., Seidl, A. H., et al. (2012). Astrocyte-secreted factors modulate the developmental distribution of inhibitory synapses in nucleus laminaris of the avian auditory brainstem. *J. Comp. Neurol.* 520, 1262–1277. doi: 10.1002/cne.22786

Kullmann, D. M. (2011). Interneuron networks in the hippocampus. *Curr. Opin. Neurobiol.* 21, 709–716. doi: 10.1016/j.conb.2011.05.006

Lee, E., Lee, J., and Kim, E. (2017). Excitation/inhibition imbalance in animal models of autism spectrum disorders. *Biol. Psychiatry* 81, 838–847. doi: 10.1016/j.biopsych.2016.05.011

Lewitus, G. M., Konefal, S. C., Greenhalgh, A. D., Pribiag, H., Augereau, K., and Stellwagen, D. (2016). Microglial TNF-α suppresses cocaine-induced plasticity and behavioral sensitization. *Neuron* 90, 483–491. doi: 10.1016/j.neuron.2016.03.030

Li, K., Wei, Q., Liu, F.-F., Hu, F., Xie, A.-J., Zhu, L.-Q., et al. (2017). Synaptic dysfunction in Alzheimer's disease: aβ, tau, and epigenetic alterations. *Mol. Neurobiol.* doi: 10.1007/s12035-017-0533-3 [Epub ahead of print].

Lim, S. H., Park, E., You, B., Jung, Y., Park, A. R., Park, S. G., et al. (2013). Neuronal synapse formation induced by microglia and interleukin 10. *PLoS One* 8:e81218. doi: 10.1371/journal.pone.0081218

Lin, S.-C., and Bergles, D. E. (2004). Synaptic signaling between GABAergic interneurons and oligodendrocyte precursor cells in the hippocampus. *Nat. Neurosci.* 7, 24–32. doi: 10.1038/nn1162

Lin, S.-C., Huck, J. H. J., Roberts, J. D. B., Macklin, W. B., Somogyi, P., and Bergles, D. E. (2005). Climbing fiber innervation of NG2-expressing glia in the mammalian cerebellum. *Neuron* 46, 773–785. doi: 10.1016/j.neuron.2005.04.025

Liu, Q. Y., Schaffner, A. E., Chang, Y. H., Vaszil, K., and Barker, J. L. (1997). Astrocytes regulate amino acid receptor current densities in embryonic rat hippocampal neurons. *J. Neurobiol.* 33, 848–864. doi: 10.1002/(sici)1097-4695(19971120)33:6<848::aid-neu11>3.0.co;2-0

Liu, Q. Y., Schaffner, A. E., Li, Y. X., Dunlap, V., and Barker, J. L. (1996). Upregulation of $GABA_A$ current by astrocytes in cultured embryonic rat hippocampal neurons. *J. Neurosci.* 16, 2912–2923.

Muthukumar, A. K., Stork, T., and Freeman, M. R. (2014). Activity-dependent regulation of astrocyte GAT levels during synaptogenesis. *Nat. Neurosci.* 17, 1340–1350. doi: 10.1038/nn.3791

Nagler, K., Mauch, D. H., and Pfrieger, F. W. (2001). Glia-derived signals induce synapse formation in neurones of the rat central nervous system. *J. Physiol.* 533, 665–679. doi: 10.1111/j.1469-7793.2001.00665.x

Neniskyte, U., and Gross, C. T. (2017). Errant gardeners: glial-cell-dependent synaptic pruning and neurodevelopmental disorders. *Nat. Rev. Neurosci.* 18, 658–670. doi: 10.1038/nrn.2017.110

Ortinski, P. I., Dong, J., Mungenast, A., Yue, C., Takano, H., Watson, D. J., et al. (2010). Selective induction of astrocytic gliosis generates deficits in neuronal inhibition. *Nat. Neurosci.* 13, 584–591. doi: 10.1038/nn.2535

Paolicelli, R. C., Bolasco, G., Pagani, F., Maggi, L., Scianni, M., Panzanelli, P., et al. (2011). Synaptic pruning by microglia is necessary for normal brain development. *Science* 333, 1456–1458. doi: 10.1126/science.1202529

Parkhurst, C. N., Yang, G., Ninan, I., Savas, J. N., Yates, J. R. III, Lafaille, J. J., et al. (2013). Microglia promote learning-dependent synapse formation through brain-derived neurotrophic factor. *Cell* 155, 1596–1609. doi: 10.1016/j.cell.2013.11.030

Pascual, O., Ben Achour, S., Rostaing, P., Triller, A., and Bessis, A. (2012). Microglia activation triggers astrocyte-mediated modulation of excitatory neurotransmission. *Proc. Natl. Acad. Sci. U S A* 109, E197–E205. doi: 10.1073/pnas.1111098109

Penzes, P., Cahill, M. E., Jones, K. A., VanLeeuwen, J.-E., and Woolfrey, K. M. (2011). Dendritic spine pathology in neuropsychiatric disorders. *Nat. Neurosci.* 14, 285–293. doi: 10.1038/nn.2741

Perea, G., Navarrete, M., and Araque, A. (2009). Tripartite synapses: astrocytes process and control synaptic information. *Trends Neurosci.* 32, 421–431. doi: 10.1016/j.tins.2009.05.001

Perea, G., Yang, A., Boyden, E. S., and Sur, M. (2014). Optogenetic astrocyte activation modulates response selectivity of visual cortex neurons *in vivo*. *Nat. Commun.* 5:3262. doi: 10.1038/ncomms4262

Pfrieger, F. W., and Barres, B. A. (1996). New views on synapse—glia interactions. *Curr. Opin. Neurobiol.* 6, 615–621. doi: 10.1016/s0959-4388(96)80093-6

Pizzorusso, T., Medini, P., Berardi, N., Chierzi, S., Fawcett, J. W., and Maffei, L. (2002). Reactivation of ocular dominance plasticity in the adult visual cortex. *Science* 298, 1248–1251. doi: 10.1126/science.1072699

Pyka, M., Wetzel, C., Aguado, A., Geissler, M., Hatt, H., and Faissner, A. (2011). Chondroitin sulfate proteoglycans regulate astrocyte-dependent synaptogenesis and modulate synaptic activity in primary embryonic hippocampal neurons. *Eur. J. Neurosci.* 33, 2187–2202. doi: 10.1111/j.1460-9568.2011.07690.x

Risher, W. C., Patel, S., Kim, I. H., Uezu, A., Bhagat, S., Wilton, D. K., et al. (2014). Astrocytes refine cortical connectivity at dendritic spines. *Elife* 3:e04047. doi: 10.7554/eLife.04047

Schafer, D. P., Lehrman, E. K., Kautzman, A. G., Koyama, R., Mardinly, A. R., Yamasaki, R., et al. (2012). Microglia sculpt postnatal neural circuits in an activity and complement-dependent manner. *Neuron* 74, 691–705. doi: 10.1016/j.neuron.2012.03.026

Seifert, G., Schilling, K., and Steinhauser, C. (2006). Astrocyte dysfunction in neurological disorders: a molecular perspective. *Nat. Rev. Neurosci.* 7, 194–206. doi: 10.1038/nrn1870

Shemer, A., Erny, D., Jung, S., and Prinz, M. (2015). Microglia plasticity during health and disease: an immunological perspective. *Trends Immunol.* 36, 614–624. doi: 10.1016/j.it.2015.08.003

Shigetomi, E., Tong, X., Kwan, K. Y., Corey, D. P., and Khakh, B. S. (2012). TRPA1 channels regulate astrocyte resting calcium and inhibitory synapse efficacy through GAT-3. *Nat. Neurosci.* 15, 70–80. doi: 10.1038/nn.3000

Sorg, B. A., Berretta, S., Blacktop, J. M., Fawcett, J. W., Kitagawa, H., Kwok, J. C. F., et al. (2016). Casting a wide net: role of perineuronal nets in neural plasticity. *J. Neurosci.* 36, 11459–11468. doi: 10.1523/JNEUROSCI.2351-16.2016

Stevens, B., Allen, N. J., Vazquez, L. E., Howell, G. R., Christopherson, K. S., Nouri, N., et al. (2007). The classical complement cascade mediates CNS synapse elimination. *Cell* 131, 1164–1178. doi: 10.1016/j.cell.2007.10.036

Stipursky, J., Romão, L., Tortelli, V., Neto, V. M., and Gomes, F. C. A. (2011). Neuron-glia signaling: implications for astrocyte differentiation and synapse formation. *Life Sci.* 89, 524–531. doi: 10.1016/j.lfs.2011.04.005

Tan, Z., Liu, Y., Xi, W., Lou, H.-F., Zhu, L., Guo, Z., et al. (2017). Glia-derived ATP inversely regulates excitability of pyramidal and CCK-positive neurons. *Nat. Commun.* 8:13772. doi: 10.1038/ncomms13772

Tremblay, M.-È., Stevens, B., Sierra, A., Wake, H., Bessis, A., and Nimmerjahn, A. (2011). The role of microglia in the healthy brain. *J. Neurosci.* 31, 16064–16069. doi: 10.1523/JNEUROSCI.4158-11.2011

Tsai, H.-H., Li, H., Fuentealba, L. C., Molofsky, A. V., Taveira-Marques, R., Zhuang, H., et al. (2012). Regional astrocyte allocation regulates CNS synaptogenesis and repair. *Science* 337, 358–362. doi: 10.1126/science.1222381

Ullian, E. M., Harris, B. T., Wu, A., Chan, J. R., and Barres, B. A. (2004). Schwann cells and astrocytes induce synapse formation by spinal motor neurons in culture. *Mol. Cell. Neurosci.* 25, 241–251. doi: 10.1016/j.mcn.2003.10.011

Ullian, E. M., Sapperstein, S. K., Christopherson, K. S., and Barres, B. A. (2001). Control of synapse number by glia. *Science* 291, 657–661. doi: 10.1126/science.291.5504.657

Um, J. W., and Ko, J. (2013). LAR-RPTPs: synaptic adhesion molecules that shape synapse development. *Trends Cell Biol.* 23, 465–475. doi: 10.1016/j.tcb.2013.07.004

van Berckel, B. N., Bossong, M. G., Boellaard, R., Kloet, R., Schuitemaker, A., Caspers, E., et al. (2008). Microglia activation in recent-onset schizophrenia: a quantitative (*R*)-[^{11}C]PK11195 positron emission tomography study. *Biol. Psychiatry* 64, 820–822. doi: 10.1016/j.biopsych.2008.04.025

Vitellaro-Zuccarello, L., Calvaresi, N., and De Biasi, S. (2003). Expression of GABA transporters, GAT-1 and GAT-3, in the cerebral cortex and thalamus of the rat during postnatal development. *Cell Tissue Res.* 313, 245–257. doi: 10.1007/s00441-003-0746-9

Voineagu, I., Wang, X., Johnston, P., Lowe, J. K., Tian, Y., Horvath, S., et al. (2011). Transcriptomic analysis of autistic brain reveals convergent molecular pathology. *Nature* 474, 380–384. doi: 10.1038/nature10110

Volterra, A., and Meldolesi, J. (2005). Astrocytes, from brain glue to communication elements: the revolution continues. *Nat. Rev. Neurosci.* 6, 626–640. doi: 10.1038/nrn1722

Wu, Y., Dissing-Olesen, L., MacVicar, B. A., and Stevens, B. (2015). Microglia: dynamic mediators of synapse development and plasticity. *Trends Immunol.* 36, 605–613. doi: 10.1016/j.it.2015.08.008

Xia, M., Zhu, S., Shevelkin, A., Ross, C. A., and Pletnikov, M. (2016). DISC1, astrocytes and neuronal maturation: a possible mechanistic link with implications for mental disorders. *J. Neurochem.* 138, 518–524. doi: 10.1111/jnc.13663

Yang, J., Yang, H., Liu, Y., Li, X., Qin, L., Lou, H., et al. (2016). Astrocytes contribute to synapse elimination via type 2 inositol 1,4,5-trisphosphate receptor-dependent release of ATP. *Elife* 5:e15043. doi: 10.7554/eLife.15043

Zhang, J.-M., Wang, H.-K., Ye, C.-Q., Ge, W., Chen, Y., Jiang, Z.-L., et al. (2003). ATP released by astrocytes mediates glutamatergic activity-dependent heterosynaptic suppression. *Neuron* 40, 971–982. doi: 10.1016/s0896-6273(03)00717-7

Zoghbi, H. Y., and Bear, M. F. (2012). Synaptic dysfunction in neurodevelopmental disorders associated with autism and intellectual disabilities. *Cold Spring Harb. Perspect. Biol.* 4:a009886. doi: 10.1101/cshperspect.a009886

Conflict of Interest Statement: The author declares that the research was conducted in the absence of any commercial or financial relationships that could be construed as a potential conflict of interest.

frontiers in Molecular Neuroscience

ORIGINAL RESEARCH
published: 13 October 2017
doi: 10.3389/fnmol.2017.00327

LAR-RPTP Clustering Is Modulated by Competitive Binding between Synaptic Adhesion Partners and Heparan Sulfate

Seoung Youn Won[1†], Cha Yeon Kim[2†], Doyoun Kim[3], Jaewon Ko[4], Ji Won Um[4], Sung Bae Lee[4], Matthias Buck[5], Eunjoon Kim[3,6], Won Do Heo[6,7], Jie-Oh Lee[1]* and Ho Min Kim[3,8]**

[1]Department of Chemistry, Korea Advanced Institute of Science and Technology (KAIST), Daejeon, South Korea, [2]Graduate School of Nanoscience and Technology, Korea Advanced Institute of Science and Technology (KAIST), Daejeon, South Korea, [3]Center for Synaptic Brain Dysfunctions, Institute for Basic Science (IBS), Daejeon, South Korea, [4]Department of Brain & Cognitive Sciences, Daegu Gyeongbuk Institute of Science and Technology (DGIST), Daegu, South Korea, [5]Department of Physiology and Biophysics, Case Western Reserve University, School of Medicine, Cleveland, OH, United States, [6]Department of Biological Sciences, Korea Advanced Institute of Science and Technology (KAIST), Daejeon, South Korea, [7]Center for Cognition and Sociality, Institute for Basic Science (IBS), Daejeon, South Korea, [8]Graduate School of Medical Science & Engineering, Korea Advanced Institute of Science and Technology (KAIST), Daejeon, South Korea

OPEN ACCESS

Edited by:
Chen Zhang,
Peking University, China

Reviewed by:
Davide Comoletti,
Rutgers University, The State University of New Jersey, United States
Alexander Dityatev,
German Center for Neurodegenerative Diseases (HZ), Germany

***Correspondence:**
Ho Min Kim
hm_kim@kaist.ac.kr
Jie-Oh Lee
jieoh@kaist.ac.kr
Won Do Heo
wondo@kaist.ac.kr

[†]These authors have contributed equally to this work.

Received: *05 August 2017*
Accepted: *28 September 2017*
Published: *13 October 2017*

Citation:
Won SY, Kim CY, Kim D, Ko J, Um JW, Lee SB, Buck M, Kim E, Heo WD, Lee J-O and Kim HM (2017) LAR-RPTP Clustering Is Modulated by Competitive Binding between Synaptic Adhesion Partners and Heparan Sulfate. Front. Mol. Neurosci. 10:327. doi: 10.3389/fnmol.2017.00327

The leukocyte common antigen-related receptor protein tyrosine phosphatases (LAR-RPTPs) are cellular receptors of heparan sulfate (HS) and chondroitin sulfate (CS) proteoglycans that direct axonal growth and neuronal regeneration. LAR-RPTPs are also synaptic adhesion molecules that form *trans*-synaptic adhesion complexes by binding to various postsynaptic adhesion ligands, such as Slit- and Trk-like family of proteins (Slitrks), IL-1 receptor accessory protein-like 1 (IL1RAPL1), interleukin-1 receptor accessory protein (IL-1RAcP) and neurotrophin receptor tyrosine kinase C (TrkC), to regulate synaptogenesis. Here, we determined the crystal structure of the human LAR-RPTP/IL1RAPL1 complex and found that lateral interactions between neighboring LAR-RPTP/IL1RAPL1 complexes in crystal lattices are critical for the higher-order assembly and synaptogenic activity of these complexes. Moreover, we found that LAR-RPTP binding to the postsynaptic adhesion ligands, Slitrk3, IL1RAPL1 and IL-1RAcP, but not TrkC, induces reciprocal higher-order clustering of *trans*-synaptic adhesion complexes. Although LAR-RPTP clustering was induced by either HS or postsynaptic adhesion ligands, the dominant binding of HS to the LAR-RPTP was capable of dismantling pre-established LAR-RPTP-mediated *trans*-synaptic adhesion complexes. These findings collectively suggest that LAR-RPTP clustering for synaptogenesis is modulated by a complex synapse-organizing protein network.

Keywords: LAR-RPTPs, postsynaptic ligand, synaptic adhesion molecules, higher-order clustering, heparan sulfate, crystal structure

INTRODUCTION

Synapses, the fundamental functional elements of the nervous system, are formed via a highly orchestrated process called synaptogenesis. This dynamic process involves several steps, starting from axon-dendrite target selection and leading ultimately to the final assembly, differentiation and stabilization of a mature synapse (Giagtzoglou et al., 2009). Synaptic adhesion molecules play a central role in this process by forming *trans*-synaptic adhesion complexes.

These complexes not only physically connect pre- and post-synaptic neuronal membranes, they also initiate bidirectional cellular signaling. The leukocyte common antigen-related receptor protein tyrosine phosphatases (LAR-RPTPs), including LAR, PTPσ and PTPδ in vertebrates, and dLAR in *Drosophila*, have recently emerged as a major family of synaptic adhesion molecules (Han et al., 2016a). Presynaptic LAR-RPTPs induce synaptic differentiation by binding several postsynaptic partners, including members of the Slit- and Trk-like family of proteins (Slitrks), interleukin-1 receptor accessory protein (IL-1RAcP), IL-1 receptor accessory protein-like 1 (IL1RAPL1), neurotrophin receptor tyrosine kinase C (TrkC), netrin-G ligand-3 (NGL-3), synaptic adhesion-like molecule 3 (SALM3) and synaptic adhesion-like molecule 5 (SALM5; Woo et al., 2009; Mah et al., 2010; Takahashi et al., 2011; Yoshida et al., 2011, 2012; Yim et al., 2013; Choi et al., 2016). LAR-RPTPs contain multiple splice sites—designated mini-exons A-D (MeA-D), that produce diverse LAR-RPTP variants with and without short peptide inserts (Pulido et al., 1995). Recent progress in the structural characterization of *trans*-synaptic adhesion complexes, including LAR-RPTPs bound to Slitrks, TrkC, IL1RAPL1 or IL-1RAcP, have revealed the interaction interface of these complexes as well as the significant role of splice inserts, particularly that of MeA and MeB, in their selective binding (Coles et al., 2014; Um et al., 2014; Yamagata et al., 2015b). Each *trans*-synaptic adhesion complex appears to be formed through interactions with different affinity, a selectivity that permits fine-tuned modulation of synapse organization. Interestingly, our previous report on the three-dimensional structure of the LAR-RPTPs/Slitrk1 complex have demonstrated that Slitrk1 mediates presynaptic differentiation through direct binding to LAR-RPTPs and subsequent formation of clusters of LAR-RPTP/Slitrk1 complexes (Um et al., 2014). It remains elusive, however, that other Slitrk members and/or other postsynaptic adhesion partners (e.g., IL1RAPL1, IL-1RAcP and TrkC) can induce the LAR-RPTP clustering required for synapse differentiation.

In addition to their role as synaptic adhesion molecules at neuronal synapses, LAR-RPTPs regulate neuronal extension and guidance at neuronal growth cones through direct binding to heparan sulfate proteoglycans (HSPGs) or chondroitin sulfate proteoglycans (CSPGs; Aricescu et al., 2002; Shen et al., 2009; Coles et al., 2011). HSPG binding to PTPσ induces PTPσ clustering at the neuronal growth cone and promotes neurite outgrowth, whereas CSPG binding does not induce PTPσ clustering and inhibits neuronal extension and nerve regeneration. In addition to these functions in neurogenesis and axonal guidance (Johnson et al., 2004; Rawson et al., 2005), HSPGs, particularly glypican-4 (GPC-4), has been reported to play a role in synaptogenesis. GPC-4 mediates excitatory synapse development by interacting with both LRRTM4 in the postsynaptic membrane and with PTPσ in the presynaptic membrane in a heparan sulfate (HS)-dependent manner (Siddiqui et al., 2013; de Wit et al., 2013; Ko et al., 2015). This suggests that HSPGs play a critical role not only in neuronal growth at axonal growth cones, but also in the regulation of synaptic strength and synaptogenesis at neuronal synapses. Furthermore, it is likely that switching between neuronal growth and synapse formation is tightly regulated by a highly orchestrated process involving complex synapse-organizing proteins and an HSPG network. However, we did not yet know whether HSPGs affect the formation of LAR-RPTP-mediated *trans*-synaptic adhesion complexes and subsequent synaptogenesis.

Here, we determined the crystal structure of the human LAR-RPTP (PTPδ)/IL1RAPL1 complex and identified the lateral molecular interactions between neighboring LAR-RPTP (PTPδ)/IL1RAPL1 complexes in the crystal-packing lattices. Notably, these interactions were found to be essential for the formation of higher-order *trans*-synaptic adhesion complex assemblies (PTPδ/IL1RAPL1 complexes) and for IL1RAPL1-mediated presynaptic differentiation. Likewise, the binding of LAR-RPTPs to other postsynaptic adhesion molecules—Slitrk3 and IL-1RAcP (but not TrkC)—induces the formation of higher-order *trans*-synaptic adhesion complex assemblies. We also provide compelling evidence that HSPG, but not CSPG, inhibits the interactions of LAR-RPTPs with their postsynaptic ligands (Slitrk1, IL1RAPL1 and IL-1RAcP) and that HSPGs can even disrupt pre-established LAR-RPTP-mediated *trans*-synaptic adhesion complexes. Our results suggest that the competitive advantage of HSPGs over postsynaptic adhesion partners for LAR-RPTP binding can modulate LAR-RPTP-mediated synaptogenesis.

MATERIALS AND METHODS

Construction of Expression Vectors

The constructs used in this study are summarized in Supplementary Table S1. Briefly, for cell adhesion assays, the extracellular domains of LAR-RPTPs and their postsynaptic adhesion partners, Slitrk1 LRR1/2 (or Slitrk1 LRR1), Slitrk3 LRR1/2, TrkC LRR-Ig1-2 (or TrkC LRR-Ig1), IL1RAPL1 Ig1-3, or IL-1RAcP Ig1-3, were cloned into the *Bgl*II and *Sal*I sites of the pDisplay vector (Invitrogen). For live-cell imaging, these extracellular domains followed by the PDFGR transmembrane domain were cloned into the *Eco*RI and *Bam*HI sites of the pEGFP-N1 vector (Clontech). For protein expression of LAR-RPTPs and their postsynaptic adhesion partners, Slitrk1 LRR1, Slitrk3 LRR1, TrkC LRR-Ig1-2 (or TrkC LRR-Ig1), IL1RAPL1 Ig1-3 and IL-1RAcP Ig1-3, the indicated regions of each target gene were cloned into modified pAcGP67A or pVL1393 vectors (BD Biosciences), which encode either protein A derived from pEZZ18 (GE Healthcare Life Sciences) or the Fc domain of human IgG for affinity purification.

Expression and Purification of Recombinant Proteins

Recombinant proteins were expressed in High Five insect cells (Invitrogen) by transfecting them with the corresponding P4 baculovirus and incubating them at 28°C for 3 days.

After pelleting cells by centrifugation, the supernatants were pooled and loaded onto IgG Sepharose resins (GE Healthcare Life Sciences) to purify protein A-fused proteins, or protein A Sepharose resins (GE Healthcare Life Sciences) to purify Fc-fused proteins. The protein-bound resins were then washed with 20 mM Tris-HCl pH 8.0, 200 mM NaCl and treated with thrombin (0.5% (v/v)) in 20 mM Tris-HCl pH 8.0, 200 mM NaCl at 4°C overnight to remove the C-terminal tags (protein A or the Fc domain). To generate the Fc-fusion proteins used for treating cells during live-cell imaging, we eluted Fc-fused proteins with 100 mM glycine, pH 2.7 and immediately neutralized the resulting solution with 100 mM Tris-HCl, pH 8.0 instead of thrombin cleavage. The proteins were then further purified by gel filtration chromatography on a Superdex 200 column (GE Healthcare Life Sciences) using a buffer containing 20 mM Tris-HCl pH 8.0, 200 mM NaCl. The human PTPδ Ig1-3(+/+)/IL1RAPL1 Ig1-3 complex was produced by mixing purified PTPδ Ig1-3(+/+) with IL1RAPL1 Ig1-3 at a 1:1 molar ratio for 3 h at 4°C. Any unbound IL1RAPL1 Ig1-3 was removed by gel filtration chromatography (buffer: 20 mM Tris-HCl pH 8.0, 200 mM NaCl). Fractions containing PTPδ Ig1-3(+/+)/IL1RAPL1 Ig1-3 complexes were pooled and further concentrated to 5 mg/ml for crystallization.

Crystallization and Structural Determination

The sitting-drop vapor-diffusion method was used to grow crystals of the PTPδ Ig1-3(+/+)/IL1RAPL1 Ig1-3 complex at 296 K. For this, 0.2 μl of protein (5 mg/ml) was mixed with 0.2 μl of crystallization buffer (100 mM Tris-HCl pH 7.5, 200 mM zinc acetate, 10% PEG8K [v/v]). For data collection at 100 K, crystals were transferred to a cryo-protective solution (100 mM Tris-HCl pH 7.5, 200 mM zinc acetate, 13% PEG8K [v/v], 30% glycerol [v/v]) and flash-frozen in liquid nitrogen. We found the PTPδ Ig1-3(+/+)/IL1RAPL1 Ig1-3 complex crystals belonged to the space group $P3_212$ and had the following unit cell constants: a = 110.4 Å, b = 110.4 Å, c = 210.5 Å, α = 90°, β = 90°, γ = 120°. After diffraction data were collected at beamline 7A (Pohang Accelerator Laboratory), they were reduced and integrated using the program HKL2000 (Otwinowski and Minor, 1997), and the initial phases were calculated by molecular replacement using PHASER (McCoy et al., 2005). The structures of the Ig1-2 domains from PTPδ (PDB: 4RCA; Um et al., 2014) and IL1RAPL1 (PDB: 3O4O; Wang et al., 2010) were used as search probes for structure determination. After several iterative rounds of model building and refinement for the Ig1-2 domains of PTPδ and IL1RAPL1 using COOT (Emsley and Cowtan, 2004) and PHENIX (Adams et al., 2002), atomic models for the Ig3 domains of both PTPδ and IL1RAPL1 were manually built and refined. The statistics used for data collection and refinement are summarized in Supplementary Table S2. A Ramachandran plot analysis of the PTPδ Ig1-3(+/+)/IL1RAPL1 Ig1-3 complex structure showed that 96.4%, 2.9% and 0.7% of residues were in favored regions, allowed regions and outlier regions, respectively. All structural figures were depicted using PyMOL (Molecular Graphics System).

Live-Cell Imaging

For live-cell imaging, cultured COS-7 cells (ATCC) were cultured in 96-well plates and transfected with 100 ng/well of the indicated constructs using Lipofectamine LTX (Invitrogen). For LAR-RPTP clustering analysis, cells were transfected with PTPδ Ig1-FN3(+/+)-PDGFR_TM-EGFP or PTPσ Ig1-FN3(−/−)-PDGFR_TM-EGFP. For postsynaptic adhesion molecule clustering analysis, cells were transfected with the indicated IL1RAPL1 Ig1-3-PDGFR_TM-EGFP variants (wild type (WT) or E87A/E137R/N138A/R342D/H344D mutant), Slitrk1 LRR1/2-PDGFR_TM-EGFP, Slitrk3 LRR1/2-PDGFR_TM-EGFP, IL-1RAcP Ig1-3-PDGFR_TM-EGFP, or TrkC LRR-Ig1-2-PDGFR_TM-EGFP. After 12–18 h, cells were washed with Dulbecco's phosphate-buffered saline (DPBS) containing glucose (Invitrogen) and then treated with 50 μg/ml of the indicated Fc-fused proteins or Fc alone. Cells were then imaged once every 1 min for 10–20 min using a confocal microscope (Nikon A1) at 60× magnification. Clusters were detected by monitoring fluorescent puncta formed by EGFP fused to the C-termini of LAR-RPTPs or the indicated postsynaptic adhesion molecules. ImageJ (NIH) was used to quantify accumulated clusters on COS-7 cell membranes. For quantification, clusters were defined as discrete puncta of EGFP fluorescence that satisfied criteria of size (>2 pixel) and circularity (0.1–1.0). The number of clusters per cell corresponding to each figure was presented as means ± SEM (n = 7–10 COS-7 cells).

Cell Adhesion Assays

Cell adhesion assays were performed using L cells (ATCC). First, two groups of L cells in 6-well plates were transfected with 2 μg of the indicated expression vectors. After 36 h, the transfected cells were trypsinized and re-suspended in Dulbecco's Modified Eagle Medium (DMEM) containing 10% fetal bovine serum (FBS) and 1% antibiotics. The two groups of L cells—one expressing EGFP and the indicated postsynaptic adhesion partner and the other expressing DsRed and the indicated LAR-RPTP—were mixed and rotated at room temperature for 2 h to allow the cells to aggregate. Thereafter, mixtures were spotted onto 4-well culture slides (SPL), and the extent of cell aggregation was imaged by confocal microscopy (LSM 510; Zeiss). The effect of HS or chondroitin sulfate (CS) on pre-formed *trans*-synaptic adhesion complexes was measured by treating mixed cell aggregates with or without 0.5 mg/ml HS (Amsbio, GAG-HS01) or CS (Sigma, C4384) and then incubating them for an additional 2 h. For quantification, cell aggregates were defined as clusters containing at least two or more cells that included at least one green (EGFP) and one red (DsRed) cell. MetaMorph Software (Molecular Devices) was used to measure the area of each region of cell aggregates. The size of cell aggregates was presented as means ± SEM (n = 12–15 fields from at least three independent experiments). Areas smaller than the average size of a single cell were

excluded from the analysis based on the definition of cell aggregates.

Rat Hippocampal Neuron Culture

Cultured primary hippocampal neurons were prepared from embryonic day 18 (E18) Sprague-Dawley rat brains (KOATECK). Neurons were seeded on 25-mm poly-L-lysine (1 mg/ml)-coated coverslips and cultured in neurobasal media (Gibco) containing penicillin-streptomycin and 0.5 mM GlutaMax (Gibco) supplemented with 2% B-27 (Gibco) and 0.5% FBS (Hyclone). All procedures were conducted according to the guidelines and protocols for rodent experimentation approved by the Institutional Animal Care and Use Committee of KAIST.

Heterologous Synapse-Formation Assays

Heterologous synapse-formation assays were performed using HEK293T cells (ATCC). Briefly, HEK293T cells were transfected with EGFP (negative control), IL1RAPL1-WT (IL1RAPL1 Ig1-3-PDGFR_TM-EGFP), or IL1RAPL1 mutant (IL1RAPL1 Ig1-3-PDGFR_TM-EGFP [E87A/E137R/N138A/R342D/H344D]) using Lipofectamine LTX (Invitrogen). After 48 h, transfected cells were trypsinized, seeded onto hippocampal neuron cultures at 10 days *in vitro* (DIV10), and co-cultured for an additional 48 h. At DIV12, cultured cells were fixed and permeabilized by serially incubating in 1% paraformaldehyde and pre-chilled 100% methanol (5 min each). Cells were then incubated first with primary antibodies against EGFP (#1996; Choi et al., 2006) and synapsin I (EMD Millipore), and then with Cy3- and FITC-conjugated secondary antibodies (Jackson ImmunoResearch). Images were acquired using a confocal microscope (LSM780; Carl Zeiss). In quantifying the acquired images, the contours of transfected HEK293T cells were set as the region of interest. The fluorescence intensity of immunoreactive puncta was normalized with respect to each HEK293T cell area, and then MetaMorph Software (Molecular Devices) was used to quantify both red and green channels. The data are presented as means ± SEM (n = 15–20 HEK293T cells).

Grid Preparation for Negative-Stain Transmission Electron Microscopy

A total of 40 ng of PTPδ Ig1-FN8(+/+) or PTPσ Ig1-FN3(+/+) was applied to a glow-discharged carbon-coated 400 mesh copper grid (Electron Microscopy Science). For complex structures containing HS or CS, PTPδ Ig1-FN8(+/+) or PTPσ Ig1-FN3(+/+) were incubated with a 2-fold molar excess of HS (Amsbio, GAG-HS01) or CS (Sigma, C4384) at 4°C for 1 h, and then this mixture was applied to a glow-discharged carbon-coated 400 mesh copper grid. After staining the grid with 0.75% uranyl formate solution (Electron Microscopy Science) as previously described (Booth et al., 2011), images were acquired using a Tecnai T12 Bio-TWIN transmission electron microscope equipped with a FEI Eagle 4K by 4K CCD camera, operating at 120 kV.

Size-Exclusion Chromatography

Trans-synaptic adhesion complexes were formed by incubating Slitrk1 LRR1, IL1RAPL1 Ig1-3, or IL-1RAcP Ig1-3 with the indicated LAR-RPTP Ig1-3s (PTPσ Ig1-3(+/+) or PTPδ Ig1-3(+/+)) at a 1:1 molar ratio at 4°C for 3 h. After incubation, the mixtures were applied to a Superdex 200 10/300 GL column (GE Healthcare Life Sciences) in a buffer consisting of 20 mM Tris-HCl (pH 8.0) and 50 mM NaCl. The formation of *trans*-synaptic adhesion complexes was then detected as forward shifts in the size-exclusion chromatography peaks of each individual protein. The effect of HS or CS on pre-formed *trans*-synaptic adhesion complexes were analyzed by incubating each pre-formed *trans*-synaptic adhesion complex with a 2-fold molar excess of HS (Amsbio, GAG-HS01) or CS (Sigma, C4384) at 4°C for an additional 3 h, followed by size exclusion chromatography on a Superdex 200 10/300 GL column (GE Healthcare Life Sciences) with a buffer consisting of 10 mM Tris-HCl (pH 8.0) and 50 mM NaCl. To determine whether HS inhibits the binding of LAR-RPTPs to their postsynaptic adhesion partners, we pre-incubated LAR-RPTP Ig1-3s (PTPσ Ig1-3(+/+) or PTPδ Ig1-3(+/+)) with a 2-fold molar excess of HS at 4°C for 3 h. We then incubated HS-bound PTPσ Ig1-3 or PTPδ Ig1-3 with the same molar concentration of Slitrk1 LRR1, IL1RAPL1 Ig1-3, or IL-1RAcP Ig1-3 for an additional 3 h, followed by size-exclusion chromatography, as described above. HS used in this study (Amsbio, GAG-HS01) consists of three major disaccharide units—GlcA-GlcNAc, IdoA-GlcNS and GlcA-GlcNS, of which the number of N-sulfates per 100 disaccharides are 65 and the ratio of N-sulfation and O-sulfation is 0.73. CS from shark cartilage (Sigma, C4384) is composed of alternating units of GalNAc and GlcA that can be sulfated at 6 and/or 4-position of the GalNAc. Therefore, the distribution of sulfate groups (typically one to two per disaccharide) along CS chains is relatively uniform, whereas HS has high-sulfation regions (three groups per disaccharide).

Statistical Analysis

All quantifiable data in this study are presented as means ± SEM. We performed each experiment on ≥3 independent cultures and used ANOVAs followed by Tukey's *post hoc* tests to analyze the results ($^{*}P < 0.05$, $^{**}P < 0.01$, $^{***}P < 0.001$). For analysis of the data and representation of bar graphs, Prism5 (GraphPad) was used.

Data Availability

The accession number for the coordinate of human PTPδ/human IL1RAPL1 complex reported in this article is PDB: 5WY8.

RESULTS

Novel Lateral Interactions in the Human PTPδ/IL1RAPL1 Complex

The previously reported crystal structure of mouse PTPδ/IL1RAPL1 revealed that the synaptic adhesion molecule, IL1RAPL1, may specifically bind to LAR-RPTPs through an interaction in which splice inserts (both MeA and MeB) play a critical role (Yamagata et al., 2015b). However, it was

not yet clear whether binding of IL1RAPL1 to LAR-RPTPs induces clustering of this *trans*-synaptic adhesion complex in a manner similar to that of the LAR-RPTP/Slitrk1 complex (Um et al., 2014). To address this, we determined the crystal structure of human PTPδ Ig1-3 in complex with IL1RAPL1 Ig1-3 at 3.08 Å resolution (**Figure 1A**, Supplementary Figure S1A and Supplementary Table S2). We found that IL1RAPL1 Ig1-3 exhibits an L-shaped configuration and that the V-shaped configuration of PTPδ Ig1-2 is clamped between the IL1RAPL1 Ig1 and Ig3 domains via Ig1, Ig2 and Ig3 patches (**Figure 1B** and Supplementary Figure S1B). Overall, our structure of human PTPδ Ig1-3, IL1RAPL1 Ig1-3 and their complex was not substantially different from the mouse structure (PDB: 4YH7; Yamagata et al., 2015b). The Cα root mean squared deviations for PTPδ Ig1-3 alone, IL1RAPL1 Ig1-3 alone and the PTPδ Ig1-3/IL1RAPL1 Ig1-3 complex were 1.41, 1.00 and 2.01 Å, respectively (Supplementary Figures S1C–E). The Ig1 patch is formed mainly by hydrophilic interactions between positively charged clusters on PTPδ (K59, N66, R68, R88, R91 and R117) and negatively charged clusters on IL1RAPL1 (E291, D292, E300 and E337; **Figure 1B**, red box). These hydrophilic interaction networks are stabilized by the hydrophobic interaction of P90 on PTPδ with Y282 and F289 on IL1RAPL1. The Ig2 patch consists of both hydrophobic and hydrophilic interactions (**Figure 1B**, yellow box). M130, L146, A148, L178, P187 and A191 on PTPδ form a hydrophobic network with W34, I38 and Y59 on IL1RAPL1. E181 and R189 on PTPδ interact, respectively, with R61 and D37 on IL1RAPL1 through ionic interactions. E181, T186 and P187 in the MeA splice site of PTPδ stabilize the other Ig2 patch interactions. The Ig3 patch is formed primarily by a broad range of hydrophobic interactions that include those between P263, M264, Y266, M282, I284 and M305 on PTPδ, and M75, Y77, F85, P88 and A90 on IL1RPAL1 (**Figure 1B**, green box). In addition, S73 on IL1RAPL1 forms hydrogen bonds with E279 on PTPδ.

Intriguingly, we identified novel, discrete crystal packing interactions between the adjacent PTPδ Ig1-3/IL1RAPL1 Ig1-3 complexes along the a-axis of our crystal structure's unit cell (**Figure 1C** and Supplementary Figure S2), neither of which were observed in the structure of the mouse PTPδ Ig1-2/IL1RAPL1 Ig1-3 complex (PDB: 5Y32) or the mouse PTPδ full ECD/IL1RAPL1 Ig1-3 complex (PDB: 4YH7). Each PTPδ Ig1 and IL1RAPL1 Ig3 pair forms a symmetrical interaction interface with a neighboring PTPδ Ig1* and IL1RAPL1 Ig3* pair (**Figure 1D**), where the asterisk denotes domains or residues in the neighboring complex. We designated this lateral interaction, Interface I, which has a buried interaction surface area of 972.7 Å (**Figure 1D** and Supplementary Figure S3A). In Interface I, R342 and H344 of IL1RAPL1 form reciprocal ionic interactions with E97* and E106* of PTPδ*, whereas D32 and R112 on PTPδ interact with R112* and D32* on PTPδ*. We also defined a second symmetrical lateral interaction between neighboring PTPδ Ig1-3/IL1RAPL1 Ig1-3 complexes, designated Interface II, which is formed by the PTPδ Ig3 and IL1RAPL1 Ig1 domains (**Figure 1E** and Supplementary Figure S3B). In Interface II, E87 and E137 on IL1RAPL1 Ig1 interact with the main-chain of Q111* on IL1RAPL1* and R232* on PTPδ*, respectively. Interestingly, glycans (NAG2-BMA-MAN, shown in orange stick in **Figure 1E**) attached to N138 on IL1RAPL1 also participate in a broad range of interactions with the PTPδ* Ig3 domain. A sequence conservation analysis was performed on the sequences listed in Supplementary Table S3, using the AL2CO (Pei and Grishin, 2001; Pettersen et al., 2004). It showed that the key residues at Interface I and Interface II involved in the lateral interaction are highly conserved (Supplementary Figure S3C).

Lateral Clustering of PTPδ/IL1RAPL1 Complexes Is Critical for Synaptogenesis

To further investigate the potential biological significance of the lateral interactions observed in crystal packing, we first examined whether PTPδ clustering is induced upon binding to the postsynaptic partner, IL1RAPL1. To this end, we transiently transfected COS-7 cells with a construct encoding the chimeric protein, PTPδ Ig1-FN3-PDGFR_TM-EGFP, composed of the extracellular Ig1-FN3 domain of PTPδ, the transmembrane domain of PDGFR, and the intracellular EGFP. We then treated the cells with Fc-fused IL1RAPL1 Ig1-3 (IL1RAPL1-Fc) and measured the formation of PTPδ clusters by monitoring the increase in EGFP puncta by live-cell imaging (**Figure 2A**). We found that, similar to Slitrk1-mediated LAR-RPTP clustering in our previous study (Um et al., 2014), IL1RAPL1-Fc induced significant clustering of PTPδ in the cell membrane (**Figure 2A**, left panel, and **Figure 2D**). However, the Fc-fused IL1RAPL1 Ig1-3 mutant, E87A/E137R/N138A/R342D/H344D, which disrupts lateral interactions, did not induce membrane clustering of PTPδ (**Figure 2A**, right panel and **Figure 2D**), despite the fact that the IL1RAPL1 mutant folds properly and maintains its ability to bind PTPδ (**Figures 2B,E**).

Next, we investigated whether IL1RAPL1 mutants defective for PTPδ clustering are also defective for LAR-RPTP–mediated synaptogenic activity in heterologous synapse-formation assays. In these experiments, HEK293T cells were transfected with wild-type IL1RAPL1 (IL1RAPL1-WT) or E87A/E137R/N138A/R342D/H344D mutant IL1RAPL1, and co-cultured with hippocampal neurons for 2 days. Formation of heterologous synapses mediated by IL1RAPL1 was monitored by immunofluorescence detection of the presynaptic marker protein, synapsin I (**Figures 2C,F**). The IL1RAPL1 mutant exhibited significantly decreased presynaptic differentiation activity compared with IL1RAPL1-WT, suggesting that the lateral interaction interfaces we identified in the crystal packing lattice are the primary mediators of PTPδ/IL1RAPL1 complex clustering and their subsequent promotion of synaptogenesis.

Mutual Clustering of *Trans*-Synaptic Adhesion Complexes, Except TrkC

Since we have shown here and previously (Um et al., 2014) that both IL1RAPL1 and Slitrk1 induce clustering of LAR-

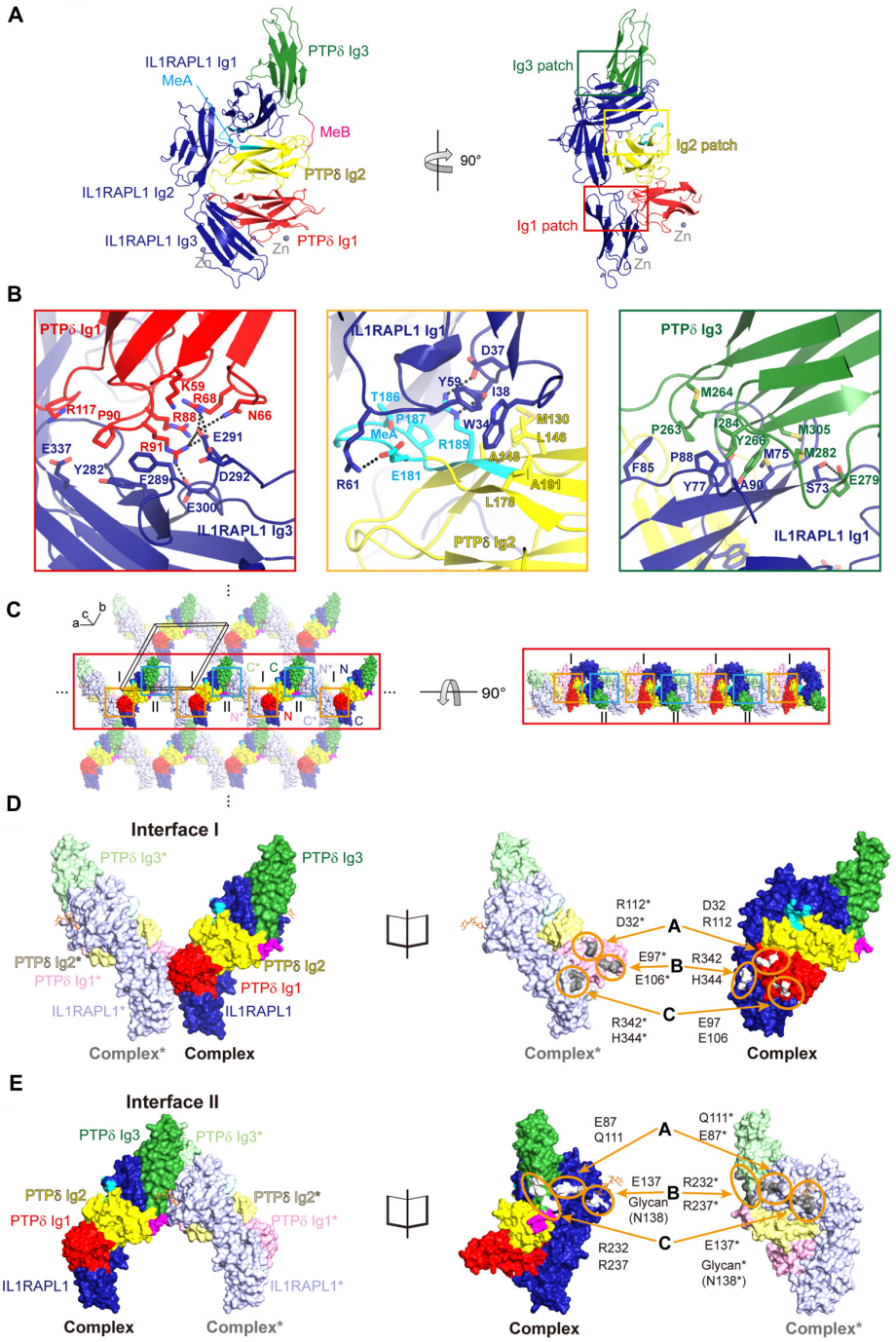

FIGURE 1 | Structure of the Human PTPδ/IL-1 receptor accessory protein-like 1 (IL1RAPL1) complex and lateral interactions between neighboring complexes. **(A)** Overall structure of the human PTPδ Ig1-3/IL1RAPL1 Ig1-3 complex. Cartoon representations of PTPδ Ig1, Ig2 and Ig3 domains, and IL1RAPL1 Ig1-3 domain are colored red, yellow, green and dark-blue, respectively. The MeA and MeB splice inserts are shown in cyan and magenta, respectively. The interaction patches, divided into Ig1, Ig2 and Ig3 patches, are boxed in red, yellow and green, respectively. Zinc ions found in the crystal are shown as gray spheres. **(B)** Three binding interfaces—Ig1, Ig2 and Ig3 patches—of the human PTPδ Ig1-3/IL1RAPL1 Ig1-3 complex. The residues involved in the interaction are shown as sticks and labeled, and hydrogen/ionic interactions are indicated by black dashed lines. **(C)** Packing interactions in the crystal lattice of the PTPδ Ig1-3/IL1RAPL1 Ig1-3 complex. For clarity, the two alternating PTPδ Ig1-3/IL1RAPL1 Ig1-3 complex are represented as deep (complex) and light (neighboring complex*) colored surface, respectively. The color scheme of complex is the same as that described in **(A)**. The black box represents a unit cell. Lateral interactions in the crystal-packing lattice are boxed in orange and light blue. The middle line of lateral oligomers is highlighted for clarity. **(D,E)** Close-up views of the crystallographic packing interactions shown in **(C)** at Interface I (orange boxes) **(D)** and Interface II (light blue boxes) **(E)**. PTPδ Ig1-3/IL1RAPL1 Ig1-3 complex and neighboring complex* in crystal lattice are presented as surfaces (left) and open book views (right). The interacting regions and key residues at Interface I and Interface II are highlighted by orange circles and labeled.

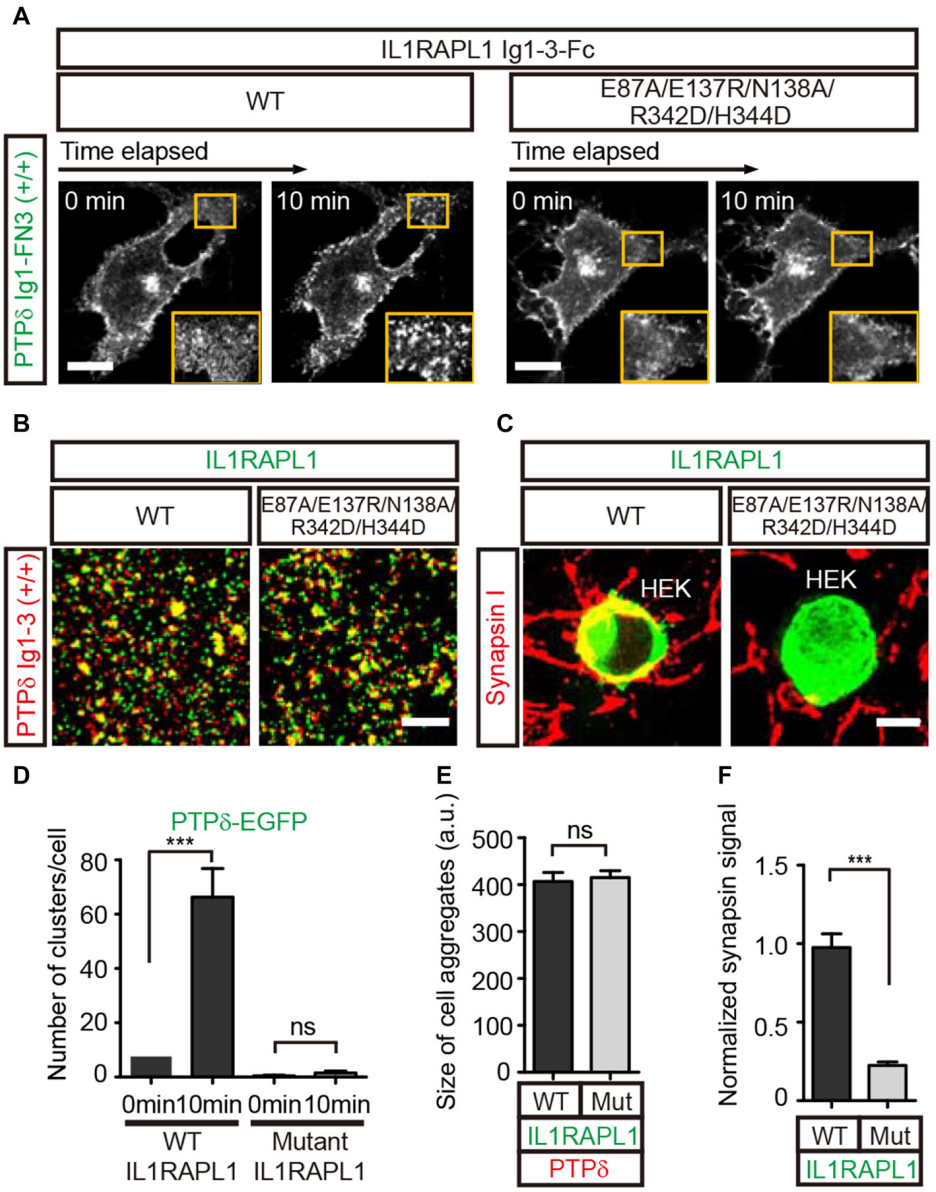

FIGURE 2 | Lateral interactions between PTPδ/IL1RAPL1 complexes are critical for their clustering and synapse formation. **(A)** Analysis of LAR-RPTP clustering upon binding of Fc-fused IL1RAPL1 variants (wild type (WT) or E87A/E137R/N138A/R342D/H344D mutant). Confocal time-lapse images of PTPδ clustering induced by IL1RAPL1 Ig1-3-Fc in COS-7 cells. PTPδ clustering was examined by treating COS-7 cells expressing PTPδ Ig1-FN3-PDGFR_TM-EGFP with 50 μg/ml of the indicated IL1RAPL1 Ig1-3-Fc variant (WT or E87A/E137R/N138A/R342D/H344D mutant). Representative cell images before and 10 min after treatment are shown. A magnified view of the yellow boxed area appears in the lower right corner of each image. Scale bars = 20 μm. **(B)** Representative images (left) and summary bar graph (right) for cell adhesion assays. For these assays, one group of L cells co-expressing DsRed and pDis-PTPδ(+/+) was mixed with a second group of L cells co-expressing EGFP and pDis-IL1RAPL1 WT (left) or pDis-IL1RAPL1 mutant (right). Scale bars = 200 μm. **(C)** Representative images of heterologous synapse-formation assays. HEK293T cells expressing IL1RAPL1-WT (IL1RAPL1 Ig1-3-PDGFR_TM-EGFP) or IL1RAPL1 mutant (IL1RAPL1 Ig1-3-PDGFR_TM-EGFP [E87A/E137R/N138A/R342D/H344D]) were co-incubated with cultured hippocampal neurons. After 48 h, co-cultured cells were immunostained with antibodies against the excitatory presynaptic marker synapsin and EGFP. Scale bars = 10 μm. **(D–F)** Quantification of data presented in **(A–C)**. Error bars represent SEM for COS-7 cells (**D**; n = 7–10), L cells (**E**; n = 12–15) and HEK 293T cells (**F**; n = 15–20) from three independent experiments. Statistical significance was assessed by ANOVA followed by Tukey's *post hoc* tests **(D)** or Student's t-test **(E,F)** (***$P < 0.001$).

RPTP, we further examined whether the clustering of LAR-RPTPs is mediated by other postsynaptic adhesion partners, namely Slitrk3, IL-1RAcP and TrkC. We first transiently transfected COS-7 cells with a construct encoding a chimeric protein composed of the extracellular Ig1-FN3 domain of LAR-RPTP (either PTPδ or PTPσ), the transmembrane

domain of PDGFR, and the intracellular EGFP. We paired these with the splice isoforms that showed the strongest affinity for each postsynaptic ligand; these were PTPσ Ig1-FN3 MeA−MeB− for TrkC, and PTPδ Ig1-FN3 MeA+MeB+ for Slitrk3 and IL-1RAcP (Han et al., 2016a; **Figure 3A**). Hereafter, we denote MeA+MeB+, MeA+MeB−, MeA−MeB+ and MeA−MeB− splice isoforms in chimeric constructs as +/+, +/−, −/+ and −/−, respectively. We treated cells expressing LAR-RPTP Ig1-FN3 (PTPσ Ig1-FN3(−/−)-PDGFR_TM-EGFP or PTPδ Ig1-FN3(+/+)-PDGFR_TM-EGFP) with the Fc-fused postsynaptic adhesion partners, Slitrk3 LRR1-Fc, TrkC LRR-Ig1-2-Fc or IL-1RAcP Ig1-3-Fc, or Fc alone (negative control), and measured the formation of LAR-RPTP clusters by monitoring the increase in EGFP puncta. We found that both Slitrk3-Fc and IL-1RAcP-Fc also induced significant clustering of PTPδ in the cell membrane (**Figure 3B**, top and **Figure 3C**). Surprisingly, we observed no significant clustering of PTPσ upon treatment with TrkC-Fc (**Figure 3B**, middle left and **Figure 3C**). Neurotrophin-3 (NT-3) was recently reported to exert its modulatory effects on synaptogenesis by enhancing interactions between axonal PTPσ and dendritic TrkC (Ammendrup-Johnsen et al., 2015; Han et al., 2016b). We therefore asked whether the dimeric NT-3/ecto-TrkC (TrkC LRR-Ig1-2 domain) complex is capable of inducing the clustering of PTPσ Ig1-FN3. Since the Fc dimer might hinder NT-3–mediated dimerization of TrkC, we removed the Fc tag from TrkC LRR-Ig1-2-Fc by digesting it with thrombin and then produced dimeric NT-3/ecto-TrkC complexes. Treatment of PTPσ-expressing cells with dimeric NT-3/ecto-TrkC complexes does not induce PTPσ clustering, indicating that TrkC fails to promote complex clustering, even in the presence of NT-3 (**Figure 3B**, middle right and **Figure 3C**).

Next, we examined whether binding of LAR-RPTPs reciprocally induces clustering of post-synaptic adhesion partners. To this end, we applied LAR-RPTP Ig1-3-Fc to COS-7 cells expressing Slitrk1 LRR1/2, Slitrk3 LRR1/2, TrkC LRR-Ig1-2, IL1RAPL1 Ig1-3, or IL-1RAcP Ig1-3 attached to the PDGFR transmembrane domain and an intracellular EGFP. The first three Ig domains (Ig1-3) of LAR-RPTPs constitute the minimal binding region, but the binding of LAR-RPTPs to Slitrks, TrkC, IL1RAPL1, or IL-1RAcP depends on a specific LAR-RPTP splice insert. Accordingly, we used PTPδ Ig1-3(+/+)-Fc for Slitrk3, IL1RAPL1 and IL-1RAcP, and PTPσ Ig1-3(−/−)-Fc for TrkC. We observed a gradual clustering of the postsynaptic adhesion molecules, Slitrk1, Slitrk3, IL1RAPL1 and IL-1RAcP at the cell membrane after treatment with the LAR-RPTP-Fc isoforms (**Figure 3D**, top and **Figure 3F**). In contrast, TrkC showed no clustering in response to PTPσ Ig1-3-Fc (**Figures 3E,F**). Fc alone did not induce any meaningful clustering of LAR-RPTPs or postsynaptic adhesion partners (**Figures 3B,D,E**, bottom). These results suggest that LAR-RPTP–mediated *trans*-synaptic adhesion complexes mutually induce their own lateral clustering in both presynaptic and postsynaptic membranes, although TrkC appears to be the exception to this rule.

Competitive Inhibition of LAR-RPTP *Trans*-Synaptic Adhesion Complex Formation by HS

Negative-stain electron microscopy and cluster assays on the cell membrane confirmed that HS promotes clustering not only of PTPσ, the reported cellular receptor for HSPG, but also of PTPδ. In contrast, CS did not induce PTPσ or PTPδ clustering in solution or on the cell membrane (Supplementary Figure S4), a finding consistent with a previous report (Coles et al., 2011). Because both HS and the postsynaptic adhesion molecules Slitrks, IL1RAPL1 and IL-1RAcP can induce oligomerization of LAR-RPTPs in the membrane, we asked whether the LAR-RPTP clustering elicited by these different ligands (i.e., postsynaptic adhesion partners and HSPG) is cooperative or competitive. The crystal structures of PTPδ/Slitrk1, PTPδ/IL1RAPL1 and PTPδ/IL-1RAcP *trans*-synaptic adhesion complexes showed that the HS-binding surfaces of the LAR-RPTP Ig1 domains are distinct from the Slitrk1- and IL-1RAcP-binding surfaces and only partially overlap with the IL1RAPL1-binding surface (**Figure 4A**; Um et al., 2014; Yamagata et al., 2015a,b).

We therefore examined whether LAR-RPTPs can form a ternary complex with HS and the postsynaptic adhesion molecules Slitrk1, IL1RAPL1 and IL-1RAcP by monitoring peak position in size-exclusion chromatography analysis after mixing HS with *trans*-synaptic adhesion complexes (i.e., PTPδ/Slitrk1, PTPδ/IL1RAPL1, or PTPδ/IL-1RAcP). Surprisingly, following incubation of the PTPσ/Slitrk1 complex with a 2-fold excess of HS, we observed a peak shift in the chromatography profile toward oligomeric PTPσ Ig1-3 species (**Figure 4B**, blue curve, left), with a corresponding dissociation of Slitrk1 LRR1 (**Figure 4B**, blue box, right). This result suggests that HS binding to PTPσ induces dissociation of the PTPσ/Slitrk1 complex, despite the fact that the HS-binding and Slitrk1-binding surfaces in PTPσ do not overlap. Next, we mixed HS with PTPσ to induce oligomerization of PTPσ Ig1-3, and then incubated the resulting complexes with Slitrk1 (**Figure 4B**, black curve, left); this completely inhibited PTPσ/Slitrk1 complex formation (**Figure 4B**, black box, right). Interestingly, the addition of CS to PTPσ/Slitrk1 *trans*-synaptic adhesion complexes did not affect the binding of Slitrk1 to PTPσ or induce any higher-order oligomerization (**Figure 4B**, green curve and box). Similarly, we found that HS treatment induced dissociation of the PTPδ/IL1RAPL1 and PTPδ/IL-1RAcP *trans*-synaptic adhesion complexes, whereas CS treatment did not (**Figures 4C,D** and Supplementary Figure S5). These results indicate that dominant binding of HS to the LAR-RPTP induces the dissociation of postsynaptic adhesion molecules from their *trans*-synaptic adhesion complexes, PTPδ/Slitrk1, PTPδ/IL1RAPL1 and PTPδ/IL-1RAcP.

We further performed cell adhesion assays to examine this HS-induced dissociation of *trans*-synaptic adhesion complexes on the cell membrane. To this end, we incubated L cells co-expressing each postsynaptic ligand and EGFP with another group of cells co-expressing the corresponding LAR-RPTP

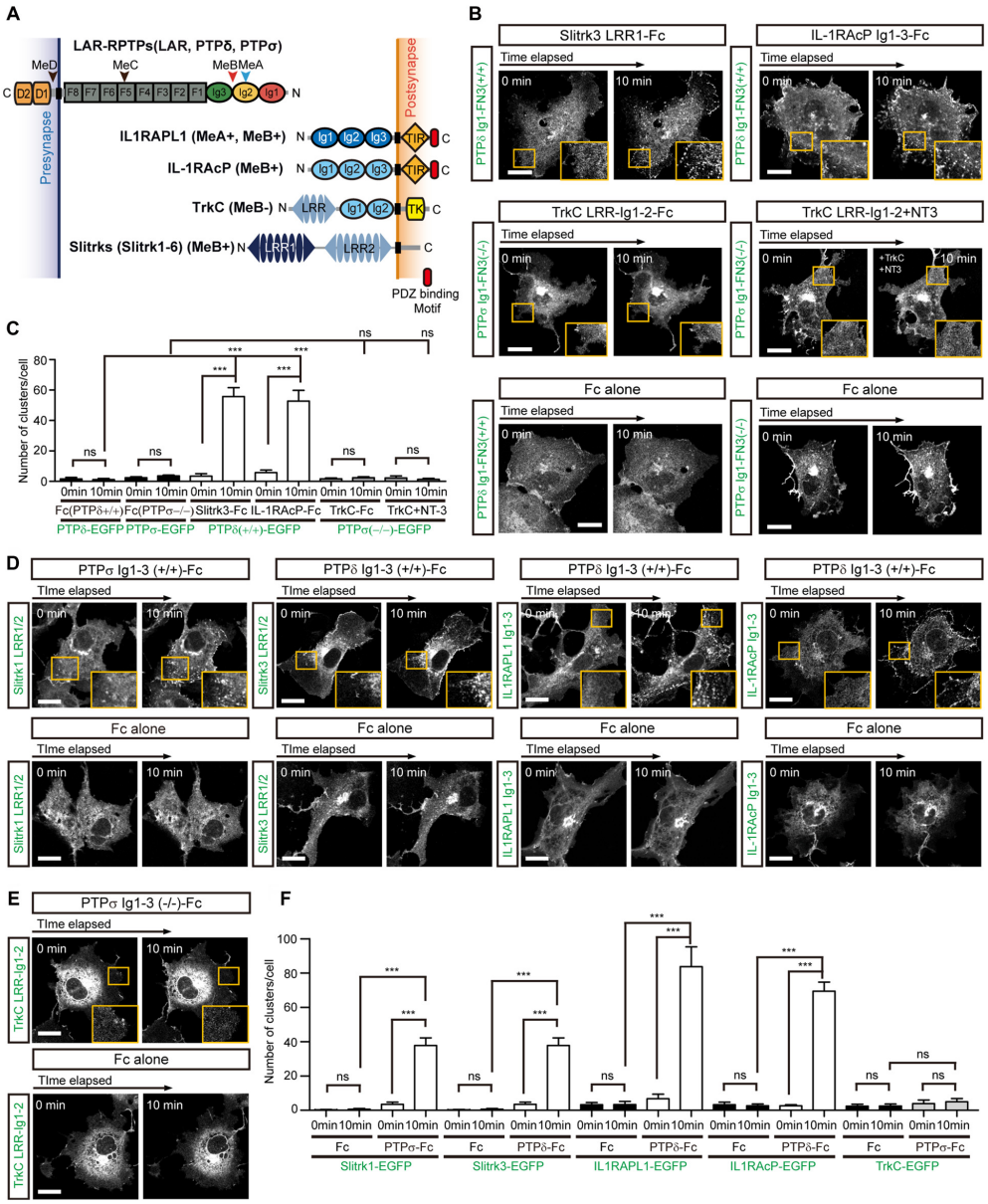

FIGURE 3 | Complex Formation between LAR-RPTPs and postsynaptic adhesion partners induces mutual clustering. **(A)** Schematic domain structure of LAR-RPTPs and their postsynaptic adhesion partners. Abbreviations: Ig, Ig-like domain (Ig1, red; Ig2, yellow; and Ig3, green); F, fibronectin-like domain (gray); D1 and D2, phosphatase domains; N, N-termini; C, C-termini; LRR, leucine-rich repeat; TIR, Toll/interleukin-1 receptor homology; TK, tyrosine kinase. The LRR1 and LRR2 domains of Slit- and Trk-like family of proteins (Slitrks) are shown in dark blue and light blue, respectively. The relative positions of the MeA, MeB, MeC and MeD splice inserts are indicated by arrowheads. **(B)** Postsynaptic adhesion partner binding induces LAR-RPTP clustering. Confocal time-lapse images of LAR-RPTP clustering in COS-7 cells induced by the addition of Fc-fused postsynaptic adhesion partners. COS-7 cells expressing PTPδ Ig1-FN3(+/+)-PDGFR_TM-EGFP (top) or PTPσ Ig1-FN3(−/−)-PDGFR_TM-EGFP (middle) were treated with 50 μg/ml of the indicated Fc-fused postsynaptic adhesion partner. COS-7 cells expressing PTPδ Ig1-FN3(+/+)-PDGFR_TM-EGFP or PTPσ Ig1-FN3(−/−)-PDGFR_TM-EGFP were treated with Fc alone as a control (bottom). Representative cell images before and 10 min after the treatment are shown. A magnified view of the yellow boxed area appears in the lower right corner of each image. Scale bars = 20 μm. **(C)** Quantification of data presented in **(B)**. A summary bar graph corresponding to the number of clusters accumulated in COS-7 cells is shown. Error bars in bar graphs represent SEM from 7 to 10 different cells from three independent experiments. Statistical significance was assessed by ANOVA followed by Tukey's *post hoc* test (***$P < 0.001$). **(D,E)** LAR-RPTP binding induces postsynaptic adhesion partner clustering. Confocal time-lapse images of postsynaptic adhesion partner clustering in COS-7 cells induced by the addition of Fc-fused LAR-RPTPs. COS-7 cells expressing Slitrk1 LRR1/2-PDGFR_TM-EGFP, Slitrk3 LRR1/2-PDGFR_TM-EGFP, IL-1RAPL1 Ig1-3-PDGFR_TM-EGFP, IL-1RAcP Ig1-3-PDGFR_TM-EGFP **(D)** or TrkC LRR-Ig1-2-PDGFR_TM-EGFP **(E)** were treated with 50 μg/ml of Fc alone or Fc-fused LAR-RPTPs, as indicated. Representative cell images before and 10 min after treatment are shown. A magnified view of the yellow boxed area appears in the lower right corner of each image. Scale bars = 20 μm. **(F)** Quantification of data presented in **Figures 3D,E**. Summary bar graph corresponding to the number of clusters accumulated in COS-7 cells is shown. Error bars in bar graphs represent SEM from 7 to 10 different cells from three independent experiments. Statistical significance was assessed by ANOVA followed by Tukey's *post hoc* tests (***$P < 0.001$).

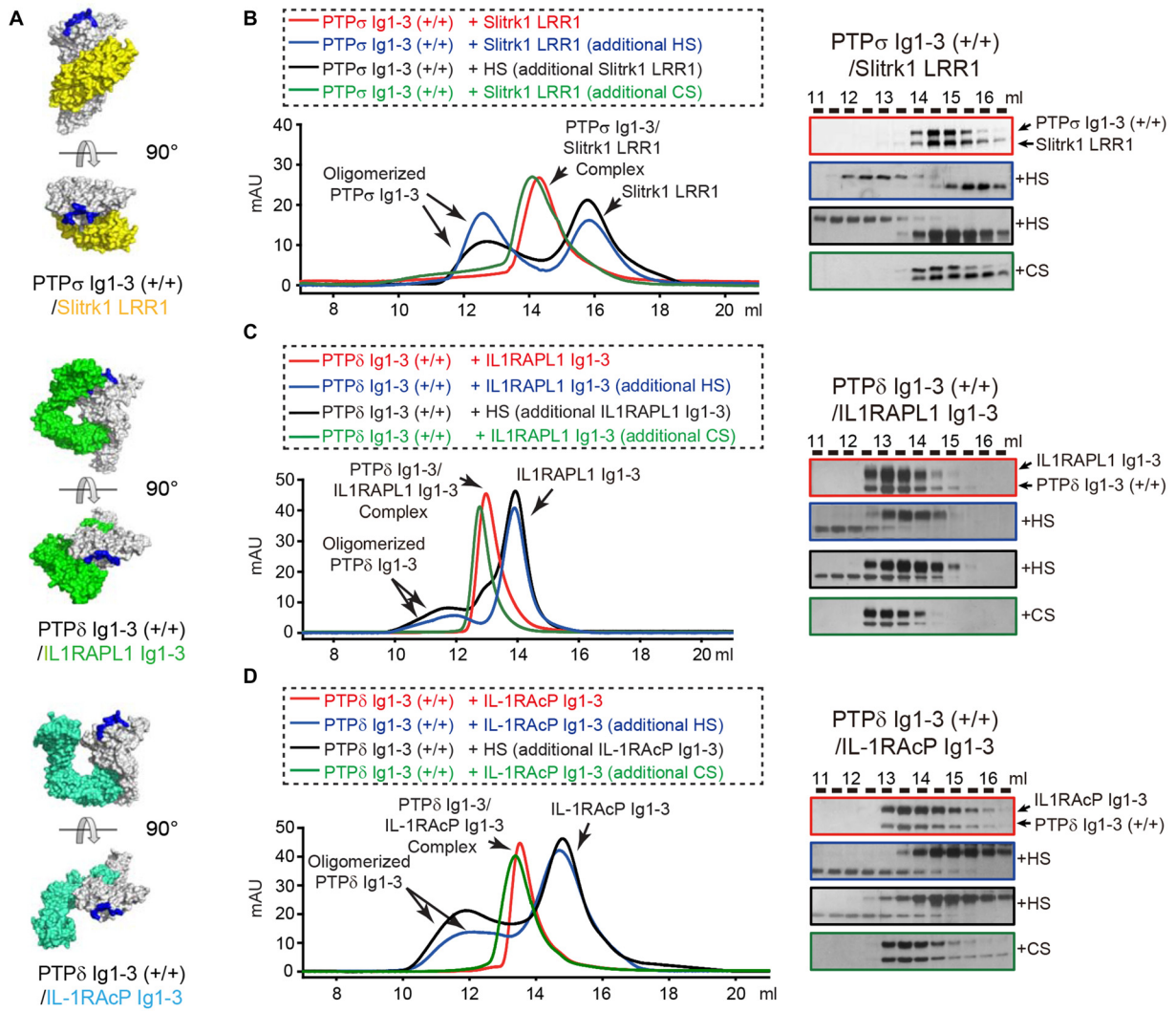

FIGURE 4 | Dissociation of *Trans*-synaptic adhesion complexes by heparan sulfate (HS). **(A)** Surface views of the crystal structures of the *trans*-synaptic adhesion complexes, PTPδ Ig1-3/Slitrk1 LRR1 (PDB: 4RCA), PTPδ Ig1-3/IL1RAPL1 Ig1-3 (PDB: 5Y32 and 5WY8) and PTPδ Ig1-3/IL-1RAcP Ig1-3(PDB: 4YFD). PTPδ and PTPσ are colored white. Slitrk1, IL1RAPL1 and IL-1RAcP are colored yellow, green and cyan, respectively. Potential HS-binding lysine patches on PTPδ and PTPσ (i.e., K68/K69/K71/K72 for PTPσ and K59A/K60A/K62A/K63A for PTPδ) are colored blue. **(B–D)** Size-exclusion chromatography (SEC) analysis to monitor the effects of HS and chondroitin sulfate (CS) on the interactions between the LAR-RPTPs, PTPσ Ig1-3 **(B)** or PTPδ Ig1-3 **(C,D)**, and their corresponding postsynaptic adhesion partners, Slitrk1 LRR1 **(B)**, IL1RAPL1 Ig1-3 **(C)** and IL-1RAcP Ig1-3 **(D)** (left). *Trans*-synaptic adhesion complexes (red), *trans*-synaptic adhesion complexes incubated with 2-fold molar excess of HS (blue), *trans*-synaptic adhesion complexes incubated with 2-fold molar excess of CS (green), and HS/LAR-RPTP complexes incubated with postsynaptic adhesion partners (black) were applied to a Superdex 200 10/300 GL column, and gel-filtration fractions were analyzed by SDS-PAGE and visualized by silver staining (right). Retention volumes are indicated above the gel images.

isoform and DsRed for 2 h at room temperature. In this assay, an increase in cell aggregation appears as an increase in fluorescence co-localization (yellow), indicating the presence of *trans* interactions between LAR-RPTPs and their postsynaptic adhesion partners (i.e., Slitrk1, IL1RAPL1, or IL-1RAcP; **Figures 5A–C**, WT control). To measure the effects of HS and CS on these *trans*-synaptic adhesion complexes, we incubated pre-formed cell aggregates with 0.5 mg/ml HS or CS for an additional 2 h. Consistent with our biochemical (size-exclusion chromatography) results (see **Figure 4**), we found that HS induced dissociation of pre-formed cell aggregates mediated by PTPσ/Slitrk1, PTPδ/IL1RAPL1 and PTPδ/IL-1RAcP *trans*-synaptic adhesion complexes. In contrast, CS had no effect (**Figures 5A–C**, WT+HS and WT+CS and **Figures 5D–F**).

To confirm that the specific binding of HS to LAR-RPTPs mediates the observed disruption of *trans*-synaptic adhesion complexes, we performed an additional round of cell adhesion assays using LAR-RPTPs containing HS-binding site mutations (K68A/K69A/K71A/K72A for PTPσ and K59A/K60A/K62A/K63A for PTPδ; Aricescu et al., 2002; Coles et al., 2011). These LAR-RPTP HS-binding-site mutants

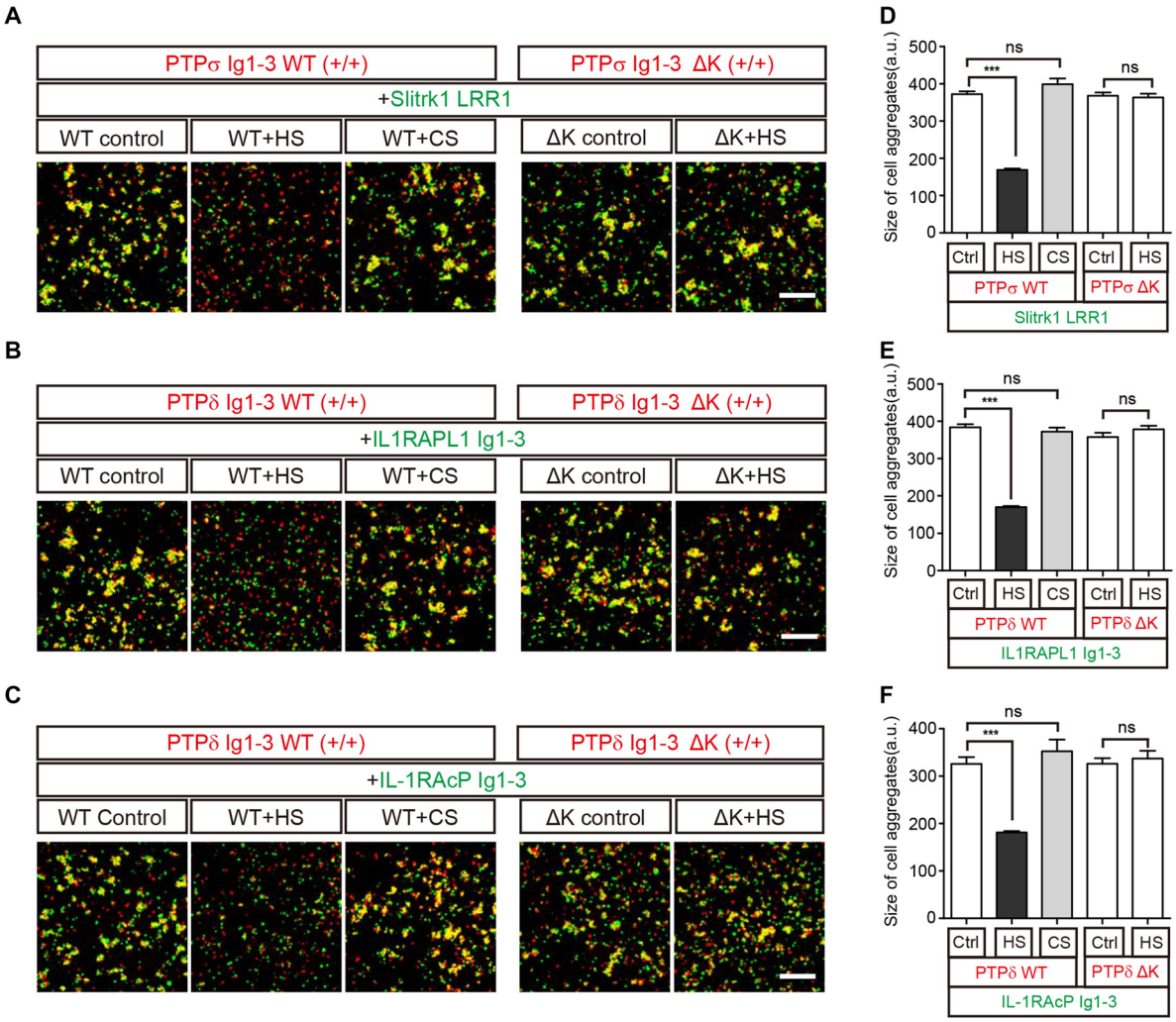

FIGURE 5 | HS Inhibits *Trans* interactions between cells expressing LAR-RPTPs and postsynaptic ligands. **(A–F)** Representative images **(A–C)** and summary bar graphs **(D–F)** for cell adhesion assays. In these assays, one group of L cells co-expressing DsRed and the indicated LAR-RPTP variant (pDis-PTPσ WT(+/+), pDis-PTPδ WT(+/+), pDis-PTPσΔK(+/+) or pDis-PTPδΔK(+/+)) was mixed with a second group of L cells co-expressing EGFP and the indicated postsynaptic adhesion partner (pDis-Slitrk1, pDis-IL1RAPL1, or pDis-IL-1RAcP) without HS. The effect of HS or CS on pre-formed *trans*-synaptic adhesion complexes was measured by treating mixed cell aggregates with 0.5 mg/ml HS or CS. Scale bars = 200 μm. Error bars represent SEM for 12–15 different cells from three independent experiments. Statistical significance was assessed by ANOVA with a Tukey's *post hoc* test (***$P < 0.001$).

are hereafter referred to as LAR-RPTPΔKs. LAR-RPTPΔKs were able to form normal *trans*-synaptic interactions with their postsynaptic synaptic adhesion partners (**Figures 5A–C**, ΔK control and **Figures 5D–F**) because the mutated HS-binding lysine residues do not participate in these interactions (Coles et al., 2014; Um et al., 2014; Yamagata et al., 2015b). In contrast to findings obtained with WT LAR-RPTPs, HS treatment had no effect on the appearance of pre-formed aggregates between cells expressing LAR-RPTPΔKs and their postsynaptic adhesion partners (**Figures 5A–C**, ΔK+HS and **Figures 5D–F**), probably because HS are unable to bind LAR-RPTPΔK. This indicates that the specific binding of HS to the LAR-RPTP disturbs the *trans*-synaptic interactions between presynaptic LAR-RPTPs and their postsynaptic adhesion partners, leading to dissociation of cell-to-cell contacts.

Together, our results indicate that HS binding to LAR-RPTPs is favored, although the higher-order assembly of LAR-RPTPs can be induced either by HS or the postsynaptic adhesion molecules, Slitrks, IL1RAPL1 and IL-1RAcP (**Figure 6**).

DISCUSSION

The higher-order assembly of adhesion complexes, like those formed by β-neurexin/neuroligin (Dean et al., 2003; Tanaka et al., 2012), Eph receptor/ephrin (Himanen et al., 2010; Seiradake et al., 2010), cadherins (Harrison et al., 2011) and SynCAM1 (Fogel et al., 2011), is a general hallmark

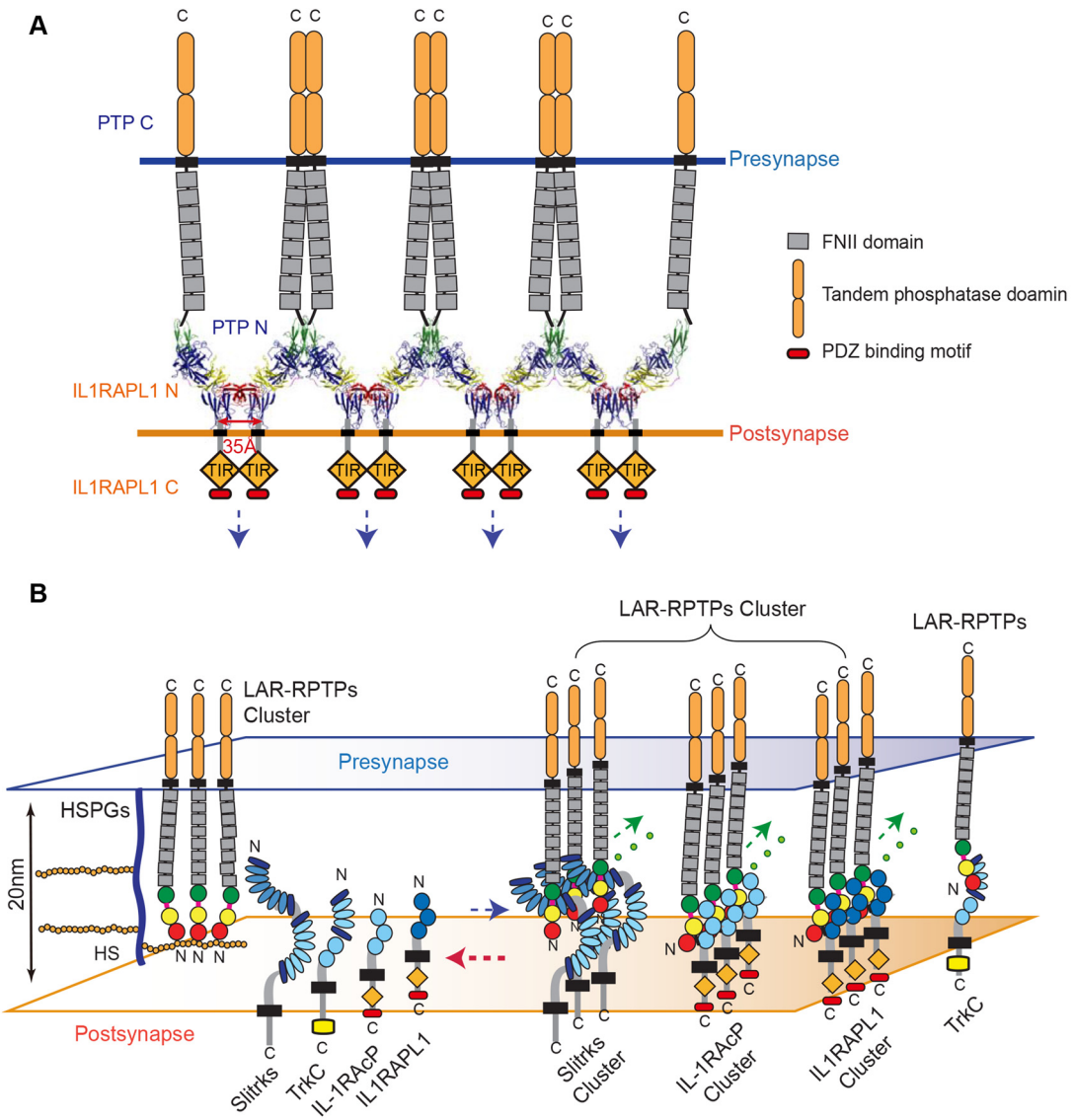

FIGURE 6 | Model for the modulation of LAR-RPTP clustering by both heparan sulfate proteoglycans (HSPGs) and postsynaptic adhesion partners. **(A)** A schematic representation of the lateral clustering of a *trans*-synaptic PTPδ Ig1-3/IL1RAPL1 Ig1-3 complex. The crystal structures of PTPδ Ig1-3/IL1RAPL1 Ig1-3 complexes are depicted as cartoons in the synaptic cleft. **(B)** The local concentration of HS or HSPG controls the state of LAR-RPTPs in a manner that blocks physical access to various postsynaptic adhesion partners (left). When the HS or HSPG level is decreased, postsynaptic adhesion partners bind to LAR-RPTPs, inducing the clustering of *trans*-synaptic adhesion complexes and subsequent synaptogenesis (right). **(A,B)** Fibronectin III domains and cytosolic tandem phosphatase domains of the LAR-RPTP are represented by gray and rounded orange boxes, respectively. The cytosolic TIR domains of IL1RAPL1 and IL-1RAcP are represented by orange rhombuses and labeled.

of adhesion-mediated cellular processes. Assembly of such oligomeric complexes is initiated by *trans*-interactions between the ecto-domains of adhesion partners in opposing membranes. These complexes, in turn, undergo lateral (*cis*) clustering, leading to the higher-order assembly of *trans*-adhesion complexes.

In this study, we determined the crystal structure of the human PTPδ Ig1-3/IL1RAPL1 complex, revealing that novel lateral interaction interfaces between neighboring *trans*-synaptic adhesion complexes are crucial for the clustering of PTPδ/IL1RAPL1 complexes as well as their synaptogenic activity, similar to the case for LAR-RPTP/Slitrk1 *trans*-synaptic adhesion complexes (Um et al., 2014). Interestingly, binding of either IL1RAPL1 or Slitrk1 induced LAR-RPTP clustering, but the critical residues for the clustering of these *trans*-synaptic adhesion complexes were not identical (Supplementary Figure S2), suggesting that the specific interface that drives their clustering is dependent on the post-synaptic adhesion ligand.

The higher-order assembly of the *trans*-synaptic adhesion complex, LAR-RPTP/IL1RAPL1, not only sheds light on the adhesion architecture of these complexes, but also provides clues about the potential mechanism of signal transduction that

occurs upon cell adhesion. IL1RAPL1, which belongs to a novel class of the TIR (Toll/IL-1 receptor domain) family, consists of three Ig-like domains, a single transmembrane segment, the TIR domain, and a C-terminal domain (Yoshida et al., 2011). In general, the intracellular TIR domain of TIR family receptors, such as Toll-like receptors (TLRs) and IL-17Rs, are juxtaposed upon ligand binding and subsequent dimerization, thereby activating a cytoplasmic signaling cascade. Interestingly, we noted that C-termini of neighboring IL1RAPL1 extracellular domains in the crystal lattice of the PTPδ Ig1-3/IL1RAPL1 Ig1-3 complex lie ∼35 Å apart (**Figure 6A**). This coincides with the distance between the two TIR domains of a ligand-bound TLR dimer as well as the distance between each intracellular TIR domain in the structure of the dimeric IL1RAPL1 TIR domain (PDB: 1T3G; Khan et al., 2004; Park et al., 2009). We therefore speculate that when the LAR-RPTP binds IL1RAPL1 and induces lateral clustering of *trans*-synaptic adhesion complexes, it brings the cytosolic TIR domains of neighboring IL1RAPL1s into close enough proximity to induce the recruitment of downstream adaptor molecules. As is the case for typical dimerization of the TIR domain, this would activate downstream signaling cascades in the postsynaptic neuron. Moreover, the clustering of LAR-RPTPs induced by various postsynaptic adhesion partners (i.e., Slitrks, IL1RAPL1 and IL-1RAcP) may facilitate the efficient organization of the presynaptic liprin-α/CASK/liprin-β–mediated supramolecular signaling complex (Wei et al., 2011) to regulate diverse presynaptic cellular signaling and differentiation processes. Further experiments will be necessary to fully explore this hypothesis.

TrkC binds neurotrophin NT-3 through its Ig2 domain and presynaptic PTPσ through its LRR and Ig1 domains (**Figure 3A**; Takahashi et al., 2011). The fact that these domains do not overlap suggests that TrkC can interact simultaneously with NT-3 and PTPσ. Although the requirement of NT-3 binding to the PTPσ/TrkC complex for glutamatergic postsynaptic differentiation is somewhat controversial (Takahashi et al., 2011; Ammendrup-Johnsen et al., 2015; Han et al., 2016b), we found here that neither TrkC alone nor the TrkC/NT-3 complex promoted higher-order assemblies of *trans*-synaptic adhesion PTPσ/TrkC complexes. This result is radically different from findings obtained with the other postsynaptic adhesion partners, Slitrk1, Slitrk3, IL1RAPL1 and IL-1RAcP (**Figure 3**). According to Takahashi et al. (2011) however, the artificial surface aggregation of TrkC using beads coated with either anti-TrkC antibody or PTPσ induces co-clustering of PSD-95 and the NMDA receptor NR1 subunit, leading to glutamatergic postsynaptic differentiation. Therefore, we cannot exclude the possibility that TrkC binding to PTPσ alone, or with the aid of additional factors (e.g., NT-3), might mediate lateral clustering of *trans*-synaptic adhesion complexes (PTPσ/TrkC) and activation of the bi-directional signaling necessary for synaptogenesis.

Knockout mice deficient for HS synthesis are known to exhibit specific brain malformations (Inatani et al., 2003). In the *Drosophila* neuromuscular junction, knockdown of two different enzymes that regulate HSPG sulfation induce opposing effects, either weakening or strengthening neurotransmission (Dani et al., 2012). HS- and CS-bound PTPσ in axons exert opposing effects on neuronal extension (Coles et al., 2011), suggesting that HS/HSPGs and CS/CSPGs modulate distinct downstream signaling pathways during neuronal growth depending on their modulation of the oligomeric status of LAR-RPTPs. Interestingly, HS on presynaptic GPC-4 mediates the interactions between presynaptic LAR-RPTPs and postsynaptic LRRTM4 for excitatory synaptic transmission (Ko et al., 2015). It has also been suggested that HSPG in association with polysialylated neural cell adhesion molecule (NCAM) can activate FGF receptors (FGFR), thus stimulating differentiation of presynaptic specializations (Dityatev et al., 2004; Dityatev and El-Husseini, 2006). Accumulating evidence clearly suggests that HS moieties in HSPGs regulate the strength of a neuronal adhesion and thus affect neuronal connectivity. In this study, we found that HS affected LAR-RPTP-mediated *trans*-synaptic adhesion complexes. LAR-RPTPs interacted exclusively with HS or the postsynaptic adhesion partners Slitrks, IL1RAPL1 and IL-1RAcP, but the dominant binding of HS to LAR-RPTPs effectively disrupted pre-formed LAR-mediated *trans*-synaptic adhesion complexes (**Figures 4**, **5**). Although the detailed molecular mechanisms underlying these observations should be further explored, the islands of high sulfation present in HS, but not CS, may promote close packing and clustering of LAR-RPTP (Coles et al., 2011), leading to a potential clash between postsynaptic adhesion partners and neighboring LAR-RPTPs, and the subsequent dissociation of postsynaptic adhesion partners from *trans*-synaptic adhesion complexes. Therefore, we speculate that LAR-RPTPs transit between HS-bound oligomers and *trans*-synaptic adhesion complexes, depending on the amount of HSPGs or soluble HS in the synaptic cleft (**Figure 6B**). In other words, HS or HSPGs can serve as molecular modulators of the initiation and/or termination of synaptic connections mediated by presynaptic LAR-RPTPs and their postsynaptic adhesion partners Slitrks, IL1RAPL1, IL-1RAcP and TrkC. It is also conceivable that HSPG may induce the LAR-RPTPs to exchange their postsynaptic adhesion partners from Slitrks, IL1RAPL1, IL-1RAcP, or TrkC to members of the LRRTM or FGFR for synaptogenesis and activity-dependent remodeling of synapses. It would be of great interest to investigate the ability of glycans to disrupt *trans*-synaptic adhesion as a function of HS and CS concentration, degree of sulfation and polymerization. Furthermore, an interesting question for future research would be to determine whether LAR-RPTP binding to HS/HSPGs or different postsynaptic adhesion partners (Slitrks, IL1RAPL1, IL-1RAcP, or TrkC) transmits distinct signals toward pre- or postsynaptic compartments and whether the properties of synapses induced by direct trans-synaptic adhesion can be different from those induced through incorporation of HSPGs.

In conclusion, LAR-RPTP clustering can be induced by either HS or the postsynaptic adhesion ligands Slitrks, IL1RAPL1 and IL-1RAcP (but not TrkC), but the dominant binding of HS to LAR-RPTPs can dismantle pre-established LAR-RPTP–mediated *trans*-synaptic adhesion complexes. Our results emphasize the complexity of the protein networks at

synapses and highlight our need to understand how they organize neuronal synapses. Such understanding would likely contribute to the future development of therapeutic interventions for cognitive and neuropsychiatric diseases, especially autism spectrum disorders, which have been linked to patient mutations in LAR-RPTPs, their postsynaptic adhesion partners, and HSPGs.

AUTHOR CONTRIBUTIONS

HMK: conceptualization; HMK, SYW, CYK, DK, EK and J-OL: methodology; SYW, CYK, DK, JK, JWU, SBL and MB: investigation; HMK, SYW, DK and MB: writing original draft; HMK, DK, EK, MB and WDH: funding acquisition; HMK, J-OL and WDH: supervision.

ACKNOWLEDGMENTS

This work was supported by grants from the National Research Foundation of Korea (NRF), Ministry of Science, ICT and Future Planning, Korea (NRF-2015R1A2A2A01005533 to HMK) and by the Institute for Basic Science (IBS; IBS-R002-D1 to HMK, DK and EK; IBS-R001-G1 to WDH). MB is supported by Foundation for the National Institutes of Health (NIH) grant R01GM112491.

SUPPLEMENTARY MATERIAL

The Supplementary Material for this article can be found online at: https://www.frontiersin.org/articles/10.3389/fnmol.2017.00327/full#supplementary-material

REFERENCES

Adams, P. D., Grosse-Kunstleve, R. W., Hung, L.-W., Ioerger, T. R., McCoy, A. J., Moriarty, N. W., et al. (2002). *PHENIX*: building new software for automated crystallographic structure determination. *Acta Crystallogr. D Biol. Crystallogr.* 58, 1948–1954. doi: 10.1107/s0907444902016657

Ammendrup-Johnsen, I., Naito, Y., Craig, A. M., and Takahashi, H. (2015). Neurotrophin-3 enhances the synaptic organizing function of TrkC-protein tyrosine phosphatase σ in rat hippocampal neurons. *J. Neurosci.* 35, 12425–12431. doi: 10.1523/JNEUROSCI.1330-15.2015

Aricescu, A. R., McKinnell, I. W., Halfter, W., and Stoker, A. W. (2002). Heparan sulfate proteoglycans are ligands for receptor protein tyrosine phosphatase σ. *Mol. Cell. Biol.* 22, 1881–1892. doi: 10.1128/mcb.22.6.1881-1892.2002

Booth, D. S., Avila-Sakar, A., and Cheng, Y. (2011). Visualizing proteins and macromolecular complexes by negative stain EM: from grid preparation to image acquisition. *J. Vis. Exp.* 58:e3227. doi: 10.3791/3227

Choi, S., Ko, J., Lee, J.-R., Lee, H. W., Kim, K., Chung, H. S., et al. (2006). ARF6 and EFA6A regulate the development and maintenance of dendritic spines. *J. Neurosci.* 26, 4811–4819. doi: 10.1523/JNEUROSCI.4182-05.2006

Choi, Y., Nam, J., Whitcomb, D. J., Song, Y. S., Kim, D., Jeon, S., et al. (2016). SALM5 trans-synaptically interacts with LAR-RPTPs in a splicing-dependent manner to regulate synapse development. *Sci. Rep.* 6:26676. doi: 10.1038/srep26676

Coles, C. H., Mitakidis, N., Zhang, P., Elegheert, J., Lu, W., Stoker, A. W., et al. (2014). Structural basis for extracellular *cis* and *trans* RPTPσ signal competition in synaptogenesis. *Nat. Commun.* 5:5209. doi: 10.1038/ncomms6209

Coles, C. H., Shen, Y., Tenney, A. P., Siebold, C., Sutton, G. C., Lu, W., et al. (2011). Proteoglycan-specific molecular switch for RPTPσ clustering and neuronal extension. *Science* 332, 484–488. doi: 10.1126/science.1200840

Dani, N., Nahm, M., Lee, S., and Broadie, K. (2012). A targeted glycan-related gene screen reveals heparan sulfate proteoglycan sulfation regulates WNT and BMP trans-synaptic signaling. *PLoS Genet.* 8:e1003031. doi: 10.1371/journal.pgen.1003031

de Wit, J., O'Sullivan, M. L., Savas, J. N., Condomitti, G., Caccese, M. C., Vennekens, K. M., et al. (2013). Unbiased discovery of glypican as a receptor for LRRTM4 in regulating excitatory synapse development. *Neuron* 79, 696–711. doi: 10.1016/j.neuron.2013.06.049

Dean, C., Scholl, F. G., Choih, J., DeMaria, S., Berger, J., Isacoff, E., et al. (2003). Neurexin mediates the assembly of presynaptic terminals. *Nat. Neurosci.* 6, 708–716. doi: 10.1038/nn1074

Dityatev, A., Dityateva, G., Sytnyk, V., Delling, M., Toni, N., Nikonenko, I., et al. (2004). Polysialylated neural cell adhesion molecule promotes remodeling and formation of hippocampal synapses. *J. Neurosci.* 24, 9372–9382. doi: 10.1523/JNEUROSCI.1702-04.2004

Dityatev, A., and El-Husseini, A. (2006). *Molecular Mechanisms of Synaptogenesis.* New York, NY: Springer.

Emsley, P., and Cowtan, K. (2004). Coot: model-building tools for molecular graphics. *Acta Crystallogr. D Biol. Crystallogr.* 60, 2126–2132. doi: 10.1107/s0907444904019158

Fogel, A. I., Stagi, M., Perez de Arce, K., and Biederer, T. (2011). Lateral assembly of the immunoglobulin protein SynCAM 1 controls its adhesive function and instructs synapse formation. *EMBO J.* 30, 4728–4738. doi: 10.1038/emboj.2011.336

Giagtzoglou, N., Ly, C. V., and Bellen, H. J. (2009). Cell adhesion, the backbone of the synapse: "vertebrate" and "invertebrate" perspectives. *Cold Spring Harb. Perspect. Biol.* 1:a003079. doi: 10.1101/cshperspect.a003079

Han, K. A., Jeon, S., Um, J. W., and Ko, J. (2016a). Emergent synapse organizers: LAR-RPTPs and their companions. *Int. Rev. Cell Mol. Biol.* 324, 39–65. doi: 10.1016/bs.ircmb.2016.01.002

Han, K. A., Woo, D., Kim, S., Choii, G., Jeon, S., Won, S. Y., et al. (2016b). Neurotrophin-3 regulates synapse development by modulating TrkC-PTPσ synaptic adhesion and intracellular signaling pathways. *J. Neurosci.* 36, 4816–4831. doi: 10.1523/JNEUROSCI.4024-15.2016

Harrison, O. J., Jin, X., Hong, S., Bahna, F., Ahlsen, G., Brasch, J., et al. (2011). The extracellular architecture of adherens junctions revealed by crystal structures of type I cadherins. *Structure* 19, 244–256. doi: 10.1016/j.str.2010.11.016

Himanen, J. P., Yermekbayeva, L., Janes, P. W., Walker, J. R., Xu, K., Atapattu, L., et al. (2010). Architecture of Eph receptor clusters. *Proc. Natl. Acad. Sci. U S A* 107, 10860–10865. doi: 10.1073/pnas.1004148107

Inatani, M., Irie, F., Plump, A. S., Tessier-Lavigne, M., and Yamaguchi, Y. (2003). Mammalian brain morphogenesis and midline axon guidance require heparan sulfate. *Science* 302, 1044–1046. doi: 10.1126/science.1090497

Johnson, K. G., Ghose, A., Epstein, E., Lincecum, J., O'Connor, M. B., and Van Vactor, D. (2004). Axonal heparan sulfate proteoglycans regulate the distribution and efficiency of the repellent slit during midline axon guidance. *Curr. Biol.* 14, 499–504. doi: 10.1016/j.cub.2004.02.005

Khan, J. A., Brint, E. K., O'Neill, L. A., and Tong, L. (2004). Crystal structure of the Toll/interleukin-1 receptor domain of human IL-1RAPL. *J. Biol. Chem.* 279, 31664–31670. doi: 10.1074/jbc.m403434200

Ko, J. S., Pramanik, G., Um, J. W., Shim, J. S., Lee, D., Kim, K. H., et al. (2015). PTPσ functions as a presynaptic receptor for the glypican-4/LRRTM4 complex and is essential for excitatory synaptic transmission. *Proc. Natl. Acad. Sci. U S A* 112, 1874–1879. doi: 10.1073/pnas.1410138112

Mah, W., Ko, J., Nam, J., Han, K., Chung, W. S., and Kim, E. (2010). Selected SALM (synaptic adhesion-like molecule) family proteins regulate synapse formation. *J. Neurosci.* 30, 5559–5568. doi: 10.1523/JNEUROSCI.4839-09.2010

McCoy, A. J., Grosse-Kunstleve, R. W., Storoni, L. C., and Read, R. J. (2005). Likelihood-enhanced fast translation functions. *Acta Crystallogr. D Biol. Crystallogr.* 61, 458–464. doi: 10.1107/s0907444905001617

Otwinowski, Z., and Minor, W. (1997). Processing of X-ray diffraction data collected in oscillation mode. *Meth. Enzymol.* 276, 307–326. doi: 10.1016/S0076-6879(97)76066-X

Park, B. S., Song, D. H., Kim, H. M., Choi, B. S., Lee, H., and Lee, J. O. (2009). The structural basis of lipopolysaccharide recognition by the TLR4-MD-2 complex. *Nature* 458, 1191–1195. doi: 10.1038/nature07830

Pei, J., and Grishin, N. V. (2001). AL2CO: calculation of positional conservation in a protein sequence alignment. *Bioinformatics* 17, 700–712. doi: 10.1093/bioinformatics/17.8.700

Pettersen, E. F., Goddard, T. D., Huang, C. C., Couch, G. S., Greenblatt, D. M., Meng, E. C., et al. (2004). UCSF Chimera—a visualization system for exploratory research and analysis. *J. Comput. Chem.* 25, 1605–1612. doi: 10.1002/jcc.20084

Pulido, R., Serra-Pages, C., Tang, M., and Streuli, M. (1995). The LAR/PTP δ/PTP σ subfamily of transmembrane protein-tyrosine-phosphatases: multiple human LAR, PTP δ, and PTP σ isoforms are expressed in a tissue-specific manner and associate with the LAR-interacting protein LIP.1. *Proc. Natl. Acad. Sci. U S A* 92, 11686–11690. doi: 10.1073/pnas.92.25.11686

Rawson, J. M., Dimitroff, B., Johnson, K. G., Rawson, J. M., Ge, X., Van Vactor, D., et al. (2005). The heparan sulfate proteoglycans Dally-like and Syndecan have distinct functions in axon guidance and visual-system assembly in *Drosophila*. *Curr. Biol.* 15, 833–838. doi: 10.1016/j.cub.2005.03.039

Seiradake, E., Harlos, K., Sutton, G., Aricescu, A. R., and Jones, E. Y. (2010). An extracellular steric seeding mechanism for Eph-ephrin signaling platform assembly. *Nat. Struct. Mol. Biol.* 17, 398–402. doi: 10.1038/nsmb.1782

Shen, Y., Tenney, A. P., Busch, S. A., Horn, K. P., Cuascut, F. X., Liu, K., et al. (2009). PTPσ is a receptor for chondroitin sulfate proteoglycan, an inhibitor of neural regeneration. *Science* 326, 592–596. doi: 10.1126/science.1178310

Siddiqui, T. J., Tari, P. K., Connor, S. A., Zhang, P., Dobie, F. A., She, K., et al. (2013). An LRRTM4-HSPG complex mediates excitatory synapse development on dentate gyrus granule cells. *Neuron* 79, 680–695. doi: 10.1016/j.neuron.2013.06.029

Takahashi, H., Arstikaitis, P., Prasad, T., Bartlett, T. E., Wang, Y. T., Murphy, T. H., et al. (2011). Postsynaptic TrkC and presynaptic PTPσ function as a bidirectional excitatory synaptic organizing complex. *Neuron* 69, 287–303. doi: 10.1016/j.neuron.2010.12.024

Tanaka, H., Miyazaki, N., Matoba, K., Nogi, T., Iwasaki, K., and Takagi, J. (2012). Higher-order architecture of cell adhesion mediated by polymorphic synaptic adhesion molecules neurexin and neuroligin. *Cell Rep.* 2, 101–110. doi: 10.1016/j.celrep.2012.06.009

Um, J. W., Kim, K. H., Park, B. S., Choi, Y., Kim, D., Kim, C. Y., et al. (2014). Structural basis for LAR-RPTP/Slitrk complex-mediated synaptic adhesion. *Nat. Commun.* 5:5423. doi: 10.1038/ncomms6423

Wang, D., Zhang, S., Li, L., Liu, X., Mei, K., and Wang, X. (2010). Structural insights into the assembly and activation of IL-1β with its receptors. *Nat. Immunol.* 11, 905–911. doi: 10.1038/ni.1925

Wei, Z., Zheng, S., Spangler, S. A., Yu, C., Hoogenraad, C. C., and Zhang, M. (2011). Liprin-mediated large signaling complex organization revealed by the liprin-α/CASK and liprin-α/liprin-β complex structures. *Mol. Cell* 43, 586–598. doi: 10.1016/j.molcel.2011.07.021

Woo, J., Kwon, S. K., Choi, S., Kim, S., Lee, J. R., Dunah, A. W., et al. (2009). Trans-synaptic adhesion between NGL-3 and LAR regulates the formation of excitatory synapses. *Nat. Neurosci.* 12, 428–437. doi: 10.1038/nn.2279

Yamagata, A., Sato, Y., Goto-Ito, S., Uemura, T., Maeda, A., Shiroshima, T., et al. (2015a). Structure of Slitrk2-PTPδ complex reveals mechanisms for splicing-dependent trans-synaptic adhesion. *Sci. Rep.* 5:9686. doi: 10.1038/srep09686

Yamagata, A., Yoshida, T., Sato, Y., Goto-Ito, S., Uemura, T., Maeda, A., et al. (2015b). Mechanisms of splicing-dependent trans-synaptic adhesion by PTPδ-IL1RAPL1/IL-1RAcP for synaptic differentiation. *Nat. Commun.* 6:6926. doi: 10.1038/ncomms7926

Yim, Y. S., Kwon, Y., Nam, J., Yoon, H. I., Lee, K., Kim, D. G., et al. (2013). Slitrks control excitatory and inhibitory synapse formation with LAR receptor protein tyrosine phosphatases. *Proc. Natl. Acad. Sci. U S A* 110, 4057–4062. doi: 10.1073/pnas.1209881110

Yoshida, T., Shiroshima, T., Lee, S. J., Yasumura, M., Uemura, T., Chen, X., et al. (2012). Interleukin-1 receptor accessory protein organizes neuronal synaptogenesis as a cell adhesion molecule. *J. Neurosci.* 32, 2588–2600. doi: 10.1523/JNEUROSCI.4637-11.2012

Yoshida, T., Yasumura, M., Uemura, T., Lee, S. J., Ra, M., Taguchi, R., et al. (2011). IL-1 receptor accessory protein-like 1 associated with mental retardation and autism mediates synapse formation by trans-synaptic interaction with protein tyrosine phosphatase δ. *J. Neurosci.* 31, 13485–13499. doi: 10.1523/JNEUROSCI.2136-11.2011

Conflict of Interest Statement: The authors declare that the research was conducted in the absence of any commercial or financial relationships that could be construed as a potential conflict of interest.

The handling editor is currently editing a Research Topic with one of the authors JK, and confirms the absence of any other collaboration.

frontiers in Molecular Neuroscience

ORIGINAL RESEARCH
published: 31 August 2017
doi: 10.3389/fnmol.2017.00281

Distinct Activities of Tfap2A and Tfap2B in the Specification of GABAergic Interneurons in the Developing Cerebellum

Norliyana Zainolabidin[1,2], *Sandhya P. Kamath*[1,2], *Ayesha R. Thanawalla*[1,2] *and Albert I. Chen*[1,2,3]*

[1]School of Biological Sciences, Nanyang Technological University (NTU), Singapore, Singapore, [2]School of Life Sciences, University of Warwick, Coventry, United Kingdom, [3]A*STAR, Institute of Molecular and Cell Biology, Singapore, Singapore

GABAergic inhibitory neurons in the cerebellum are subdivided into Purkinje cells and distinct subtypes of interneurons from the same pool of progenitors, but the determinants of this diversification process are not well defined. To explore the transcriptional regulation of the development of cerebellar inhibitory neurons, we examined the role of Tfap2A and Tfap2B in the specification of GABAergic neuronal subtypes in mice. We show that Tfap2A and Tfap2B are expressed in inhibitory precursors during embryonic development and that their expression persists into adulthood. The onset of their expression follows Ptf1a and Olig2, key determinants of GABAergic neuronal fate in the cerebellum; and, their expression precedes Pax2, an interneuron-specific factor. Tfap2A is expressed by all GABAergic neurons, whereas Tfap2B is selectively expressed by interneurons. Genetic manipulation via *in utero* electroporation (IUE) reveals that Tfap2B is necessary for interneuron specification and is capable of suppressing the generation of excitatory cells. Tfap2A, but not Tfap2B, is capable of inducing the generation of interneurons when misexpressed in the ventricular neuroepithelium. Together, our results demonstrate that the differential expression of Tfap2A and Tfap2B defines subtypes of GABAergic neurons and plays specific, but complementary roles in the specification of interneurons in the developing cerebellum.

Keywords: Tfap2A, Tfap2B, cerebellum, GABAergic interneurons, transcription factors, development

OPEN ACCESS

Edited by:
Jaewon Ko,
Daegu Gyeongbuk Institute of Science and Technology (DGIST), South Korea

Reviewed by:
Kathleen Millen,
Seattle Children's Hospital, United States
Sandra Blaess,
University of Bonn, Germany

***Correspondence:**
Albert I. Chen
albert.chen@ntu.edu.sg

Received: *27 May 2017*
Accepted: *18 August 2017*
Published: *31 August 2017*

Citation:
Zainolabidin N, Kamath SP, Thanawalla AR and Chen AI (2017) Distinct Activities of Tfap2A and Tfap2B in the Specification of GABAergic Interneurons in the Developing Cerebellum. Front. Mol. Neurosci. 10:281. doi: 10.3389/fnmol.2017.00281

INTRODUCTION

The cerebellum plays a critical role in sensory-motor integration and is important for the precise coordination of body, limb and eye movements as well as adaptation and learning of motor skills (Eccles et al., 1967; Thach and Bastian, 2004; Ito, 2006). The ability of the cerebellum to carry out these tasks relies on the specification of distinct classes of cerebellar neurons and the assembly of these neurons into functional circuits during development. Despite consisting of less than 10 percent of all neurons in the cerebellum (Andersen et al., 1992; Korbo et al., 1993), the different subtypes of inhibitory neurons play important roles in cerebellar function by providing feedback and feedforward inhibition (Eccles et al., 1967; Ito, 2006). Cerebellar cortical inhibitory neurons use gamma-aminobutyric acid (GABA) and/or glycine and are made up of four major subtypes: stellate, basket, Purkinje and Golgi cells (Miale and Sidman, 1961; Sillitoe and Joyner, 2007). Stellate and basket cells provide feedforward inhibition to Purkinje cells

and together regulate motor learning and adaptation as well as fine motor movements (Eccles et al., 1967; De Zeeuw et al., 1998; Wulff et al., 2009; Heiney et al., 2014). Golgi cells, on the other hand, provide feedback inhibition to granule cells to regulate motor coordination and compound movement (Watanabe et al., 1998; D'Angelo et al., 2013). Even though the electrophysiological and morphological properties as well as, to some extent, functional relevance of cerebellar inhibitory neurons have been examined (Palay and Chan-Palay, 1974; Ito, 2006), the molecular mechanisms underlying the diversification of distinct subtypes of cerebellar inhibitory neurons are not well defined.

There is growing evidence that the specification of inhibitory neuronal identity in the cerebellum is controlled by the expression of a set of transcription factors (Pascual et al., 2007; Zordan et al., 2008; Hori and Hoshino, 2012; Hoshino, 2012; Leto and Rossi, 2012). GABAergic neurons of the cerebellar cortex originate from the ventricular neuroepithelium and express basic helix-loop-helix (bHLH) transcription factor Ptf1a, which is required for generation of stellate, basket, Purkinje and Golgi cells (Hoshino et al., 2005; Pascual et al., 2007; Yamada et al., 2014). GABAergic projection neurons, the Purkinje cells, are generated by progenitors within the cerebellar ventricular zone (VZ) and require Corl2/Skor2 for differentiation (Minaki et al., 2008; Nakatani et al., 2014). Another bHLH transcription factor, Olig2, is expressed in the embryonic VZ, and some Olig2-expressing cells differentiate into Purkinje cells (Seto et al., 2014b; Ju et al., 2016). GABAergic interneurons in the cerebellar cortex, which include stellate, basket and Golgi cells, and in the deep cerebellar nuclei (DCN), are generated in the same region and express Pax2 as GABAergic interneuron precursors that proliferate in the white matter (WM) layer (Maricich and Herrup, 1999; Leto et al., 2006, 2009; Weisheit et al., 2006). A set of homeobox transcription factors Lhx1/5 is expressed by all GABAergic postmitotic neurons, however, deletion of Lhx1 and Lhx5 results only in the loss of Purkinje cells, but not GABAergic interneurons (Zhao et al., 2007). Even though a transcriptional program for cerebellar GABAergic neuronal specification is emerging, whether differentially expressed transcription factors have the capability to specify GABAergic interneurons has not yet been identified.

Transcriptome analysis has revealed a number of transcription factors that are regulated by Ptf1a including Lhx1, Lhx5, Corl2, Ngn2 and Pax2 (Borromeo et al., 2014; Russ et al., 2015). Also included in this list are two members of the Transcription Factor AP-2 (Tfap2) family of proteins Tfap2A and Tfap2B (Meredith et al., 2013; Borromeo et al., 2014; Jin et al., 2015; Russ et al., 2015). Tfap2A and Tfap2B have been demonstrated to play important roles for the development of a variety of tissues including the nervous system, kidney, skeleton, skin, limbs and the eye (Schorle et al., 1996; Zhang et al., 1996; Nottoli et al., 1998; West-Mays et al., 1999; Eckert et al., 2005; Seberg et al., 2017). For instance, in the developing nervous system, Tfap2A and Tfap2B are required for the survival of sympathetic and sensory ganglia progenitors (Schmidt et al., 2011). In the developing mouse retina, Tfap2A and Tfap2B have been shown to promote the differentiation of GABAergic and glycinergic amacrine cells (Jin et al., 2015). Thus, these two members of the Tfap2 family of transcription factors appear to regulate proliferation and survival of various cell types and may also be involved in the specification of distinct neuronal subtypes during development.

In addition to the sympathetic and sensory ganglia, both *Tfap2A* and *Tfap2B* transcripts are expressed in the developing and mature mouse cerebellum (Moser et al., 1995, 1997; Shimada et al., 1999), but the neuronal subtypes within the cerebellum that express these transcription factors have not yet been determined. Moreover, the functional significance of these transcription factors in the specification of cerebellar neuronal subtypes is not known. In this study, we examine the expression pattern and function of Tfap2A and Tfap2B in the mouse cerebellum. First, we assessed the spatial-temporal expression of Tfap2A and Tfap2B across embryonic and postnatal stages. Next, we compared their expression with cell type-specific and developmental markers. Finally, using *in utero* electroporation (IUE), we explored the functional significance of Tfap2A and Tfap2B during the development of cerebellar GABAergic neuronal subtypes.

MATERIALS AND METHODS

Animals

C57BL/6JInv mice were used in this study. All mice were housed and bred in Agency for Science, Technology and Research Biological Resource Centre on a 12 h light/dark cycle with free access to food and water. This study was carried out in accordance with the recommendations of Agency for Science, Technology and Research Biological Resource Centre. All protocols were approved by the Institute of Animal Care and Use Committee in accordance with the National Advisory Committee for Laboratory Animal Research guidelines.

Immunohistochemistry

Mice were anesthetized with 2.5% Avertin [0.025 g/mL 2,2-2 Tribomoethanol (Sigma) in 2-Methyl-2-butanol (Sigma)] prior to perfusion with 0.9% saline and 4% paraformaldehyde (Sigma). Early postnatal tissues were then post-fixed for 1 h while adult tissues were post-fixed overnight in 4% paraformaldehyde. Pregnant mice were euthanized using carbon dioxide gas chamber and confirmed through cervical dislocation. Embryos were collected in 4% paraformaldehyde and post-fixed for 30 min. All tissues were preserved overnight in 30% sucrose (1st BASE) and stored in −80°C in O.C.T compound (Sakura Finetek). All tissues were sectioned at 16–20 μm using a cryostat (ThermoScientific).

Tissue sections were permeabilized with 0.3% Triton-X (OmniPur) in phosphate buffered saline (PBS; 1st Base) for 10 min and blocked for 1 h with 2% horse serum (Invitrogen) and 0.1% Triton-X in PBS. The sections were then incubated with primary antibodies overnight in 4°C. On the following day, the tissues were washed with 0.1% Triton-X in PBS for 3 min three times and incubated with secondary antibodies for 1 h. Tissue sections were again washed and stained with DAPI before being mounted with a coverslip.

Primary antibodies used were as follows: rabbit anti-Tfap2B (1:10,000; gift from T. Jessell, Columbia University), rabbit anti-Ptf1a (1:1000; gift from C. Wright, Vanderbilt University), rabbit anti-Tfap2A (1:500; Santa Cruz Bio Technology), goat anti-Pax6 (1:500; Santa Cruz Bio Technology) and mouse anti-Pax2 (1:500; Santa Cruz Bio Technology), mouse anti-Tfap2A (2 μg/mL; developed by T. Williams, Developmental Studies Hybridoma Bank) and mouse anti-Lhx1/5 (2 μg/mL; developed by T. Jessell, Developmental Studies Hybridoma Bank), goat anti-Olig2 (1:250; R&D), mouse anti-Calbindin (1:5000; Swant) and goat anti-Parvalbumin (1:5000; Swant), rat anti-green fluorescent protein (GFP) (1:1000; Nacalai Tesque) and rat anti-RFP (1:500; Chromotek). Secondary antibodies used were as follows: Donkey anti-Rabbit Alexa Fluor 488, Donkey anti-Rabbit Alexa Fluor 647, Donkey anti-Goat Alexa Fluor 555, Donkey anti-Mouse Alexa Fluor 647, Donkey anti-Rat Alexa Fluor 488 and Donkey anti-Rat Alexa Fluor 555 (1:1000; Molecular Probes).

Generation of Expression Constructs

For overexpression (OE) studies, pCDH lentivector (p*EF1*-MCS-IRES-RFP) was used (System Bioscience, #CD531A-2). Individual transfer vectors containing open reading frames of *Tfap2A* and *Tfap2B* (GeneArt Invitrogen) were sub-cloned into multiple cloning site (MCS) of pCDH lentivector. Plasmids were digested with *Xba*I and *Not*I (New England Biolabs) restriction enzymes and isolated on 1% agarose gel. Digested plasmids were ligated using T7 DNA ligase (New England Biolabs) for 20–22 h at 16°C. For knockdown studies, pLL3.7 lentivector (p*U6*-MCS-*CMV*-GFP; Addgene) was used to express target short hairpin RNA (shRNA) under *U6* promoter and GFP reporter controlled by *cytomegalovirus* (*CMV*) promoter. DNA oligonucleotides which will be transcribed into shRNA were designed using Invitrogen BLOCK-iT$_{TM}$ RNAi Designer. It comprised of *Xho*I overhang (5′ TCGA 3′) on the 5′ end of the antisense strand and a short hairpin loop (5′ TTCAAGAGA 3′). Targeting sequence used for scramble is 5′ TGCCCTACCACCGAGGTCAA 3′, for Tfap2A knockdown is 5′ TGACAACATTCCGATCCCAATG 3′ and for Tfap2B knockdown is 5′ TGCATGGACAAGATGTTCTTGA 3′. Forty micromolar of sense and antisense oligonucleotides diluted in 1X T4 DNA ligase buffer (New England Biolabs) were annealed by boiling at 100°C for 10 min and cooled to room temperature. Subsequently, both the pLL3.7 and annealed oligonucleotides were digested, separately, with *Xho*I and *Hpa*I (New England Biolabs). Ligation was carried out similar to the OE construct. Cloned vectors were sequenced by Institute of Molecular and Cellular Biology, DNA Sequencing Facility.

Western Blot

Human embryonic kidney 293T (HEK-293T) cells were seeded at a density of 500,000 cells per well in a 6-well tissue culture plate a day before transfection. OPTI-MEM reduced serum media (Gibco) was used to dilute 1 μg of DNA as well as Lipofectamine 2000 reagent (Invitrogen). Lipid-DNA mixture was introduced into the cells and was incubated for 48 h before protein isolation.

Cells were washed once with PBS before proteins were isolated using M-PER mammalian protein extraction reagent (Pierce) which is supplemented with phosphatase inhibitor tablet (Pierce) and protease inhibitor cocktail (Sigma). Proteins were subsequently quantified via colorimetric assay (Bio-Rad) according to manufacturer's protocol. Twenty microgram of proteins were used for fractionation by SDS-PAGE and transferred to a PVDF membrane using iBlot® Dry Blotting System (Invitrogen). After incubation with 2% Bovine Serum Albumin (BSA) diluted in TBS-T (10 mM Tris [pH 8.0], 150 mM NaCl, 0.5% Tween 20) for an hour, this blocking buffer was decanted and primary antibodies were incubated overnight at 4°C.

The primary antibodies used were as follows: rabbit anti-Tfap2A (1:500; Santa Cruz Bio Technology), rabbit anti-Tfap2B (1:500; Santa Cruz Bio Technology), and mouse anti-GAPDH (0.05 μg/mL; Sigma). On the next day, membranes were washed with TBS-T thrice, for 10 min each before being incubated with appropriate secondary antibodies. The secondary antibodies used were diluted in blocking buffer as follows: anti-mouse IgG fragment-peroxidase antibody produced in goat (1:3000; Sigma) and anti-rabbit IgG fragment-peroxidase antibody produced in goat (1:3000; Sigma). Membrane was washed again, similarly, before being developed with the ECL system (Cell Signaling) according to manufacturer's protocol.

In Utero Electroporation

C57BL/6J pregnant mice were anesthetized with 2% isoflurane throughout the procedure and were kept warm using a homeothermic blanket. Hair on the abdomen area was shaved and skin cleaned with cotton swabs soaked in 70% ethanol. A small incision (5–10 mm) on the abdomen through the midline was done and gauze moistened with 42°C 0.9% saline was placed around the incision. Another incision on the muscle was made and both of the uterine horns were carefully placed on the gauze. From time to time, the exposed embryos were moistened with warm saline. 2–5 μL of purified plasmids (1 μg/μL) with Fastgreen Dye (0.1 mg/mL) were delivered into the fourth ventricle using a glass capillary. Electrodes were positioned in between the ventricles and five pulses of 250 mV for 50 ms each, were delivered. Uterine horns were returned into the peritoneal cavity and warm saline was added before the lining of cavity and the skin was sutured. Mice were given Meloxicam for post-operative pain management.

Image and Cell Count Analysis

Confocal images from immunohistochemistry were captured using Zeiss LSM-710 Confocal Microscope System (Axio Imager Z2 Stand) on ZEN2011. All images were processed with ImageJ (National Institute of Health).

For the Tfap2-Pax2 cell count analysis, two sagittal sections were obtained from the vermis region of each of the three brains and cells were counted, Using ImageJ, specific regions of interest were manually drawn around all nuclei positive for Tfap2A, Tfap2B and Pax2 and were subsequently scored. Immuno-positive neurons were then grouped and percentages were calculated.

Analysis for *in utero* electroporation experiments was assessed by counting all, transfected cells in the WM layer from multiple sagittal sections (approximately 10–25 sections, 100–500 cells) were counted for three brains. Cells were scored for the respective molecular markers and percentages were calculated. Experimental groups were compared against control groups.

Statistical Analysis

A non-parametric student's *t*-test was carried out in all the experiments that require statistical analysis. Data represents mean ± SEM. All data was analyzed with GraphPad Prism 6. The statistical data are described in each figure legend.

RESULTS

Analysis of the Spatial Expression Pattern of Tfap2A and Tfap2B in the Developing and Mature Cerebellum

In order to uncover the involvement of Tfap2 transcription factors in the development of GABAergic neurons and determine their functional relevance, we analyzed the expression of Tfap2A and Tfap2B in the developing mouse cerebellum. We first assessed whether Tfap2A and Tfap2B are expressed in the rhombic lip (RL) and the intermediate domain of rhombomere (r)1, where the first cerebellar neurons such as glutamatergic DCN neurons and GABAergic Purkinje cells are generated at embryonic day (E) 10.5 (Hoshino et al., 2005; Machold and Fishell, 2005; Wang et al., 2005). The expression of both Tfap2A and Tfap2B was not detected in either of these regions at this stage (**Figures 1A,B**). At E12.5, we observed expression of Tfap2A and Tfap2B in the WM layer of the cerebellum, located superior to the VZ where GABAergic neurons are produced (**Figures 1C,D**; Hoshino et al., 2005). The expression of Tfap2B appears to be more widespread than Tfap2A at this stage which may reflect the expression of Tfap2B in non-cerebellar cell types (**Figures 1C–F**). Since GABAergic neurons transit in the WM before they reassemble to specific layers in the cerebellar cortex (Zhang and Goldman, 1996; Maricich and Herrup, 1999; Leto et al., 2009), our results suggest that Tfap2A$^+$ and Tfap2B$^+$ cells partake a GABAergic neuron migratory pathway and are expressed by GABAergic precursors in the embryonic cerebellum.

To determine whether the expression of Tfap2A and Tfap2B is maintained during late embryogenesis through postnatal stages, we analyzed their expression in perinatal and postnatal cerebellar tissues. The spatial expression pattern of Tfap2A and Tfap2B at E15.5 and P0 supports our earlier observations that Tfap2A and Tfap2B are expressed by GABAergic neurons (**Figures 1E–H**). In P10 and adult cerebellum, we found Tfap2A$^+$ neurons in the molecular layer (ML), Purkinje cell layer (PCL) and internal granular layer (IGL; **Figures 1I,K**). Tfap2A is expressed by a subset of calbindin$^+$ Purkinje cells in the developing cerebellum suggesting that it could mark early-onset Purkinje cell clusters which disperse after birth (**Figure 1G**, **Supplementary Figures S1A–D**). However, colocalization analysis in the coronal orientation in the adult cerebellum revealed that Tfap2A is uniformly expressed in parvalbumin$^+$ Purkinje cells (**Supplementary Figures S1E–H**). These results indicate Tfap2A is expressed in a subset of Purkinje

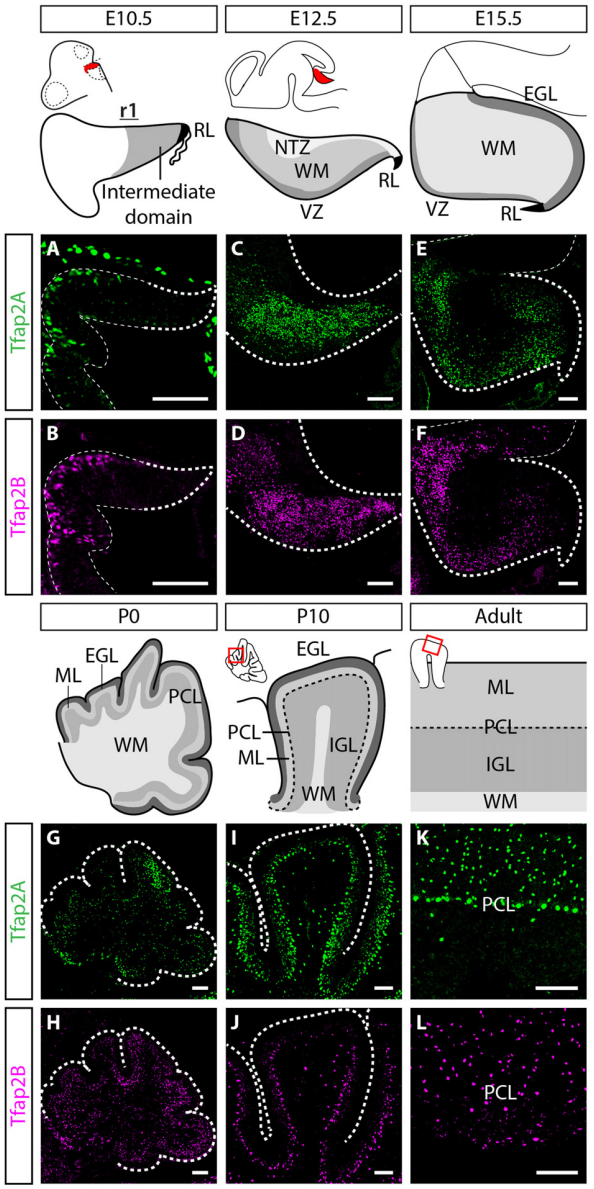

FIGURE 1 | Spatiotemporal expression pattern of Tfap2A and Tfap2B in the cerebellum. **(A,B)** Expression of both Tfap2A (green, **A**) and Tfap2B (magenta, **B**) is not detected in the cerebellar derivatives in r1 at E10.5. **(C–H)** Expression of Tfap2A and Tfap2B is detected in the underlying WM at E12.5 **(C,D)** and E15.5 **(E,F)** where inhibitory neurons transit after exiting the VZ. At early postnatal stages, P0 and P10, Tfap2A, but not Tfap2B, is expressed in the PCL **(G,I)**. In addition, by P10 both Tfap2A$^+$ **(I)** and Tfap2B$^+$ cells **(J)** have entered the lower half of the ML and the IGL. **(K,L)** In the mature cerebellum at P150, Tfap2A expression **(K)** is detected in the ML, PCL and IGL whereas Tfap2B expression **(L)** is restricted to the ML and IGL. Analysis performed on cerebellar vermal region of sagittal sections. Abbreviations: EGL, external germinal layer; IGL, internal granular layer; ML, molecular layer; NTZ, nuclear transitory zone; PCL, Purkinje cell layer; RL, rhombic lip; r1, rhombomere 1; VZ, ventricular zone; WM, white matter. Scale bar = 100 μm.

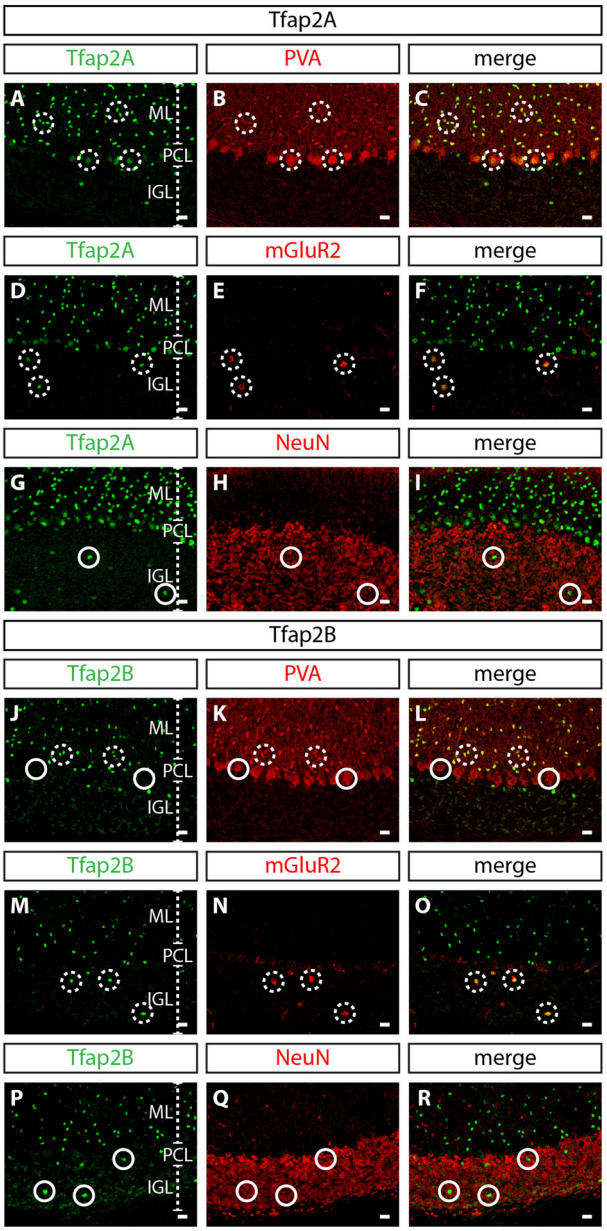

FIGURE 2 | Expression of Tfap2A and Tfap2B is restricted to GABAergic neuronal subtypes in the adult cerebellum. **(A–R)** Analysis of the expression of Tfap2A and Tfap2B with cell type-specific molecular markers in the adult cerebellar cortex. At P60, Tfap2A (green) is coexpressed with PVA (red) in the ML and PCL **(A–C)** and with mGluR2 (red) in the IGL **(D–F)**. Tfap2B (green) is coexpressed with PVA (red) only observed in the ML **(J–L)** and with mGluR2 (red) in the IGL **(M–O)**. No Tfap2A **(G–I)** or Tfap2B **(P–R)** expression (green) is detected in NeuN$^+$ granule cells (red) in the IGL. Analysis performed on cerebellar vermal region of sagittal sections. Broken circles indicate cells with colocalized expression, continuous circles indicate no colocalization. Abbreviations: IGL, internal granular layer; ML, molecular layer; PCL, Purkinje cell layer. Scale bar = 10 μm.

cells during development, but is expressed by all Purkinje cells in the adult cerebellum. Tfap2B$^+$ neurons, on the other hand, are only detected in the ML and IGL (**Figures 1J,L**). Thus, due to their overlapping expression pattern, we compared the expression of Tfap2A and Tfap2B with cell-type specific molecular markers in the adult cerebellum. We show that Tfap2A is found in stellate, basket and Purkinje cells, which are all labeled by parvalbumin (**Figures 2A–C**). Tfap2A is also found in Golgi cells, which are labeled by mGluR2 (**Figures 2D–F**). Tfap2B, on the other hand, is expressed only by stellate, basket and Golgi cells (**Figures 2J–O**). Neither Tfap2A nor Tfap2B is observed in NeuN$^+$ granule cells (**Figures 2G–I,P–R**). Additionally, analysis of the DCN also shows that Tfap2A, but not Tfap2B, labels small GABAergic neurons in all three nuclei (**Supplementary Figure S2**). Thus, analysis of the temporal and spatial expression pattern of Tfap2A and Tfap2B indicates that they are expressed as early as E12.5 in the cerebellum when GABAergic neurons are produced, and that their expression persists into adulthood.

Molecular Distinctions between Tfap2A$^+$ and Tfap2B$^+$ Neurons in the Developing Cerebellum

To define the identity of Tfap2A$^+$ and Tfap2B$^+$ cells in the early developing cerebellum, we differentiated regions of the embryonic cerebellum with relevant molecular markers of GABAergic lineage at E12.5. The VZ can be demarcated by Ptf1a, a transcription factor responsible for differentiation of neural precursors into GABAergic neuron precursors (Hoshino et al., 2005; Yamada et al., 2014). The cerebellar VZ can also be marked by two other transcription factors namely Olig2 and Pax2 which contribute to Purkinje cell and interneuron development (Seto et al., 2014a,b; Ju et al., 2016). We observed an overlap in the expression of Ptf1a and Olig2 which demonstrates that Olig2-expressing cells are GABAergic precursors (**Figures 3A–C**). Therefore, Tfap2A and Tfap2B are primarily expressed by cells in the VZ and WM (**Figures 3D–F**). However, we observed some Tfap2B$^+$ cells which do not express Tfap2A in the VZ (**Figures 3D–F**). Thus, the expression pattern at E12.5 indicates that Tfap2A$^+$ cells consist of a subset of Tfap2B$^+$ cells and suggests that their expression defines distinct neuronal subpopulations.

To determine whether Tfap2A and Tfap2B are expressed by mitotic or postmitotic GABAergic neurons, we assessed whether these cells express transcription factors Lhx1/5 (postmitotic), Olig2 and Pax2 (both mitotic and postmitotic; Maricich and Herrup, 1999; Chizhikov et al., 2006; Morales and Hatten, 2006; Zhao et al., 2007). In the VZ, most Tfap2A$^+$ cells express both Olig2 and Lhx1/5, indicating that these cells in the VZ are early postmitotic GABAergic neurons (**Figures 3G–J**). In contrast, some Tfap2B$^+$ cells in the VZ express Olig2 while others express both Olig2 and Lhx1/5 (**Figures 3K–N**). Thus, ∼50% of Olig2-expressing cells express Tfap2A while ∼100% of Olig2-expressing cells express Tfap2B (**Figures 3G–N**; data not shown). Together, these numbers suggest that Tfap2B$^+$ cells in the VZ consist of both mitotic as well as early postmitotic GABAergic cells. Tfap2A$^+$ and Tfap2B$^+$ cells in the WM only express Lhx1/5 indicating that they are postmitotic GABAergic neurons (**Figures 3G–N**). These results show that Tfap2A$^+$ and Tfap2B$^+$

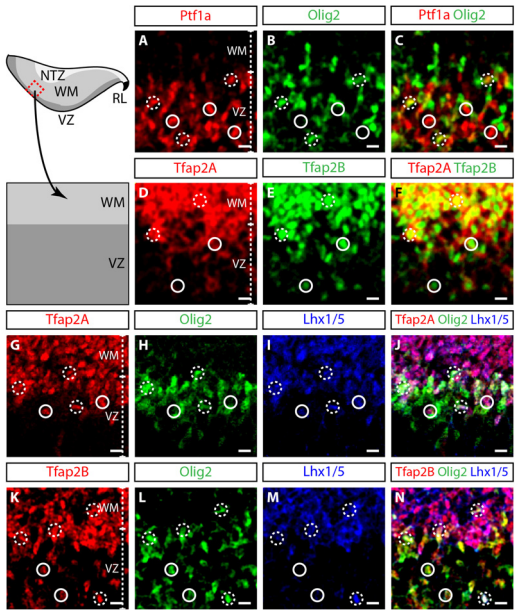

FIGURE 3 | Tfap2A and Tfap2B are expressed in GABAergic precursors. **(A–C)** At E12.5, Ptf1a (red, **A**) and Olig2 (green, **B**) expression is predominantly localized in the VZ. Overlapping Ptf1a and Olig2 expression is observed in the intermediary region of the VZ (broken circle). **(D–F)** Tfap2A (red, **D**) and Tfap2B (green, **E**) are coexpressed in the VZ and WM. **(G–J)** Expression of Tfap2A (red) colocalizes with Olig2 (green) and Lhx1/5 (blue) in the VZ (broken circle). However, not all Olig2-expressing cells in the VZ express Tfap2A (continuous circle, **J**). **(K–N)** The expression of Tfap2B also colocalizes with Olig2 and Lhx1/5 (broken circle). In addition, all Olig2-expressing cells express Tfap2B (circle). Analysis performed on cerebellar vermal region of sagittal sections. Broken circles indicate cells with colocalized expression, continuous circles indicate no colocalization. Abbreviations: VZ, ventricular zone; WM, white matter. Scale bar = 10 μm.

cells at E12.5 are GABAergic, and Tfap2A labels postmitotic cells while Tfap2B labels both mitotic and postmitotic cells in the VZ.

Hierarchical Expression of Ptf1a, Tfap2A/B and Pax2 in the Developing Cerebellum

The expression of Tfap2A and Tfap2B is not observed in the VZ delineated by Ptf1a, but is expressed together with Olig2, suggesting Ptf1a expression precedes Tfap2A and Tfap2B (**Figures 3G–N**; Hoshino et al., 2005). In addition, Tfap2A$^+$ and Tfap2B$^+$ cells also overlap with Pax2 indicating that these cells identify for interneuron precursors (**Supplementary Figure S3**). To determine the temporal expression pattern of Tfap2A and Tfap2B in relation to cerebellar neuronal markers, we compared their expression at E15.5 and E18.5 with Pax2 and RORα, molecular markers for GABAergic interneuron precursors and postmitotic Purkinje cells, respectively (Nakagawa et al., 1997; Maricich and Herrup, 1999; Ino, 2004; Weisheit et al., 2006). Purkinje cells are specified in the VZ while interneurons diversifies later in the WM (Miale and Sidman, 1961; Palay and Chan-Palay, 1974; Leto et al., 2006, 2009). At E15.5, RORα expression is localized in the dorsal region and spreads under the external germinal layer (EGL; **Figures 4A,C,D,F**). On the other hand, Pax2 expression is more limited to the

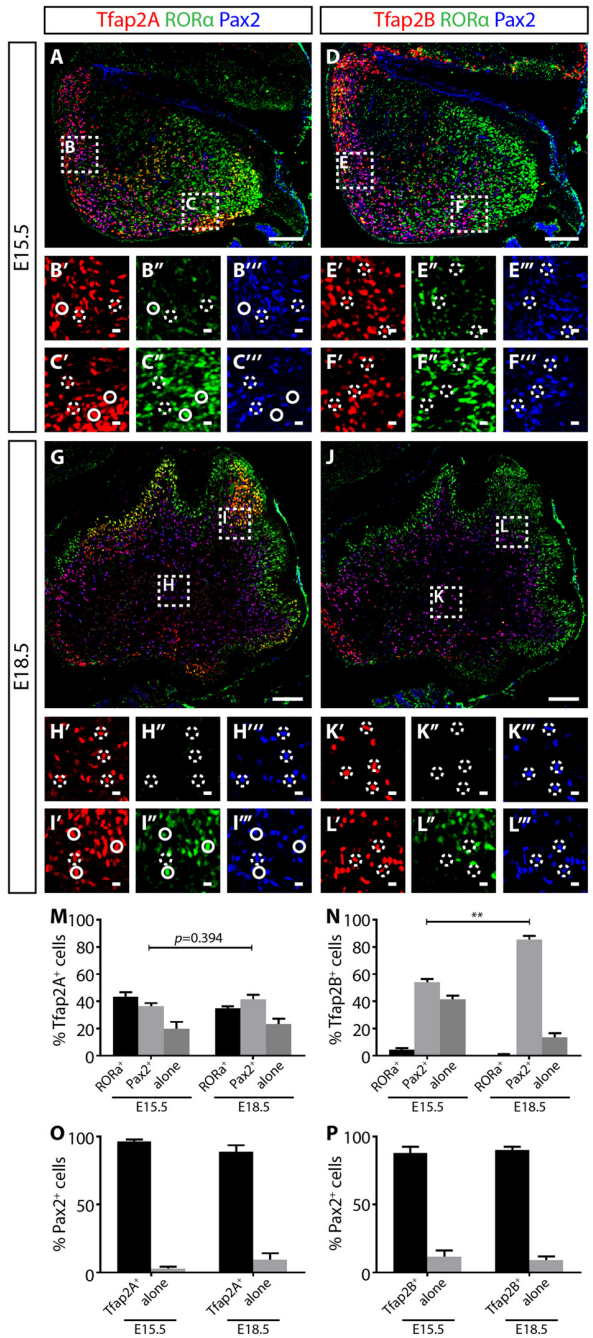

FIGURE 4 | Tfap2A and Tfap2B expression precedes Pax2 in the developing cerebellum. **(A–F‴)** At E15.5, Tfap2A is expressed by a subset of RORα$^+$ Purkinje cells (green) and Pax2$^+$ interneurons (blue) **(A)** while Tfap2B is expressed by only Pax2$^+$ interneurons **(D)**. Expression of RORα is localized mostly at the dorsal region of the cerebellum **(B′–B‴, E′–E‴)** while the expression of Pax2 is localized near the ventral region **(C′–C‴,F′–F‴)**. **(G–L‴)** At E18.5, the same Tfap2A$^+$ and Tfap2B$^+$ subpopulations persist, but with different distributions. **(M)** Quantification of three Tfap2A$^+$ neuronal subpopulations (E15.5: Tfap2A$^+$/RORα$^+$ = 43 ± 3%, Tfap2A$^+$/Pax2$^+$ = 37 ± 2%, Tfap2A$^+$-alone = 20 ± 5%; E18.5: Tfap2A$^+$/RORα$^+$ = 35 ± 1%, Tfap2A$^+$/Pax2$^+$ = 42 ± 3%, Tfap2A$^+$-alone = 23 ± 4%). **(N)** Quantification of two Tfap2B$^+$ neuronal

(*Continued*)

FIGURE 4 | Continued
subpopulations (E15.5: Tfap2B$^+$/Pax2$^+$ = 54 ± 3%, Tfap2B$^+$-alone = 42 ± 3%; E18.5: Tfap2B$^+$/Pax2$^+$ = 86 ± 3%, Tfap2B$^+$-alone = 14 ± 3%). **(O,P)** Analysis of Pax2$^+$ neuronal population indicates that most Pax2$^+$ interneurons express Tfap2A (E15.5: 97 ± 1%, E18.5: 89 ± 4%) and Tfap2B (E15.5: 88 ± 4%, E18.5: 90 ± 2%) at both E15.5 and E18.5. Analysis performed on cerebellar vermal region of sagittal sections. Continuous circles indicate colocalization of Tfap2 with RORα and broken circles indicate colocalization of Tfap2 with Pax2. Values represent mean ± SEM, n = 3 mice, 2 sections per mouse, $^*p \leq 0.05$, $^{**}p \leq 0.01$. Scale bar = 100 μm **(A,D,G,J)**, 10 μm (cropped images).

ventral region (**Figures 4A,B,D,E**). In E18.5 cerebellum, RORα is expressed in the PCL while Pax2 expression is restricted to the WM (**Figures 4H,I,K,L**). This pattern of expression defines the migrating status of Purkinje cells and GABAergic interneuron precursors from the VZ to the WM and finally to the cerebellar cortex providing us with the basis for analysis of Tfap2A and Tfap2B expression during this process.

At both E15.5 and E18.5, we identified three Tfap2A subpopulations (Tfap2A$^+$/Pax2$^+$, Tfap2A$^+$/RORα$^+$ and Tfap2A$^+$-alone) consisting of Purkinje cells and interneurons (**Figures 4A–C,G–I**). At these stages, we also identified two Tfap2B subpopulations (Tfap2B$^+$/Pax2$^+$ and Tfap2B$^+$-alone) made up of only interneurons, but not Purkinje cells, consistent with the lack of Tfap2B expression in Purkinje cells in the adult cerebellum (**Figures 4D–F,J–L**, see also **Figures 2J–L**). To examine the expression dynamics of Tfap2A and Tfap2B subpopulations, we analyzed sagittal sections of the cerebellum and examined the changes in the distribution of each subpopulation. Between E15.5 to E18.5, we detected a 5% increase in Tfap2A$^+$/Pax2$^+$ cells and a 3% increase in cells expressing only Tfap2A, although these changes are not statistically significant (p = 0.394; **Figure 4M**). We observed an increase in Tfap2B$^+$/Pax2$^+$ cells from 54% to 86% and a decrease in cells expressing only Tfap2B from 42% to 14% ($p \leq 0.01$; **Figure 4N**). These changes suggests that cells previously expressing only Tfap2A or Tfap2B are now also expressing Pax2, and that, perhaps, Tfap2A$^+$ and Tfap2B$^+$ cells become GABAergic interneurons expressing Pax2 as they mature in the WM. Analysis of changes in Pax2 expression between E15.8 and E18.5 revealed that ∼92% of Pax2$^+$ cells express Tfap2A and ∼89% express Tfap2B, indicating majority of Pax2$^+$ interneurons express Tfap2A and Tfap2B (**Figures 4O,P**). Together, these results provide evidence that the expression of Tfap2A and Tfap2B precedes the expression of Pax2 and raise the possibility that Tfap2A and Tfap2B regulate the expression of Pax2.

Manipulation of the Expression of Tfap2A and Tfap2B in GABAergic Precursors

To investigate the functional relevance of Tfap2A and Tfap2B during the development of GABAergic neuronal subtypes, we set out to manipulate the expression of Tfap2A and Tfap2B via IUE. We first generated knockdown constructs containing short hairpin RNA (shRNA) under mouse *U6* promoter and GFP under *CMV* promoter (p*U6*-shRNA-*CMV*-GFP; **Figure 5A**). We also generated cDNA constructs expressing either *Tfap2A* or *Tfap2B* and red fluorescent protein (RFP) separated by Internal Ribosomal Entry Site (IRES) sequence under the *elongation factor 1* (*EF1*) promoter (p*EF1*-cDNA-IRES-RFP; **Figure 5B**). To determine the efficiency and specificity of these constructs, knockdown and OE plasmids were co-transfected into HEK-293T cells which do not normally express either of these transcription factors. Following that, western blot was carried out to identify the most efficient and specific shRNA that targets the respective member of Tfap2. We found that pU6-2Ash2 and pU6-2Bsh2 to be most efficient and specific in targeting Tfap2A and Tfap2B expression, respectively, so they were subsequently used for *in vivo* experiments (**Figures 5C,D**).

For IUE experiments, plasmid constructs were delivered into the fourth ventricle (4v) of E12.5 wild-type (WT) embryos. Cells lining the 4v, which includes the VZ and RL with sparse Tfap2A and Tfap2B expression, were transfected via electroporation (**Figures 5E,F**, **Supplementary Figure S4**). After 3 days, transfected neurons from the VZ migrate anteriorly into the WM while neurons originating from the RL migrate tangentially over the cerebellar surface before descending into the WM (**Figure 5G**). Therefore, we analyzed the identity of transfected cells which have migrated into the WM. In control or scrambled experiments, ∼33% of GFP$^+$ cells express Tfap2A while ∼22% express Tfap2B (**Figures 5H,J,N,P**). In knockdown experiments, Tfap2A knockdown reduces the percentage of transfected cells expressing Tfap2A by 10-fold while Tfap2B knockdown reduces the percentage of transfected cells expressing Tfap2B by 20-fold (**Figures 5H–J,N–P**). In the OE experiments, we observed a ∼three-fold and five-fold increase in the number of transfected cells expressing Tfap2A and Tfap2B, respectively (**Figures 5K–M,Q–S**). This strategy provides means to manipulate Tfap2 expression *in vivo* through suppression and induction of their expression.

Consequences of Manipulating Tfap2A and Tfap2B Expression on Specification of GABAergic Interneurons

Ptf1a is a major determinant of specification of GABAergic neuronal fate (Pascual et al., 2007; Hori and Hoshino, 2012; Yamada et al., 2014), but determinants of GABAergic interneurons vs. GABAergic projection neurons are limited. To assess the capability of Tfap2A and Tfap2B in directing the specification of GABAergic neuronal subtypes, we analyzed consequences of misexpressing each transcription factor on the expression of neuronal markers, Pax2, Pax6 and CBP which correspond to GABAergic interneurons, glutamatergic neurons and Purkinje cells, respectively. We first examined whether misexpression of Tfap2A or Tfap2B is sufficient to regulate Pax2 expression. We did not observe any changes in the number of Pax2$^+$ interneurons in Tfap2B-misexpressed cells compared to control (**Figures 6A,C,D**). Interestingly, we observed a ∼16% decrease in the number of Pax6$^+$ excitatory cells within Tfap2B-misexpressed cells compared to control (**Figures 6E,G,H**). Next, we assessed consequences of misexpressing Tfap2A. Despite the inability of Tfap2B to change the number of Pax2$^+$

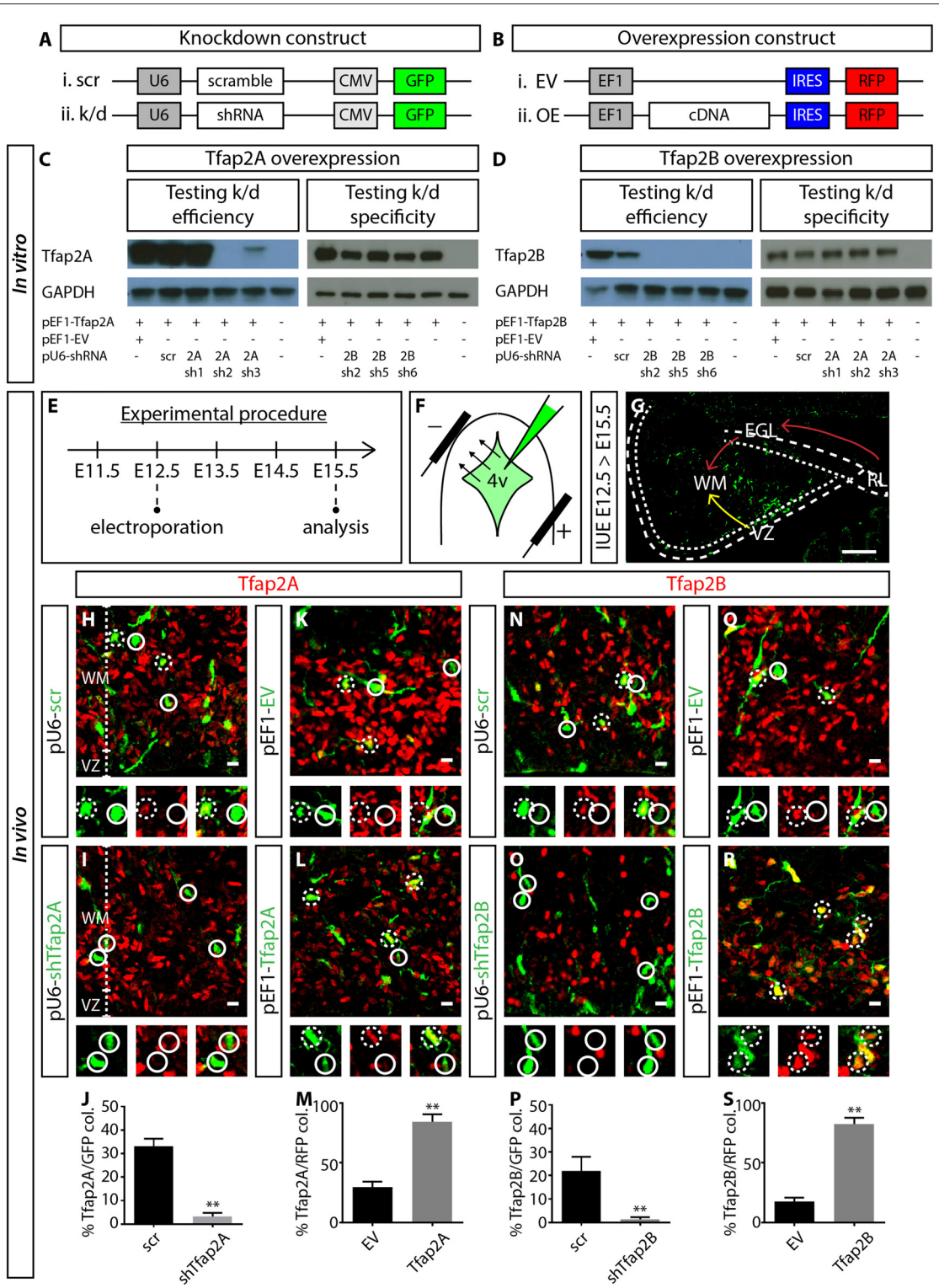

FIGURE 5 | Manipulating the expression of Tfap2A and Tfap2B. **(A,B)** Plasmid constructs used to manipulate the expression of Tfap2A and Tfap2B. **(C,D)** Testing OE and knockdown constructs *in vitro* in human embryonic kidney 293T (HEK-293T) cells. Co-transfection revealed that 2Ash2 and 2Bsh2 are the most efficient (left) and specific (right) in knocking down Tfap2A **(C)** and Tfap2B **(D)** expression respectively. **(E–G)** Strategy for manipulating Tfap2A and Tfap2B expression *in utero* and experimental timeline. Transfected cells originating from the VZ migrate into the WM (yellow arrow, **G**) while cells originating from the RL migrate tangentially along the external germinal layer (EGL) before descending into the WM (red arrow, **G**). **(H–M)** Tfap2A-knockdown abolishes Tfap2A expression (3 ± 2% vs. 33 ± 3% in

(*Continued*)

FIGURE 5 | Continued
controls, $p \leq 0.01$; **(H–J)** control: $n = 3$ mice, 115 cells in 11 sections; 2A k/d: $n = 3$ mice, 187 cells in 14 sections) while ectopic expression of Tfap2A results in an increase in Tfap2A$^+$ cells (84 ± 6% vs. 30 ± 4% in controls, $p \leq 0.01$; **(K–M)** control: $n = 3$ mice, 372 cells in 17 sections; 2A OE: $n = 3$ mice, 276 cells in 12 sections). **(N–S)** Similarly Tfap2B-knockdown abolishes Tfap2B expression (1 ± 1% vs. 22 ± 6% in controls, $p \leq 0.01$; **(N–P)** control: $n = 3$ mice, 121 cells in 11 sections; 2B k/d: $n = 3$ mice, 192 cells in 12 sections) while ectopic expression of Tfap2B results in an increase in Tfap2B$^+$ cells (82 ± 5% vs. 18 ± 3% in controls, $p \leq 0.01$; **(Q–S)** control: $n = 3$ mice, 276 cells in 12 sections; 2B OE: $n = 3$ mice, 366 cells in 13 sections). Continuous circles indicate a lack of colocalization and broken circles indicate colocalization of transfected cells with respective markers. Abbreviations: 4v, 4th ventricle; EGL, external germinal layer; EV, empty vector; k/d, knockdown; OE, overexpression; RL, rhombic lip; WM, scr, scramble; white matter; VZ, ventricle zone. Values represent the mean ± SEM, $^*p \leq 0.05$, $^{**}p \leq 0.01$. Scale bar = 100 μm **(G)**, 10 μm **(H,I,K,L,N,O,Q,R)**.

interneurons, we found a two-fold increase in the number of Pax2$^+$ interneurons in Tfap2A-misexpressed cells relative to control in the WM (**Figures 6A,B,D**). No change was observed in the number of Pax6$^+$ RL-derived cells within Tfap2A-misexpressed cells (**Figures 6E,F,H**). Additionally, misexpression of Tfap2A or Tfap2B had no impact on the expression of CBP (**Figures 6I–L**). Together we show that the expression of Tfap2A, but not Tfap2B, has the ability to direct specification of Pax2$^+$ GABAergic interneurons. Conversely, the expression of Tfap2B, but not Tfap2A can suppress the expression of Pax6.

To determine the requirements of Tfap2 for specification of GABAergic neurons, we assessed the effects of knocking down the expression of Tfap2A or Tfap2B on the expression of Pax2, Pax6 and CBP at E15.5. We found a ∼15% reduction in the number of Pax2$^+$ interneurons in Tfap2B-knockdown cells in the WM (**Figures 7A,C,D**). In contrast, no change in number of Pax2$^+$ interneurons were observed in Tfap2A-knockdown cells (**Figures 7A,B,D**). Knockdown of Tfap2A or Tfap2B had no impact on the expression of Pax6 as predicted (**Figures 7E–H**). Knockdown of Tfap2B results in a modest reduction in the number of CBP$^+$ Purkinje cells, although Purkinje cells do not typically express Tfap2B (**Figures 2, 7J–L**). No change in number of CBP$^+$ cells was detected following Tfap2A knockdown (**Figures 7I,K,L**). Moreover, because Purkinje cells are scarcely transfected at E12.5 (**Figure 7L**), our results suggest that Tfap2A and Tfap2B are unable to influence CBP expression. Knockdown of Tfap2B in the VZ of the developing cerebellum at E12.5 results in a decrease of Pax2 expression, indicating that Tfap2B is necessary for the specification of cerebellar GABAergic interneurons. Together, our results demonstrate that Tfap2A and Tfap2B have independent roles in directing the diversification of cerebellar GABAergic neuronal subtypes in the cerebellum. Moreover, our results indicate that only Tfap2B is indispensable for the specification of cerebellar GABAergic interneurons.

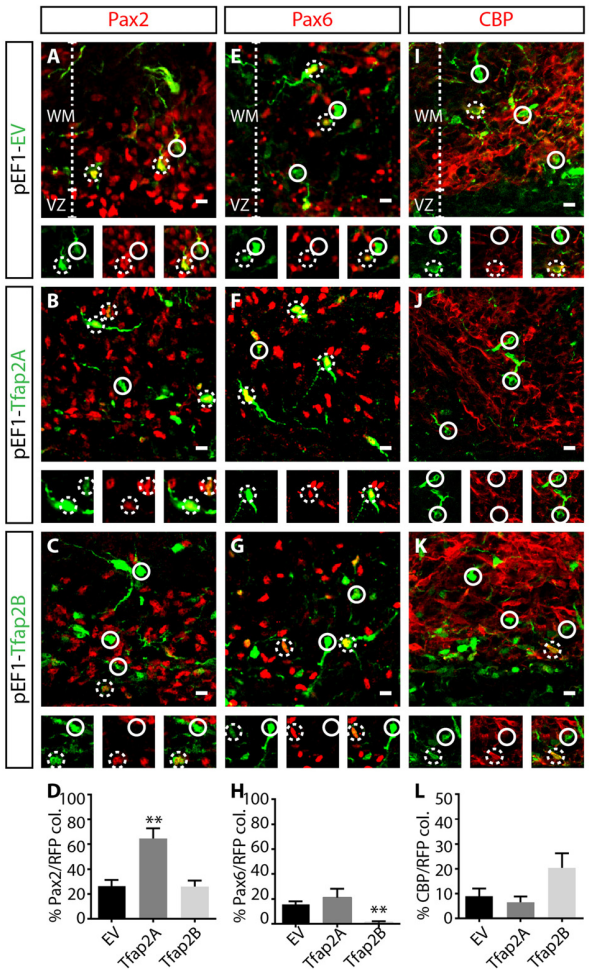

FIGURE 6 | Tfap2A misexpression results in an increase in Pax2 expression, while Tfap2B misexpression results in a decrease in the expression of Pax6. **(A–L)** Consequences of Tfap2A and Tfap2B misexpression on generation of cerebellar neuronal subpopulations. Misexpression of Tfap2A results in an increase in the number of Pax2$^+$ cells (54 ± 11% vs. 26 ± 5% in controls, $p \leq 0.01$; **(A,B,D)** control: $n = 3$ mice, 347 cells in 13 sections; 2A OE: $n = 3$ mice, 130 cells in 14 sections), but misexpression of Tfap2B did not change the number of Pax2$^+$ cells compared to controls (24 ± 6% vs. 26 ± 5% in controls, $p = 0.88$; **(B–D)** control: $n = 3$ mice, 347 cells in 12 sections; 2B OE: $n = 3$ mice, 212 cells in 12 sections). Misexpression of Tfap2B, but not Tfap2A, results in a decrease in the number of Pax6$^+$ cells (Tfap2B: 1 ± 1% vs. 16 ± 3% in controls, $p \leq 0.01$; **(F–H)** Tfap2A: 19 ± 8% vs. 16 ± 3% in controls, $p = 0.66$; **(E,G,H)** control: $n = 3$ mice, 542 cells in 14 sections; 2A OE: $n = 3$ mice, 65 cells in 8 sections; 2B OE: $n = 3$ mice, 337 cells in 13 sections). Misexpression of Tfap2A and Tfap2B has no impact on the number of CBP$^+$ Purkinje cells (Tfap2A: 6 ± 2% vs. 9 ± 3% in controls, $p = 0.85$; **(I,K,L)** Tfap2B: 20 ± 6% vs. 9 ± 3% in controls, $p = 0.063$; **(J–L)** control: $n = 3$ mice, 365 cells in 15 sections; 2A OE: $n = 3$ mice 160 cells in 10 sections; 2B OE: $n = 261$ cells in 9 sections). Continuous circles indicate lack of colocalization and broken circles indicate colocalization of transfected cells with respective markers. Abbreviations: VZ, ventricular zone; WM, white matter. Values represent the mean ± SEM, $^*p \leq 0.05$, $^{**}p \leq 0.01$. Scale bar = 10 μm.

DISCUSSION

GABAergic neurons in the cerebellar cortex are subdivided into projection neurons and interneurons, consisting of at least four subtypes derived from the same pool of multipotent progenitors (Hoshino et al., 2005; Pascual et al., 2007; Yamada et al., 2014), but the transcriptional program that directs this diversification is not well defined. To explore determinants of the

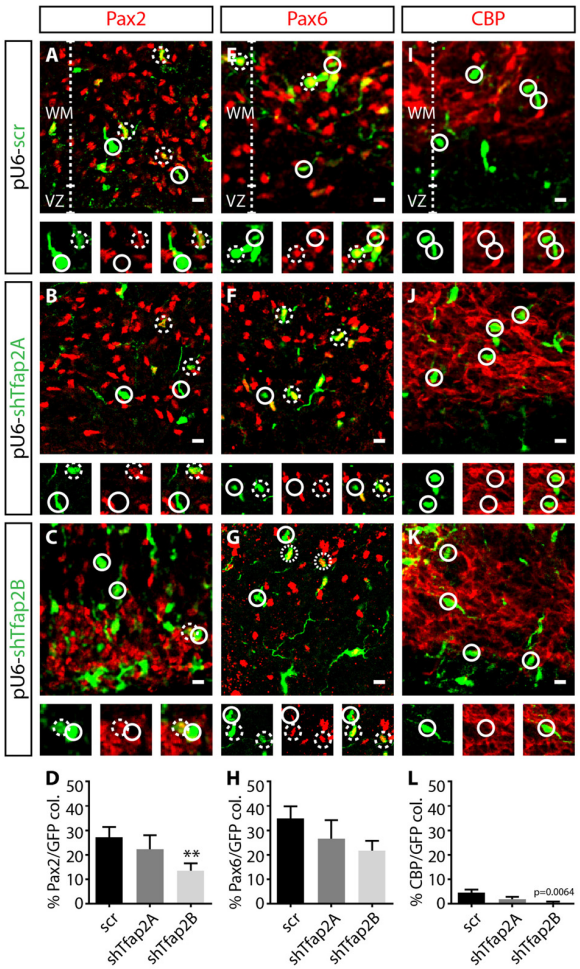

FIGURE 7 | Knockdown of the expression of Tfap2B, but not Tfap2A, results in a reduction in Pax2 expression. **(A–H)** Knockdown of Tfap2A expression in the VZ does not affect the number of Pax2$^+$ cells (22 ± 6% vs. 27 ± 4% in controls, $p = 0.53$; **(A,B,D)** control: $n = 3$ mice, 153 cells in 12 sections; 2A k/d: $n = 3$ mice, 87 cells in 14 sections) or number of Pax6$^+$ cells compared to controls (27 ± 8% vs. 34 ± 4% in controls, $p = 0.29$; **(E,F,H)** control: $n = 3$ mice, 241 cells in 13 sections; 2A k/d: $n = 3$ mice, 188 cells in 13 sections). However, knockdown of Tfap2B expression results in a significant decrease in number of Pax2$^+$ cells (13 ± 3% vs. 27 ± 4% in controls, $p \leq 0.01$; **(A,C,D)** control: $n = 3$ mice, 153 cells in 12 sections; 2B k/d: $n = 3$ mice, 391 cells in 26 sections), without affecting the number of Pax6$^+$ cells (22 ± 4% vs. 34 ± 4% in controls, $p = 0.054$; **(E,G,H)** control: $n = 3$ mice, 241 cells in 13 sections; 2B k/d: $n = 3$ mice, 211 cells in 12 sections). **(I–L)** A scant percentage of CBP$^+$ Purkinje cells are transfected, although knockdown of Tfap2B, but not Tfap2A, slightly decreased this subpopulation (Tfap2B: 0.5 ± 0.5% vs. 4 ± 1% in controls, $p = 0.0064$; **(J–L)** Tfap2A: 2 ± 1% vs. 4 ± 1% in controls, $p = 0.067$; **(I,J,L)** control: $n = 3$ mice, 307 cells in 13 sections; 2A k/d: $n = 3$ mice, 206 cells in 14 sections; 2B k/d: $n = 3$ mice, 253 cells in 13 sections). Continuous circles indicate lack of colocalization and broken circles indicate colocalization of transfected cells with respective markers. Abbreviations: VZ, ventricular zone; WM, white matter. Values represent the mean ± SEM, $^*p \leq 0.05$, $^{**}p \leq 0.01$. Scale bar = 10 μm.

specification of GABAergic neuron progenitors into GABAergic neuronal subtypes, we examined the expression and function of Tfap2 family of transcription factors (summarized in **Figure 8**). We discuss how the differential expression of Tfap2A and Tfap2B defines GABAergic neuronal subtypes and their contribution to the generation and specification of cerebellar GABAergic neurons.

Combinatorial Expression of Tfap2 Transcription Factors and Cerebellar GABAergic Neuronal Subtypes

There is emerging evidence that GABAergic neuronal subtypes are defined by their unique expression of transcription factors (Helms and Johnson, 2003; Wonders and Anderson, 2006; Hoshino, 2012; Achim et al., 2014). In the cortex, for instance, GABAergic interneurons are derived from Nkx2.1 domain of the medial ganglionic eminence and ventral caudal ganglionic eminence (Cobos et al., 2006; Wonders and Anderson, 2006). Subsequently, GABAergic neuronal subtypes can be differentiated by their distinct combinatorial expression of Dlx1/2, Dlx5/6 and Lhx6 (Cobos et al., 2006; Wonders and Anderson, 2006). In more caudal regions of the nervous system, the differential expression of Lbx1, Lhx1/5, Pax2, Gsh1/2, Dbx2 and GATA2/3 defines GABAergic interneuron subtypes in the spinal cord; Lhx1/5 is expressed by all GABAergic neurons and Pax2 is expressed only by interneurons in the cerebellum (Helms and Johnson, 2003; Hori and Hoshino, 2012). Additionally, Ptf1a is expressed by all early GABAergic precursors in both the cerebellum and spinal cord (Hori and Hoshino, 2012). Thus, in comparison to the cortex and spinal cord, there are less distinguishing molecular features for labeling and monitoring of GABAergic neuronal subtypes in the cerebellum.

We show in this study that the combinatorial expression of Tfap2A and Tfap2B may distinguish GABAergic projection neurons from interneurons in the developing cerebellum. In the adult cerebellum, Tfap2A is expressed in all GABAergic neurons, whereas Tfap2B is selectively expressed in the interneuronal population (**Figure 2**). In contrast to Ptf1a and Olig2, whose expression is extinguished by E13.5 (Pascual et al., 2007; Seto et al., 2014a; Ju et al., 2016), the expression of Tfap2 transcription factors persists into adulthood. However, Tfap2B might be transiently expressed in early Purkinje cells during embryonic development (**Figure 3**). Our discovery that Tfap2 transcription factors are dynamically and, perhaps, differentially expressed by GABAergic neuronal subtypes in the cerebellum, provides a novel set of molecular markers that can complement a growing list of genetic tools for future characterization and lineage analysis of these neurons. There is now a number of mouse lines for the tagging and monitoring of cerebellar GABAergic neurons: *Gad67*::GFP and *Ptf1a*::Cre label all GABAergic neurons (Yamanaka et al., 2004; Pascual et al., 2007; Yamada et al., 2014), *Corl2*::GFP and *Olig2*::Cre mark projection neurons (Nakatani et al., 2014; Seto et al., 2014b; Ju et al., 2016) and *Pax2*::GFP selectively labels GABAergic interneurons (Leto et al., 2006; Weisheit et al., 2006). The emergence of these tools will permit a systematic examination of the development, function as well as molecular profile of cerebellar GABAergic neuronal subtypes.

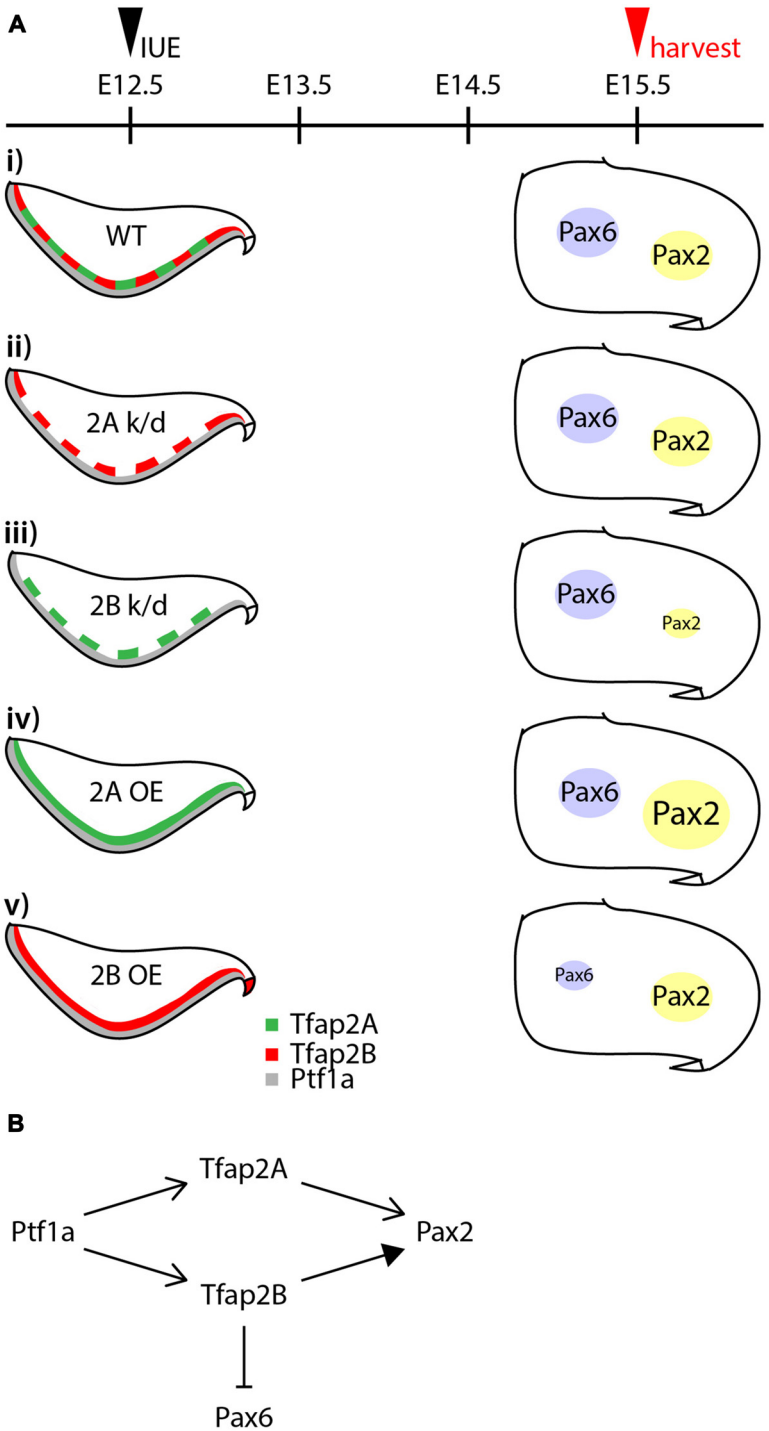

FIGURE 8 | Summary of the activities of Tfap2A and Tfap2B in GABAergic interneuron specification. **(A)** Summary of results from knocking down and ectopic expression of Tfap2A and Tfap2B. **(Ai)** In a wild-type, expression of Tfap2A and Tfap2B occur in an overlapping manner in the ventricular zone at E12.5 which is observed superior to Ptf1a territory. Some expression of Pax6 and Pax2 is observed in the white matter of the developing cerebellum at E15.5. Knockdown of Tfap2A does not show any changes in the expression of Pax2 or Pax6 **(Aii)**. Knockdown of Tfap2B results in a decrease in Pax2 expression **(Aiii)**. Ectopic expression of Tfap2A results in an increase in Pax2 expression **(Aiv)**, while ectopic expression of Tfap2B results in a decrease in Pax6 expression **(Av)**. **(B)** Proposed activities of Tfap2A and Tfap2B in the development of cerebellar neurons. Expression of Tfap2A and Tfap2B downstream of Ptf1a play distinct roles to ensure generation of $Pax2^{+}$ interneurons. Tfap2A may also function to produce Purkinje cells, but at earlier developmental stages. In addition to generation of GABAergic interneurons, Tfap2B plays a role in the suppression of Pax6 expression. Abbreviations: IUE, *in utero* electroporation; k/d, knockdown; OE, overexpression; RL, rhombic lip; VZ, ventricular zone; WT, wild-type.

Distinct Roles of Tfap2A and Tfap2B in Establishment of GABAergic Neuronal Subtype Identity

Tfap2 family of transcription factors regulates a myriad of developmental processes in the nervous system, kidney, skeleton, limbs, skin and eye (Schorle et al., 1996; Zhang et al., 1996; Moser et al., 1997; Nottoli et al., 1998; West-Mays et al., 1999; Eckert et al., 2005; Seberg et al., 2017). Members of this family exhibit functional redundancy in zebrafish. For instance, Tfap2A and Tfap2E are redundant in their regulation of melanophore development (Van Otterloo et al., 2010). Additionally, Tfap2A and Tfap2C are redundant in their induction of neural crest development (Hoffman et al., 2007; Li and Cornell, 2007). In the mouse, however, members of this family appear to play more discrete roles in developmental processes. For example, Tfap2A is indispensable for craniofacial, eye, and limb development (Schorle et al., 1996; Nottoli et al., 1998); and, Tfap2B is indispensable for kidney development (Moser et al., 1997). Consistently, our results indicate that Tfap2A and Tfap2B play independent roles in the specification of GABAergic interneurons during mouse cerebellar development.

There is growing evidence that, in addition to Ptf1a, Tfap2A and Tfap2B play a crucial role in the specification of GABAergic neuronal subtypes (**Figures 6**, **7**). The expression of Ptf1a in neural precursors directs generation of GABAergic neurons and suppresses generation of glutamatergic neurons in the cerebellum, spinal cord and retina (Glasgow et al., 2005; Hoshino et al., 2005; Nakhai et al., 2007; Pascual et al., 2007). Tfap2A and Tfap2B expression is dependent on Ptf1a in the retina (Jin et al., 2015). Both transcription factors have the ability to promote generation of GABAergic/glycinergic amacrine cells and concomitantly suppress the generation of excitatory photoreceptors and bipolar cells (Jin et al., 2015). In this study, we show that following determination of GABAergic fate of neural precursors in the VZ by Ptf1a, Tfap2A and Tfap2B subsequently serve to ensure generation of GABAergic neurons and suppression of excitatory neurons. Tfap2A alone has the ability to promote generation of GABAergic interneurons while Tfap2B, but not Tfap2A, can suppress the generation of excitatory cells. Thus, Tfap2A and Tfap2B appear to have distinct roles in the specification of GABAergic/glycinergic neurons in the cerebellum, and may serve to delegate the activities of Ptf1a similar to the function of Tfap2A/B in the retina (**Figure 8B**).

Distinguishing molecular features of GABAergic interneurons vs. GABAergic projection neurons in the cerebellum have not be well defined. A set of bHLH transcription factors Ascl1 and Ngn1 may be involved in specification of interneurons and projection neurons, respectively. Ascl1 is required for generation of $Pax2^+$ interneurons, but not Purkinje cells, whereas Ngn1 is required for generation of Purkinje cells, but not $Pax2^+$ interneurons (Grimaldi et al., 2009; Lundell et al., 2009). Lim homeodomain transcription factors Lhx1 and Lhx5 and their cofactor Ldb1 are required for production of Purkinje cells, but not $Pax2^+$ interneurons (Zordan et al., 2008). Additionally, the transcription factor Corl2 plays a role in maturation of Purkinje cells (Wang et al., 2011). Besides Ascl1, cerebellar GABAergic interneurons are dependent on cyclin D2 and cell-cycle dynamics (Huard et al., 1999; Leto et al., 2011). In this study, we add to this list members of Tfap2 family of transcription factors whose expression defines cerebellar GABAergic projection vs. interneurons, and acts to ensure specification of GABAergic interneurons, but not projection neurons.

AUTHOR CONTRIBUTIONS

NZ and AIC designed the studies and prepared the manuscript with comments from all authors. NZ performed all the experiments and analyzed the data. SPK carried out *in utero* electroporation experiments and revised the manuscript. ART carried out analysis in the DCN.

ACKNOWLEDGMENTS

We are grateful to Thomas Jessell and Susan Brenner-Morton for Tfap2B antibody, and Chris Wright for Ptf1a antibody. We thank Guo Lanboling for advice on *in utero* electroporation. We thank J. Nicholas Betley, Toh Hean Ch'ng and Mark Featherstone for comments on the manuscript.

SUPPLEMENTARY MATERIAL

The Supplementary Material for this article can be found online at: http://journal.frontiersin.org/article/10.3389/fnmol.2017.00281/full#supplementary-material

FIGURE S1 | Tfap2A is selectively expressed in the Purkinje cell layer during development but is uniformly expressed in the adult cerebellum. **(A–D)** Colocalization of Tfap2A (red, **B′,C′,D′,B‴,C‴,D‴**) and CBP (green, **B″,C″,D″,B‴,C‴,D‴**) at early post-natal day 7 show selective Purkinje cell expression in the developing cerebellum. **(E–H)** The expression of Tfap2A (red, **F′,G′,H′,F‴,G‴,H‴**) and PVA (green, **F″,G″,H″,F‴,G‴,H‴**) in Purkinje cells from different regions of the cerebellum does not show a medio-lateral distribution pattern. Analysis was performed on coronal sections of the cerebellum from P60 mice. Broken circles indicate cells with colocalized expression, continuous circles indicate no colocalization. Abbreviations: CBP, calbindin; DCN, deep cerebellar nuclei; IGL, internal granular layer ML, molecular layer; PCL, Purkinje cell layer; PVA, parvalbumin. Scale bar = 1000 μm **(A,E)**, 20 μm **(B′–D‴,F′–H‴)**.

FIGURE S2 | Tfap2A, but not Tfap2B, is expressed in GABAergic neurons in the DCN. **(A–F)** Expression of Tfap2A (green, **A–C**) is restricted to small GABAergic neurons of the DCN, marked by MAP2 (red) and Gad67 (blue). Tfap2B expression, on the other hand, is absent in all three nuclei in the DCN. Scale bar = 10 μm.

FIGURE S3 | Tfap2A and Tfap2B are expressed by GABAergic interneuron precursors in the embryonic cerebellum. **(A–C)** Delineation of the E12.5 cerebellum with Ptf1a (red, **A**), a molecular marker that labels the ventricular zone, and Pax2 (green, **B**), a GABAergic interneuron precursor marker. **(D–I)** A subset of Tfap2A **(D)** and Tfap2B **(G)** colocalizes with Pax2 interneuron marker in the embryonic cerebellum. Abbreviations: VZ, ventricular zone; WM, white matter. Scale bar = 10 μm.

FIGURE S4 | *In utero* electroporation of the cerebellum at E12.5 transfects cells of the ventricular zone and rhombic lip. **(A,B)** Summary of targeted regions and strategy for *in utero* electroporation. **(C–I)** Schematic diagram of the expression of respective molecular markers in the embryonic cerebellum at E13.5. **(C′–E″)** GABAergic molecular markers, Ptf1a and Olig2, label the ventricular zone while Pax2 labels the white matter layer. **(F′–G″)** Glutamatergic molecular markers, Pax6 and calretinin, label transfected cells that arise from the rhombic lip. **(H′–I″)** Tfap2A and Tfap2B cells are mostly found in the white matter layer which are preferentially targeted during *in utero* electroporation. Abbreviations: NTZ, nuclear transitory zone; RL, rhombic lip; WM, white matter; VZ, ventricular zone. Scale bar = 10 μm.

REFERENCES

Achim, K., Salminen, M., and Partanen, J. (2014). Mechanisms regulating GABAergic neuron development. *Cell. Mol. Life Sci.* 71, 1395–1415. doi: 10.1007/s00018-013-1501-3

Andersen, B. B., Korbo, L., and Pakkenberg, B. (1992). A quantitative study of the human cerebellum with unbiased stereological techniques. *J. Comp. Neurol.* 326, 549–560. doi: 10.1002/cne.903260405

Borromeo, M. D., Meredith, D. M., Castro, D. S., Chang, J. C., Tung, K. C., Guillemot, F., et al. (2014). A transcription factor network specifying inhibitory versus excitatory neurons in the dorsal spinal cord. *Development* 141, 2803–2812. doi: 10.1242/dev.105866

Chizhikov, V. V., Lindgren, A. G., Currle, D. S., Rose, M. F., Monuki, E. S., and Millen, K. J. (2006). The roof plate regulates cerebellar cell-type specification and proliferation. *Development* 133, 2793–2804. doi: 10.1242/dev.02441

Cobos, I., Long, J. E., Thwin, M. T., and Rubenstein, J. L. (2006). Cellular patterns of transcription factor expression in developing cortical interneurons. *Cereb. Cortex* 16, i82–i88. doi: 10.1093/cercor/bhk003

D'Angelo, E., Solinas, S., Mapelli, J., Gandolfi, D., Mapelli, L., and Prestori, F. (2013). The cerebellar Golgi cell and spatiotemporal organization of granular layer activity. *Front. Neural Circuits* 7:93. doi: 10.3389/fncir.2013.00093

De Zeeuw, C. I., Hansel, C., Bian, F., Koekkoek, S. K., van Alphen, A. M., Linden, D. J., et al. (1998). Expression of a protein kinase C inhibitor in Purkinje cells blocks cerebellar LTD and adaptation of the vestibulo-ocular reflex. *Neuron* 20, 495–508. doi: 10.1016/s0896-6273(00)80990-3

Eccles, J. C., Ito, M., and Szentágothai, J. (1967). *The Cerebellum as a Neuronal Machine*. Berlin, New York, NY: Springer-Verlag.

Eckert, D., Buhl, S., Weber, S., Jäger, R., and Schorle, H. (2005). The AP-2 family of transcription factors. *Genome Biol.* 6:246. doi: 10.1186/gb-2005-6-13-246

Glasgow, S. M., Henke, R. M., Macdonald, R. J., Wright, C. V., and Johnson, J. E. (2005). Ptf1a determines GABAergic over glutamatergic neuronal cell fate in the spinal cord dorsal horn. *Development* 132, 5461–5469. doi: 10.1242/dev.02167

Grimaldi, P., Parras, C., Guillemot, F., Rossi, F., and Wassef, M. (2009). Origins and control of the differentiation of inhibitory interneurons and glia in the cerebellum. *Dev. Biol.* 328, 422–433. doi: 10.1016/j.ydbio.2009.02.008

Heiney, S. A., Kim, J., Augustine, G. J., and Medina, J. F. (2014). Precise control of movement kinematics by optogenetic inhibition of Purkinje cell activity. *J. Neurosci.* 34, 2321–2330. doi: 10.1523/jneurosci.4547-13.2014

Helms, A. W., and Johnson, J. E. (2003). Specification of dorsal spinal cord interneurons. *Curr. Opin. Neurobiol.* 13, 42–49. doi: 10.1016/s0959-4388(03)00010-2

Hoffman, T. L., Javier, A. L., Campeau, S. A., Knight, R. D., and Schilling, T. F. (2007). Tfap2 transcription factors in zebrafish neural crest development and ectodermal evolution. *J. Exp. Zool. B Mol. Dev. Evol.* 308, 679–691. doi: 10.1002/jez.b.21189

Hori, K., and Hoshino, M. (2012). GABAergic neuron specification in the spinal cord, the cerebellum and the cochlear nucleus. *Neural Plast.* 2012:921732. doi: 10.1155/2012/921732

Hoshino, M. (2012). Neuronal subtype specification in the cerebellum and dorsal hindbrain. *Dev. Growth Differ.* 54, 317–326. doi: 10.1111/j.1440-169x.2012.01330.x

Hoshino, M., Nakamura, S., Mori, K., Kawauchi, T., Terao, M., Nishimura, Y. V., et al. (2005). Ptf1a, a bHLH transcriptional gene, defines GABAergic neuronal fates in cerebellum. *Neuron* 47, 201–213. doi: 10.1016/j.neuron.2005.06.007

Huard, J. M., Forster, C. C., Carter, M. L., Sicinski, P., and Ross, M. E. (1999). Cerebellar histogenesis is disturbed in mice lacking cyclin D2. *Development* 126, 1927–1935.

Ino, H. (2004). Immunohistochemical characterization of the orphan nuclear receptor RORα in the mouse nervous system. *J. Histochem. Cytochem.* 52, 311–323. doi: 10.1177/002215540405200302

Ito, M. (2006). Cerebellar circuitry as a neuronal machine. *Prog. Neurobiol.* 78, 272–303. doi: 10.1016/j.pneurobio.2006.02.006

Jin, K., Jiang, H., Xiao, D., Zou, M., Zhu, J., and Xiang, M. (2015). Tfap2a and 2b act downstream of Ptf1a to promote amacrine cell differentiation during retinogenesis. *Mol. Brain* 8:28. doi: 10.1186/s13041-015-0118-x

Ju, J., Liu, Q., Zhang, Y., Liu, Y., Jiang, M., Zhang, L., et al. (2016). Olig2 regulates Purkinje cell generation in the early developing mouse cerebellum. *Sci. Rep.* 6:30711. doi: 10.1038/srep30711

Korbo, L., Andersen, B. B., Ladefoged, O., and Møller, A. (1993). Total numbers of various cell types in rat cerebellar cortex estimated using an unbiased stereological method. *Brain Res.* 609, 262–268. doi: 10.1016/0006-8993(93)90881-m

Leto, K., Bartolini, A., Di Gregorio, A., Imperiale, D., De Luca, A., Parmigiani, E., et al. (2011). Modulation of cell-cycle dynamics is required to regulate the number of cerebellar GABAergic interneurons and their rhythm of maturation. *Development* 138, 3463–3472. doi: 10.1242/dev.064378

Leto, K., Bartolini, A., Yanagawa, Y., Obata, K., Magrassi, L., Schilling, K., et al. (2009). Laminar fate and phenotype specification of cerebellar GABAergic interneurons. *J. Neurosci.* 29, 7079–7091. doi: 10.1523/jneurosci.0957-09.2009

Leto, K., Carletti, B., Williams, I. M., Magrassi, L., and Rossi, F. (2006). Different types of cerebellar GABAergic interneurons originate from a common pool of multipotent progenitor cells. *J. Neurosci.* 26, 11682–11694. doi: 10.1523/jneurosci.3656-06.2006

Leto, K., and Rossi, F. (2012). Specification and differentiation of cerebellar GABAergic neurons. *Cerebellum* 11, 434–435. doi: 10.1007/s12311-011-0324-8

Li, W., and Cornell, R. A. (2007). Redundant activities of Tfap2a and Tfap2c are required for neural crest induction and development of other non-neural ectoderm derivatives in zebrafish embryos. *Dev. Biol.* 304, 338–354. doi: 10.1016/j.ydbio.2006.12.042

Lundell, T. G., Zhou, Q., and Doughty, M. L. (2009). Neurogenin1 expression in cell lineages of the cerebellar cortex in embryonic and postnatal mice. *Dev. Dyn.* 238, 3310–3325. doi: 10.1002/dvdy.22165

Machold, R., and Fishell, G. (2005). Math1 is expressed in temporally discrete pools of cerebellar rhombic-lip neural progenitors. *Neuron* 48, 17–24. doi: 10.1016/j.neuron.2005.08.028

Maricich, S. M., and Herrup, K. (1999). Pax-2 expression defines a subset of GABAergic interneurons and their precursors in the developing murine cerebellum. *J. Neurobiol.* 41, 281–294. doi: 10.1002/(sici)1097-4695(19991105)41:2<281::aid-neu10>3.0.co;2-5

Meredith, D. M., Borromeo, M. D., Deering, T. G., Casey, B. H., Savage, T. K., Mayer, P. R., et al. (2013). Program specificity for Ptf1a in pancreas versus neural tube development correlates with distinct collaborating cofactors and chromatin accessibility. *Mol. Cell. Biol.* 33, 3166–3179. doi: 10.1128/MCB.00364-13

Miale, I. L., and Sidman, R. L. (1961). An autoradiographic analysis of histogenesis in the mouse cerebellum. *Exp. Neurol.* 4, 277–296. doi: 10.1016/0014-4886(61)90055-3

Minaki, Y., Nakatani, T., Mizuhara, E., Inoue, T., and Ono, Y. (2008). Identification of a novel transcriptional corepressor, Corl2, as a cerebellar Purkinje cell-selective marker. *Gene Exp. Patterns* 8, 418–423. doi: 10.1016/j.gep.2008.04.004

Morales, D., and Hatten, M. E. (2006). Molecular markers of neuronal progenitors in the embryonic cerebellar anlage. *J. Neurosci.* 26, 12226–12236. doi: 10.1523/JNEUROSCI.3493-06.2006

Moser, M., Imhof, A., Pscherer, A., Bauer, R., Amselgruber, W., Sinowatz, F., et al. (1995). Cloning and characterization of a second AP-2 transcription factor: AP-2β. *Development* 121, 2779–2788.

Moser, M., Pscherer, A., Roth, C., Becker, J., Mücher, G., Zerres, K., et al. (1997). Enhanced apoptotic cell death of renal epithelial cells in mice lacking transcription factor AP-2β. *Genes Dev.* 11, 1938–1948. doi: 10.1101/gad.11.15.1938

Nakagawa, S., Watanabe, M., and Inoue, Y. (1997). Prominent expression of nuclear hormone receptor RORα in Purkinje cells from early development. *Neurosci. Res.* 28, 177–184. doi: 10.1016/s0168-0102(97)00042-4

Nakatani, T., Minaki, Y., Kumai, M., Nitta, C., and Ono, Y. (2014). The c-Ski family member and transcriptional regulator Corl2/Skor2 promotes early differentiation of cerebellar Purkinje cells. *Dev. Biol.* 388, 68–80. doi: 10.1016/j.ydbio.2014.01.016

Nakhai, H., Sel, S., Favor, J., Mendoza-Torres, L., Paulsen, F., Duncker, G. I., et al. (2007). Ptf1a is essential for the differentiation of GABAergic and glycinergic amacrine cells and horizontal cells in the mouse retina. *Development* 134, 1151–1160. doi: 10.1242/dev.02781

Nottoli, T., Hagopian-Donaldson, S., Zhang, J., Perkins, A., and Williams, T. (1998). AP-2-null cells disrupt morphogenesis of the eye, face, and limbs in chimeric mice. *Proc. Natl. Acad. Sci. U S A* 95, 13714–13719. doi: 10.1073/pnas.95.23.13714

Palay, S. L., and Chan-Palay, V. (1974). *Cerebellar Cortex: Cytology and Organization*. Berlin, Heidelberg, New York, NY: Springer.

Pascual, M., Abasolo, I., Mingorance-Le Meur, A., Martínez, A., Del Rio, J. A., Wright, C. V., et al. (2007). Cerebellar GABAergic progenitors adopt an external granule cell-like phenotype in the absence of Ptf1a transcription factor expression. *Proc. Natl. Acad. Sci. U S A* 104, 5193–5198. doi: 10.1073/pnas.0605699104

Russ, J. B., Borromeo, M. D., Kollipara, R. K., Bommareddy, P. K., Johnson, J. E., and Kaltschmidt, J. A. (2015). Misexpression of ptf1a in cortical pyramidal cells *in vivo* promotes an inhibitory peptidergic identity. *J. Neurosci.* 35, 6028–6037. doi: 10.1523/JNEUROSCI.3821-14.2015

Schmidt, M., Huber, L., Majdazari, A., Schütz, G., Williams, T., and Rohrer, H. (2011). The transcription factors AP-2β and AP-2α are required for survival of sympathetic progenitors and differentiated sympathetic neurons. *Dev. Biol.* 355, 89–100. doi: 10.1016/j.ydbio.2011.04.011

Schorle, H., Meier, P., Buchert, M., Jaenisch, R., and Mitchell, P. J. (1996). Transcription factor AP-2 essential for cranial closure and craniofacial development. *Nature* 381, 235–238. doi: 10.1038/381235a0

Seberg, H. E., Van Otterloo, E., Loftus, S. K., Liu, H., Bonde, G., Sompallae, R., et al. (2017). TFAP2 paralogs regulate melanocyte differentiation in parallel with MITF. *PLoS Genet.* 13:e1006636. doi: 10.1371/journal.pgen.1006636

Seto, Y., Ishiwata, S., and Hoshino, M. (2014a). Characterization of Olig2 expression during cerebellar development. *Gene Exp. Patterns* 15, 1–7. doi: 10.1016/j.gep.2014.02.001

Seto, Y., Nakatani, T., Masuyama, N., Taya, S., Kumai, M., Minaki, Y., et al. (2014b). Temporal identity transition from Purkinje cell progenitors to GABAergic interneuron progenitors in the cerebellum. *Nat. Commun.* 5:3337. doi: 10.1038/ncomms4337

Shimada, M., Konishi, Y., Ohkawa, N., Ohtaka-Maruyama, C., Hanaoka, F., Makino, Y., et al. (1999). Distribution of AP-2 subtypes in the adult mouse brain. *Neurosci. Res.* 33, 275–280. doi: 10.1016/s0168-0102(99)00017-6

Sillitoe, R. V., and Joyner, A. L. (2007). Morphology, molecular codes, and circuitry produce the three-dimensional complexity of the cerebellum. *Annu. Rev. Cell Dev. Biol.* 23, 549–577. doi: 10.1146/annurev.cellbio.23.090506.123237

Thach, W. T., and Bastian, A. J. (2004). Role of the cerebellum in the control and adaptation of gait in health and disease. *Prog. Brain Res.* 143, 353–366. doi: 10.1016/s0079-6123(03)43034-3

Van Otterloo, E., Li, W., Bonde, G., Day, K. M., Hsu, M. Y., and Cornell, R. A. (2010). Differentiation of zebrafish melanophores depends on transcription factors AP2alpha and AP2 epsilon. *PLoS Genet.* 6:e1001122. doi: 10.1371/journal.pgen.1001122

Wang, B., Harrison, W., Overbeek, P. A., and Zheng, H. (2011). Transposon mutagenesis with coat color genotyping identifies an essential role for Skor2 in sonic hedgehog signaling and cerebellum development. *Development* 138, 4487–4497. doi: 10.1242/dev.067264

Wang, V. Y., Rose, M. F., and Zoghbi, H. Y. (2005). Math1 expression redefines the rhombic lip derivatives and reveals novel lineages within the brainstem and cerebellum. *Neuron* 48, 31–43. doi: 10.1016/j.neuron.2005.08.024

Watanabe, D., Inokawa, H., Hashimoto, K., Suzuki, N., Kano, M., Shigemoto, R., et al. (1998). Ablation of cerebellar Golgi cells disrupts synaptic integration involving GABA inhibition and NMDA receptor activation in motor coordination. *Cell* 95, 17–27. doi: 10.1016/s0092-8674(00)81779-1

Weisheit, G., Gliem, M., Endl, E., Pfeffer, P. L., Busslinger, M., and Schilling, K. (2006). Postnatal development of the murine cerebellar cortex: formation and early dispersal of basket, stellate and Golgi neurons. *Eur. J. Neurosci.* 24, 466–478. doi: 10.1111/j.1460-9568.2006.04915.x

West-Mays, J. A., Zhang, J., Nottoli, T., Hagopian-Donaldson, S., Libby, D., Strissel, K. J., et al. (1999). AP-2α transcription factor is required for early morphogenesis of the lens vesicle. *Dev. Biol.* 206, 46–62. doi: 10.1006/dbio.1998.9132

Wonders, C. P., and Anderson, S. A. (2006). The origin and specification of cortical interneurons. *Nat. Rev. Neurosci.* 7, 687–696. doi: 10.1038/nrn1954

Wulff, P., Schonewille, M., Renzi, M., Viltono, L., Sassoè-Pognetto, M., Badura, A., et al. (2009). Synaptic inhibition of Purkinje cells mediates consolidation of vestibulo-cerebellar motor learning. *Nat. Neurosci.* 12, 1042–1049. doi: 10.1038/nn.2348

Yamada, M., Seto, Y., Taya, S., Owa, T., Inoue, Y. U., Inoue, T., et al. (2014). Specification of spatial identities of cerebellar neuron progenitors by ptf1a and atoh1 for proper production of GABAergic and glutamatergic neurons. *J. Neurosci.* 34, 4786–4800. doi: 10.1523/JNEUROSCI.2722-13.2014

Yamanaka, H., Yanagawa, Y., and Obata, K. (2004). Development of stellate and basket cells and their apoptosis in mouse cerebellar cortex. *Neurosci. Res.* 50, 13–22. doi: 10.1016/j.neures.2004.06.008

Zhang, L., and Goldman, J. E. (1996). Generation of cerebellar interneurons from dividing progenitors in white matter. *Neuron* 16, 47–54. doi: 10.1016/s0896-6273(00)80022-7

Zhang, J., Hagopian-Donaldson, S., Serbedzija, G., Elsemore, J., Plehn-Dujowich, D., McMahon, A. P., et al. (1996). Neural tube, skeletal and body wall defects in mice lacking transcription factor AP-2. *Nature* 381, 238–241. doi: 10.1038/381238a0

Zhao, Y., Kwan, K. M., Mailloux, C. M., Lee, W. K., Grinberg, A., Wurst, W., et al. (2007). LIM-homeodomain proteins Lhx1 and Lhx5, and their cofactor Ldb1, control Purkinje cell differentiation in the developing cerebellum. *Proc. Natl. Acad. Sci. U S A* 104, 13182–13186. doi: 10.1073/pnas.0705464104

Zordan, P., Croci, L., Hawkes, R., and Consalez, G. G. (2008). Comparative analysis of proneural gene expression in the embryonic cerebellum. *Dev. Dyn.* 237, 1726–1735. doi: 10.1002/dvdy.21571

Conflict of Interest Statement: The authors declare that the research was conducted in the absence of any commercial or financial relationships that could be construed as a potential conflict of interest.

frontiers in Molecular Neuroscience

ORIGINAL RESEARCH
published: 28 August 2017
doi: 10.3389/fnmol.2017.00269

Loss of FMRP Impaired Hippocampal Long-Term Plasticity and Spatial Learning in Rats

Yonglu Tian[1,2†], Chaojuan Yang[1†], Shujiang Shang[1†], Yijun Cai[3†], Xiaofei Deng[4†], Jian Zhang[1], Feng Shao[5], Desheng Zhu[1], Yunbo Liu[6], Guiquan Chen[7], Jing Liang[4], Qiang Sun[3]*, Zilong Qiu[3]* and Chen Zhang[1,8]**

[1] State Key Laboratory of Membrane Biology, School of Life Sciences, Peking University-IDG/McGovern Institute for Brain Research, Peking University, Beijing, China, [2] Peking-Tsinghua Center for Life Sciences, Academy for Advanced Interdisciplinary Studies, Peking University, Beijing, China, [3] CAS Key Laboratory of Primate Neurobiology, Institute of Neuroscience, Chinese Academy of Sciences, Shanghai, China, [4] Key Laboratory of Mental Health, Institute of Psychology, Chinese Academy of Sciences, Beijing, China, [5] Department of Psychology, Peking University, Beijing, China, [6] Institute of Laboratory Animal Science, Peking Union Medical College/Chinese Academy of Medical Sciences, Beijing, China, [7] MOE Key Laboratory of Model Animal for Disease Study, Model Animal Research Center, Nanjing University, Nanjing, China, [8] Key Laboratory for Neuroscience, Ministry of Education/National Health and Family Planning Commission, Peking University, Beijing, China

OPEN ACCESS

Edited by:
Eunjoon Kim,
Institiue for Basic Science (IBS) and Korea Advanced Institute of Science and Technology (KAIST), Korea

Reviewed by:
Kihoon Han,
Korea University College of Medicine, South Korea
Hyunsoo Shawn Je,
Duke-NUS Medical School, Singapore

***Correspondence:**
Jing Liang
liangj@psych.ac.cn
Qiang Sun
qsun@ion.ac.cn
Zilong Qiu
zqiu@ion.ac.cn
Chen Zhang
ch.zhang@pku.edu.cn

[†] These authors have contributed equally to this work.

Received: 10 June 2017
Accepted: 09 August 2017
Published: 28 August 2017

Citation:
Tian Y, Yang C, Shang S, Cai Y, Deng X, Zhang J, Shao F, Zhu D, Liu Y, Chen G, Liang J, Sun Q, Qiu Z and Zhang C (2017) Loss of FMRP Impaired Hippocampal Long-Term Plasticity and Spatial Learning in Rats. Front. Mol. Neurosci. 10:269. doi: 10.3389/fnmol.2017.00269

Fragile X syndrome (FXS) is a neurodevelopmental disorder caused by mutations in the *FMR1* gene that inactivate expression of the gene product, the fragile X mental retardation 1 protein (FMRP). In this study, we used clustered regularly interspaced short palindromic repeats (CRISPR)/CRISPR-associated protein 9 (Cas9) technology to generate *Fmr1* knockout (KO) rats by disruption of the fourth exon of the *Fmr1* gene. Western blotting analysis confirmed that the FMRP was absent from the brains of the *Fmr1* KO rats ($Fmr1^{exon4-KO}$). Electrophysiological analysis revealed that the theta-burst stimulation (TBS)–induced long-term potentiation (LTP) and the low-frequency stimulus (LFS)–induced long-term depression (LTD) were decreased in the hippocampal Schaffer collateral pathway of the $Fmr1^{exon4-KO}$ rats. Short-term plasticity, measured as the paired-pulse ratio, remained normal in the KO rats. The synaptic strength mediated by the α-amino-3-hydroxy-5-methyl-4-isoxazolepropionic acid receptor (AMPAR) was also impaired. Consistent with previous reports, the $Fmr1^{exon4-KO}$ rats demonstrated an enhanced 3,5-dihydroxyphenylglycine (DHPG)–induced LTD in the present study, and this enhancement is insensitive to protein translation. In addition, the $Fmr1^{exon4-KO}$ rats showed deficits in the probe trial in the Morris water maze test. These results demonstrate that deletion of the *Fmr1* gene in rats specifically impairs long-term synaptic plasticity and hippocampus-dependent learning in a manner resembling the key symptoms of FXS. Furthermore, the $Fmr1^{exon4-KO}$ rats displayed impaired social interaction and macroorchidism, the results consistent with those observed in patients with FXS. Thus, $Fmr1^{exon4-KO}$ rats constitute a novel rat model of FXS that complements existing mouse models.

Keywords: FXS, hippocampus, long-term plasticity, spatial learning, intellectual disability

INTRODUCTION

Fragile X syndrome (FXS) is the most common heritable cause of mental retardation and intellectual disability in humans (Pieretti et al., 1991). The prevalence of FXS is about 1 in 4,000 men and 1 in 6,000–8,000 women (de Vries et al., 1997). Approximately 85% of male and 25% of female patients with FXS show significant intellectual and developmental disability (Lozano et al., 2016). Fragile X mental retardation protein (FMRP) is enriched in the brain and testes (Devys et al., 1993; Bakker et al., 2000), in accordance with the mental retardation and macroorchidism exhibited by most patients with FXS (Hagerman, 1987; Martin and Arici, 2008; Saldarriaga et al., 2014).

The most studied FXS animal model is the *Fmr1* knockout (KO) mouse, which is generated by disrupting either exon 5 (The Dutch-Belgian Fragile X Consortium, 1994) or exon 1 and the promoter region (Mientjes et al., 2006) of the *Fmr1* gene. Both *Fmr1* KO mouse lines lack FMRP in the brain and show diverse behavioral phenotypes and synaptic physiology deficits, some of which recapitulate the clinical symptoms of patients with FXS [reviewed in (Kazdoba et al., 2014)]. *Fmr1* KO mice with transgenic expression of the human *FMR1* gene have demonstrated reduced anxiety and increased exploratory behavior in addition to the correction of some KO behavior phenotypes (Peier et al., 2000; Spencer et al., 2008). Mouse models with expansion of the CGG trinucleotide repeat in the *Fmr1* gene have also been developed to mimic the genetic changes observed in humans with FXS (Bontekoe et al., 2001). However, mouse FXS models have yielded mixed results or failed to reproduce several core FXS clinical phenotypes, including global cognitive dysfunction. For example, *Fmr1* KO mice showed normal behavior in the probe trial in the Morris water maze test, with the exception of a subtle change during the reversal trial when the platform was changed to the opposite position (The Dutch-Belgian Fragile X Consortium, 1994; Kooy et al., 1996). In the radial arm maze test, *Fmr1* KO mice exhibited a normal working memory in comparison with that of the wild-type (WT) mice (Yan et al., 2004). Long-term potentiation (LTP) is a major type of long-lasting synaptic plasticity and is associated with learning and memory. Protein synthesis-dependent late-phase LTP in the hippocampus of *Fmr1* KO mice is still controversial (Hu et al., 2008; Shang et al., 2009; Koga et al., 2015).

Rats are genetically more similar than mice to humans. The usage of rats in scientific research began in the middle of the 19th century (Baker et al., 1979). Rats are widely used in studies of neurological disorders, such as epilepsy, depression, Parkinson's disease, stroke, and vascular brain disorders (Kerkerian-Le Goff et al., 2009; Melani et al., 2010; Bailey et al., 2011; Nabika et al., 2012; Tayebati et al., 2012; Liao et al., 2013; Russo et al., 2013). Inactivation of the *Fmr1* gene in rats via zinc finger nuclease (ZFN) technology targeting of the junction region between intron 7 and exon 8 was recently reported (Hamilton et al., 2014) in a three-chamber test in which 21 amino acids were deleted from the FMRP. This line of KO rats ($Fmr1^{exon8-KO}$) displayed social dysfunction, an autism-related phenotype. Further studies of $Fmr1^{exon8-KO}$ rats revealed abnormal neuronal morphology in the superior olivary complex and impaired sound processing (Engineer et al., 2014; Ruby et al., 2015), as well as increased metabotropic glutamate receptor (mGluR)-dependent hippocampal long-term depression (Till et al., 2015). Juvenile $Fmr1^{exon8-KO}$ rats showed dysfunction in regulating the circuit state in the visual cortex (Berzhanskaya et al., 2016, 2017).

Fragile X mental retardation 1 protein is highly expressed in neurons, and dysregulation of FMRP causes impairment of synaptic strength and neural circuit development. In the present study, a KO rat model was generated by specifically targeting exon 4 using clustered regularly interspaced short palindromic repeats (CRISPR)/CRISPR-associated protein 9 (Cas9) technology, ensuring that regions downstream of exon 4, including the full RNA binding sequence, were not translated. We examine the physiology in hippocampal CA1 pyramidal neurons of the $Fmr1^{exon4-KO}$ rat. Loss of FMRP can lead to deficits in basal synaptic transmission and long-term synaptic plasticity, including theta burst stimulation (TBS)–induced LTP, a low-frequency stimulus (LFS)–induced long-term depression (LTD), and a 3,5-dihydroxyphenylglycine (DHPG)–induced LTD in the $Fmr1^{exon4-KO}$ rat. The knockout (KO) *Fmr1* gene in rats also contributes to abnormal cognitive behaviors.

MATERIALS AND METHODS

Animals

Fmr1 KO rats were produced by the CRISPR/Cas9 method and maintained in the laboratory animal center of Peking University. This line was created via the outbred Sprague-Dawley background. The KO rat lines were maintained with heterozygous female and WT male breeding pairs. The genotypes of the animals were identified. KO and WT rats aged 8–12 weeks were used in the study. The rats were kept in a temperature- and relative-humidity-controlled environment (22 ± 2°C, 40–70%) with a 12-h light/dark cycle and free access to food and water. All animal studies were conducted in accordance with the *Guide for the Care and Use of Laboratory Animals* (8th edition) and approved by the Institutional Animal Care and Use Committee of Peking University. All tests were performed using WT and KO littermates derived from breeding heterozygous female rats with Sprague-Dawley WT male rats. All behavioral tests were conducted in a temperature-controlled (24 ± 2°C) test room between 14:00 and 18:00. After each test, the apparatus and the test area were cleaned with 75% ethanol to remove olfactory cues. In all the behavioral assays, the light intensity was 15–20 lx, and the sound intensity was less than 60 dB. All the behavior tests and electrophysiological measurements were performed in a blinded manner.

DNA Analysis and Genotyping

DNA was obtained from rat-toe tissue samples by incubation with 500 μg/mL proteinase K (Amresco, Solon, OH, United States) in 400 μL lysis buffer [10 mM Tris–HCl, 5 mM EDTA, 0.2% sodium dodecyl sulfate (SDS), 200 mM NaCl] for 6–8 h at 55°C. After incubation, 400 μL isopropyl alcohol

was added to precipitate DNA. The suspensions were centrifuged at 13,000 rpm for 10 min, after which the supernatant was removed. Next, 1 mL of 70% ethanol was added to the sample, which was centrifuged at 13,000 rpm for 10 min, after which all ethanol was removed, and the tube was dried. The DNA was dissolved in 100 μL 5 mM Tris buffer (pH 8.0) for 30 min at 55°C. PCR genotyping was performed using 2× *Taq* PCR Mix (Aidlab, Beijing, China), *Fmr1* forward primer (5′-CCG TGA GTT CTC AAG TTG TTT CCA-3′), and *Fmr1* reverse primer (5′-GGG ATT AAG AGC ATG CAT CAC CAT-3′). Polymerase chain reaction (PCR) was performed with the following protocol on a MyCycler Thermal Cycler™ (Bio-Rad, Hercules, CA, United States): 95°C for 4 min, 95°C for 30 s, 60°C for 30 s (lowered 0.5°C per cycle), 72°C for 30 min (30 cycles); 95°C for 30 s, 45 °C for 30 s, 72°C for 30 min (30 cycles); 72°C for 7 min, and a final hold at 4°C. PCR products were run on 1% agarose gel. The amplicon was approximately 500 bp. The amplicon was sequenced to determine the genotypes of the rats.

Western Blot Analysis

The brains of the WT and *Fmr1* KO rats were homogenized in phosphate-buffered saline (PBS) containing 0.1 mM ethylene glycol-bis (β-aminoethyl ether)-N,N,N′,N′-tetraacetic acid (EGTA), 1 mM phenylmethylsulfonyl fluoride (PMSF), 1 μg/mL pepstatin, 1 μg/mL leupeptin, 2 μg/mL protinin, and 1% Triton X-100. Proteins in the homogenate were extracted for 2 h at 4°C, after which insoluble material was removed with centrifugation (1 h at 100,000 × *g*). Protein concentrations were determined using a BCA Protein Assay Kit (Thermo Scientific, Carlsbad, CA, United States). Each protein sample (100 μg) was boiled in sodium dodecyl sulfate (SDS)-loading buffer, subjected to electrophoresis on a 10% SDS-polyacrylamide gel, and electroblotted onto a nitrocellulose membrane as described previously (Wei et al., 2017). FMRP was detected using a rabbit antibody (Cell Signaling Technology, Danvers, MA, United States, #4317, 1:1,000) as the primary antibody. GAPDH was detected using a rabbit antibody (Abmart, Shanghai, China, P30008, 1:1,000) as the primary antibody. IRDye 800CW-labeled anti-rabbit IgG was used as the secondary antibody and was detected with an Odyssey Infrared Imager System (LI-COR, Lincoln, NE, United States).

RNA Isolation and Quantitative RT-PCR

Total RNA was isolated from the hippocampus and cortex samples that were collected from three WT rats and three *Fmr1* KO rats at approximately 8–12 weeks of age. The samples were homogenized in a glass-Teflon® homogenizer according to the protocol supplied with TRIzol® Reagent (Life Technologies, Carlsbad, CA, United States). The concentration of RNA was measured with spectrophotometry. The reaction volume consisted of 2 μg of total RNA, 5× buffer (Takara, Kusatsu, Japan), Rt enzyme mix (Takara), oligo (dT) (Takara), Random6 primer (Takara), and RNase-free H_2O (to a final volume of 20 μL). The amplification program was as follows: 37°C for 15 min, 85°C for 5 s, and a final hold at 4°C. Quantitative PCR was carried out in an MX 3000P™ (Agilent Stratagene, Palo Alto, CA, United States) real-time PCR system with 2× SYBR Green qPCR Mix (Aidlab, PC3302) using designed primers. Three primer pairs were designed for the *Fmr1* amplicon: a pair crossing exons 1, 2, and 3 (forward primer: 5′-GGC TCC AAT GGC GCT TTC TA-3′; reverse primer: 5′-TAA CCT ACA GGT GGT GGG-3′); a pair crossing exons 4 and 5 (forward primer: 5′-TAA CCT ACA GGT GGT GGG-3′); reverse primer: 5′-TGT GAC AAT TTC ATT GTA TG-3′); and a pair crossing exons 7 and 8 (forward primer: 5′-GAA ATG AAG AAG CCA GTA A-3′; reverse primer: 5′-AAT CAA TAG CAG TGA CCC-3′). GAPDH was used as an internal control (forward primer: 5′-CCT GGA GAA ACC TGC CAA GTA T-3′; reverse primer: 5′-CCC TCA GAT GCC TGC TTC A-3′) (Mientjes et al., 2006). Relative expression levels were calculated using the $2^{-\Delta\Delta CT}$ method.

Three-Chamber Sociability Test

The experiment was executed as described previously (Chung et al., 2015; Xu et al., 2015; Lo et al., 2016). WT ($n = 8$) and KO ($n = 11$) male rats aged 8–12 weeks were tested in a three-chamber apparatus (40 cm × 34 cm × 24 cm) with each side chamber connected to the middle chamber by a corridor (10 cm × 10 cm × 15 cm). Before the test day, the animals were allowed to habituate the environment for 60 min. At the beginning of the test, each rat was placed into the middle chamber and allowed to move freely through all three chambers for 5 min. For the sociability tested, a novel rat (stranger1) locked in a small cage was placed in one of the side chambers, and an empty cage of the same size and design was placed in the other side chamber. The test animal was monitored and allowed to explore both chambers for 10 min, and the total time spent in each chamber was measured. The intruder was randomly assigned to one of the side chambers to avoid a side bias. In the social novelty tested, a new unfamiliar rat (stranger2) was enclosed in the cage that had been empty during the sociability test. All model rats were male and were the same age as the testing rat but had no previous contact with each other. Data were analyzed with one-way analysis of variance (ANOVA), and a two-sided Student's *t*-test was used to perform the preference index analysis.

Assessment of Motor Activity Using a Force-Plate Actometer

A force-plate actometer (Bioanalytical Systems, West Lafayette, IN, United States) was used as an open field to evaluate hyperactivity and motor function. The actometer consisted of a Plexiglas® enclosure (33 cm high), a 44 cm × 44 cm plate, four force transducers, and a recording and analysis system. The area was defined as the center point to 11.64 cm, and the outer area was defined as the zone from 11.64 to 44.00 cm. The animals were placed in a force-plate actometer chamber (44 cm × 44 cm) in a dark and sound-attenuating cabinet for 60 min. Data were collected and stored during time units of 40.96 frames, with a sampling frequency of 100 points/s. The distance traveled, the tremor index, focused stereotypy, bouts of low mobility (BLM; 10 s within a 20 mm radius), and time spent in the center field were recorded. The temperature of the test room was controlled (24 ± 2°C). Before the test, rats were allowed to adapt to the environment for 1 h.

Morris Water Maze Assay

Tests were conducted in a circular black tank 150 cm in diameter containing 22 cm of water (24 ± 2°C). A circular platform (8 cm in diameter) was placed 2 cm beneath the water level. The swim paths of the rats were tracked, digitized, and stored for later behavioral analysis using Ethovision (Noldus, Wageningen, Netherlands). The water maze was divided into four quadrants (I, II, III, and IV). The rats were given four trials per day (30 min inter-trial intervals, ITIs) for four consecutive days during the spatial learning phase. During the learning phase, each animal was randomly placed in a different quadrant, with the exception of the quadrant where the platform was placed in each trial. The maximum trial length was 60 s. When a rat did not find the platform within 60 s, the latency time was calculated as 60 s. After the rats were taken out of the pool, they were dried with towels and returned to their cages. The platform was removed during the probe test. During the reverse training phase, the platform was placed in the third quadrant, which was opposite that used during the learning phase.

Elevated Plus Maze

The elevated plus maze (EPM) was used to assess anxiety-like behavior. The black-painted maze consisted of four arms (50 cm length × 10 cm width). Two opposite open arms without walls and two opposite closed arms with 35 cm high walls formed a "+" shape. The maze was elevated 76 cm above the floor by four metal legs under each arm. Each rat was placed at the junction of the open and closed arms, facing an open arm. The rat was allowed to freely explore the entire maze for 5 min. The time spent in the open arms and closed arms were recorded using the Xeye Aba V3.2 tracking system.

Slice Physiology

Hippocampal slices (400 μm) were produced from 8-week-old male WT and *Fmr1* KO rats as previously (Wei et al., 2016). Animals were anesthetized using pentobarbital (10 mg/mL, 0.1 mL/10 g) and euthanized via decapitation. The brain was quickly removed to an ice-cold dissection solution with a pH of 7.3–7.4. The solution contained 213 mM sucrose, 10 mM glucose, 3 mM KCl, 1 mM NaH_2PO_4, 0.5 mM $CaCl_2$, 5 mM $MgCl_2$, and 26 mM $NaHCO_3$. Transverse slices were cut in ice-cold dissection solution on a vibrating blade microtome (Leica VT-1200s, Wetzlar, Germany). Slices were maintained for 1 h at room temperature in artificial cerebrospinal fluid (ACSF) containing the following: 10 mM glucose, 125 mM NaCl, 5 mM KCl, 2 mM NaH_2PO_4, 2.6 mM $CaCl_2$, 1.3 mM $MgCl_2$, and 26 mM $NaHCO_3$ (pH 7.3–7.4). The ACSF and dissection solution were gassed with 95% O_2 and 5% CO_2. For the recordings, slices were individually transferred to the recording chamber and mounted on the stage of an upright microscope (Olympus BX51WI, Tokyo, Japan). The bathing solution was kept at room temperature and constantly exchanged through a gravity-driven perfusion system with a flow rate of approximately 2 mL/min during the experiment. Stimuli was delivered to the slice via a concentric bipolar electrode (CBBEB75, FHC, Bowdoin, ME, United States). Microelectrodes filled with ACSF (4–7 MΩ) were used to record field excitatory postsynaptic potentials (fEPSPs) from the stratum radiatum of the CA1 region. An EPC10 Patch Clamp Amplifier (HEKA, Lambrecht, Germany) was used to record fEPSPs, the values of which were calculated by measuring the onset (a 30–70% rising phase) slope of the fEPSP. TBSs were used to induce LTP as described previously (Zhang C. et al., 2009; Zhang et al., 2010). Each TBS was composed of five episodes of stimulation delivered at 0.1 Hz, whereas each episode contained 10 stimuli trains of five pulses (100 Hz) delivered at 5 Hz. The average response was expressed as a percentage of the pre-TBS response. A LTD was induced with low-frequency stimulation (1 Hz, 900 pulses) or DHPG (100 μM, 10 min, Tocris, Bristol, United Kingdom). Anisomycin (20 μM, MedChemExpress, Monmouth Junction, NJ, United States) was added to the ACSF 1 h before recording and throughout the recordings. The synaptic ratio was calculated as the percentage of the second fEPSP slope vs. the first slope in individual slices.

Histology

Cresyl violet (Nissl) staining was used to evaluate the cytoarchitecture in the hippocampal regions. The rats were deeply anesthetized with tribromoethanol (240 mg/kg, Sigma–Aldrich, St. Louis, MO, United States) and transcardially with 4% paraformaldehyde (PFA) (w/v) in PBS. The brains were removed and dipped into fresh 4% PFA for an additional 48 to 72 h to be post-fixed at room temperature. Then the samples were embedded in paraffin and sectioned. Four-micron-thick sections were used for staining. The tissue slides were dried for 30 min at 55°C and then rewarmed at room temperature. The sections were washed at the time for distilled water and stained with a 0.5% Cresyl violet solution for 10 min. Then, the sections were washed again with distilled water, dehydrated in a graded ethanol series (95%, 1 min; 95%, 30 s; 100%, 1 min; and 100%, 1 min), and subsequently soaked three times in xylene, 5 min per time. Using the mounting medium, the sections were covered with a coverslip. Finally, an Axio Scan.Z1 (Zeiss, Oberkochen, Germany) digital slide scanner with an X20 objective was used for image acquisition.

RESULTS

Generation of *Fmr1* KO Rats with CRISPR/Cas9-Mediated Genome Editing

In the present study, the CRISPR/Cas9 system was used to introduce deletions or mutations in exon 4 of the *Fmr1* gene in rats (**Figure 1A**). Sanger sequencing showed that one of the offspring lines carried a deletion of five amino acids and a G-A mutation in the *Fmr1* gene (**Figure 1B**). This genetic modification resulted in a frame-shift starting from the second Agenet-like 2 domain in FMRP (**Figure 1C**). RT-PCR analyses of the expression of the *Fmr1* transcript in the hippocampus and the cortex were conducted using three pairs of primers: one pair upstream of exon 4 of the *Fmr1* gene in rats and two pairs downstream of the gene. Similar to the expression of the *Fmr1* transcript in KO mice (Mientjes et al., 2006), expression of the *Fmr1* transcript in $Fmr1^{exon4-KO}$ rats was approximately 18.58–33.78% of that of

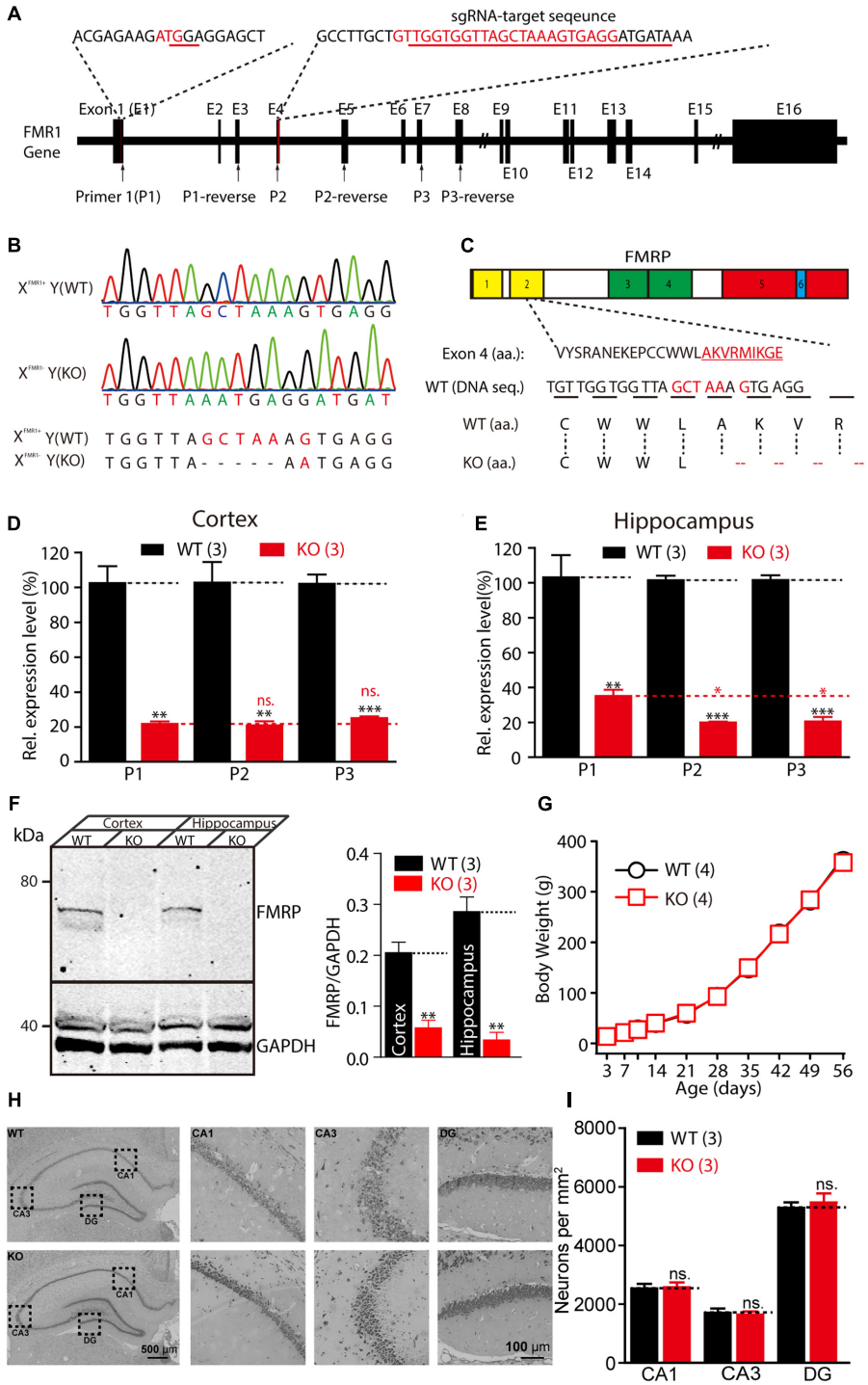

FIGURE 1 | Generation of *Fmr1* knockout (KO) rats using the CRISPR/Cas9 method. **(A)** Targeting of the *Fmr1* gene. **(B)** Genotypes of the *Fmr1* KO rats were determined with sequencing of polymerase chain reaction (PCR) products amplified from tail DNA. **(C)** Localization of the deletion in FMRP. Domains in FMRP: Agenet-like 1 (no. 1, yellow), Agenet-like 2 (no. 2, yellow), KH 1 (no. 3, green), and KH 2 (no. 4, green), interaction with RANBP9 (no. 5, red) and RNA-binding RGG box (no. 6, blue). **(D,E)** Relative expression levels of *Fmr1* transcripts in the cerebral cortex **(D)** and hippocampus **(E)** were measured. Student's *t*-test was used to compare the expression levels of the two groups. **(F)** *Fmr1* KO brain lacking expression of the fragile X mental retardation 1 protein (FMRP). Brain homogenates (100 µg) were subjected to western blot analysis (left). Normalized expression levels of FMRP in rat brain homogenate (right). **(G)** *Fmr1* KO rats showed a normal developmental curve. **(H)** Hippocampal regions stained with Nissl staining and the cellular layer in CA1, CA3, and DG region of the hippocampus of the WT and KO rats. **(I)** Neuron densities were calculated in the CA1, CA3, and DG region of hippocampus. All data are presented as mean ± standard error of the mean (SEM). (***$p < 0.001$, **$p < 0.01$, *$p < 0.05$; ns., not significant, two-sided Student's *t*-test was used).

the WT rats (**Figures 1D,E**). The primers targeting the sequence upstream of exon 4 yielded statistically significant increases in the transcript expression levels in the hippocampus that were slightly higher than those of the two primer pairs targeting regions downstream of exon 4 (**Figure 1E**). Western blotting, using specific anti-FMRP antibodies, confirmed the presence of FMRP in the cortex and hippocampus lysate of the WT [$X^{Fmr1(+)}Y$] rats but not in that of the KO rats [$X^{Fmr1(-)}Y$] (**Figure 1F** and **Supplementary Figure S1**, cortex: WT, 0.21 ± 0.02, KO, 0.06 ± 0.01, $n = 3$, $p < 0.01$; hippocampus: WT, 0.29 ± 0.03, KO, 0.03 ± 0.02, $n = 3$, $p < 0.01$). When $X^{Fmr1(+)}Y$ rats were crossed with $X^{Fmr1(+)}X^{Fmr1(-)}$ rats, 50.24% of the male offspring were KO rats (109 of 211 male animals from eight breeding pairs), which is consistent with the expected Mendelian ratio. The male KO rats showed normal development curves (**Figure 1G**). The brains of the KO rats exhibited normal histology of hippocampal and neuron densities (**Figures 1H,I**, CA1: WT, 2533 ± 163.3, KO, 2578 ± 164.8, $n = 3$, $p > 0.05$; CA3: WT, 1711 ± 145.7, KO, 1644 ± 104.2, $n = 3$, $p > 0.05$; DG: WT, 5289 ± 185.9, KO, 5467 ± 312.7, $n = 3$, $p > 0.05$), suggesting that FMRP deletion did not cause prenatal lethality or pervasive developmental deficits.

Impaired Basal Synaptic Transmission and Synaptic Plasticity in *Fmr1* KO Rats

Patients with FXS exhibit severe mental retardation that is caused by synaptic dysfunction. We first examined synaptic transmission and plasticity in the hippocampal Schaffer collateral pathway in acute slice preparation. Extracellular recordings were performed to monitor the fEPSP elicited by the stimulation of Schaffer collateral/CA1 glutamatergic fibers. The slope of the input-output curve of the α-amino-3-hydroxy-5-methyl-4-isoxazolepropionic acid receptor (AMPAR)–mediated fEPSP was statistically significantly decreased in the *Fmr1* KO rats compared with that of the WT littermate controls (**Figure 2A**, $slope_{WT} = 0.015 \pm 0.001$, $slope_{KO} = 0.009 \pm 0.001$, $p < 0.001$), demonstrating impairment of the basal synaptic transmission

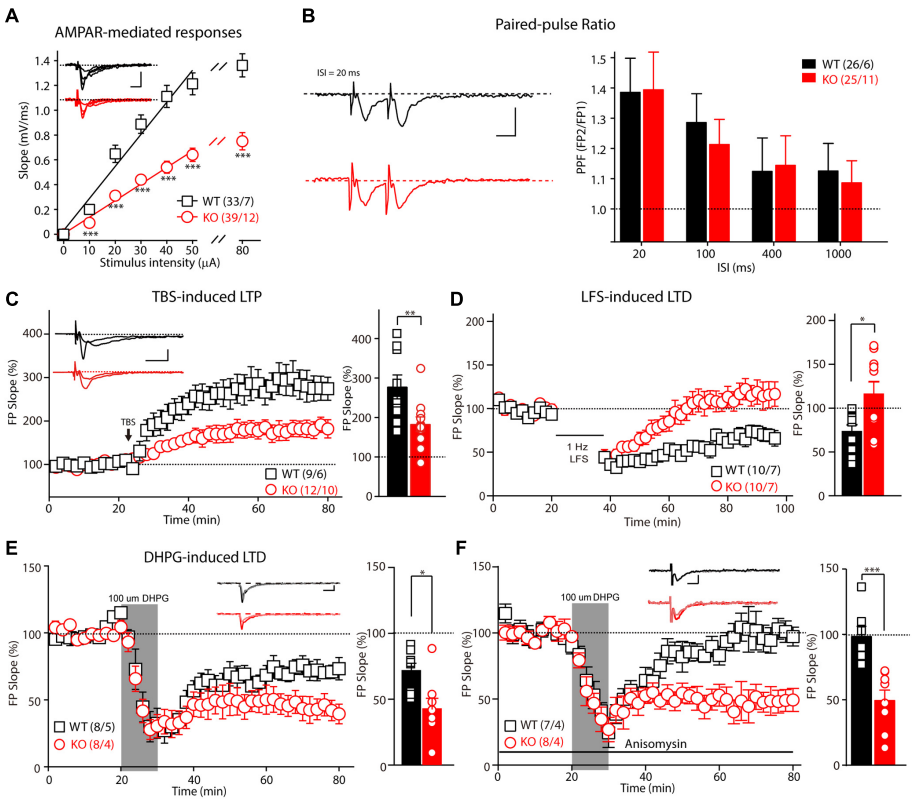

FIGURE 2 | Impaired basic synaptic transmission and long-term plasticity in hippocampal CA3–CA1 synapses in *Fmr1* KO rats. **(A)** The α-amino-3-hydroxy-5-methyl-4-isoxazolepropionic acid receptor(AMPAR)–mediated field excitatory postsynaptic potential (fEPSP) and the input-output curve were reduced in 8-week-old *Fmr1* knockout (KO) rats. The initial slopes of the evoked fEPSP were plotted as a function of the stimulus intensity. **(B)** Left: Representative fEPSP traces from the control and *Fmr1* KO rats evoked by two consecutive stimuli with a 20-ms ISI. Right: Paired-pulse facilitation was normal in the 8-week-old KO rats. **(C)** The theta-burst stimulation (TBS)–induced long-term potentiation (LTP) was impaired in the 8-week-old KO rats. The inset (left panel) shows representative traces before and after LTP induction. The mean fEPSP slopes averaged 50–60 min after LTP induction in the wild-type (WT) and KO rats (Student's *t*-test; right). **(D)** The low-frequency stimulus (LFS)–induced long-term depression (LTD) was impaired in the 8-week-old KO rats. **(E)** *Fmr1* KO rats showed an enhanced 3,5-dihydroxyphenylglycine (DHPG)–induced LTD (left: represented traces of WT and KO rats). **(F)** The protein synthesis inhibitor anisomycin blocks the DHPG-induced LTD of the WT rats but has no effect on the *Fmr1* KO rats. All data are presented as mean ± standard error of the mean (SEM). The scale bars represent 10 ms, 1 mV (*$p < 0.05$, **$p < 0.01$, ***$p < 0.001$; ns., not significant. The number of hippocampal slices (left) and rats (right) used in each experiment is indicated in parentheses).

at the CA3–CA1 excitatory synapses. Next, we measured the synaptic facilitation induced by two identical stimuli separated by various intervals, which is an indicator of short-term plasticity. As shown in **Figure 2B**, paired-pulse facilitation was normal in the *Fmr1* KO rats when compared with that of the control rats. We next examined the effect of FMRP inactivation in CA3 neurons on TBS-induced LTP in the Schaffer collateral pathway. The amplitude of TBS-induced LTP (slope averaged 50–60 min post-TBS stimulation) was markedly impaired in the *Fmr1* KO rats (**Figure 2C**, WT: 277.8 ± 30.3%; KO: 183.4 ± 18.5%, $t = 2.770$, df = 18, $p < 0.01$), demonstrating a critical role of FMRP in regulating LTP at CA3–CA1 synapses. Therefore, we next asked whether the loss of FMRP in rats alters the maintenance of long-term depression. The LFS-induced LTD was statistically significantly reduced in $Fmr1^{\text{exon4-KO}}$ rats (**Figure 2D**, WT: 73.5 ± 7.2%; KO: 116.2 ± 13.7%, $t = 2.752$, df = 18, $p < 0.05$). The magnitude of the mGluRs-dependent LTD elicited by directly activating group I mGluRs with the agonist DHPG was statistically significantly greater in slices from the *Fmr1* KO rats compared with their control littermates (**Figure 2E**, WT: 71.7 ± 5.7%; KO: 42.7 ± 8.1%, $t = 2.948$, df = 14, $p < 0.05$). Moreover, treating the slice with anisomycin (20 μM), a protein synthesis inhibitor, prevented the maintenance of the mGluR-dependent LTD of the WT rats (98.38 ± 7.602%) but not that of the KO rats (49.49 ± 7.954%, **Figure 2F**). This result suggested that a DHPG-induced LTD does not require protein synthesis in $Fmr1^{\text{exon4-KO}}$ rats. Thus, FMRP differentially regulates the LTP and LTD in the hippocampal CA3-CA1 synapses in an induction-specific manner.

Fmr1 KO Rats Exhibit Altered Learning in the Morris Water Maze Test

Altered *Fmr1* gene function is the major cause of mental retardation in patients with FXS. To test whether deletion of the *Fmr1* gene affects the spatial learning ability of KO rats, their

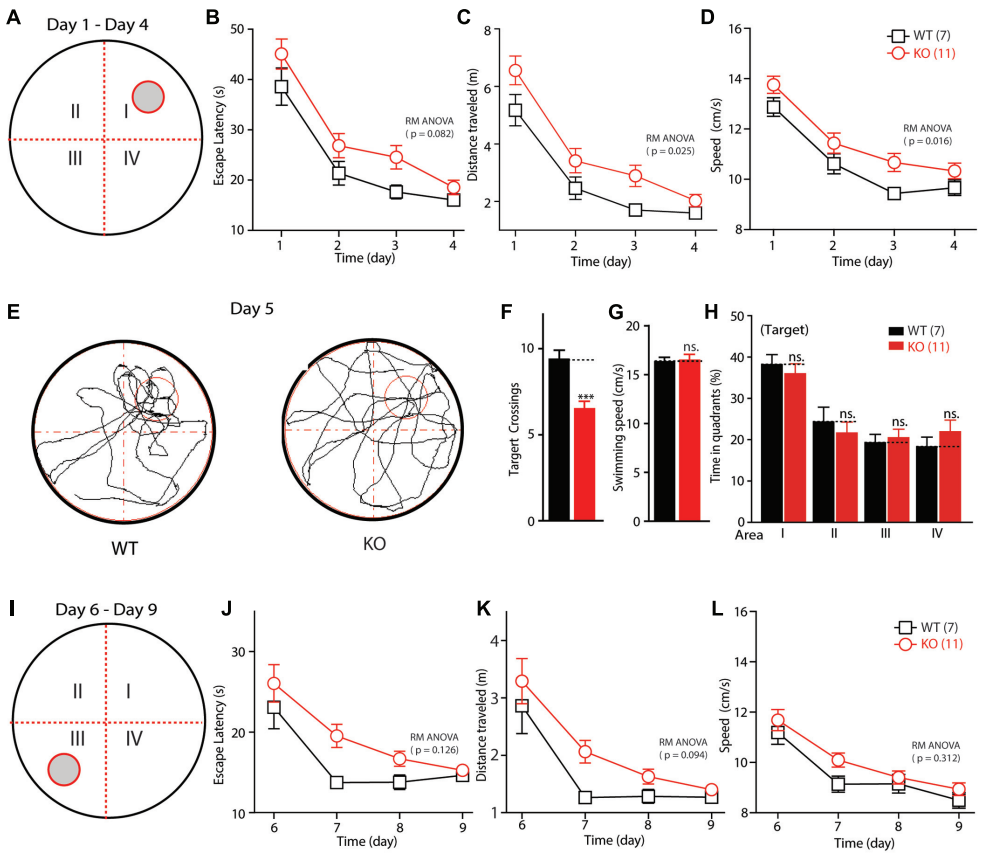

FIGURE 3 | Impaired spatial learning and memory in *Fmr1* KO rats in the Morris water maze. **(A)** Schematic diagram of the apparatus. **(B)** Plot of escape latency. **(C)** Plot of travel distance. **(D)** Plot of swimming speed required for the rats to find the visible platform during the learning phase. **(E)** Representative movement traces. The empty red circles (left) indicate the location of the former platform, which was removed in the probe test. **(F)** Summary of the number of crosses of the former platform area. **(G)** Swimming speed in the probe test. **(H)** Time in each quadrant during the probe test ($p < 0.001$ target quadrant vs. Q2, Q3, or Q4). **(I)** Schematic diagram of the apparatus. The visible platform was placed in the third quadrant, which was opposite to that used during the learning phase (the first quadrant). **(J)** Plot of escape latency. **(K)** Plot of travel distance. **(L)** Plot of swimming speed required for the rats to find the visible platform during the reverse learning phase. All data are presented as mean ± SEM. Repeated-measures analysis of variance (RM ANOVA) was used to evaluate the difference between the two curves in **(A–D)** and **(J–L)**. Student's *t*-test was used to compare the two groups **(F,G)**. *Post hoc* analysis was used to analyze the statistically significant ANOVA results **(H)** (***$p < 0.001$; ns., not significant).

performance was evaluated in a Morris water maze. The training time comprised 1-min periods over 4 days (**Figure 3A**). The escape latency and the travel distance of the WT and KO rats were statistically significantly reduced on days 1–4 (the training period) compared with these measurements on the test days [**Figures 3B–D**; escape latency: $F_{(3,48)} = 64.655$, $p < 0.001$; distance traveled: $F_{(3,48)} = 64.941$, $p < 0.001$; swimming speed: $F_{(3,48)} = 45.650$, $p < 0.001$]. Furthermore, in the KO rats, the escape latency was lengthened in comparison with that of the WT animals [**Figure 3B**, genotype $F_{(1,16)} = 3.435$, $p = 0.082$], the distance traveled before finding the hidden platform was longer [**Figure 3C**, genotype $F_{(1,16)} = 6.083$, $p = 0.025$], and swimming speed was statistically significantly increased [**Figure 3D**, genotype $F_{(1,16)} = 7.186$, $p = 0.016$]. After 4 days of training, the rats were tested in the same maze but without the platform (the probe test phase of memory; **Figure 3E**). As shown in **Figure 3F**, the KO rats crossed the target area statistically significantly less often than did the WT controls (WT: 9.43 ± 0.48, $n = 7$; KO: 6.55 ± 0.39, $n = 11$, $p < 0.001$); this difference was not due to impaired motor function, as the swimming speeds of the rats of each genotype did not differ statistically significantly (**Figure 3G**, WT: 16.38 ± 0.39, $n = 7$; KO: 16.55 ± 0.52, $n = 11$, $p > 0.05$). The time in each quadrant of the KO and WT littermate controls was not statistically significantly different (**Figures 3H,I**: WT: 38.17 ± 2.42, $n = 7$, KO: 35.99 ± 2.40, $n = 11$, $p > 0.05$; II: WT: 24.31 ± 3.60, $n = 7$, KO: 21.63 ± 2.64, $n = 11$, $p > 0.05$; III: WT: 19.25 ± 2.07, $n = 7$, KO: 20.46 ± 2.12, $n = 11$, $p > 0.05$; IV: WT: 18.26 ± 2.38, $n = 7$; KO: 21.92 ± 2.83, $n = 11$, $p > 0.05$). The WT and KO rats spent more time in the target quadrant. After the probe test phase, the rats were subjected to reverse learning, and the hidden platform was switched to the opposite quadrant to test behavioral flexibility (**Figure 3I**). The WT rats consistently found the new hidden platform more quickly than did the KO rats, but there was no statistically significant difference between the two groups [**Figures 3J–L**; escape latency: reversal training day, $F_{(3,48)} = 24.566$, $p < 0.001$; genotype, $F_{(1,16)} = 2.605$, $p = 0.126$; distance traveled: reversal training day, $F_{(3,48)} = 27.113$, $p < 0.001$; genotype, $F_{(1,16)} = 3.160$, $p = 0.094$; swimming speed: reversal training day, $F_{(3,48)} = 60.115$, $p < 0.001$; genotype, $F_{(1,16)} = 1.089$, $p = 0.312$]. These results show that deletion of FMRP in rats impaired their ability to obtain spatial learning and memory and to maintain a normal ability to retain memories.

Fmr1 KO Rats Display Impaired Social Interaction

Social dysfunction has been observed in patients with FXS and the animal models of FXS. To determine whether *Fmr1* KO rats display social deficits, we monitored the behavior of the rats in the three-chamber apparatus (Nadler et al., 2004), in which the social approach of a rat toward a stranger rat trapped in a wire cage can be measured. We first tested the WT and KO rats in three empty chambers; the two genotypes showed no difference (**Figures 4A,B**, WT: left: 98.86 ± 7.4, center: 93.9 ± 4.5, right: 107.2 ± 4.8, $p > 0.05$; KO: left: 93.7 ± 6.5, center: 96.2 ± 6.1, right: 110.1 ± 9.5, $p > 0.05$). In the sociability test, a novel object was placed in one side chamber, and a novel, same-sex rat (stranger1) was placed in the other side of the chamber. The WT and KO rats showed normal performance as measured by the amount of time spent in each chamber (**Figure 4C**, WT: stranger1: 346.3 ± 46.5 s, object: 177.9 ± 36.2 s, $p < 0.05$; KO: stranger1: 391.8 ± 41.7 s, object: 147.4 ± 35.5 s, $p < 0.001$), the preference index derived from these parameters (**Figure 4D**, WT: 28.06 ± 13.7, KO: 40.72 ± 12.8, $p > 0.05$), and the frequency of subject entry into each side chamber from the center chamber (**Figure 4E**, WT: stranger1: 6.4 ± 1.5, object: 5.8 ± 1.5, $p > 0.05$; KO: stranger1: 5.5 ± 0.9, object: 4.6 ± 0.9 s, $p > 0.05$). However, in the social novelty test, when the inanimate object was replaced with another stranger rat (stranger2), stranger1 was observed to be a familiar stimulus. The *Fmr1* KO rats spent less time with stranger2 compared to the amount of time spent with stranger1 (**Figure 4F**, WT: stranger1: 168.7.3 ± 34.0 s, stranger2: 356.0 ± 44.0 s, $p < 0.05$; KO: stranger1: 336.3 ± 53.2 s, stranger2: 183.5 ± 41.1 s, $p < 0.05$). The preference index derived from these parameters was also different (**Figure 4G**, WT: 31.23 ± 12.9, KO: −25.46 ± 15.4, $p < 0.05$), but the frequency of subject entry into each side chamber from the center chamber of the KO rats was similar to that obtained from the WT rats (**Figure 4H**, WT: stranger1: 4.4 ± 1.3, stranger2: 4.1 ± 1.0, $p > 0.05$; KO: stranger1: 4.3 ± 0.9, stranger2: 4.1 ± 1.0, $p > 0.05$). These results suggest that *Fmr1* KO rats are impaired in terms of social novelty recognition but display normal sociability or social anxiety.

Fmr1 KO Rats Demonstrate Normal Locomotor Activity and Normal Anxiety Levels

To test whether motor dysfunction might contribute to the learning deficits observed in the Morris water maze test, the locomotor activity of *Fmr1* KO rats was measured on a force-plate actometer (Fowler et al., 2001). The travel distances and the number of BLM of the KO and WT littermate controls were not statistically significantly different (**Figures 5A,B**, distance: WT: 133.25 ± 8.93 m, $n = 7$; KO: 136.64 ± 15.25 m, $n = 11$, $p > 0.05$; BLM: WT: 197.25 ± 20.45, $n = 7$; KO: 199.33 ± 19.9, $n = 11$, $p > 0.05$). Furthermore, the KO rats spent essentially the same percentage of time in the center area (23.2 cm × 23.2 cm; **Figure 5C** left, WT: 18.82 ± 2.83, $n = 7$; KO: 17.39 ± 6.26, $n = 11$, $p > 0.05$) and made a similar number of leaps over the center (**Figure 5C** right, WT: 830.43 ± 141.42, $n = 7$; KO: 601.64 ± 136.52, $n = 11$, $p > 0.05$). The tremor index of the KO and WT rats (calculated from the power spectra data using Fourier analysis) was also not statistically significantly different (**Figure 5D**, tremor index 1: WT: 0.18 ± 0.03, $n = 7$; KO: 0.17 ± 0.03, $n = 11$, $p > 0.05$; tremor index 2: WT: −0.41 ± 0.08, $n = 7$; KO: −0.30 ± 0.10, $n = 11$, $p > 0.05$). The frequency of stereotypical behavior declined over time after the WT and KO rats were placed on the force plate, but there were no genotypic differences [**Figure 5E**, genotype, $F_{(1,160)} = 0.1110$, $p = 0.7395$; time block, $F_{(9,160)} = 1.310$, $p = 0.2354$]. These results demonstrate that deletion of FMRP in rats had no detectable effects on motor function.

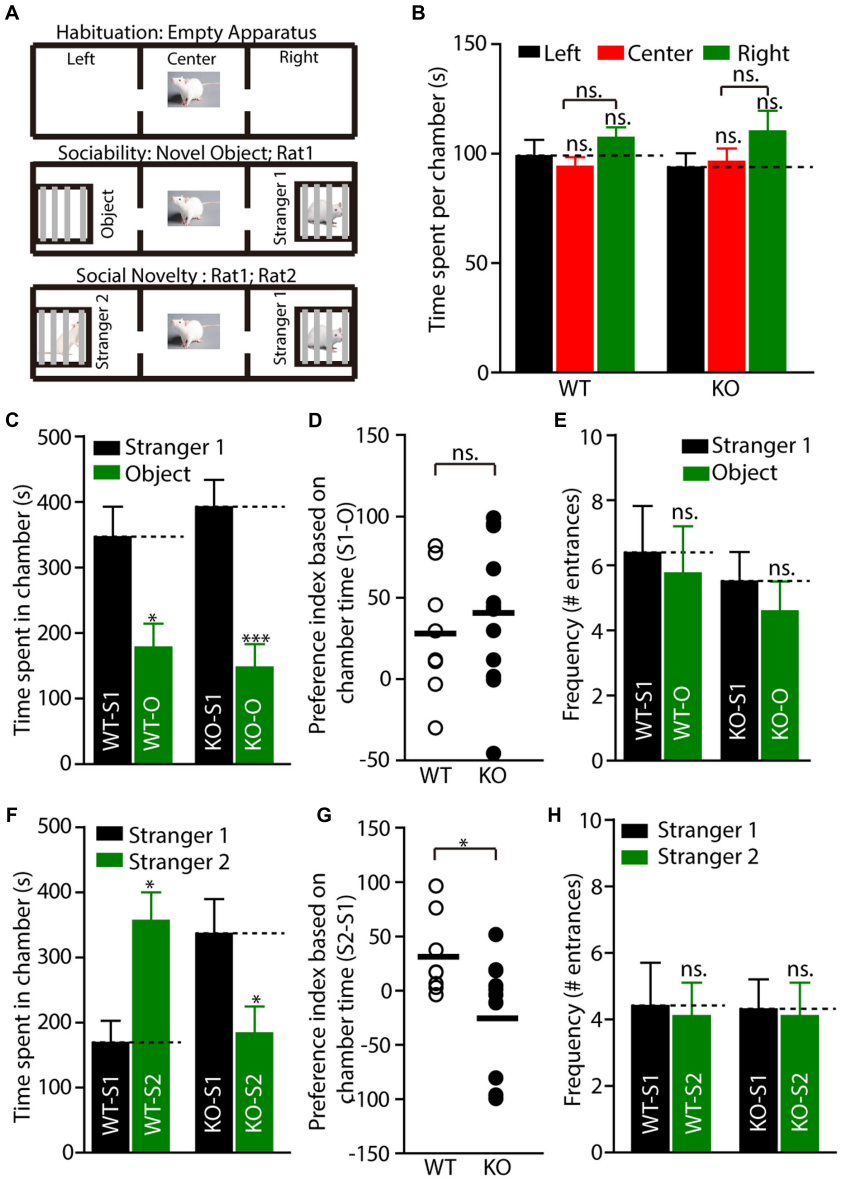

FIGURE 4 | *Fmr1* KO rats display impaired social interaction in the three-chamber test. **(A)** Diagram of the testing apparatus with two outer side chambers, each housing a novel object or stranger rat behind perforated Plexiglas, and the center chamber where the subject was started. Two doorways allowed the subject to move freely between all chambers. **(B)** A WT or KO subject was allowed to explore the apparatus. The mean total duration each subject spent per chamber (including time at partitions within side chambers) is shown, WT: $n = 8$; KO: $n = 12$. **(C–E)** Quantification of the results in **(A)** (middle), as shown by the amount of time spent in chamber **(C)** with a novel rat (stranger1, S1) vs. an inanimate object (O), or the preference index derived from the numerical difference between the time spent in chamber **(D)** with S1 and O divided by total time spent × 100. Frequency of subject entry into each side chamber from the center chamber is shown **(E)**. **(F–H)** Quantification of the results in **(A)** (bottom). S2 (stranger2) and S1 (stranger1). All data are presented mean ± SEM. [$^{*}p < 0.05$, $^{***}p < 0.001$; ns., not significant; one-way analysis of variance (ANOVA) and two-sided Student's *t*-test were used].

To explore whether the KO rats showed anxiety and hyperactivity, we performed the EPM test. The time spent in open arms and close arms were not different between genotypes (**Figures 5F,G**, open arms: WT vs. KO, 23.25 ± 4.85 s vs. 20.93 ± 3.83 s; close arms: WT vs. KO, 193.50 ± 21.09 s vs. 218.50 ± 16.09 s, WT: $n = 13$, KO: $n = 12$). These results indicated that the *Fmr1* KO rats showed normal anxiety level with the WT rats.

Fmr1 KO Rats Show Macroorchidism

Macroorchidism, one of the hallmark symptoms experienced by patients with FXS, is also observed in several FXS animal models (Hamilton et al., 2014). Therefore, we examined the weight of the testes from 5-week-old to 5-month-old rats. As mentioned above, there were no differences in the average body weights of the WT and KO rats (**Figure 6A** left: WT 152.92 ± 6.10 g, $n = 5$; KO 147.26 ± 3.41 g, $n = 5$, $p > 0.05$; **Figure 6B** left:

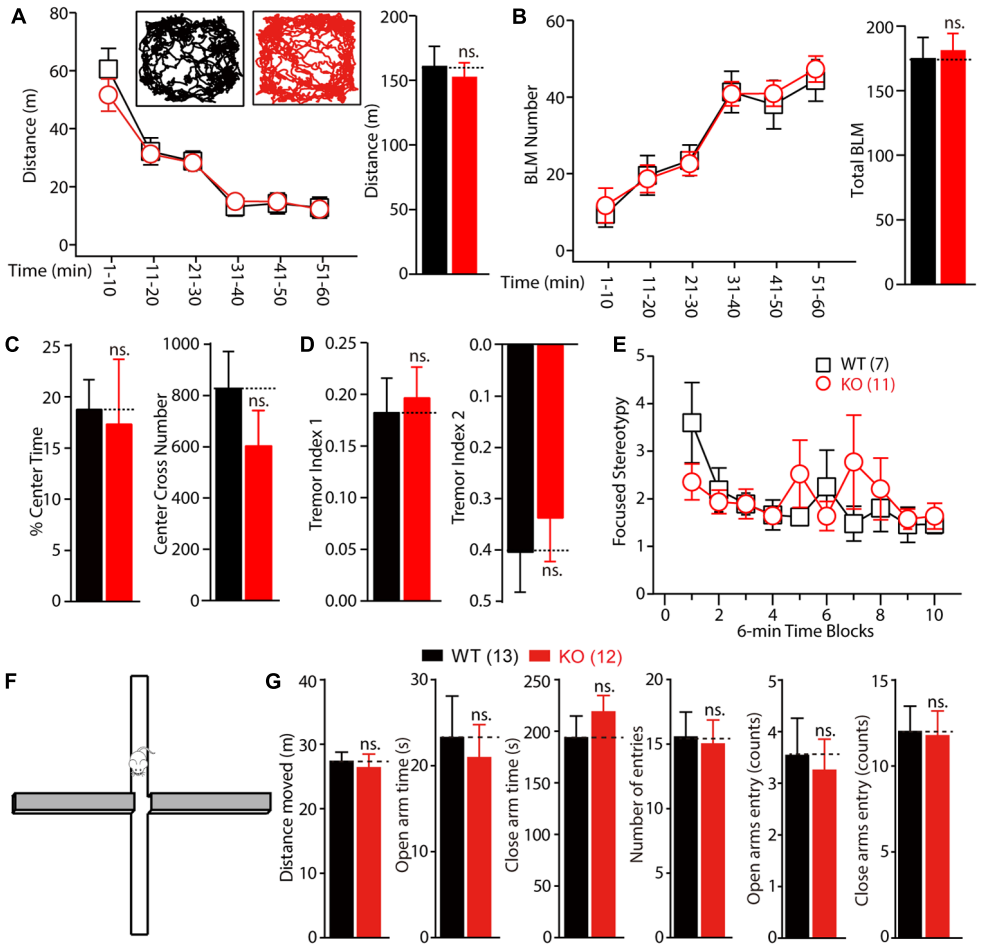

FIGURE 5 | Normal locomotor activity and anxiety of *Fmr1* KO rats in force plate actometer and elevated plus maze test. **(A,B)** *Fmr1* KO rats showed normal exploratory behavior **(A)** and bouts of low mobility (BLM) **(B)** on the force plate. Rats were allowed to move freely on the force plate actometer for 60 min. Distance traveled and BLM were quantified every 10 min (left) and for the total 60 min period (right). The inset shows the representative movement trajectories of the WT and KO rats. **(C)** The percentage of time spent in the center field of the force plate and the number of crosses of the center field were measured. **(D)** KO rats showed normal whole-body tremor, which was quantified from the force variation data. **(E)** The focused stereotypy scores of the KO rats were similar to those of their WT littermate controls. The focused stereotypy scores were calculated from the intense rhythmic movement data of the rats on the force plate. **(F)** Diagram of the elevated plus maze test apparatus. **(G)** The distance the rats moved, in open and close arm time; there was no statistically significant difference in the open and close arm entries between the WT and KO rats. All data are presented as mean ± standard error of the mean (SEM). (ns., not significant, two-way ANOVA and two-sided Student's *t*-test were used).

WT 511.26 ± 9.79 g, $n = 9$; KO 519.39 ± 8.89 g, $n = 10$, $p > 0.05$). No differences were observed in the testes of KO rats at the age of 5 weeks, in either net weight (**Figure 6A** middle: total: WT 1.4 ± 0.04 g, KO 1.4 ± 0.05 g, $p > 0.05$; left: WT 0.72 ± 0.04 g, KO 0.72 ± 0.04 g, $p > 0.05$; right: WT 0.68 ± 0.02 g, KO 0.70 ± 0.03 g, $p > 0.05$) or organ relative weight (**Figure 6A** right: total: WT 0.92 ± 0.02%, KO 0.97 ± 0.04%, $p > 0.05$; left: WT 0.47 ± 0.01%, KO 0.49 ± 0.02%, $p > 0.05$; right: WT 0.45 ± 0.02%, KO 0.48 ± 0.03%, $p > 0.05$). However, the net weight of the 5-month-old *Fmr1* KO rats' testes was statistically significantly heavier than that of the WT rats (**Figure 6B** middle: total: WT 3.77 ± 0.12 g, KO 4.37 ± 0.11 g, $p < 0.01$; left: WT 1.85 ± 0.07 g, KO 2.17 ± 0.06 g, $p < 0.01$; right: WT 1.92 ± 0.06 g, KO 2.20 ± 0.06 g, $p < 0.01$), and the organ relative weight was also heavier than that of the WT rats (**Figure 6B** right: total: WT 0.74 ± 0.02%, KO 0.84 ± 0.02%, $p < 0.01$; left: WT 0.36 ± 0.01%, KO 0.42 ± 0.01%, $p < 0.01$; right: WT 0.38 ± 0.01%, KO 0.42 ± 0.01%, $p < 0.01$). These results demonstrate that *Fmr1* KO rats display macroorchidism at the age of 5 months.

DISCUSSION

In this study, we identified hippocampal physiology, hippocampal-dependent, and social behavior of *Fmr1* KO rats, which were generated by creating a five amino acid deletion in exon 4 of the *Fmr1* gene of a rat using the CRISPR/CAS9 method. FMRP consists of several protein domains: nuclear localization signal (NLS), two hnRNP-K-homology (KH)

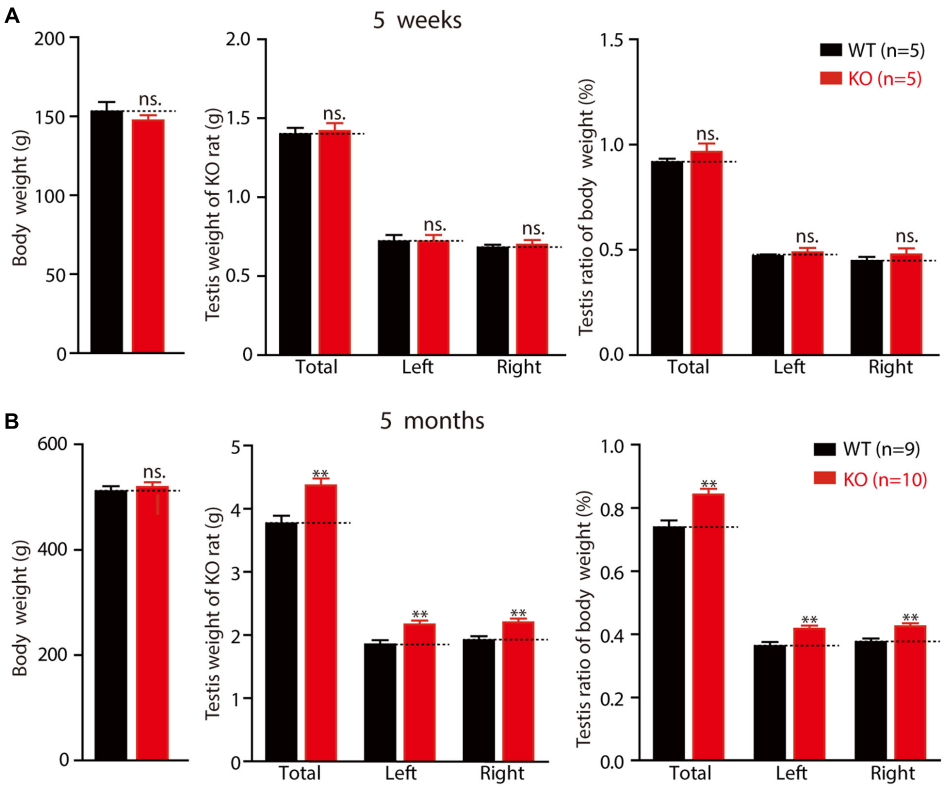

FIGURE 6 | *Fmr1* KO rats exhibit macroorchidism. **(A)** *Fmr1* KO rats' body weight, testis weight and testis ratio of body in 5-week-old *Fmr1* KO rats. **(B)** *Fmr1* KO rats' body weight, testis weight and testis ratio of body in 5-month-old *Fmr1* KO rats. All data are presented as mean ± SEM (**$p < 0.01$, two-sided Student's *t*-test was used).

domains (KH1 and KH2), nuclear export signal (NES), and arginine-glycine-glycine (RGG box). FMRP regulates protein translation by binding to approximately 4% of the mRNA in the mammalian brain through the two KH domains and the RGG box (Ashley et al., 1993; Siomi et al., 1993). In the present study, the genomic modification caused a frame-shift, but not an in-frame deletion in exon 4, ensuring that the remaining transcript, if any, would not generate a truncated FMRP with functional domains (**Figures 1A–C**). Western blotting analysis confirmed the absence of FMRP in the brains of KO rats (**Figure 1F**). The *Fmr1*$^{exon4-KO}$ rats exhibited grossly normal development (**Figure 1G**) and normal locomotor activity, as reflected by normal activity in the open field test and the force plate tests and a normal anxiety level in the EPM test (**Figure 5**). These observations demonstrate that inactivation of the *Fmr1* gene in rats does not cause global motor dysfunction.

The normal function of the hippocampus, including LTP at the hippocampal Schaffer collateral pathway, is essential for learning during the Morris water maze test (Nosten-Bertrand et al., 1996; Lu et al., 1997; Moser et al., 1998; Jia et al., 2001). In *Fmr1* KO mice, LTP induced by either TBS or high-frequency stimulation remained unaltered at the hippocampal Schaffer collateral pathway (Godfraind et al., 1996; Zhang J. et al., 2009; Yun and Trommer, 2011; Bostrom et al., 2015), while the LTD was consistently enhanced in the *Fmr1* KO mouse and rat models (Godfraind et al., 1996; Huber et al., 2002; Li et al., 2002; Till et al., 2015). The dependence of the hippocampal LTP on FMRP had not been investigated in rats before this study. In the present study, electrophysiological analysis revealed that the TBS-induced LTP was severely reduced in hippocampal CA3–CA1 synapses, providing a plausible explanation for the learning deficits observed in the *Fmr1* KO rats (**Figure 2D**). Furthermore, basal synaptic transmission, as measured by the slope of the input–output curve, was statistically significantly reduced in the *Fmr1* KO rats, whereas short-term plasticity, a presynaptic phenomenon, was unchanged. These data imply that postsynaptic plasticity might be affected more severely than presynaptic plasticity at *Fmr1* KO synapses. The *Fmr1*$^{exon4-KO}$ rats exhibited an enhanced DHPG-induced LTD (**Figure 2E**), and this enhancement is independent of protein synthesis (**Figure 2F**), similar to previous studies of KO mice (Nosyreva and Huber, 2006; Till et al., 2015). Consistent with previous studies with another line of *Fmr1* KO rats, which was generated by SAGE Lab using ZFN technology to target intron 7 and exon 8 of *Fmr1* (Hamilton et al., 2014), both lines exhibited an enhanced DHPG-induced LTD, and social dysfunction in the three-chamber test (Till et al., 2015). Interestingly, *Fmr1*$^{exon4-KO}$ rats exhibited some distinct disease-related symptoms, including a reduced TBS-induced LTP (**Figure 2C**) and an LFS-induced LTD (**Figure 2D**)

and learning disability in Morris water maze test (**Figure 3**). FMRP regulates the translation of the protein that is necessary for the induction and expression of synaptic plasticity and can impact synaptic plasticity through FMRP's control of protein translation (Sidorov et al., 2013). Loss of FMRP may to some extent impact the interaction of the protein with AMPAR trafficking and then result in a reduced LTP and LTD through a postsynaptic mechanism.

In the Morris water maze test, an apparatus used to measure hippocampus-dependent spatial learning and memory (Schenk and Morris, 1985; Terry, 2009), *Fmr1*$^{\text{exon4-KO}}$ rats demonstrated slower learning and statistically significantly poorer performance during the probe test phase and the reversal leaning phase. These results are consistent with the fact that the majority of patients with FXS are diagnosed with a learning disability (Skinner et al., 2005; Hall et al., 2008). The probe trial difference in the *Fmr1*$^{\text{exon4-KO}}$ rats is intriguing and has not been observed in most of the *Fmr1* KO mouse lines. Studies using *Fmr1* KO mice have consistently revealed normal trial performance, whereas mixed results have been reported with respect to the memory acquisition and reversal learning processes (The Dutch-Belgian Fragile X Consortium, 1994; Kooy et al., 1996; D'Hooge et al., 1997; Paradee et al., 1999; Baker et al., 2010; Uutela et al., 2012). Results obtained using *Fmr1* KO mice do not correspond well with clinical observations of the symptoms of patients with FXS. Another explanation for differences in mouse and rat models of FXS might be differences in behavior-training paradigms, which seem to contribute to the performance difference in the probe trial. The *Fmr1*$^{\text{exon8-KO}}$ rats showed normal performance in the Morris water maze test when trained with an enhanced training paradigm (Till et al., 2015), suggesting that *Fmr1* KO rats may maintain spatial learning ability to some extent but have difficulty with complex spatial learning tasks. In the present study, we increased the training difficulty by hiding the platform underneath the water throughout the experiments, instead of using a visible platform as in the previous report (Till et al., 2015). Moreover, two *FMR1* paralogs, *FXR1P* and *FXR2P*, share a high domain homology with FMRP in mammals (Kaufmann et al., 2002). Functional compensation by *Fxr1p* and *Fxr2p* in the KO rats may also allow them to perform relatively well in easy tasks. Cooperation of FMRP and FXR2P in regulating synaptic plasticity has been observed in comparisons of *Fmr1* knockout, *Fxr2p* knockout, and *Fmr1/Fxr2p* double-knockout mice (Zhang J. et al., 2009). Therefore, it might be worthwhile to examine the cognitive ability and synaptic plasticity of *Fmr1*- and *Fxrps-compound* mutant rats. Thus, based on behavior and electrophysiological phenotypes, *Fmr1*$^{\text{exon4-KO}}$ rats constitute an ideal model with which to further explore the mechanisms underlying cognitive impairment in patients with FXS, which are directly related to the pathogenesis of FXS.

Patients with FXS exhibit abnormalities in social, communication, and stereotypic behaviors. In this study, *Fmr1*$^{\text{exon4-KO}}$ rats displayed normal social recognition but abnormal social novelty behavior in the three-chamber test. In the sociability test, the wild-type and *Fmr1*$^{\text{exon4-KO}}$ rats preferred to explore the first novel rat (stranger1) over an object relatively, and there was a lack of genotype effect. However, the *Fmr1*$^{\text{exon4-KO}}$ rats spent less time with the novel rat (stranger 2) in the social novelty test compared to the control rats, which is consistent with previous reports (McNaughton et al., 2008; Liu and Smith, 2009; Mines et al., 2010; Heitzer et al., 2013). These results are analogous to the abnormalities in individuals with FXS who display social withdrawal and anxiety (Demark et al., 2003; Cohen et al., 2005; Hatton et al., 2006). These results indicate that basal synaptic transmission in the Schaffer collateral pathway of *Fmr1*$^{\text{exon4-KO}}$ rats is deficit. The loss of long-term plasticity may constitute an essential mechanism in the Morris water maze test.

AUTHOR CONTRIBUTIONS

YT, CY, SS, YC, and XD contributed equally to this work. YT, CY, SS, YC, and XD carried out the experiments. JZ, FS, DZ, YL, GC, JL, QS, ZQ, and CZ contributed to the planning of the work. ZQ and CZ wrote the paper.

ACKNOWLEDGMENTS

This work was supported by grants from the National Key Research and Development Program of China (2017YFA0105201, 2012YQ03026004 and 2014CB942804), the National Science Foundation of China (31670842), Beijing Municipal Science and Technology Commission (Z161100002616021, Z161100000216154), and the Seeding Grant for Medicine and Life Sciences of Peking University (Grant 2014-MB-11).

SUPPLEMENTARY MATERIAL

The Supplementary Material for this article can be found online at: http://journal.frontiersin.org/article/10.3389/fnmol.2017.00269/full#supplementary-material

FIGURE S1 | Full image of western blot.

REFERENCES

Ashley, C. T., Sutcliffe, J. S., Kunst, C. B., Leiner, H. A., Eichler, E. E., Nelson, D. L., et al. (1993). Human and murine *FMR-1*: alternative splicing and translational initiation downstream of the CGG-repeat. *Nat. Genet.* 4, 244–251. doi: 10.1038/ng0793-244

Bailey, E. L., Smith, C., Sudlow, C. L., and Wardlaw, J. M. (2011). Is the spontaneously hypertensive stroke prone rat a pertinent model of sub cortical ischemic stroke? A systematic review. *Int. J. Stroke* 6, 434–444. doi: 10.1111/j.1747-4949.2011.00659.x

Baker, H. J., Lindsey, J. R., and Weisbroth, S. H. (1979). *The Laboratory Rat*. New York, NY: Academic Press.

Baker, K. B., Wray, S. P., Ritter, R., Mason, S., Lanthorn, T. H., and Savelieva, K. V. (2010). Male and female Fmr1 knockout mice on C57 albino background exhibit spatial learning and memory impairments. *Genes Brain Behav.* 9, 562–574. doi: 10.1111/j.1601-183X.2010.00585.x

Bakker, C. E., de Diego Otero, Y., Bontekoe, C., Raghoe, P., Luteijn, T., Hoogeveen, A. T., et al. (2000). Immunocytochemical and biochemical characterization of FMRP, FXR1P, and FXR2P in the mouse. *Exp. Cell Res.* 258, 162–170. doi: 10.1006/excr.2000.4932

Berzhanskaya, J., Phillips, M. A., Gorin, A., Lai, C., Shen, J., and Colonnese, M. T. (2017). Disrupted Cortical State Regulation in a Rat Model of Fragile X Syndrome. *Cereb. Cortex* 27, 1386–1400. doi: 10.1093/cercor/bhv331

Berzhanskaya, J., Phillips, M. A., Shen, J., and Colonnese, M. T. (2016). Sensory hypo-excitability in a rat model of fetal development in Fragile X Syndrome. *Sci. Rep.* 6:30769. doi: 10.1038/srep30769

Bontekoe, C. J., Bakker, C. E., Nieuwenhuizen, I. M., van der Linde, H., Lans, H., de Lange, D., et al. (2001). Instability of a (CGG)98 repeat in the Fmr1 promoter. *Hum. Mol. Genet.* 10, 1693–1699. doi: 10.1093/hmg/10.16.1693

Bostrom, C. A., Majaess, N. M., Morch, K., White, E., Eadie, B. D., and Christie, B. R. (2015). Rescue of NMDAR-dependent synaptic plasticity in Fmr1 knock-out mice. *Cereb. Cortex* 25, 271–279. doi: 10.1093/cercor/bht237

Chung, W., Choi, S. Y., Lee, E., Park, H., Kang, J., Choi, Y., et al. (2015). Social deficits in IRSp53 mutant mice improved by NMDAR and mGluR5 suppression. *Nat. Neurosci.* 18, 435–443. doi: 10.1038/nn.3927

Cohen, D., Pichard, N., Tordjman, S., Baumann, C., Burglen, L., Excoffier, E., et al. (2005). Specific genetic disorders and autism: clinical contribution towards their identification. *J. Autism Dev. Disord.* 35, 103–116. doi: 10.1007/s10803-004-1038-2

de Vries, B. B., van den Ouweland, A. M., Mohkamsing, S., Duivenvoorden, H. J., Mol, E., Gelsema, K., et al. (1997). Screening and diagnosis for the fragile X syndrome among the mentally retarded: an epidemiological and psychological survey. Collaborative Fragile X Study Group. *Am. J. Hum. Genet.* 61, 660–667. doi: 10.1086/515496

Demark, J. L., Feldman, M. A., and Holden, J. J. (2003). Behavioral relationship between autism and fragile x syndrome. *Am. J. Ment. Retard.* 108, 314–326. doi: 10.1352/0895-8017(2003)108<314:BRBAAF>2.0.CO;2

Devys, D., Lutz, Y., Rouyer, N., Bellocq, J. P., and Mandel, J. L. (1993). The FMR-1 protein is cytoplasmic, most abundant in neurons and appears normal in carriers of a fragile X premutation. *Nat. Genet.* 4, 335–340. doi: 10.1038/ng0893-335

D'Hooge, R., Nagels, G., Franck, F., Bakker, C. E., Reyniers, E., Storm, K., et al. (1997). Mildly impaired water maze performance in male Fmr1 knockout mice. *Neuroscience* 76, 367–376. doi: 10.1016/S0306-4522(96)00224-2

Engineer, C. T., Centanni, T. M., Im, K. W., Rahebi, K. C., Buell, E. P., and Kilgard, M. P. (2014). Degraded speech sound processing in a rat model of fragile X syndrome. *Brain Res.* 1564, 72–84. doi: 10.1016/j.brainres.2014.03.049

Fowler, S. C., Birkestrand, B. R., Chen, R., Moss, S. J., Vorontsova, E., Wang, G., et al. (2001). A force-plate actometer for quantitating rodent behaviors: illustrative data on locomotion, rotation, spatial patterning, stereotypies, and tremor. *J. Neurosci. Methods* 107, 107–124. doi: 10.1016/S0165-0270(01)00359-4

Godfraind, J. M., Reyniers, E., De Boulle, K., D'Hooge, R., De Deyn, P. P., Bakker, C. E., et al. (1996). Long-term potentiation in the hippocampus of fragile X knockout mice. *Am. J. Med. Genet.* 64, 246–251. doi: 10.1002/(SICI)1096-8628(19960809)64:2<246::AID-AJMG2>3.0.CO;2-S

Hagerman, R. J. (1987). Fragile X syndrome. *Curr. Probl. Pediatr.* 17, 621–674. doi: 10.1016/0045-9380(87)90011-9

Hall, S. S., Burns, D. D., Lightbody, A. A., and Reiss, A. L. (2008). Longitudinal changes in intellectual development in children with Fragile X syndrome. *J. Abnorm. Child Psychol.* 36, 927–939. doi: 10.1007/s10802-008-9223-y

Hamilton, S. M., Green, J. R., Veeraragavan, S., Yuva, L., McCoy, A., Wu, Y., et al. (2014). Fmr1 and Nlgn3 knockout rats: novel tools for investigating autism spectrum disorders. *Behav. Neurosci.* 128, 103–109. doi: 10.1037/a0035988

Hatton, D. D., Sideris, J., Skinner, M., Mankowski, J., Bailey, D. B. Jr., Roberts, J., et al. (2006). Autistic behavior in children with fragile X syndrome: prevalence, stability, and the impact of FMRP. *Am. J. Med. Genet. A* 140A, 1804–1813. doi: 10.1002/ajmg.a.31286

Heitzer, A. M., Roth, A. K., Nawrocki, L., Wrenn, C. C., and Valdovinos, M. G. (2013). Brief report: altered social behavior in isolation-reared Fmr1 knockout mice. *J. Autism Dev. Disord.* 43, 1452–1458. doi: 10.1007/s10803-012-1670-1

Hu, H., Qin, Y., Bochorishvili, G., Zhu, Y., van Aelst, L., and Zhu, J. J. (2008). Ras signaling mechanisms underlying impaired GluR1-dependent plasticity associated with fragile X syndrome. *J. Neurosci.* 28, 7847–7862. doi: 10.1523/JNEUROSCI.1496-08.2008

Huber, K. M., Gallagher, S. M., Warren, S. T., and Bear, M. F. (2002). Altered synaptic plasticity in a mouse model of fragile X mental retardation. *Proc. Natl. Acad. Sci. U.S.A.* 99, 7746–7750. doi: 10.1073/pnas.122205699

Jia, Z., Lu, Y. M., Agopyan, N., and Roder, J. (2001). Gene targeting reveals a role for the glutamate receptors mGluR5 and GluR2 in learning and memory. *Physiol. Behav.* 73, 793–802. doi: 10.1016/S0031-9384(01)00516-9

Kaufmann, W. E., Cohen, S., Sun, H. T., and Ho, G. (2002). Molecular phenotype of Fragile X syndrome: FMRP, FXRPs, and protein targets. *Microsc. Res. Tech.* 57, 135–144. doi: 10.1002/jemt.10066

Kazdoba, T. M., Leach, P. T., Silverman, J. L., and Crawley, J. N. (2014). Modeling fragile X syndrome in the Fmr1 knockout mouse. *Intractable Rare Dis. Res.* 3, 118–133. doi: 10.5582/irdr.2014.01024

Kerkerian-Le Goff, L., Bacci, J. J., Jouve, L., Melon, C., and Salin, P. (2009). Impact of surgery targeting the caudal intralaminar thalamic nuclei on the pathophysiological functioning of basal ganglia in a rat model of Parkinson's disease. *Brain Res. Bull.* 78, 80–84. doi: 10.1016/j.brainresbull.2008.08.010

Koga, K., Liu, M. G., Qiu, S., Song, Q., O'Den, G., Chen, T., et al. (2015). Impaired presynaptic long-term potentiation in the anterior cingulate cortex of Fmr1 knock-out mice. *J. Neurosci.* 35, 2033–2043. doi: 10.1523/JNEUROSCI.2644-14.2015

Kooy, R. F., D'Hooge, R., Reyniers, E., Bakker, C. E., Nagels, G., De Boulle, K., et al. (1996). Transgenic mouse model for the fragile X syndrome. *Am. J. Med. Genet.* 64, 241–245. doi: 10.1002/(SICI)1096-8628(19960809)64:2<241::AID-AJMG1>3.0.CO;2-X

Li, J., Pelletier, M. R., Perez Velazquez, J. L., and Carlen, P. L. (2002). Reduced cortical synaptic plasticity and GluR1 expression associated with fragile X mental retardation protein deficiency. *Mol. Cell. Neurosci.* 19, 138–151. doi: 10.1006/mcne.2001.1085

Liao, S. J., Huang, R. X., Su, Z. P., Zeng, J. S., Mo, J. W., Pei, Z., et al. (2013). Stroke-prone renovascular hypertensive rat as an animal model for stroke studies: from artery to brain. *J. Neurol. Sci.* 334, 1–5. doi: 10.1016/j.jns.2013.07.2517

Liu, Z. H., and Smith, C. B. (2009). Dissociation of social and nonsocial anxiety in a mouse model of fragile X syndrome. *Neurosci. Lett.* 454, 62–66. doi: 10.1016/j.neulet.2009.02.066

Lo, S. C., Scearce-Levie, K., and Sheng, M. (2016). Characterization of social behaviors in caspase-3 deficient mice. *Sci. Rep.* 6:18335. doi: 10.1038/srep18335

Lozano, R., Azarang, A., Wilaisakditipakorn, T., and Hagerman, R. J. (2016). Fragile X syndrome: a review of clinical management. *Intractable Rare Dis. Res.* 5, 145–157. doi: 10.5582/irdr.2016.01048

Lu, Y. M., Jia, Z., Janus, C., Henderson, J. T., Gerlai, R., Wojtowicz, J. M., et al. (1997). Mice lacking metabotropic glutamate receptor 5 show impaired learning and reduced CA1 long-term potentiation (LTP) but normal CA3 LTP. *J. Neurosci.* 17, 5196–5205.

Martin, J. R., and Arici, A. (2008). Fragile X and reproduction. *Curr. Opin. Obstet. Gynecol.* 20, 216–220. doi: 10.1097/GCO.0b013e3282fe7254

McNaughton, C. H., Moon, J., Strawderman, M. S., Maclean, K. N., Evans, J., and Strupp, B. J. (2008). Evidence for social anxiety and impaired social cognition in a mouse model of fragile X syndrome. *Behav. Neurosci.* 122, 293–300. doi: 10.1037/0735-7044.122.2.293

Melani, A., Cipriani, S., Corti, F., and Pedata, F. (2010). Effect of intravenous administration of dipyridamole in a rat model of chronic cerebral ischemia. *Ann. N. Y. Acad. Sci.* 1207, 89–96. doi: 10.1111/j.1749-6632.2010.05732.x

Mientjes, E. J., Nieuwenhuizen, I., Kirkpatrick, L., Zu, T., Hoogeveen-Westerveld, M., Severijnen, L., et al. (2006). The generation of a conditional Fmr1 knock out mouse model to study Fmrp function in vivo. *Neurobiol. Dis.* 21, 549–555. doi: 10.1016/j.nbd.2005.08.019

Mines, M. A., Yuskaitis, C. J., King, M. K., Beurel, E., and Jope, R. S. (2010). GSK3 influences social preference and anxiety-related behaviors during social interaction in a mouse model of fragile X syndrome and autism. *PLoS ONE* 5:e9706. doi: 10.1371/journal.pone.0009706

Moser, E. I., Krobert, K. A., Moser, M. B., and Morris, R. G. (1998). Impaired spatial learning after saturation of long-term potentiation. *Science* 281, 2038–2042. doi: 10.1126/science.281.5385.2038

Nabika, T., Ohara, H., Kato, N., and Isomura, M. (2012). The stroke-prone spontaneously hypertensive rat: still a useful model for post-GWAS genetic studies? *Hypertens. Res.* 35, 477–484. doi: 10.1038/hr.2012.30

Nadler, J. J., Moy, S. S., Dold, G., Trang, D., Simmons, N., Perez, A., et al. (2004). Automated apparatus for quantitation of social approach behaviors in mice. *Genes Brain Behav.* 3, 303–314. doi: 10.1111/j.1601-183X.2004.00071.x

Nosten-Bertrand, M., Errington, M. L., Murphy, K. P., Tokugawa, Y., Barboni, E., Kozlova, E., et al. (1996). Normal spatial learning despite regional inhibition of LTP in mice lacking Thy-1. *Nature* 379, 826–829. doi: 10.1038/379826a0

Nosyreva, E. D., and Huber, K. M. (2006). Metabotropic receptor-dependent long-term depression persists in the absence of protein synthesis in the mouse model of fragile X syndrome. *J. Neurophysiol.* 95, 3291–3295. doi: 10.1152/jn.01316.2005

Paradee, W., Melikian, H. E., Rasmussen, D. L., Kenneson, A., Conn, P. J., and Warren, S. T. (1999). Fragile X mouse: strain effects of knockout phenotype and evidence suggesting deficient amygdala function. *Neuroscience* 94, 185–192. doi: 10.1016/S0306-4522(99)00285-7

Peier, A. M., McIlwain, K. L., Kenneson, A., Warren, S. T., Paylor, R., and Nelson, D. L. (2000). (Over)correction of FMR1 deficiency with YAC transgenics: behavioral and physical features. *Hum. Mol. Genet.* 9, 1145–1159. doi: 10.1093/hmg/9.8.1145

Pieretti, M., Zhang, F. P., Fu, Y. H., Warren, S. T., Oostra, B. A., Caskey, C. T., et al. (1991). Absence of expression of the FMR-1 gene in fragile X syndrome. *Cell* 66, 817–822. doi: 10.1016/0092-8674(91)90125-I

Ruby, K., Falvey, K., and Kulesza, R. J. (2015). Abnormal neuronal morphology and neurochemistry in the auditory brainstem of Fmr1 knockout rats. *Neuroscience* 303, 285–298. doi: 10.1016/j.neuroscience.2015.06.061

Russo, E., Citraro, R., Davoli, A., Gallelli, L., Di Paola, E. D., and De Sarro, G. (2013). Ameliorating effects of aripiprazole on cognitive functions and depressive-like behavior in a genetic rat model of absence epilepsy and mild-depression comorbidity. *Neuropharmacology* 64, 371–379. doi: 10.1016/j.neuropharm.2012.06.039

Saldarriaga, W., Tassone, F., Gonzalez-Teshima, L. Y., Forero-Forero, J. V., Ayala-Zapata, S., and Hagerman, R. (2014). Fragile X syndrome. *Colomb. Med.* 45, 190–198.

Schenk, F., and Morris, R. G. (1985). Dissociation between components of spatial memory in rats after recovery from the effects of retrohippocampal lesions. *Exp. Brain Res.* 58, 11–28. doi: 10.1007/BF00238949

Shang, Y., Wang, H., Mercaldo, V., Li, X., Chen, T., and Zhuo, M. (2009). Fragile X mental retardation protein is required for chemically-induced long-term potentiation of the hippocampus in adult mice. *J. Neurochem.* 111, 635–646. doi: 10.1111/j.1471-4159.2009.06314.x

Sidorov, M. S., Auerbach, B. D., and Bear, M. F. (2013). Fragile X mental retardation protein and synaptic plasticity. *Mol. Brain* 6:15. doi: 10.1186/1756-6606-6-15

Siomi, H., Siomi, M. C., Nussbaum, R. L., and Dreyfuss, G. (1993). The protein product of the fragile X gene, *FMR1*, has characteristics of an RNA-binding protein. *Cell* 74, 291–298. doi: 10.1016/0092-8674(93)90420-U

Skinner, M., Hooper, S., Hatton, D. D., Roberts, J., Mirrett, P., Schaaf, J., et al. (2005). Mapping nonverbal IQ in young boys with fragile X syndrome. *Am. J. Med. Genet. A* 132A, 25–32. doi: 10.1002/ajmg.a.30353

Spencer, C. M., Graham, D. F., Yuva-Paylor, L. A., Nelson, D. L., and Paylor, R. (2008). Social behavior in Fmr1 knockout mice carrying a human FMR1 transgene. *Behav. Neurosci.* 122, 710–715. doi: 10.1037/0735-7044.122.3.710

Tayebati, S. K., Tomassoni, D., and Amenta, F. (2012). Spontaneously hypertensive rat as a model of vascular brain disorder: microanatomy, neurochemistry and behavior. *J. Neurol. Sci.* 322, 241–249. doi: 10.1016/j.jns.2012.05.047

Terry, A. V. Jr. (2009). "Spatial navigation (water maze) tasks," in *Methods of Behavior Analysis in Neuroscience*, 2nd Edn, ed. J. J. Buccafusco (Boca Raton, FL: CRC Press).

The Dutch-Belgian Fragile X Consortium. (1994). Fmr1 knockout mice: a model to study fragile X mental retardation. The Dutch-Belgian Fragile X Consortium. *Cell* 78, 23–33.

Till, S. M., Asiminas, A., Jackson, A. D., Katsanevaki, D., Barnes, S. A., Osterweil, E. K., et al. (2015). Conserved hippocampal cellular pathophysiology but distinct behavioural deficits in a new rat model of FXS. *Hum. Mol. Genet.* 24, 5977–5984. doi: 10.1093/hmg/ddv299

Uutela, M., Lindholm, J., Louhivuori, V., Wei, H., Louhivuori, L. M., Pertovaara, A., et al. (2012). Reduction of BDNF expression in Fmr1 knockout mice worsens cognitive deficits but improves hyperactivity and sensorimotor deficits. *Genes Brain Behav.* 11, 513–523. doi: 10.1111/j.1601-183X.2012.00784.x

Wei, M., Jia, M., Zhang, J., Yu, L., Zhao, Y., Chen, Y., et al. (2017). The inhibitory effect of alpha/beta-hydrolase domain-containing 6 (ABHD6) on the surface targeting of GluA2- and GluA3-containing AMPA receptors. *Front. Mol. Neurosci.* 10:55. doi: 10.3389/fnmol.2017.00055

Wei, M., Zhang, J., Jia, M., Yang, C., Pan, Y., Li, S., et al. (2016). alpha/beta-Hydrolase domain-containing 6 (ABHD6) negatively regulates the surface delivery and synaptic function of AMPA receptors. *Proc. Natl. Acad. Sci. U.S.A.* 113, E2695–E2704. doi: 10.1073/pnas.1524589113

Xu, X. J., Zhang, H. F., Shou, X. J., Li, J., Jing, W. L., Zhou, Y., et al. (2015). Prenatal hyperandrogenic environment induced autistic-like behavior in rat offspring. *Physiol. Behav.* 138, 13–20. doi: 10.1016/j.physbeh.2014.09.014

Yan, Q. J., Asafo-Adjei, P. K., Arnold, H. M., Brown, R. E., and Bauchwitz, R. P. (2004). A phenotypic and molecular characterization of the fmr1-tm1Cgr fragile X mouse. *Genes Brain Behav.* 3, 337–359. doi: 10.1111/j.1601-183X.2004.00087.x

Yun, S. H., and Trommer, B. L. (2011). Fragile X mice: reduced long-term potentiation and N-Methyl-D-aspartate receptor-mediated neurotransmission in dentate gyrus. *J. Neurosci. Res.* 89, 176–182. doi: 10.1002/jnr.22546

Zhang, C., Wu, B., Beglopoulos, V., Wines-Samuelson, M., Zhang, D., Dragatsis, I., et al. (2009). Presenilins are essential for regulating neurotransmitter release. *Nature* 460, 632–636. doi: 10.1038/nature08177

Zhang, D., Zhang, C., Ho, A., Kirkwood, A., Sudhof, T. C., and Shen, J. (2010). Inactivation of presenilins causes pre-synaptic impairment prior to post-synaptic dysfunction. *J. Neurochem.* 115, 1215–1221. doi: 10.1111/j.1471-4159.2010.07011.x

Zhang, J., Hou, L., Klann, E., and Nelson, D. L. (2009). Altered hippocampal synaptic plasticity in the FMR1 gene family knockout mouse models. *J. Neurophysiol.* 101, 2572–2580. doi: 10.1152/jn.90558.2008

Conflict of Interest Statement: The authors declare that the research was conducted in the absence of any commercial or financial relationships that could be construed as a potential conflict of interest.

frontiers in Molecular Neuroscience

ORIGINAL RESEARCH
published: 28 August 2017
doi: 10.3389/fnmol.2017.00274

Insm1a Regulates Motor Neuron Development in Zebrafish

Jie Gong[1†], Xin Wang[2†], Chenwen Zhu[2], Xiaohua Dong[3], Qinxin Zhang[3], Xiaoning Wang[2], Xuchu Duan[1], Fuping Qian[2,4], Yunwei Shi[2], Yu Gao[2], Qingshun Zhao[3], Renjie Chai[2,4*] and Dong Liu[2*]*

[1] School of Life Science, Nantong University, Nantong, China, [2] Co-innovation Center of Neuroregeneration, Key Laboratory of Neuroregeneration of Jiangsu and Ministry of Education, Nantong University, Nantong, China, [3] MOE Key Laboratory of Model Animal for Disease Study, Model Animal Research Center, Nanjing University, Nanjing, China, [4] Key Laboratory for Developmental Genes and Human Disease, Ministry of Education, Institute of Life Sciences, Southeast University, Nanjing, China

Insulinoma-associated1a (insm1a) is a zinc-finger transcription factor playing a series of functions in cell formation and differentiation of vertebrate central and peripheral nervous systems and neuroendocrine system. However, its roles on the development of motor neuron have still remained uncovered. Here, we provided evidences that *insm1a* was a vital regulator of motor neuron development, and provided a mechanistic understanding of how it contributes to this process. Firstly, we showed the localization of *insm1a* in spinal cord, and primary motor neurons (PMNs) of zebrafish embryos by *in situ* hybridization, and imaging analysis of transgenic reporter line *Tg(insm1a: mCherry)*^{ntu805}. Then we demonstrated that the deficiency of *insm1a* in zebrafish larvae lead to the defects of PMNs development, including the reduction of caudal primary motor neurons (CaP), and middle primary motor neurons (MiP), the excessive branching of motor axons, and the disorganized distance between adjacent CaPs. Additionally, knockout of *insm1* impaired motor neuron differentiation in the spinal cord. Locomotion analysis showed that swimming activity was significantly reduced in the *insm1a*-null zebrafish. Furthermore, we showed that the *insm1a* loss of function significantly decreased the transcript levels of both *olig2* and *nkx6.1*. Microinjection of *olig2* and *nkx6.1* mRNA rescued the motor neuron defects in *insm1a* deficient embryos. Taken together, these data indicated that *insm1a* regulated the motor neuron development, at least in part, through modulation of the expressions of *olig2* and *nkx6.1*.

Keywords: *insm1a*, motor neuron, differentiation, zebrafish, development

Edited by:
Chen Zhang,
Peking University, China

Reviewed by:
Zhiqiang Yan,
Fudan University, China
Jie He,
Institute of Neuroscience, Shanghai Institutes for Biological Sciences (CAS), China

***Correspondence:**
Qingshun Zhao
qingshun@nju.edu.cn
Renjie Chai
renjiec@seu.edu.cn
Dong Liu
liudongtom@gmail.com

† These authors have contributed equally to this work.

Received: *01 July 2017*
Accepted: *14 August 2017*
Published: *28 August 2017*

Citation:
Gong J, Wang X, Zhu C, Dong X, Zhang Q, Wang X, Duan X, Qian F, Shi Y, Gao Y, Zhao Q, Chai R and Liu D (2017) Insm1a Regulates Motor Neuron Development in Zebrafish. Front. Mol. Neurosci. 10:274. doi: 10.3389/fnmol.2017.00274

INTRODUCTION

In vertebrates, motor neurons have precise subtype identities that characterized by a number of morphological criteria, such as soma location, and shape, axon path, and target muscle innervation (Shirasaki and Pfaff, 2002; Lewis and Eisen, 2003). Meanwhile, motor neurons generally extend their axonal trajectory with a highly stereotyped manner during the nervous system development (Eisen, 1991; Palaisa and Granato, 2007). It has been reported that in chick and bullfrog, their motor neuron axons always followed the conservative pathways in order to project to appropriate regions of target musculatures (Landmesser, 1980; Farel and Bemelmans, 1985). In the embryo and larva of zebrafish, there are two different kinds of spinal motor neurons, which are called primary

motor neurons (PMNs), and secondary motor neuron (SMNs) (Myers, 1985; Myers et al., 1986). The PMNs can be further classified into three groups, caudal primary motor neurons (CaP), middle primary motor neurons (MiP), and rostral primary motor neurons (RoP), by the positions of somata in the spinal cord, and the trajectory of neuron axons (Myers et al., 1986; Westerfield et al., 1986). CaPs, whose somata locate in the middle of each spinal cord hemisegment, can innervate ventral axial muscle, and have been well-studied because of their easy observation and distinct axon projection (Myers et al., 1986; Rodino-Klapac and Beattie, 2004). MiPs project axons to innervate the dorsal axial muscle, while RoPs project axons to control the middle muscle (Rodino-Klapac and Beattie, 2004). Although the somata of the three identifiable PMNs are localized in different position in the spinal cord, their axons pioneer to the myoseptum through a mutual exit point (Eisen et al., 1986). Due to the identifiability of the three kinds of PMNs, they have already become an excellent system to study motor axon guidance and their intraspinal navigation (Beattie et al., 2002).

The insulinoma-associated 1 (*insm1*) gene, which is first isolated from an subtraction cDNA library of insulinoma tumor cells, encodes a DNA-binding zinc finger transcription factor with SNAG repressor motifs in N-terminal as well as Cys2-His2 Zn finger motifs in C-terminal, and widely expresses in the developing nervous system, endocrine cells, pancreatic cells, and related neuroendocrine tumor cells (Goto et al., 1992; Xie et al., 2002; Jacob et al., 2009; Lan and Breslin, 2009; Jia et al., 2015b). Consequently, extensive studies focused on the biological function of *insm1* in nervous, and endocrine cell proliferation, differentiation, and transformation have been reported in the model organisms (Farkas et al., 2008; Wildner et al., 2008; Lan and Breslin, 2009; Ramachandran et al., 2012; Jia et al., 2015a,b). For example, in the *insm1* knockout mice, its endocrine progenitor in the developing pancreas were less differentiated, meanwhile hormone production, and cell migration also exhibited seriously defects (Osipovich et al., 2014). Farkas et al. reported that compared to the wild type and heterozygous mice, the number of basal progenitors in the *insm1* null dorsal telencephalon (dTel) was decreased almost half, and the radial thickness of dTel cortical plate as well as the neurogenesis in the neocortex were also predominantly reduced after lacking *insm1* gene (Farkas et al., 2008). In the zebrafish, *insm1a* can regulate a series of related genes, which are necessary for the Müller glia (MG) formation, and differentiation as well as the zone definition of injury-responsive MG to participate in the retina regeneration (Ramachandran et al., 2012). Moreover, it was also reported that during the development of zebrafish retina, *insm1* could regulate cell cycle kinetics and differentiation of the progenitor cells by acting the upstream of the basic helix-loop-helix (bHLH) transcription factors, and the photoreceptor specification genes (Forbes-Osborne et al., 2013). Although *insm1a* is widely detected in the nervous system and its necessity in the brain and retina development have been also illuminated well, little is known about the function and molecular mechanisms of *insm1a* on the formation and development of other neuronal types, especially in the zebrafish.

The zebrafish has become an excellent model system to investigate the mechanisms of the neuron formation and its axonal pathfinding due to the accessible observation of motor neurons from the initial stages of embryo development (Zelenchuk and Bruses, 2011). Here, we examined the function of *insm1a* in the primary motor neurons development by CRISPR/Cas9-mediated knockout in the *Tg(mnx1:GFP)*^{ml2} transgenic zebrafish and investigated the possible transcriptional network during this process.

MATERIALS AND METHODS

Zebrafish Line and Breeding

The zebrafish embryos and adults were maintained in zebrafish Center of Nantong University under conditions in accordance with our previous protocols (Xu et al., 2014; Wang et al., 2016). The transgenic zebrafish line, *Tg(mnx1:GFP)*^{ml2}, has been described in the previous work (Zelenchuk and Bruses, 2011).

RNA Isolation, Reverse Transcription and Quantitative PCR

Total RNA was extracted from zebrafish embryos by TRIzol reagent according to the manufacturer's instructions (Invitrogen, USA). Genomic contaminations were removed by DNaseI, and then 2 μg total RNA was reversely transcribed using a reversed first strand cDNA synthesis kit (Fermentas, USA) and stored at −20°C. qRT-PCR was performed using the corresponding primers (Supplementary Table 1) in a 20 μl reaction volume with 10 μl SYBR premix (Takara, Japan) and *elongation factor 1a* (*ef1a*) was used as the internal control. All samples were analyzed in triplicate.

Whole Mount *In situ* Hybridization

A 501 bp cDNA fragment of *insm1a* was amplified from the cDNA library that established from wild type (WT) AB embryos using the specific primers of *insm1a* F1 and *insm1a* R1 (Supplementary Table 1). Digoxigenin-labeled sense and antisense probes were synthesized using linearized pGEM-T-easy vector subcloned with this *insm1a* fragment by *in vitro* transcription with DIG-RNA labeling Kit (Roche, Switzerland). Zebrafish embryos and larvae were collected and fixed with 4% paraformaldehyde (PFA) in phosphate-buffered saline (PBS) for one night. The fixed samples were then dehydrated through a series of increasing concentrations of methanol and stored at −20°C in 100% methanol eventually. Whole mount *in situ* hybridization was subsequently performed as described in the previous study (Huang et al., 2013).

Establishment of *Tg(insm1a: EGFP)*^{ntu804} and *Tg(insm1a: mCherry)*^{ntu805} Transgenic Line

Transgenic zebrafish were created using the Tol2kit transgenesis system and Gateway vectors. The *insm1a* promoter was cloned and insert into the p5E-MCS entry vector. A multiSite Gateway vector construction reaction (Invitrogen, USA) was conducted with the resulting p5E-insm1a together with pME-EGFP (or mCherry) and p3E-polyA subcloned into the

pDestTol2pA2 to produce *insm1a: EGFP* or *insm1a: mCherry* construct. Subsequently, this construct was co-injected with *tol2-transposase* mRNAs into zebrafish one to two-cell-stage embryos to create the *Tg(insm1a: EGFP)^{ntu804}* and *Tg(insm1a: mCherry)^{ntu805}* transgenic line.

sgRNA/ Cas9 mRNA Synthesis and Injection

Cas9 mRNA was obtained by *in vitro* transcription with the linearized plasmid pXT7-Cas9 according to the procedure previously described. The sgRNAs were transcribed from the DNA templates that amplified by PCR with a pT7 plasmid as the template, a specific forward primer and a universal reverse primer (Supplementary Table 1) (Chang et al., 2013; Qi et al., 2016). Transgenic zebrafish lines *Tg(mnx1:GFP)^{ml2}*, were natural mated to obtain embryos for microinjection. One to two-cell stage zebrafish embryos were injected with 2–3 nl of a solution containing 250 ng/μl Cas9 mRNA and 15 ng/μl sgRNA. At 24 h post fertilization (hpf), zebrafish embryos were randomly sampled for genomic DNA extraction according to the previous methods to determine the indel mutations by sequencing.

Morpholino and mRNAs Injections

Translation blocking antisense Morpholino (MOs; Gene Tools) against the ATG-containing sequence was designed (5′-AAA TCCTCTGGGCATCTTCGCCAGC-3′) to target the translation start site according to the manufacturer's instruction and the other MO oligo (5′-CCTCTTACCTCAGTTACAATTTATA-3′) was used as standard control. The MOs were diluted to 0.3 mM with RNase-free water and injected into the yolk of one to two-cell stage embryos and then raised in E3 medium at 28.5°C.

The cDNAs containing the open reading frame of the target genes were cloned into PCS2^{+} vector respectively and then were transcribed *in vitro* using the mMESSAGE mMACHIN Kit (Ambion, USA) after the recombinant plasmids linearized with NotI Restriction Enzyme (NEB, England), and then the capped mRNAs were purified by RNeasy Mini Kit (Qiagen, Germany). 2 nl target genes and *mCherry* mRNA mixture (1:1) were injected at 20 ng/μl into 1/2-cell stage embryos.

Locomotion Analysis in Zebrafish Larvae

To determine whether the deficiency of *insm1a* affect spontaneous movement, knockout, and normal larvae were raised in a 24-well-culture plate with one larva in each well-filled with 1 ml E3 medium. The 24-well-culture plate was transferred to the Zebralab Video-Track system (Zebrabox, France) equipped with a sealed opaque plastic box that kept insulated from laboratory environment, an infrared filter and a monochrome camera. After adapting for 30 min, traveled distances of the larvae were videotaped with every 5 mins forming a movement distance and trajectory by the linked software.

Microscopy and Statistical Analysis

Zebrafish embryos were anesthetized with E3/0.16 mg/mL tricaine/1% 1-phenyl-2-thiourea (Sigma, USA) and embedded in 0.8% low melt agarose, and then were examined with a Leica TCS-SP5 LSM confocal imaging system. For the results of *in situ* hybridization, Photographs were taken using an Olympus stereomicroscope MVX10. Statistical comparisons of the data were carried out by student's *t*-test or one-way analysis of variance (ANOVA) followed by Duncan's test, and $P < 0.05$ were considered statistically significant. All statistical analysis was performed using the SPSS 13.0 software (SPSS, USA).

RESULT

Insm1a is Expressed in Spinal Cord and PMNs of Zebrafish

To analyze the expression of *insm1a* in zebrafish nervous system, we performed the whole amount *in situ* hybridization (WISH) analysis with a digoxigenin-labeled *insm1a* probe. Similar to the previous study (Lukowski et al., 2006), at late somitogenesis (24 hpf) *insm1a* transcripts were apparently localized in ventral part of the neurons in the spinal cord, where most of the motor neurons located at this stage (**Figure 1A**).

To further determine the localization of *insm1a*, we generated the *Tg(insm1a: EGFP)^{ntu804}* and *Tg(insm1a: mCherry)^{ntu805}* transgenic zebrafish lines, in which the *insm1a* promoter directed expression of EGFP or mCherry respectively. It was shown that at 30 hpf the *insm1a:mCherry* and *insm1a:EGFP* expression was observed in the spinal cord, retina and brain, which was similar with the results of *in situ* hybridization (**Figures 1B,B'**; Supplementary Figures 1A,A') (Lukowski et al., 2006). In addition, we found that *insm1a:EGFP* expression was highly activated in Müller glia of injury sites in adult zebrafish retina (Supplementary Figure 1B), which was consistent with the ISH data carried out by other researchers (Ramachandran et al., 2012). These results suggested that the transgenes recapitulated the endogenous *insm1a* expression.

To investigate whether *insm1a* is expressed in motor neurons, we outcrossed *Tg(insm1a: mCherry)^{ntu805}* transgenic line with *Tg(mnx1:GFP)^{ml2}* line, in which motor neurons were labeled with GFP (Zelenchuk and Bruses, 2011). We found that the GFP^{+} motor neurons were also labeled with mCherry fluorescence (**Figures 1C–C"**), suggesting *insm1a* was expressed in motor neurons.

Knockout of *insm1a* Caused Primary Motor Neurons Developmental Defect

In order to examine whether *insm1a* is required for the development of motor neuron, the CRISPR/Cas9 system was utilized to knockout *insm1a* in *Tg(mnx1:GFP)^{ml2}* transgenic zebrafish line. To ensure complete disruption of functional proteins, we chose the target sites near the translation start codon (ATG) in the exon1 of zebrafish *insm1a* (Supplementary Figure 2A). The selected gRNA-Cas9 system efficiently induced mutations in the targeting site with four types of mutations were identified (Supplementary Figure 2B). The mutated alleles included a 5-bp deletion, an 8-bp deletion and two 10-bp deletions, which all resulted in reading frame shift and premature translation termination (Supplementary Figure 2C). In addition,

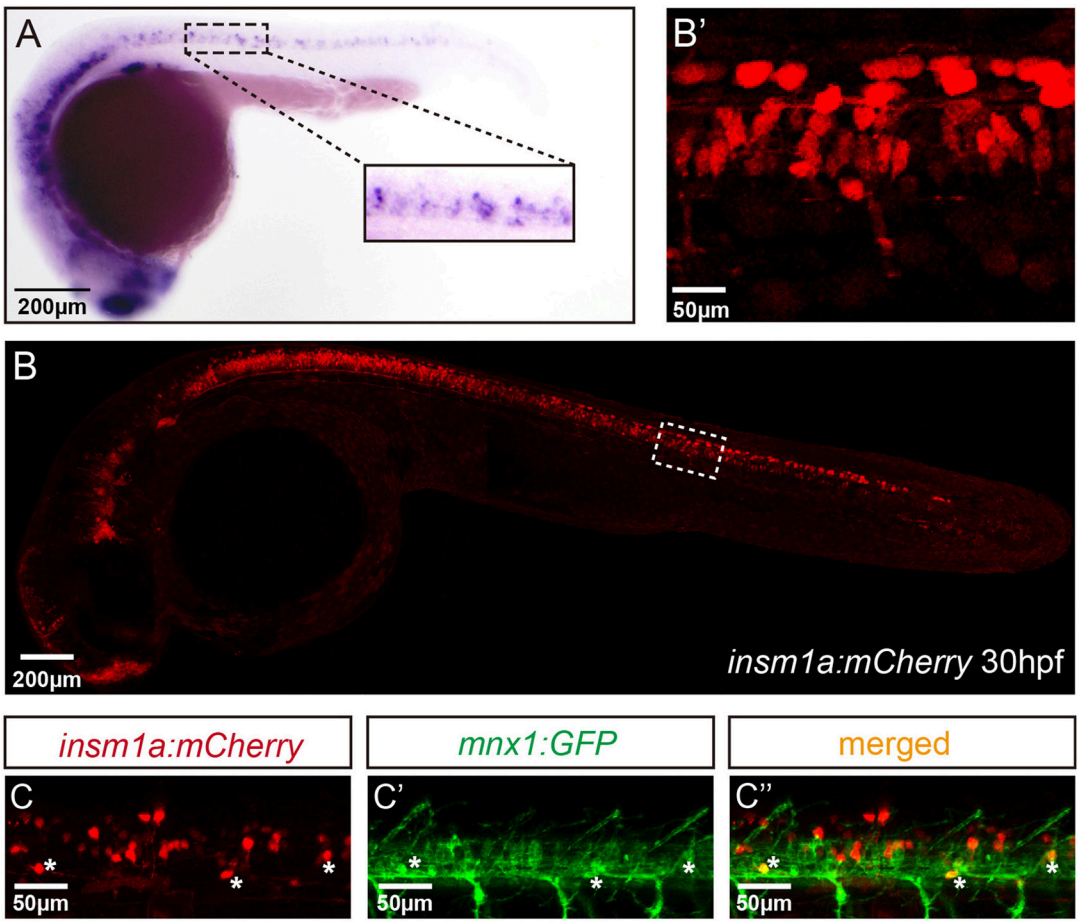

FIGURE 1 | *Insm1a* expression in embryonic zebrafish spinal cord and primary motor neurons. **(A)** At 24 hpf, the *in situ* hybridization signal of insm1a is localized in the spinal cord., Scale bar = 200 μm. **(B)** The confocal imaging analysis of the transgene *insm1a:mCherry* expression at 30 hpf. Square in dash line indicates the magnified region in **(B')** Scale bar = 50 μm. **(C,C',C")**. Confocal imaging analysis of *Tg(mnx1:GFP)*^{ml2} × *Tg(insm1a: mCherry)*^{ntu805} transgenic line.

these lines showed the same phenotypes and the 8-bp deletion mutant line was used for the following experiments.

It was observed that *insm1a* knockout caused obvious developmental defect of motor neurons (**Figure 2**). Firstly, the number of MiPs and CaPs were significantly reduced in the *insm1a* mutants (**Figure 2A**). We counted the number of Caps and classified the zebrafish embryo into three categories by its defective degree: severe group with over 80% loss of Caps, moderate group with <80% loss and normal group with <20% loss (In the following statistical analysis, the zebrafish with <20% loss was defined as normal, whereas, it was abnormal). These results revealed that 48.1% severe and 32.1% moderate defect were found in the *insm1a* mutants, while there was only 7.9% moderate defect in the control group (**Figure 2B**). Similarly, the MiPs were also obviously impaired in *insm1a* knockout embryos (**Figures 2A,F**). Importantly, we found that these abnormal phenotypes of motor neurons could not recover at later stages we checked (Supplementary Figure 3).

Moreover, the morphology of motor neurons was significantly affected in the *insm1a* mutants (**Figures 2A,D,E**). The axons of Caps in *insm1a* mutants were shorter and failed to reach the ventral musculatures. The branches density of the Caps in *insm1a* mutants was higher than that in control. For example, in the *insm1a* mutants, there were around 34 branch points of per 1 mm CaP axon at 48 hpf, while only 31 in control embryos (**Figure 2E**). With the larvae development, the excess branching became more, and more pronounced (Supplementary Figure 3). In addition, statistical analysis revealed that the average length of each CaP anon in the *insm1a* mutants was 707.9 μm at 48 hpf, while in control embryos it increased to 1367.9 μm (**Figure 2D**). Interestingly, we also found that the distances between adjacent CaPs were significantly variant in *insm1a* mutants (**Figure 2C**).

In order to validate the developmental defects of motor neuron was specifically caused by the *insm1a* inactivation, further experiments were carried out. The embryos that injected with an *insm1a* translation blocking morpholino displayed the similar motor neuron with that observed in the *insm1a* mutants (Supplementary Figure 4). To confirm phenotypic specificity induced by the *insm1a* MO injection, we performed rescue experiment by co-injection of 50 ng of *insm1a* mRNA with

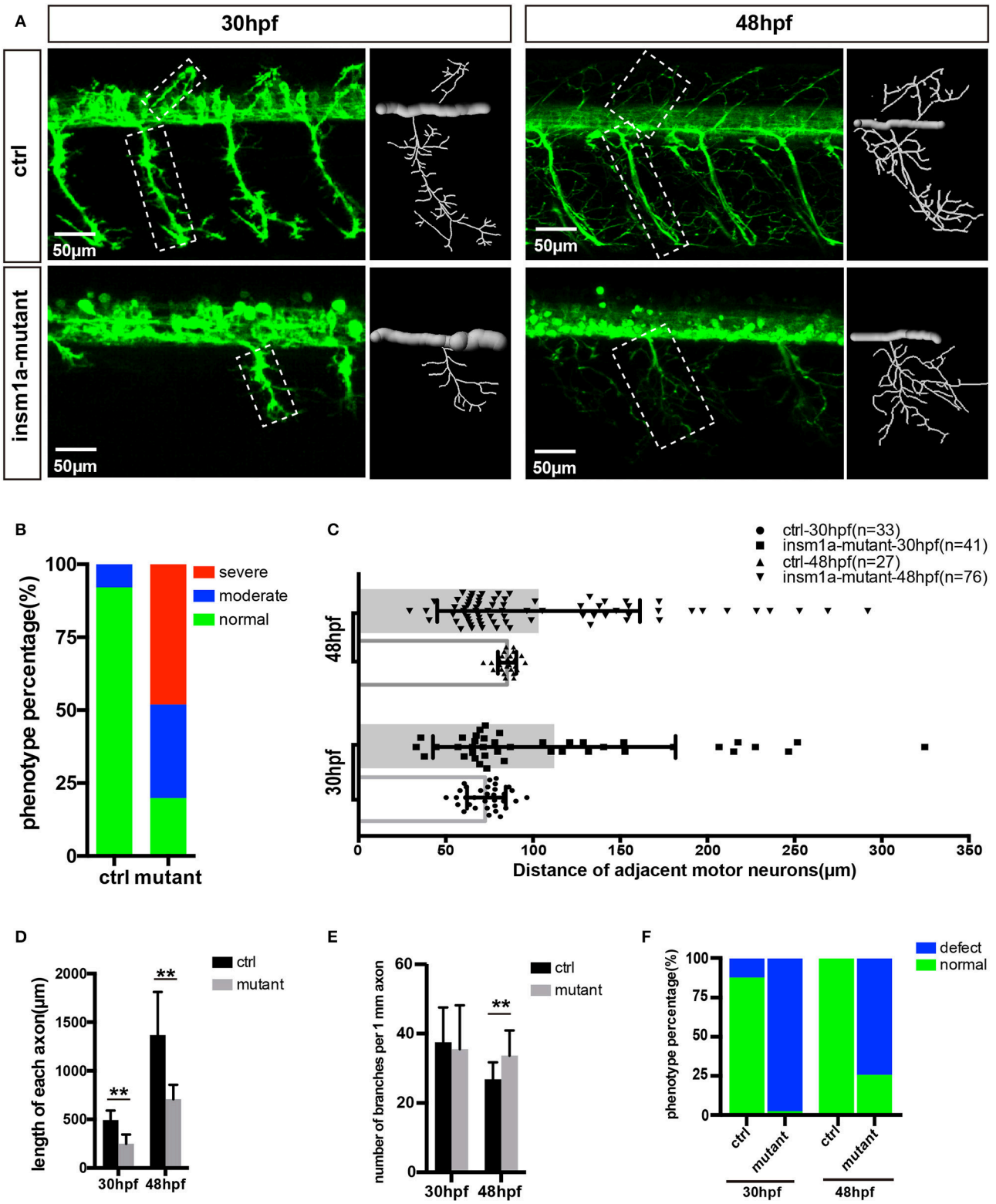

FIGURE 2 | Primary motor neuron morphogenesis defects in the *insm1a* mutant zebrafish embryos. **(A)** Confocal imaging analysis of primary motor neuron in control group and *insm1a* mutant groups at 30 hpf and 48 hpf *Tg(mnx1:GFP)*^{ml2}. Caps in dash line are showed in diagrams. Scale bar = 50 μm. **(B)** Quantification of zebrafish embryos with abnormal Caps. The zebrafish embryos are classified into three categories according to its loss degree: severe group with over 80% loss of

(Continued)

FIGURE 2 | Continued
Cap primary motor neuron, moderate group with <80% loss, and normal group with <20% loss. **(C)** Quantification of distance between adjacent motor neurons (μm) in control group and *insm1a* mutant groups at 30 hpf ($n = 33$ and 41 respectively) and 48 hpf ($n = 27$ and 76 respectively). **(D,E)** The length and branching number of Cap axons in control group and *insm1a* mutant groups at 30 and 48 hpf. Asterisks above the bars indicate significant differences (**$P < 0.01$). **(F)** Quantification of zebrafish embryos with abnormal Caps at 30 and 48 hpf.

insm1a MO into zebrafish embryos, and the results showed that the co-injection significantly decreased the loss, and premature branching of PMNs (Supplementary Figure 4E). Taken together, these results indicated those motor neuron developmental defects were caused by loss of *insm1a*.

Insm1a Deficiency Suppressed Neuronal Cells Differentiation

The confocal imaging analysis discovered that there were a number of round and not well-differentiated GFP positive cells in *Tg(mnx1:GFP)*^{ml2} *insm1a* mutants (**Figure 3A**). Statistical analysis showed that at 30 and 48 hpf the number of these undifferentiated cell in the *insm1a* deficiency zebrafish was significantly higher than that in the control fish (**Figure 3B**). We also observed these undifferentiated cells in *insm1a* morphants, however the number was less than that in mutants (**Figures 3A,B**).

To further investigate the cellular mechanism underlying the motor neuronal defects in *insm1a* deficient embryos, we performed confocal time-lapse imaging analysis. It was found that in control embryos the axon of CaP sprouted from the spinal cord, and extended toward to the ventral muscle (**Figure 3C**). In control embryos the axon of CaP started to branch when it passed through the midline, while in *insm1a* mutants the axon initiated to branch once it came out from the spinal cord (**Figures 3A,C**, Supplementary Movies 1, 2). In addition, we found that those round GFP positive cells did not develop neuronal projections (**Figures 3A,C**, Supplementary Movie 1).

Knockout of *insm1a* Reduced the Zebrafish Swimming Activity

In order to investigate whether the motor neuron defects affects the motor ability, *insm1a* mutant zebrafish larvae were further performed for 40-min free-swimming activity test independent of any stimuli at 7 and 10 dpf. It demonstrated that the movement trajectory and swimming distance per 5 mins, which could reflect the swimming speed, of *insm1a* mutant zebrafish larvae were significantly decreased compared to that in the control (**Figure 4**). The movie in the Supplementary Material showed that swimming behavior could be easily discovered in the control group, while the zebrafish in mutant group kept involuntomotory (Supplementary Movie 3). Additionally, we also discovered that under the stereoscopic microscope the mutant zebrafish became insensitive to the touch stimuli (data not shown).

The *insm1a* Deficiency Caused Alteration of Gene Expression Involved in Motor Neuron Development

Since insm1a is a transcription factor, we supposed that motor neuron developmental defects in *insm1a* deficient embryos were associated with altered expression of downstream genes of *insm1a* or the genes participating in the motor neuron development. Based on the previous studies, *NNR2a*, *NNR2b*, *islet2*, *Asci1a*, *Asci1b*, *shh*, *Ngn2*, *Nkx6.1,* and *olig2* were selected to do the qRT-PCR analysis in wild-type (WT) and *insm1a* deficiency zebrafish embryos (Park et al., 2002; Hutchinson et al., 2007; Davis-Dusenbery et al., 2014; Barreiro-Iglesias et al., 2015). The results showed that expressions of *NNR2a*, *NNR2b*, *islet2*, *Asci1a,* and *Asci1b* were significantly influenced in the *insm1a* deficiency zebrafish compared to the control (Supplementary Figure 5). We also found that the expression of *shh* was obviously elevated in *insm1a* mutants at 19, 24, and 36 hpf (Supplementary Figure 5). Interestingly, *olig2* and *nkx6.1* transcripts dramatically decreased in *insm1a* deficient embryos (**Figures 5A,B**).

Olig2 and *nkx6.1* Over Expression Rescued the Motor Neuron Defects in *insm1a* Deficient Embryos

As the downregulation of *olig2* and *nkx6.1* in *insm1a* loss of function embryos, we reasoned that insm1a might bind the transcriptional regulatory elements of these two genes. Based on the JASPAR 2016 database (Mathelier et al., 2016) analysis, we found that both *olig2* and *nkx6.1* contained the putative binding sites of Insm1a, suggesting Insm1a directly regulates the expression of *olig2,* and *nkx6.1* during PMNs development. To investigate whether the motor neuronal defects in *insm1a* deficient embryos were caused by reduced expression of *olig2* and *nkx6.1*, we tried to rescue the phenotype with olig2 and nkx6.1 gain of function in *insm1a* deficient embryos. It was shown that co-injection both *olig2 and nkx6.1* mRNA respectively with *insm1a* MO significantly reduced the motor neuronal defects caused by loss of *insm1a* (**Figures 5C,D**). 69.6% zebrafish embryos injected with *insm1a* MO at 48 hpf had the motor neuron developmental defects, while only 42.1% had the motor neuronal phenotype in the *olig2* mRNA and *insm1a* MO co-injection group (**Figure 5D**). Similarly, after *nkx6.1* mRNA and *insm1a* MO co-injection, the ratio of motor neuronal phenotype decreased to 38.6% (**Figure 5D**).

DISCUSSION

As one of the most conserved zinc-finger transcriptional factor, insm1a plays important roles in various biological processes in vertebrates (Wildner et al., 2008; Jacob et al., 2009; Forbes-Osborne et al., 2013; Osipovich et al., 2014; Jia et al., 2015b; Lorenzen et al., 2015). Previous studies have identified its role in regulating the endocrine cells divisions of the pancreas, the neuroendocrine development, the differentiation of retina progenitors and neurogenesis of nervous system (Gierl et al., 2006; Duggan et al., 2008; Farkas et al., 2008; Jacob et al., 2009;

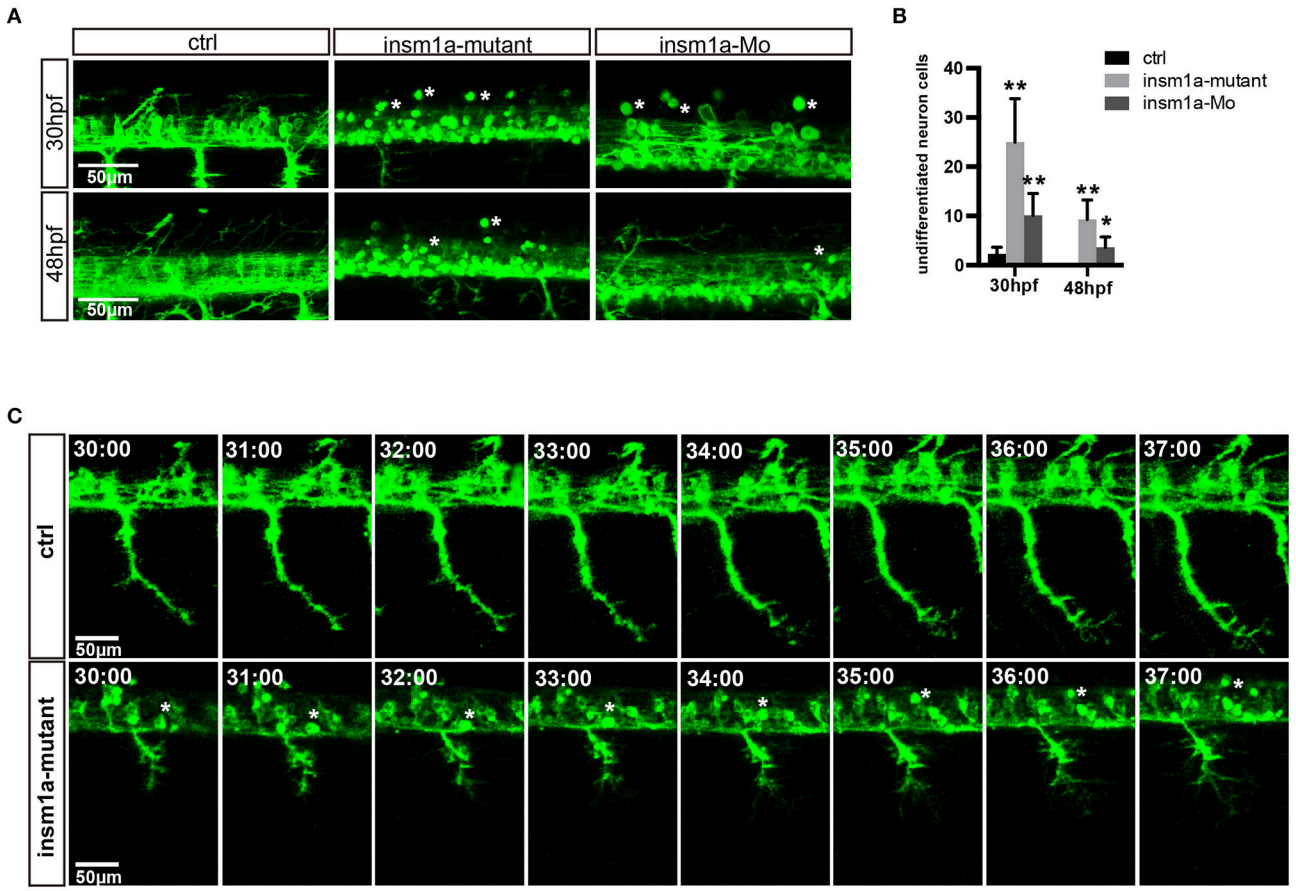

FIGURE 3 | *Insm1a* deficiency suppressed neuronal cells differentiation. **(A)** Confocal imaging analysis of primary motor neuron in control group, *insm1a* mutant group and morphant group at 30 and 48 hpf *Tg(mnx1:GFP)*^{ml2}. Phenotypes of neuronal cells in the spinal cord in control group, morphant group, and insm1a mutant groups at 30 hpf and 48 hpf. Asterisks indicate undifferentiated neuronal cells. Scale bar = 50 μm. **(B)** Quantification of the undifferentiated neuronal cell in the *insm1a* different treatment zebrafish. Asterisks above the bars indicate significant differences (*$P < 0.05$, **$P < 0.01$). **(C)** Time-lapse imaging analysis of the primary motor neuron in control group and insm1a mutant groups. Asterisks represent undifferentiated neuronal cells. Scale bar = 50 μm

Lan and Breslin, 2009; Ramachandran et al., 2012). Currently, our data in this study provided with new insights into the role of insm1a in motor neuron development.

Our WISH data and previous study (Ramachandran et al., 2012) demonstrated that *insm1a* transcripts were detected in retina and spinal cord at 24 hpf. Furthermore, imaging analysis of our established transgenic reporter line *Tg(insm1a: EGFP)*^{ntu804} *and Tg(insm1a: mCherry)*^{ntu805} verified the results of *in situ* hybridization, and revealed the expression of EGFP or mCherry that were driven by *insm1a* promoter in the PMNs. It is well-known that the spinal cord contains PMNs which project their axons out of the spinal cord to the terminal musculature with the embryo development (Davis-Dusenbery et al., 2014). Taken together, the localization data of *insm1a* from both *in situ* hybridization analysis and the study based on transgenic reporter line suggested that *insm1a* might participate in the regulation of PMNs development.

To test whether *insm1a* was required for formation of PMNs, we generated CRISPR/Cas9-mediated *insm1a* mutants, and showed that obvious motor neuron loss and defects of the PMNs axons. Moreover, we also performed *insm1a* knockdown, and the results showed similar PMNs defects as the ones produced by the *insm1a* knockout. In wild embryos, exuberant side branches developed at around 72 hpf, and then invaded into myotome to form distributed neuromuscular synapses (Liu and Westerfield, 1990; Downes and Granato, 2004). These results suggested that *insm1a* was pivotal for the primary motor axon development to block precociously extending into muscle territories. Additionally, locomotion analysis displayed a typical low activity swimming behavior in *insm1a* mutant zebrafish. It was known motor neuron was a major kind of cell type that regulated swimming behavior in zebrafish during early development (Brustein et al., 2003). Previous studies also showed a significant involvement of motor neuron in the overall locomotor behavior (Flanagan-Steet et al., 2005; Levin et al., 2009). Currently, the decrease of swimming activity in this study was consistent with the motor neuron defects in the *insm1a* knockout zebrafish.

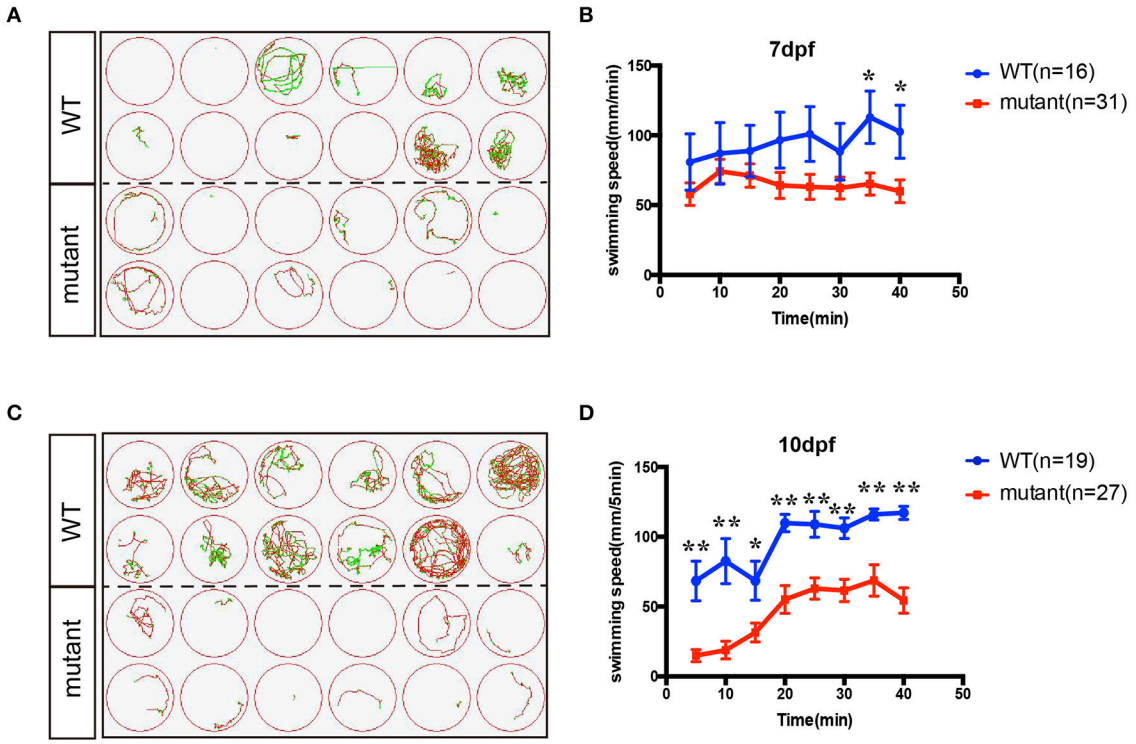

FIGURE 4 | The swimming behavior analysis of control and *insm1a* mutant zebrafish embryos at 7 and 10 dpf. **(A,C)**. The swimming trajectory of the control and *insm1a* mutant zebrafish embryos at 7 and 10 dpf. **(B,D)**. Quantification of the swimming distance of control and *insm1a* mutant zebrafish embryos at 7 and 10 dpf per 5 mins ($n = 36$ in each group). Asterisks indicate the significant difference (*$P < 0.05$, **$P < 0.01$).

Another prominent phenotype in the *insm1a* deficiency zebrafish was the disorganized distance between adjacent Caps, which might be caused by the ectopic departure of motor axons from the spinal cord (Palaisa and Granato, 2007). During the zebrafish PMNs development, the three kinds of PMN axons firstly longitudinally migrated toward a segmental spinal cord exit point, and then diverged to individual-specific trajectories (Eisen et al., 1986; Myers et al., 1986). It has been reported that axonal exit sites at the spinal cord might be restricted and conserved (Niederlander and Lumsden, 1996). However, the change of distance between adjacent motor axon and the formation of abnormal axons in our study suggested that the motor axons could form exit points at any positions along entire length of spinal cord in *insm1a* mutants. The similar phenotypes were also showed in *plexin A3* and *semaphorin 3A* morphants (Feldner et al., 2007; Palaisa and Granato, 2007; Tanaka et al., 2007). Additionally, Birely et al. reported the phenotype that motor axons departed from the spinal cord at the ectopic points accompanied with defects in slow muscle fiber development (Birely et al., 2005). These studies suggested that the low activity swimming behavior in *insm1a* mutant zebrafish might be involved in the ectopic departure of motor axons from the spinal cord.

In this study we also found that loss function of Insm1a obviously impaired the motor neuronal differentiation. Similarly, It was shown that Insm1a regulated cell differentiation and migration in zebrafish retinal development and regeneration (Ramachandran et al., 2012; Forbes-Osborne et al., 2013). In vertebrates, Insm1 stimulates cell cycle exit by suppressing expression of cell proliferation related genes and relieving repression of p57kip2, a cyclin kinase inhibitor that along with p27kip1 drives cell cycle exit (Dyer and Cepko, 2001). One consequence of insm1a driven cell cycle exit is progenitor differentiation (Ramachandran et al., 2012). The undifferentiated cells in the spinal cord of *insm1a* mutants confirmed the role of this transcriptional factor in cell differentiation in more cell types.

A series of genes have been identified to contribute to motor neuron formation and development (Park et al., 2002; Cheesman et al., 2004). It has been reported that *nkx6.1* and *olig2* were dynamically expressed in zebrafih motor neuron and required for motor neuron development. Downregulation of the two genes lead to developmental defect of motor neuron, which was similar with that in *insm1a* mutant (Park et al., 2002; Cheesman et al., 2004; Hutchinson et al., 2007). Conversely, overexpression of *nkx6.1* or *olig2* by mRNA injection could significantly promote the development of the PMNs (Park et al., 2002; Hutchinson et al., 2007). Current study revealed that the inactivation of *insm1a* resulted in the significant decrease of *nkx6.1* and *olig2* expression levels. Furthermore, *olig2,* and *nkx6.1* overexpression rescued the motor neuron defects in *insm1a* deficient embryos. These data suggested that *insm1a* regulated the motor neuron development, at least in part, by regulating the expressions of *olig2,* and *nkx6.1*.

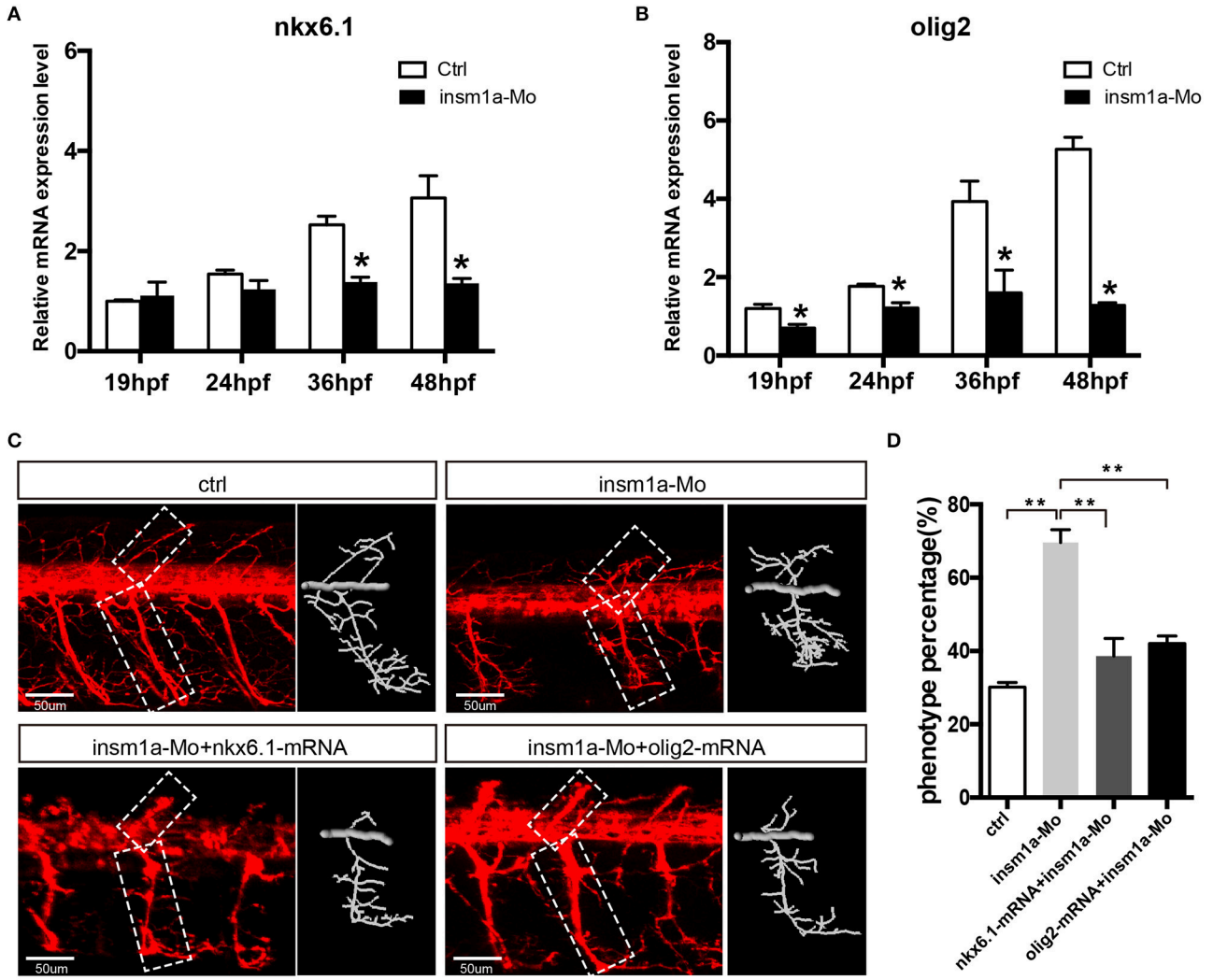

FIGURE 5 | Over expressions of *nkx6.1* and *olig2* rescued the motor neuron defects in *insm1a* deficient embryos. **(A,B)**. Effects of *insm1a* knockdown on the expressions of *nkx6.1* and *olig2* at 19, 24, 36, and 48 hpf. Asterisks indicate significant differences (*$P < 0.05$). **(C)** Abnormal Caps in insm1a knockdown zebrafish embryos were restored by co-injection of *nkx6.1* or *olig2* mRNA. Diagrams of Caps in dash line are displayed near the corresponding confocal image. Scale bar = 50 μm. **(D)** Quantification of zebrafish embryos with abnormal Cap primary motor neuron. Asterisks indicate significant differences (**$P < 0.01$).

ETHICS STATEMENT

All animal experimentation was carried out in accordance with the NIH Guidelines for the care and use of laboratory animals (http://oacu.od.nih.gov/regs/index.htm) and ethically approved by the Administration Committee of Experimental Animals, Jiangsu Province, China [Approval ID: SYXK (SU) 2007–0021].

AUTHOR CONTRIBUTIONS

DL, RC, and QSZ conceived the project. JG, XW, CZ, XNW, XCD, FQ, YS, and YG performed most of the experiments. XHD and QXZ generated the mutants. DL, JG, and XW analyzed the data and prepared the manuscript. All authors commented and approved the manuscript.

ACKNOWLEDGMENTS

This study was supported by grants from the National Natural Science Foundation of China (31400918, 41606169, 81570447, 81622013, 81470692, 31500852); Natural Science Foundation of Jiangsu Province (BK20160418, BK20150022, BK20140620); the National Key Research Development Program of China (2017YFA0103900, 2015CB965000, 2017YFA0103903); the Yingdong Huo Education Foundation; and the Fundamental Research Funds for the Central Universities.

SUPPLEMENTARY MATERIAL

The Supplementary Material for this article can be found online at: http://journal.frontiersin.org/article/10.3389/fnmol.2017.00274/full#supplementary-material

REFERENCES

Barreiro-Iglesias, A., Mysiak, K. S., Scott, A. L., Reimer, M. M., Yang, Y., Becker, C. G., et al. (2015). Serotonin promotes development and regeneration of spinal motor neurons in Zebrafish. *Cell Rep.* 13, 924–932. doi: 10.1016/j.celrep.2015.09.050

Beattie, C. E., Granato, M., and Kuwada, J. Y. (2002). Cellular, genetic and molecular mechanisms of axonal guidance in the zebrafish. *Results Probl. Cell Differ.* 40, 252–269. doi: 10.1007/978-3-540-46041-1_13

Birely, J., Schneider, V. A., Santana, E., Dosch, R., Wagner, D. S., Mullins, M. C., et al. (2005). Genetic screens for genes controlling motor nerve-muscle development and interactions. *Dev. Biol.* 280, 162–176. doi: 10.1016/j.ydbio.2005.01.012

Brustein, E., Saint-Amant, L., Buss, R. R., Chong, M., McDearmid, J. R., and Drapeau, P. (2003). Steps during the development of the zebrafish locomotor network. *J. Physiol. Paris* 97, 77–86. doi: 10.1016/j.jphysparis.2003.10.009

Chang, N., Sun, C., Gao, L., Zhu, D., Xu, X., Zhu, X., et al. (2013). Genome editing with RNA-guided Cas9 nuclease in zebrafish embryos. *Cell Res.* 23, 465–472. doi: 10.1038/cr.2013.45

Cheesman, S. E., Layden, M. J., Von Ohlen, T., Doe, C. Q., and Eisen, J. S. (2004). Zebrafish and fly Nkx6 proteins have similar CNS expression patterns and regulate motoneuron formation. *Development* 131, 5221–5232. doi: 10.1242/dev.01397

Davis-Dusenbery, B. N., Williams, L. A., Klim, J. R., and Eggan, K. (2014). How to make spinal motor neurons. *Development* 141, 491–501. doi: 10.1242/dev.097410

Downes, G. B., and Granato, M. (2004). Acetylcholinesterase function is dispensable for sensory neurite growth but is critical for neuromuscular synapse stability. *Dev. Biol.* 270, 232–245. doi: 10.1016/j.ydbio.2004.02.027

Duggan, A., Madathany, T., de Castro, S. C., Gerrelli, D., Guddati, K., and Garcia-Anoveros, J. (2008). Transient expression of the conserved zinc finger gene INSM1 in progenitors and nascent neurons throughout embryonic and adult neurogenesis. *J. Comp. Neurol.* 507, 1497–1520. doi: 10.1002/cne.21629

Dyer, M. A., and Cepko, C. L. (2001). $p27^{Kip1}$ and $p57^{Kip2}$ regulate proliferation in distinct retinal progenitor cell populations. *J. Neurosci.* 21, 4259–4271. Available online at: http://www.jneurosci.org/content/21/12/4259.long

Eisen, J. S. (1991). Determination of primary motoneuron identity in developing zebrafish embryos. *Science* 252, 569–572. doi: 10.1126/science.1708527

Eisen, J. S., Myers, P. Z., and Westerfield, M. (1986). Pathway selection by growth cones of identified motoneurones in live zebra fish embryos. *Nature* 320, 269–271. doi: 10.1038/320269a0

Farel, P. B., and Bemelmans, S. E. (1985). Specificity of motoneuron projection patterns during development of the bullfrog tadpole (*Rana catesbeiana*). *J. Comp. Neurol.* 238, 128–134. doi: 10.1002/cne.902380112

Farkas, L. M., Haffner, C., Giger, T., Khaitovich, P., Nowick, K., Birchmeier, C., et al. (2008). Insulinoma-associated 1 has a panneurogenic role and promotes the generation and expansion of basal progenitors in the developing mouse neocortex. *Neuron* 60, 40–55. doi: 10.1016/j.neuron.2008.09.020

Feldner, J., Reimer, M. M., Schweitzer, J., Wendik, B., Meyer, D., Becker, T., et al. (2007). PlexinA3 restricts spinal exit points and branching of trunk motor nerves in embryonic zebrafish. *J. Neurosci.* 27, 4978–4983. doi: 10.1523/JNEUROSCI.1132-07.2007

Flanagan-Steet, H., Fox, M. A., Meyer, D., and Sanes, J. R. (2005). Neuromuscular synapses can form *in vivo* by incorporation of initially a neural postsynaptic specializations. *Development* 132, 4471–4481. doi: 10.1242/dev.02044

Forbes-Osborne, M. A., Wilson, S. G., and Morris, A. C. (2013). Insulinoma-associated 1a (Insm1a) is required for photoreceptor differentiation in the zebrafish retina. *Dev. Biol.* 380, 157–171. doi: 10.1016/j.ydbio.2013.05.021

Gierl, M. S., Karoulias, N., Wende, H., Strehle, M., and Birchmeier, C. (2006). The zinc-finger factor Insm1 (IA-1) is essential for the development of pancreatic beta cells and intestinal endocrine cells. *Genes Dev.* 20, 2465–2478. doi: 10.1101/gad.381806

Goto, Y., De Silva, M. G., Toscani, A., Prabhakar, B. S., Notkins, A. L., and Lan, M. S. (1992). A novel human insulinoma-associated cDNA, IA-1, encodes a protein with zinc-finger DNA-binding motifs. *J. Biol. Chem.* 267, 15252–15257.

Huang, Y., Wang, X., Wang, X., Xu, M., Liu, M., and Liu, D. (2013). Nonmuscle myosin II-B (myh10) expression analysis during zebrafish embryonic development. *Gene Expr. Patterns* 13, 265–270. doi: 10.1016/j.gep.2013.04.005

Hutchinson, S. A., Cheesman, S. E., Hale, L. A., Boone, J. Q., and Eisen, J. S. (2007). Nkx6 proteins specify one zebrafish primary motoneuron subtype by regulating late islet1 expression. *Development* 134, 1671–1677. doi: 10.1242/dev.02826

Jacob, J., Storm, R., Castro, D. S., Milton, C., Pla, P., Guillemot, F., et al. (2009). Insm1 (IA-1) is an essential component of the regulatory network that specifies monoaminergic neuronal phenotypes in the vertebrate hindbrain. *Development* 136, 2477–2485. doi: 10.1242/dev.034546

Jia, S., Ivanov, A., Blasevic, D., Muller, T., Purfurst, B., Sun, W., et al. (2015a). Insm1 cooperates with Neurod1 and Foxa2 to maintain mature pancreatic beta-cell function. *EMBO J.* 34, 1417–1433. doi: 10.15252/embj.201490819

Jia, S., Wildner, H., and Birchmeier, C. (2015b). Insm1 controls the differentiation of pulmonary neuroendocrine cells by repressing Hes1. *Dev. Biol.* 408, 90–98. doi: 10.1016/j.ydbio.2015.10.009

Lan, M. S., and Breslin, M. B. (2009). Structure, expression, and biological function of INSM1 transcription factor in neuroendocrine differentiation. *FASEB J.* 23, 2024–2033. doi: 10.1096/fj.08-125971

Landmesser, L. T. (1980). The generation of neuromuscular specificity. *Annu. Rev. Neurosci.* 3, 279–302. doi: 10.1146/annurev.ne.03.030180.001431

Levin, E. D., Aschner, M., Heberlein, U., Ruden, D., Welsh-Bohmer, K. A., Bartlett, S., et al. (2009). Genetic aspects of behavioral neurotoxicology. *Neurotoxicology* 30, 741–753. doi: 10.1016/j.neuro.2009.07.014

Lewis, K. E., and Eisen, J. S. (2003). From cells to circuits: development of the zebrafish spinal cord. *Prog. Neurobiol.* 69, 419–449. doi: 10.1016/S0301-0082(03)00052-2

Liu, D. W., and Westerfield, M. (1990). The formation of terminal fields in the absence of competitive interactions among primary motoneurons in the zebrafish. *J. Neurosci.* 10, 3947–3959.

Lorenzen, S. M., Duggan, A., Osipovich, A. B., Magnuson, M. A., and Garcia-Anoveros, J. (2015). Insm1 promotes neurogenic proliferation in delaminated otic progenitors. *Mech. Dev.* 138(Pt 3), 233–245. doi: 10.1016/j.mod.2015.11.001

Lukowski, C. M., Ritzel, R. G., and Waskiewicz, A. J. (2006). Expression of two insm1-like genes in the developing zebrafish nervous system. *Gene Expr. Patterns* 6, 711–718. doi: 10.1016/j.modgep.2005.12.008

Mathelier, A., Fornes, O., Arenillas, D. J., Chen, C. Y., Denay, G., Lee, J., et al. (2016). JASPAR 2016: a major expansion and update of the open-access database of transcription factor binding profiles. *Nucleic Acids Res.* 44, D110–D115. doi: 10.1093/nar/gkv1176

Myers, P. Z. (1985). Spinal motoneurons of the larval zebrafish. *J. Comp. Neurol.* 236, 555–561. doi: 10.1002/cne.902360411

Myers, P. Z., Eisen, J. S., and Westerfield, M. (1986). Development and axonal outgrowth of identified motoneurons in the zebrafish. *J. Neurosci.* 6, 2278–2289.

Niederlander, C., and Lumsden, A. (1996). Late emigrating neural crest cells migrate specifically to the exit points of cranial branchiomotor nerves. *Development* 122, 2367–2374.

Osipovich, A. B., Long, Q., Manduchi, E., Gangula, R., Hipkens, S. B., Schneider, J., et al. (2014). Insm1 promotes endocrine cell differentiation by modulating the expression of a network of genes that includes Neurog3 and Ripply3. *Development* 141, 2939–2949. doi: 10.1242/dev.104810

Palaisa, K. A., and Granato, M. (2007). Analysis of zebrafish sidetracked mutants reveals a novel role for Plexin A3 in intraspinal motor axon guidance. *Development* 134, 3251–3257. doi: 10.1242/dev.007112

Park, H. C., Mehta, A., Richardson, J. S., and Appel, B. (2002). olig2 is required for zebrafish primary motor neuron and oligodendrocyte development. *Dev. Biol.* 248, 356–368. doi: 10.1006/dbio.2002.0738

Qi, J., Dong, Z., Shi, Y., Wang, X., Qin, Y., Wang, Y., et al. (2016). NgAgo-based fabp11a gene knockdown causes eye developmental defects in zebrafish. *Cell Res.* 26, 1349–1352. doi: 10.1038/cr.2016.134

Ramachandran, R., Zhao, X. F., and Goldman, D. (2012). Insm1a-mediated gene repression is essential for the formation and differentiation of Muller glia-derived progenitors in the injured retina. *Nat. Cell Biol.* 14, 1013–1023. doi: 10.1038/ncb2586

Rodino-Klapac, L. R., and Beattie, C. E. (2004). Zebrafish topped is required for ventral motor axon guidance. *Dev. Biol.* 273, 308–320. doi: 10.1016/j.ydbio.2004.06.007

Shirasaki, R., and Pfaff, S. L. (2002). Transcriptional codes and the control of neuronal identity. *Annu. Rev. Neurosci.* 25, 251–281. doi: 10.1146/annurev.neuro.25.112701.142916

Tanaka, H., Maeda, R., Shoji, W., Wada, H., Masai, I., Shiraki, T., et al. (2007). Novel mutations affecting axon guidance in zebrafish and a role for plexin signalling in the guidance of trigeminal and facial nerve axons. *Development* 134, 3259–3269. doi: 10.1242/dev.004267

Wang, X., Ling, C. C., Li, L., Qin, Y., Qi, J., Liu, X., et al. (2016). MicroRNA-10a/10b represses a novel target gene mib1 to regulate angiogenesis. *Cardiovasc. Res.* 110, 140–150. doi: 10.1093/cvr/cvw023

Westerfield, M., McMurray, J. V., and Eisen, J. S. (1986). Identified motoneurons and their innervation of axial muscles in the zebrafish. *J. Neurosci.* 6, 2267–2277.

Wildner, H., Gierl, M. S., Strehle, M., Pla, P., and Birchmeier, C. (2008). Insm1 (IA-1) is a crucial component of the transcriptional network that controls differentiation of the sympatho-adrenal lineage. *Development* 135, 473–481. doi: 10.1242/dev.011783

Xie, J., Cai, T., Zhang, H., Lan, M. S., and Notkins, A. L. (2002). The zinc-finger transcription factor INSM1 is expressed during embryo development and interacts with the Cbl-associated protein. *Genomics* 80, 54–61. doi: 10.1006/geno.2002.6800

Xu, M., Liu, D., Dong, Z., Wang, X., Wang, X., Liu, Y., et al. (2014). Kinesin-12 influences axonal growth during zebrafish neural development. *Cytoskeleton* 71, 555–563. doi: 10.1002/cm.21193

Zelenchuk, T. A., and Bruses, J. L. (2011). *In vivo* labeling of zebrafish motor neurons using an mnx1 enhancer and Gal4/UAS. *Genesis* 49, 546–554. doi: 10.1002/dvg.20766

Conflict of Interest Statement: The authors declare that the research was conducted in the absence of any commercial or financial relationships that could be construed as a potential conflict of interest.

frontiers in Molecular Neuroscience

HYPOTHESIS AND THEORY
published: 09 August 2017
doi: 10.3389/fnmol.2017.00255

Membrane Receptor-Induced Changes of the Protein Kinases A and C Activity May Play a Leading Role in Promoting Developmental Synapse Elimination at the Neuromuscular Junction

Josep M. Tomàs†, Neus Garcia*†, Maria A. Lanuza†, Laura Nadal, Marta Tomàs, Erica Hurtado, Anna Simó and Víctor Cilleros*

Unitat d'Histologia i Neurobiologia (UHN), Facultat de Medicina i Ciències de la Salut, Universitat Rovira i Virgili, Reus, Spain

Synapses that are overproduced during histogenesis in the nervous system are eventually lost and connectivity is refined. Membrane receptor signaling leads to activity-dependent mutual influence and competition between axons directly or with the involvement of the postsynaptic cell and the associated glial cell/s. Presynaptic muscarinic acetylcholine (ACh) receptors (subtypes mAChR; M_1, M_2 and M_4), adenosine receptors (AR; A_1 and A_{2A}) and the tropomyosin-related kinase B receptor (TrkB), among others, all cooperate in synapse elimination. Between these receptors there are several synergistic, antagonic and modulatory relations that clearly affect synapse elimination. Metabotropic receptors converge in a limited repertoire of intracellular effector kinases, particularly serine protein kinases A and C (PKA and PKC), to phosphorylate protein targets and bring about structural and functional changes leading to axon loss. In most cells A_1, M_1 and TrkB operate mainly by stimulating PKC whereas A_{2A}, M_2 and M_4 inhibit PKA. We hypothesize that a membrane receptor-induced shifting in the protein kinases A and C activity (inhibition of PKA and/or stimulation of PKC) in some nerve endings may play an important role in promoting developmental synapse elimination at the neuromuscular junction (NMJ). This hypothesis is supported by: (i) the tonic effect (shown by using selective inhibitors) of several membrane receptors that accelerates axon loss between postnatal days P5–P9; (ii) the synergistic, antagonic and modulatory effects (shown by paired inhibition) of the receptors on axonal loss; (iii) the fact that

OPEN ACCESS

Edited by:
Chen Zhang,
Peking University, China

Reviewed by:
Weiwen Wang,
Institute of Psychology (CAS), China
Chuang Wang,
Ningbo University, China

***Correspondence:**
Josep M. Tomàs
josepmaria.tomas@urv.cat
Neus Garcia
mariadelesneus.garcia@urv.cat

†These authors have contributed equally to this work.

Received: *04 May 2017*
Accepted: *27 July 2017*
Published: *09 August 2017*

Citation:
Tomàs JM, Garcia N, Lanuza MA, Nadal L, Tomàs M, Hurtado E, Simó A and Cilleros V (2017) Membrane Receptor-Induced Changes of the Protein Kinases A and C Activity May Play a Leading Role in Promoting Developmental Synapse Elimination at the Neuromuscular Junction. Front. Mol. Neurosci. 10:255. doi: 10.3389/fnmol.2017.00255

Abbreviations: AC, adenyl cyclase; ACh, acetylcholine; AR, adenosine receptors; A_1adenosine receptor; A_{2A}adenosine receptor; βIV_{5-3}, translocation inhibitor peptide, beta I βIV_{5-3}; CaC, calphostin C; Ca_v, voltage-gated calcium; cPKCα, alpha protein kinase C isoform; cPKCβI, beta I protein kinase C isoform; DPCPX, 8-Cyclopentyl-1,3-IP3, inositol triphosphate; IP3, inositol triphosphate; LAL, Levator auris longus muscle; M_1, M_1-type muscarinic acetylcholine receptor; M_2, M_2-type muscarinic acetylcholine receptor; M_4, M_4-type muscarinic acetylcholine receptor; mAChR, muscarinic acetylcholine receptor; MET, methoctramine; nAChR, nicotinic acetylcholine receptor; nAChRδ, delta nicotinic acetylcholine receptor subunit; nAChRε, epsilon nicotinic acetylcholine receptor subunit; NMJ, neuromuscular junction; nPKCε, epsilon protein kinase C isoform; nPKCθ, theta protein kinase C isoform; NTR, neurotrophin receptor; OXO, oxotremorine; PIR, pirenzepine; PKA, protein kinase A; PKC, protein kinase C; PLC, phospholipase C; SCH58261, 2-(2-Furanyl)-7-(2-phenylethyl)-7*H*-pyrazolo[4,3-*e*][1,2,4]triazolo[1,5-*c*]pyrimidin-5-amine; TrkB, tropomyosin-related kinase B receptor; TrkB-Fc, inhibitor recombinant human TrkB-Fc Chimera.

the coupling of these receptors activates/inhibits the intracellular serine kinases; and (iv) the increase of the PKA activity, the reduction of the PKC activity or, in most cases, both situations simultaneously that presumably occurs in all the situations of singly and paired inhibition of the mAChR, AR and TrkB receptors. The use of transgenic animals and various combinations of selective and specific PKA and PKC inhibitors could help to elucidate the role of these kinases in synapse maturation.

Keywords: motor end-plate, postnatal synapse elimination, acetylcholine release, muscarinic acetylcholine receptors, adenosine receptors, neurotrophins, PKC, PKA

DEVELOPMENTAL AXONAL LOSS AND SYNAPSE ELIMINATION

When the nervous system develops, the neurons and synapses involved in circuitry wiring and connectivity are overproduced. However, Hebbian competition between nerve processes and endings eliminates redundant synapses and refines the specificity of the functional circuits (Purves and Lichtman, 1980; Jansen and Fladby, 1990; Sanes and Lichtman, 1999). Synapses are lost throughout the nervous system during histogenesis (Bourgeois and Rakic, 1993). In the visual system, thalamocortical axons disconnect from cortical layer IV cells (Hubel et al., 1977; Huberman, 2007), in the cerebellum, climbing fibers disconnect from Purkinje cells (Daniel et al., 1992; Hashimoto and Kano, 2005) and in autonomic ganglia, preganglionic inputs disconnect from ganglion cells (Lichtman, 1997). Developmental axonal loss also occurs in neuromuscular junction (NMJ), the paradigmatic model of neuroscience. Most axonal elimination occurs during the first 2 weeks after birth. At birth, the NMJs are initially polyinnervated but, by the end of the axonal competition, the motor endplates are innervated by a solitary axon (Benoit and Changeux, 1975; O'Brien et al., 1978; Liu et al., 1994; Ribchester and Barry, 1994; Nguyen and Lichtman, 1996; Chang and Balice-Gordon, 1997; Sanes and Lichtman, 1999; Herrera and Zeng, 2003; Nelson et al., 2003; Wyatt and Balice-Gordon, 2003; Buffelli et al., 2004; **Figure 1**).

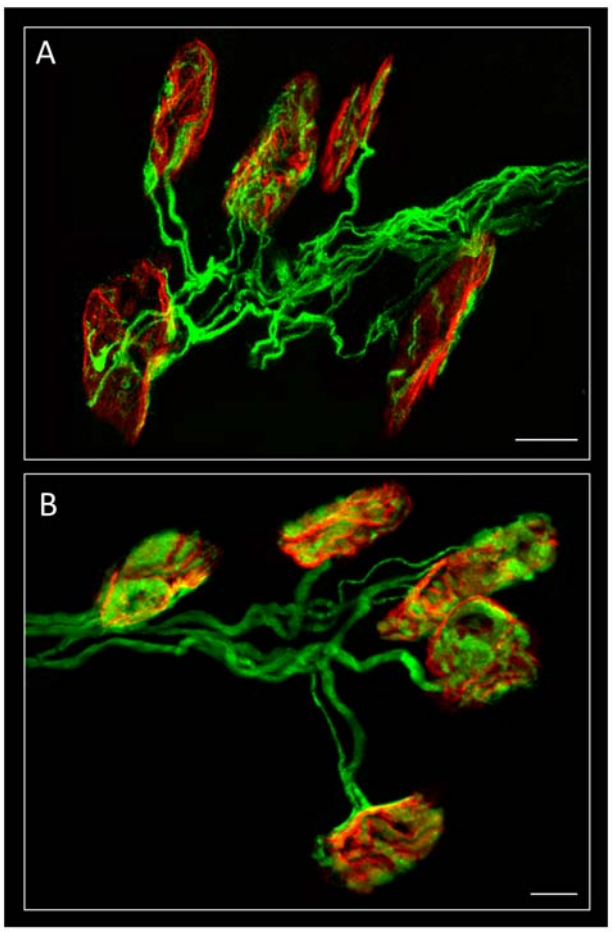

FIGURE 1 | Confocal immunofluorescence. The image shows mono-innervated and polyinnervated synapses from C57BL/6J P7 **(A)** and YFP **(B)** control mice. The Levator auris longus muscle (LAL) neuromuscular junctions (NMJs) (in **A**) show the axons stained green by 200-kD neurofilament antibody and the postsynaptic nicotinic acetylcholine receptors (nAChR) clusters (both in **A,B**) stained red by TRITC-α-BTX. Scale bar: 10 μm. Image **(A)** has been adapted from Figure 1 in the original article (Tomàs et al., 2017). The original article is an open access article distributed under the terms of the Creative Commons Attribution License (http://creativecommons.org/licenses/by/2.0), which permits unrestricted use, distribution and reproduction in any medium, provided the original work is properly cited.

MEMBRANE RECEPTORS IN AXONAL LOSS

Membrane receptor signaling can play a role in axonal competition by allowing the various nerve endings to have an activity-dependent influence on one another directly or with the involvement of the postsynaptic cell and the associated glial cell/s (Keller-Peck et al., 2001; Tomàs et al., 2014). We observed that presynaptic muscarinic acetylcholine receptors (mAChR; subtypes M_1, M_2 and M_4), adenosine receptors (AR; A_1 and A_{2A}) and the neurotrophin receptor (NTR) tropomyosin-related kinase B receptor (TrkB) all cooperate in the developmental synapse elimination process at this synapse [NMJ from the *Levator auris longus*—LAL—muscle of the B6.Cg-Tg (Thy1-YFP)16 Jrs/J mice (hereinafter YFP mice), and from C57BL/6J P7 mice] by favoring axonal competition and loss (Nadal et al., 2016a,b, 2017; Tomàs et al., 2017). Other receptors, for example glutamate receptors at the mice NMJ (Waerhaug and Ottersen, 1993) may collaborate because developmental synapse loss is slowed by reducing activation of the glutamate-NMDA receptor pathway (Personius et al., 2016).

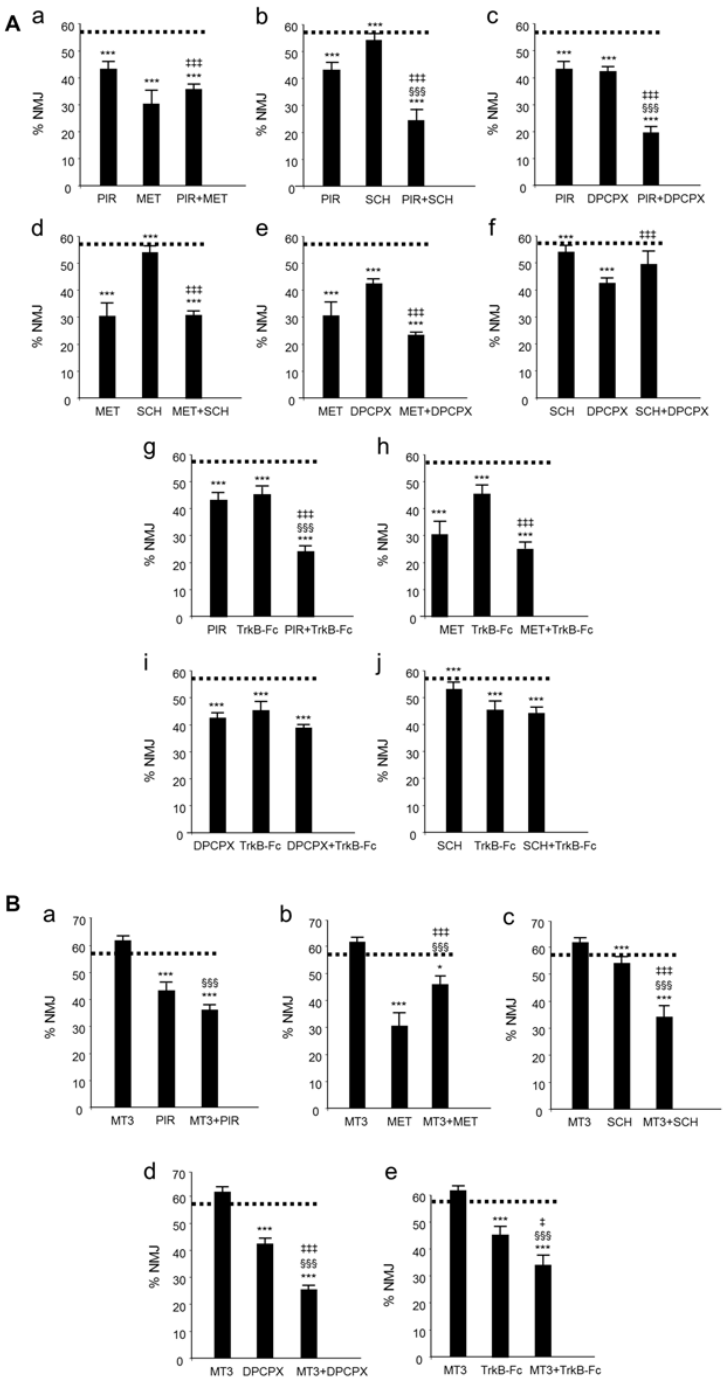

FIGURE 2 | Changes in polyneuronal innervation of the NMJ after inhibiting the muscarinic ACh autoreceptors (mAChR), adenosine receptors (AR) and the tropomyosin-related kinase B receptor (TrkB) signaling in the YFP mice. **(Aa–j)** shows the percentage of monoinnervated NMJs in controls (PBS, dotted lines) and after exposure (four applications, one application every day after P5) to one inhibitor or after simultaneous inhibition of two receptors that individually affect axon loss (all inhibitors but MT3). The associations of MT3 with the other substances are represented in **(Ba–e)**. The symbols indicate: $^{*}P < 0.05$, $^{***}P < 0.005$ when the corresponding antagonist or combinations of two substances are compared with control PBS. $^{§§§}P < 0.005$ when the combination of two substances is compared with the first substance. $^{‡}P < 0.05$, $^{‡‡‡}P < 0.005$ when the combination of two substances is compared with the second. The selective inhibitors are: methoctramine (MET), M_2 inhibitor; pirenzepine (PIR), M_1 inhibitor; 8-Cyclopentyl-1,3-IP3, inositol triphosphate (DPCPX), A_1 inhibitor; SCH58261, A_{2A} inhibitor and inhibitor recombinant human TrkB-Fc Chimera (TrkB-Fc), TrkB inhibitor: this figure has been adapted and redrawn from Figures 3,4 in the original article by Nadal et al. (2016a). The original article is an open access article distributed under the terms of the Creative Commons Attribution License (http://creativecommons.org/licenses/by/2.0), which permits unrestricted use, distribution and reproduction in any medium, provided the original work is properly cited. The paired inhibition data of the AR and TrkB shown in the histograms i and j have not been previously published.

We have used the term cooperation above to define the collaboration between mAChR, AR and TrkB receptor pathways in controlling axonal loss. Cooperation requires the receptors to work together: (i) additively or synergistically; or (ii) occlusively or antagonically. We simultaneously applied two inhibitors (two selective antagonists from two different receptors) to reveal the possible additive or occlusive crosstalk effects between the corresponding pathways. The histograms in **Figure 2** show the individual and the paired effects of these inhibitors on axonal loss at P9 (percentage of the monoinnervated synapses after exposure to blockers (data drawn from previous studies: Nadal et al., 2016a,b, 2017; Tomàs et al., 2017). The paired inhibition data of the AR and TrkB shown in histograms i and j from **Figure 2A** have not been previously published).

SYNERGISTIC AND ANTAGONIC EFFECTS OF THE mAChR, AR AND TrkB THAT AFFECT DEVELOPMENTAL SYNAPSE ELIMINATION

The receptors (**Figure 2A**) with the exception of the M_4 subtype (**Figure 2B**), directly accelerate axon loss at P9 (when selectively blocked between P5 and P8, axonal elimination is reduced and this shows their tonic effect in normal conditions). All diagrams in **Figure 3** (taken from previous articles, except some unpublished data in **Figure 3D**, see below; Nadal et al., 2016b, 2017), show the effect of the selective inhibitors in order of their ability to finally delay monoinnervation and keep a high percentage of synapses innervated by two or more axons (methoctramine (MET), M_2 inhibitor; PIR, M_1 inhibitor; 8-Cyclopentyl-1,3-IP3, inositol triphosphate (DPCPX), A_1 inhibitor; SCH58261, A_{2A} inhibitor; inhibitor recombinant human TrkB-Fc Chimera (TrkB-Fc), TrkB inhibitor). The red arrows show approximately how effective the selective blockers are at delaying axonal elimination (the thicker they are, the greater their effect, although their absolute pharmacological potency cannot be directly compared). In this case, only the M_4 blocker MT3 is unable to significantly change the percentage of monoinnervation (see the data in **Figure 2B**), which shows that there is no direct effect of M_4 on axonal loss at this time (black arrow in **Figures 3A–D**).

Diagrams also show the cooperation links between the receptors as judging by the effect of the corresponding paired inhibitors exposition (gray circles mean there is no change, green circles mean there is a synergistic effect and red circles mean there is an antagonic effect).

Synergistic Role of the M_1 Subtype

Figure 3A shows the synergistic role of the M_1 mAChR, which potentiates the effect of both AR (A_1, 58% and A_{2A} 36%) and TrkB (25%) on axonal elimination. Only a small antagonic effect is observed on the potent M_2 function and in this case the final effect is no different from the individual M_1 effect on axon loss.

Modulatory Role of the M_4 Subtype

This receptor is not directly involved in axonal loss. **Figure 3B** shows, however, that it strongly potentiates the effect of AR (A_1, 33% and A_{2A} 32%) and TrkB (23%) and also slightly inhibits the potent M_2 effect. In fact, although M_4 does not act directly

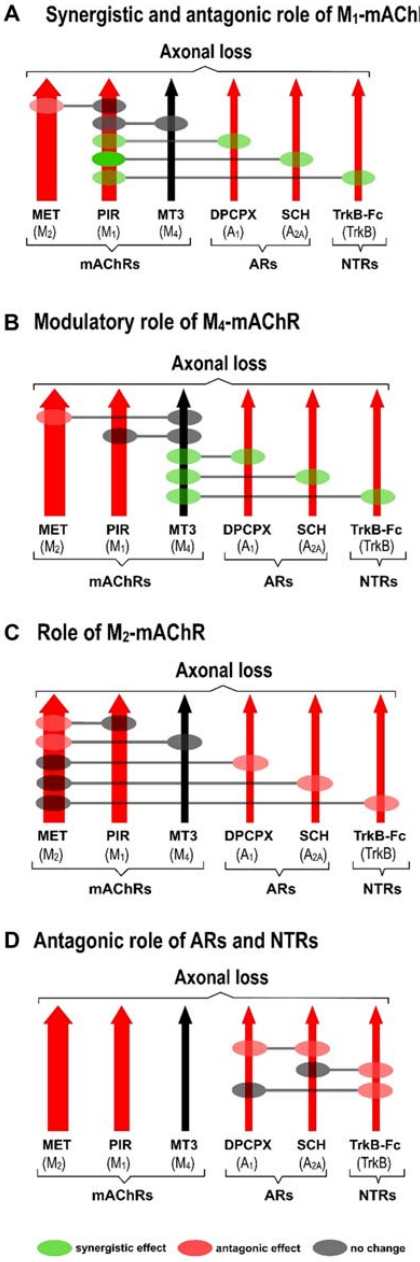

FIGURE 3 | Cooperation between mAChR, AR and TrkB receptors. All diagrams **(A–D**; redrawn from previous work, except some unpublished data in diagram **(D)**, Nadal et al., 2016b, 2017), show the effect of the selective inhibitors in order of their ability to finally delay monoinnervation and keep a high percentage of synapses innervated by two or more axons (MET, M_2 inhibitor; PIR, M_1 inhibitor; DPCPX, A_1 inhibitor; SCH58261, A_{2A} inhibitor; TrkB-Fc, TrkB inhibitor). The red arrows show how effective the blockers are at delaying elimination (the thicker they are, the greater their effect). Only the M_4 blocker MT3 is unable to change axonal loss (black arrow in the figures). Diagrams show the cooperation links between the receptors as judging by the effect of the corresponding paired inhibition (gray circles mean there is no change, green circles mean there is a synergistic effect and red circles mean there is an antagonic effect between the receptors).

by itself, its regulatory functions are similar to those of the M_1 subtype. Therefore, M_4 has a modulatory function. We think that though insufficient to promote an effect by itself, the M4 pathway may realize some priming action on the other pathways to facilitate them (the AR and the TrkB pathways) or to obstruct them (the M2 pathway).

Role of M_2 Subtype

M_2 has a powerful effect on axon loss and only the other mAChRs, M_1 and M_4, can slightly reduce its potency (**Figure 3C**).

Antagonic Effects between AR and TrkB

Figure 3D shows that when the inhibitor recombinant human TrkB-Fc Chimera (TrkB-Fc) is associated with one of the AR inhibitors DPCPX or SCH58261, the effect is just the same as the individual effect of one of them on axon loss (in the graph, we have chosen to represent the position of the red circles only on the TrkB pathway for purposes of simplicity. These data have not been previously published). When both AR are blocked simultaneously, occlusion is complete and the final result is no different from that of the untreated control.

Thus, several synergistic, antagonic and modulatory relations are clearly observed between the receptors, which affect synapse elimination.

SERINE KINASES IN AXONAL LOSS

Metabotropic membrane receptors converge in a limited repertoire of intracellular effector kinases (mainly serine protein kinases A and C [PKA and PKC]) to phosphorylate protein targets and bring about structural and functional changes that lead to axon loss. The nerve endings that lose the competitive process progressively weaken by diminishing the quantal content of the evoked ACh release in parallel with the progressive loss of nicotinic acetylcholine receptors (nAChR) from the postsynaptic muscle cell (Caulfield, 1993; Felder, 1995; Caulfield and Birdsall, 1998; Nathanson, 2000; Lanuza et al., 2001, 2002; Santafé et al., 2004; Garcia et al., 2010; Tomàs et al., 2014). Receptors and kinases may regulate coordinately these changes.

In the postsynaptic component, the phosphorylation of the nAChR delta and epsilon (delta nicotinic acetylcholine receptor subunit (nAChRδ) and epsilon nicotinic acetylcholine receptor subunit (nAChRε)) subunits may help the nAChR cluster to mature, which may also affect synapse loss during postnatal development. nPKCθ produces nAChR instability and loss by phosphorylating the delta subunit, while PKA reverses this effect and increases receptor stability by phosphorylating the epsilon subunit. Moreover, PKA and PKC may phosphorylate differently the nAChR in the different axon terminals (with different activity) that are in competition in the same synaptic site. PKC-induced dispersion under the weakest nerve terminals and a PKA-induced catching and stabilization under the more active axon terminals results in the differentiation of the postsynaptic gutters (Nelson et al., 2003; Lanuza et al., 2006, 2010, 2014). Also, protein phosphorylation is an important posttranslational modification of group I metabotropic glutamate receptors. Evidences indicate that PKA and PKC directly interact with mGluR1/5, phosphorylate specific serine or threonine sites and thereby regulate trafficking, distribution, and function of phosphorylated receptors (Mao and Wang, 2016).

In the presynaptic component, intracellular serine kinases, both PKA and PKC in the nerve terminals, could be directly involved in modulating calcium-dependent ACh release at the NMJ (Santafé et al., 2006, 2007a,b, 2009b; Tomàs et al., 2011). Specifically, PKC [alpha protein kinase C isoform (cPKCα), beta I protein kinase C isoform (cPKCβI) and epsilon protein kinase C isoform (nPKCε) isoforms are the candidates (Besalduch et al., 2010; Lanuza et al., 2010; Obis et al., 2015)] is able to reduce the ACh release capacity of the weak axons in developing polyinnervated synapses (Santafé et al., 2003, 2004, 2007b, 2009a,b; Tomàs et al., 2011). This effect on transmitter release may also be related with axonal loss because the competitive force of these nerve endings decreases.

In other molecular mechanisms PKA and PKC can phosphorylate the same molecule in different residues. For instance, SNAP25 is phosphorylated by PKA (in T138) and PKC (in S187) whereas Munc18 is only phosphorylated by PKC in the modulation steps of the ACh release (Leenders and Sheng, 2005).

However, not always PKA and PKC cooperate in phosphorylating the same molecule or different subunits of the same complex. There are molecules and coupled functions modulated only by PKA. It seems that only PKA is involved in the desensitization induced by 5-HT in rat serotonergic neurons (Yao et al., 2010). Other molecules are modulated only by PKC. Spinal sigma-1 receptor-induced mechanical and thermal hypersensitivity are mediated by an increase in NO-induced PKC-dependent but PKA-independent expression of the spinal NMDA receptor GluN1 subunit (Roh et al., 2011). PKC isozymes modulate voltage-gated calcium (Ca_v) currents through $Ca_v2.2$ and $Ca_v2.3$ channels by targeting serine/threonine (Ser/Thr) phosphorylation sites of $Ca_v\alpha_1$ subunits. Stimulatory (Thr-422, Ser-2108 and Ser-2132) and inhibitory (Ser-425) sites were identified in the $Ca_v2.2\alpha_1$ subunits to PKCs βII and ε. Net PKC effect may be the difference between the responses of the stimulatory and inhibitory sites (Rajagopal et al., 2017).

MEMBRANE RECEPTORS AND SERINE KINASES

In most cells A_1, M_1 and TrkB operate mainly by stimulating the phospholipase C gamma (PLCγ) and, therefore, the PKC pathways and the inositol triphosphate (IP3) pathway, whereas A_{2A}, M_2 and M_4 inhibit the adenyl cyclase (AC) and PKA pathway (Caulfield, 1993; Felder, 1995; Marala and Mustafa, 1995; Caulfield and Birdsall, 1998; Nathanson, 2000; De Lorenzo et al., 2004; Nishizaki, 2004; Oliveira and Correia-de-Sá, 2005).

In considering the synergistic, antagonic and modulatory effects of the receptors on axonal loss (**Figures 2**, **3**), we believe that an inhibition of PKA and/or stimulation of PKC in some nerve endings may play a leading role in promoting synapse elimination. Therefore, the left-hand side of **Figure 4** shows how the individual use of selective inhibitors changes PKA

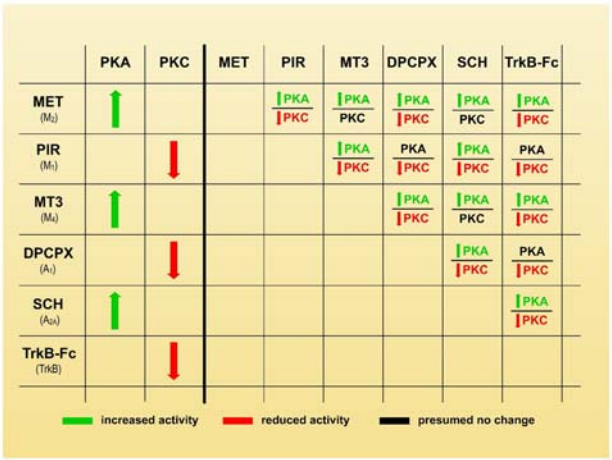

FIGURE 4 | Membrane receptors and serine kinases. The left-hand side of the figure shows how the individual use of selective inhibitors changes protein kinase A (PKA) and protein kinase C (PKC) activity (green arrows mean stimulation, red arrows mean inhibition). The right-hand side of the figure shows that when two blockers are associated, PKA activity generally increases (green characters) or is unaffected in the cases of PIR-DPCPX, PIR-TrkB and DPCPX-TrkB associations (black characters). However, PKC activity is generally reduced (red characters) or unaffected in MET-MT3, MET-SCH58261 and MT3-SCH58261 dual inhibition (black characters also). Therefore, a higher PKA/PKC ratio can be produced by selective inhibitors and this coincide with a delay in axonal loss.

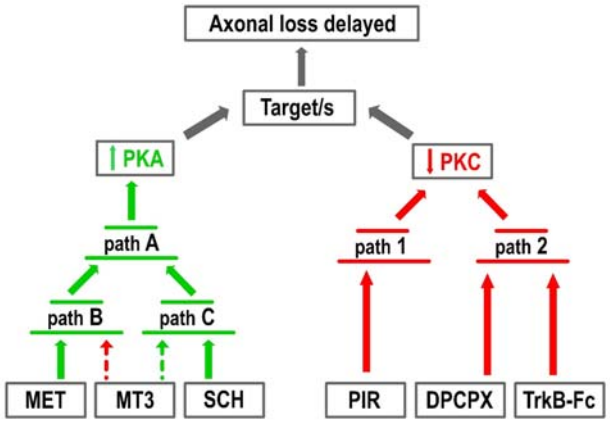

FIGURE 5 | Pathways resulting in increased PKA and decreased PKC activity. The figure represents the two groups of receptor inhibitors: those that reduce PKC activity (right-hand side of the figure, red arrows) and those that increase PKA activity (left-hand side, green arrows). In terms of PKC, the effect of PIR is synergistic with the DPCPX and the TrkB-Fc effects although these last two substances are mutually occlusive. This suggests that PKC activity can be reduced by two parallel pathways (paths 1 and 2). In terms of PKA, the effects of MET and SCH58261 seem to converge on the final path A through the respective paths B and C, which cannot be summed even though they are in turn respectively modulated negatively (dotted red arrow) and positively (dotted green arrow) by MT3.

and PKC activity in many cells (Caulfield, 1993; Felder, 1995; Calabresi et al., 1998; Caulfield and Birdsall, 1998; Nathanson, 2000; Santafé et al., 2006, 2007a; Salgado et al., 2007; Ansari et al., 2009; Tomàs et al., 2011; Rodrigues et al., 2014; Hughes et al., 2015; Obis et al., 2015). Theoretically, when two inhibitors are associated (right side of the **Figure 4**), PKA activity is generally increased (or unaffected in the cases of PIR-DPCPX, PIR-TrkB and DPCPX-TrkB associations, black characters). However, PKC activity is generally reduced (or unaffected in MET-MT3, MET-SCH58261 and MT3-SCH58261 dual inhibition, black characters). Therefore, the selective inhibitors would give a higher PKA/PKC ratio and delay axonal loss, which means that, in normal conditions without inhibitors, all the considered receptor pathways join together to give a lower PKA/PKC ratio and accelerate axonal loss.

However, although PKA and PKC are involved in synapse elimination, and changes in their respective activity seems relevant, a specific decrease of the PKA/PKC activity ratio would be not the best manner to describe their complementary role. Therefore, we hypothesize that "a membrane receptor-induced shifting in the PKA and PKC activity (inhibition of PKA and/or stimulation of PKC) in some nerve endings may play an important role in promoting developmental synapse elimination at the NMJ".

In addition, the use of inhibitors show only the tonic effect of the molecule that is inhibited in basal conditions but the supposition that without the presence of the inhibitor the molecule play in all cases this tonic effect is a further deduction that will be considered as forming part of the hypothesis and analyzed with caution.

Although in 12 out of 15 simultaneous inhibitions with two drugs PKC activity is reduced and remains unchanged in only three (the same numbers applie for PKA activity increase and maintenance respectively, see **Figure 4**), it seems that a higher PKA/PKC ratio is the main factor in the paired receptors signaling inhibition. In this regard, there is no clear difference between the situations in which PKA presumably increases or is unchanged or when PKC decreases or remains unchanged in relation to axonal loss. This means that in paired inhibition conditions (two different receptors are blocked), the presumed relevant fact to influence axon loss seems to be the increase of the PKA activity only, the reduction of the PKC activity only or, in most cases, both situations simultaneously.

For instance, axon loss is also partially occluded between TrkB and both AR pathways (A_1 and A_{2A}) even when PKA would be not affected by blocking TrkB and A_1 and PKA would increase by blocking TrkB and A_{2A}. Also, a strong decrease in PKC while PKA remains stable can result in a synergistic effect of the inhibitors (PIR and DPCPX) or in an occlusion between them (DPCPX and TrkB). Therefore, the increase in the PKA/PKC ratio is the parameter that seems to change after all the direct and crossed inhibitions of the mAChR, AR and TrkB had been checked.

Figure 5 shows the two groups of receptor inhibitors separately: those that reduce PKC activity (right-hand side of the figure) and those that increase PKA activity (left-hand side). In terms of PKC, the effect of PIR is synergistic and can be added to the DPCPX and the TrkB-Fc effects although these last two substances are mutually occlusive. This suggests that PKC activity can be reduced by two parallel pathways (path 1 and 2 in the figure). Paths 1 and 2 can be summed but the pathways

converging on path 2 cannot. In terms of PKA, the effects of MET and SCH58261 seem to converge on the final path A through their respective paths B and C, which cannot be summed even though they are in turn respectively modulated negatively and positively by MT3. Interestingly, a reduction in PKC (PIR) and an increase in PKA (SCH58261) can have a synergistic effect (**Figure 2Ab**). However, there is only one situation in which the inhibitors DPCPX (PKC reduction) and SCH58261 (PKA increase) fully antagonize each other (**Figure 2Af**). This suggests that, downstream of the AR, there is a common link that is inversely regulated by the two subtypes.

Therefore, in basal conditions, a reduction in PKA activity, an increase in PKC activity or, in most cases, both situations simultaneously, would accelerate synapse elimination.

There are many molecular targets of the membrane receptors-kinases phosphorylation pathways involved in transmitter release and nerve terminal stability. Their analysis is out of the scope here. However, during developmental axonal competition and loss, the nerve endings achieve differences in ACh release capacity and in the functional expression of several related molecules. Specifically, in the weakest endings (those that evoke small synaptic potentials) in polyinnervated NMJ, M_1 receptors reduce release through the PKC pathway due to an excess of Ca^{2+} inflow through P-, N- and L-type calcium channels (L channel is only present in the weak endings). However, in the strongest and mature endings, the coupling of M_1 to PKC activity results in ACh release potentiation using Ca^{2+} inflow through the P-channel. The PKA-linked M_2 subtype is also present in the weakest endings, it is related only to P and N channels to potentiate release (Santafé et al., 2009a; see also Santafé et al., 2003, 2004, 2007a,b, 2009a,b; Tomàs et al., 2011). It is tempting to speculate on the relevance of the PKA and PKC phosphorylation of the Ca^{2+} channels in the differential control of transmitter release during axonal competition and nerve terminal loss.

CONCLUSION AND HYPOTHESIS

We suggest that a membrane receptor-induced shifting in the PKA and PKC activity may play an important role in promoting developmental synapse elimination at the NMJ. This hypothesis is supported by: (i) the tonic effect (shown by using selective inhibitors) of several membrane receptors that accelerates axon loss between P5 and P9; (ii) the synergistic, antagonic and modulatory effects (shown by paired inhibition) of the receptors on axonal loss; (iii) the fact that the coupling of these receptors activates/inhibits the intracellular serine kinases; and (iv) the increase of the PKA activity, the reduction of the PKC activity or, in most cases, both situations simultaneously that presumably occurs in all the situations of singly and paired inhibition of the mAChR, AR and TrkB receptors.

The use of transgenic animals and various combinations of selective and specific PKA and PKC inhibitors could help to elucidate the role of these kinases in synapse maturation.

Transgenic Mice

The transgenic mouse B6.Cg-Tg(Camk2a-Prkaca)426Tabe/J has a 50% reduction in basal cAMP-dependent PKA. Also, we found that nPKCε and cPKCβI isoforms are exclusively located in the motor nerve terminals of the adult rat NMJ and are involved in transmitter release (Besalduch et al., 2010; Lanuza et al., 2010; Obis et al., 2015). Thus, the use of the B6.129S4-*Prkce*^{tm1Msg}/J mouse, homozygous for the *Prkce*^{tm1Msg} which is a nPKCε mutant mouse, may be useful.

Selective and Specific PKA and PKC Modulators

The classic PKA antagonists H-89 and KT-5720 (De Lorenzo et al., 2006; Martinez-Pena y Valenzuela et al., 2013) and the agonist Dibutyryl-cAMP (Nelson et al., 2003) together with the PKC antagonists Calphostin C (CaC) and Go 6976 (Lanuza et al., 2002; Nili et al., 2006) and the PKC agonists phorbol 12-myristate 13-acetate and Bryostatin 1 (Lanuza et al., 2002; Sun and Alkon, 2006; Hage-Sleiman et al., 2015), will be useful tools. More importantly, the use of specific peptides that affect PKC translocation and activity may help us to understand what role these kinases play in axonal loss. For instance, the nPKCε-specific translocation inhibitor peptide, epsilon V1–2 (εV_{1-2}; [Brandman et al., 2007; Obis et al., 2015]), the specific agonist peptide εV_{1-7} (Johnson et al., 1996), and the cPKCβI-specific translocation inhibitor peptide, betaI V5–3 (βIV_{5-3}; Liu et al., 1999) together with the specific cPKCβI agonist dPPA (Rigor et al., 2010) will be helpful.

Exposure of these substances on the LAL surface during the synapse elimination period and counting the axons could be a simple and productive procedure (Nadal et al., 2016a,b, 2017).

ETHICS APPROVAL

The mice were cared for in accordance with the guidelines of the European Community's Council Directive of 24 November 1986 (86/609/EEC) for the humane treatment of laboratory animals. All experiments on animals have been reviewed and approved by the Animal Research Committee of the Universitat Rovira i Virgili (Reference number: 0233).

AUTHOR CONTRIBUTIONS

LN, EH, AS, VC and MT: data collection, quantitative analysis; literature search, data interpretation and graphic design; NG and MAL: statistics; JMT, NG and MAL: conception and design, literature search, data interpretation and manuscript preparation.

ACKNOWLEDGMENTS

This work was supported by a grant from the Catalan Government (2014SGR344) and a grant from MINECO (SAF2015-67143-P). We thank the reviewers for their careful reading of our manuscript and their many insightful comments.

REFERENCES

Ansari, H. R., Teng, B., Nadeem, A., Roush, K. P., Martin, K. H., Schnermann, J., et al. (2009). A_1 adenosine receptor-mediated PKC and p42/p44 MAPK signaling in mouse coronary artery smooth muscle cells. *Am. J. Physiol. Heart Circ. Physiol.* 297, H1032–H1039. doi: 10.1152/ajpheart.00374.2009

Brandman, R., Disatnik, M. H., Churchill, E., and Mochly-Rosen, D. (2007). Peptides derived from the C2 domain of protein kinase C epsilon (epsilon PKC) modulate epsilon PKC activity and identify potential protein-protein interaction surfaces. *J. Biol. Chem.* 282, 4113–4123. doi: 10.1074/jbc.M608521200

Benoit, P., and Changeux, J. P. (1975). Consequences of tenotomy on the evolution of multiinnervation in developing rat soleus muscle. *Brain Res.* 99, 354–358. doi: 10.1016/0006-8993(75)90036-0

Besalduch, N., Tomàs, M., Santafé, M. M., Garcia, N., Tomàs, J., and Lanuza, M. A. (2010). Synaptic activity-related classical protein kinase C isoform localization in the adult rat neuromuscular synapse. *J. Comp. Neurol.* 518, 211–228. doi: 10.1002/cne.22220

Bourgeois, J. P., and Rakic, P. (1993). Changes of synaptic density in the primary visual cortex of the macaque monkey from fetal to adult stage. *J. Neurosci.* 13, 2801–2820.

Buffelli, M., Busetto, G., Bidoia, C., Favero, M., and Cangiano, A. (2004). Activity dependent synaptic competition at mammalian neuromuscular junctions. *News Physiol. Sci.* 19, 85–91. doi: 10.1152/nips.01464.2003

Calabresi, P., Centonze, D., Gubellini, P., Pisani, A., and Bernardi, G. (1998). Endogenous ACh enhances striatal NMDA-responses via M1-like muscarinic receptors and PKC activation. *Eur. J. Neurosci.* 10, 2887–2895. doi: 10.1111/j.1460-9568.1998.00294.x

Caulfield, M. P. (1993). Muscarinic receptors—characterization, coupling and function. *Pharmacol. Ther.* 58, 319–379. doi: 10.1016/0163-7258(93)90027-b

Caulfield, M. P., and Birdsall, N. J. (1998). International Union of Pharmacology. XVII. Classification of muscarinic acetylcholine receptors. *Pharmacol. Rev.* 50, 279–290.

Chang, Q., and Balice-Gordon, R. J. (1997). Nip and tuck at the neuromuscular junction: a role for proteases in developmental synapse elimination. *Bioessays* 19, 271–275. doi: 10.1002/bies.950190402

Daniel, H., Hemart, N., Jaillard, D., and Crepel, F. (1992). Coactivation of metabotropic glutamate receptors and of voltage-gated calcium channels induces long-term depression in cerebellar Purkinje cells *in vitro*. *Exp. Brain Res.* 90, 327–331. doi: 10.1007/bf00227245

De Lorenzo, S., Veggetti, M., Muchnik, S., and Losavio, A. (2004). Presynaptic inhibition of spontaneous acetylcholine release induced by adenosine at the mouse neuromuscular junction. *Br. J. Pharmacol.* 142, 113–124. doi: 10.1038/sj.bjp.0705656

De Lorenzo, S., Veggetti, M., Muchnik, S., and Losavio, A. (2006). Presynaptic inhibition of spontaneous acetylcholine release mediated by P2Y receptors at the mouse neuromuscular junction. *Neuroscience* 142, 71–85. doi: 10.1016/j.neuroscience.2006.05.062

Felder, C. C. (1995). Muscarinic acetylcholine receptors: signal transduction through multiple effectors. *FASEB J.* 9, 619–625.

Garcia, N., Tomàs, M., Santafé, M. M., Besalduch, N., Lanuza, M. A., and Tomàs, J. (2010). The interaction between tropomyosin-related kinase B receptors and presynaptic muscarinic receptors modulates transmitter release in adult rodent motor nerve terminals. *J. Neurosci.* 30, 16514–16522. doi: 10.1523/JNEUROSCI.2676-10.2010

Hage-Sleiman, R., Hamze, A. B., Reslan, L., Kobeissy, H., and Dbaibo, H. (2015). The novel PKCθ from benchtop to clinic. *J. Immunol. Res.* 2015:348798. doi: 10.1155/2015/348798

Hashimoto, K., and Kano, M. (2005). Postnatal development and synapse elimination of climbing fiber to Purkinje cell projection in the cerebellum. *Neurosci. Res.* 53, 221–228. doi: 10.1016/j.neures.2005.07.007

Herrera, A. A., and Zeng, Y. (2003). Activity-dependent switch from synapse formation to synapse elimination during development of neuromuscular junctions. *J. Neurocytol.* 32, 817–833. doi: 10.1023/b:neur.0000020626.29900.fb

Hubel, D. H., Wiesel, T. N., and LeVay, S. (1977). Plasticity of ocular dominance columns in monkey striate cortex. *Philos. Trans. R. Soc. Lond. B Biol. Sci.* 278, 377–409. doi: 10.1098/rstb.1977.0050

Huberman, A. D. (2007). Mechanisms of eye-specific visual circuit development. *Curr. Opin. Neurobiol.* 17, 73–80. doi: 10.1016/j.conb.2007.01.005

Hughes, S. J., Cravetchi, X., Vilas, G., and Hammond, J. R. (2015). Adenosine A1 receptor activation modulates human equilibrative nucleoside transporter 1 (hENT1) activity via PKC-mediated phosphorylation of serine-281. *Cell Signal.* 27, 1008–1018. doi: 10.1016/j.cellsig.2015.02.023

Johnson, J. A., Gray, M. O., Chen, C. H., and Mochly-Rosen, D. A. (1996). Protein kinase C translocation inhibitor as an isozyme-selective antagonist of cardiac function. *J. Biol. Chem.* 271, 24962–24966. doi: 10.1074/jbc.271.40.24962

Jansen, J. K., and Fladby, T. (1990). The perinatal reorganization of the innervation of skeletal muscle in mammals. *Prog. Neurobiol.* 34, 39–90. doi: 10.1016/0301-0082(90)90025-c

Keller-Peck, C. R., Feng, G., Sanes, J. R., Yan, Q., Lichtman, J. W., and Snider, W. D. (2001). Glial cell line-derived neurotrophic factor administration in postnatal life results in motor unit enlargement and continuous synaptic remodeling at the neuromuscular junction. *J. Neurosci.* 21, 6136–6146.

Lanuza, M. A., Besalduch, N., González, C., Santafé, M. M., Garcia, N., Tomàs, M., et al. (2010). Decreased phosphorylation of δ and ε subunits of the acetylcholine receptor coincides with delayed postsynaptic maturation in PKC θ deficient mouse. *Exp. Neurol.* 225, 183–195. doi: 10.1016/j.expneurol.2010.06.014

Lanuza, M. A., Garcia, N., Santafé, M., González, C. M., Alonso, I., Nelson, P. G., et al. (2002). Pre- and postsynaptic maturation of the neuromuscular junction during neonatal synapse elimination depends on protein kinase C. *J. Neurosci. Res.* 67, 607–617. doi: 10.1002/jnr.10122

Lanuza, M. A., Garcia, N., Santafé, M., Nelson, P. G., Fenoll-Brunet, M. R., and Tomàs, J. (2001). Pertussis toxin-sensitive G-protein and protein kinase C activity are involved in normal synapse elimination in the neonatal rat muscle. *J. Neurosci. Res.* 63, 330–340. doi: 10.1002/1097-4547(20010215)63:4<330::aid-jnr1027>3.0.co;2-w

Lanuza, M. A., Gizaw, R., Viloria, A., González, C. M., Besalduch, N., Dunlap, V., et al. (2006). Phosphorylation of the nicotinic acetylcholine receptor in myotube-cholinergic neuron cocultures. *J. Neurosci. Res.* 83, 1407–1414. doi: 10.1002/jnr.20848

Lanuza, M. A., Santafe, M. M., Garcia, N., Besalduch, N., Tomàs, M., Obis, T., et al. (2014). Protein kinase C isoforms at the neuromuscular junction: localization and specific roles in neurotransmission and development. *J. Anat.* 224, 61–73. doi: 10.1111/joa.12106

Leenders, A. G. M., and Sheng, Z. H. (2005). Modulation of neurotransmitter release by the second messenger activated protein kinases: implications for presynaptic plasticity. *Pharmacol. Ther.* 105, 69–84. doi: 10.1016/j.pharmthera.2004.10.012

Lichtman, J. W. (1997). The reorganization of synaptic connexions in the rat submandibular ganglion during post-natal development. *J. Physiol.* 273, 155–177. doi: 10.1113/jphysiol.1977.sp012087

Liu, Y., Fields, R. D., Festoff, B. W., and Nelson, P. G. (1994). Proteolytic action of thrombin is required for electrical activity-dependent synapse reduction. *Proc. Natl. Acad. Sci. U S A* 91, 10300–10304. doi: 10.1073/pnas.91.22.10300

Liu, Y., Liu, Y. C., Meller, N., Giampa, L., Elly, C., Doyle, M., et al. (1999). Protein kinase C activation inhibits tyrosine phosphorylation of Cbl and its recruitment of Src homology 2 domain-containing proteins. *J. Immunol.* 162, 7095–7101.

Mao, L. M., and Wang, Q. (2016). Phosphorylation of group I metabotropic glutamate receptors in drug addiction and translational research. *J. Transl. Neurosci.* 1, 17–23. doi: 10.3868/j.issn.2096-0689.01.002

Marala, R. B., and Mustafa, S. J. (1995). Modulation of protein kinase C by adenosine: involvement of adenosine A_1 receptor-pertussis toxin sensitive nucleotide binding protein system. *Mol. Cell. Biochem.* 149–150, 51–58. doi: 10.1007/978-1-4615-2015-3_6

Martinez-Pena y Valenzuela, I., Pires-Oliveira, M., and Akaaboune, M. (2013). PKC and PKA regulate AChR dynamics at the neuromuscular junction of living mice. *PLoS One* 8:e81311. doi: 10.1371/journal.pone.0081311

Nadal, L., Garcia, N., Hurtado, E., Simó, A., Tomàs, M., Lanuza, M. A., et al. (2016a). Presynaptic muscarinic acetylcholine autoreceptors (M_1, M_2 and M_4 subtypes), adenosine receptors (A_1 and A_{2A}) and tropomyosin-related kinase B receptor (TrkB) modulate the developmental synapse elimination process at the neuromuscular junction. *Mol. Brain* 9:67. doi: 10.1186/s13041-016-0248-9

Nadal, L., Garcia, N., Hurtado, E., Simó, A., Tomàs, M., Lanuza, M. A., et al. (2016b). Synergistic action of presynaptic muscarinic acetylcholine receptors and adenosine receptors in developmental axonal competition at the neuromuscular junction. *Dev. Neurosci.* 38, 407–419. doi: 10.1159/000458437

Nadal, L., Garcia, N., Hurtado, H., Simó, A., Tomàs, M., Lanuza, M. A., et al. (2017). Presynaptic muscarinic acetylcholine receptors and TrkB receptor cooperate in the elimination of redundant motor nerve terminals during development. *Front. Aging Neurosci.* 9:24. doi: 10.3389/fnagi.2017.00024

Nathanson, N. M. (2000). A multiplicity of muscarinic mechanisms: enough signaling pathways to take your breath away. *Proc. Natl. Acad. Sci. U S A* 97, 6245–6247. doi: 10.1073/pnas.97.12.6245

Nelson, P. G., Lanuza, M. A., Jia, M., Li, M. X., and Tomàs, J. (2003). Phosphorylation reactions in activity-dependent synapse modification at the neuromuscular junction during development. *J. Neurocytol.* 32, 803–816. doi: 10.1023/b:neur.0000020625.70284.a6

Nili, U., de Wit, H., Gulyas-Kovacs, A., Toonen, R. F., Sørensen, J. B., Verhage, M., et al. (2006). Munc18–1 phosphorylation by protein kinase C potentiates vesicle pool replenishment in bovine chromaffin cells. *Neuroscience* 143, 487–500. doi: 10.1016/j.neuroscience.2006.08.014

Nishizaki, T. (2004). ATP- and adenosine-mediated signaling in the central nervous system: adenosine stimulates glutamate release from astrocytes via A_{2a} adenosine receptors. *J. Pharmacol. Sci.* 94, 100–102. doi: 10.1254/jphs.94.100

Nguyen, Q. T., and Lichtman, J. W. (1996). Mechanism of synapse disassembly at the developing neuromuscular junction. *Curr. Opin. Neurobiol.* 6, 104–112. doi: 10.1016/s0959-4388(96)80015-8

Obis, T., Besalduch, N., Hurtado, E., Nadal, L., Santafé, M. M., Garcia, N., et al. (2015). The novel protein kinase C epsilon isoform at the adult neuromuscular synapse: location, regulation by synaptic activity-dependent muscle contraction through TrkB signaling and coupling to ACh release. *Mol. Brain* 8:80. doi: 10.1186/s13041-015-0098-x

O'Brien, R. A., Ostberg, A. J., and Vrbová, G. (1978). Observations on the elimination of polyneuronal innervation in developing mammalian skeletal muscle. *J. Physiol.* 282, 571–582. doi: 10.1113/jphysiol.1978.sp012482

Oliveira, L., and Correia-de-Sá, P. (2005). Protein kinase A and Ca_v1 (L-Type) channels are common targets to facilitatory adenosine A_{2A} and muscarinic M_1 receptors on rat motoneurons. *Neurosignals* 14, 262–272. doi: 10.1159/000088642

Personius, K. E., Slusher, B. S., and Udin, S. B. (2016). Neuromuscular NMDA receptors modulate developmental synapse elimination. *J. Neurosci.* 36, 8783–8789. doi: 10.1523/JNEUROSCI.1181-16.2016

Purves, D., and Lichtman, J. W. (1980). Elimination of synapses in the developing nervous system. *Science* 210, 153–157. doi: 10.1126/science.7414326

Rajagopal, S., Burton, B. K., Fields, B. L., El, I. O., and Kamatchi, G. L. (2017). Stimulatory and inhibitory effects of PKC isozymes are mediated by serine/threonine PKC sites of the $Ca_v2.3\alpha_1$ subunits. *Arch. Biochem. Biophys.* 621, 24–30. doi: 10.1016/j.abb.2017.04.002

Ribchester, R. R., and Barry, J. A. (1994). Spatial versus consumptive competition at polyneuronally innervated neuromuscular junctions. *Exp. Physiol.* 79, 465–494. doi: 10.1113/expphysiol.1994.sp003781

Rigor, R. R., Hawkins, B. T., and Miller, D. S. (2010). Activation of PKC isoform β_I at the blood-brain barrier rapidly decreases P-glycoprotein activity and enhances drug delivery to the brain. *J. Cereb. Blood Flow Metab.* 30, 1373–1383. doi: 10.1038/jcbfm.2010.21

Rodrigues, T. M., Jerónimo-Santos, A., Sebastião, A. M., and Diógenes, M. J. (2014). Adenosine A_{2A} receptors as novel upstream regulators of BDNF-mediated attenuation of hippocampal long-term depression (LTD). *Neuropharmacology* 79, 389–398. doi: 10.1016/j.neuropharm.2013.12.010

Roh, D.-H., Choi, S.-R., Yoon, S.-Y., Kang, S.-Y., Moon, J.-Y., Kwon, S.-G., et al. (2011). Spinal neuronal NOS activation mediates sigma-1 receptor-induced mechanical and thermal hypersensitivity in mice: involvement of PKC-dependent GluN1 phosphorylation. *Br. J. Pharmacol.* 163, 1707–1720. doi: 10.1111/j.1476-5381.2011.01316.x

Salgado, H., Bellay, T., Nichols, J. A., Bose, M., Martinolich, L., Perrotti, L., et al. (2007). Muscarinic M_2 and M_1 receptors reduce GABA release by Ca^{2+} channel modulation through activation of PI_3K/Ca^{2+}-independent and PLC/Ca^{2+}-dependent PKC. *J. Neurophysiol.* 98, 952–965. doi: 10.1152/jn.00060.2007

Sanes, J. R., and Lichtman, J. W. (1999). Development of the vertebrate neuromuscular junction. *Annu. Rev. Neurosci.* 22, 389–442. doi: 10.1146/annurev.neuro.22.1.389

Santafé, M. M., Garcia, N., Lanuza, M. A., and Tomàs, J. (2007a). Protein kinase C activity affects neurotransmitter release at polyinnervated neuromuscular synapses. *J. Neurosci. Res.* 85, 1449–1457. doi: 10.1002/jnr.21280

Santafé, M. M., Lanuza, M. A., Garcia, N., Tomàs, M., and Tomàs, J. (2007b). Coupling of presynaptic muscarinic autoreceptors to serine kinases in low and high release conditions on the rat motor nerve terminal. *Neuroscience* 148, 432–440. doi: 10.1016/j.neuroscience.2007.06.017

Santafé, M. M., Garcia, N., Lanuza, M. A., Tomàs, M., Besalduch, N., and Tomàs, J. (2009a). Presynaptic muscarinic receptors, calcium channels and protein kinase C modulate the functional disconnection of weak inputs at polyinnervated neonatal neuromuscular synapses. *J. Neurosci. Res.* 87, 1195–1206. doi: 10.1002/jnr.21934

Santafé, M. M., Garcia, N., Lanuza, M. A., Tomàs, M., and Tomàs, J. (2009b). Interaction between protein kinase C and protein kinase A can modulate transmitter release at the rat neuromuscular synapse. *J. Neurosci. Res.* 87, 683–690. doi: 10.1002/jnr.21885

Santafé, M. M., Salon, I., Garcia, N., Lanuza, M. A., Uchitel, O. D., and Tomàs, J. (2003). Modulation of ACh release by presynaptic muscarinic autoreceptors in the neuromuscular junction of the newborn and adult rat. *Eur. J. Neurosci.* 17, 119–127. doi: 10.1046/j.1460-9568.2003.02428.x

Santafé, M. M., Salon, I., Garcia, N., Lanuza, M. A., Uchitel, O. D., and Tomàs, J. (2004). Muscarinic autoreceptors related with calcium channels in the strong and weak inputs at polyinnervated developing rat neuromuscular junctions. *Neuroscience* 123, 61–73. doi: 10.1016/j.neuroscience.2003.09.012

Santafé, M. M., Lanuza, M. A., Garcia, N., and Tomàs, J. (2006). Muscarinic autoreceptors modulate transmitter release through protein kinase C and protein kinase A in the rat motor nerve terminal. *Eur. J. Neurosci.* 23, 2048–2056. doi: 10.1111/j.1460-9568.2006.04753.x

Sun, M. K., and Alkon, D. L. (2006). Bryostatin-1: pharmacology and therapeutic potential as a CNS drug. *CNS Drug Rev.* 12, 1–8. doi: 10.1111/j.1527-3458.2006.00001.x

Tomàs, J., Garcia, N., Lanuza, M. A., Santafé, M. M., Tomàs, M., Nadal, L., et al. (2017). Presynaptic membrane receptors modulate ACh release, axonal competition and synapse elimination during neuromuscular junction development. *Front. Mol. Neurosci.* 10:132. doi: 10.3389/fnmol.2017.00132

Tomàs, J., Santafé, M. M., Garcia, N., Lanuza, M. A., Tomàs, M., Besalduch, N., et al. (2014). Presynaptic membrane receptors in acetylcholine release modulation in the neuromuscular synapse. *J. Neurosci. Res.* 92, 543–554. doi: 10.1002/jnr.23346

Tomàs, J., Santafé, M. M., Lanuza, M. A., García, N., Besalduch, N., and Tomàs, M. (2011). Silent synapses in neuromuscular junction development. *J. Neurosci. Res.* 89, 3–12. doi: 10.1002/jnr.22494

Waerhaug, O., and Ottersen, O. P. (1993). Demonstration of glutamate-like immunoreactivity at rat neuromuscular junctions by quantitative electron microscopic immunocytochemistry. *Anat. Embryol.* 188, 501–513. doi: 10.1007/bf00190144

Wyatt, R. M., and Balice-Gordon, R. J. (2003). Activity-dependent elimination of neuromuscular synapses. *J. Neurocytol.* 32, 777–794. doi: 10.1023/b:neur.0000020623.62043.33

Yao, Y., Bergold, P. J., and Penington, N. J. (2010). Acute Ca^{2+}-dependent desensitization of $5\text{-}HT_{1A}$ receptors is mediated by activation of protein kinase A (PKA) in rat serotonergic neurons. *Neuroscience* 169, 87–97. doi: 10.1016/j.neuroscience.2010.04.042

Conflict of Interest Statement: The authors declare that the research was conducted in the absence of any commercial or financial relationships that could be construed as a potential conflict of interest.

frontiers in Cellular Neuroscience

ORIGINAL RESEARCH
published: 26 July 2017
doi: 10.3389/fncel.2017.00212

The FOXP2-Driven Network in Developmental Disorders and Neurodegeneration

Franz Oswald[1†], Patricia Klöble[1†], André Ruland[1], David Rosenkranz[2], Bastian Hinz[2,3], Falk Butter[4], Sanja Ramljak[5], Ulrich Zechner[3,6‡] and Holger Herlyn[2‡]*

[1] Center for Internal Medicine, Department of Internal Medicine I, University Medical Center Ulm, Ulm, Germany, [2] Institut für Organismische und Molekulare Evolutionsbiologie, Johannes Gutenberg-University Mainz, Mainz, Germany, [3] Institute of Human Genetics, University Medical Center Mainz, Mainz, Germany, [4] Institute of Molecular Biology, Mainz, Germany, [5] Sciema UG, Mainz, Germany, [6] Dr. Senckenbergisches Zentrum für Humangenetik, Frankfurt, Germany

The transcription repressor FOXP2 is a crucial player in nervous system evolution and development of humans and songbirds. In order to provide an additional insight into its functional role we compared target gene expression levels between human neuroblastoma cells (SH-SY5Y) stably overexpressing *FOXP2* cDNA of either humans or the common chimpanzee, Rhesus monkey, and marmoset, respectively. RNA-seq led to identification of 27 genes with differential regulation under the control of human *FOXP2*, which were previously reported to have FOXP2-driven and/or songbird song-related expression regulation. RT-qPCR and Western blotting indicated differential regulation of additional 13 new target genes in response to overexpression of human *FOXP2*. These genes may be directly regulated by FOXP2 considering numerous matches of established FOXP2-binding motifs as well as publicly available FOXP2-ChIP-seq reads within their putative promoters. Ontology analysis of the new and reproduced targets, along with their interactors in a network, revealed an enrichment of terms relating to cellular signaling and communication, metabolism and catabolism, cellular migration and differentiation, and expression regulation. Notably, terms including the words "neuron" or "axonogenesis" were also enriched. Complementary literature screening uncovered many connections to human developmental (autism spectrum disease, schizophrenia, Down syndrome, agenesis of corpus callosum, trismus-pseudocamptodactyly, ankyloglossia, facial dysmorphology) and neurodegenerative diseases and disorders (Alzheimer's, Parkinson's, and Huntington's diseases, Lewy body dementia, amyotrophic lateral sclerosis). Links to deafness and dyslexia were detected, too. Such relations existed for single proteins (e.g., DCDC2, NURR1, PHOX2B, MYH8, and MYH13) and groups of proteins which conjointly function in mRNA processing, ribosomal recruitment, cell–cell adhesion (e.g., CDH4), cytoskeleton organization, neuro-inflammation, and processing of amyloid precursor protein. Conspicuously, many links pointed to an involvement of the FOXP2-driven network in JAK/STAT signaling and the regulation of the ezrin–radixin–moesin complex. Altogether, the applied phylogenetic perspective substantiated FOXP2's

OPEN ACCESS

Edited by:
Jaewon Ko,
Daegu Gyeongbuk Institute of Science and Technology (DGIST), South Korea

Reviewed by:
Cedric Boeckx,
Institució Catalana de Recerca i Estudis Avançats (ICREA), Spain
Kihoon Han,
Korea University College of Medicine, South Korea

***Correspondence:**
Holger Herlyn
herlyn@uni-mainz.de

†Shared first authorship
‡Shared senior authorship

Received: 24 March 2017
Accepted: 04 July 2017
Published: 26 July 2017

Citation:
Oswald F, Klöble P, Ruland A, Rosenkranz D, Hinz B, Butter F, Ramljak S, Zechner U and Herlyn H (2017) The FOXP2-Driven Network in Developmental Disorders and Neurodegeneration. Front. Cell. Neurosci. 11:212. doi: 10.3389/fncel.2017.00212

importance for nervous system development, maintenance, and functioning. However, the study also disclosed new regulatory pathways that might prove to be useful for understanding the molecular background of the aforementioned developmental disorders and neurodegenerative diseases.

Keywords: language, speech, brain, schizophrenia, Parkinson's disease, Alzheimer's disease, Huntington's disease, neuronal circuitry

INTRODUCTION

The high complexity clearly sets apart human verbal communication from vocalization repertoires of other primate species. Yet, despite this importance we are still at the beginning of understanding the molecular pathways behind the evolutionary and developmental acquisition of speech and language. Probably, the most advancement was made in respect to the role of the gene coding for forkhead box P2 (FOXP2; O15409; also CAGH44). The encoded transcription repressor spans 715 amino acids (aa) in human isoform I, thereby containing the eponymous forkhead box domain with DNA-binding ability at the C-terminus, a central expression suppression domain with zinc finger and leucine zipper motifs, and a glutamine-enriched N-terminus, with the longest poly-glutamine stretch spanning 40 aa (**Figure 1A**; e.g., Vernes and Fisher, 2009; Enard, 2011).

FOXP2's relevance for verbal communication became obvious when a missense mutation in the coding gene (p.R553H) which lowers the DNA binding capability was recognized to associate with speech-language disorder 1 (SPCH1, OMIM #602081), also known as developmental verbal dyspraxia (DVD) and childhood apraxia of speech (CAS). Affected family members suffered from deficits in virtually every aspect of expressive and receptive language. They especially showed disturbed orofacial motor coordination affecting tongue, lips, jaw and palate, which together led to impaired lingual articulation and non-lingual sound-production (e.g., Vernes and Fisher, 2009). The subsequent recognition of associations between other *FOXP2* mutations and communication disorders further substantiated the importance of the gene for the acquisition of full speech and language competence (Vernes and Fisher, 2009; Palka et al., 2012). *FOXP2* has additionally been implicated in the etiology of mental diseases such as autism spectrum disorder (ASD; Bowers and Konopka, 2012) and schizophrenia (SCZD; e.g., Jamadar et al., 2011; Li et al., 2013). Notably, also these disorders are frequently accompanied by language and speech deficits (e.g., Stephane et al., 2007; Abrahams and Geschwind, 2010; Kupferberg, 2010) so that studies on *FOXP2* hold out the prospect of elucidating the evolution and development of speech and language (e.g., Marcus and Fisher, 2003; Bolhuis et al., 2010; Enard, 2011).

The *FOXP2* gene is expressed in multiple tissues including fetal and adult brain (e.g., Vernes and Fisher, 2009; Enard, 2011) whereby haploinsufficiency and thus lowered levels of transcript and protein are commonly assumed to elicit the aforementioned diseases and disorders (e.g., Enard, 2011). In support of this view, all documented patients were heterozygous for the etiological mutation (Vernes and Fisher, 2009) in either the gene itself (point mutations, deletions, chromosomal rearrangements; e.g., Turner et al., 2013 and references therein) or downstream regulatory elements (e.g., Adegbola et al., 2015). Random mono-allelic expression (RMAE) with some cells having half the *FOXP2* dosage and others expressing none at all (Adegbola et al., 2015) and mosaic deletion with some cells possessing two functional alleles and others none (Palka et al., 2012) also play a role. Either way, minimum expression of one functional allele in at least part of the cells seems indispensable to life, a condition that is additionally demonstrated by early post-natal death of mice homozygous for a *Foxp2* null allele (French et al., 2007; Vernes et al., 2007; Rousso et al., 2012).

FOXP2's influence on human vocalization skills has a stunning parallel in non-primate vocal-learners. In songbirds, brain *FOXP2* levels positively associate with vocal learning and singing activity whereas knockdown impairs song learning (see, e.g., Bolhuis et al., 2010; Pfenning et al., 2014). In line with this, *FOXP2* belonged to the highly supported genes in a genome-wide screen for singing-related transcriptional changes in male zebra finch brains (see Hilliard et al., 2012). Investigation of other bird and additional mammalian species underlined a general pattern confirming that normal development of vocal learning and vocalization skills requires fine-tuned regulation of FOXP2 expression in brain (e.g., Bolhuis et al., 2010; Pfenning et al., 2014).

The human–bird parallel demonstrates that FOXP2's origin predates the split of Mammalia and Sauropsida about 320 million years ago (timetree.org estimate). Yet, regardless of hundreds of millions of years of independent evolution zebra finch FOXP2 still shows 98% identity with the human ortholog (Haesler et al., 2004). Evolutionary conservation of FOXP2 also prevailed throughout the divergence of primates, though with a notable exception: Thus, two aa substitutions, p.T303N and p.N325S (rs753394697 SNP), occurred on the human branch after the split from the chimpanzee lineage. These two exchanges reside inside the transcription repression domain (**Figure 1A**) and potentially were exposed to positive selection (reviewed in Enard, 2011; also, e.g., Mozzi et al., 2016). However, according to genome-wide evidence the selective sweep was not complete (Mallick et al., 2016) so that *FOXP2* evolution in primates and especially in humans was probably more complex than previously thought. In any case, the two aa exchanges known from humans seem to be functional. Thus, mice homozygous for a *Foxp2* version mutated for both human exchanges had reduced dopamine concentration in all investigated brain regions and their striatal medium spiny neurons showed

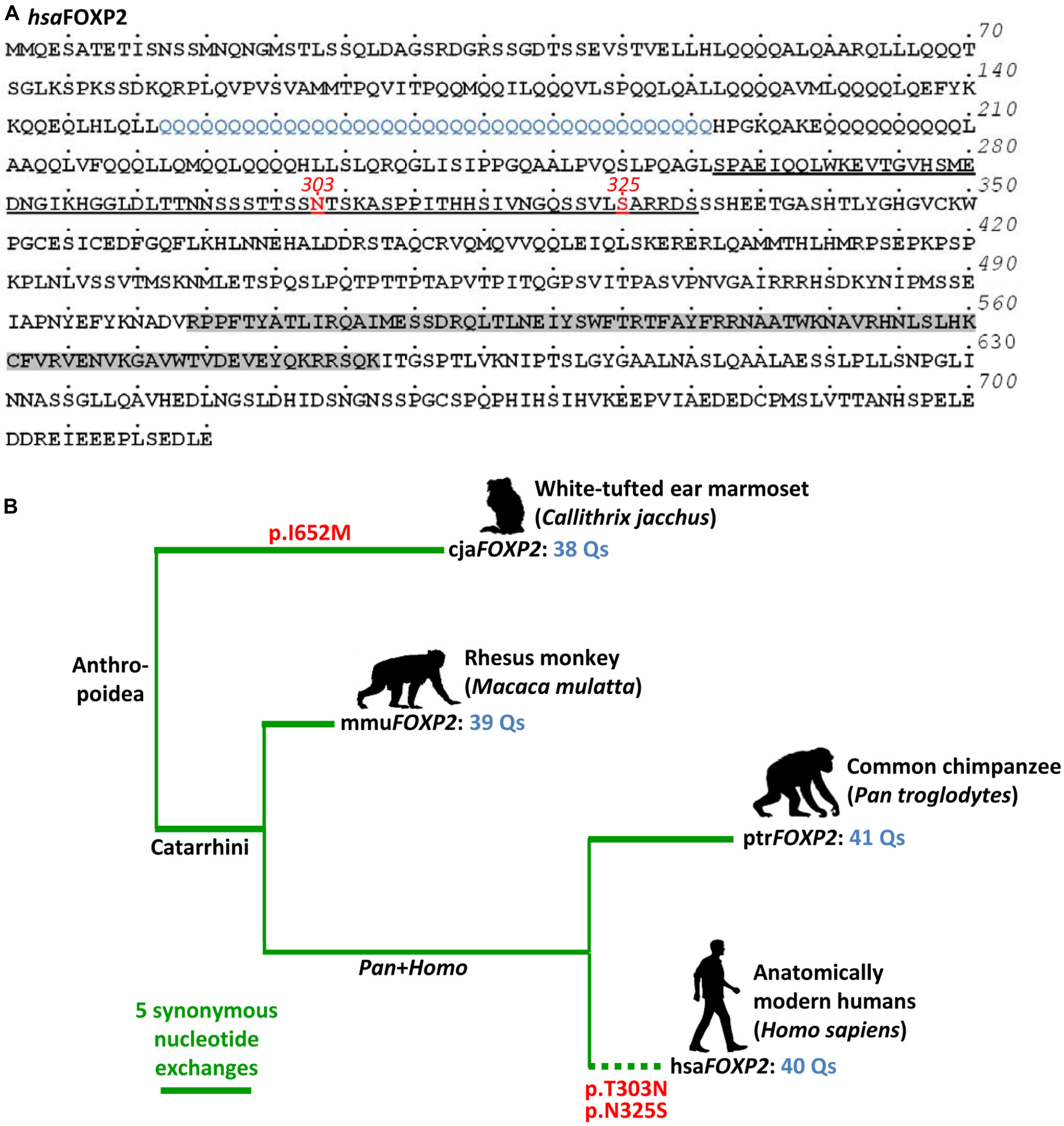

FIGURE 1 | Evolution of *FOXP2* in primates (Anthropoidea). **(A)** Human FOXP2 protein (*hsa*FOXP2: NP_055306) with two characteristic amino acids at positions 303 and 325 highlighted in red. Underlining broadly defines the transcription repression domain. The FOX domain is shown in gray (domains after Zhang et al., 2002). Blue labeling highlights the longest poly-glutamine stretch within the glutamine-enriched N-terminus. Dots above the amino acid sequence indicate increments of five amino acids, each. Numbers on the right give the total number of amino acids. **(B)** *FOXP2* gene tree (Primates, Anthropoidea). Horizontal branch lengths (thick green lines) correspond to the number of synonymous exchanges. Red labels indicate two non-synonymous exchanges, which occurred on the human branch (dotted line). The respective amino acid exchanges occured inside the transcription repression domain, as shown in **(A)**. Another non-synonymous exchange took place on the lineage to the marmoset. A detailed list of the branch-specific exchanges is given in Supplementary Table 1.1. *FOXP2* cDNAs (cja*FOXP2* etc.) are designated according to the Latin species names (cja, *Callithrix jacchus* etc.).

increased dendrite length, synaptic plasticity, and long term depression (Enard et al., 2009). A related study substantiated the relevance of both aa exchanges for dendrite length of neurons in cortico-basal ganglia circuits (Reimers-Kipping et al., 2011).

The investigation of how mutations that associate with verbal dyspraxia affect FOXP2 expression, subcellular localization, DNA-binding and transactivation properties in human neuron-related cells (SH-SY5Y) inspired a series of further *in vitro* analyses (Vernes et al., 2006). Two of the sequel studies identified diverse FOXP2 target candidates in SH-SY5Y cells that were transfected with either human *FOXP2* cDNA or empty vector (Spiteri et al., 2007; Vernes et al., 2007). Based on the same *in vitro* approach, one of the follow-up studies determined retinoic acid signaling as an important pathway in FOXP2-driven neuronal differentiation (Devanna et al., 2014). Another investigation addressed potential regulatory changes in humans by comparing target gene expression levels between

SH-SY5Y cells overexpressing either human *FOXP2* cDNA or a variant in which both human-specific non-synonymous substitutions were mutated to acquire the chimpanzee-specific aa content at the respective sites (*FOXP2*^{chimp} in Konopka et al., 2009). The latter study as well as additional ones with a focus on the effect of both human-specific aa substitutions in mutated mice (*Foxp2*^{hum} in Enard et al., 2009 and follow-up studies) generated valuable data on FOXP2/Foxp2 functioning. However, the interpretability of the data is fairly challenging from an evolutionary point of view, due to the following: Understanding the evolutionary meaning behind differential target gene expression levels in a pair of models representing two extant species requires considerable assumptions in regard to expression levels in an unknown ancestor. Without such assumptions it is not possible to certainly assign an evolutionary change to either one or the other lineage. Neither parental cells nor cells carrying empty vector can appropriately model the ancestral condition as they rather reflect baseline expression levels in extant species as do wild-type animals in respective comparisons. Moreover, the mutated *FOXP2*/*Foxp2* variants which merge states of two species in a single cDNA (*FOXP2*^{chimp}, *Foxp2*^{hum}) have no counterparts in living species and it is questionable if they have ever existed in any human ancestor. This is due to additional synonymous (silent) and non-synonymous nucleotide substitutions in the human–mouse and human–chimpanzee comparison (see, e.g., Enard et al., 2002). Variant lengths of the CAG/CAA repeats coding for the N-terminal FOXP2 poly-glutamine tracts additionally contribute to this discrepancy (**Figure 1A**). Yet, the outlined restraints in terms of evolutionary interpretability can be overcome in a broader phylogenetic context which addresses the effect of human *FOXP2* relative to naturally occurring cDNAs of chimpanzee and at least one further non-human species. In such a phylogenetic approach unidirectional differences in target gene expression levels between the human model on the one hand and the non-human models on the other give an approximation of potential expressional changes in human evolution.

Synonymous exchanges might indeed have functional relevance on FOXP2 expression, namely through nucleotide (Debatisse et al., 2004) and tRNA availability (Wohlgemuth et al., 2013). It is also conceivable that extension of the longest of N-terminal poly-glutamine tracts is functionally relevant. The respective stretch spans 40 aa in the human reference (*Homo sapiens* FOXP2, hsaFOXP2) whereas it has 41, 39, and 38 glutamines in the FOXP2 of common chimpanzee (*Pan troglodytes*, ptrFOXP2), Rhesus monkey (*Macaca mulatta*, mmuFOXP2), and white-tufted ear marmoset (*Callithrix jacchus*, cjaFOXP2), respectively (**Figure 1B**). Although these interspecific differences may appear negligible they seem to evolve under functional constraint as suggested by a general tendency of repeat length conservation in humans (Bruce and Margolis, 2002). In support of this view, mutations decreasing the number of N-terminal glutamines in FOXP2 were found to occur in speech and sound disorder (SSD) patients. Also, the fact that a deletion of glutamines from the FOXP2 N-terminus alters expression of the language gene *CNTNAP2* suggests that the extension of the respective stretches is functionally relevant (Zhao et al., 2015; for language association, see Abrahams and Geschwind, 2010; Kato et al., 2014). Functional relevance of poly-glutamine tract extension could be anticipated given that poly-glutamine tract expansion in other genes account for several diseases (e.g., Fan et al., 2014). On that premise, some of FOXP2's functional implications in human evolution and development might still await their discovery.

The present study investigates FOXP2's role by adopting a broader phylogenetic perspective. To the best of our knowledge, this approach takes into account for the first time the entire spectrum of differences that distinguish human *FOXP2* gene from its non-human primate counterparts. In detail, we compared expression levels between SH-SY5Y cells stably overexpressing hsa*FOXP2* with corresponding levels in cells that were alternatively transfected with ptr*FOXP2*, mmu*FOXP2*, and cja*FOXP2*. The species sample behind covers the major lineages inside extant anthropoid primates (New World monkeys, Old World monkeys, and Hominoidea) and at the same time allows for the identification of changes on the human branch (for phylogenetic relationships, see **Figure 1B**). We investigated which of the genes with specific expression regulation under hsa*FOXP2* control already showed FOXP2/Foxp2-driven and/or songbird song-related expression regulation in previous studies. Additional attention was payed to the question if the FOXP2-driven network might be more comprehensive than known so far. We finally addressed which of the functional implications of the proteins in our network confirm previous knowledge, and which pathways might have been not observed before.

MATERIALS AND METHODS

Cell Culture and Transfection

We evaluated pcDNA3-constructs in HEK293 human embryonic kidney cells (ATCC no. CRL-1573) that were cultivated in DMEM (Gibco) supplemented with 10% FCS (Biochrom) and 1% Penicillin–Streptomycin (Gibco) at 37°C and 5% CO_2. After RT-PCR detected only minimum amount of endogenous *FOXP2* transcript (Supplementary Image 1), cells (1×10^6 cells, seeded in 8 cm dishes) were transiently transfected with Nanofectin (PAA) with 8 μg of either empty pcDNA3 expression vector (Thermo Fisher) or constructs carrying alternative primate *FOXP2* cDNAs. The custom-synthesized (BlueHeron) cDNAs used for transfection were species-specific and coded for human FOXP2 isoform I (715 aa; ENST00000350908; *Homo sapiens*, hsa) and FOXP2s in common chimpanzee (AY064549; *Pan troglodytes*, ptr), Rhesus monkey (ENSMMUT00000011202; *Macaca mulatta*, mmu), and white-tufted ear marmoset (XM_002751707; *Callithrix jacchus*, cja). Full-length transcription and translation of hsa*FOXP2*, ptr*FOXP2*, mmu*FOXP2*, and cja*FOXP2* was verified through specific molecular weights (plus/minus FLAG tag: higher/lower molecular weight) in Western blots 24 h after transfection (Supplementary Image 2). For the subsequent generation of

stable transfectants we used *FOXP2*-specific expression plasmids without N-terminal FLAG tag.

Parental SH-SY5Y neuroblastoma cells (ATCC no. CRL-2266) were grown in DMEM containing 15% FCS and 1% Penicillin–Streptomycin. After RT-PCR (Supplementary Image 1) detected no endogenous *FOXP2* transcript, SH-SY5Y cells were transfected with 2 μg of either linearized empty plasmid (pcDNA3) or *FOXP2*-specific pcDNA3-constructs (see above), using the Amaxa Cell Line Nucleofector V Kit (Lonza) according to the manufacturer's instructions. This was done three times, thus generating three biological replicates per condition (designated I-III). Cells were cultivated in selection medium supplemented with 600 μg/ml geneticin (G-418; PAA; optimized concentration according to toxicity testing) to enforce stable transfection. Stable expression of FOXP2 protein was repeatedly monitored by Western blotting (see: Immunoblotting). Efficiency and persistence of transfection were additionally monitored in SH-SY5Y cells carrying pcDNA3-eGFP constructs, by fluorescence microscopy and through Western blotting using anti-eGFP (mouse monoclonal IgG, cat 11814460001, Roche; peroxidase conjugated sheep anti-mouse IgG, NA931V, GE Healthcare).

RT-PCR and Sanger Sequencing

Coding DNAs were generated with SuperScript II (Invitrogen; random primers) from total RNAs extracted with RNeasy Mini Kit (Qiagen). Subsequent standard PCR (Taq DNA Polymerase; Invitrogen) used primers hybridizing to evolutionary conserved sites of *FOXP2* cDNA (forward: 5′-AACAGAGACCACTGCAGGTGCC-3′; reverse: 5′-TCCCT GACGCTGAAGGCTGAG-3′). For assessing levels of endogenous *FOXP2* transcription in parental HEK293 and SH-SY5Y cell lines, PCR reactions were separated on an ethidium bromide-stained agarose gel, documented under UV light, and evaluated by eye. For validating transfection of SH-SY5Y cells with the intended pcDNA3 construct, RT-PCR set the start for subsequent gel extraction of *FOXP2* bands (Gel Extraction Kit, Qiagen), ligation into TOPO vector (TOPO TA, Invitrogen), cloning into *Escherichia coli* XL1-Blue (Stratagene), plasmid preparation (Wizard Plus, Promega), and Sanger sequencing with vector primer M13 (Sequiserve).

RNA Sequencing

Barcoded mRNA-seq cDNA libraries were prepared from 600 ng of total RNA of biological replicates I and II per each condition, using Illumina's TruSeq RNA Sample Preparation Kit. mRNA was isolated using oligo(d)T magnetic beads. Isolated mRNA was fragmented using divalent cations and heat and converted into cDNA using random primers and SuperScript II, followed by second strand synthesis. cDNA was end repaired, 3′ adenylated and single T-overhang Illumina multiplex specific adapters were ligated to the cDNA fragments, followed by an enrichment PCR. All cleanups were done using Agencourt AMPure XP magnetic beads. The quantity of the resulting cDNA mRNA-Seq libraries was measured using Qubit. Barcoded mRNA-Seq libraries were clustered on the cBot using the TruSeq PE cluster kit V3 (10 pM) and 2 × 50 bp were sequenced on the Illumina HiSeq 2500 (TruSeq SBS V3 kit; 50 cycles). Raw and processed data of RNA-seq have been deposited at NCBI's Gene Expression Omnibus (GEO) under accession number GSE100291.

The raw output data of the HiSeq was preprocessed according to the Illumina standard protocol. This includes filtering for low quality reads and demultiplexing. Sequence reads were aligned to the reference genomic sequence (hg19) using STAR[1]. The alignment coordinates were compared to the exon coordinates of the UCSC transcripts[2] and for each transcript the counts of overlapping alignments were recorded. The read counts were normalized to numbers of bases which map per kb of exon model per million mapped bases (BPKM; see Mortazavi et al., 2008) for each transcript. Comparisons between alternatively transfected cells were conducted on the basis of BPKM values as averaged over the transcripts identified.

Reverse Transcription Quantitative PCR

Coding DNA was synthesized from 2 μg total RNA of biological replicates I and II (per each condition) by reverse transcription using oligo(d)T and random primers with SuperScript III (Invitrogen) according to the manufacturer's instructions. The cDNA samples were diluted 1:40, and 7.5 μl of the diluted cDNA was used for reverse transcription quantitative PCR (RT-qPCR) of the candidate genes (for primers, see Supplementary Table 1.2) with QuantiTect SYBR Green Master Mix (Qiagen) on a StepOnePlus Real-Time PCR System (Life Technologies). Data was first explored with LinRegPCR[3] for calculating PCR efficiency. Subsequently, relative expression was calculated using the $2^{-2\Delta\Delta Ct}$ method (Livak and Schmittgen, 2001). Measurements were carried out thrice per biological replicate. For data normalization, we measured mRNA levels of the reference genes *GAPDH* and *RPLP* (for primers, see Supplementary Table 1.2).

Immunoblotting

We focused on proteins for which commercially available antibodies yielded specific bands of the expected molecular weight in Western blots. These analyses were carried out on the basis of all three biological replicates that we prepared per condition (I-III). Protein isolation, protein quantification, SDS-PAGE, Western blotting (PVDF, Millipore), blocking and incubation with antibodies, and Enhanced Chemiluminescence (ECL, GE Healthcare) followed standard protocols. FOXP2 protein expression in transiently transfected HEK293 cells was monitored by ECL in Western blots (primary antibody: anti FOXP2 polyclonal goat anti-human, ab1307, Abcam; secondary antibody: peroxidase-conjugated rabbit anti-goat IgG, Jackson ImmunoResearch). Protein levels in stably transfected SH-SY5Y cells (all without FLAG tag) were assessed by Western blotting and ECL using the following antibodies: anti-FOXP2 (monoclonal rabbit anti-human IgG, F9050-02C, Biomol,

[1]https://github.com/alexdobin/STAR/releases

[2]https://genome.ucsc.edu/

[3]www.hartfaalcentrum.nl

secondary antibody: peroxidase-conjugated donkey anti-rabbit IgG, NA934V, GE Healthcare), anti-BACE2 (mouse monoclonal IgG, sc271286, Santa Cruz Biotechnology, secondary antibody: peroxidase-conjugated sheep anti-mouse IgG, NA931V, GE Healthcare), anti-MSN (monoclonal rabbit IgG, ab52490, Abcam, secondary antibody: NA934V, GE Healthcare), anti-CDH4 (polyclonal rabbit IgG, sc7941, Santa Cruz Biotechnology, secondary antibody: NA934V, GE Healthcare). The anti-human FOXP2 antibody was raised against a peptide sequence which is conserved across the species included. Beta-actin (β-actin) served as a standard for protein loading (anti-β-actin antibody: mouse monoclonal IgG, A1978, Sigma, secondary antibody: NA931V). For densitometric analysis, signal intensity was scanned at least twice (two technical replicates) from Western blots of three biological replicates using the ImageJ software[4].

Bioinformatics and Statistics

Gene and protein symbols accord to the recommendations of the Human Gene Nomenclature Committee.

Branch-specific synonymous (silent) and aa altering exchanges in *FOXP2* were inferred by Codeml, as implemented in the PAML package v. 4.7 (Yang, 2007). For meeting the demands of PAML, we compiled a species tree with three equally ranking branches leading to the zebra finch (*Taeniopygia guttata*), the European house mouse (*Mus musculus*), and the four primate species considered (Anthropoidea). The relationships amongst the four anthropoid species reflected the commonly accepted phylogeny (e.g., Perelman et al., 2011). Codeml analysis additionally used an alignment (ClustalX implemented in BioEdit; Hall, 1999) of the corresponding four anthropoid cDNAs (for accession numbers, see above) and of their murine (ENSMUST00000115477.7) and zebra finch (AY549148.1) orthologs.

We screened BPKM values from RNA-seq for genes whose expression levels differed in the same direction (up-/down) between each of the hsa*FOXP2*-overexpressing SH-SY5Y transfectants and every transfectant overexpressing a non-human primate *FOXP2* cDNA or carrying empty vector. This entry criterion was tightened for new FOXP2 targets which additionally had to show at least twofold differential expression levels between the human and every other tested condition (mean *versus* mean). Statistical significance of expression levels in hsa*FOXP2*-overexpressing *versus* non-human primate *FOXP2*-overexpressing cells was then assessed employing the two-tailed *t*-test in SPSS v. 23.0 (IMB). The same test was applied to relative expression levels (RT-qPCR) and densitometric values (Western blotting).

Expression analyses included an evaluation of the magnitude of the effect, which stable overexpression of hsa*FOXP2* had on target gene transcription and translation in SH-SY5Y cells relative to the alternative treatment with non-human primate *FOXP2* cDNAs. In detail, we calculated the correlation coefficient *r*, thereby taking into account inhomogeneous variances between samples and unequal sample sizes (Cohen, 1988). The *r*-values were also used for *post hoc* analyses of the power of *t*-tests, which were carried out with the aid of G*Power 3.1.9.2 (Faul et al., 2009). Following the convention, we regarded *r*-values of at least 0.5 and power estimates of >80% as approximate benchmarks of large effect size and acceptable test power, respectively (Cohen, 1988).

As detailed in the legend of present Supplementary Table 2.1, we matched our RNA-seq data with previously published lists of potential targets of human FOXP2 and murine Foxp2 as identified by Spiteri et al. (2007, their Table 1), Vernes et al. (2007, their Table 1), Enard et al. (2009, their Figures S8A,B, right panel), Konopka et al. (2009, their Supplementary Table 1), and Vernes et al. (2011, their Table S1). We additionally checked our data for matches with genes that showed singing-related expression regulation in zebra finch brain (Hilliard et al., 2012, their Table S2: only genes where *q*-values indicated significant support).

In addition, we mapped publicly available FOXP2-binding sequences on putative promoter sequences (5,000 bp upstream of transcription start) of the newly defined FOXP2 candidate genes. The down-loaded sequences were generated by chromatin immunoprecipitation with an antibody against 127 C-terminal aa of human FOXP2, followed by sequencing (FOXP2-ChIP-seq). The respective DNA was isolated from human neuroblastoma SK-N-MC cells (GEO project GSM803353: SRR351544; see also Nelson et al., 2013). The mapping results were normalized for the number of hits across the human genome (GRCh38.p7). The putative promoter sequences of the same genes were also screened for established FOXP2-binding motifs (see Stroud et al., 2006; Vernes et al., 2007, 2011; Nelson et al., 2013). This was done with the aid of SeqMap v. 1.0.3 (Jiang and Wong, 2008), without allowing for any mismatch.

Following others (e.g., Boeckx and Benítez-Burraco, 2014a,b) we employed the STRING server (v. 10.0[5]) for the reconstruction of a protein–protein interaction (PPI) network as well as for PPI enrichment and gene ontology (GO) enrichment analyses. Thresholds for the acceptance of a PPI were alternatively set to low (≥0.15), medium (≥0.4), high (≥0.7), and maximum combined confidence scores (≥0.9). We inferred node degree values per protein (= number of direct edges a protein has) with the aid of Cytoscape v. 3.2.1 and the plugin NetworkAnalyzer 1[6].

We consulted brainspan.org for assessing spatiotemporal gene expression of new FOXP2 target genes in human brain. Sequences of all target genes (new and reproduced ones) and the encoded proteins can be retrieved from the ENSEMBL database via the identifiers (IDs) given in **Table 1**, amongst others. The same IDs lead to the rate ratios of synonymous to non-synonymous substitution rates (dN/dS) of the FOXP2 target genes and genes coding for interactors in the Rhesus monkey–human and Rhesus monkey–common chimpanzee comparison, which we retrieved from the ENSEMBL pages. The sampled dN/dS values were compared with a two-tailed Mann–Whitney *U* (MWU) test as implemented in

[4]https://imagej.nih.gov/ij/index.html

[5]http://string-db.org

[6]www.cytoscape.org

TABLE 1 | Proteins used for network reconstruction and GO enrichment analysis.

Subsample	Symbol	ENSEMBL ID	Subsample	Symbol	ENSEMBL ID
Encoded by reproduced FOXP2 targets	ADAP1	ENSP00000265846	Added interactors	CFTR	ENSP00000003084
	ALG11	ENSP00000430236		DICER1	ENSP00000343745
	APH1A	ENSP00000358105		EIF2C1	ENSP00000362300
	CDH11	ENSP00000268603		EIF2C2	ENSP00000220592
	DNMBP	ENSP00000315659		EIF2C3	ENSP00000362287
	ERP44	ENSP00000262455		EIF2C4	ENSP00000362306
	GPR160	ENSP00000348161		EIF4E	ENSP00000425561
	HSD17B3	ENSP00000364412		EIF4G1	ENSP00000338020
	IFI30	ENSP00000384886		EZR	ENSP00000338934
	IL4R	ENSP00000170630		HSP90AA1	ENSP00000335153
	LONRF1	ENSP00000381298		IL13	ENSP00000304915
	LRP3	ENSP00000253193		IL13RA1	ENSP00000360730
	LRRTM2	ENSP00000274711		IL2RG	ENSP00000363318
	MAFF	ENSP00000345393		IL4	ENSP00000231449
	MARVELD1	ENSP00000441365		JAK1	ENSP00000343204
	MGST2	ENSP00000265498		JAK2	ENSP00000371067
	MRPS6	ENSP00000382250		JAK3	ENSP00000391676
	NEU1	ENSP00000364782		KEAP1	ENSP00000171111
	PCDHB16	ENSP00000354293		KIF13B	ENSP00000427900
	PIM1	ENSP00000362608		LRRK2	ENSP00000298910
	SEMA6D	ENSP00000324857		MRPS10	ENSP00000053468
	SERPINH1	ENSP00000350894		MRPS16	ENSP00000362036
	SETBP1	ENSP00000282030		MRPS2	ENSP00000241600
	TBX22	ENSP00000362390		MRPS5	ENSP00000272418
	TMEM5	ENSP00000261234		NFATC1	ENSP00000327850
	TNRC6C	ENSP00000336783		NFE2L2	ENSP00000380252
	ZDHHC3	ENSP00000296127		PABPC1	ENSP00000313007
Encoded by new FOXP2 targets	BACE2	ENSP00000332979		PAIP1	ENSP00000302768
	CDH4	ENSP00000353656		PAN3	ENSP00000370345
	DCDC2	ENSP00000367715		RHOA	ENSP00000400175
	FOXL1	ENSP00000326272		ROCK1	ENSP00000382697
	GABRE	ENSP00000359353		SLC9A3R1	ENSP00000262613
	MSN	ENSP00000353408		SOCS5	ENSP00000305133
	MYH13	ENSP00000252172		STAT3	ENSP00000264657
	MYH8	ENSP00000384330		STAT5A	ENSP00000341208
	NURR1	ENSP00000344479		STAT5B	ENSP00000293328
	PHOX2B	ENSP00000226382		STAT6	ENSP00000300134
	PTPRQ	ENSP00000266688		TARBP2	ENSP00000266987
	SEBOX	ENSP00000416240		TNRC6A	ENSP00000379144
	TMEM200A	ENSP00000296978		TNRC6B	ENSP00000401946

SPSS (see above). *P*-values from *t*-tests (expressional analyses) were transformed into false discovery rates (FDRs), thus accounting for multiple testing (see, e.g., Vernes et al., 2007). FDRs in GO enrichment analysis as generated by Cytoscape were multiplied by the factor of two, thus conservatively adjusting for parallel testing of two datasets. *P*-values from PPI enrichment testing (network analysis) were adjusted in the same manner. Significance thresholds applied were <0.01 for GO enrichment analysis and <0.05 for all other tests. Data on sample sizes refer to the numbers of cell lines overexpressing either hsa*FOXP2* (N) or different non-human *FOXP2* cDNAs (M).

RESULTS

Evaluation of the Study System

RT-PCR detected only minimal endogenous *FOXP2* transcript in parental HEK293 cells (Supplementary Image 1). In further support of their suitability for subsequent validation steps, no FOXP2 band appeared in lanes loaded with lysate from parental HEK293 cells (Western blotting). In contrast, anti-FOXP2 antibody recognized protein bands of two different molecular weights in transiently transfected HEK293 cells, which overexpressed either human or one of the non-human primate *FOXP2* cDNAs. These differences correlated with

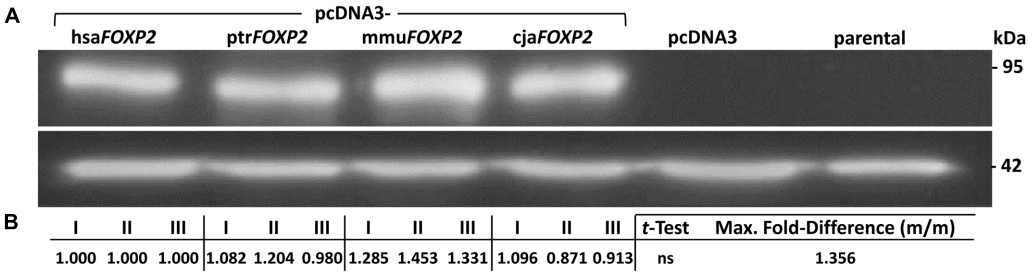

FIGURE 2 | FOXP2 protein expression in SH-SY5Y cells. **(A)** Representative Western blot illustrating that anti-FOXP2 antibody detected no protein in parental cells, indicative of absent endogenous expression. Moreover, there was no FOXP2 detectable in cells carrying empty vector (pcDNA3). In contrast, bands were recognized in SH-SY5Y cells stably transfected with pcDNA3-hsa*FOXP2*, -ptr*FOXP2*, -mmu*FOXP*, and -cja*FOXP2* (all without FLAG tag), thereby indicating similar levels of exogenous FOXP2 expression. Purified lysates were run on an SDS-PAGE gel, transferred to PVDF membrane, and successively hybridized with the respective antibodies. Lower panel: β-actin served as a standard for protein load. **(B)** Densitometric analysis of FOXP2 levels. The given measurements refer to biological replicates I–III (with two technical replicates, each) of the conditions labeled in **(A)**. Maximum (Max.) fold-difference corresponds to the ratio of the most extreme pair of mean expression levels (m/m) between hsa*FOXP2*-overexpressing cells and cells expressing non-human *FOXP2* (here: mmu*FOXP2*). cja, marmoset (*Callithrix jacchus*); hsa, human (*Homo sapiens*); mmu, Rhesus monkey (*Macaca mulatta*); ptr, chimpanzee (*Pan troglodytes*).

the extension and non-extension of the different FOXP2 sequences with a C-terminal FLAG tag, thus indicating full length transcription and translation of exogenously expressed *FOXP2* (Supplementary Image 2). After having shown the functionality of the pcDNA3-*FOXP2* constructs we turned to our actual study system, i.e., SH-SY5Y cells. RT-PCR confirmed previous notions of absent endogenous *FOXP2* transcription in parental SH-SY5Y cells (Supplementary Image 1; see also, e.g., Zhao et al., 2015). Consistently, no FOXP2 protein was contained in lysates prepared from parental and pcDNA3-transfected SH-SY5Y cells, according to Western blotting (**Figure 2**). Thus, detection of *FOXP2*/FOXP2 in cells stably transfected with pcDNA3-*FOXP2* constructs can be assigned to exogenous expression. Thereby, we ensured by Sanger sequencing that the different transfectants overexpressed the intended human, chimpanzee, Rhesus monkey, and marmoset FOXP2 cDNA, respectively (not shown). Notably, densitometric analysis suggested about equal FOXP2 protein amounts in hsa*FOXP2*-overexpressing cells on the one hand and SH-SY5Y cells transfected with ptr*FOXP2*, mmu*FOXP2*, and cja*FOXP2* cDNAs on the other (**Figure 2**). Consequently, downstream analyses of target gene expression levels should not be biased by unequal FOXP2 amounts across the cell lines compared.

Matching of RNA-seq Data with Results of Previous Studies

Preliminary analysis of BPKM values from present RNA-seq (GSE100291) revealed differential expression levels of altogether 898 genes in hsa*FOXP2*-overexpressing SH-SY5Y cells relative to the cells alternatively transfected with ptr*FOXP2*, mmu*FOXP2*, cja*FOXP2* cDNAs, and empty vector (biological replicates I and II per each condition). As to be expected from upstream experiments *FOXP2* was not amongst these differentially regulated genes. However, the sample contained 122 genes that were previously reported to be potential FOXP2/Foxp2 targets (Spiteri et al., 2007; Vernes et al., 2007, 2011; Enard et al., 2009; Konopka et al., 2009) and/or to have singing-related expression regulation in male zebra finch brain (Hilliard et al., 2012). In 27 out of these 122 reproduced genes support for differential BPKM levels under hsa*FOXP2* control was significant according to FDRs <0.05 in the *t*-tests conducted (Supplementary Table 2.1). The corresponding *r* values indicated a large effect size (>0.5) for all 27 comparisons. Consequently, the test power estimates by G*Power constantly overshot the threshold of acceptability, i.e., 80% (Supplementary Table 2.1). The detailed power estimates even ranged from 94 to 100% between the cells overexpressing hsa*FOXP2* ($N = 2$) and non-human *FOXP2* ($M = 6$). This fact, along with the appearance of these 27 genes in the reference studies, suggested that the inclusion of additional replicates should not alter the results. Consequently, we retained all 27 reproduced genes for downstream analyses (Supplementary Table 2.1 and **Table 1**).

New FOXP2 Targets and Validation by RT-qPCR

Subsequently, we addressed the question if the significance testing of RNA-seq data might have led to an underestimation of the extent of the (hsa)FOXP2-driven network. In order to get an estimate, we selected 13 additional genes out of the aforementioned preliminary set of 898 loci (Supplementary Table 2.2). The genes under scrutiny had low to moderate expression levels but at the same time showed more than twofold differential expression under hsa*FOXP2* control relative to any other condition (mean *versus* mean). Furthermore, they were protein-coding and displayed expression in brain in at least some phase of human life[7]. The 13 genes selected did not receive significant statistical support for FOXP2/Foxp2-driven and/or songbird song-related expression regulation in any of the six reference studies mentioned in the previous paragraph. Thus, we herein refer to the respective genes as to new FOXP2 targets.

[7]brainspan.org

TABLE 2 | Target gene expression levels (RT-qPCR) in SH-SY5Y cells overexpressing human *FOXP2* relative to cells overexpressing non-human primate *FOXP2*.

	pcDNA3-											
	hsa*FOXP2*		ptr*FOXP2*		mu*FOXP2*		cja*FOXP2*					
Symbol	**I**	**II**	**I**	**II**	**I**	**II**	**I**	**II**	**FDR *t*-test**	**Min. fold-change (m/m)**	***r***	**Power**
BACE2	0.177	0.211	1.875	1.973	1.598	1.999	0.595	0.497	<0.001	0.355	0.735	0.725
	0.177	0.211	1.875	1.973	1.598	1.999	–	–	<0.05	0.108	0.986	1.000
DCDC2	0.289	0.230	0.562	0.879	0.433	0.474	0.889	0.800	<0.01	0.572	0.767	0.803
CDH4	0.284	0.387	1.128	1.661	3.003	3.565	2.437	2.154	<0.05	0.241	0.808	0.895
FOXL1	0.378	0.308	3.404	2.443	3.140	3.661	2.235	1.790	<0.001	0.170	0.897	0.997
GABRE	0.014	0.012	0.423	0.455	0.606	0.562	0.361	0.348	<0.01	0.037	0.933	1.000
MSN	0.111	0.180	1.217	1.825	0.981	1.237	1.391	1.474	<0.01	0.131	0.931	1.000
MYH8	0.253	0.293	1.369	1.620	1.337	1.285	1.974	2.067	<0.01	0.208	0.923	1.000
MYH13	0.044	0.049	1.011	0.897	0.565	0.536	0.808	0.826	<0.01	0.084	0.922	1.000
NURR1	0.092	0.131	2.742	2.331	3.386	3.915	0.840	1.007	ns	0.121	0.743	0.745
	0.092	0.131	2.742	2.331	3.386	3.915	–	–	0.01	0.044	0.943	0.999
PHOX2B	0.091	0.083	0.942	0.598	0.877	0.447	2.598	3.094	<0.05	0.131	0.589	0.411
	0.091	0.083	0.942	0.598	0.877	0.447	–	–	<0.05	0.131	0.873	0.899
PTPRQ	0.147	0.131	0.401	0.300	1.357	1.119	0.331	0.377	<0.05	0.397	0.556	0.357
	0.147	0.131	0.401	0.300	–	–	0.331	0.377	<0.01	0.397	0.950	1.000
SEBOX	4.423	4.172	0.105	0.143	0.143	0.169	0.153	0.182	<0.05	25.657	0.998	1.000
TMEM200A	0.124	0.088	1.110	0.839	1.567	1.207	0.326	0.483	ns	0.262	0.731	0.715
	0.124	0.088	1.110	0.839	1.567	1.207	–	–	<0.05	0.109	0.921	0.987

*Two biological replicates (I, II) were measured per condition. Values were corrected for signal intensity of reference genes and normalized for expression levels in cells carrying empty expression vector. Minimum (Min.) fold-difference refers to the ratio of the least extreme pair of mean expression levels between hsaFOXP2-overexpressing cell lines and their counterparts overexpressing one of the non-human FOXP2 cDNA. Power estimates according to G*Power v. 3.1.9.2. FDR, false discovery rate; cja, marmoset (Callithrix jacchus); hsa, human (Homo sapiens); mmu, Rhesus monkey (Macaca mulatta); ns, not significant; ptr, chimpanzee (Pan troglodytes); r, correlation coefficient.*

RT-qPCR confirmed up- (1 gene) and down-regulation (12 genes) of expression under hsa*FOXP2* control in SH-SY5Y cells for all 13 genes measured (**Table 2**). The effect of hsa*FOXP2* overexpression on target gene expression was again large, as indicated by *r*-values >0.5 in all of the comparisons between hsa*FOXP2* and non-human *FOXP2*-overexpressing cells (biological replicates I and II per each condition). In twelve cases, RT-qPCR corroborated the results of RNA-seq of at least twofold up- or down-regulation (mean *versus* mean) under hsa*FOXP2* control relative to any other condition. We noticed the strongest regulation in *SEBOX*, whereby the minimum fold-change between hsa*FOXP2* and non-human primate *FOXP2*-overexpressing cells was >25 (with $N = 2$, $M = 6$), indicating a strong up-regulation of transcription in response to hsa*FOXP2* overexpression (**Table 2**). The corresponding values for *BACE2*, *CDH4*, *FOXL1*, *GABRE*, *MSN*, *MYH8*, *MYH13*, *NURR1*, *PHOX2B*, *PTPRQ*, and *TMEM200A* ranged between 0.037 and 0.397, which corresponds to a considerable down-regulation of transcription for each of these loci. *DCDC2* failed the twofold-threshold in the comparison of the hsa*FOXP2*-overexpressing cells with any other condition (0.572) but down-regulation of expression under hsa*FOXP2* control was nonetheless significant (**Table 2**). Significant FDRs (<0.05, *t*-test) were also reached in the human/non-human comparison of the other new FOXP2 target candidates, except for *NURR1* and *TMEM200A* (all with $N = 2$ and $M = 6$). The latter two genes missed the 5% threshold of significance in the first place, despite their strong down-regulation in hsa*FOXP2*-overexpressing cells and the correspondingly increased *r*-values (>0.7).

This discrepancy between effect size and significance testing in *NURR1* and *TMEM200A* apparently reflected an increased variation across the non-human models due to conspicuous values under cja*FOXP2* control. However, the inclusion of models for the Rhesus monkey and marmoset besides the chimpanzee condition was a rather conservative approach with respect to our prime goal of detecting expressional changes in the human model cell lines (compare **Figure 1B**). In *NURR1* and *TMEM200A*, the consideration of the complete species sample might even have obscured actually relevant changes in response to hsa*FOXP2* overexpression. Accordingly, we found the expression levels of *NURR1* and *TMEM200A* to differ significantly under hsa*FOXP2* control when the data were re-analyzed under exclusion of the values measured in the cja*FOXP2*-overexpressing cells (thus, with $N = 2$ and $M = 4$; **Table 2**). The reduction in the species sample associated with an increase of the corresponding *r* values and power estimates for the *t*-tests carried out on *NURR1* and *TMEM200A*. Similarly, the power estimates overshot the 80% threshold of acceptability when the levels of *BACE2*, *PHOX2B*, and *PTPRQ* transcripts were compared between hsa*FOXP2*-overexpressing cells and a reduced sample of non-human primate models (**Table 2**). Thus, *post hoc* analysis of *t*-tests underlined that significant support for expressional changes under hsa*FOXP2*

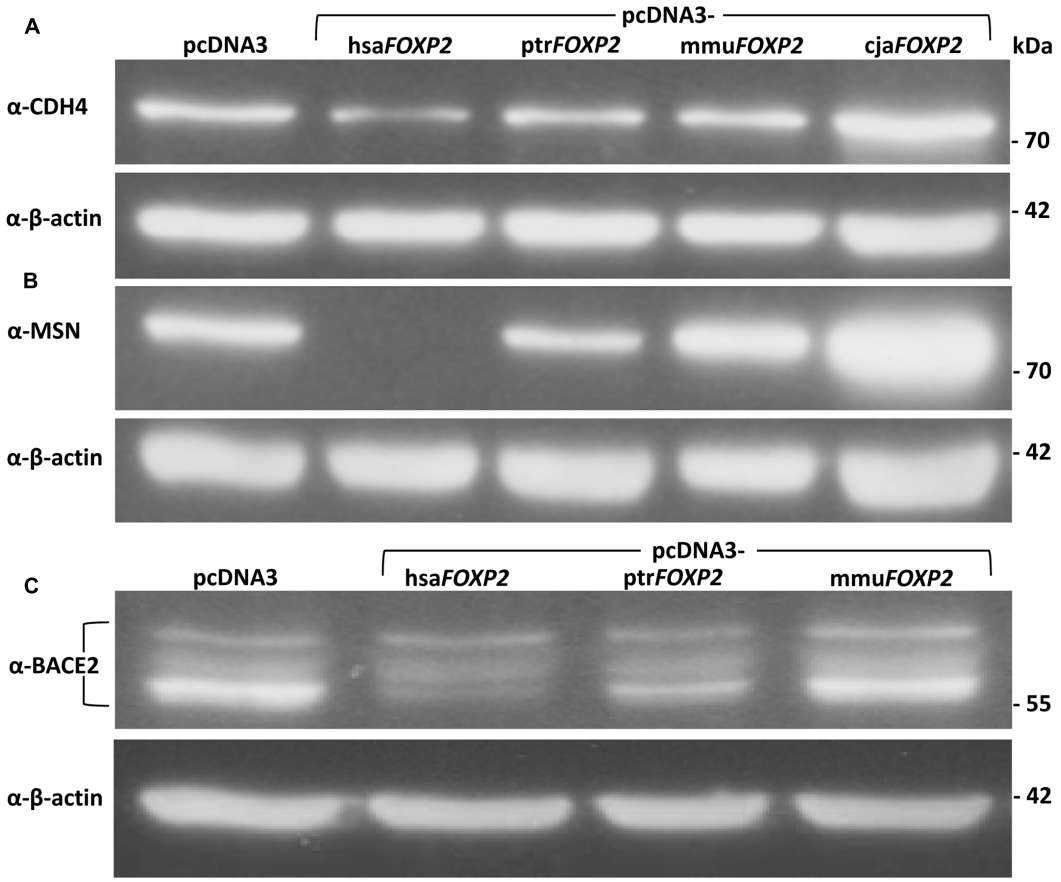

FIGURE 3 | Representative Western blots showing expression levels of FOXP2 targets in SH-SY5Y cells. **(A)** Anti-CDH4 detected significantly less protein quantity in response to hsa*FOXP2* overexpression relative to the cells overexpressing one of the three non-human primate *FOXP2* cDNAs (all without FLAG tag). **(B)** No MSN was discernible in hsa*FOXP2*-overexpressing cell lines, whereas protein expression was obvious in cell lines either overexpressing one of the tested non-human primate *FOXP2* cDNAs or carrying empty vector (pcDNA3). **(C)** Anti-BACE2 recognized one band at about 56 kDa and additional ones at higher molecular weights, which presumably represent differently glycosylated variants of the membrane protein (Acquati et al., 2000). In particular, the lowest band appeared to be down-regulated under hsa*FOXP2* control relative to the non-human models included, but all the bands were used for densitometric analysis. Purified lysates were run on an SDS-PAGE gel, transferred to PVDF membrane, and successively hybridized with the respective antibodies. Lower panels: β-actin served as a standard for protein load in all experiments. Results of densitometric analyses are given in **Table 3**. cja, marmoset (*Callithrix jacchus*); hsa, human (*Homo sapiens*); mmu, Rhesus monkey (*Macaca mulatta*); ptr, chimpanzee (*Pan troglodytes*).

control could be correlated with acceptable power estimates in all 13 new target genes – at least after obscuring signal was excluded from the comparison. However, high power estimates suggest that the alternative hypothesis of unequal means (here: expression levels) is true. Consequently, additional biological replicates should reproduce the findings without bringing an essential gain of new information – a prediction that we tested on the protein level.

Western Blotting of Proteins Encoded by New FOXP2 Targets

The three proteins selected for Western blot analyses represented loci, for which the power of *t*-tests was >80% when contrasting transcript amounts (RT-qPCR) in hsa*FOXP2*-overexpressing SH-SY5Y cells with the corresponding levels in either the complete (*CDH4*, *MSN*) or a reduced set of non-human models (*BACE2*). Densitometric analysis confirmed significant down-regulation under hsa*FOXP2* control for all three tested proteins, when taking the same two biological replicates per condition as used for transcriptome measurements (I and II). As in transcriptomic analyses, the *r* values exceeded the threshold of large effect size in all of the three comparisons of densitometric values (**Figure 3** and **Table 3**). Correspondingly, the power estimates for the conducted *t*-tests was constantly >80%, so that the inclusion of additional replicates should not alter the results. In line with this expectation, *t*-tests confirmed a significant down-regulation of protein expression after addition of a third biological replicate (III), thus increasing sample sizes to $N = 3$ and $M = 9$ for CDH4 and MSN, and to $N = 3$ and $M = 6$ for BACE2 (**Figure 3** and **Table 3**). We interpreted these findings as a confirmation that SH-SY5Y cells translated different transcript amounts of FOXP2 targets into corresponding protein quantities. The findings further demonstrated that large effect size and high power values appeared to be reliable predictors of the

TABLE 3 | Densitometric analyses of Western blots: CDH4, MSN, and BACE2 abundance in SH-SY5Y cells overexpressing human *FOXP2* relative to cells overexpressing non-human primate *FOXP2*.

	Overexpression of														
	hsa*FOXP2*			ptr*FOXP2*			mmu*FOXP2*			cja*FOXP2*					
Protein	**I**	**II**	**III**	**I**	**II**	**III**	**I**	**II**	**III**	**I**	**II**	**III**	**FDR *t*-test**	***r***	**Power**
CDH4	0.431	0.650	–	0.952	1.171	–	1.018	1.045	–	1.336	1.213	–	<0.01	0.861	0.976
	0.431	0.650	0.514	0.952	1.171	0.960	1.018	1.045	2.499	1.336	1.213	2.691	<0.05	–	–
MSN	0.051	0.116	–	0.695	0.728	–	2.046	1.694	–	2.562	2.228	–	<0.05	0.775	0.822
	0.051	0.116	0.077	0.695	0.728	0.595	2.046	1.694	1.759	2.562	2.228	2.204	<0.001	–	–
BACE2	0.358	0.348	–	0.749	0.731	–	1.071	0.989	–	–	–	–	<0.001	0.900	0.958
	0.358	0.348	0.344	0.749	0.731	0.974	1.071	0.989	1.164	–	–	–	<0.05	–	–

*Two and three biological replicates per condition (I–III) were included in t-tests. Values were corrected for β-actin levels and normalized for protein levels of the respective protein in cells carrying empty vector. See **Figure 3** for representative Western blots. cja, marmoset (Callithrix jacchus); hsa, human (Homo sapiens); mmu, Rhesus monkey (Macaca mulatta); ptr, chimpanzee (Pan troglodytes).*

reproducibility of *t*-test results, even when sample sizes were comparably small. In retrospect, therefore, the sample sizes in the transcriptome analyses seemed acceptable.

Mapping of FOXP2-Binding Motifs and FOXP2-ChIP-seq Reads to Putative Promoter Sequences of New FOXP2 Targets

After having shown differential expression under hsa*FOXP2* control for all 13 new candidate genes we investigated their regulatory sequences. Screening the 5 kb upstream the transcription start of the human orthologs we found numerous matches with publicly available FOXP2-ChIP-seq reads (SRR351544). The same putative promoter sequences additionally contained previously published FOXP2-binding motifs (see Stroud et al., 2006; Vernes et al., 2007; Nelson et al., 2013). The number of matches further increased when extra motifs overrepresented in murine Foxp2 target gene promoters were taken into account (see Vernes et al., 2011). Overall, we detected between seven and 48 FOXP2/Foxp2-binding motifs within the putative human promoter sequences (Supplementary Table 2.3). Furthermore, we observed juxtaposition and overlaps of motifs and the matching positions of FOXP2-ChIP-seq reads in the promoter sequences of all 13 new target genes (see **Figure 4** for *CDH4*, *MSN*, and *BACE2*; see Supplementary Image 3 for the other genes). Thus, the expression of all 13 new candidate genes might be directly regulated by FOXP2. Whether in terms of a direct or indirect regulation through FOXP2 we accepted all 13 genes scrutinized for downstream network reconstruction.

Network Reconstruction, Gene Ontology Enrichment Analysis, and Evolutionary Analysis

For network reconstruction, we merged our 13 new with the 27 reproduced target genes, thus generating an initial sample of 40 genes with empirical evidence for FOXP2/Foxp2-driven expression regulation. In order to reach a meaningful size for network and GO analyses, the STRING server was enabled to add best-supported 40 interactors so that the final dataset contained 80 proteins (**Table 1** and Supplementary Tables 2.4, 2.5). Interestingly, these interactors contained nine additional proteins whose coding genes were previously shown to be FOXP2/Foxp2 targets and/or to associate with singing in male zebra finch brains (Supplementary Table 2.4). Thus, altogether 49 nodes in the network correlated with empirical support for FOXP2/Foxp2-driven and/or songbird song-related expression regulation (nodes with rays in **Figure 5**). Disregarding six genes with only songbird song-related expression regulation a total of 43 nodes in our network associated with experimental evidence for FOXP2/Foxp2-driven expression regulation (**Table 1** and Supplementary Tables 2.1, 2.4). For this reason, we further refer to the network as to the FOXP2-driven network (**Figure 5**).

The number of PPIs was significantly increased relative to the expectation whichever confidence threshold was applied (*FDR* = 0, each; Supplementary Tables 2.6, 2.7). Fifty-three percent of the interactions were recognized with at least medium confidence (≥0.4). Confidence was still high (≥0.7) in 43% and highest (≥0.9) in 36% of the edges (**Figure 5** and Supplementary Table 2.7). Self-interactions were not detected. Six of the proteins were not engaged in any interaction. The remaining 74 proteins were constituents of the largest connected component (LCC), thereby having 11.342 PPI partners on average (see **Figure 5**). With 36 PPIs, the chaperone HSP90AA1 was the most connected protein in the LCC. Out of the new FOXP2 targets, MSN was the only one with an above-average node degree (= 15; **Figure 5** and Supplementary Table 2.6).

Kinases with high node degrees such as LRRK2 and Janus kinases JAK1-3 but also above-average connected PIM1 and average-connected ROCK1 pointed to a general involvement of our network in the regulation of protein activity. The same is true for ROCK1's highly connected upstream regulator RHOA, and for the phosphatase PTPRQ. Also the regulation of conductivity was represented by our network, namely through CFTR and GABRE (compare **Figure 5**; see Discussion for detailed protein functions). Additional functional implications emerged when testing our 80 protein sample for the enrichment

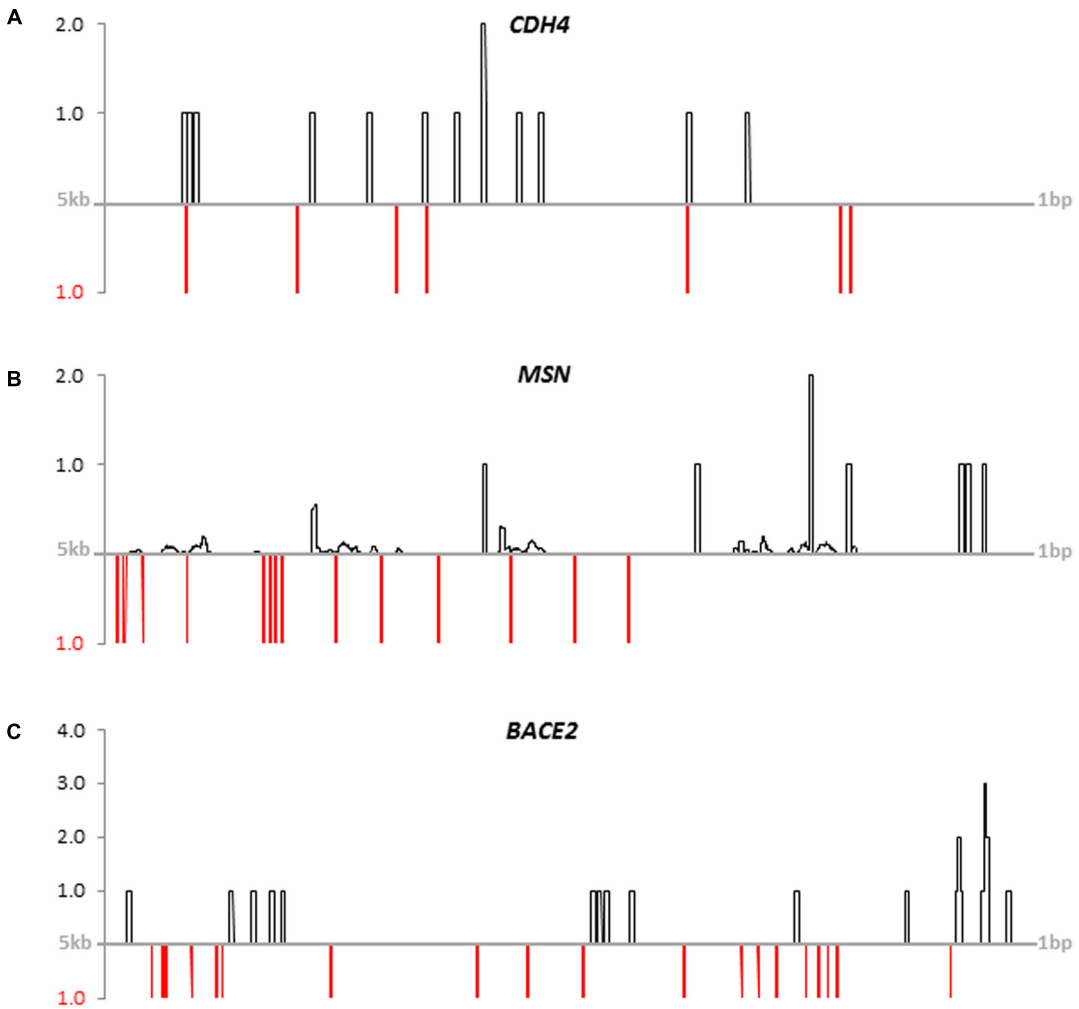

FIGURE 4 | Coverage of publicly available FOXP2-ChIP-seq reads (black lines) and FOXP2-binding motifs (red lines) on putative promoter sequences. **(A)** *CDH4*, **(B)** *MSN,* and **(C)** *BACE2*. Putative promoter sequences of human genes spanned 5 kb upstream of the transcription start sites. FOXP2-ChIP-seq reads were down-loaded from NCBI's GEO database (GSM803353: SRR351544). Hits were normalized for the genome-wide background (GRCh38.p7). See Supplementary Table 2.3 for sequence IDs and motifs. Mapping results for the other eleven new FOXP2 targets are given in Supplementary Image 3.

of GO terms (STRING). Applying a 1% FDR, 153 biological process GOs were overrepresented in our sample relative to the genome-wide background (**Figure 5** and Supplementary Table 2.8). When individual terms were combined to larger entities, cellular signaling and communication appeared as the largest category (number of GO terms = 59; **Figure 6** and Supplementary Table 2.8). This category contained members of the JAK/STAT cascade (statins, Janus kinases, and SOCS5) as well as MSN and EZR as constituents of the ezrin–radixin–moesin complex (ERM). Also cell–cell adhesion-mediating cadherins (CDH4, CDH11) were sorted into this category. Twenty-five GOs demonstrated importance for metabolic and catabolic processes as illustrated by ZDDH3, KEAP1, and LRRK2. Seventeen GOs reflected a strong involvement in transcriptional control (**Figure 6**). The latter category included transcriptionally active proteins like MAFF, NFATC1, and TBX22 as well as proteins encoded by the new FOXP2 targets *NURR1*, *PHOX2B*, *FOXL1*, and *SEBOX*. High relevance for post-transcriptional expression regulation was suggested by altogether eleven respective GOs. Proteins acting in ribosome recruitment (EIF4E, EIF4G1, and PABPC1) fell under this category. The same applied to highly connected DICER1, TARBP2, TRNC6A-C, and four RISC members (EIF2C1-4) which conjointly function in gene silencing. Actually, terms relating to gene silencing received the highest support from GO enrichment analysis (Supplementary Table 2.8). Five mitochondrial ribosomal proteins pointed to an engagement in protein synthesis as an additional layer of post-transcriptional expression regulation. Twenty-nine GOs indicated increased pertinence for development and cellular differentiation, migration, and motility. Notably, 10 out of these 29 GOs were directly relating to nervous system development and to neuron differentiation, projection, morphogenesis (inclusively axonogenesis and neurotrophin signaling) and survival (**Figure 6**). The 26 proteins matching

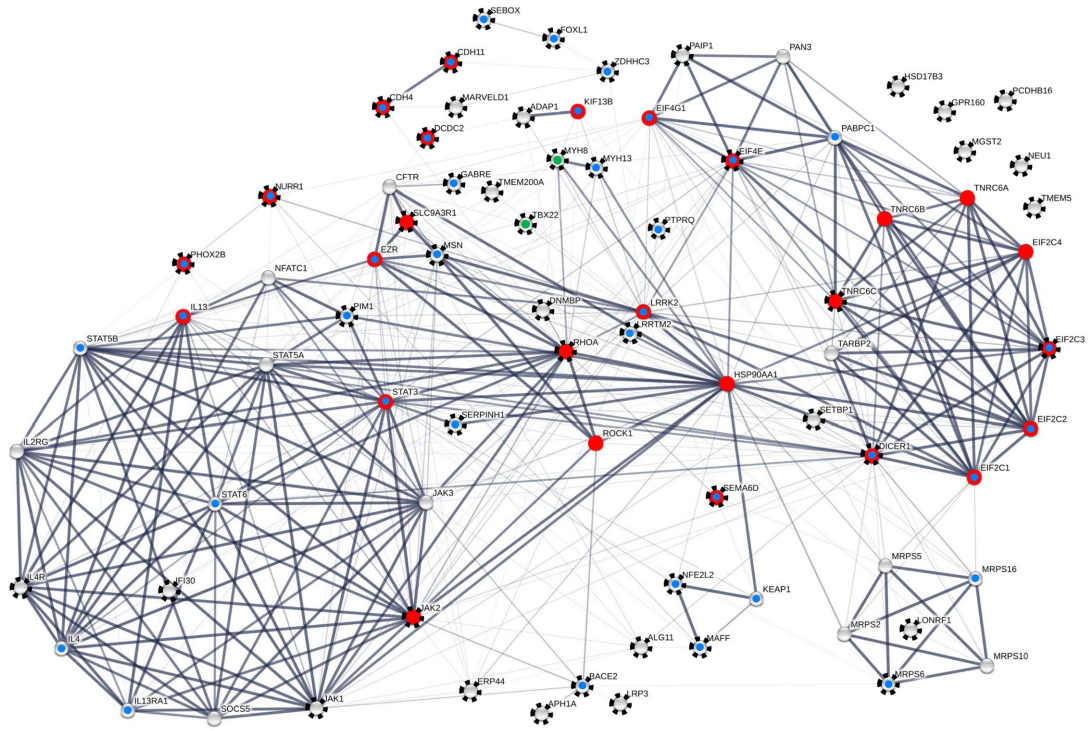

FIGURE 5 | FOXP2-driven protein–protein interaction (PPI) network including 80 proteins. Seventy-four nodes are contained in the largest connected component (LCC). Black rays highlight 49 proteins with empirical evidence for FOXP2/Foxp2-driven and/or songbird-song-related expression regulation from the present and previous analyses (see **Tables 2**, **3** as well as Supplementary Tables 2.1, 2.4 for details). Red dots highlight proteins that matched with neuron-related GO terms in enrichment analysis (see Supplementary Table 2.8). Blue dots indicate nodes whose implication in neuronal and neural functions and/or diseases and disorders is detailed in the Discussion. This is a conservative estimate as exemplified by ERP44 which might have neural relevance (see Discussion) but is not categorized as such in this scheme. Green dots refer to an involvement in trismus-pseudocamptodactyly (MYH8) and X-linked cleft palate and ankyloglossia (TBX22). Proteins in the LCC have 11.342 direct interactors (node degree) on average. Thickness of edges correlates with confidence scores ≥0.90, ≥0.7, ≥0.4, and ≥0.15. The clustering coefficient varied between 0.616 and 0.831 depending on the confidence threshold applied. The network was constructed with the aid of STRING v. 10.0 and analyzed with the aid of Cytoscape v. 3.2.1 and the NetworkAnalyzer plugin. For individual node degrees and additional network statistics see Supplementary Tables 2.6, 2.7.

these "nervous system terms" are highlighted by red dots in **Figure 5** (compare Supplementary Table 2.8).

For assessing the impact of the newly detected FOXP2 targets we repeated network and GO enrichment analyses under exclusion of the respective 13 proteins, thus starting with the 27 reproduced loci only. After addition of 40 interactors STRING again detected significantly more nodes than expected, no matter which confidence threshold was applied (Supplementary Tables 3.1, 3.2). About 82% of the previously recognized enriched GO terms were also reproduced. However, with the exception of a single GO term (neurotrophin TRK receptor signaling pathway) there was no enrichment of terms literally relating to neuronal relevance anymore. In particular, terms containing the words "neuron" or "axonogenesis" were not enriched in the 67 protein sample (Supplementary Table 3.3). Thus, the inclusion of the new FOXP2 targets significantly affected the results of GO enrichment analysis.

Lastly, we analyzed the sequence evolution of the 80 protein sample on the basis of 59 protein-coding genes for which the respective values were available at the time of the study (ENSEMBL). Taking dN/dS as a measure we found overall similar evolutionary rates in the Rhesus monkey–human and Rhesus monkey–chimpanzee comparison. This was evidenced at the level of mean dN/dS values (0.202 *versus* 0.200, respectively) as well as medians (0.148 *versus* 0.141, respectively; $P = 0.957$, MWU test). The single dN/dS values were all <1.0 (Supplementary Table 2.9), thus illustrating that negative selection and hence selection against aa exchanges prevailed in the evolution of the present FOXP2-driven network.

DISCUSSION

Comparing human neuronal cells (SH-SY5Y) stably overexpressing species-specific primate *FOXP2* cDNAs, we detected 40 genes with differential expression levels in response to hsa*FOXP2* overexpression. We refer to 27 of these genes as to reproduced FOXP2 targets as they have been already reported to show FOXP2/Foxp2-driven and/or songbird sing-related expression regulation in several reference studies (Spiteri et al., 2007; Vernes et al., 2007, 2011; Enard et al., 2009; Konopka et al., 2009; Hilliard et al., 2012). The remaining 13 genes with

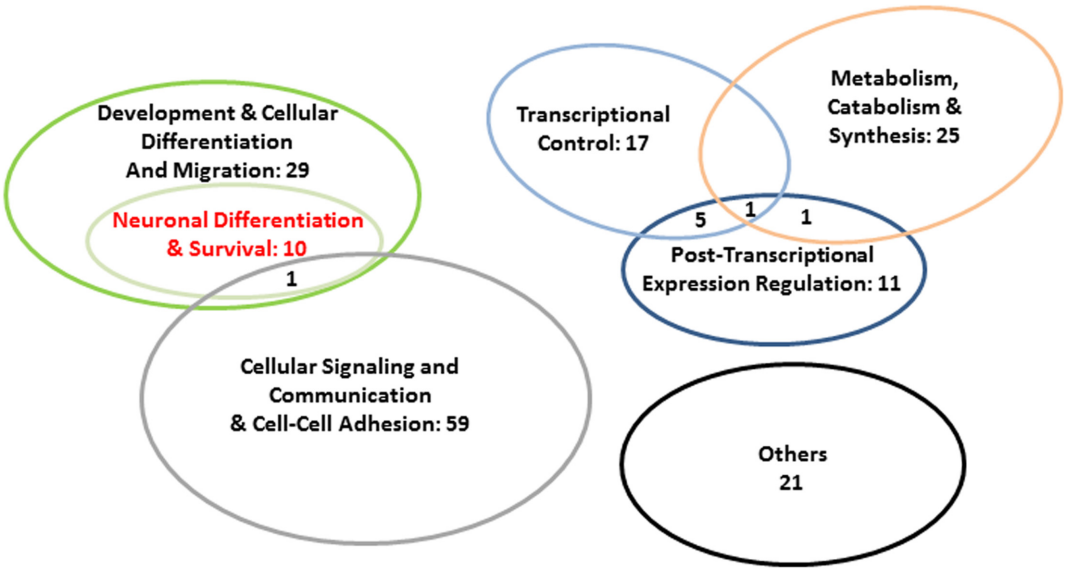

FIGURE 6 | Abundance of super-ordinate categories of the enriched biological process GOs in our 80 protein sample. GO enrichment analysis was carried out with STRING v. 10.0 (FDR < 0.01). For detailed results of GO analysis, see Supplementary Table 2.8.

differential expression levels controlled by hsa*FOXP2* did not show significantly differential regulation in any of the references and hence are termed new FOXP2 targets herein.

In support of the validity of the findings, *post hoc* analyses revealed that the recognition of transcriptional changes under hsa*FOXP2* control associated with acceptable power (>80%) of the conducted *t*-tests. This might be surprising on the first sight, considering that mRNA-based measurements involved comparably few cell lines modeling the human and non-human conditions, with a total sample size of mostly 8 and exceptionally 6 (**Table 2** and Supplementary Table 2.1). However, such high power estimates fully agree with the results of a simulation study which demonstrated that *t*-tests can reach acceptable power despite small sample sizes ($N = 2$; $M = 5$; thus, with a total sample size of 7), when the corresponding effect sizes are high (de Winter, 2013). The precondition of large effect size was indeed fulfilled in present transcriptome analyses (**Table 2** and Supplementary Table 2.1). As high power estimates suggest that the alternative hypothesis of unequal means is true, the inclusion of additional biological replicates should not have altered the results in present transcriptome analyses (see Cohen, 1988; Open Science Collaboration, 2012) – an assessment which we found confirmed for a selection of proteins encoded by new FOXP2 targets (**Table 3**). Therefore, it seemed justifiable to us to take all 40 genes which showed differential transcription under hsa*FOXP2* control as a starting sample for network reconstruction and evolutionary analysis.

The resulting FOXP2-driven network contained altogether 80 proteins. Matching the newly added interactors with the reference studies increased the number of nodes with FOXP2/Foxp2-driven and/or songbird song-related expression regulation in the network to a total of 49 (nodes with rays in **Figure 5**). Forty-three of them correlated with experimental evidence for FOXP2/Foxp2-driven expression regulation from the present and several reference studies (see Results). Considering FOXP2's role in impairment of verbal communication (see Introduction), our FOXP2-driven network might have played a contributory role in human evolution, potentially even in the acquisition of speech and language (**Figures 1**, **5**). However, adaptive aa substitutions were apparently of minor importance in this context as illustrated by prevalent signatures of negative selection, i.e., selection disfavoring aa exchanges, in genes coding for the proteins in our network (Supplementary Table 2.9). The codons of the respective genes might even evolve under stronger constraint than it is the case across the entire genome. Thus, the mean dN/dS of the genes encoding our network members was 0.202 in the Rhesus monkey-human comparison, while the genome-wide mean should be in the range of 0.26 or higher according to the dN and dS values, which Wolf et al. (2009) reported for the same species pair. This could point to an increased functional relevance of the FOXP2-driven network in primate evolution. If true, this seems to be a general principle as we observed similar evolutionary rates of the genes encoding our network members, whether the Rhesus monkey orthologs were compared with their counterparts in humans or common chimpanzee (Supplementary Table 2.9). On the contrary, our data do not suggest noteworthy changes in the evolutionary rates of the members of the FOXP2-driven network on the human branch (compare **Figure 1B**). This does not change the fact that adaptive evolution of some genes influenced hominization as it is the case for FOXP2 itself (Mallick et al., 2016; also, e.g., Enard et al., 2002; Mozzi et al., 2016). Still, present results of RNA-seq, RT-qPCR, and Western blotting rather emphasize the prominent role of expression regulation changes in human evolution (**Tables 2**, **3** and Supplementary Tables 2.1, 2.2), thus lending support to respective postulates from about 30 years ago

(e.g., King and Wilson, 1975). The changes in fine-tuning might have affected cellular signaling and communication, protein and nucleotide metabolism and catabolism, expression regulation, development and cellular differentiation and migration, and especially neuronal differentiation and survival (**Figure 6**). For reasons of space limitations we will focus in the following on the respective implications of the LCC in the present FOXP2-driven PPI network (**Figure 5**).

Cytoskeleton: MSN, the ERM Complex, and the Actin Scaffold

Above-average connected moesin (MSN, also MOE) was expressed at markedly lower levels in SH-SY5Y cells stably transfected with hsa*FOXP2* relative to cells overexpressing non-human primate *FOXP2* cDNAs (**Figures 3B**, **5** and **Tables 2**, **3**). In support of its neuronal relevance, MSN protein levels were previously reported to be down-regulated in fetal Down syndrome brains (Lubec et al., 2001) whereas levels of a *MSN*-binding non-coding RNA (*MSNP1AS*) showed up-regulation in ASD cortices (Kerin et al., 2012). Such associations might reflect the central role of the protein in the remodeling of the cell cortex during mitosis and also its activation by the phosphatase PTEN (see Roubinet et al., 2011; also Georgescu et al., 2014). Hence, PTEN is a critical regulator of neuron development and survival, axonal regeneration, and synaptic plasticity and is implicated in AD, PD, and ALS (Ismail et al., 2012). Recent observations in the mouse model fit in with the presumed functional association of the three proteins. Thus, mislocalization of Pten in murine brain was observed to correlate with down-regulation of *Foxp2* and upregulation of *Msn* (Tilot et al., 2016).

Although MSN seems to function on its own (e.g., Fehon et al., 2010; Roubinet et al., 2011), it is also active through its participation in the ERM complex which additionally contains RDX and the present LCC member EZR (**Figure 5**). The ERM complex bridges the plasma membrane with the actin cytoskeleton, thus being involved in cell–cell recognition, signaling, and motility of diverse cell types as well as the formation and collapse of filopodia, microvilli, and microspikes (e.g., Fehon et al., 2010; Antoine-Bertrand et al., 2011; Roubinet et al., 2011; Georgescu et al., 2014). Accordingly, MSN and EZR matched in the present enrichment analysis with more general GO terms such as movement of cell or subcellular component and membrane to membrane docking (Supplementary Table 2.8). Nonetheless, the functional spectrum of the ERM complex also covers regulation of neurite outgrowth, neuron motility and growth cone morphology (e.g., Antoine-Bertrand et al., 2011 and references therein). These functions obviously substantiate the neuronal relevance of the present FOXP2-driven network – and of its LCC.

Activation of the complex through phosphorylation (pERM) involves three additional members of our LCC (**Figure 5**), i.e., RHOA, RHOA's downstream effector and regulator ROCK1 (Antoine-Bertrand et al., 2011; Tang et al., 2012), and LRRK2 (Parisiadou et al., 2009). ROCK1 is implicated in neuronal regeneration and neuritogenesis (Da Silva et al., 2003; Tang et al., 2012). Moreover, mutations in *LRRK2* gene represent the most frequent genetic cause of late-onset PD (Paisan-Ruiz et al., 2008), possibly due to negative effects on neuritogenesis and survival of nigrostriatal dopaminergic neurons (Han et al., 2008; Xiao et al., 2015). The links between our LCC and neurodegeneration are even more manifest when considering that pERM is required for proteolytic processing of amyloid precursor protein (APP) by α-secretases into the neuroprotective soluble APP ectodomain (sAPPα) (Darmellah et al., 2012). Yet, the alternative cleavage of APP into neurotoxic amyloid-β (Aβ) is catalyzed by a γ-secretase containing present LCC member APH1A (Zhao et al., 2010) (**Figure 5**). Another APP processing pathway involves the aspartic protease encoded by the new FOXP2 target *BACE2* (β-site APP-cleaving enzyme 2; also *CEAP1*, *DRAP*) which resides inside the so-called 'Down critical region' in 21q22.3 (Acquati et al., 2000; O'Brien and Wong, 2011) (**Figures 3C**, **5** and **Table 2**). In line with the expectation for BACE2's ability to cleave APP, certain variants of the coding gene associate with neurodegeneration, namely with AD (Myllykangas et al., 2005). However, the connections of our LCC with APP metabolism are not confined to the cleaving enzymes. Thus, the present LCC also contains the chaperone SERPINH1 (also HSP47) which has been demonstrated to regulate Aβ formation and the growth of amyloid plaques (**Figure 5**) (Bianchi et al., 2011).

Cytoskeleton: Myosins and Microtubules

The two myosin heavy chain proteins in the present LCC, both encoded by new FOXP2 targets (**Figure 5** and **Table 2**), might have an influence on hard tissue development. Thus, *MYH8* levels were found to be up- and down-regulated in retrognathia and prognathia patients, respectively (Oukhai et al., 2011). Furthermore, a recurrent mutation in *MYH8* gene associates with trismus-pseudocamptodactyly syndrome (TPS) involving joint contracture and the inability of patients to open the mouth fully (also Dutch-Kentucky or Hecht-Beal syndrome; e.g., Toydemir et al., 2006). Strikingly, a recent study demonstrated the expression of *Foxp2* (and *Foxp1*) in the developing temporomandibular joint of mice (Cesario et al., 2016). Consequently, disturbed FOXP2-regulated expression of *MYH8* might indeed play a role in the pathogenesis of TPS. Also MYH13 seems to be important for the development of the anatomical basis of speaking. The protein might especially be involved in the acquisition of adult larynx properties as suggested by cease of laryngeal MYH13 expression during or after childhood (Périé et al., 2000). *MYH13* seems further to be involved in the pathogenesis of age-related neurodegenerative disorders (e.g., Cacabelos et al., 2012) and in formal thought disorder, or disorganized speech (Wang et al., 2012).

Besides, our FOXP2-driven network contributes to the organization of the microtubule scaffold. In particular, the new FOXP2 target *DCDC2* codes for a protein (**Figure 5** and **Table 2**) which directs neuronal migration by stabilizing microtubules (e.g., Meng et al., 2005). This functional implication might have importance for human communication skills as suggested by mutations in *DCDC2* that associate with a recessive form of deafness (DFNB66), variation of gray matter volume in language-related brain regions of schizophrenia patients, reading disability (RD), and dyslexia (DYX2) (Meng et al., 2005; Jamadar

et al., 2011; Newbury et al., 2011; Grati et al., 2015). In line with these associations in humans, *DCDC2* is co-expressed in certain regions of the marmoset brain with other speech- and language-related genes like *FOXP2* itself, but also with *ROBO1*, *CMIP*, *KIAA03319*, and *CNTNAP2*. The spatiotemporal overlap includes thalamus and basal ganglia and, especially, substantia nigra pars compacta and pars reticulata (Kato et al., 2014; see also Vernes et al., 2008). Yet, nigrostriatal and thalamocortical-basal ganglia circuits function in voluntary motor control in marmoset (Kato et al., 2014) and dysfunction in humans can lead to oromandibular, lingual, and laryngeal spasms (Colosimo et al., 2010). Thus, *DCDC2* and the co-expressed speech- and language genes exemplify that the study of marmoset can improve our understanding of the molecular and neural basis of human communication. At the same time, *DCDC2* exemplifies that the differences in the communication skills between humans and marmoset might be due to changes in expression levels, which occurred on the human branch (compare **Figure 1B**).

Similar to DCDC2, MARVELD1 has a rather peripheral position in our LCC. Nonetheless, also this protein has importance for the organization of microtubules as demonstrated for the murine ortholog (Zeng et al., 2011). Microtubules are further the basis for the functioning of present LCC member KIF13B (**Figure 5**). The protein moves along microtubules to the tips of neurites where it promotes neurite outgrowth (Yoshimura et al., 2010). Notably, the murine protein has been shown to be a negative regulator of PIK3K/AKT-mediated myelination in central and peripheral nervous system (Noseda et al., 2016). Yet, phosphatidylinositol-mediated signaling was one of the enriched GO terms in our protein sample (Supplementary Table 2.8). Moreover, PIK3K/AKT signaling could also link the new FOXP2 target *PTPRQ* (DFNB84A) (**Table 2**). The gene is another deafness susceptibility locus in our LCC (**Figure 5**) and codes for a phosphatidylinositol phosphatase (e.g., Schraders et al., 2010) which has been implicated in the organization of the actin cytoskeleton again (see, e.g., Nayak et al., 2007).

Transcriptional Regulation: Transcription Factors

A number of proteins in our LCC support FOXP2's previously stated influence on neuronal development and maintenance through downstream transcriptional regulators (**Figures 5**, **6**). Thereby, the transcription factor encoded by the new FOXP2 target *NURR1* (also *NR4A2*, *NOT*) (**Figure 5** and **Table 2**) seems to be of special importance for normal dopaminergic functioning. Thus, stimulation of NURR1 improves behavioral deficits associated with the degeneration of dopamine neurons in PD model mice – an effect which involves enhanced *trans*-repression of neurotoxic pro-inflammatory genes in microglia and increased transcriptional activation of midbrain dopaminergic (mDA) neurons (Kim et al., 2015). *Nurr1* knockout mice even fail to develop dopamine neurons (e.g., Zetterström et al., 1997). Therefore, it is not surprising that several mutations in human *NURR1* coincide with dopamine-related diseases, namely SCZD, Lewy body dementia (LBD), AD, and PD (e.g., Chen et al., 2001; Zheng et al., 2003; Chu et al., 2006). The involvement of the present LCC in neuronal maintenance is also reflected by MAFF (**Figure 5**), i.e., another transcription factor, which has also been implicated in PD (reviewed in Kannan et al., 2012).

Four additional proteins further substantiate FOXP2's effectivity through downstream regulators of transcription (**Figures 5**, **6** and see **Tables 2**, **3** for new and reproduced FOXP2 targets). Corresponding evidence is particularly strong with respect to PHOX2B: Murine Phox2b regulates the differentiation of hindbrain visceral and branchial motor neurons (see Hirsch et al., 2013). *Phox2b* knockout mice even lack the facial motor nucleus which is an important source of Slit ligands for Robo receptor-expressing pontine neurons in wild-type mice (Geisen et al., 2008). Yet, the essentiality of SLIT1/ROBO signaling for neuron migration and axon guidance is well established (see, e.g., Geisen et al., 2008; Boeckx and Benítez-Burraco, 2014a,b; Pfenning et al., 2014), and *SLIT1* belongs to the already known FOXP2 targets (Konopka et al., 2009; Devanna et al., 2014). The second protein out of this group of four, SEBOX is involved in postnatal brain maturation as suggested by corresponding evidence in the mouse model (Cinquanta et al., 2000). Seeing the remarkable up-regulation of *SEBOX* under hsa*FOXP2* control (**Table 2**) the encoded protein might indeed have importance for human brain development and evolution. The third one, FOXL1 could play a role in (mid)brain development as suggested by respective observations in the zebrafish (Nakada et al., 2006). Similarly, the functioning of the transcription factor TBX22 has a morphogenetic dimension: Loss-of-function mutations in the coding gene cause X-linked cleft palate and ankyloglossia, a developmental disorder which decreases the motility of the tongue, thus leading to problems with feeding and speech. The disorder also affects dentition, hearing, and psychological development (Braybrook et al., 2001) Thus, the transcriptional cascades controlled by FOXP2 are essential for neural and neuronal maintenance and development as well as for normal development of the anatomical underpinning of speech.

Transcriptional Regulation: JAK/STAT Signaling

JAK/STAT signaling, represented in the present LCC by highly connected three Janus kinases (JAK1-3) and four statins (STAT3, STAT5A, STAT5B, STAT6) (**Figures 5**, **6**), is commonly connoted with immune reaction (see Supplementary Table 2.8). However, a growing body of data points to a contributory role of the JAK/STAT cascade in the pathogenesis of Down syndrome, neuro-inflammatory diseases, and dopaminergic neurodegeneration (Lee et al., 2016; Qin et al., 2016). In agreement with the symptoms associated with these pathologies, present LCC members STAT3, STAT5B, and STAT6 modulate neuron survival, synaptic plasticity, and neurite outgrowth (Deboy et al., 2006; Georganta et al., 2013; Tyzack et al., 2014).

The JAK/STAT cascade additionally includes interleukins, their receptors, and members of the suppressor of cytokine signaling (SOCS) protein family (also STAT-induced STAT inhibitor family). For example, interaction of Socs5 with Il4r inhibits Il4-dependent activation of Stat6 in the mouse model (Seki et al., 2002), and expression of Il4 can again be induced by Nfatc1 (Monticelli and Rao, 2002). Yet, the respective human

proteins belong to our LCC (**Figure 5**), thereby displaying about average to high connectivity.

Interestingly, the rodent orthologs of IL4 and of the second interleukin in our LCC, IL13, have been implicated in neuron survival, protection, and recovery (Pan et al., 2013; Walsh et al., 2015). IL4 and IL13 further share anti-inflammatory properties (Mori et al., 2016) and their common receptor comprises a subunit, IL13RA1 which has above-average connectivity in our network (**Figure 5**). The coding gene *IL13RA1* resides in the PD susceptibility locus PARK12 and its murine counterpart is expressed in dopaminergic neurons of the ventral tegmental area and the substantia nigra pars compacta (Morrison et al., 2012). Thus, also IL13RA1/Il13ra1 relegate to dopaminergic neurodegeneration.

Confirmation of a JAK/STAT-mediated implication of our network and especially of the LCC in neuroprotection and neurodegeneration comes from HSP90AA1 (also HSP90). Not only that this chaperone had the most direct PIPs in our LCC but HSP90AA1 also interacts with STAT3 in human cells (Sato et al., 2003) (**Figure 5**). This again stabilizes the folding of another protein in our network, i.e., the phosphatase PIM1 (Shen et al., 2014), which once more builds the bridge to neuron survival: Pim1 inhibition rescues Aβ and Tau pathology in murine brain (Velazquez et al., 2016), and inhibition of human PIM1 induces the neuroprotective transcription factor NFE2L2 (also NRF2; McMahon et al., 2014). Yet, NFE2L2 and its inhibitor KEAP1 (see Yamazaki et al., 2015) are further components of the present LCC (**Figure 5**).

Post-transcriptional Expression Regulation

The present network and its LCC are additionally linked to gene silencing, namely through average- to highly connected proteins such as TARBP2, DICER1, and EIF2C1-4 (also AGO1-4) (**Figures 5**, **6**; see also Vernes et al., 2011). This pathway will affect the expression of a wide range of indirect FOXP2 targets but also gene silencing of *FOXP2* itself is in the range of possible. In support of the latter, *Foxp2* showed premature expression in the embryonic neocortex of mice whose *Dicer* gene was knocked out (Clovis et al., 2012; but see Haesler et al., 2007). Whether in the one direction or just the other way around balanced gene silencing is certainly important for normal development. This is demonstrated by deletions involving *EIF2C1* and *EIF2C3* which were recently reported to associate with facial dysmorphologies, speech and motor delay, and also with moderate intellectual disability (Tokita et al., 2015). In addition, DICER1 and EIF2C2 appear to be connected with the pathogenesis of Huntington's disease (HD; e.g., Banez-Coronel et al., 2012; see also Batassa et al., 2010), thus providing an additional link between our LCC and dopamine imbalance (Chen et al., 2013).

The regulatory subunit PAN3 of the poly(A) nuclease PAN suggests an influence of our LCC on post-transcriptional expression regulation through mRNA decay (**Figures 5**, **6**) (Uchida et al., 2004). The LCC is additionally pertinent to ribosome recruitment (compare, e.g., Vernes et al., 2011), as exemplified by PAIP1, PAIP1-binding PABPC1, and the highly connected eukaryotic translation initiation factors EIF4E and EIF4G1 (e.g., Craig et al., 1998) (**Figure 5**). Yet, also ribosome recruitment is certainly vital for normal neural functioning as illustrated by late-onset motor incoordination in model mice upon sequestration of Pabpc1 (Damrath et al., 2012). Accordingly, mutations in *EIF4G1* have been recognized to associate with PD, and deregulation of *EIF4E* activity seems to increase susceptibility to autism (AUTS19) (Neves-Pereira et al., 2009; Chartier-Harlin et al., 2011).

Five moderately connected mitochondrial ribosomal subunits (MRPSs) underline that our LCC contributes to mitochondrial protein synthesis (**Figure 5**). The significance of this process for neuronal survival is exhibited by differential *MRPS6* levels in PD patients relative to unaffected individuals (Papapetropoulos et al., 2006). Moreover, a mutation in the *MRPS16* gene induces respiratory chain dysfunction with fatal consequences including agenesis of corpus callosum and death (Miller et al., 2004; Emdadul Haque et al., 2008). In further support of an effect of FOXP2 upon nervous system development through mitochondrial translation, murine isoform Foxp2Ex12+ has been localized to mitochondria in Purkinje cells – especially in cellular buds giving rise to dendrites (Tanabe et al., 2012). Yet, Purkinje cells have been reported to show altered synapse plasticity in mice carrying humanized *Foxp2* (Reimers-Kipping et al., 2011).

Mitochondrial translation also builds the bridge to another LCC member, namely ERP44 (also ERp44; **Figure 5**). This chaperone regulates, along with other proteins, the association of mitochondria with the endoplasmatic reticulum (ER). The establishment and maintenance of this interface is pivotal for cellular survival due to its influence on lipid transport, energy metabolism, and Ca^{2+} signaling (Hayashi et al., 2009). In particular, the latter implication might involve an inhibitory effect of ERP44 upon inositol-1,4,5-trisphosphate (IP3) receptors as demonstrated in mouse cerebellar microsomes (Higo et al., 2005). Yet, the implication of the LCC in phosphatidylinositol-mediated signaling was already mentioned, and Ca^{2+} release from the ER through IP3 receptors is altered in AD, HD, and ASD patients (see Schmunk et al., 2015 and references therein).

Membrane Conductivity and Cell–Cell Adhesion

Present evidence for differential regulation of *GABRE* under hsa*FOXP2* control corroborates previous findings stressing the importance of GABAergic circuitry for the evolution of speech and language (e.g., Boeckx and Benítez-Burraco, 2014a,b) (**Figure 5** and **Table 2**). *GABRE* shows wide tissue distribution but appropriately spliced mRNA was exclusively detected in the hypothalamic region and hippocampus and, to a much lesser degree, in heart tissue (Whiting et al., 1999). Consequently, *GABRE* might have more importance for nervous system functioning than known to date. Besides GABRE, it is ZDHHC3 (also GODZ) which links our LCC with GABAergic wiring (**Figure 5**). The Golgi-specific DHHC zinc finger protein palmitoylates the γ2 subunit of GABA(A) receptors in neurons as demonstrated for the murine brain (Keller et al., 2004). Membrane conductivity is also modulated by present LCC member CFTR (**Figure 5**), which regulates chloride (and HCO3-)

currents (Weyler et al., 1999). Interestingly, CFTR interacts with the abovementioned pERM and with another LCC member, i.e., SLC9A3R1 (also NHERF1) (**Figure 5**) (Alshafie et al., 2014). However, binding of SLC9A3R1 stabilizes the ERM complex and its kinase PTEN (Georgescu et al., 2014), whose neuronal and neural implications have been discussed above.

Importance for nervous system development through cell–cell adhesion has been found for diverse cadherins including CDH4 (also R-cadherin) which is encoded by one of the new FOXP2 targets (**Figures 3A**, **5** and **Table 2**; e.g., Oblander and Brady-Kalnay, 2010). Supporting the neural relevance of these Ca^{2+}-dependent proteins, *CDH4* along with the gene coding for LCC member CDH11 (also OB-cadherin; **Figure 5**) was found to display differential spatial and temporal expression in developing marmoset brain (Matsunaga et al., 2015). In accordance, murine *Cdh4* and *Cdh11* seem to be essential for the association and migration of neurons during embryogenesis (Kimura et al., 1995; Hertel and Redies, 2011). Such relevance might partly reflect their interaction with other members of the cadherin family (e.g., Paulson et al., 2014). For instance, murine Cdh4 interacts with Cdh2 (N-cadherin) whose neuronal relevance is well-established (Matsunami et al., 1993). Moreover, *Cdh11* and *Cdh2* at least have overlapping functions including the regulation of β-catenin abundance and β-catenin-dependent gene expression (Di Benedetto et al., 2010). Yet, *Cdh2* is another Foxp2 target, whose regulation has been shown to affect the detachment of differentiating neurons from the neuroepithelium (e.g., Rousso et al., 2012).

FOXP2's likely influence on neuronal development is further reflected by transmembrane LRRTM2, i.e., another member of the present LCC (**Figure 5**), which presumably regulates synapse formation through neurexin binding (Ko et al., 2009). An involvement in neurite formation and synapse formation is likewise probable for the transmembrane semaphorin SEMA6D (**Figure 5**) as suggested by observations in different model systems (e.g., Leslie et al., 2011). Congruously, the murine gene was previously reported to show Foxp2-driven expression regulation during neurite outgrowth (Vernes et al., 2011). It is thus unsurprising that SEMA6D matched with all neuron-related GO terms that were enriched in the present analysis, despite its peripheral position in our LCC (**Figure 5** and Supplementary Table 2.8).

CONCLUSION

In the present study, we compared expression levels between SH-SY5Y cell lines stably overexpressing human *FOXP2* cDNA with cell lines stably transfected with *FOXP2* cDNAs of marmoset, macaque, and chimpanzee (**Figure 1**). Using RNA-seq, RT-qPCR, and Western blotting, we identified 13 new FOXP2 targets with differential expression levels under hsa*FOXP2* control (**Tables 2**, **3**; also **Figure 3**). The putative promoter sequences of all new target genes contained previously published FOXP2/FOXP2-binding motifs. Multiple matches of publicly available FOXP2-ChIP-seq reads with fragments inside the same promoter sequences additionally pointed to a potential direct binding of FOXP2. Thus, down-regulation of expression might reflect that hsaFOXP2 represses the respective target genes more efficiently than any of the non-human FOXP2s studied. The opposite might be true for transcription of *SEBOX*, the only gene amongst the new targets that showed hsaFOXP2-driven up-regulation. Whether their transcription is directly or indirectly regulated by FOXP2, the detection of 13 new targets denotes that the extent of the FOXP2-driven network is greater than currently known. It is further conceivable that the extent of the FOXP2-driven network was underestimated so far especially at the expense of target genes with moderate or even low transcription rates.

The 13 new FOXP2 targets, along with 27 reproduced ones set the start point for the reconstruction of a PPI network (**Figure 5**). The resulting network contained in total 80 proteins, thereof 43 with confirmed experimental evidence for FOXP2/Foxp2-driven expression regulation. Altogether 49 proteins in the network showed FOXP2/Foxp2-driven and/or songbird song-related expression regulation (**Figure 3**, **Tables 2**, **3**, and Supplementary Tables 2.1, 2.4; see also Spiteri et al., 2007; Vernes et al., 2007, 2011; Hilliard et al., 2012). In-depth literature screening and GO analysis underlined a general pattern showing that FOXP2 is effective also indirectly through signaling cascades and other transcriptionally and post-transcriptionally active proteins (**Figure 6** and Supplementary Table 2.8; also, e.g., Marcus and Fisher, 2003; Konopka et al., 2009). Additional functional domains whose fine-tuning might have had a considerable effect on hominization are as follows: regulation of cellular signaling and communication, protein and nucleotide metabolism and catabolism, as well as cellular migration, differentiation and development inclusively neuronal differentiation and survival (**Figure 6**). In particular, the neural and neuronal relevance of FOXP2 was demonstrated before (see, e.g., Enard et al., 2009; Konopka et al., 2009). However, the present study illustrates that also less connected proteins with only moderate to low expression levels can significantly alter our understanding of FOXP2's role in neural and neuronal development, maintenance, and functioning: Thus, GO terms including the words "neuron" or "axonogenesis" (thus excluding "neurotrophin") only appeared to be enriched as long as the 13 new FOXP2 targets were included (compare Supplementary Tables 2.8, 3.3). Nonetheless, the numerous connections between the present network and neuritogenesis, neuron differentiation, etc. were by no means restricted to the new FOXP2 targets (see Discussion for details).

It is further worthwhile that we identified comparably few genes (see present Supplementary Table 2.1: genes without significant support) that were previously reported as differentially expressed between SH-SY5Y cells overexpressing either human *FOXP2* cDNA or a "chimpanized" variant (*FOXP2*^{chimp}; see Konopka et al., 2009, their Supplementary Table 1). The same applies with respect to an earlier examination of the effect of the two human-specific aa substitutions in mice carrying humanized *Foxp2* (*Foxp2*^{hum}; see Enard et al., 2009; their Figures S8A,B, right panel). On the contrary, the overlap was much higher between the present protein sample and the lists of targets that were identified by FOXP2-ChIP-seq in human tissues and in SH-SY5Y cells stably overexpressing human FOXP2 (Spiteri et al., 2007, their Table 1; Vernes et al., 2007; their Table 1). The

overlap increased when expanding the comparison to Foxp2 targets identified by ChIP-seq in wild type murine brain (Vernes et al., 2011, their Table S1). The number of reproduced loci further rose when genes with songbird song-related expression regulation were considered (Hilliard et al., 2012, their Table S2). These differences in overlap might partially reflect the different size of the gene lists taken as references. Nonetheless, there seems to be a trend displaying that we primarily re-identified genes from the studies that used non-mutated cDNAs rather than mutated ones combining states of two species. From our point of view this supports the suitability of species-specific cDNAs with counterparts in nature for studying FOXP2's role in evolution.

The present study differs from others especially with respect to the phylogenetic concept applied. Yet, this conceptual extension is not only of theoretical value as illustrated by the special case of *PHOX2B*. This gene was already a candidate for FOXP2-mediated expression regulation in a previous study which compared expression levels in SH-SY5Y cells overexpressing human FOXP2 *versus* cells carrying empty vector (Spiteri et al., 2007). Although RT-qPCR indicated down-regulation of transcription in the overexpressing cells the difference was not significant. In contrast, the present approach yielded significant support for down-regulation of *PHOX2B* expression in hsa*FOXP2*-overexpressing cells relative to cells overexpressing ptr*FOXP2* and mmu*FOXP2*. In our opinion this illustrates the usefulness of a phylogenetic approach including at least one additional non-human model besides human and chimpanzee models in order to unmask changes in the fine-tuning of target gene expression that might have importance for human evolution and health.

In this way, we determined multiple connections of the FOXP2-driven network and its LCC to developmental (ASD, SCZD, Down syndrome, agenesis of corpus callosum, trismus-pseudocamptodactyly, ankyloglossia, facial dysmorphology) and neurodegenerative disorders and diseases (AD, PD, HD, LBD, ALS), deafness, and dyslexia (for details, see Discussion). In particular, the links to AD, PD, and HD pathologies but also diverse connections to the affected neuron types and brain regions substantiate the importance of FOXP2 for dopaminergic wiring and neurodegeneration (see Discussion for details; also, e.g., Reimers-Kipping et al., 2011; Hilliard et al., 2012; Devanna et al., 2014; Pfenning et al., 2014; Schreiweis et al., 2014). Moreover, reported communication deficits in at least some cases of AD, PD, HD, LBD, ALS, ASD, SCZD, and Down syndrome (Murray, 2000; Yoder and Warren, 2004; Stephane et al., 2007; Abrahams and Geschwind, 2010; Kupferberg, 2010; Reilly et al., 2010; Ferris and Farlow, 2013) confirm the well-established involvement of FOXP2 in the evolutionary and developmental acquisition of speech and language (see, e.g., Vernes and Fisher, 2009; Bolhuis et al., 2010; Enard, 2011; but see Mallick et al., 2016).

However, the present approach did not only confirm and substantiate previous knowledge. Thus, we were able to delineate new pathways of how human FOXP2 governs neurogenesis, neurite outgrowth, synapse plasticity, neuron migration, and the regulation of conductivity. These involve: (i) transcription regulation through NURR1, PHOX2B, TBX22, SEBOX, and FOXL1, (ii) cadherin-mediated cell–cell adhesion (CDH4, CDH11), (iii) gene silencing through DICER1 and RISC, (iv) JAK/STAT signaling and neuro-inflammation, and (v) the organization of the microtubule (DCDC2, KIF13B), myosin (MYH8, MYH13), and actin cytoskeleton (PTPRQ, MSN and ERM complex). Single interactors of gene silencing, the ERM complex and JAK/STAT signaling also appeared in other FOXP2-directed studies (e.g., RDX in Figure 3 of Konopka et al., 2009; Dicer1 and Jak1 in Table S1 of Vernes et al., 2011). Yet, such implications of FOXP2 seemingly did not emerge with the same clarity before. In this way, we regard also gene silencing, JAK/STAT signaling, and the regulation of the ERM complex as novel FOXP2-driven pathways.

We hope that these novel insights may open up new avenues toward a better understanding of the molecular causes of the aforementioned developmental disorders, of communication deficits and especially of neurodegenerative diseases. With respect to the latter it would be advantageous to further investigate if down-regulation of newly detected FOXP2 targets such as *DCDC2*, *MYH8*, and *MYH13* under hsa*FOXP2* control is due to direct FOXP2-binding. FOXP2-ChIP-qPCR could be a good way to answer this question, and also for validating the expressional differences which we observed in RNA-seq, RT-qPCR, and Western blot analyses. The entire spectrum of techniques could further be applied to transiently transfected SH-SY5Y cells, which overexpress different primate FOXP2 cDNAs. Reproduction of our findings in such cell lines would rule out that inestimable effects of the foreign DNA integrates (pcDNA3-constructs) into the genomes of SH-SY5Y cells have biased our results. This seems especially relevant considering that the integration sites and the number of integrated plasmids can vary between stably transfected cells and their descendants, due to the random integration of plasmids (e.g., Mitin et al., 2001). In genes such as *PHOX2B* and *NURR1* further steps could involve animal studies to verify if their established implication in brain development and maintenance is FOXP2-driven or not. Lastly, in cases where the present study evidenced down-regulated expression at the protein level (CDH4, MSN, BACE2) the next steps could involve the investigation of murine knock-outs against the background of neurodegenerative disease phenotypes. Preliminary data on *Cdh4* seem promising in this respect: A viable knock-out reportedly decreased activity, amongst others (see MGI:99218). However, if this change ultimately reflects changes in *Foxp2* expression or Foxp2 activity and if the behavioral data associate with an alteration in neuronal wiring are questions waiting for an answer.

AUTHOR CONTRIBUTIONS

FO, PK, and AR generated the pcDNA3-*FOXP2* constructs and cultivated, transfected, and characterized HEK293 and SH-SY5Y cells. The same authors carried out immunoblotting and densitometric analysis. BH, UZ, and HH conducted and analyzed RT-qPCR measurements. DR and HH analyzed

RNA-seq data as well as previously published FOXP2-ChIP-seq data, and searched putative target gene promoters for established FOXP2/FOXP2-binding motifs. FB assisted in data analysis. HH conducted network reconstruction, gene ontology analysis, in-depth literature screening, and evolutionary analysis. HH, UZ, FO, and SR conceived the study. HH wrote the manuscript. SR, FO, UZ, DR, and FB co-wrote the manuscript. All authors were involved in the scientific interpretation of the results.

FUNDING

This work was supported by the German Research Foundation (DFG, collaborative research grant SFB 1074/A3), and by the BMBF (research nucleus SyStAR) to FO.

ACKNOWLEDGMENTS

We want to thank S. Schirmer and R. Rittelmann (University Medical Center Ulm, Germany) for excellent technical assistance. Our thanks go further to H. Zischler (Institut für Organismische und Molekulare Evolutionsbiologie, Mainz, Germany) for fruitful discussions. We apologize to all whose contributions could not be cited for reasons of space limitations.

SUPPLEMENTARY MATERIAL

The Supplementary Material for this article can be found online at: http://journal.frontiersin.org/article/10.3389/fncel.2017.00212/full#supplementary-material

REFERENCES

Abrahams, B. S., and Geschwind, D. H. (2010). Connecting genes to brain in the autism spectrum disorders. *Arch. Neurol.* 67, 395–399. doi: 10.1001/archneurol.2010.47

Acquati, F., Accarino, M., Nucci, C., Fumagalli, P., Jovine, L., Ottolenghi, S., et al. (2000). The gene encoding DRAP (BACE2), a glycosylated transmembrane protein of the aspartic protease family, maps to the down critical region. *FEBS Lett.* 468, 59–64. doi: 10.1016/S0014-5793(00)01192-3

Adegbola, A. A., Cox, G. F., Bradshaw, E. M., Hafler, D. A., Gimelbrant, A., and Chess, A. (2015). Monoallelic expression of the human *FOXP2* speech gene. *Proc. Natl. Acad. Sci. U.S.A.* 112, 6848–6854. doi: 10.1073/pnas.1411270111

Alshafie, W., Chappe, F. G., Li, M., Anini, Y., and Chappe, V. M. (2014). VIP regulates CFTR membrane expression and function in Calu-3 cells by increasing its interaction with NHERF1 and P-ERM in a VPAC1- and PKCepsilon-dependent manner. *Am. J. Physiol. Cell. Physiol.* 307, C107–C119. doi: 10.1152/ajpcell.00296.2013

Antoine-Bertrand, J., Ghogha, A., Luangrath, V., Bedford, F. K., and Lamarche-Vane, N. (2011). The activation of ezrin-radixin-moesin proteins is regulated by netrin-1 through Src kinase and RhoA/Rho kinase activities and mediates netrin-1-induced axon outgrowth. *Mol. Biol. Cell* 22, 3734–3746. doi: 10.1091/mbc.E10-11-0917

Banez-Coronel, M., Porta, S., Kagerbauer, B., Mateu-Huertas, E., Pantano, L., Ferrer, I., et al. (2012). A pathogenic mechanism in Huntington's disease involves small CAG-repeated RNAs with neurotoxic activity. *PLoS Genet.* 8:e1002481. doi: 10.1371/journal.pgen.1002481

Batassa, E. M., Costanzi, M., Saraulli, D., Scardigli, R., Barbato, C., Cogoni, C., et al. (2010). RISC activity in hippocampus is essential for contextual memory. *Neurosci. Lett.* 471, 185–188. doi: 10.1016/j.neulet.2010.01.038

Bianchi, F. T., Camera, P., Ala, U., Imperiale, D., Migheli, A., Boda, E., et al. (2011). The collagen chaperone HSP47 is a new interactor of APP that affects the levels of extracellular beta-amyloid peptides. *PLoS ONE* 6:e22370. doi: 10.1371/journal.pone.0022370

Boeckx, C., and Benítez-Burraco, A. (2014a). Globularity and language-readiness: generating new predictions by expanding the set of genes of interest. *Front. Psychol.* 5:1324. doi: 10.3389/fpsyg.2014.01324

Boeckx, C., and Benítez-Burraco, A. (2014b). The shape of the language-ready brain. *Front. Psychol* 5:282. doi: 10.3389/fpsyg.2014.00282

Bolhuis, J. J., Okanoya, K., and Scharff, C. (2010). Twitter evolution: converging mechanisms in birdsong and human speech. *Nat. Rev. Neurosci.* 11, 747–759. doi: 10.1038/nrn2931

Bowers, J. M., and Konopka, G. (2012). The role of the FOXP family of transcription factors in ASD. *Dis. Markers* 33, 251–260. doi: 10.3233/DMA-2012-0919

Braybrook, C., Doudney, K., Marcano, A. C., Arnason, A., Bjornsson, A., Patton, M. A., et al. (2001). The T-box transcription factor gene *TBX22* is mutated in X-linked cleft palate and ankyloglossia. *Nat. Genet.* 29, 179–183. doi: 10.1038/ng730

Bruce, H. A., and Margolis, R. L. (2002). *FOXP2*: novel exons, splice variants, and CAG repeat length stability. *Hum. Genet.* 111, 136–144. doi: 10.1007/s00439-002-0768-5

Cacabelos, R., Martinez, R., Fernandez-Novoa, L., Carril, J. C., Lombardi, V., Carrera, I., et al. (2012). Genomics of dementia: *APOE*- and *CYP2D6*-related pharmacogenetics. *Int. J. Alzheimers Dis.* 2012:518901. doi: 10.1155/2012/518901

Cesario, J. M., Almaidhan, A. A., and Jeong, J. (2016). Expression of forkhead box transcription factor genes Foxp1 and *Foxp2* during jaw development. *Gene Expr. Patterns* 20, 111–119. doi: 10.1016/j.gep.2016.03.001

Chartier-Harlin, M.-C., Dachsel, J. C., Vilarino-Guell, C., Lincoln, S. J., Lepretre, F., Hulihan, M. M., et al. (2011). Translation initiator *EIF4G1* mutations in familial Parkinson disease. *Am. J. Hum. Genet.* 89, 398–406. doi: 10.1016/j.ajhg.2011.08.009

Chen, J. Y., Wang, E. A., Capeda, C., and Levine, M. S. (2013). Dopamine imbalance in Huntington's disease: a mechanism for the lack of behavioral flexibility. *Front. Neurosci.* 7:114. doi: 10.3389/fnins.2013.00114

Chen, Y. H., Tsai, M. T., Shaw, C. K., and Chen, C. H. (2001). Mutation analysis of the human NR4A2 gene, an essential gene for midbrain dopaminergic neurogenesis, in schizophrenic patients. *Am. J. Med. Genet.* 105, 753–757. doi: 10.1002/ajmg.10036

Chu, Y., Le, W., Kompoliti, K., Jankovic, J., Mufson, E. J., and Kordower, J. H. (2006). Nurr1 in Parkinson's disease and related disorders. *J. Comp. Neurol.* 494, 495–514. doi: 10.1002/cne.20828

Cinquanta, M., Rovescalli, A. C., Kozak, C. A., and Nirenberg, M. (2000). Mouse *Sebox* homeobox gene expression in skin, brain, oocytes, and two-cell embryos. *Proc. Natl. Acad. Sci. U.S.A.* 97, 8904–8909. doi: 10.1073/pnas.97.16.8904

Clovis, Y. M., Enard, W., Marinaro, F., Huttner, W. B., and De Pietri Tonelli, D. (2012). Convergent repression of Foxp2 3′UTR by miR-9 and miR-132 in embryonic mouse neocortex: implications for radial migration of neurons. *Development* 139, 3332–3342. doi: 10.1242/dev.078063

Cohen, J. (1988). *Statistical Power Analysis for the Behavioral Sciences*, 2nd Edn. New York, NY: Lawrence Erlbaum Associates.

Colosimo, C., Suppa, A., Fabbrini, G., Bologna, M., and Berardelli, A. (2010). Craniocervical dystonia: clinical and pathophysiological features. *Eur. J. Neurol.* 17(Suppl. 1), 15–21. doi: 10.1111/j.1468-1331.2010.03045.x

Craig, A. W., Haghighat, A., Yu, A. T., and Sonenberg, N. (1998). Interaction of polyadenylate-binding protein with the eIF4G homologue PAIP enhances translation. *Nature* 392, 520–523. doi: 10.1038/33198

Da Silva, J. S., Medina, M., Zuliani, C., Di Nardo, A., Witke, W., and Dotti, C. G. (2003). RhoA/ROCK regulation of neuritogenesis via profilin IIa-mediated control of actin stability. *J. Cell. Biol.* 162, 1267–1279. doi: 10.1083/jcb.200304021

Damrath, E., Heck, M. V., Gispert, S., Azizov, M., Nowock, J., Seifried, C., et al. (2012). ATXN2-CAG42 sequesters PABPC1 into insolubility and induces FBXW8 in cerebellum of old ataxic knock-in mice. *PLoS Genet.* 8:e1002920. doi: 10.1371/journal.pgen.1002920

Darmellah, A., Rayah, A., Auger, R., Cuif, M.-H., Prigent, M., Arpin, M., et al. (2012). Ezrin/radixin/moesin are required for the purinergic P2X7 receptor (P2X7R)-dependent processing of the amyloid precursor protein. *J. Biol. Chem.* 287, 34583–34595. doi: 10.1074/jbc.M112.400010

de Winter, J. C. F. (2013). Using the Student's t-test with extremely small sample sizes. *Pract. Assess. Res. Eval.* 18, 1–12.

Debatisse, M., Toledo, F., and Anglana, M. (2004). Replication initiation in mammalian cells: changing preferences. *Cell Cycle* 3, 19–21. doi: 10.4161/cc.3.1.628

Deboy, C. A., Xin, J., Byram, S. C., Serpe, C. J., Sanders, V. M., and Jones, K. J. (2006). Immune-mediated neuroprotection of axotomized mouse facial motoneurons is dependent on the *IL-4*/STAT6 signaling pathway in CD4(+) T cells. *Exp. Neurol.* 201, 212–224. doi: 10.1016/j.expneurol.2006.04.028

Devanna, P., Middelbeek, J., and Vernes, S. C. (2014). FOXP2 drives neuronal differentiation by interacting with retinoic acid signaling pathways. *Front. Cell. Neurosci.* 8:305. doi: 10.3389/fncel.2014.00305

Di Benedetto, A., Watkins, M., Grimston, S., Salazar, V., Donsante, C., Mbalaviele, G., et al. (2010). N-cadherin and cadherin 11 modulate postnatal bone growth and osteoblast differentiation by distinct mechanisms. *J. Cell Sci.* 123, 2640–2648. doi: 10.1242/jcs.067777

Emdadul Haque, M., Grasso, D., Miller, C., Spremulli, L. L., and Saada, A. (2008). The effect of mutated mitochondrial ribosomal proteins S16 and S22 on the assembly of the small and large ribosomal subunits in human mitochondria. *Mitochondrion* 8, 254–261. doi: 10.1016/j.mito.2008.04.004

Enard, W. (2011). FOXP2 and the role of cortico-basal ganglia circuits in speech and language evolution. *Curr. Opin. Neurobiol.* 21, 415–424. doi: 10.1016/j.conb.2011.04.008

Enard, W., Gehre, S., Hammerschmidt, K., Holter, S. M., Blass, T., Somel, M., et al. (2009). A humanized version of Foxp2 affects cortico-basal ganglia circuits in mice. *Cell* 137, 961–971. doi: 10.1016/j.cell.2009.03.041

Enard, W., Przeworski, M., Fisher, S. E., Lai, C. S. L., Wiebe, V., Kitano, T., et al. (2002). Molecular evolution of *FOXP2*, a gene involved in speech and language. *Nature* 418, 869–872. doi: 10.1038/nature01025

Fan, H.-C., Ho, L.-I., Chi, C.-S., Chen, S.-J., Peng, G.-S., Chan, T.-M., et al. (2014). Polyglutamine (PolyQ) diseases: genetics to treatments. *Cell Transplant.* 23, 441–458. doi: 10.3727/096368914X678454

Faul, F., Erdfelder, E., Buchner, A., and Lang, A. G. (2009). Statistical power analyses using G*Power 3.1: tests for correlation and regression analyses. *Behav. Res. Methods* 41, 1149–1160. doi: 10.3758/BRM

Fehon, R. G., McClatchey, A. I., and Bretscher, A. (2010). Organizing the cell cortex: the role of ERM proteins. *Nat. Rev. Mol. Cell Biol.* 11, 276–287. doi: 10.1038/nrm2866

Ferris, S. H., and Farlow, M. (2013). Language impairment in Alzheimer's disease and benefits of acetylcholinesterase inhibitors. *Clin. Interv. Aging* 8, 1007–1014. doi: 10.2147/CIA.S39959

French, C. A., Groszer, M., Preece, C., Coupe, A.-M., Rajewsky, K., and Fisher, S. E. (2007). Generation of mice with a conditional *Foxp2* null allele. *Genesis* 45, 440–446. doi: 10.1002/dvg.20305

Geisen, M. J., Di Meglio, T., Pasqualetti, M., Ducret, S., Brunet, J.-F., Chedotal, A., et al. (2008). *Hox* paralog group 2 genes control the migration of mouse pontine neurons through slit-robo signaling. *PLoS Biol.* 6:e142. doi: 10.1371/journal.pbio.0060142

Georganta, E.-M., Tsoutsi, L., Gaitanou, M., and Georgoussi, Z. (2013). δ-opioid receptor activation leads to neurite outgrowth and neuronal differentiation via a STAT5B-Gαi/o pathway. *J. Neurochem.* 127, 329–341. doi: 10.1111/jnc.12386

Georgescu, M.-M., Cote, G., Agarwal, N. K., and White, C. L. (2014). NHERF1/EBP50 controls morphogenesis of 3D colonic glands by stabilizing PTEN and ezrin-radixin-moesin proteins at the apical membrane. *Neoplasia* 16, 365–374.e2. doi: 10.1016/j.neo.2014.04.004

Grati, M., Chakchouk, I., Ma, Q., Bensaid, M., Desmidt, A., Turki, N., et al. (2015). A missense mutation in DCDC2 causes human recessive deafness DFNB66, likely by interfering with sensory hair cell and supporting cell cilia length regulation. *Hum. Mol. Genet.* 24, 2482–2491. doi: 10.1093/hmg/ddv009

Haesler, S., Rochefort, C., Georgi, B., Licznerski, P., Osten, P., and Scharff, C. (2007). Incomplete and inaccurate vocal imitation after knockdown of *FoxP2* in songbird basal ganglia nucleus Area X. *PLoS Biol.* 5:e321. doi: 10.1371/journal.pbio.0050321

Haesler, S., Wada, K., Nshdejan, A., Morrisey, E. E., Lints, T., Jarvis, E. D., et al. (2004). *FoxP2* expression in avian vocal learners and non-learners. *J. Neurosci.* 24, 3164–3175. doi: 10.1523/JNEUROSCI.4369-03.2004

Hall, T. A. (1999). BioEdit: a user-friendly biological sequence alignment editor and analysis program for Windows 95/98/NT. *Nucl. Acids Symp. Ser.* 41, 95–98.

Han, B.-S., Iacovitti, L., Katano, T., Hattori, N., Seol, W., and Kim, K.-S. (2008). Expression of the LRRK2 gene in the midbrain dopaminergic neurons of the substantia nigra. *Neurosci. Lett.* 442, 190–194. doi: 10.1016/j.neulet.2008.06.086

Hayashi, T., Rizzuto, R., Hajnoczky, G., and Su, T.-P. (2009). MAM: more than just a housekeeper. *Trends Cell Biol.* 19, 81–88. doi: 10.1016/j.tcb.2008.12.002

Hertel, N., and Redies, C. (2011). Absence of layer-specific cadherin expression profiles in the neocortex of the reeler mutant mouse. *Cereb. Cortex* 21, 1105–1117. doi: 10.1093/cercor/bhq183

Higo, T., Hattori, M., Nakamura, T., Natsume, T., Michikawa, T., and Mikoshiba, K. (2005). Subtype-specific and ER lumenal environment-dependent regulation of inositol 1,4,5-trisphosphate receptor type 1 by ERp44. *Cell* 120, 85–98. doi: 10.1016/j.cell.2004.11.048

Hilliard, A. T., Miller, J. E., Fraley, E. R., Horvath, S., and White, S. A. (2012). Molecular microcircuitry underlies functional specification in a basal ganglia circuit dedicated to vocal learning. *Neuron* 73, 537–552. doi: 10.1016/j.neuron.2012.01.005

Hirsch, M.-R., d'Autreaux, F., Dymecki, S. M., Brunet, J.-F., and Goridis, C. (2013). A Phox2b:FLPo transgenic mouse line suitable for intersectional genetics. *Genesis* 51, 506–514. doi: 10.1002/dvg.22393

Ismail, A., Ning, K., Al-Hayani, A., Sharrack, B., and Azzouz, M. (2012). *PTEN*: a molecular target for neurodegenerative disorders. *Transl. Neurosci.* 3, 132–142. doi: 10.2478/s13380-012-0018-9

Jamadar, S., Powers, N. R., Meda, S. A., Gelernter, J., Gruen, J. R., and Pearlson, G. D. (2011). Genetic influences of cortical gray matter in language-related regions in healthy controls and schizophrenia. *Schizophr. Res.* 129, 141–148. doi: 10.1016/j.schres.2011.03.027

Jiang, H., and Wong, W. H. (2008). SeqMap: mapping massive amount of oligonucleotides to the genome. *Bioinformatics* 24, 2395–2396. doi: 10.1093/bioinformatics/btn429

Kannan, M. B., Solovieva, V., and Blank, V. (2012). The small MAF transcription factors MAFF, MAFG and MAFK: current knowledge and perspectives. *Biochim. Biophys. Acta* 1823, 1841–1846. doi: 10.1016/j.bbamcr.2012.06.012

Kato, M., Okanoya, K., Koike, T., Sasaki, E., Okano, H., Watanabe, S., et al. (2014). Human speech- and reading-related genes display partially overlapping expression patterns in the marmoset brain. *Brain Lang.* 133, 26–38. doi: 10.1016/j.bandl.2014.03.007

Keller, C. A., Yuan, X., Panzanelli, P., Martin, M. L., Alldred, M., Sassoe-Pognetto, M., et al. (2004). The γ2 subunit of GABA(A) receptors is a substrate for palmitoylation by GODZ. *J. Neurosci.* 24, 5881–5891. doi: 10.1523/JNEUROSCI.1037-04.2004

Kerin, T., Ramanathan, A., Rivas, K., Grepo, N., Coetzee, G. A., and Campbell, D. B. (2012). A noncoding RNA antisense to moesin at 5p14.1 in autism. *Sci. Transl. Med.* 4:128ra40. doi: 10.1126/scitranslmed.3003479

Kim, C.-H., Han, B.-S., Moon, J., Kim, D.-J., Shin, J., Rajan, S., et al. (2015). Nuclear receptor Nurr1 agonists enhance its dual functions and improve behavioral deficits in an animal model of Parkinson's disease. *Proc. Natl. Acad. Sci. U.S.A.* 112, 8756–8761. doi: 10.1073/pnas.1509742112

Kimura, Y., Matsunami, H., Inoue, T., Shimamura, K., Uchida, N., Ueno, T., et al. (1995). Cadherin-11 expressed in association with mesenchymal morphogenesis in the head, somite, and limb bud of early mouse embryos. *Dev. Biol.* 169, 347–358. doi: 10.1006/dbio.1995.1149

King, M. C., and Wilson, A. C. (1975). Evolution at two levels in humans and chimpanzees. *Science* 188, 107–116. doi: 10.1126/science.1090005

Ko, J., Fuccillo, M. V., Malenka, R. C., and Sudhof, T. C. (2009). LRRTM2 functions as a neurexin ligand in promoting excitatory synapse formation. *Neuron* 64, 791–798. doi: 10.1016/j.neuron.2009.12.012

Konopka, G., Bomar, J. M., Winden, K., Coppola, G., Jonsson, Z. O., Gao, F., et al. (2009). Human-specific transcriptional regulation of CNS development genes by FOXP2. *Nature* 462, 213–217. doi: 10.1038/nature08549

Kupferberg, G. (2010). Language in schizophrenia part 1: an introduction. *Lang. Linguist. Compass.* 4, 576–589. doi: 10.1111/j.1749-818X.2010.00216.x

Lee, H.-C., Tan, K.-L., Cheah, P.-S., and Ling, K.-H. (2016). Potential role of JAK-STAT signaling pathway in the neurogenic-to-gliogenic shift in Down syndrome brain. *Neural Plast.* 2016:7434191. doi: 10.1155/2016/7434191

Leslie, J. R., Imai, F., Fukuhara, K., Takegahara, N., Rizvi, T. A., Friedel, R. H., et al. (2011). Ectopic myelinating oligodendrocytes in the dorsal spinal cord as a consequence of altered semaphorin 6D signaling inhibit synapse formation. *Development* 138, 4085–4095. doi: 10.1242/dev.066076

Li, T., Zeng, Z., Zhao, Q., Wang, T., Huang, K., Li, J., et al. (2013). *FoxP2* is significantly associated with schizophrenia and major depression in the Chinese Han population. *World J. Biol. Psychiatry* 14, 146–150. doi: 10.3109/15622975.2011.615860

Livak, K. J., and Schmittgen, T. D. (2001). Analysis of relative gene expression data using real-time quantitative PCR and the 2(-Delta Delta C(T)) Method. *Methods* 25, 402–408. doi: 10.1006/meth.2001.1262

Lubec, B., Weitzdoerfer, R., and Fountoulakis, M. (2001). Manifold reduction of moesin in fetal Down syndrome brain. *Biochem. Biophys. Res. Commun.* 286, 1191–1194. doi: 10.1006/bbrc.2001.5520

Mallick, S., Li, H., Lipson, M., Mathieson, I., Gymrek, M., Racimo, F., et al. (2016). The simons genome diversity project: 300 genomes from 142 diverse populations. *Nature* 538, 201–206. doi: 10.1038/nature18964

Marcus, G. F., and Fisher, S. E. (2003). FOXP2 in focus: what can genes tell us about speech and language? *Trends Cogn. Sci.* 7, 257–262. doi: 10.1016/S1364-6613(03)00104-9

Matsunaga, E., Nambu, S., Oka, M., and Iriki, A. (2015). Complex and dynamic expression of cadherins in the embryonic marmoset cerebral cortex. *Dev. Growth Differ.* 57, 474–483. doi: 10.1111/dgd.12228

Matsunami, H., Miyatani, S., Inoue, T., Copeland, N. G., Gilbert, D. J., Jenkins, N. A., et al. (1993). Cell binding specificity of mouse R-cadherin and chromosomal mapping of the gene. *J. Cell Sci.* 106, 401–409.

McMahon, M., Campbell, K. H., MacLeod, A. K., McLaughlin, L. A., Henderson, C. J., and Wolf, C. R. (2014). HDAC inhibitors increase NRF2-signaling in tumour cells and blunt the efficacy of co-adminstered cytotoxic agents. *PLoS ONE* 9:e114055. doi: 10.1371/journal.pone.0114055

Meng, H., Smith, S. D., Hager, K., Held, M., Liu, J., Olson, R. K., et al. (2005). *DCDC2* is associated with reading disability and modulates neuronal development in the brain. *Proc. Natl. Acad. Sci. U.S.A.* 102, 17053–17058. doi: 10.1073/pnas.0508591102

Miller, C., Saada, A., Shaul, N., Shabtai, N., Ben-Shalom, E., Shaag, A., et al. (2004). Defective mitochondrial translation caused by a ribosomal protein (MRPS16) mutation. *Ann. Neurol.* 56, 734–738. doi: 10.1002/ana.20282

Mitin, N., Ramocki, M. B., Konieczny, S. F., and Taparowsky, E. J. (2001). "Ras regulation of skeletal muscle differentiation and gene expression," in *Methods in Enzymology, Regulators and Effectors of Small GTPases*, Vol. 333, eds W. E. Balch and C. J. Der (New York: Springer), 232–246.

Monticelli, S., and Rao, A. (2002). NFAT1 and NFAT2 are positive regulators of IL-4 gene transcription. *Eur. J. Immunol.* 32, 2971–2978. doi: 10.1002/1521-4141(2002010)32:10<2971::AID-IMMU2971>3.0.CO;2-G

Mori, S., Maher, P., and Conti, B. (2016). Neuroimmunology of the interleukins 13 and 4. *Brain Sci.* 6, E18. doi: 10.3390/brainsci6020018

Morrison, B. E., Marcondes, M. C. G., Nomura, D. K., Sanchez-Alavez, M., Sanchez-Gonzalez, A., Saar, I., et al. (2012). Cutting edge: IL-13Ralpha1 expression in dopaminergic neurons contributes to their oxidative stress-mediated loss following chronic peripheral treatment with lipopolysaccharide. *J. Immunol.* 189, 5498–5502. doi: 10.4049/jimmunol.1102150

Mortazavi, A., Williams, B. A., McCue, K., Schaeffer, L., and Wold, B. (2008). Mapping and quantifying mammalian transcriptomes by RNA-Seq. *Nat. Methods* 5, 621–628. doi: 10.1038/nmeth.1226

Mozzi, A., Forni, D., Clerici, M., Pozzoli, U., Mascheretti, S., Guerini, F. R., et al. (2016). The evolutionary history of genes involved in spoken and written language: beyond *FOXP2*. *Sci. Rep.* 6:22157. doi: 10.1038/srep22157

Murray, L. L. (2000). Spoken language production in Huntington's and Parkinson's diseases. *J. Speech Lang. Hear. Res.* 43, 1350–1366. doi: 10.1044/jslhr.4306.1350

Myllykangas, L., Wavrant-De Vrieze, F., Polvikoski, T., Notkola, I.-L., Sulkava, R., Niinisto, L., et al. (2005). Chromosome 21 *BACE2* haplotype associates with Alzheimer's disease: a two-stage study. *J. Neurol. Sci.* 236, 17–24. doi: 10.1016/j.jns.2005.04.008

Nakada, C., Satoh, S., Tabata, Y., Arai, K.-I., and Watanabe, S. (2006). Transcriptional repressor foxl1 regulates central nervous system development by suppressing shh expression in zebra fish. *Mol. Cell. Biol.* 26, 7246–7257. doi: 10.1128/MCB.00429-06

Nayak, G. D., Ratnayaka, H. S., Goodyear, R. J., and Richardson, G. P. (2007). Development of the hair bundle and mechanotransduction. *Int. J. Dev. Biol.* 51, 597–608. doi: 10.1387/ijdb.072392gn

Nelson, C. S., Fuller, C. K., Fordyce, P. M., Greninger, A. L., Li, H., and DeRisi, J. L. (2013). Microfluidic affinity and ChIP-seq analyses converge on a conserved FOXP2-binding motif in chimp and human, which enables the detection of evolutionarily novel targets. *Nucleic Acids Res.* 41, 5991–6004. doi: 10.1093/nar/gkt259

Neves-Pereira, M., Muller, B., Massie, D., Williams, J. H. G., O'Brien, P. C. M., Hughes, A., et al. (2009). Deregulation of EIF4E: a novel mechanism for autism. *J. Med. Genet.* 46, 759–765. doi: 10.1136/jmg.2009.066852

Newbury, D. F., Paracchini, S., Scerri, T. S., Winchester, L., Addis, L., Richardson, A. J., et al. (2011). Investigation of dyslexia and SLI risk variants in reading- and language-impaired subjects. *Behav. Genet.* 41, 90–104. doi: 10.1007/s10519-010-9424-3

Noseda, R., Guerrero-Valero, M., Alberizzi, V., Previtali, S. C., Sherman, D. L., Palmisano, M., et al. (2016). Kif13b regulates PNS and CNS myelination through the Dlg1 scaffold. *PLoS Biol.* 14:e1002440. doi: 10.1371/journal.pbio.1002440

Oblander, S. A., and Brady-Kalnay, S. M. (2010). Distinct PTPmu-associated signaling molecules differentially regulate neurite outgrowth on E-, N-, and R-cadherin. *Mol. Cell. Neurosci.* 44, 78–93. doi: 10.1016/j.mcn.2010.02.005

O'Brien, R. J., and Wong, P. C. (2011). Amyloid precursor protein processing and Alzheimer's disease. *Annu. Rev. Neurosci.* 34, 185–204. doi: 10.1146/annurev-neuro-061010-113613

Open Science Collaboration. (2012). An open, large-scale, collaborative effort to estimate the reproducibility of psychological science. *Perspect. Psychol. Sci.* 7, 657–660. doi: 10.1177/1745691612462588

Oukhai, K., Maricic, N., Schneider, M., Harzer, W., and Tausche, E. (2011). Developmental myosin heavy chain mRNA in masseter after orthognathic surgery: a preliminary study. *J. Craniomaxillofac. Surg.* 39, 401–406. doi: 10.1016/j.jcms.2010.06.001

Paisan-Ruiz, C., Nath, P., Washecka, N., Gibbs, J. R., and Singleton, A. B. (2008). Comprehensive analysis of LRRK2 in publicly available Parkinson's disease cases and neurologically normal controls. *Hum. Mutat.* 29, 485–490. doi: 10.1002/humu.20668

Palka, C., Alfonsi, M., Mohn, A., Cerbo, R., Guanciali Franchi, P., Fantasia, D., et al. (2012). Mosaic 7q31 deletion involving *FOXP2* gene associated with language impairment. *Pediatrics* 129, e183–e188. doi: 10.1542/peds.2010-2094

Pan, H. C., Yang, C. N., Hung, Y. W., Lee, W. J., Tien, H. R., Shen, C. C., et al. (2013). Reciprocal modulation of C/EBP-α and C/EBP-β by IL-13 in activated microglia prevents neuronal death. *Eur. J. Immunol.* 43, 2854–2865. doi: 10.1002/eji.201343301

Papapetropoulos, S., Ffrench-Mullen, J., McCorquodale, D., Qin, Y., Pablo, J., and Mash, D. C. (2006). Multiregional gene expression profiling identifies MRPS6 as a possible candidate gene for Parkinson's disease. *Gene Expr.* 13, 205–215. doi: 10.3727/000000006783991827

Parisiadou, L., Xie, C., Cho, H. J., Lin, X., Gu, X.-L., Long, C.-X., et al. (2009). Phosphorylation of ezrin/radixin/moesin proteins by LRRK2 promotes the rearrangement of actin cytoskeleton in neuronal morphogenesis. *J. Neurosci.* 29, 13971–13980. doi: 10.1523/JNEUROSCI.3799-09.2009

Paulson, A. F., Prasad, M. S., Thuringer, A. H., and Manzerra, P. (2014). Regulation of cadherin expression in nervous system development. *Cell Adh. Migr.* 8, 19–28. doi: 10.4161/cam.27839

Perelman, P., Johnson, W. E., Roos, C., Seuánez, H. N., Horvath, J. E., Moreira, M. A. M., et al. (2011). A molecular phylogeny of living primates. *PLoS Genet.* 7:e1001342. doi: 10.1371/journal.pgen.1001342

Périé, S., Agbulut, O., St Guily, J. L., and Butler-Browne, G. S. (2000). Myosin heavy chain expression in human laryngeal muscle fibers. A biochemical study. *Ann. Otol. Rhinol. Laryngol.* 109, 216–220. doi: 10.1177/000348940010900218

Pfenning, A. R., Hara, E., Whitney, O., Rivas, M. V., Wang, R., Roulhac, P. L., et al. (2014). Convergent transcriptional specializations in the brains of humans and song-learning birds. *Science* 346:1256846. doi: 10.1126/science.1256846

Qin, H., Buckley, J. A., Li, X., Liu, Y., Fox, T. H., Meares, G. P., et al. (2016). Inhibition of the JAK/STAT pathway protects against α-synuclein-induced neuroinflammation and dopaminergic neurodegeneration. *J. Neurosci.* 36, 5144–5159. doi: 10.1523/JNEUROSCI.4658-15.2016

Reilly, J., Rodriguez, A., Lamy, M., and Neils-Strunjas, J. (2010). Cognition, language, and clinical pathological features of non-Alzheimer's dementias: an overview. *J. Commun. Disord.* 43, 438–452. doi: 10.1016/j.jcomdis.2010.04.011

Reimers-Kipping, S., Hevers, W., Pääbo, S., and Enard, W. (2011). Humanized *Foxp2* specifically affects cortico-basal ganglia circuits. *Neuroscience* 175, 75–84. doi: 10.1016/j.neuroscience.2010.11.042

Roubinet, C., Decelle, B., Chicanne, G., Dorn, J. F., Payrastre, B., Payre, F., et al. (2011). Molecular networks linked by Moesin drive remodeling of the cell cortex during mitosis. *J. Cell Biol.* 195, 99–112. doi: 10.1083/jcb.201106048

Rousso, D. L., Pearson, C. A., Gaber, Z. B., Miquelajauregui, A., Li, S., Portera-Cailliau, C., et al. (2012). Foxp-mediated suppression of N-cadherin regulates neuroepithelial character and progenitor maintenance in the CNS. *Neuron* 74, 314–330. doi: 10.1016/j.neuron.2012.02.024

Sato, N., Yamamoto, T., Sekine, Y., Yumioka, T., Junicho, A., Fuse, H., et al. (2003). Involvement of heat-shock protein 90 in the interleukin-6-mediated signaling pathway through STAT3. *Biochem. Biophys. Res. Commun.* 300, 847–852. doi: 10.1016/S0006-291X(02)02941-8

Schmunk, G., Boubion, B. J., Smith, I. F., Parker, I., and Gargus, J. J. (2015). Shared functional defect in IP(3)R-mediated calcium signaling in diverse monogenic autism syndromes. *Transl. Psychiatry* 5:e643. doi: 10.1038/tp.2015.123

Schraders, M., Oostrik, J., Huygen, P. L. M., Strom, T. M., van Wijk, E., Kunst, H. P. M., et al. (2010). Mutations in *PTPRQ* are a cause of autosomal-recessive nonsyndromic hearing impairment DFNB84 and associated with vestibular dysfunction. *Am. J. Hum. Genet.* 86, 604–610. doi: 10.1016/j.ajhg.2010.02.015

Schreiweis, C., Bornschein, U., Burguiere, E., Kerimoglu, C., Schreiter, S., Dannemann, M., et al. (2014). Humanized Foxp2 accelerates learning by enhancing transitions from declarative to procedural performance. *Proc. Natl. Acad. Sci. U.S.A.* 111, 14253–14258. doi: 10.1073/pnas.1414542111

Seki, Y.-I., Hayashi, K., Matsumoto, A., Seki, N., Tsukada, J., Ransom, J., et al. (2002). Expression of the suppressor of cytokine signaling-5 (SOCS5) negatively regulates IL-4-dependent STAT6 activation and Th2 differentiation. *Proc. Natl. Acad. Sci. U.S.A.* 99, 13003–13008. doi: 10.1073/pnas.202477099

Shen, H., Zhu, H., Song, M., Tian, Y., Huang, Y., Zheng, H., et al. (2014). A selenosemicarbazone complex with copper efficiently down-regulates the 90-kDa heat shock protein HSP90AA1 and its client proteins in cancer cells. *BMC Cancer* 14:629. doi: 10.1186/1471-2407-14-629

Spiteri, E., Konopka, G., Coppola, G., Bomar, J., Oldham, M., Ou, J., et al. (2007). Identification of the transcriptional targets of *FOXP2*, a gene linked to speech and language, in developing human brain. *Am. J. Hum. Genet.* 81, 1144–1157. doi: 10.1086/522237

Stephane, M., Pellizzer, G., Fletcher, C. R., and McClannahan, K. (2007). Empirical evaluation of language disorder in schizophrenia. *J. Psychiatry. Neurosci.* 32, 250–258.

Stroud, J. C., Wu, Y., Bates, D. L., Han, A., Nowick, K., Paabo, S., et al. (2006). Structure of the forkhead domain of FOXP2 bound to DNA. *Structure* 14, 159–166. doi: 10.1016/j.str.2005.10.005

Tanabe, Y., Fujiwara, Y., Matsuzaki, A., Fujita, E., Kasahara, T., Yuasa, S., et al. (2012). Temporal expression and mitochondrial localization of a Foxp2 isoform lacking the forkhead domain in developing Purkinje cells. *J. Neurochem.* 122, 72–80. doi: 10.1111/j.1471-4159.2011.07524.x

Tang, A. T., Campbell, W. B., and Nithipatikom, K. (2012). ROCK1 feedback regulation of the upstream small GTPase RhoA. *Cell. Signal.* 24, 1375–1380. doi: 10.1016/j.cellsig.2012.03.005

Tilot, A. K., Bebek, G., Niazi, F., Altemus, J., Todd, R., Frazier, T. W., et al. (2016). Neural transcriptome of constitutional Pten dysfunction in mice and its relevance to human idiopathic Autism Spectrum Disorder. *Mol. Psychiatry* 21, 118–125. doi: 10.1038/mp.2015.17

Tokita, M. J., Chow, P. M., Mirzaa, G., Dikow, N., Maas, B., Isidor, B., et al. (2015). Five children with deletions of 1p34.3 encompassing *AGO1* and *AGO3*. *Eur. J. Hum. Genet.* 23, 761–765. doi: 10.1038/ejhg.2014.202

Toydemir, R. M., Chen, H., Proud, V. K., Martin, R., van Bokhoven, H., Hamel, B. C. J., et al. (2006). Trismus-pseudocamptodactyly syndrome is caused by recurrent mutation of MYH8. *Am. J. Med. Genet. A* 140, 2387–2393. doi: 10.1002/ajmg.a.31495

Turner, S. J., Hildebrand, M. S., Block, S., Damiano, J., Fahey, M., Reilly, S., et al. (2013). Small intragenic deletion in *FOXP2* associated with childhood apraxia of speech and dysarthria. *Am. J. Med. Genet. A* 161A, 2321–2326. doi: 10.1002/ajmg.a.36055

Tyzack, G. E., Sitnikov, S., Barson, D., Adams-Carr, K. L., Lau, N. K., Kwok, J. C., et al. (2014). Astrocyte response to motor neuron injury promotes structural synaptic plasticity via STAT3-regulated TSP-1 expression. *Nat. Commun.* 5:4294. doi: 10.1038/ncomms5294

Uchida, N., Hoshino, S.-I., and Katada, T. (2004). Identification of a human cytoplasmic poly(A) nuclease complex stimulated by poly(A)-binding protein. *J. Biol. Chem.* 279, 1383–1391. doi: 10.1074/jbc.M309125200

Velazquez, R., Shaw, D. M., Caccamo, A., and Oddo, S. (2016). Pim1 inhibition as a novel therapeutic strategy for Alzheimer's disease. *Mol. Neurodegener.* 11:52. doi: 10.1186/s13024-016-0118-z

Vernes, S. C., and Fisher, S. E. (2009). Unravelling neurogenetic networks implicated in developmental language disorders. *Biochem. Soc. Trans.* 37, 1263–1269. doi: 10.1042/BST0371263

Vernes, S. C., Newbury, D. F., Abrahams, B. S., Winchester, L., Nicod, J., Groszer, M., et al. (2008). A functional genetic link between distinct developmental language disorders. *N. Engl. J. Med.* 359, 2337–2345. doi: 10.1056/NEJMoa0802828

Vernes, S. C., Nicod, J., Elahi, F. M., Coventry, J. A., Kenny, N., Coupe, A.-M., et al. (2006). Functional genetic analysis of mutations implicated in a human speech and language disorder. *Hum. Mol. Genet.* 15, 3154–3167. doi: 10.1093/hmg/ddl392

Vernes, S. C., Oliver, P. L., Spiteri, E., Lockstone, H. E., Puliyadi, R., Taylor, J. M., et al. (2011). Foxp2 regulates gene networks implicated in neurite outgrowth in the developing brain. *PLoS Genet.* 7:e1002145. doi: 10.1371/journal.pgen.1002145

Vernes, S. C., Spiteri, E., Nicod, J., Groszer, M., Taylor, J. M., Davies, K. E., et al. (2007). High-throughput analysis of promoter occupancy reveals direct neural targets of *FOXP2*, a gene mutated in speech and language disorders. *Am. J. Hum. Genet.* 81, 1232–1250. doi: 10.1086/522238

Walsh, J. T., Hendrix, S., Boato, F., Smirnov, I., Zheng, J., Lukens, J. R., et al. (2015). MHCII-independent CD4+ T cells protect injured CNS neurons via IL-4. *J. Clin. Invest.* 125, 699–714. doi: 10.1172/JCI76210

Wang, K.-S., Zhang, Q., Liu, X., Wu, L., and Zeng, M. (2012). PKNOX2 is associated with formal thought disorder in schizophrenia: a meta-analysis of two genome-wide association studies. *J. Mol. Neurosci.* 48, 265–272. doi: 10.1007/s12031-012-9787-4

Weyler, R. T., Yurko-Mauro, K. A., Rubenstein, R., Kollen, W. J., Reenstra, W., Altschuler, S. M., et al. (1999). CFTR is functionally active in GnRH-expressing GT1-7 hypothalamic neurons. *Am. J. Physiol.* 277, C563–C571.

Whiting, P. J., Bonnert, T. P., McKernan, R. M., Farrar, S., Le Bourdelles, B., Heavens, R. P., et al. (1999). Molecular and functional diversity of the expanding GABA-A receptor gene family. *Ann. N. Y. Acad. Sci.* 868, 645–653. doi: 10.1111/j.1749-6632.1999.tb11341.x

Wohlgemuth, S. E., Gorochowski, T. E., and Roubos, J. A. (2013). Translational sensitivity of the *Escherichia coli* genome to fluctuating tRNA availability. *Nucleic Acids Res.* 41, 8021–8033. doi: 10.1093/nar/gkt602

Wolf, J. B. W., Kunstner, A., Nam, K., Jakobsson, M., and Ellegren, H. (2009). Nonlinear dynamics of nonsynonymous (dN) and synonymous (dS)

substitution rates affects inference of selection. *Genome Biol. Evol.* 1, 308–319. doi: 10.1093/gbe/evp030

Xiao, Q., Yang, S., and Le, W. (2015). G2019S LRRK2 and aging confer susceptibility to proteasome inhibitor-induced neurotoxicity in nigrostriatal dopaminergic system. *J. Neural. Transm. (Vienna)* 122, 1645–1657. doi: 10.1007/s00702-015-1438-9

Yamazaki, H., Tanji, K., Wakabayashi, K., Matsuura, S., and Itoh, K. (2015). Role of the Keap1/Nrf2 pathway in neurodegenerative diseases. *Pathol. Int.* 65, 210–219. doi: 10.1111/pin.12261

Yang, Z. (2007). PAML 4: a program package for phylogenetic analysis by maximum likelihood. *Mol. Biol. Evol.* 24, 1586–1591. doi: 10.1093/molbev/mst179

Yoder, P. J., and Warren, S. F. (2004). Early predictors of language in children with and without Down syndrome. *Am. J. Ment. Retard.* 109, 285–300. doi: 10.1352/0895-8017

Yoshimura, Y., Terabayashi, T., and Miki, H. (2010). Par1b/MARK2 phosphorylates kinesin-like motor protein GAKIN/KIF13B to regulate axon formation. *Mol. Cell. Biol.* 30, 2206–2219. doi: 10.1128/MCB.01181-09

Zeng, F., Tian, Y., Shi, S., Wu, Q., Liu, S., Zheng, H., et al. (2011). Identification of mouse MARVELD1 as a microtubule associated protein that inhibits cell cycle progression and migration. *Mol. Cells* 31, 267–274. doi: 10.1007/s10059-011-0037-3

Zetterström, R. H., Solomin, L., Jansson, L., Hoffer, B. J., Olson, L., and Perlmann, T. (1997). Dopamine neuron agenesis in Nurr1-deficient mice. *Science* 276, 248–250. doi: 10.1126/science.276.5310.248

Zhang, J., Webb, D. M., and Podlaha, O. (2002). Accelerated protein evolution and origins of human-specific features: Foxp2 as an example. *Genetics* 162, 1825–1835.

Zhao, G., Liu, Z., Ilagan, M. X. G., and Kopan, R. (2010). γ-secretase composed of PS1/Pen2/Aph1a can cleave notch and amyloid precursor protein in the absence of nicastrin. *J. Neurosci.* 30, 1648–1656. doi: 10.1523/JNEUROSCI.3826-09.2010

Zhao, Y., Liu, X., Sun, H., Wang, Y., Yang, W., and Ma, H. (2015). Contactin-associated proteinlike 2 expression in SHSY5Y cells is upregulated by a *FOXP2* mutant with a shortened polyglutamine tract. *Mol. Med. Rep.* 12, 8162–8168. doi: 10.3892/mmr.2015.4483

Zheng, K., Heydari, B., and Simon, D. K. (2003). A common NURR1 polymorphism associated with Parkinson disease and diffuse Lewy body disease. *Arch. Neurol.* 60, 722–725. doi: 10.1001/archneur.60.5.722

Conflict of Interest Statement: The authors declare that the research was conducted in the absence of any commercial or financial relationships that could be construed as a potential conflict of interest.

frontiers in Molecular Neuroscience

REVIEW
published: 16 May 2017
doi: 10.3389/fnmol.2017.00132

Presynaptic Membrane Receptors Modulate ACh Release, Axonal Competition and Synapse Elimination during Neuromuscular Junction Development

Josep Tomàs†, Neus Garcia*†, Maria A. Lanuza†, Manel M. Santafé†, Marta Tomàs, Laura Nadal, Erica Hurtado, Anna Simó and Víctor Cilleros*

Unitat d'Histologia i Neurobiologia (UHN), Facultat de Medicina i Ciències de la Salut, Universitat Rovira i Virgili, Reus, Spain

During the histogenesis of the nervous system a lush production of neurons, which establish an excessive number of synapses, is followed by a drop in both neurons and synaptic contacts as maturation proceeds. Hebbian competition between axons with different activities leads to the loss of roughly half of the neurons initially produced so connectivity is refined and specificity gained. The skeletal muscle fibers in the newborn neuromuscular junction (NMJ) are polyinnervated but by the end of the competition, 2 weeks later, the NMJ are innervated by only one axon. This peripheral synapse has long been used as a convenient model for synapse development. In the last few years, we have studied transmitter release and the local involvement of the presynaptic muscarinic acetylcholine autoreceptors (mAChR), adenosine autoreceptors (AR) and trophic factor receptors (TFR, for neurotrophins and trophic cytokines) during the development of NMJ and in the adult. This review article brings together previously published data and proposes a molecular background for developmental axonal competition and loss. At the end of the first week postnatal, these receptors modulate transmitter release in the various nerve terminals on polyinnervated NMJ and contribute to axonal competition and synapse elimination.

Keywords: postnatal synapse elimination, axonal competition, acetylcholine release, voltage-dependent calcium channels, muscarinic acetylcholine receptors, protein kinases, TrkB, PKC

OPEN ACCESS

Edited by:
Chen Zhang,
Peking University, China

Reviewed by:
Osvaldo D. Uchitel,
University of Buenos Aires, Argentina
Hyunsoo Shawn Je,
Duke NUS Graduate Medical School, Singapore

***Correspondence:**
Josep Tomàs
josepmaria.tomas@urv.cat
Neus Garcia
mariadelesneus.garcia@urv.cat

†*These authors have contributed equally to this work.*

Received: *07 February 2017*
Accepted: *20 April 2017*
Published: *16 May 2017*

Citation:
Tomàs J, Garcia N, Lanuza MA, Santafé MM, Tomàs M, Nadal L, Hurtado E, Simó A and Cilleros V (2017) Presynaptic Membrane Receptors Modulate ACh Release, Axonal Competition and Synapse Elimination during Neuromuscular Junction Development. Front. Mol. Neurosci. 10:132. doi: 10.3389/fnmol.2017.00132

Abbreviations: ACh, acetylcholine; AR, adenosine receptors; AT, atropine; BDNF, Brain-derived neurotrophic factor; CaC, calphostin C; Che, chelerythrine; CF, climbing fiber; CNTF, Ciliary neurotrophic factor; DAG, diacylglycerol; EPP, evoke endplate potentials; GDNF, Glial cell line-derived neurotrophic factor; mGluR1, glutamate receptor; LAL, Levator auris longus muscle; mAChR, muscarinic acetylcholine receptor; nAChR, nicotinic acetylcholine receptor; MT-3, muscarinic toxin 3; MT-7, muscarinic toxin 7; M_1, M_1-type muscarinic acetylcholine receptor; M_2, M_2-type muscarinic acetylcholine receptor; M_4, M_4-type muscarinic acetylcholine receptor; MET, methoctramine; NIT, nitrendipine; NMJ, neuromuscular junction; NTR, neurotrophin receptors; NT-4, neurotrophin-4; OXO, oxotremorine; PIR, pirenzepine; PKA, protein kinase A; PKC, protein kinase C; PLC, phospholipase C; PC, Purkinje cells; TrkB, tropomyosin-related kinase B receptor; TRO, tropicamide; VDCC, voltage-dependent calcium channels; ω-AGA, ω-agatoxin; ω-CON, ω-conotoxin.

INTRODUCTION

"During the development of the nervous system there is an initial overproduction of synapses" (Lanuza et al., 2014) that promotes wide-ranging connectivity and which is followed by an activity-dependent reduction in their number (Thompson, 1985; Bourgeois and Rakic, 1993). "This refines connectivity and increases specificity" (Nadal et al., 2016). Hebbian competition between nerve endings with different activities (the less active result eliminated) is the fundamental feature of the process which leads to the elimination of half of the contacts produced and the strengthening of the remaining contacts (Fields and Nelson, 1992; Sanes and Lichtman, 1999; Zorumski and Mennerick, 2000). Synaptic contacts are lost throughout the nervous tissues during histogenesis (Bourgeois and Rakic, 1993). In the visual system, thalamic axons detach from cortical cells (Hubel et al., 1977; Huberman, 2007); in the cerebellum, climbing fibers (CFs) disconnect from Purkinje cells (PC; Daniel et al., 1992; Hashimoto and Kano, 2005); in autonomic ganglia, axonal inputs disconnect from ganglionar neurons (Lichtman, 1977); and at the neuromuscular junction (NMJ), motor nerve endings disconnect from muscle cells (Benoit and Changeux, 1975; O'Brien et al., 1978). In some neural circuits a given presynaptic axon type innervates only one postsynaptic cell at the end of the competition process (i.e., only one climbing axon persists over the dendritic arbor of a PC in the cerebellar cortex). However, most neurons were polyinnervated by various axons in the adult and the mechanism of axonal competition and selection of some nerve endings was even more sophisticated.

In newborn animals, skeletal muscle fibers are polyinnervated in the NMJ by several motor axons (Redfern, 1970; Brown et al., 1976; Ribchester and Barry, 1994), but at the end of the competitive interactions between the nerve endings, endplates are innervated by a solitary axon (Benoit and Changeux, 1975; O'Brien et al., 1978; Jansen and Fladby, 1990; Sanes and Lichtman, 1999). This peripheral synapse has long been used as a paradigm for studying the principles of synapse development and function (Keller-Peck et al., 2001; Lanuza et al., 2002; Santafé et al., 2009a; Garcia et al., 2011; Lichtman and Tapia, 2013). There is evidence to suggest that several presynaptic receptors (muscarinic acetylcholine autoreceptors (mAChR), adenosine autoreceptors (AR) and tropomyosin-related kinase B receptor (TrkB)) play an important role by allowing the nerve terminals to communicate in the competition that leads to synapse loss in the NMJ (Santafé et al., 2006; Amaral and Pozzo-Miller, 2012; Nadal et al., 2016). The mAChR may be of particular importance. The involvement of mAChR in the elimination process "may allow direct competitive interaction between nerve endings through differential activity-dependent acetylcholine (ACh) release. The more active endings may directly punish the less active ones or reward themselves" (Nadal et al., 2016). Differences in the amount of activity of the terminal axons in competition but also their timing is important. Asynchronous activity promotes synapse elimination whereas synchronous activity prevents it (Favero et al., 2012). Our results indicate that the weakest nerve endings (those that evoke endplate potentials (EPP) with the least quantal content in dual junctions) have an ACh release inhibition mechanism, based on muscarinic autoreceptors and coupled to protein kinase C (PKC) and voltage-dependent calcium channels (VDCC), that can depress the ACh release capacity in these endings and even contribute to functionally disconnect the synapse (Santafé et al., 2003, 2004, 2007a, 2009a,b; Tomàs et al., 2011). We suggest that this muscarinic "mechanism plays a central role in the elimination of redundant neonatal synapses because functional axonal withdrawal can indeed be temporarily reversed by mAChR, VDCC or PKC block" (Santafé et al., 2007b, 2009a; Tomàs et al., 2011). In addition, M_1, M_2 and M_4 muscarinic subtypes cooperate to favor axonal competition at the end of the first postnatal week and promote the full sequence of axonal loss and synapse elimination shortly thereafter (Nadal et al., 2016).

However, different local effectivenesses and motorneuron activities are key to eventual success or failure, since an axon that fails at one muscle cell can win the competition at another (Keller-Peck et al., 2001), which suggests the participation of other signaling pathways and possible postsynaptic muscle cell-derived factors. Our results suggest that TrkB receptor-mediated, brain derived neurotrophic factor (BDNF) signaling plays this role and cooperates with muscarinic signaling (Tomàs et al., 2011; Nadal et al., 2016, 2017b).

This review article collects and reevaluates previously published data on the local involvement of the presynaptic mAChR and TrkB pathway in ACh release and axonal elimination. We propose a molecular background for developmental axonal loss.

EXPERIMENTAL CONDITIONS

We attempted to characterize the funcional capacity of the various motor axons that are in competition at the polyinnervated NMJ. "The homogeneity of the experimental conditions needs to be carefully defined in a review study such as this one" (Tomàs et al., 2014). For the electrophysological experiments, only *ex vivo Levator auris longus* (LAL) muscles from P6-P7 mice (Swiss mice) or rat (Sprague-Dawley) were studied and the basic procedures have been extensively described (Santafé et al., 2003, 2004, 2009a; Tomàs et al., 2011). Briefly, to prevent stimulation-induced contractions, neonatal muscles were paralyzed with μ-CgTX-GIIB or occasionally cut on either side of the main intramuscular nerve branch. "The nerve was stimulated with increasing intensity from zero until an EPP was observed. If the size and latency of the EPP remained constant as the stimulus was increased, we concluded that the endplate was mono-innervated (*M* endings). In endplates with polyneuronal innervation, increasing the stimulus amplitude caused one or more axons to be recruited, which produced a stepwise increment in the EPP" (Redfern, 1970). Specifically, "with dually innervated fibers (the most affordable polyinnervation condition), a second EPP can appear after the first one when the intensity of the electrical stimulus is increased. This compound EPP is built by recruiting two axons. We calculated the EPP amplitude of the second axon response by subtracting the first EPP amplitude

from the compound EPP" (Garcia et al., 2010b). Usually, these EPPs have different amplitudes because "the size of an EPP is not related to the threshold of the axon" (Santafé et al., 2009a) that produces it. "We refer to the axon terminals that produce these synaptic potentials as the weak (*W*, smallest EPP) and strong (*S*, largest EPP) nerve endings (and their synapses)". In addition, we observed (Santafé et al., 2009a; Tomàs et al., 2011) that some nerve terminals go silent (do not evoke EPP on stimulation) before they completely retract and before the end of the functional elimination period, "but retain certain capabilities for evoked release that can be pharmacologically recovered (*R*, recovered endings)" (Tomàs et al., 2011). In polyinnervated synapses, "quantal responses clearly decrease in both size and number before axonal withdrawal is completed (Dunia and Herrera, 1993; Colman et al., 1997). Neurotransmitter release from the axon that survives is characterized by a greater quantal content, whereas the efficiency of the input(s) removed decreases progressively, since a small quantal content is associated with reduced postsynaptic receptor density (Colman et al., 1997; Culican et al., 1998)" (see Santafé et al., 2002). "Imposed changes in synaptic activity can accelerate or delay this developmental synapse elimination process (Jansen and Fladby, 1990), and in most cases, deviations from the normal physiological tempo are for several hours or even days" (see also Nelson, 2005; Tomàs et al., 2011). However, when we studied the *R* endings, we observed a fast response (1 h) of some motor nerve terminals, which recovered ACh release by acute exposure to modulators of certain molecular pathways involved in neurotransmission. "We used intracellular recordings of the evoked synaptic potentials to observe the number of functional inputs for a large number of NMJs. Then we calculated the mean value, defined as the polyinnervation index of the muscle studied (PI)" in control P6-P7 rodent muscles the PI was 1.63 ± 0.14 with a 47.92% ± 2.08 of monoinnervated junctions (Lanuza et al., 2001; Santafé et al., 2001), and finally we studied the "effect on PI of blocking or activating several key molecules involved in ACh release" (Tomàs et al., 2011). A rapid increase in PI can indicate the recruitment of some silent nerve endings that transitorily recover transmission (*R* endings).

In summary, we analyzed how neurotransmission is affected by interfering with muscarinic and neurotrophin signaling in *M, S and W* P7 synaptic contacts on dual junctions, and the possible appearance of silent contacts (*R*) and compared these cases with neurotransmission in the mature adult NMJ (P30; *A* nerve endings; Santafé et al., 2001, 2002, 2004, 2009b; Garcia et al., 2010d; Tomàs et al., 2011).

Finally, we performed direct "axonal counts in confocal LAL preparations (average number of axonal connections per NMJ) from B6.Cg-Tg (Thy1-YFP)16 Jrs/J mice (hereinafter YFP). Transgenic mice express spectral variants of GFP (yellow-YFP) at high levels in motor neurons and axons are brightly fluorescent all the way to the terminals" (Nadal et al., 2016). In most cases, we checked the results with C57BL/6J mice and the axons were shown with an antibody against 200-kD neurofilament protein. LAL muscles were processed to detect the postsynaptic nicotinic ACh receptors (nAChRs) with TRITC-α- BTX (**Figure 1**). In these histological preparations we counted "the percentage of singly-, dually- and triply- (or more) innervated synapses at P7, P9 and P15 postnatal days with no experimental manipulation (control), and also after two (days 5, 6), four (days 5–8) and 10 (days 5–14) subcutaneous applications of muscarinic and TrkB receptor signaling-related substances" (Nadal et al., 2016; see also Nadal et al., 2017a,b).

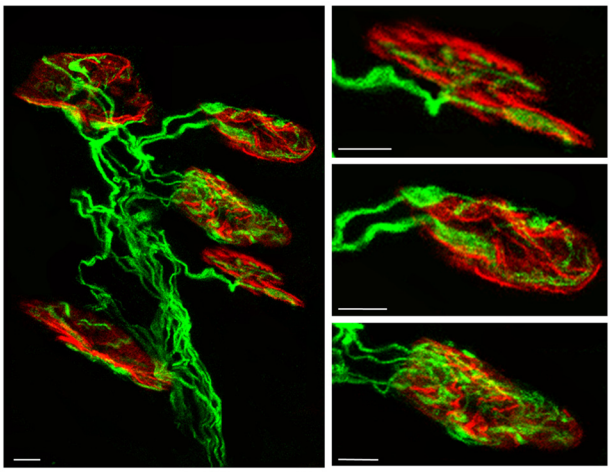

FIGURE 1 | Confocal immunofluorescence images. The pictures show representative confocal fluorescence images of monoinnervated and polyinnervated synapses from C57BL/6J P7 control mice. The levator auris longus (LAL) neuromuscular junctions (NMJs) show the axons stained by 200-kD neurofilament antibody in green and the postsynaptic nicotinic acetylcholine receptor (nAChR) clusters stained in red with TRITC-α- BTX. Scale bar: 10 μm.

MUSCARINIC SIGNALING

mAChR in the NMJ

There is no consensus about which mAChR subtypes are present in the nerve terminals on the NMJ (Garcia et al., 2005; Wright et al., 2009). In immunohistochemistry assays, most antibodies seemed to detect more than one subtype but in knockout mice their specificity was not clearly determined (Jositsch et al., 2009). Some studies (Wright et al., 2009) only unquestionably observed the M_2 subtype in the adult nerve endings. In adult and newborn NMJs, we observed the probable presence of M_1, M_2, M_3 and M_4 subtypes in the cells that construct the synapse (Garcia et al., 2005). In addition, intracellular recording of the synaptic transmission using selective and unselective muscarinic agonists and blockers show that some of these receptors have a regulatory influence on ACh release in developing (Santafé et al., 2001, 2002, 2003, 2004, 2007b, 2009a) and adult synapses (Santafé et al., 2005, 2006, 2007b). Using genetic approaches, it has been observed that motor axon terminals are unstable without M_2. Some loss of terminal branches occurs in the M_2 KO mice (Wright et al., 2009). In this context, the neuronal connectivity in the visual cortex was altered by the absence of M_2/M_4 mAChR (Groleau et al., 2014).

mAChR in ACh Release

The diagram in **Figure 2A** shows the effect of several subtype-selective muscarinic substances on ACh release in developing (P7; *M, S, W*) and mature (P30; *A*) nerve endings. The effect of the muscarinic substances on the PI of these treated muscles can be seen in R and the effect on the axonal loss rate can be seen in the outermost concentric layer.

In the adult (*A* contacts), M_1 and M_2 receptors modulate "evoked transmitter release by positive and negative feedback, respectively (Slutsky et al., 1999; Minic et al., 2002; Santafé et al., 2003, 2006). The M_2 receptor inhibits ACh release because its selective block with methoctramine (MET) or AFX-116 increases release whereas the M_1 receptor increases release because its selective block with pirenzepine (PIR) or MT-7 reduces it. Both M_1- and M_2-mediated mechanisms operate in parallel" (Tomàs et al., 2014), with some predominance of M_2, because their simultaneous non-specific stimulation (oxotremorine, OXO) decreases release and the non-specific block (atropine, AT) increases transmitter output (data not represented in the figure, see Santafé et al., 2003). The M_3 (4-DAMP) and M_4 (tropicamide [TRO] and MT-3) blockers do not affect evoked ACh release. Thus, in the adult, mAChR signaling seems to "save the synapse function by decreasing the extent of evoked release" (Santafé et al., 2015) in basal conditions. Changes in synaptic activity may lead to subtypes playing different funcional roles (Minic et al., 2002; Santafé et al., 2003, 2006).

During developmental synapse elimination, the involvement of mAChR in ACh release is different. At P6-P7 roughly half of the NMJs are monoinnervated because one nerve terminal wins the axonal competition (Lanuza et al., 2002; Santafé et al., 2002). In these axons (*M* contacts), all the selective M_1 and M_2 blockers tested reduce release. Notably, the same occurs in the strongest endings of the dual junctions still in competition (*S* contacts). This suggests that a positive value of the winning axons is that all functional mAChR are committed to improve ACh release (in *M* and *S* contacts, the M_3 and M_4 blockers do not affect release). Using this autocrine mechanism the strongest ending may reinforce itself. However, in the weakest nerve contact in dual junctions (*W* contacts), only the M_2 blockers reduce release whereas M_1 and M_4 blockers can lead to increases in the EPP evoked by these weak axons (Santafé et al., 2003, 2004, 2007b, 2009a,b; Tomàs et al., 2011). Thus, during NMJ synaptogenesis, the functional significance of the subtypes differs from the adult's. M_2 receptors promote release in all nerve endings independently of their ACh release level or maturation state whereas M_1 and M_4 receptors reduce release in the weakest endings on dual junctions. This suggests that the weak, presumably loser axon may be negatively influenced by ACh release from the strongest axons through M_1 and M_4 subtype pathways.

Role of mAChR in the Recovery of Silent Synapses

In electrophysiological experiments, an increase in PI indicates the rapid recruitment of some silent synaptic contacts (*R* endings) that transitorily recover transmission. In P6-P7 muscles, we observed that blocking M_2 with MET results in a percentage increase in the NMJ with 3–4 inputs and higher PI (**Figure 2A**). This was not the case for MT-7 (M_1 blocker) or MT3 (M_4 blocker). Thus, M_2 seems to play a role in the recovery of silent synapses and might be involved in promoting the last step of the functional axonal disconnection (Tomàs et al., 2011). Whereas M_2 may stimulate release in *M*, *S* and *W* axons, it seems to reduce it in silent endings because blocking M_2 (MET) increases the ACh release in these endings just to become functionally recovered.

mAChR in Axonal Loss

By counting axons in P6-P7 YFP mice "we observed that M_1 and M_4 mAChR subtypes are involved in a mechanism that delays axonal elimination" (Nadal et al., 2016) because when M_1 or M_4 receptors are selectively blocked (with PIR and MT3 respectively), axonal loss is accelerated and causes a fast three-to-one axon transition (see the most external concentric layer in **Figures 2A**, **3**). Interestingly, M_2 does not change axonal loss rate in this period.

However, when we analyzed the effect of muscarinic agents at P9, we observed that the inhibitors PIR and MET (but not MT3) delay axonal loss (**Figure 3**, Nadal et al., 2016). Thus, "the M_1-M_2 subtype pair (in substitution of the M_1-M_4 pair) cooperates in favoring the full sequence of synapse elimination (the three-to-one axon transition)" (Nadal et al., 2016). Thus, mAChRs seem to play an important role in NMJ maturation and may affect ACh release capacity and the competitive strength of the different axons. Interestingly, even with the continued presence of the M_1 and M_2 inhibitors (PIR and MET, which delay axonal loss at P9), the axonal loss process comes to its normal end by the second postnatal week (P15; Nadal et al., 2016). This further suggests that other signaling pathways between the nerve terminals in competition cooperate to resolve the correct synaptic connectivity in a multifactorial process.

Relation between mAChR-Mediated Changes in Axonal Loss and ACh Release

How are mAChR subtypes related to the ACh release ability of the *S* and *W* endings in polyinnervated synapses and the final loss of some axons? At P7, the ACh release capacity of the *W* endings (those that produce the smallest EPP) in dual junctions was increased by the M_1 and M_4 selective inhibitors PIR and MT3, whereas ACh release from the *S* nerve terminal was reduced (by PIR) or unaffected (by MT3; Santafé et al., 2003). Thus, these interferences reduce the difference in ACh release between *S* and *W* nerve endings in competition. This may mean a reduction in the competitive balance between these nerve terminals in terms of ACh release and a delay in axon elimination may be hypothetically expected. However, both PIR and MT3 accelerate axon loss at P7 and how this is related to the presumed lesser activity-related competition is not clear. A plausible interpretation is that in this developmental stage (P7), mAChR-mediated competition is fully operative in the NMJ of untreated muscles, and some axons, engaged in competition, have not been fully lost. If competition is reduced or unbalanced by, for instance, blocking M_1 or M_4 the loss of these axons

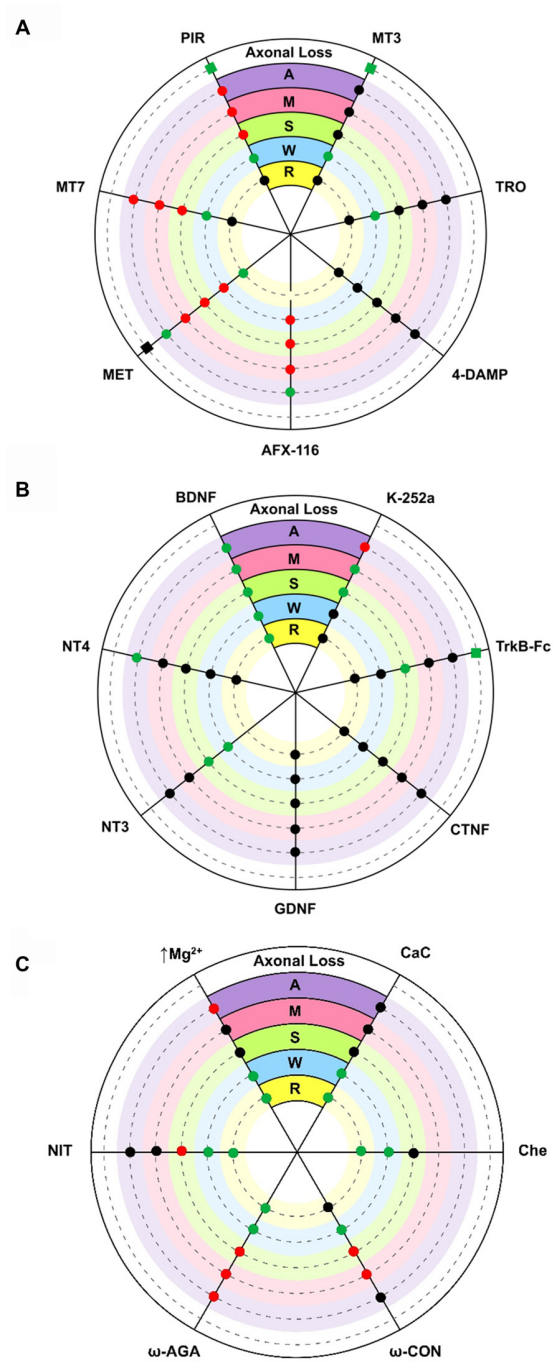

FIGURE 2 | Diagrams showing an overall representation of the data. The diagrams show the effect of several substances on acetylcholine (ACh) release (evoke endplate potential, EPP size represented by circles: increase [green], decrease [red] and no change [black] with respect to untreated controls) in developing (P7) single axons on monoinnervated junctions [M], the strong [S] and weak [W] synaptic contacts on dual junctions and in adult (P30) nerve endings [A]. Silent synaptic contacts [R] can be observed in some NMJs (*Continued*)

FIGURE 2 | Continued
in treated muscles after recovering ACh release. Here, R shows the effect of some substances on the polyinnervation index (PI, the mean number of axons per synapse) of these treated muscles (green = increased PI, black = no change). The axonal loss rate (represented with squares in the outermost concentric layer in **A** and **B**) is quantified by direct axonal counts in confocal LAL preparations from B6.Cg-Tg (Thy1-YFP)16 Jrs/J mice. In these histological preparations we counted the percentage of singly-, dually- and triply- (or more) innervated synapses at P7 after 2 days of subcutaneous applications of several muscarinic and TrkB substances. Delayed axon loss in red squares, accelerated loss in green and no change in black. **(A)** shows the effect of several subtype-selective muscarinic substances. The M_2 receptor is selectively blocked with methoctramine (MET) or AFX-116. The M_1 receptor is selectively blocked with pirenzepine (PIR) or muscarinic toxin 7 (MT7). The M_3 subtype is blocked with 4-DAMP and the M_4 subtype is blocked with tropicamide (TRO) or muscarínic toxin 3 (MT3). **(B)** shows the effect of neurotrophins and trophic cytokines (Brain-derived neurotrophic factor, BDNF, NT4, NT3, GDNF and CNTF) and related substances (TrkB-Fc chimera and k-252a). **(C)** shows the effect of voltage-dependent calcium channels (VDCC) blockers (nitrendipine [L type], ω-AGA [P type] and ω-CON [N type]), ion concentration change (0.5 mM magnesium) and PKC blockers (calphostin C (CaC) and chelerythrine (Che)). In all cases, significance is at $P < 0.05$.

accelerates. Also, in dual junctions ACh release is reduced by the M_2 blocker MET in both the weak and strong endings suggesting that the axonal difference in release is the same but axons are not as strong or have less competitive force. In this case, as may be expected, MET does not affect axonal elimination at P7.

Between P7–P9, the percentage of multiinnervated NMJ changes only by a 10% and all NMJs are not finally monoinnervated until P15 (Lanuza et al., 2001, 2002; Santafé et al., 2001; Nelson et al., 2003). Also, the mAChR in the monoinnervated synapses does not mature functionally until P15 (Santafé et al., 2003) suggesting that the competitive interactions between axons and their release capacity may not be very different between P7 and P9. If this is so, "the reduction (at P9) in the competitive advantage (or disadvantage) linked to ACh release between the strong and weak endings produced by PIR and the reduccion of the strength of the different axons produced by MET" (Nadal et al., 2016), may result in a relevant delay in axonal loss and we found that this is the case. Thus, the relation between the ACh release capacity of the endings in competition and the rate of axonal loss in multiinnervated junctions seems best observed at P9 when, judging by the effects of PIR and MET, the receptors M_1 and M_2 play a role in accelerating axonal loss. The functional effect on ACh release of these receptors may reinforce the strongest endings and be detrimental to the weak endings in dual junctions.

NEUROTROPHIN SIGNALING

The agents that modify the mAChR response can alter the time course of the axons loss process but not the end point at P15 (Nadal et al., 2016). Likewise, experimental manipulations of the PKC/PKA intracellular pathways (for instance, blocking or stimulating PKC with Calphostin C (CaC) or phorbol esters, respectively) also change the time course but not the final synapse loss around P15 (Lanuza et al., 2002; Nelson et al., 2003),

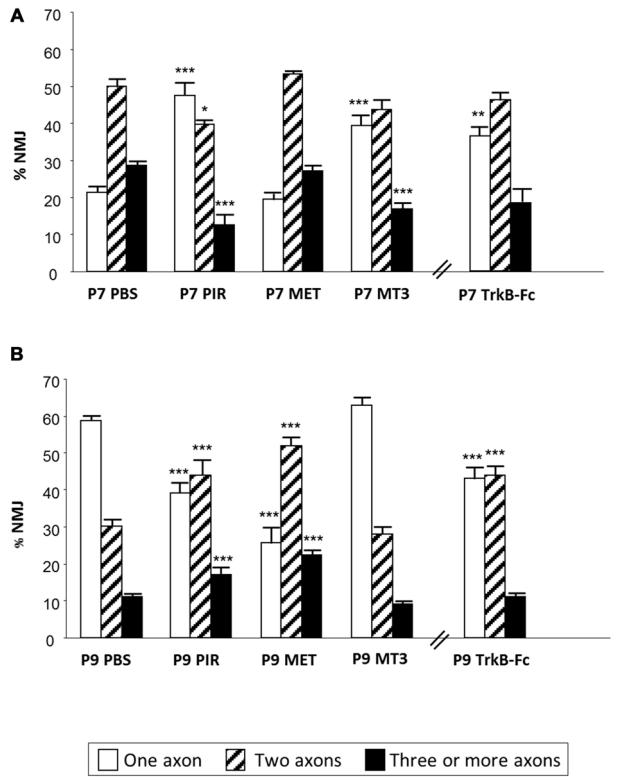

FIGURE 3 | Changes in polyneuronal innervation of the NMJ after inhibiting the mAChR and blocking the TrKB signaling. The figure shows the percentage of singly-, doubly- and triply (or more) innervated NMJs in untreated YFP control mice (exposed to PBS applications) and after two (P7 in **A**) and four (P9 in **B**) applications (one application each day after P5) of the mAChR antagonists PIR, MET and MT3. The figure also shows the effect of the TrkB blocking pathway agent TrkB-Fc. $^{***}p < 0.001$,$^{**}p < 0.01$, $^{*}p < 0.05$. This figure has been adapted and redrawn from the Figures 3, 4 in the original article "[Presynaptic muscarinic ACh autoreceptors (M1, M2 and M4 subtypes), adenosine receptors (A_1 and A^{2A}) and tropomyosin-related kinase B receptor (TrkB) modulate the developmental synapse elimination process at the NMJ]" by Nadal et al. (2016). The original article is an open access article distributed under the terms of the Creative Commons Attribution License http://creativecommons.org/licenses/by/2.0, which permits unrestricted use, distribution and reproduction in any medium, provided the original work is properly cited.

indicating that several receptors and their coupled intracellular mechanisms can be used for redundant synapse elimination (Nadal et al., 2016, 2017a,b).

Neurotrophin Receptors in NMJ

Neurotrophins and their receptors have been shown to be expressed in muscle and nerve tissues both during development and in the adult (Funakoshi et al., 1993, 1995; Griesbeck et al., 1995; Gonzalez et al., 1999; Ip et al., 2001; Nagano and Suzuki, 2003; Pitts et al., 2006; Garcia et al., 2010c). Electrophysiology procedures show that some of these receptors influence ACh release in the NMJ in the same time periods (Stoop and Poo, 1996; Poo et al., 1999; Poo, 2001; Garcia et al., 2010b,d; Santafé et al., 2014).

Neurotrophin Receptors in ACh Release

In the NMJ of adult rodents, exogenously added BDNF (or neurotrophin-4, NT-4) increases evoked ACh release after 3 h (Mantilla et al., 2004; Garcia et al., 2010d). This presynaptic effect can be prevented by preincubation with TrkB-Fc chimera or by pharmacologically blocking TrkB signaling (k-252a or the blocker antibody 47TrkB). Low doses of BDNF quickly promote (within minutes) a TrkB-dependent potentiation of transmitter release at developing NMJs in *Xenopus laevis* in culture (Stoop and Poo, 1996; Poo et al., 1999; Poo, 2001). In P7 developing muscles *ex vivo* (**Figure 2B**), exogenous BDNF (10 nM for 3 h or 50 nM for 1 h) potentiates release in all endings also with the involvement of TrkB receptors (Garcia et al., 2010c). NT-3 potentiates release only in the *W* and *S* endings in dual junctions (Garcia et al., 2010d), and NT-4 only in adult NMJs. The Glial cell line-derived neurotrophic factor (GDNF) and Ciliary neurotrophic factor (CNTF), on the other hand, do not directly modify ACh release in any nerve endings (Garcia et al., 2010a).

Thus, "exogenous BDNF acts on a section of the release mechanism that is operative and potentiates neurotransmission in all nerve endings" (Garcia et al., 2010b) that are in developmental competition (regardless of their particular state of maturation). However, when we analyzed the possible effect of endogenously produced BDNF during synaptic maturation, we found that blocking TrkB (k-252a) or neutralizing endogenous BDNF (TrkB-Fc) does not change the quantal content of the *W* endings although surprisingly it does increase release in the S endings (Garcia et al., 2010d; see **Figure 2B**). Therefore, although the BDNF-TrkB pathway seems ready to be stimulated by exogenous BDNF to potentiate release in all nerve terminals during development, endogenous BDNF does not affect the weak ending at P7 but, in this period, may help to reduce release in the *S* nerve terminal (Garcia et al., 2010d). The effect of BDNF on *S* endings may be related to the relative involvement and generally opposing actions of truncated and full-length TrkB and $p75^{NTR}$ receptors, and proBDNF and mature BDNF on the postnatal polyinnervated synapses.

Neurotrophin Receptors in Silent Synapses. Role of TrkB in Recovery of Silent Synapses

Blocking TrkB, using TrkB-Fc to prevent endogenous BDNF action or stimulating with several neurotrophins (NT-4, NT-3, GDNF or CNTF) does not change mean PI. However, stimulation with exogenous BDNF (1 h in the bath) transitorily increases PI, considerably reduces monoinnervated junctions and increases the number of junctions with 2–3 functional inputs (Tomàs et al., 2011); the innermost concentric layer in **Figure 2B**). This suggests that there are a number of silent inputs on the boundary that can be recovered (to produce an EPP) by BDNF. In fact, BDNF stabilizes silent synapses at mice NMJs during development (Kwon and Gurney, 1996; Garcia et al., 2010d). It can be hypothesized that the lack of activity in the weakest endings means that little BDNF is produced and it does not work locally on these endings

(the absence of tonic change in ACh release by TrkB block or by using the neutralizing fusion protein TrkB-Fc suggests that endogenous BDNF does not work on the weak and silent synapses). However, exogenous BDNF may reach the weak endings close to elimination and induce some release recovery. As previously stated, downregulation of M_2 (MET) produces the same effect as TrkB stimulation with exogenous BDNF (that is to say, PI increases because silent endings recover some of their transmitter release capacity). ACh from the strong more active terminals may reach M_2 in the neighbor silent endings thus punishing them.

Neurotrophin Receptors in Developmental Axonal Loss

We used TrkB-Fc to sequester endogenous BDNF and NT-4 and, at P7, morphologically observed a clear acceleration of the three-to-two rate in axon loss, well matched by the acceleration of the two-to-one rate (see the outermost concentric layer in **Figures 2B**, **3**, and also Nadal et al., 2016) although, as stated above, the funcional PI does not change significantly. This seems to suggest that some of the axonal endings eliminated are not functional at this time (the opposite of what occurs with MET—see above—which has no effect on the number of axons at P7 but increases the percentage of functional ones). Interestingly, using a chemical-genetic approach to block TrkB signaling during NMJ development, it has been found that "inhibition of TrkB signaling by daily injection of 1NMPP1 to TrkBF616A knock-in mice accelerated synapse elimination at P7" (Je et al., 2013). This fastened synapse elimination is similar to the described here in developing NMJ at P7. Therefore, in normal conditions the physiological role of the BDNF-TrkB pathway at P7 seems to delay the axonal loss process although endogenous BDNF does not affect ACh release in the W endings, as stated above, and transmitter release seems to be somewhat independent. This result partially agrees with a proposed model in which proBDNF and mature BDNF (mBDNF) serve as potencial "punishment" and "reward" signals for the less active and more active nerve endings, respectively *in vivo*. Exogenous proBDNF promoted synapse elimination by activating $p75^{NTR}$ receptors, whereas mBDNF infusion substantially delayed synapse elimination in the mouse LAL muscle (Je et al., 2013). The postsynaptic secretion of "proBDNF stabilizes or eliminates presynaptic axon terminals, depending on its proteolytic conversion at synapses" (Je et al., 2013). "Pharmacological inhibition of the proteolytic conversion of proBDNF to mBDNF accelerated synapse elimination via activation of $p75^{NTR}$ receptors. Furthermore, the inhibition of both $p75^{NTR}$ receptors and sortilin signaling attenuated synapse elimination" (Je et al., 2013). "It seems that proBDNF-mediated synaptic retraction requires simultaneous activation of $p75^{NTR}$ receptors and the complementary receptor sortilin, a coreceptor that binds to pro-neurotrophins" (Je et al., 2013; see also Nykjaer et al., 2004; Teng et al., 2005; Jansen et al., 2007). Also, in the LAL muscle of the mouse, blocking the $p75^{NTR}$ receptors delays axonal loss and some nerve terminals even regrow (Garcia et al., 2011).

However, "at P9, neurotrophin signaling seems to reverse their coupling to the axonal loss process (**Figure 3**) because TrkB-Fc considerably delays elimination (resulting in more dual and fewer monoinnervated NMJs), which indicates that in a normal situation the role of BDNF/NT-4 mediators changes at this time (P9) and accelerates elimination, as has been described above for the muscarinic mechanism" (Nadal et al., 2016). In PC, the deficiency of TrkB has a consequence in the developmental detach and loss of redundant CF synaptic contacts. It can be observed "an abnormal multiple CF innervation in PC in trkB-deficient mice" Bosman et al., 2006) in the second postnatal week (see also Watanabe and Kano, 2010). This delay in synapse elimination is similar to the described by us in developing NMJ (at P9) treated with TrkB-Fc.

Thus, also in this case, it seems that the BDNF-TrkB pathway plays a biphasic role during the critical period of synapse loss. The progressive maturation of the NMJ at P9 may change the operating conditions of the BDNF-TrkB pathway to a more mature endogenous BDNF production and release promoting effect in certain nerve terminals resulting in more efficient competitive interactions and axonal loss.

RELATION BETWEEN MUSCARINIC AND NEUROTROPHIN SIGNALING

"Synapse operation is largely the logical outcome of the confluence of several metabotropic receptors and signaling" (Tomàs et al., 2014). In the adult NMJ, "the activity of a given receptor can modulate a given combination of spontaneous, evoked and activity-dependent ACh release parameters" (Tomàs et al., 2014). Specifically, the mAChR generally seems to protect the synapse from resources depletion by decreasing the extent of evoked ACh secretion (mainly an M_2 action) and decreasing activity-dependent depression (Santafé et al., 2003). One of the main roles of TrkB is to keep the spontaneous quantal leak of ACh low and potentiate evoked release (Garcia et al., 2010d). Thus, some functions in the adult synapses can be balanced by the opposing actions of different receptors.

Changes in how some of these receptors and pathways operate affect the normal coupling of the other complementary molecules to transmitter release. "Consecutive incubations with two substances (for instance, a muscarinic blocker followed by a TrkB blocker) can be used as a pharmacological tool to investigate the possible occlusive or additive crosstalk effects between two receptors" (Tomàs et al., 2014). In the adult NMJ, we found a link between mAChR and TrkB pathways because the normal function of the mAChR is a requirement for the TrkB to couple to ACh release and vice versa (Garcia et al., 2010d; Santafé et al., 2014). It is know that mAChR and TrkB pathways are related and share a link mediated by phospholipase C (PLC)-phosphatidylinositol 4,5-bisphosphate (PIP2)-diacylglycerol (DAG)-PKC, which modulates P/Q-type VDCC (Santafé et al., 2006; Amaral and Pozzo-Miller, 2012). Also, "the PLC-generated DAG regulates the vesicle priming protein Munc13–1 and recruits ACh-containing vesicles for the immediately releasable pool" (see Bauer et al., 2007; Tomàs et al., 2014). Thus, the relations between these signaling

pathways contribute to modulate the VDCC and synaptic vesicles, and then neurotransmission (Takamori, 2012). The inflow of Ca^{2+} needed for ACh release is modulated by the presynaptic M_1 mAChR (Santafé et al., 2006) interacting with the BDNF-TrkB pathway (Amaral and Pozzo-Miller, 2012). In the adult skeletal NMJ, the M_1 mAChR contribute to adjust the M_2 mAChR subtype, which is a protein kinase A (PKA)-mediated inhibitor of ACh secretion (Santafé et al., 2006). This balance is further adjusted by adenosine coreleased with ACh at the NMJ (Oliveira et al., 2009; Garcia et al., 2013; Santafé et al., 2015) and TrkB (Garcia et al., 2010c). However, when neuromuscular transmission is low (as it is during synaptic development) or defective, "the balance between them shifts in favor of the M_1 mAChR, partly because of an M_2 mAChR-mediated switch from PKA to PKC activation" (see Santafé et al., 2007a; Garcia et al., 2010b; Tomàs et al., 2014).

The complementary function of these receptors in the adult NMJ neurotransmission provides further evidence of their coordinated involvement in developmental synaptic elimination. Thus, PKC, and VDCC can also be expected to have a role in developmental axonal loss. PKC is not coupled to modify transmitter release in basal conditions because its inhibition with, for instance, CaC does not influence the quantal content of the EPP. This is the situation in adult motor nerve endings, and also in the strong endings of dually innervated NMJ and in the ending in the recently monoinnervated junctions during maturation (Santafé et al., 2007a, 2008); see also **Figure 2C**). In these nerve terminals, however, PKC couples to potentiate ACh release during synaptic activity (Santafé et al., 2007a). Interestingly however, a tonic PKC coupling reduces release in the weakest axons in dual junctions because their inhibition (with CaC or chelerythrine, Che) increases ACh release in these endings and even recovers *R* endings (**Figure 2C**). Therefore, PKC may be decisive for the axonal loss control (Lanuza et al., 2002; Nelson et al., 2003; Santafé et al., 2009a). As far as the VDCC and calcium inflow are concerned, our results show (judging by the effect of the inhibitors used, **Figure 2C**) that a part of the calcium entry through the P/Q-, N- or L-type VDCC reduces ACh release in the weak endings of dual junctions (Santafé et al., 2009a) and even also recover *R* endings. Therefore, our results indicate that during NMJ development "there is a release inhibition mechanism based on a mAChR-PKC-VDCC intracellular cascade. When it is fully active in certain weak motor axons, it can depress ACh release and even disconnect synapses" (Santafé et al., 2009a). Blocking PKCs, VDCCs (P/Q-type with ω-Agatoxin [ω-AGA], N-type with ω-Conotoxin [ω-CON] or L-type with nitrendipine [NIT]) and/or calcium influx (moderately increasing Mg^{2+}) or mAChR (M_1- and/or M_4-subtypes) "can lead to similar percentage increases in the size of the synaptic potentials evoked by weak axons in developing polyinnervated synapses and even, in most cases, the functional recovery of previously disconnected synapses" (Santafé et al., 2009a; see also Santafé et al. 2003; 2004; 2007b; 2009b; Tomàs et al., 2011). "We suggest that this mechanism plays a central role in the elimination of redundant neonatal synapses" (Lanuza et al., 2014). However, at P7, M_1, M_4 and TrkB receptors delay axon loss while M_1 and M_4 reduce ACh release in the weakest axon terminals, which suggests some independence between transmitter release and elimination. We interpret that at this developmental point the activity-dependent competitive interactions in most junctions are at their peak and this may delay axon loss. The accelerating effect of these receptors on axon loss is much clearer at P9.

Cerebellar CF to PC synapses in rodents provides "a good model to study elimination of redundant synapses in the central nervous system. At birth, each PC is innervated by multiple CFs but at the end of the third postnatal week, most PCs become innervated by single CFs" (Hashimoto and Kano, 2005; see also Kano and Hashimoto, 2009). In the early phase of CF synapse elimination, CF differential activities results in Ca^{2+} influx through the P/Q- type VDCC in an activity-dependent manner. This promotes competition among CF inputs allowing the strongest CF to segregate in the dendrites, whereas the weaker fibers "remain on the soma until their perisomatic synapses are massively eliminated" (Watanabe and Kano, 2010). A signaling cascade from a glutamate receptor (mGluR1) to PKCγ is involved in this late phase of CF synapse loss. Mutant mice deficient at some point in the pathway show reduced CF synaptic loss (Kano et al., 1995, 1997, 1998; Levenes et al., 1997; Offermanns et al., 1997; Hashimoto et al., 2000, 2001; Ichise et al., 2000). Interestingly, mice deficient in "P/Q-type Ca^{2+} channel have persistent multiple CF innervation on the PC soma" (Miyazaki et al., 2004). This fact agrees with our observation that, in the NMJ, a fraction of the Ca^{2+} entry through the P/Q-, N- or L-type VDCC reduces ACh release in the weak endings of dual junctions (Santafé et al., 2009a) relating Ca^{2+} inflow, transmitter release and synapse loss.

Interestingly, mAChR (Garcia et al., 2005) and TrkB receptors (Garcia et al., 2010d) are present also in the postsynaptic membrane contributing to their organization (Gonzalez et al., 1999; Belluardo et al., 2001; Loeb et al., 2002; Peng et al., 2003). In this postsynaptic membrane, selective nAChR-phosphorylation by PKC (in the delta subunit) and PKA (epsilon subunit) is a major cause of nAChR dispersion and stability, respectively (Nishizaki and Sumikawa, 1994; Li et al., 2004; Lanuza et al., 2010). PKC-induced dispersion under the weakest nerve terminals and a PKA-induced catching and stabilization under the more active axon terminals results in the differentiation of the postsynaptic gutters. In our blocking experiments of these receptors, we observed that prolonged M_1, M_2 and TrkB block produce a delay in postsynaptic maturation at P15. This indicates a role for these receptors in the postsynaptic component. Nevertheless, this occurs when axon loss has been completed, suggesting independent regulation (Nadal et al., 2016).

Interestingly, glutamate and mGluR1 also mediate transmission at the NMJ (Waerhaug and Ottersen, 1993; Malomouzh et al., 2011; Walder et al., 2013). Glutamate at the NMJ is derived from the motor nerve terminal (Marmiroli and Cavaletti, 2012). Postsynaptic NMDA receptors at the end plate have been documented in rodent myotubes (Lück et al., 2000).

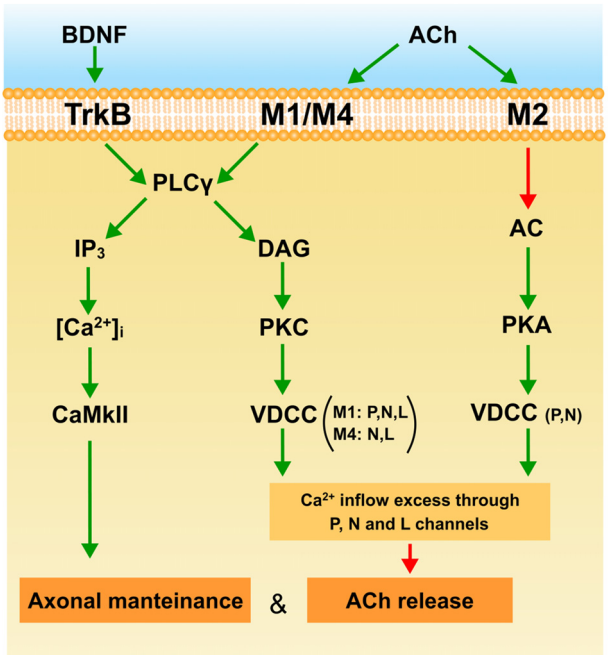

FIGURE 4 | The figure is a plausible interpretation of the role of mAChR (M_1, M_2 and M_4) and the BDNF-TrkB pathways in the process of eliminating the weakest endings around P7. The explanation can be found in the conclusion to the main text. Green arrows indicate activation or stimulation, and red arrows inhibition.

It has been found that developmental synapse loss in mice is slowed at P11 by reducing activation of the glutamate-NMDA receptor pathway (Personius et al., 2016). This is in accordance with our observation of the effect of mAChR and TrkB receptors block delaying axonal loss at P9 and postsynaptic gutters maturation around P15. The involvement of the mGluR1s in synapse elimination at the NMJ emphasize the complexity of a multireceptor mechanism.

CONCLUSION

The diagram in **Figure 4** shows a plausible interpretation of the role of mAChR and BDNF-TrkB pathways in the elimination of the supernumerary endings in the NMJ at the end of the first week postnatal (P7). ACh released from *W* and *S* axons in the common synaptic cleft could stimulate M_1, M_4 and M_2 muscarinic types in *W* endings. M_1 receptors reduce release through the PKC pathway due to an excess of Ca^{2+} inflow (through P, N and L VDCC) or because a selective inflow through L channel (only present in *W* endings) targeted to restrain the release machinery. The coupling of M_1 to PKC activity in the *W* endings differs from the coupling of the mature and adult (*M* and *A*) synapses where release is potentiated using Ca^{2+} inflow through the P-channel. The presence of M_4 and the L and N channels in the *W* contacts may have something to do with this difference. The PKA-linked M_2 subtype is also present in the *W* axons. It is related only to P and N channels and here potentiates ACh release which, in this case also, differs from the adult where M_2 inhibits release. Thus, the weak and presumably loser axon may be negatively influenced by their neighboring strongest one through M_1 and M_4 subtypes. The axons that win the competition (*M* and *S* contacts) have their functional mAChR (M_1, M_2) committed to improve ACh release. Using this autocrine mechanism the strongest ending may reinforce themselve. However, when axon loss is analyzed at P7, the M_1-M_4 pair reduces the synapse elimination rate. This effect may be produced by the IP3-CaMKII pathway which is known to promote axonal maintenance and growth. It seems that at P7, mAChRs contribute to the development of activity-dependent competition but that, at this time, these competitive interactions can delay axon loss.

At P7 the BDNF-TrkB pathway is operative and ready to be stimulated by exogenous BDNF to favor ACh release in all axonal endings during development (*W*, *S* and *M* endings and even transitorily recover some silent axons and increase PI). This effect may be produced by the IP3 branch of the PLC because endogenous BDNF does not affect ACh release in the weak ending. Interestingly, at P7 the BDNF-TrkB pathway delays axonal loss in the same way as mAChR signaling does. This effect may also be mediated by the CaMKII pathway.

Thus at P7, TrkB, M_1 and M_4 promote axonal maintenance. This coincides with mAChR reducing ACh release in the weakest axon in dual NMJs, which may result in their being competitively handicapped. However, some days later at P9, the mAChR subtype pair M_1-M_2 and the BDNF pathway cooperate to favor the full sequence of axonal loss and synapse elimination.

AUTHOR CONTRIBUTIONS

LN, EH, AS, VC and MT: data collection, quantitative analysis; literature search, data interpretation, design graphic; NG, MAL and MMS: statistics; JT, NG, MAL and MMS: conception and design, literature search, data interpretation, manuscript preparation.

ETHICS STATEMENT

The mice were cared for in accordance with the guidelines of the European Community's Council Directive of 24 November 1986 (86/609/EEC) for the humane treatment of laboratory animals. All experiments on animals have been reviewed and approved by the Animal Research Committee of the Universitat Rovira i Virgili (Reference number: 0233).

ACKNOWLEDGMENTS

This work was supported by a grant from the Catalan Government (2014SGR344) and a grant from Ministerio de Economia y Competitividad (MINECO; SAF2015-67143-P). We thank the reviewers for their careful reading of our manuscript and their many insightful comments.

REFERENCES

Amaral, M. D., and Pozzo-Miller, L. (2012). Intracellular Ca^{2+} stores and Ca^{2+} influx are both required for BDNF to rapidly increase quantal vesicular transmitter release. *Neural Plast.* 2012:203536. doi: 10.1155/2012/203536

Bauer, C. S., Woolley, R. J., Teschemacher, A. G., and Seward, E. P. (2007). Potentiation of exocytosis by phospholipase C-coupled G-protein-coupled receptors requires the priming protein Munc13–1. *J. Neurosci.* 27, 212–219. doi: 10.1523/JNEUROSCI.4201-06.2007

Belluardo, N., Westerblad, H., Mudó, G., Casabona, A., Bruton, J., Caniglia, G., et al. (2001). Neuromuscular junction disassembly and muscle fatigue in mice lacking neurotrophin-4. *Mol. Cell. Neurosci.* 18, 56–67. doi: 10.1006/mcne.2001.1001

Benoit, P., and Changeux, J. P. (1975). Consequences of tenotomy on the evolution of multiinnervation in developing rat soleus muscle. *Brain Res.* 99, 354–358. doi: 10.1016/0006-8993(75)90036-0

Bosman, L. W., Hartmann, J., Barski, J. J., Lepier, A., Noll-Hussong, M., Reichardt, L. F., et al. (2006). Requirement of TrkB for synapse elimination in developing cerebellar Purkinje cells. *Brain Cell Biol.* 35, 87–101. doi: 10.1007/s11068-006-9002-z

Bourgeois, J. P., and Rakic, P. (1993). Changes of synaptic density in the primary visual cortex of the macaque monkey from fetal to adult stage. *J. Neurosci.* 13, 2801–2820.

Brown, M. C., Jansen, J. K., and Van Essen, D. (1976). Polyneuronal innervation of skeletal muscle in new-born rats and its elimination during maturation. *J. Physiol.* 261, 387–422.

Colman, H., Nabekura, J., and Lichtman, J. W. (1997). Alterations in synaptic strength preceding axon withdrawal. *Science* 275, 356–361. doi: 10.1126/science.275.5298.356

Culican, S. M., Nelson, C. C., and Lichtman, J. W. (1998). Axon withdrawal during synapse elimination at the neuromuscular junction is accompanied by disassembly of the postsynaptic specialization and withdrawal of Schwann cell processes. *J. Neurosci.* 18, 4953–4965.

Daniel, H., Hemart, N., Jaillard, D., and Crepel, F. (1992). Coactivation of metabotropic glutamate receptors and of voltage-gated calcium channels induces long-term depression in cerebellar Purkinje cells *in vitro*. *Exp. Brain Res.* 90, 327–331. doi: 10.1007/bf00227245

Dunia, R., and Herrera, A. A. (1993). Synapse formation and elimination during growth of the pectoral muscle in *Xenopus laevis*. *J. Physiol.* 469, 501–509. doi: 10.1113/jphysiol.1993.sp019825

Favero, M., Busetto, G., and Cangiano, A. (2012). Spike timing plays a key role in synapse elimination at the neuromuscular junction. *Proc. Natl. Acad. Sci. U S A* 109, E1667–E1675. doi: 10.1073/pnas.1201147109

Fields, R. D., and Nelson, P. G. (1992). Activity-dependent development of the vertebrate nervous system. *Int. Rev. Neurobiol.* 34, 133–214. doi: 10.1016/S0074-7742(08)60098-7

Funakoshi, H., Belluardo, N., Arenas, E., Yamamoto, Y., Casabona, A., Persson, H., et al. (1995). Muscle-derived neurotrophin-4 as an activity-dependent trophic signal for adult motor neurons. *Science* 268, 1495–1499. doi: 10.1126/science.7770776

Funakoshi, H., Frisén, J., Barbany, G., Timmusk, T., Zachrisson, O., Verge, V. M., et al. (1993). Differential expression of mRNAs for neurotrophins and their receptors after axotomy of the sciatic nerve. *J. Cell Biol.* 123, 455–465. doi: 10.1083/jcb.123.2.455

Garcia, N., Priego, M., Obis, T., Santafé, M. M., Tomàs, M., Besalduch, N., et al. (2013). Adenosine A_1 and A_{2A} receptor-mediated modulation of acetylcholine release in the mice neuromuscular junction. *Eur. J. Neurosci.* 38, 2229–2241. doi: 10.1111/ejn.12220

Garcia, N., Santafé, M. M., Salon, I., Lanuza, M. A., and Tomàs, J. (2005). Expression of muscarinic acetylcholine receptors (M1-, M2-, M3- and M4-type) in the neuromuscular junction of the newborn and adult rat. *Histol. Histopathol.* 20, 733–743. doi: 10.14670/HH-20.733

Garcia, N., Santafé, M. M., Tomàs, M., Lanuza, M. A., Besalduch, N., Priego, M., et al. (2010a). The glial cell line-derived neurotrophic factor (GDNF) does not acutely change acetylcholine release in developing and adult neuromuscular junction. *Neurosci. Lett.* 480, 127–131. doi: 10.1016/j.neulet.2010.06.022

Garcia, N., Santafé, M. M., Tomàs, M., Lanuza, M. A., Besalduch, N., and Tomàs, J. (2010b). Involvement of brain-derived neurotrophic factor (BDNF) in the functional elimination of synaptic contacts at polyinnervated neuromuscular synapses during development. *J. Neurosci. Res.* 88, 1406–1419. doi: 10.1002/jnr.22320

Garcia, N., Tomàs, M., Santafé, M. M., Besalduch, N., Lanuza, M. A., and Tomàs, J. (2010c). The interaction between tropomyosin-related kinase B receptors and presynaptic muscarinic receptors modulates transmitter release in adult rodent motor nerve terminals. *J. Neurosci.* 30, 16514–16522. doi: 10.1523/JNEUROSCI.2676-10.2010

Garcia, N., Tomàs, M., Santafé, M. M., Lanuza, M. A., Besalduch, N., and Tomàs, J. (2010d). Localization of brain-derived neurotrophic factor, neurotrophin-4, tropomyosin-related kinase b receptor and p75 NTR receptor by high-resolution immunohistochemistry on the adult mouse neuromuscular junction. *J. Peripher. Nerv. Syst.* 15, 40–49. doi: 10.1111/j.1529-8027.2010.00250.x

Garcia, N., Tomàs, M., Santafé, M. M., Lanuza, M. A., Besalduch, N., and Tomàs, J. (2011). Blocking p75 (NTR) receptors alters polyinnervationz of neuromuscular synapses during development. *J. Neurosci. Res.* 89, 1331–1341. doi: 10.1002/jnr.22620

Gonzalez, M., Ruggiero, F. P., Chang, Q., Shi, Y. J., Rich, M. M., Kraner, S., et al. (1999). Disruption of Trkb-mediated signaling induces disassembly of postsynaptic receptor clusters at neuromuscular junctions. *Neuron* 24, 567–583. doi: 10.1016/s0896-6273(00)81113-7

Griesbeck, O., Parsadanian, A. S., Sendtner, M., and Thoenen, H. (1995). Expression of neurotrophins in skeletal muscle: quantitative comparison and significance for motoneuron survival and maintenance of function. *J. Neurosci. Res.* 42, 21–33. doi: 10.1002/jnr.490420104

Groleau, M., Nguyen, H. N., Vanni, M. P., Huppé-Gourgues, F., Casanova, C., and Vaucher, E. (2014). Impaired functional organization in the visual cortex of muscarinic receptor knock-out mice. *Neuroimage* 98, 233–242. doi: 10.1016/j.neuroimage.2014.05.016

Hashimoto, K., and Kano, M. (2005). Postnatal development and synapse elimination of climbing fiber to Purkinje cell projection in the cerebellum. *Neurosci. Res.* 53, 221–228. doi: 10.1016/j.neures.2005.07.007

Hashimoto, K., Miyata, M., Watanabe, M., and Kano, M. (2001). Roles of phospholipase Cβ4 in synapse elimination and plasticity in developing and mature cerebellum. *Mol. Neurobiol.* 23, 69–82. doi: 10.1385/MN:23:1:69

Hashimoto, K., Watanabe, M., Kurihara, H., Offermanns, S., Jiang, H., Wu, Y., et al. (2000). Limbing fiber synapse elimination during postnatal cerebellar development requires signal transduction involving Gαq and phospholipase Cβ4. *Prog. Brain Res.* 124, 31–48. doi: 10.1016/S0079-6123(00)24006-5

Hubel, D. H., Wiesel, T. N., and LeVay, S. (1977). Plasticity of ocular dominance columns in monkey striate cortex. *Philos. Trans. R Soc. Lond. B Biol. Sci.* 278, 377–409. doi: 10.1098/rstb.1977.0050

Huberman, A. D. (2007). Mechanisms of eye-specific visual circuit development. *Curr. Opin. Neurobiol.* 17, 73–80. doi: 10.1016/j.conb.2007.01.005

Ichise, T., Kano, M., Hashimoto, K., Yanagihara, D., Nakao, K., Shigemoto, R., et al. (2000). mGluR1 in cerebellar Purkinje cells essential for long-term depression, synapse elimination and motor coordination. *Science* 288, 1832–1835. doi: 10.1126/science.288.5472.1832

Ip, F. C., Cheung, J., and Ip, N. Y. (2001). The expression profiles of neurotrophins and their receptors in rat and chicken tissues during development. *Neurosci. Lett.* 301, 107–110. doi: 10.1016/s0304-3940(01)01603-2

Jansen, J. K., and Fladby, T. (1990). The perinatal reorganization of the innervation of skeletal muscle in mammals. *Prog. Neurobiol.* 34, 39–90. doi: 10.1016/0301-0082(90)90025-c

Jansen, P., Giehl, K., Nyengaard, J. R., Teng, K., Lioubinsk, O., Sjoegaard, S. S., et al. (2007). Roles for the proneurotrophin receptor sortilin in neuronal development, aging and brain injury. *Nat. Neurosci.* 10, 1449–1457. doi: 10.1038/nn2000

Je, H. S., Yang, F., Ji, Y., Potluri, S., Fu, X. Q., Luo, Z. G., et al. (2013). ProBDNF and mature BDNF as punishment and reward signals for synapse elimination at mouse neuromuscular junctions. *J. Neurosci.* 33, 9957–9962. doi: 10.1523/JNEUROSCI.0163-13.2013

Jositsch, G., Papadakis, T., Haberberger, R. V., Wolff, M., Wess, J., and Kummer, W. (2009). Suitability of muscarinic acetylcholine receptor antibodies for immunohistochemistry evaluated on tissue sections of receptor gene-deficient mice. *Naunyn. Schmiedebergs Arch. Pharmacol.* 379, 389–395. doi: 10.1007/s00210-008-0365-9

Kano, M., and Hashimoto, K. (2009). Synapse elimination in the central nervous system. *Curr. Opin. Neurobiol.* 19, 154–161. doi: 10.1016/j.conb.2009.05.002

Kano, M., Hashimoto, K., Chen, C., Abeliovich, A., Aiba, A., Kurihara, H., et al. (1995). Impaired synapse elimination during cerebellar development in PKC gamma mutant mice. *Cell* 83, 1223–1231. doi: 10.1016/0092-8674(95)90147-7

Kano, M., Hashimoto, K., Kurihara, H., Watanabe, M., Inoue, Y., Aiba, A., et al. (1997). Persistent multiple climbing fiber innervation of cerebellar Purkinje cells in mice lacking mGluR1. *Neuron* 18, 71–79. doi: 10.1016/s0896-6273(01)80047-7

Kano, M., Hashimoto, K., Watanabe, M., Kurihara, H., Offermanns, S., Jiang, H., et al. (1998). Phospholipase cβ4 is specifically involved in climbing fiber synapse elimination in the developing cerebellum. *Proc. Natl. Acad. Sci. U S A* 95, 15724–15729. doi: 10.1073/pnas.95.26.15724

Keller-Peck, C. R., Feng, G., Sanes, J. R., Yan, Q., Lichtman, J. W., and Snider, W. D. (2001). Glial cell line-derived neurotrophic factor administration in postnatal life results in motor unit enlargement and continuous synaptic remodeling at the neuromuscular junction. *J. Neurosci.* 21, 6136–6146.

Kwon, Y. W., and Gurney, M. E. (1996). Brain-derived neurotrophic factor transiently stabilizes silent synapses on developing neuromuscular junctions. *J. Neurobiol.* 29, 503–516. doi: 10.1002/(SICI)1097-4695(199604)29:4<503::AID-NEU7>3.0.CO;2-C

Lanuza, M. A., Besalduch, N., González, C., Santafé, M. M., Garcia, N., Tomàs, M., et al. (2010). Decreased phosphorylation of δ and ε subunits of the acetylcholine receptor coincides with delayed postsynaptic maturation in PKC theta deficient mouse. *Exp. Neurol.* 225, 183–195. doi: 10.1016/j.expneurol.2010.06.014

Lanuza, M. A., Garcia, N., Santafé, M., González, C. M., Alonso, I., Nelson, P. G., et al. (2002). Pre- and postsynaptic maturation of the neuromuscular junction during neonatal synapse elimination depends on protein kinase C. *J. Neurosci. Res.* 67, 607–617. doi: 10.1002/jnr.10122

Lanuza, M. A., Garcia, N., Santafé, M., Nelson, P. G., Fenoll-Brunet, M. R., and Tomàs, J. (2001). Pertussis toxin-sensitive G-protein and protein kinase C activity are involved in normal synapse elimination in the neonatal rat muscle. *J. Neurosci. Res.* 63, 330–340. doi: 10.1002/1097-4547(20010215)63:4<330::AID-JNR1027>3.0.CO;2-W

Lanuza, M. A., Santafé, M. M., Garcia, N., Besalduch, N., Tomàs, M., Obis, T., et al. (2014). Protein kinase C isoforms at the neuromuscular junction: localization and specific roles in neurotransmission and development. *J. Anat.* 224, 61–73. doi: 10.1111/joa.12106

Levenes, C., Daniel, H., Jaillard, D., Conquet, F., and Crépel, F. (1997). Incomplete regression of multiple climbing fibre innervation of cerebellar Purkinje cells in mGLuR1 mutant mice. *Neuroreport* 8, 571–574. doi: 10.1097/00001756-199701200-00038

Li, M. X., Jia, M., Yang, L. X., Jiang, H., Lanuza, M. A., Gonzalez, C. M., et al. (2004). The role of the theta isoform of protein kinase C (PKC) in activity-dependent synapse elimination: evidence from the PKC theta knock-out mouse *in vivo* and *in vitro*. *J. Neurosci.* 24, 3762–3769. doi: 10.1523/JNEUROSCI.3930-03.2004

Lichtman, J. W. (1977). The reorganization of synaptic connexions in the rat submandibular ganglion during post-natal development. *J. Physiol.* 273, 155–177. doi: 10.1113/jphysiol.1977.sp012087

Lichtman, J. W., and Tapia, J. C. (2013). "Synapse elimination," in *Fundamental Neuroscience*, 4th Edn., eds L. R. Squire, D. Berg, F. E. Bloom, S. Du Lac, A. Ghosh, and N. C. Spitzer (Amsterdam: Academic Press), 437–456.

Loeb, J. A., Hmadcha, A., Fischbach, G. D., Land, S. J., and Zakarian, V. L. (2002). Neuregulin expression at neuromuscular synapses is modulated by synaptic activity and neurotrophic factors. *J. Neurosci.* 22, 2206–2214.

Lück, G., Hoch, W., Hopf, C., and Blottner, D. (2000). Nitric oxide synthase (NOS-1) coclustered with agrin-induced AChR-specializations on cultured skeletal myotubes. *Mol. Cell. Neurosci.* 16, 269–281. doi: 10.1006/mcne.2000.0873

Malomouzh, A. I., Nikolsky, E. E., and Vyskočil, F. (2011). Purine P2Y receptors in ATP-mediated regulation of non-quantal acetylcholine release from motor nerve endings of rat diaphragm. *Neurosci. Res.* 71, 219–225. doi: 10.1016/j.neures.2011.07.1829

Mantilla, C. B., Zhan, W. Z., and Sieck, G. C. (2004). Neurotrophins improve neuromuscular transmission in the adult rat diaphragm. *Muscle Nerve* 29, 381–386. doi: 10.1002/mus.10558

Marmiroli, P., and Cavaletti, G. (2012). The glutamatergic neurotransmission in the central nervous system. *Curr. Med. Chem.* 19, 1269–1276. doi: 10.2174/092986712799462711

Minic, J., Molgó, J., Karlsson, E., and Krejci, E. (2002). Regulation of acetylcholine release by muscarinic receptors at the mouse neuromuscular junction depends on the activity of acetylcholinesterase. *Eur. J. Neurosci.* 15, 439–448. doi: 10.1046/j.0953-816x.2001.01875.x

Miyazaki, T., Hashimoto, K., Shin, H. S., Kano, M., and Watanabe, M. (2004). P/Q-type Ca^{2+} channel α1A regulates synaptic competition on developing cerebellar Purkinje cells. *J. Neurosci.* 24, 1734–1743. doi: 10.1523/JNEUROSCI.4208-03.2004

Nadal, L., Garcia, N., Hurtado, E., Simó, A., Tomàs, M., Lanuza, M. A., et al. (2016). Presynaptic muscarinic acetylcholine autoreceptors (M1, M2 and M4 subtypes), adenosine receptors (A1 and A2A) and tropomyosin-related kinase B receptor (TrkB) modulate the developmental synapse elimination process at the neuromuscular junction. *Mol. Brain* 9:67. doi: 10.1186/s13041-016-0248-9

Nadal, L., Garcia, N., Hurtado, E., Simó, A., Tomàs, M., Lanuza, M. A., et al. (2017a). Synergistic action of presynaptic muscarinic acetylcholine receptors and adenosine receptors in developmental axonal competition at the neuromuscular junction. *Dev. Neurosci.* doi: 10.1159/000458437 [Epub ahead of print].

Nadal, L., Garcia, N., Hurtado, E., Simó, A., Tomàs, M., Lanuza, M. A., et al. (2017b). Presynaptic muscarinic acetylcholine receptors and TrkB receptor cooperate in the elimination of redundant motor nerve terminals during development. *Front. Aging Neurosci.* 9:24. doi: 10.3389/fnagi.2017.00024

Nagano, M., and Suzuki, H. (2003). Quantitative analyses of expression of GDNF and neurotrophins during postnatal development in rat skeletal muscles. *Neurosci. Res.* 45, 391–399. doi: 10.1016/s0168-0102(03)00010-5

Nelson, P. G. (2005). Activity-dependent synapse modulation and the pathogenesis of Alzheimer disease. *Curr. Alzheimer Res.* 2, 497–506. doi: 10.2174/156720505774932232

Nelson, P. G., Lanuza, M. A., Jia, M., Li, M. X., and Tomàs, J. (2003). Phosphorylation reactions in activity-dependent synapse modification at the neuromuscular junction during development. *J. Neurocytol.* 32, 803–816. doi: 10.1023/B:NEUR.0000020625.70284.a6

Nishizaki, T., and Sumikawa, K. (1994). A cAMP-dependent Ca^{2+} signalling pathway at the endplate provided by the gamma to epsilon subunit switch in ACh receptors. *Mol. Brain Res.* 24, 341–346. doi: 10.1016/0169-328x(94)90148-1

Nykjaer, A., Lee, R., Teng, K. K., Jansen, P., Madsen, P., Nielsen, M. S., et al. (2004). Sortilin is essential for proNGF-induced neuronal cell death. *Nature* 427, 843–848. doi: 10.1038/nature02319

O'Brien, R. A., Ostberg, A. J., and Vrbová, G. (1978). Observations on the elimination of polyneuronal innervation in developing mammalian skeletal muscle. *J. Physiol.* 282, 571–582. doi: 10.1113/jphysiol.1978.sp012482

Offermanns, S., Hashimoto, K., Watanabe, M., Sun, W., Kurihara, H., Thompson, R. F., et al. (1997). Impaired motor coordination and persistent multiple climbing fiber innervation of cerebellar Purkinje cells in mice lacking Gαq. *Proc. Natl. Acad. Sci. U S A* 94, 14089–14094. doi: 10.1073/pnas.94.25.14089

Oliveira, L., Timóteo, M. A., and Correia-de-Sá, P. (2009). Negative crosstalk between M1 and M2 muscarinic autoreceptors involves endogenous adenosine activating A1 receptors at the rat motor endplate. *Neurosci. Lett.* 14, 127–131. doi: 10.1016/j.neulet.2009.05.001

Peng, H. B., Yang, J. F., Dai, Z., Lee, C. W., Hung, H. W., Feng, Z. H., et al. (2003). Differential effects of neurotrophins and schwann cell-derived signals on neuronal survival/growth and synaptogenesis. *J. Neurosci.* 23, 5050–5060.

Personius, K. E., Slusher, B. S., and Udin, S. B. (2016). Neuromuscular NMDA receptors modulate developmental synapse elimination. *J. Neurosci.* 36, 8783–8789. doi: 10.1523/JNEUROSCI.1181-16.2016

Pitts, E. V., Potluri, S., Hess, D. M., and Balice-Gordon, R. J. (2006). Neurotrophin and Trk-mediated signaling in the neuromuscular system. *Int. Anesthesiol. Clin.* 44, 21–76. doi: 10.1097/00004311-200604420-00004

Poo, M. M. (2001). Neurotrophins as synaptic modulators. *Nat. Rev. Neurosci.* 2, 24–32. doi: 10.1038/35049004

Poo, M., Boulanger, L., and Poo, M. M. (1999). Presynaptic depolarization facilitates neurotrophin-induced synaptic potentiation. *Nat. Neurosci.* 2, 346–351. doi: 10.1038/7258

Redfern, P. A. (1970). Neuromuscular transmission in new-born rats. *J. Physiol.* 209, 701–709. doi: 10.1113/jphysiol.1970.sp009187

Ribchester, R. R., and Barry, J. A. (1994). Spatial versus consumptive competition at polyneuronally innervated neuromuscular junctions. *Exp. Physiol.* 79, 465–494. doi: 10.1113/expphysiol.1994.sp003781

Sanes, J. R., and Lichtman, J. W. (1999). Development of the vertebrate neuromuscular junction. *Annu. Rev. Neurosci.* 22, 389–442. doi: 10.1146/annurev.neuro.22.1.389

Santafé, M. M., Salon, I., Garcia, N., Lanuza, M. A., Uchitel, O. D., and Tomàs, J. (2004). Muscarinic autoreceptors related with calcium channels in the strong and weak inputs at polyinnervated developing rat neuromuscular junctions. *Neuroscience* 123, 61–73. doi: 10.1016/j.neuroscience.2003.09.012

Santafé, M. M., Garcia, N., Lanuza, M. A., and Tomàs, J. (2007a). Protein kinase C activity affects neurotransmitter release at polyinnervated neuromuscular synapses. *J. Neurosci. Res.* 85, 1449–1457. doi: 10.1002/jnr.21280

Santafé, M. M., Lanuza, M. A., Garcia, N., Tomàs, M., and Tomàs, J. (2007b). Coupling of presynaptic muscarinic autoreceptors to serine kinases in low and high release conditions on the rat motor nerve terminal. *Neuroscience* 148, 432–440. doi: 10.1016/j.neuroscience.2007.06.017

Santafé, M. M., Garcia, N., Lanuza, M. A., Tomàs, M., Besalduch, N., and Tomàs, J. (2009a). Presynaptic muscarinic receptors, calcium channels and protein kinase C modulate the functional disconnection of weak inputs at polyinnervated neonatal neuromuscular synapses. *J. Neurosci. Res.* 87, 1195–1206. doi: 10.1002/jnr.21934

Santafé, M. M., Garcia, N., Lanuza, M. A., Tomàs, M., and Tomàs, J. (2009b). Interaction between protein kinase C and protein kinase A can modulate transmitter release at the rat neuromuscular synapse. *J. Neurosci. Res.* 87, 683–690. doi: 10.1002/jnr.21885

Santafé, M. M., Garcia, N., Lanuza, M. A., Uchitel, O. D., Salon, I., and Tomàs, J. (2002). Decreased calcium influx into the neonatal rat motor nerve terminals can recruit additional neuromuscular junctions during the synapse elimination period. *Neuroscience* 110, 147–154. doi: 10.1016/s0306-4522(01)00543-7

Santafé, M. M., Garcia, N., Lanuza, M. A., Uchitel, O. D., and Tomás, J. (2001). Calcium channels coupled to neurotransmitter release at dually innervated neuromuscular junctions in the newborn rat. *Neuroscience* 102, 697–708. doi: 10.1016/s0306-4522(00)00507-8

Santafé, M. M., Garcia, N., Tomàs, M., Obis, T., Lanuza, M. A., Besalduch, N., et al. (2014). The interaction between tropomyosin-related kinase B receptors and serine kinases modulates acetylcholine release in adult neuromuscular junctions. *Neurosci. Lett.* 561, 171–175. doi: 10.1016/j.neulet.2013.12.073

Santafé, M. M., Lanuza, M. A., Garcia, N., and Tomàs, J. (2005). Calcium inflow-dependent protein kinase C activity is involved in the modulation of transmitter release in the neuromuscular junction of the adult rat. *Synapse* 57, 76–84. doi: 10.1002/syn.20159

Santafé, M. M., Lanuza, M. A., Garcia, N., and Tomàs, J. (2006). Muscarinic autoreceptors modulate transmitter release through protein kinase C and protein kinase A in the rat motor nerve terminal. *Eur. J. Neurosci.* 23, 2048–2056. doi: 10.1111/j.1460-9568.2006.04753.x

Santafé, M. M., Priego, M., Obis, T., Garcia, N., Tomàs, M., Lanuza, M. A., et al. (2015). Adenosine receptors and muscarinic receptors cooperate in acetylcholine release modulation in the neuromuscular synapse. *Eur. J. Neurosci.* 42, 1775–1787. doi: 10.1111/ejn.12922

Santafé, M. M., Sabaté, M. M., Garcia, N., Ortiz, N., Lanuza, M. A., and Tomàs, J. (2008). Anti-GM2 gangliosides IgM paraprotein induces neuromuscular block without neuromuscular damage. *J. Neuroimmunol.* 204, 20–28. doi: 10.1016/j.jneuroim.2008.08.008

Santafé, M. M., Salon, I., Garcia, N., Lanuza, M. A., Uchitel, O. D., and Tomàs, J. (2003). Modulation of ACh release by presynaptic muscarinic autoreceptors in the neuromuscular junction of the newborn and adult rat. *Eur. J. Neurosci.* 17, 119–127. doi: 10.1046/j.1460-9568.2003.02428.x

Slutsky, I., Parnas, H., and Parnas, I. (1999). Presynaptic effects of muscarine on ACh release at the frog neuromuscular junction. *J. Physiol.* 514, 769–782. doi: 10.1111/j.1469-7793.1999.769ad.x

Stoop, R., and Poo, M. M. (1996). Synaptic modulation by neurotrophic factors. *Prog. Brain Res.* 109, 359–364. doi: 10.1016/s0079-6123(08)62118-4

Takamori, M. (2012). Structure of the neuromuscular junction: function and cooperative mechanisms in the synapse. *Ann. N Y Acad. Sci.* 1274, 14–23. doi: 10.1111/j.1749-6632.2012.06784.x

Teng, H. K., Teng, K. K., Lee, R., Wright, S., Tevar, S., Almeida, R. D., et al. (2005). ProBDNF induces neuronal apoptosis via activation of a receptor complex of p75NTR and sortilin. *J. Neurosci.* 25, 5455–5463. doi: 10.1523/JNEUROSCI.5123-04.2005

Thompson, W. J. (1985). Activity and synapse elimination at the neuromuscular junction. *Cell. Mol. Neurobiol.* 5, 167–182. doi: 10.1007/BF00711091

Tomàs, J., Santafé, M. M., Garcia, N., Lanuza, M. A., Tomàs, M., Besalduch, N., et al. (2014). Presynaptic membrane receptors in acetylcholine release modulation in the neuromuscular synapse. *J. Neurosci. Res.* 92, 543–554. doi: 10.1002/jnr.23346

Tomàs, J., Santafé, M. M., Lanuza, M. A., Garcia, N., Besalduch, N., and Tomàs, M. (2011). Silent synapses in neuromuscular junction development. *J. Neurosci. Res.* 89, 3–12. doi: 10.1002/jnr.22494

Waerhaug, O., and Ottersen, O. P. (1993). Demonstration of glutamate-like immunoreactivity at rat neuromuscular junctions by quantitative electron microscopic immunocytochemistry. *Anat. Embryol. (Berl).* 188, 501–513. doi: 10.1007/bf00190144

Walder, K. K., Ryan, S. B., Bzdega, T., Olszewski, R. T., Neale, J. H., and Lindgren, C. A. (2013). Immunohistological and electrophysiological evidence that N-acetylaspartylglutamate is a co-transmitter at the vertebrate neuromuscular junction. *Eur. J. Neurosci.* 37, 118–129. doi: 10.1111/ejn.12027

Watanabe, M., and Kano, M. (2010). Climbing fiber synapse elimination in cerebellar purkinje cells. *Eur. J. Neurosci.* 34, 1697–1710. doi: 10.1111/j.1460-9568.2011.07894.x

Wright, M. C., Potluri, S., Wang, X., Dentcheva, E., Gautam, D., Tessler, A., et al. (2009). Distinct muscarinic acetylcholine receptor subtypes contribute to stability and growth, but not compensatory plasticity, of neuromuscular synapses. *J. Neurosci.* 29, 14942–14955. doi: 10.1523/jneurosci.2276-09.2009

Zorumski, C. F., and Mennerick, S. (2000). Neural activity and survival in the developing nervous system. *Mol. Neurobiol.* 22, 41–54. doi: 10.1385/MN:22:1-3:041

Conflict of Interest Statement: The authors declare that the research was conducted in the absence of any commercial or financial relationships that could be construed as a potential conflict of interest.

frontiers in Neuroscience

ORIGINAL RESEARCH
published: 13 April 2017
doi: 10.3389/fnins.2017.00206

Spine Enlargement of Pyramidal Tract-Type Neurons in the Motor Cortex of a Rat Model of Levodopa-Induced Dyskinesia

Tatsuya Ueno[1,2]*, *Haruo Nishijima*[1,2], *Shinya Ueno*[2] and *Masahiko Tomiyama*[1,2]

[1] Department of Neurology, Aomori Prefectural Central Hospital, Aomori, Japan, [2] Department of Neurophysiology, Hirosaki University Graduate School of Medicine, Hirosaki, Japan

Growing evidence suggests that abnormal synaptic plasticity of cortical neurons underlies levodopa-induced dyskinesia (LID) in Parkinson's disease (PD). Spine morphology reflects synaptic plasticity resulting from glutamatergic transmission. We previously reported that enlargement of the dendritic spines of intratelencephalic-type (IT) neurons in the primary motor cortex (M1) is linked to the development of LID. However, the relevance of another M1 neuron type, pyramidal-tract (PT) neurons, to LID remains unknown. We examined the morphological changes of the dendritic spines of M1 PT neurons in a rat model of LID. We quantified the density and size of these spines in 6-hydroxydopamine-lesioned rats (a model of PD), 6-hydroxydopamine-lesioned rats chronically treated with levodopa (a model of LID), and control rats chronically treated with levodopa. Dopaminergic denervation alone had no effect on spine density and head area. However, the LID model showed significant increases in the density and spine head area and the development of dyskinetic movements. In contrast, levodopa treatment of normal rats increased spine density alone. Although, chronic levodopa treatment increases PT neuron spine density, with or without dopaminergic denervation, enlargement of PT neuron spines appears to be a specific feature of LID. This finding suggests that PT neurons become hyperexcited in the LID model, in parallel with the enlargement of spines. Thus, spine enlargement, and the resultant hyperexcitability of PT pyramidal neurons, in the M1 cortex might contribute to abnormal cortical neuronal plasticity in LID.

Keywords: Parkinson's disease, dyskinesia, levodopa, motor cortex, dendritic spines, plasticity, 6-hydroxydopamine, pyramidal neuron

OPEN ACCESS

Edited by:
Jaewon Ko,
Daegu Gyeongbuk Institute of Science and Technology, South Korea

Reviewed by:
Se-Young Choi,
Seoul National University, South Korea
Weien Yuan,
Shanghai Jiao Tong University, China

***Correspondence:**
Tatsuya Ueno
lacote19thg@gmail.com

Specialty section:
This article was submitted to Neurodegeneration, a section of the journal Frontiers in Neuroscience

Received: *03 February 2017*
Accepted: *27 March 2017*
Published: *13 April 2017*

Citation:
Ueno T, Nishijima H, Ueno S and Tomiyama M (2017) Spine Enlargement of Pyramidal Tract-Type Neurons in the Motor Cortex of a Rat Model of Levodopa-Induced Dyskinesia. Front. Neurosci. 11:206. doi: 10.3389/fnins.2017.00206

INTRODUCTION

Parkinson's disease (PD) is characterized by the loss of dopaminergic neurons in the substantia nigra of the midbrain, resulting in bradykinesia, muscular rigidity, rest tremor, and postural instability (Gibb and Lees, 1988). The most effective treatment for PD is oral administration of the dopamine precursor, L-3,4-dihydroxyphenylalanine (levodopa) (Olanow et al., 2006). However, long-term treatment with levodopa induces a variety of abnormal involuntary movements, termed levodopa-induced dyskinesia (LID), which represent a major treatment limitation and reduce the quality of life of PD patients (Olanow et al., 2006).

The emergence of these abnormal involuntary movements is associated with altered corticostriatal synaptic plasticity (Picconi et al., 2003). Electrophysiological recordings performed in corticostriatal slices of 6-hydroxydopamine (6-OHDA) lesioned rats with LID have shown that depotentiation at corticostriatal synapses to direct pathway striatal projection neurons (dSPN) is lost after the induction of long-term potentiation (LTP) (Shen et al., 2015). Depotentiation reverses synaptic strength from the potentiated state to pre-LTP levels, which is implicated in the mechanisms of physiological "forgetting" (Picconi et al., 2003). Consequently, the absence of depotentiation may result in the storage of unessential motor information, suggesting a key neurophysiological feature of LID (Picconi et al., 2003). Synapse strength can be determined by alteration of spine volume, or enlargement or shrinkage of spines (Kasai et al., 2010). Indeed, in a rat model of LID, we showed that dSPN dendritic spines became enlarged, suggesting supersensitivity of the corticostriatal excitatory synapses of dSPNs (Nishijima et al., 2014).

Dopaminergic signaling within the primary motor cortex (M1) is necessary for normal motor skill learning and synaptic plasticity (Molina-Luna et al., 2009). Dopaminergic projections to M1 arise from the ventral tegmental area (Hosp et al., 2011), in which neurons are also lost in PD patients (Uhl et al., 1985). Thus, progressive degeneration of dopaminergic neurons in the ventral tegmental area leads to decreased endogenous dopamine in the cortex, which affects synaptic plasticity in the M1 (Huang et al., 2011). In human studies, M1 plasticity is investigated using motor-evoked potential amplitudes elicited by transcranial magnetic stimulation (Huang et al., 2011). Using this method, PD patients with LID exhibit a lack of depotentiation-like cortical plasticity (Huang et al., 2011). This suggests that unessential motor information accounting for LID is stored in both in the striatum and the M1 (Picconi et al., 2003; Huang et al., 2011).

In rodents, corticostriatal neurons in the motor cortex are categorized into two main types: intratelencephalic (IT) and pyramidal tract (PT) neurons (Reiner et al., 2010). It has been demonstrated that IT neurons preferentially innervate dSPNs in the ipsilateral and contralateral striatum, whereas PT neurons preferentially innervate SPNs of the indirect pathway (iSPN) in the ipsilateral striatum, and send axons to the brainstem via the pyramidal tract (Reiner et al., 2010). It has been reported that dSPNs appear to play an important role in the development of LID (Picconi et al., 2003; Shen et al., 2015). In a previous study, we found enlargement of IT neuron spines in a LID model rat and proposed that IT neurons in the M1 may store abnormal information resulting in LID (Ueno et al., 2014). Furthermore, IT neurons in the M1 of the LID rat model displayed increased amplitudes of miniature excitatory postsynaptic currents (Ueno et al., 2014). These data suggest that IT neurons in dyskinesia-primed animals acquire supersensitivity to excitatory stimuli (Ueno et al., 2014).

However, it has been demonstrated that dSPNs and iSPNs are innervated by both PT and IT neurons (Kress et al., 2013; Deng et al., 2015). Thus, the preferential innervation from IT and PT neurons to SPNs remains controversial (Deng et al., 2015). Thus, it is conceivable that PT neurons also play an important role in the development of LID. Therefore, we investigated the density and size of PT neuron spines in the M1 in rat models of PD and LID.

Abbreviations: 3D, 3-dimensional; 6-OHDA, 6-hydroxydopamine; AIM, abnormal involuntary movement; dSPN, direct pathway striatal projection neurons; iSPN, indirect pathway striatal projection neurons; IT, intratelencephalic; LID, levodopa-induced dyskinesia; LTC, levodopa-treated control; LTP, long-term potentiation; M1, primary motor cortex; PD, Parkinson's disease; PT, pyramidal tract.

MATERIALS AND METHODS

Experimental Animals

Male Wistar rats (Japan Clea Co. Ltd., Tokyo, Japan) were housed in a temperature-controlled room (∼25°C) with a 12-h day/night cycle, with free access to food and water. This study was conducted in accordance with the guidelines for animal research issued by the Physiological Society of Japan and by Hirosaki University School of Medicine with the approval of Hirosaki University Animal Experimentation Committee.

Creation of Rat Models

We prepared eight 6-OHDA-lesioned hemiparkinsonian rats (PD model), eight 6-OHDA-lesioned hemiparkinsonian rats with chronic levodopa treatment (LID model), eight control rats with chronic levodopa treatment (levodopa-treated control: LTC model), and nine control rats with saline treatment (Control), as previously described (Ueno et al., 2014; **Figure 1**).

6-OHDA (8 mg/4 mL in saline with 0.01% ascorbic acid) (Sigma, San Diego, CA, USA) (PD and LID models) or saline (LTC and Control) was injected into the medial forebrain bundle (4.5 mm posterior to bregma, 1.2 mm lateral to the sagittal suture, and 8.5 mm ventral to the dural surface) in the right hemisphere of 10-week-old rats anesthetized with sodium pentobarbital (Nembutal, 50 mg/kg body weight intraperitoneally; Dainippon Sumitomo Pharma Co., Ltd., Osaka, Japan). Apomorphine (Sigma) was administered to evaluate dopaminergic denervation at 12 weeks of age. We previously reported nearly complete dopaminergic denervation in the striatum and M1 with this technique (Maeda et al., 1999; Ueno et al., 2014; **Figure 1**).

During the 4–6 weeks after the apomorphine test, both 6-OHDA-lesioned rats with dopaminergic denervation and sham-operated rats received 50 mg/kg levodopa methyl ester (Sigma) with 12.5 mg/kg benserazide (Sigma) (LID model and LTC models, respectively) or saline (PD model and Control models, respectively), twice daily (morning and evening) for 14 consecutive days (**Figure 1**). To evaluate the effects of levodopa, we measured abnormal involuntary movement (AIM) scores (Cenci and Lundblad, 2007) on days 1, 4, and 11 (**Figure 1**). The AIM score is considered comparable to LID assessments in patients with PD (Cenci and Lundblad, 2007). We observed and scored the rats every 20 min during the 2-h period following levodopa injection. We assessed and summed the scores for the three AIM subtypes (limb, axial, and orolingual) (Cenci and Lundblad, 2007).

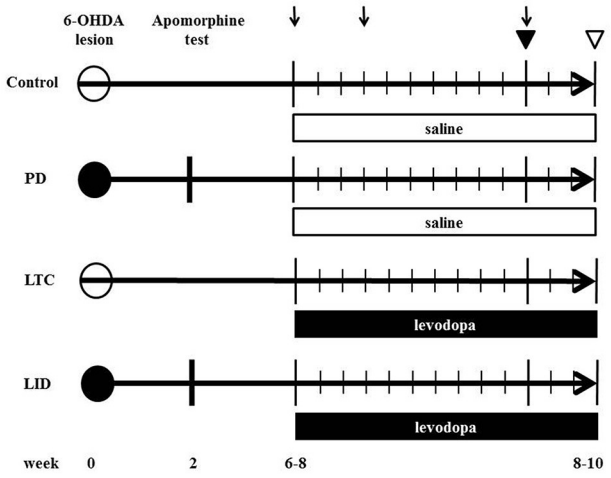

FIGURE 1 | Time chart and experimental design of the study. We injected 6-hydroxydopamine (6-OHDA) or saline into the medial forebrain bundle to induce hemiparkinsonian (levodopa-induced dyskinesia model [LID]; Parkinson's disease model [PD]) or sham-operated rats (levodopa-treated control [LTC]; Control), respectively. The number indicates the weeks post 6-OHDA lesion. At 2 weeks after 6-OHDA, dopaminergic denervation was confirmed by apomorphine test. LID and LTC rats received daily levodopa treatment for 2 weeks, while PD, and Control rats received daily saline for 2 weeks. Closed and open circles indicate 6-OHDA and saline injection, respectively. Arrows indicate abnormal involuntary movement rating sessions. Closed and open triangles indicate the days of the tracer injection and sacrifice, respectively.

Dendritic Spine Morphology

We used eight PD models, eight LID models, nine LTC models, and eight controls at 16–18 weeks of age (**Figure 1**). Our basic method has previously been described in detail (Ueno et al., 2014). To selectively label the cell bodies of PT neurons in the right M1, we stereotactically injected a retrograde tracer, Fast Blue (Polysciences, Inc., Warrington, PA, USA), over a 1-min period into the right pontine pyramidal tract (9.6 mm posterior to bregma, 0.5 mm lateral to the sagittal suture, and 10.7 mm ventral to the dural surface) on day 11 of drug treatment (Paxinos and Watson, 1998; Reiner et al., 2010) (**Figure 1**). Four days later, the rats were deeply anesthetized with sodium pentobarbital (Nembutal, >75 mg/kg intraperitoneally), intracardially perfused with 4% paraformaldehyde at 12 h after the last levodopa or saline treatment, and the brains then removed.

Serial 250-μm-thick coronal sections were cut through the M1, and Lucifer Yellow (Sigma) was injected into cell bodies of Fast Blue-labeled neurons in the right M1 under ultraviolet excitation (380–420 nm) with continuous current (up to 100 nA). Neurons were filled with Lucifer Yellow until their dendritic spines were sufficiently visible (**Figure 2A**). The tissue was examined by confocal microscopy, and images were taken with a digital camera (C1si; Nikon, Tokyo, Japan). Yellow signals (515/530 nm) were acquired from each sample using 488 nm excitation. Fluorescence projection images of somata and dendritic fields were acquired with a 60× oil-immersion lens. We selected 5–10 cells for each rat, and 1–5 horizontally projecting dendrites from each cell. We then measured the density and size of spines on the basal dendrite, 50–100 μm distal to the cell body (**Figure 2B**). Images of the spines in each dendrite were acquired with a 60× oil-immersion lens (5.0 zoom factor; 0.0064 μm^2/pixel resolution) at 0.25-μm focal steps. Image stacks were three-dimensional (3D)-deconvoluted using NIS-Elements software (Nikon) and volume rendered as 2D images to facilitate overview of the figures (**Figure 2C**). In total, we measured 9415 spines from 202 neurons in 33 motor cortices. Each spine was manually traced. The average number of spines per 10 μm of linear dendritic length was expressed as the spine density. All spines were drawn and no distinction was made between different spine types. We measured the cross-sectional area of the spine head in 2D reconstructed images. Image analysis was performed using Image J (National Institutes of Health, Bethesda, MD, USA). For analyses, we selected intracellularly injected cells (Control: 54 cells; PD model: 50 cells; LID model: 49 cells; LTC model: 49 cells) based on our previous criteria (**Table 1**; Ueno et al., 2014).

Statistics

We analyzed the spine density and the average cross-sectional area of the spine heads in each basal dendrite. Statistical analyses were performed with EZR freeware v.1.32 (Saitama Medical Center, Jichi Medical University, Saitama, Japan) (Kanda, 2013). A probability level of 5% ($P < 0.05$) was considered statistically significant. Data are presented as means ± standard error or boxplots showing medians, and 25 and 75% quartile ranges. The spine density, cross-sectional area of the spine heads, and AIM scores were examined using parametric tests (one-way analysis of variance followed by Tukey–Kramer *post-hoc* test), as the Shapiro–Wilk test indicated that the distributions were normal.

RESULTS

AIM Scores in LID and LTC Models

Dopaminergic denervation plus levodopa treatment (LID group) significantly increased AIM scores at day 4 ($P < 0.001$ cf. day 1) and day 11 ($P < 0.001$ cf. day 4), whereas levodopa treatment had no effect on AIM scores in control rats (LTC group) (**Figure 3**).

Morphological Changes in Dendritic Spines of PT Neurons

Forty-five animals underwent histological examinations with 12 excluded due to unsatisfactory histology. We analyzed the spine density and average cross-sectional area of spine heads in 619 basal dendrites (control = 162, PD = 152, LID = 153, LTC = 152) (**Table 1**; **Figure 4**). Using histograms from 9,415 cross-sectional areas of spine heads, the LID group showed significantly enlarged spine heads compared with the other groups ($P < 0.001$) (**Figure 5A**).

Levodopa treatment of the dopaminergic denervation (LID group) and control rats (LTC group) significantly increased the spine density of M1 PT neurons compared with the Control ($P < 0.05$ cf. LID; $P < 0.001$ cf. LTC) and PD groups ($P < 0.001$ cf. LID; $P < 0.001$ cf. LTC) (Control group: 7.2 ± 0.15/10 μm; PD

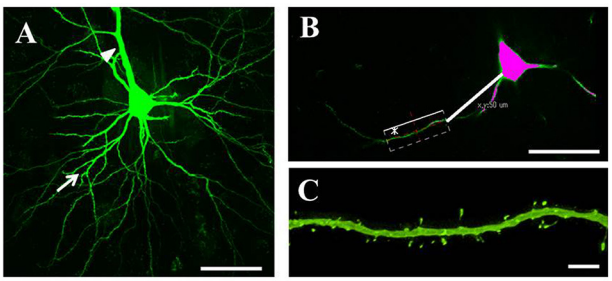

FIGURE 2 | Analysis of dendritic spines. (A) Representative confocal images of pyramidal-tract type (PT) neurons in the primary motor cortex. PT neurons were filled with Lucifer Yellow until their dendritic spines became sufficiently visible. We randomly selected several cells for each tissue slice, and several horizontally projecting dendrites for each cell. Arrows: basal dendrites; arrowhead: apical dendrite. Scale bar = 50 μm. **(B)** Dendritic spines were examined at 50–100 μm distal from the cell body. Scale bar = 50 μm. **(C)** Higher magnification view of the area indicated by asterisk in **(B)** showing a basal dendrite 50–100 μm distal from the soma. Small green dots along the basal dendrite represent dendritic spines. Scale bar = 5 μm.

TABLE 1 | Number of rat, cell, basal dendrite, and spines analyzed.

	Rat	Cell	Analyzed basal dendrite	Analyzed spine
Control	9	54	162	2,320
Parkinsonian	8	50	152	2,107
Dyskinesia	8	49	153	2,419
Levodopa treated control	8	49	152	2,569

group: 7.0 ± 0.20/10 μm; LID group: 7.9 ± 0.20/10 μm; LTC group: 8.5 ± 0.17/10 μm). However, dopaminergic denervation (PD group) had no effect on spine density of PT neurons compared with the Control group. No significant differences were observed between the LID group and the LTC group (**Figures 4**, **5B**).

Dopaminergic denervation (PD group) had no effect on the spine size of PT neurons, while dopaminergic denervation plus levodopa treatment (LID group) significantly enlarged dendritic spines compared with the Control group, the PD group, and the LTC group ($P < 0.001$) (**Figures 4**, **5C**). However, levodopa treatment of control rats (LTC group) had no effects on spine size (Control group: 0.14 ± 0.003 μm^2; PD group: 0.14 ± 0.003 μm^2; LID group: 0.16 ± 0.003 μm^2; LTC group: 0.14 ± 0.002 μm^2) (**Figures 4**, **5C**).

DISCUSSION

In this study, we demonstrated that chronic levodopa treatment in normal and LID model rats increases the spine density of PT neurons in the M1. The dendritic spines of M1 PT neurons became enlarged in the LID model, and this enlargement of spines appears to be relevant to the development of AIMs. This structural change suggests that PT neurons become supersensitive to glutamatergic inputs in dyskinetic rats.

Effect of Dopaminergic Denervation on Dendritic Spines of M1 PT Neurons

We found that dopaminergic denervation alone had no effect on M1 PT neuron spine density or size (**Figures 4**, **5B,C**). The preservation of spine density in the motor cortex after dopaminergic denervation is comparable with previous studies (Miklyaeva et al., 2007; Wang and Deutch, 2008; Ueno et al., 2014). However, Guo et al. (2015) recently reported that both spine elimination and formation of layer V pyramidal neurons of the primary motor cortex were increased in a mouse model of PD induced by 1-methyl-4-phenyl-1,2,3,6-tetrahydropyridine, resulting in a decrease in spine density in a PD mouse model. Although, the exact causes of the differences in spine density between these studies remain unclear, they may relate to whether basal or apical dendrites were analyzed. For example, no significant changes in spine density were found in three studies examining the basal dendrites of layer V pyramidal neurons (Miklyaeva et al., 2007; Wang and Deutch, 2008; Ueno et al., 2014). By contrast, Guo et al. (2015) demonstrated a decrease in the spine density of apical dendrites of layer V pyramidal neurons; a similar, but not significant, trend has also been reported (Wang and Deutch, 2008).

There were also differences between these studies in the timing of measurements after dopaminergic lesioning (Miklyaeva et al., 2007; Wang and Deutch, 2008; Ueno et al., 2014; Guo et al., 2015). Differences in the methodological approaches to visualizing spines may also be important. Although, previous studies have used the Golgi-Cox method (Miklyaeva et al., 2007; Wang and Deutch, 2008) and confocal laser scanning microscopy (Ueno et al., 2014), Guo et al. (2015) used two-photon laser scanning microscopy. The cell types examined may also result in differences. In studies other than ours, spine morphology was examined without discriminating between PT and IT neurons (Miklyaeva et al., 2007; Wang and Deutch, 2008; Ueno et al., 2014; Guo et al., 2015). As IT and PT neurons express D1 and D2 dopamine receptors, respectively, (Gee et al., 2012; Seong and Carter, 2012; Dembrow and Johnston, 2014), dopaminergic denervation may differentially impact the spine density of these cell types. Finally, differences in the methods used to induce dopaminergic denervation (e.g., local application of 6-OHDA into dopamine neurons versus generalized administration of 1-methyl-4-phenyl-1,2,3,6-tetrahydropyridine) may be an important factor contributing to these contrasting findings.

Increased Spine Density of M1 PT Neurons with Chronic Levodopa Treatment with or without Dopaminergic Denervation

Here we showed that chronic levodopa treatment with or without dopaminergic denervation increases the spine density of PT neurons in M1 (**Figures 4**, **5B**). Levodopa normalizes the increase in spine turnover in the M1 following dopaminergic denervation (Guo et al., 2015). Thus, levodopa treatment may affect spine turnover in both the dopamine-denervated M1 and the dopamine-intact M1. However, we previously reported that

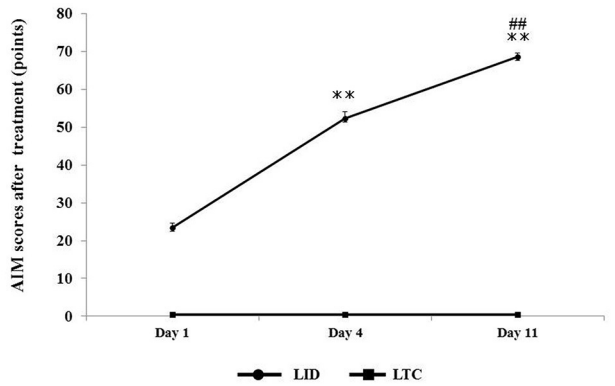

FIGURE 3 | Abnormal involuntary movement (AIM) scores in LID or LTC groups on days 1, 4, and 11 of treatment. The scores represent total scores of the three AIM subtypes (limb, axial, and orolingual) (Cenci and Lundblad, 2007). The total score of the three AIMs was significantly increased in the LID group, while no AIMS were observed in the LTC group (one-way analysis of variance followed by *post-hoc* Tukey–Kramer test: $^{**}P < 0.001$ vs. Day 1, $^{\#\#}P < 0.001$ vs. Day 4).

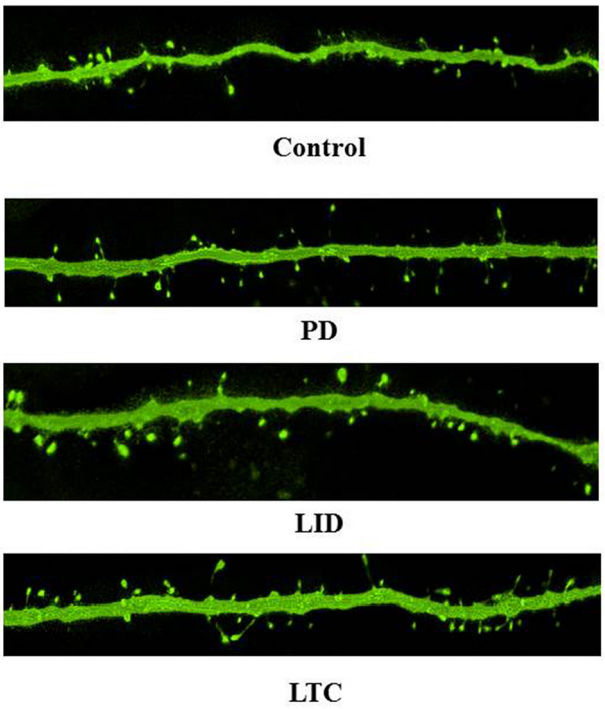

FIGURE 4 | Representative confocal microscopy images of dendritic spines on PT neurons. Scale bar = 5 μm.

chronic levodopa treatment in PD model and control rats does not change the spine density of M1 IT neurons (Ueno et al., 2014). The distribution of dopamine receptors may underlie these differences in spine density between IT and PT neurons. Although, the specific distribution of dopamine receptors in layer V pyramidal neurons of the M1 remains to be determined, IT and PT neurons in the mouse medial prefrontal cortex express D1 and D2 receptors, respectively (Gee et al., 2012; Seong and Carter, 2012; Dembrow and Johnston, 2014). D1 dopamine receptor signaling regulates spine elimination in the M1, while D2 receptor signaling controls spine formation in the M1 (Guo et al., 2015). Taken together, the differences in the effects of chronic levodopa treatment in naive rats may be dependent on the dopamine receptor type. Levodopa treatment increases dopamine levels in the motor cortex without dopaminergic denervation (Navailles et al., 2011). Thus, the increase in PT neuron spine density may be induced by the D2 receptor response in the M1. Different analysis methods may also contribute to the differences in spine density in our two studies: the spine density of each dendrite was measured in the present study, while we previously used the average spine density of each neuron, and then the average for each rat (Ueno et al., 2014).

Enlargement of Dendritic Spines of M1 PT Neurons of LID Model Rats

Dopaminergic denervation or levodopa treatment alone had no effect on dendritic spine size (**Figures 4**, **5C**). However, levodopa treatment after dopaminergic denervation enlarged dendritic spines in PT neurons, with the appearance of dyskinetic movements (**Figures 3**, **4**, **5C**). Thus, chronic levodopa treatment after dopaminergic denervation results in the enlargement of dendritic spines in both IT (Ueno et al., 2014) and PT neurons. This structural change suggests that PT neurons also acquire supersensitivity to glutamatergic inputs in dyskinesia-primed rats, as is the case for IT neurons in the M1 (Ueno et al., 2014).

We previously reported that dendritic spines become enlarged in both dSPNs in the striatum and IT neurons in the M1 cortex of the same LID model (Nishijima et al., 2014; Ueno et al., 2014). Loss of depotentiation after induction of LTP at corticostriatal synapses is a key neurophysiological feature of LID models (Picconi et al., 2003; Shen et al., 2015), and a similar loss of depotentiation-like plasticity has been demonstrated in PD patients using transcranial magnetic stimulation (Huang et al., 2011). Dendritic spines form the postsynaptic compartment of the majority of excitatory glutamatergic synapses in the brain (Murakoshi and Yasuda, 2012). Dendritic spine size is tightly correlated with synaptic strength (Matsuzaki et al., 2001), and is actively regulated during synaptic plasticity (Matsuzaki et al., 2004). Spines display long-lasting enlargement during LTP (Matsuzaki et al., 2004; Harvey and Svoboda, 2007), which results from actin polymerization and insertion of AMPA receptors into the dendritic spines (Matsuzaki et al., 2004; Rudy, 2015). These events lead to an increase in the sensitivity of postsynaptic sites to glutamate (Murakoshi and Yasuda, 2012). As enlargement of dendritic spines indicates a supersensitivity of excitatory synapses (Segal, 2010), our data support a lack of potentiation in the motor cortex in LID (Huang et al., 2011). Taken together, the loss of depotentiation may correlate with enlargement of dendritic spines in dyskinesia-primed animal models. The supersensitivity of the synapses of cortical motor neurons may contribute

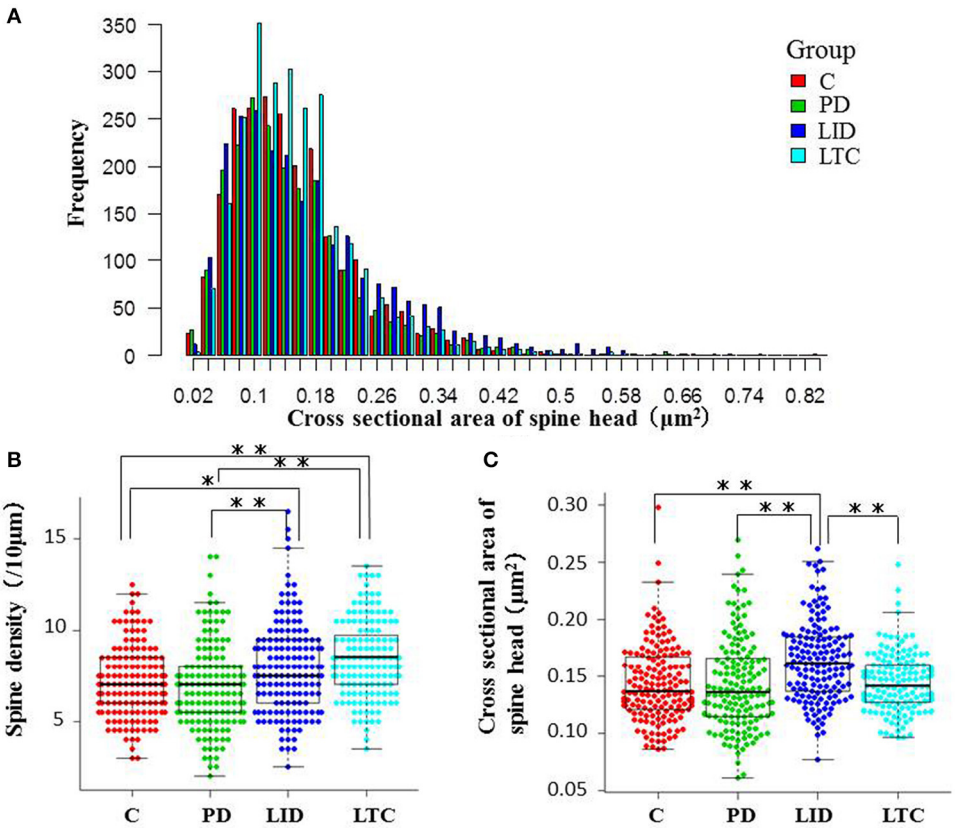

FIGURE 5 | Morphological evaluation of spines on basal dendrites. (A) Histograms of cross-sectional areas of the analyzed spine heads. The red, green, blue, and light blue bars indicate control, PD, LID, and LTC groups, respectively. The histogram shows that the cross-sectional area of the spine heads was increased in the LID group compared with the other groups. **(B)** Spine density was significantly increased in the LID and LTC groups compared with the Control and PD groups. **(C)** Spine size was significantly increased in the LID group (*$P < 0.05$, **$P < 0.001$, one-way analysis of variance followed by *post-hoc* Tukey–Kramer test). C, control.

to the strengthened signal transduction demonstrated in LID models (Ren et al., 2011; Yang et al., 2012a,b; Xie et al., 2014). Accordingly, the expression of LID is inhibited by reduction of cAMP-dependent protein kinase, dopamine and cAMP-dependent phosphoprotein of 32 kDa, and phosphorylated glutamate receptor 1 (Ren et al., 2011; Yang et al., 2012a,b; Xie et al., 2014). These molecules are essential for the activation of Ca2+/calmodulin–dependent protein kinase II, which is associated with the enlargement of dendritic spines (Yagishita et al., 2014).

Although, we did not measure the synaptic function of PT neurons using electrophysiology in this study, the spine enlargement of PT neurons probably results in supersensitivity of PT neurons to glutamatergic input in the M1 (Ueno et al., 2014), and may underlie the emergence of LID. IT-type inputs to dSPNs and PT-type inputs to iSPNs may show short-term facilitation, whereas IT-type inputs to iSPNs and PT-type inputs to dSPNs may show short-term depression (Morita, 2014). IT-dSPN and PT-iSPN synapses evoke short-term facilitation, whereas IT-iSPN and PT-dSPN synapses evoke depression (Shipp, 2017). Thus, IT and PT neurons have complementary effects on dSPNs and iSPNs. The enlargement of IT neuron spines in our previous study (Ueno et al., 2014), and of PT neuron spines in the present study, indicates the enhanced sensitivity of pyramidal neurons in the M1. This may relate to the generation of abnormal oscillation in the cortex of dyskinetic animal models (Halje et al., 2012; Dupre et al., 2016). Here, we provide further evidence for the storage of abnormal plastic information in the M1 following dyskinetic movements.

CONCLUSIONS

In the primary motor cortex, chronic levodopa treatment modifies the formation of dendritic spines in PT neurons with or without dopaminergic denervation. Furthermore, chronic levodopa treatment after dopaminergic denervation causes the enlargement of PT neuron dendritic spines. These results suggest that spine enlargement in PT neurons may be a key factor in the development of LID in the M1.

AUTHOR CONTRIBUTIONS

Conception and design of the study, data interpretation, drafting the article or revising it critically for important intellectual

content, and final approval of the version to be submitted: TU, HN, SU, and MT; Data acquisition and analysis: TU.

FUNDING

This study was supported by a grant-in-aid for scientific research from the Ministry of Education, Culture, Sports, Science and Technology of Japan (No. 22590952) to MT. The funding source had no role in study design, data collection, data analysis, data interpretation, or writing of the report.

ACKNOWLEDGMENTS

The authors thank Ms. Saeko Osanai for study support.

REFERENCES

Cenci, M. A., and Lundblad, M. (2007). Ratings of L-DOPA-induced dyskinesia in the unilateral 6-OHDA lesion model of Parkinson's disease in rats and mice. *Curr. Protoc. Neurosci.* Chapter 9:Unit 9.25. doi: 10.1002/0471142301.ns0925s41

Dembrow, N., and Johnston, D. (2014). Subcircuit-specific neuromodulation in the prefrontal cortex. *Front. Neural Circuits* 8:54. doi: 10.3389/fncir.2014.00054

Deng, Y., Lanciego, J., Kerkerian-Le-Goff, L., Coulon, P., Salin, P., Kachidian, P., et al. (2015). Differential organization of cortical inputs to striatal projection neurons of the matrix compartment in rats. *Front. Syst. Neurosci.* 9:51. doi: 10.3389/fnsys.2015.00051

Dupre, K. B., Cruz, A. V., McCoy, A. J., Delaville, C., Gerber, C. M., Eyring, K. W., et al. (2016). Effects of L-dopa priming on cortical high beta and high gamma oscillatory activity in a rodent model of Parkinson's disease. *Neurobiol. Dis.* 86, 1–15. doi: 10.1016/j.nbd.2015.11.009

Gee, S., Ellwood, I., Patel, T., Luongo, F., Deisseroth, K., and Sohal, V. S. (2012). Synaptic activity unmasks dopamine D2 receptor modulation of a specific class of layer V pyramidal neurons in prefrontal cortex. *J. Neurosci.* 32, 4959–4971. doi: 10.1523/JNEUROSCI.5835-11.2012

Gibb, W. R., and Lees, A. J. (1988). The relevance of the Lewy body to the pathogenesis of idiopathic Parkinson's disease. *J. Neurol. Neurosurg. Psychiatry* 51, 745–752. doi: 10.1136/jnnp.51.6.745

Guo, L., Xiong, H., Kim, J. I., Wu, Y. W., Lalchandani, R. R., Cui, Y., et al. (2015). Dynamic rewiring of neural circuits in the motor cortex in mouse models of Parkinson's disease. *Nat. Neurosci.* 18, 1299–1309. doi: 10.1038/nn.4082

Halje, P., Tamte, M., Richter, U., Mohammed, M., Cenci, M. A., and Petersson, P. (2012). Levodopa-induced dyskinesia is strongly associated with resonant cortical oscillations. *J. Neurosci.* 32, 16541–16551. doi: 10.1523/JNEUROSCI.3047-12.2012

Harvey, C. D., and Svoboda, K. (2007). Locally dynamic synaptic learning rules in pyramidal neuron dendrites. *Nature* 450, 1195–1200. doi: 10.1038/nature06416

Hosp, J. A., Pekanovic, A., Rioult-Pedotti, M. S., and Luft, A. R. (2011). Dopaminergic projections from midbrain to primary motor cortex mediate motor skill learning. *J. Neurosci.* 31, 2481–2487. doi: 10.1523/JNEUROSCI.5411-10.2011

Huang, Y. Z., Rothwell, J. C., Lu, C. S., Chuang, W. L., and Chen, R. S. (2011). Abnormal bidirectional plasticity-like effects in Parkinson's disease. *Brain* 134(Pt 8), 2312–2320. doi: 10.1093/brain/awr158

Kanda, Y. (2013). Investigation of the freely available easy-to-use software 'EZR' for medical statistics. *Bone Marrow Transplant.* 48, 452–458. doi: 10.1038/bmt.2012.244

Kasai, H., Fukuda, M., Watanabe, S., Hayashi-Takagi, A., and Noguchi, J. (2010). Structural dynamics of dendritic spines in memory and cognition. *Trends Neurosci.* 33, 121–129. doi: 10.1016/j.tins.2010.01.001

Kress, G. J., Yamawaki, N., Wokosin, D. L., Wickersham, I. R., Shepherd, G. M., and Surmeier, D. J. (2013). Convergent cortical innervation of striatal projection neurons. *Nat. Neurosci.* 16, 665–667. doi: 10.1038/nn.3397

Maeda, T., Kannari, K., Suda, T., and Matsunaga, M. (1999). Loss of regulation by presynaptic dopamine D2 receptors of exogenous L-DOPA-derived dopamine release in the dopaminergic denervated striatum. *Brain Res.* 817, 185–191. doi: 10.1016/S0006-8993(98)01248-7

Matsuzaki, M., Ellis-Davies, G. C., Nemoto, T., Miyashita, Y., Iino, M., and Kasai, H. (2001). Dendritic spine geometry is critical for AMPA receptor expression in hippocampal CA1 pyramidal neurons. *Nat. Neurosci.* 4, 1086–1092. doi: 10.1038/nn736

Matsuzaki, M., Honkura, N., Ellis-Davies, G. C., and Kasai, H. (2004). Structural basis of long-term potentiation in single dendritic spines. *Nature* 429, 761–766. doi: 10.1038/nature02617

Miklyaeva, E. I., Whishaw, I. Q., and Kolb, B. (2007). A golgi analysis of cortical pyramidal cells in the unilateral parkinson rat: absence of change in the affected hemisphere vs hypertrophy in the intact hemisphere. *Restor. Neurol. Neurosci.* 25, 91–99.

Molina-Luna, K., Pekanovic, A., Rohrich, S., Hertler, B., Schubring-Giese, M., Rioult-Pedotti, M. S., et al. (2009). Dopamine in motor cortex is necessary for skill learning and synaptic plasticity. *PLoS ONE*4:e7082. doi: 10.1371/journal.pone.0007082

Morita, K. (2014). Differential cortical activation of the striatal direct and indirect pathway cells: reconciling the anatomical and optogenetic results by using a computational method. *J. Neurophysiol.* 112, 120–146. doi: 10.1152/jn.00625.2013

Murakoshi, H., and Yasuda, R. (2012). Postsynaptic signaling during plasticity of dendritic spines. *Trends Neurosci.* 35, 135–143. doi: 10.1016/j.tins.2011.12.002

Navailles, S., Bioulac, B., Gross, C., and De Deurwaerdere, P. (2011). Chronic L-DOPA therapy alters central serotonergic function and L-DOPA-induced dopamine release in a region-dependent manner in a rat model of Parkinson's disease. *Neurobiol. Dis.* 41, 585–590. doi: 10.1016/j.nbd.2010.11.007

Nishijima, H., Suzuki, S., Kon, T., Funamizu, Y., Ueno, T., Haga, R., et al. (2014). Morphologic changes of dendritic spines of striatal neurons in the levodopa-induced dyskinesia model. *Mov. Disord.* 29, 336–343. doi: 10.1002/mds.25826

Olanow, C. W., Obeso, J. A., and Stocchi, F. (2006). Continuous dopamine-receptor treatment of Parkinson's disease: scientific rationale and clinical implications. *Lancet Neurol.* 5, 677–687. doi: 10.1016/S1474-4422(06)70521-X

Paxinos, G., and Watson, C. (1998). *The Rat Brain in Stereotaxic Coordinates*. San Diego, CA: Academic Press.

Picconi, B., Centonze, D., Hakansson, K., Bernardi, G., Greengard, P., Fisone, G., et al. (2003). Loss of bidirectional striatal synaptic plasticity in L-DOPA-induced dyskinesia. *Nat. Neurosci.* 6, 501–506. doi: 10.1038/nn1040

Reiner, A., Hart, N. M., Lei, W., and Deng, Y. (2010). Corticostriatal projection neurons—dichotomous types and dichotomous functions. *Front. Neuroanat.* 4:142. doi: 10.3389/fnana.2010.00142

Ren, T., Yang, X., Wu, N., Cai, Y., Liu, Z., and Yuan, W. (2011). Sustained-release formulation of levodopa methyl ester/benserazide for prolonged suppressing dyskinesia expression in 6-OHDA-leisoned rats. *Neurosci. Lett.* 502, 117–122. doi: 10.1016/j.neulet.2011.07.042

Rudy, J. W. (2015). Actin dynamics and the evolution of the memory trace. *Brain Res.* 1621, 17–28. doi: 10.1016/j.brainres.2014.12.007

Segal, M. (2010). Dendritic spines, synaptic plasticity and neuronal survival: activity shapes dendritic spines to enhance neuronal viability. *Eur. J. Neurosci.* 31, 2178–2184. doi: 10.1111/j.1460-9568.2010.07270.x

Seong, H. J., and Carter, A. G. (2012). D1 receptor modulation of action potential firing in a subpopulation of layer 5 pyramidal neurons in the prefrontal cortex. *J. Neurosci.* 32, 10516–10521. doi: 10.1523/JNEUROSCI.1367-12.2012

Shen, W., Plotkin, J. L., Francardo, V., Ko, W. K., Xie, Z., Li, Q., et al. (2015). M4 muscarinic receptor signaling ameliorates striatal plasticity deficits in models of L-DOPA-induced dyskinesia. *Neuron* 88, 762–773. doi: 10.1016/j.neuron.2015.10.039

Shipp, S. (2017). The functional logic of corticostriatal connections. *Brain Struct. Funct.* 222, 669–706. doi: 10.1007/s00429-016-1250-9

Ueno, T., Yamada, J., Nishijima, H., Arai, A., Migita, K., Baba, M., et al. (2014). Morphological and electrophysiological changes in intratelencephalic-type pyramidal neurons in the motor cortex of a rat model of levodopa-induced dyskinesia. *Neurobiol. Dis.* 64, 142–149. doi: 10.1016/j.nbd.2013.12.014

Uhl, G. R., Hedreen, J. C., and Price, D. L. (1985). Parkinson's disease: loss of neurons from the ventral tegmental area contralateral to therapeutic surgical lesions. *Neurology* 35, 1215–1218. doi: 10.1212/WNL.35.8.1215

Wang, H. D., and Deutch, A. Y. (2008). Dopamine depletion of the prefrontal cortex induces dendritic spine loss: reversal by atypical antipsychotic drug treatment. *Neuropsychopharmacology* 33, 1276–1286. doi: 10.1038/sj.npp.1301521

Xie, C. L., Wang, W. W., Zhang, S. F., Yuan, M. L., Che, J. Y., Gan, J., et al. (2014). Levodopa/benserazide microsphere (LBM) prevents L-dopa induced dyskinesia by inactivation of the DR1/PKA/P-tau pathway in 6-OHDA-lesioned Parkinson's rats. *Sci. Rep.* 4:7506. doi: 10.1038/srep07506

Yagishita, S., Hayashi-Takagi, A., Ellis-Davies, G. C., Urakubo, H., Ishii, S., and Kasai, H. (2014). A critical time window for dopamine actions on the structural plasticity of dendritic spines. *Science* 345, 1616–1620. doi: 10.1126/science.1255514

Yang, X., Chen, Y., Hong, X., Wu, N., Song, L., Yuan, W., et al. (2012a). Levodopa/benserazide microspheres reduced levodopa-induced dyskinesia by downregulating phosphorylated GluR1 expression in 6-OHDA-lesioned rats. *Drug Des. Devel. Ther.* 6, 341–347. doi: 10.2147/DDDT.S38008

Yang, X., Zheng, R., Cai, Y., Liao, M., Yuan, W., and Liu, Z. (2012b). Controlled-release levodopa methyl ester/benserazide-loaded nanoparticles ameliorate levodopa-induced dyskinesia in rats. *Int. J. Nanomed.* 7, 2077–2086. doi: 10.2147/IJN.S30463

Conflict of Interest Statement: The authors declare that the research was conducted in the absence of any commercial or financial relationships that could be construed as a potential conflict of interest.

frontiers in Molecular Neuroscience

ORIGINAL RESEARCH
published: 31 January 2017
doi: 10.3389/fnmol.2017.00024

Redundant Postsynaptic Functions of SynCAMs 1–3 during Synapse Formation

*Daniel K. Fowler[1,2], James H. Peters[2], Carly Williams[1] and Philip Washbourne[1]**

[1]*Department of Biology, Institute of Neuroscience, University of Oregon, Eugene, OR, USA,* [2]*Department of Integrative Physiology and Neuroscience, Washington State University, Pullman, WA, USA*

Investigating the roles of synaptogenic adhesion molecules during synapse formation has proven challenging, often due to compensatory functions between additional family members. The synaptic cell adhesion molecules 1–3 (SynCAM1–3) are expressed both pre- and postsynaptically, share highly homologous domains and are synaptogenic when ectopically presented to neurons; yet their endogenous functions during synaptogenesis are unclear. Here we report that SynCAM1–3 are functionally redundant and collectively necessary for synapse formation in cultured hippocampal neurons. Only triple knockdown (KD) of SynCAM1–3 using highly efficient, chained artificial microRNAs (amiRNAs) reduced synapse density and increased synapse area. Electrophysiological recordings of quantal release events supported an increase in synapse size caused by SynCAM1–3 depletion. Furthermore, a combinatorial, mosaic lentiviral approach comparing wild type (WT) and SynCAM1–3 KD neurons in the same culture demonstrate that SynCAM1–3 set synapse number and size through postsynaptic mechanisms. The results demonstrate that the redundancy between SynCAM1–3 has concealed their synaptogenic function at the postsynaptic terminal.

Keywords: redundancy, SynCAM, artificial miRNA, mosaic, hippocampus, synapse formation, knockdown, adhesion

OPEN ACCESS

Edited by:
Jaewon Ko,
Daegu Gyeongbuk Institute of Science and Technology, South Korea

Reviewed by:
Joris De Wit,
VIB, KU Leuven, Belgium
Megan E. Williams,
University of Utah, USA

****Correspondence:***
Philip Washbourne
pwash@uoneuro.uoregon.edu

Received: *07 December 2016*
Accepted: *17 January 2017*
Published: *31 January 2017*

Citation:
Fowler DK, Peters JH, Williams C and Washbourne P (2017) Redundant Postsynaptic Functions of SynCAMs 1–3 during Synapse Formation. Front. Mol. Neurosci. 10:24. doi: 10.3389/fnmol.2017.00024

INTRODUCTION

Synapse formation is initiated by physical contact of adhesion molecules between axons and dendrites which then triggers recruitment of molecular complexes to the presynaptic active zone or the postsynaptic density (PSD) (Washbourne et al., 2004). Despite considerable advances, a comprehensive understanding of how adhesion molecules orchestrate synaptogenesis is far from complete. A major obstacle in studying synapse formation is the confound of functional redundancy between key synaptic proteins. Indeed, redundancy has been observed for the synaptogenic adhesion molecule families neurexins, neuroligins and calsyntenins, such that protein reduction of at least three family members is necessary to observe certain synaptic phenotypes (Varoqueaux et al., 2006; Shipman et al., 2011; Gokce and Südhof, 2013; Um et al., 2014). Importantly, compensatory functions within protein families may hide crucial synaptic roles when manipulating single genes in isolation.

Several observations suggest that the nectin-like synaptic cell adhesion molecule (SynCAM) family may also share redundant functions during synapse formation. SynCAMs were discovered in the central nervous system by their ability to induce synapse formation *in vitro* (Biederer et al., 2002). They have been linked to autism spectrum disorder (Zhiling et al., 2008; Casey et al., 2012), and have four members (SynCAM1–4) that form homo- or heterophilic interactions in the *trans* configuration across the synaptic cleft (Fogel et al., 2007). SynCAMs 1, 2 and 3 (SynCAM1–3) are localized to excitatory synapses with both pre- and postsynaptic distributions (Fogel et al., 2007; Stagi et al., 2010; Shu et al., 2011; Cheadle and Biederer, 2012; Loh et al., 2016). The short intracellular regions of SynCAM1–3, requisite for synaptogenic activity (Biederer et al., 2002; Sara et al., 2005), contain remarkably conserved binding motifs between family members and likely interact with the same proteins during development (Biederer, 2006). While the roles of SynCAMs during synapse formation are emerging, the extent of overlap in SynCAM signaling remains unexplored.

Here we use single and chained artificial microRNAs (amiRNAs) to knock down SynCAM1–3 in cultured rat hippocampal neurons to examine functional redundancy between these gene family members. Knockdown (KD) of any single, or two SynCAMs does not affect excitatory synapse formation; rather triple KD of SynCAM1–3 shows they are necessary for and compensate to set synapse density and limit synapse size. We further investigate these phenotypes using a novel method that generates a traceable mosaic of KD and wild type (WT) cells on the same coverslip. Crucially, comparisons between these conditions allows for the differentiation of pre- and postsynaptic effects. Using this method we find that SynCAM1–3's influence on synapse number and size are through postsynaptic mechanisms. Electrophysiological recordings confirm postsynaptic effects of SynCAM1–3 KD with broadened event peaks of miniature excitatory postsynaptic currents (mEPSCs) consistent with an increase in synapse size. These results suggest that a postsynaptic mechanism for SynCAM1–3 in synaptogenesis has been heretofore concealed by overlapping functions of the gene family members.

MATERIALS AND METHODS

Cloning

The design and generation of amiRNAs targeting SynCAM1–3 and Scrambled1–3 amiRNAs, a MultiSite Gateway (Invitrogen) middle entry vector with an intronically-expressed enhanced synthetic inhibitory BIC/miR-155 RNA cloning cassette (pME-eSIBR), and insertion and chaining of amiRNAs in the cassette were described previously (Fowler et al., 2016b). SynCAM1–3 (*cadm1–3*) guide strand amiRNA targeting sequences used were *cadm1.1358*:5′-UUGAUUAUAGCUG UGUCUGCGU-3′, *cadm2.87*:5′-UUCAACAACCGUGACAUU CUGA-3′, and *cadm3.387*:5′-AUAACCAGUGAUUAUGGG UUUC-3′. Scrambled control guide strand sequences used were scrambled1: 5′-AUUCUAAUACUACGUUCCGCAU-3′, scrambled2: 5′-ACAACUUGUAUAUCGCGCAACU-3′ and scrambled3: 5′-GAUCUUAUACUCGUGAUUGAGA-3′. Gateway LR recombination reactions of pME-eSIBR vectors with single, double, or triple amiRNAs with a 5′ entry vector containing a minimal CMV (mCMV) promoter (p5E-CMVmin) and 3′ entry vector with a nlsGFP tag (p3E-nlsGFP no-pA) into a third-generation lentiviral destination vector (pEpic_Lite) were performed to create SynCAM single, double and triple KD vectors or the control Scrambled1–3 amiRNA vector were described previously (Fowler et al., 2016a). To make the memGFP-only expressing vector, a middle entry vector containing GFP with a C-terminal human H-RAS palmitoylation signal for membrane targeting (Kwan et al., 2007) was used in a MultiSite Gateway LR reaction with p5E-CMVmin, a 3′ entry vector with a hemagglutinin epitope tag (p3E-HA no-pA), and pEpic_Lite (Fowler et al., 2016a). The HA epitope is not expressed because the memGFP sequence used contains a stop codon and was used as a "filler" sequence to allow LR recombination.

Lentivirus Production and Titration

2.5×10^6 HEK293T cells (ATCC® CRL-3216) were plated per 10-cm tissue culture dishes in 10 ml of DMEM (Invitrogen), 10%FCS (Atlanta Biologicals), 25 units/ml penicillin and 25 μg/ml streptomycin (Sigma). Approximately twenty-four hours after plating, cells were transiently transfected using ProFection (Promega) calcium phosphate transfection reagents with 20 μg pEpic_Lite lentiviral vectors and packaging vectors (10 μg pMDL g/p RRE, 5 μg pRSV-Rev, 6 μg pVSV-G; Dull et al., 1998). Six to Eight hours later, media was replaced with 6 ml/plate of fresh medium. Medium was collected 48–72 h after transfection and centrifuged at 3000× g for 5 min at room temperature (RT). Supernatant was passed through a 0.45 μm syringe filter and virus was concentrated by centrifugation on a 150,000 MWCO column (Pierce). Twenty thousand HEK293T cells were plated per well of a 12-well plate and transduced with serial dilutions of concentrated lentivirus. Four to five days after transduction, titers were calculated by flow cytometry on an Attune® acoustic focusing cytometer (Applied Biosystems) for GFP+ cells. Infectious lentiviral particles/μl was calculated from viral dilutions where cells were transduced in the linear range (5%–20% GFP+ cells).

Vertebrate Animals

Studies using rats were carried out in strict accordance with the recommendations in the Guide for the Care and Use of Laboratory Animals of the National Institutes of Health. The protocols were approved by the University of Oregon and Washington State University Institutional Animal Care and Use Committee (Permit Numbers: #13-19 and #04787, respectively). Rats were anesthetized with isoflurane prior to sacrifice and culturing of neurons. Rats were housed with a 12/12 light/dark cycle according to standard protocols in the University of Oregon Animal Care Facility and Washington State University Veterinary and Biomedical Research Vivarium. Sprague-Dawley rats were obtained from Envigo.

Primary Neuron Culture

Hippocampal cultures were prepared from embryonic day 19 Sprague-Dawley rat pups as described (Brewer et al., 1993), with minimal modifications. For single-cell SynCAM immunofluorescence comparisons, 3000 dissociated hippocampal cells were plated per well of a 12-well plate. For all other experiments, cells were cultured at a density of 100,000 cells/well of a 12-well plate. For quantitative reverse transcription polymerase chain reaction (qRT-PCR) experiments cells were attached directly to plates coated with poly-L-lysine (Sigma); for all other experiments cells were cultured on glass coverslides coated with poly-L-lysine. Cells were allowed to attach to poly-L-lysine coated substrate in plating media (MEM (Invitrogen), 10% FCS, 20 mM dextrose, 25 units/ml penicillin and 25 μg/ml streptomycin) for 5–6 h. Media was then changed to maintenance media (Neurobasal medium (Invitrogen), 1× B-27 supplement (Invitrogen), 0.5 mM Glutamax (Invitrogen), 50 units/ml penicillin, 50 μg/ml streptomycin, and 0.07% β-mercaptoethanol (Sigma)). Half changes of maintenance media were performed every 3–4 days in culture. Primary hippocampal cultures were infected with lentivirus at 1–2 days *in vitro* (DIV). For saturating transduction with lentivirus, 20,000 infectious lentiviral particles (as calculated by our titration method) were added per well of a 12-well plate; for sub-saturating transduction 2000 infectious lentiviral particles were added. For studies using memGFP lentivirus, 100 infectious particles were additionally added. Cells were fixed and stained at 13–15 DIV for imaging experiments; electrophysiology recordings were made with cells at 13–16 DIV.

Quantitative Western Blotting

Standard sodium dodecyl sulfate polyacrylamide gel electrophoresis (SDS-PAGE) western blotting procedures using nitrocellulose membranes were performed as previously described (Fowler et al., 2016b). Two-color near-infrared blots were imaged with an Odyssey-Fc quantitative western blot system (LI-COR). Primary antibodies and dilutions used were mouse anti-actin 1:2000 (Millipore, clone C4) and rabbit anti-SynCAM1–3 1:1000 (Pierce, PA3-16744); secondary antibodies donkey anti-mouse IRDye 680RD and anti-rabbit IRDye 800CW (LI-COR) were used at 1:1000. Intensities were normalized to actin loading controls. KD efficiency was calculated by comparing levels relative to the Scrambled 1–3 amiRNA control conditions set to 1. The representative blot shown is a composite image made by re-arranging lanes of a single blot image at the same projection intensity.

qRT-PCR

First-strand cDNAs were synthesized from total RNA isolated from cultured hippocampal neurons using Superscript III reverse transcriptase (Invitrogen) with oligodT primers for 50 min at 50°C. Primer pairs used to measure *cadm* mRNA levels were cadm1_F: 5′-GAAGGACAGCAGGTTTCAGC-3′, cadm1_R: 5′-ACCAGGACTGTGATGGTGGT-3′, cadm2_F: 5′-TCCTGATCGAATGGTTGTGA-3′, cadm2_R: 5′-TGGGATCGTGTACAATGAGG-3′, cadm3_f: 5′-CCTGGAGAAAAGGTGACCAA-3′, cadm3_R: 5′-ATGGTTCACAGAGCACACGA-3′. qRT-PCR was performed using SYBR Green reagents (Kapa Biosystems) using standard parameters on a StepOnePlus Real-Time PCR System (Applied Biosystems). Values and relative expression levels were compared using the $\Delta\Delta C_t$ method.

Immunolabeling

Cells on glass coverslides were fixed with 4% paraformaldehyde and 4% sucrose in PBS for 15 min at 4°C. Cells were then permeabilized for 5 min with 0.25% Triton-X100 in PBS, and blocked for 1 h at RT with blocking solution (1% Roche blocking solution (Roche), 10% BSA (Sigma), 1% normal donkey serum (Jackson ImmunoResearch), and 1% normal goat serum (Jackson ImmunoResearch) in PBS). Cells were then incubated with primary antibodies in blocking solution overnight at 4°C. Primary antibodies and dilutions used were rabbit anti-Synapsin1 1:500 (EMD Millipore, AB1543), mouse anti-PSD-95 1:350 (Neuromab, clone K28/43), chicken anti-GFP 1:2000 (Aves Labs, GFP-1020), and rabbit anti-SynCAM1–3 1:500 (Pierce, PA3-16744). The next day, cells were washed 3× 5 min with PBS and incubated with secondary antibody in blocking solution for 1 h at RT. All secondary antibodies were from Jackson Laboratories and used at 1:500–goat anti-chicken Alexa Fluor 488, donkey anti-mouse or anti-rabbit Cy3, and donkey anti-rabbit Cy5. Cells were washed 3× 5 min with PBS and mounted on slides with Fluoromount G with DAPI (Southern Biotech).

Microscopic Imaging

For transduction rate experiments, neurons were imaged on a Nikon Eclipse TE300 microscope using a 20× air objective (0.45 NA), Till Photonics monochromator light source, Retiga EXi CCD camera (Q Imaging) and SimplePCI software (Hamamatsu, Inc., Houston, TX, USA). For **Figures 3B,C**, cells were imaged at 20× (**Figure 3B**) using an air (0.75 NA) objective or at 60× (**Figure 3C**) using an oil-immersion objective (1.40 NA) on an Eclipse 80i microscope with a DS-Qi1Mc camera, Intensilight C-HGFI light source and Elements software (Nikon). For **Figure 3D**, cells were imaged live in aCSF (see "Electrophysiology" Section for recipe) with a 40× water-immersion objective (0.8 NA) using an Eclipse FN1 microscope with a DS-Qi1Mc camera, Intensilight C-HGFI light source and Elements software (Nikon). All other neurons were imaged on an inverted Nikon TU-2000 confocal microscope using EZ-C1 software. For single-cell comparisons of SynCAM1–3 immunofluorescence, images were obtained using a 20× air objective (0.75 NA) and the example images in **Figures 4A,B** were obtained using a 60× water-immersion objective (1.2 NA). All other images were obtained with a 100× oil-immersion objective (1.45 NA). The presence or absence of nlsGFP was validated by visual comparison of DAPI and GFP staining. For transduction rate comparisons, 20 images of DAPI (350 nm) and corresponding GFP (488 nm) signal were taken at random positions across four coverslides per

condition. For single-cell SynCAM1–3 immunofluorescence experiments up to 20 neurons that did not overlap with neighboring cells were selected for imaging for each condition. Eight neurons were imaged for a secondary antibody-only condition for analysis of background fluorescence. Sequential scanning for each channel (488, 543 nm) was performed and the average of three scans was taken at 1024 × 1024 pixel resolution. For all other experiments, pyramidal cells were selected by morphology and cells were imaged if they had 2–3 primary or secondary small diameter dendrites (∼1–2 μm not including spines or protrusions) that originated at the soma with no further branches in a single field of view at high magnification, that terminated within a short distance of the soma (usually <100 μm), and that were visually discernable from additional GFP-positive processes and background immunofluorescence. Cells were sampled evenly between isolations. Sequential scanning for each channel (488, 543, 633 nm) was performed and the average of three scans was taken at 2048 × 2048 pixel resolution. For all experiments, images were obtained with constant pinhole, laser intensity, and detector gain settings, and the experimenter was blinded to the conditions.

Image Analysis

Each color channel was saved independently as grayscale 16-bit TIFF files. For transduction rate comparisons, the number of total cells in an image were determined by manually counting DAPI nuclei; the number of transduced cells was determined by manually counting nlsGFP+ nuclei. For single-cell SynCAM1–3 KD comparisons, binary masks were made of each neuron using Image-Pro 6.3 software (Media Cybernetics) using outlines from 488 nm images. Background debris was cleared from the masks manually using GIMP 2 software (The GIMP Team). SynCAM immunostaining intensity was calculated within the confines of the outline of the neuron defined by the binary masks using a custom program in MATLAB (Mathworks). The average fluorescence intensity for neurons in the secondary antibody only condition was used to measure background signal and was subtracted from the SynCAM staining intensity for each image. For dendrite analysis, using 488 nm images, individual basal dendrite segments averaging ∼30 μm in length were selected and binarized manually using Image-Pro 6.3 software (**Figures 2A,B**). Binary masks were then used in a custom MATLAB program to automatically detect and compare puncta from corresponding 543 nm and 633 nm images (**Figure 2B**). Briefly, the program calculated the average fluorescent intensity of corresponding images in the binarized GFP region, set a threshold for including pixels in puncta detection (1.5× the mean value for each dendrite), and automatically detected puncta that were >4 contiguous pixels within the confines of the binarized GFP mask. Only puncta >0.15 μm^2 were considered for density and size analysis. Overlapping pre- and postsynaptic puncta were counted as synapses. Dendrite lengths were measured manually using Image-Pro 6.3 software. Puncta density was calculated by dividing number of puncta by dendrite length. Puncta area was reported by our custom program. Experimenters were blinded to conditions during image analysis.

Electrophysiology

Whole cell recordings were performed on identified pyramidal neurons in hippocampal cultures using an upright Nikon FN1 microscope with fluorescence imaging capabilities. Recording electrodes (2.8–3.8 MΩ) were filled with an intracellular solution containing (mM): 6 NaCl, 4 NaOH, 130 Cs-gluconate, 11 EGTA, 1 $CaCl_2$, 1 $MgCl_2$, 10 HEPES, 2 Na_2ATP, and 0.2 Na_2GTP. The intracellular solution was pH 7.4 and 296 mOsm. All neurons were studied under voltage clamp conditions with an Axopatch 200A or MultiClamp 700A amplifier (Molecular Devices). Neurons were held at $V_H = -70$ mV using pipettes in whole cell patch configuration. Signals were filtered at 3 kHz and sampled at 30 kHz using p-Clamp software (version 10, Molecular Devices). Liquid junction potentials were not corrected. Extracellular solution (aCSF; containing (mM): 125 NaCl, 3 KCl, 1.2 KH_2PO_4, 1.2 $MgSO_4$, 25 $NaHCO_3$, 10 dextrose, and 2 $CaCl_2$) was continuously perfused and drugs were bath applied to isolate quantal glutamatergic signaling (TTX, 1 μM and Gabazine, 3 μM).

mEPSC Analysis

Digitized waveforms of quantal synaptic events were analyzed using MiniAnalysis software (Synaptosoft). Only traces from cells held under voltage clamp with a series resistance <25 MΩ were used for analysis. All events >5 pA were counted for 1–2 min of trace ∼5 min after application of drug. All events were used to calculate frequency values. The average mEPSC projection of all discrete events for each neuron was used for peak analysis measurements by automated fitting of amplitudes and decay kinetics (single exponential, 90–10%) with MiniAnalysis software. Noisy, misaligned and non-discrete events were manually removed prior to peak analysis. The experimenters were blinded to the conditions for recording and trace analysis.

Statistics

Normality of data was determined by Shapiro-Wilk tests in R (R Foundation for Statistical Computing). *P* values obtained by statistical comparisons of two sample groups used Student's two-tailed, unpaired *t*-tests in Microsoft Excel and comparisons of more than two sample groups used one-way ANOVAs followed by Tukey's *post hoc* pairwise comparisons in R.

RESULTS

Single and Multi-Gene Knockdown Lentiviral Constructs

Single and multi-gene KD was achieved through the use of inhibitory RNA (RNAi) targeting sequences in an enhanced amiRNA backbone either singly or chained in a mobile cassette (Fowler et al., 2016b). We combined amiRNAs targeting rat SynCAM1–3 in single, double and triple-gene KD combinations,

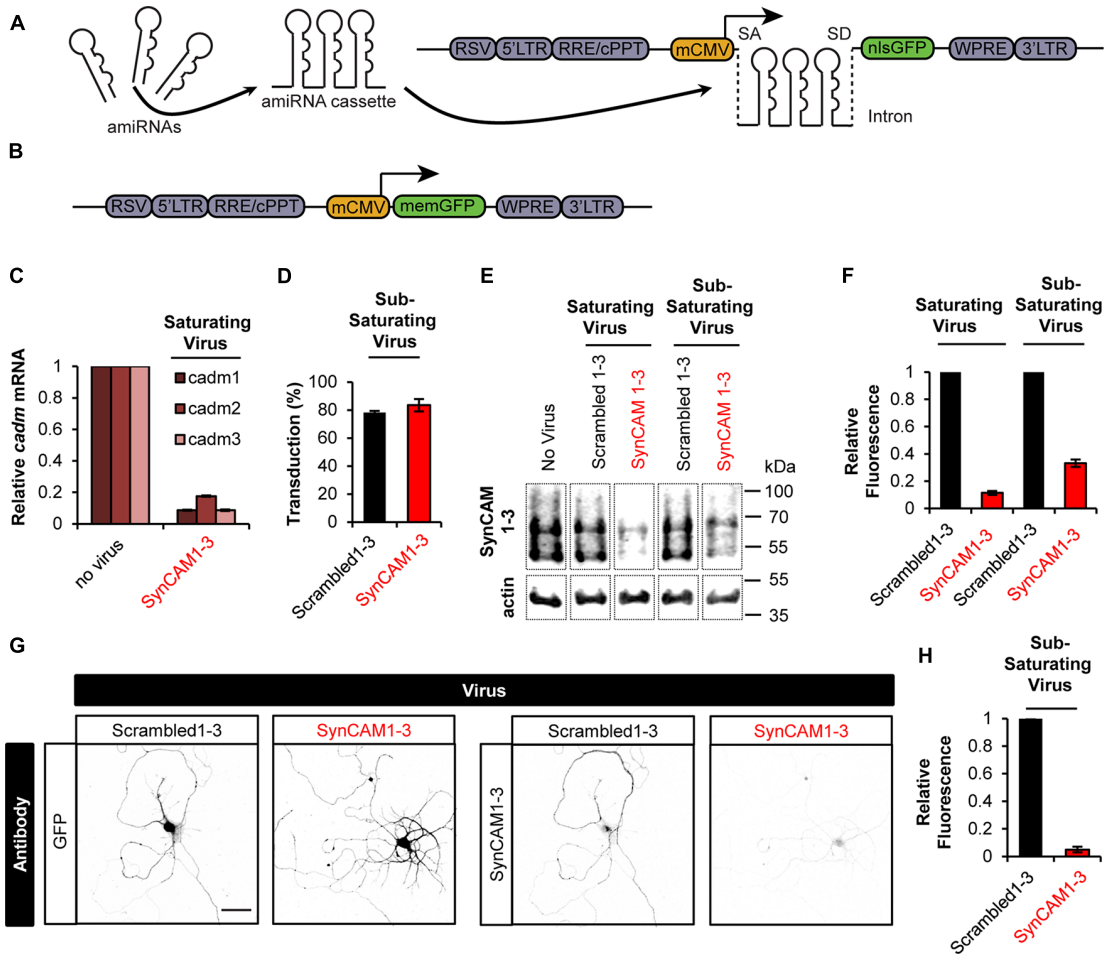

FIGURE 1 | Sub-saturating lentiviral artificial microRNA (amiRNA) transduction potently knocks down synaptic cell adhesion molecules 1–3 (SynCAM1–3) in amiRNA+ cells while keeping a subpopulation of wild type (WT) amiRNA- cells. (A) Lentiviral knockdown (KD) vectors were generated with a minimal CMV (mCMV) promoter, intronic amiRNAs, and nlsGFP. RSV, Rous sarcoma virus promoter; LTR, long-terminal repeat; RRE, Rev-response element; cPPT, central polypurine tract; WPRE, woodchuck hepatitis virus posttranscriptional regulatory element; SA, splice acceptor; SD, splice donor. **(B)** memGFP-expressing lentiviral vector for dendrite labeling. **(C)** Comparison of *cadm1–3* mRNA levels at 14–15 days *in vitro* (DIV) by quantitative reverse transcription polymerase chain reaction (qRT-PCR) in cultured rat hippocampal neurons using saturating viral titers relative to levels in uninfected control cultures. $n = 2$ experiments. **(D)** Transduction rate of cultured neurons at 14–15 DIV using sub-saturating viral titers. $n = 2$ experiments. **(E)** Representative blots and **(F)** relative SynCAM1–3 protein levels at 13–15 DIV measured by quantitative western blotting of cultured neurons following indicated amiRNA lentiviral treatments at saturating or sub-saturating viral titers compared to Scrambled1–3 amiRNA control treatments. Actin was used as a loading control. $n = 4$ (saturating) or $n = 2$ (sub-saturating) experiments. A single gel image of the same intensity was cropped as marked by dotted lines and rearranged for presentation. **(G)** Representative images and **(H)** quantification of relative SynCAM1–3 immunofluorescence at 14 DIV of individual neurons cultured at low density normalized to immunofluorescent intensity of control Scrambled 1–3 amiRNA treated neurons. Scale, 50 μm. Scrambled1–3 condition $n = 13$ cells/2 coverslips, SynCAM1–3 condition $n = 20$ cells/2 coverslips. Error bars, SEM.

as well as three scrambled amiRNA sequences targeting no known genes (Scrambled1–3), into a lentiviral destination vector with a nuclear localized GFP (nlsGFP) reporter (Fowler et al., 2016a; **Figure 1A**). These amiRNAs were expressed from an intron to prevent degradation of the mRNA to allow robust reporter expression (Chung et al., 2006). We also generated a separate lentiviral vector driving expression of a plasma membrane-localized GFP (memGFP) reporter used to label dendrites and spines (**Figure 1B**). We previously characterized these chained amiRNAs targeting SynCAM1–3, which are encoded by the cell adhesion molecule 1–3 (*cadm1–3*) genes, as highly efficient for KD of SynCAM1–3 in rat primary hippocampal cultures at 13–15 DIV by western blot (Fowler et al., 2016b). For further validation, we performed qRT-PCR for *cadm1–3* mRNA levels in hippocampal cultures following transduction with saturating levels of SynCAM1–3 amiRNAs. Results showed >90% KD of *cadm1* and *3*, and >80% KD of *cadm2* mRNAs, confirming that our amiRNAs are effective for KD of all three SynCAMs (**Figure 1C**).

Typically, Lentiviral RNAi experiments are performed at saturating transduction levels to ensure the highest level of KD. However, saturating amiRNA virus prevents a population

of non-transduced cells retaining WT SynCAM1–3 expression levels. Because we eventually wanted to compare synapse development in both WT and SynCAM1–3 KD neurons on the same coverslip, we infected cultures with sub-saturating amounts of SynCAM1–3 amiRNA or control Scrambled1–3 amiRNA virus. We counted nlsGFP+ DAPI-stained nuclei and saw that ∼80% of cells were transduced in both cases (**Figure 1D**), ensuring that ∼20% of cells retained WT SynCAM expression levels.

Because our previous characterizations of SynCAM1–3 KD by western blot (Fowler et al., 2016b) and in the current study with qPCR (**Figure 1C**) used saturating viral levels, we wanted to confirm that sub-saturating transduction still produced robust KD. Using quantitative western blotting with an antibody that recognizes SynCAM1–3 (Biederer et al., 2002), but not SynCAM4 (Fogel et al., 2007), we showed ∼90% KD with saturating and ∼70% KD with sub-saturating virus (**Figures 1E,F**). Because around 20% of cells retained WT SynCAM1–3 expression in sub-saturating virus, we reasoned that the observed 70% KD likely underrepresented the actual KD amount in SynCAM1–3 amiRNA+ cells. Therefore, we cultured cells at very low densities to allow imaging of individual cells transduced with sub-saturating concentrations of SynCAM1–3 or Scrambled1–3 amiRNA lentivirus. As measured by immunofluorescence intensity for SynCAM1–3 antibody, SynCAM1–3 amiRNA+ cells had ∼95% KD compared to Scrambled1–3 amiRNA+ cells (**Figures 1G,H**). This confirmed that sub-saturating concentrations of the amiRNA lentivirus effectively eliminated targeted protein expression in individual transduced neurons, while maintaining a subpopulation of amiRNA− cells to be used as in-culture WT controls.

SynCAM1–3 Redundantly Set Synapse Density and Size During Synaptogenesis

To test functional redundancy of SynCAM1–3 during synapse formation, we infected hippocampal cultures at sub-saturating amounts with all possible combinations of lentivirus carrying single, double, and triple amiRNAs against SynCAM1–3, as well as the Scrambled1–3 amiRNA control. We also infected a small subset of neurons (∼1%) with memGFP lentivirus to enable imaging of dendrites. To detect differences in synapse formation, we immunolabeled cultures at 13–15 DIV with antibodies to GFP, the postsynaptic protein PSD-95 and the presynaptic protein Synapsin 1 and imaged nlsGFP/amiRNA+ cells that were also labeled with memGFP using confocal microscopy (**Figure 2A**). Following manual selection of dendrites on pyramidal cells, we used automated detection of PSD-95 and Synapsin 1 puncta. We defined synapses as regions of co-localization of these pre- and postsynaptic puncta along

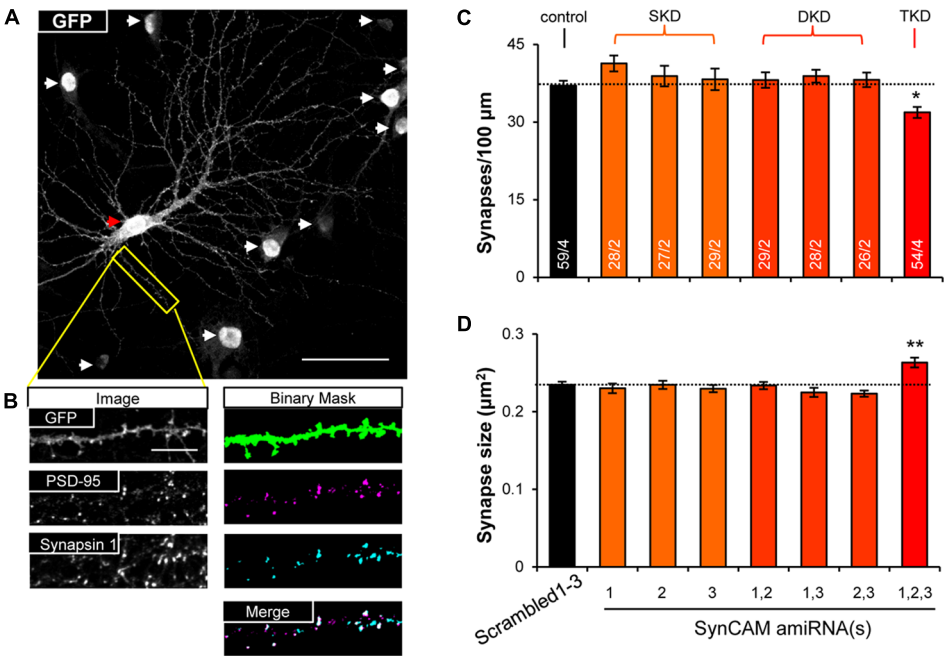

FIGURE 2 | SynCAM1–3 function redundantly to set synapse density and size. (A) Representative 60× confocal microscopy image of cultured rat hippocampal neurons at 14 DIV treated with sub-saturating lentivirus carrying Scrambled1–3 amiRNAs linked to nlsGFP, and very low titer memGFP lentivirus. An individual pyramidal cell co-labeled by memGFP and nlsGFP is marked by a red arrowhead. White arrowheads mark nuclei in the field of view only expressing nlsGFP. Scale, 50 µm. **(B)** Sample images of automated puncta and synapse detection from co-immunostaining for presynaptic protein Synapsin 1 and postsynaptic protein PSD-95 following manual selection of an individual dendrite segment from the image in **(A)**. Synapses are defined as the co-localized regions of pre- and postsynaptic puncta (white areas in merged image). Scale, 10 µm. **(C)** Average synapse density and **(D)** average synapse puncta area from 13 to 15 DIV neurons co-transduced with memGFP and sub-saturating amounts of the SynCAM amiRNAs listed or control Scrambled1–3 amiRNAs. *n* = cells/isolations is listed on the bars. SKD, single knockdown; DKD, double knockdown; TKD, triple knockdown. $^{*}p < 0.05$, $^{**}p < 0.01$, one-way analyses of variance (ANOVA) with Tukey's *post hoc* pairwise comparisons on cell average values. Error bars, SEM.

dendrites (**Figure 2B**). Only SynCAM1–3 KD, but not single or double KD, reduced synapse density by nearly 20% (**Figure 2C**) and increased the area of co-localization by ∼10% (**Figure 2D**), demonstrating that SynCAM1–3 function redundantly to set synapse number and size in developing neurons.

Mosaic Knockdown Reveals SynCAM1–3 Set Synapse Density and Size Through Postsynaptic Mechanisms

We sought to determine if the phenotypes due to SynCAM1–3 KD are caused by pre- or postsynaptic loss. Sub-saturating infection with amiRNA lentivirus results in non-transduced cells retaining WT SynCAM1–3 expression levels. Combinatorial application of memGFP lentivirus enables labeling of these WT cells for imaging, which is not possible when an RNAi payload is directly linked to the neurite-labeling fluorophore. Therefore this new methodology, named Mosaic Expression using Differentially Localized Reporters (MEDLR), allows direct comparisons of WT (memGFP+ only) and KD (memGFP+/nlsGFP+) neurons on the same coverslip (**Figure 3A**). Using MEDLR, amiRNA− WT cells were readily distinguished from amiRNA+ KD cells when visually scanned for the presence or absence of nlsGFP fluorescence in memGFP-labeled fixed cell preparations under low magnification (**Figure 3B**). The distinction between amiRNA− and amiRNA+ cells was even more apparent at higher magnifications (**Figure 3C**). Further, MEDLR was used to differentiate amiRNA− and amiRNA+ cells in live cultures (**Figure 3D**), showing that this methodology is suitable for approaches such as live cell imaging and electrophysiology.

Crucially, for proteins located on both axons and dendrites, such as SynCAM1–3, MEDLR allows the discrimination between pre- and postsynaptic sites of action. This is because in a culture infected with sub-saturating SynCAM1–3 amiRNAs, the majority of axons (∼80%) available to form connections with WT neurons have ∼5% of wildtype levels of SynCAM1–3.

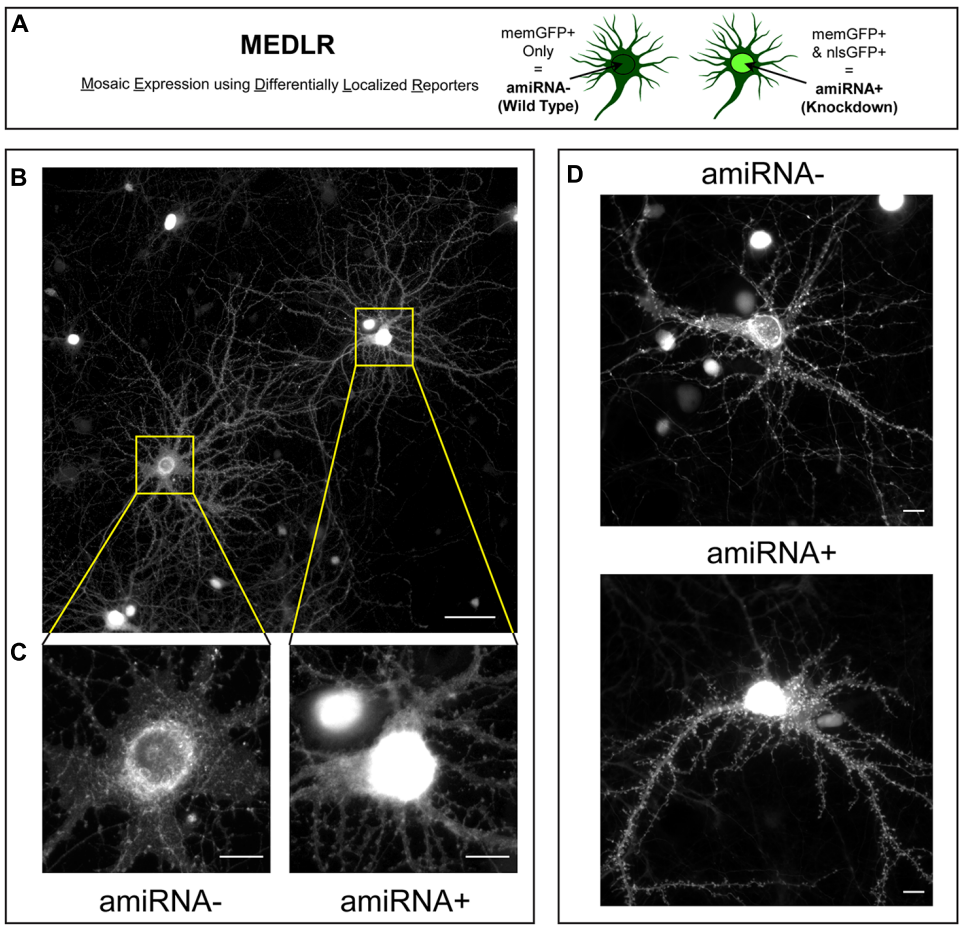

FIGURE 3 | Mosaic Expression using Differentially Localized Reporters (MEDLR) is a novel method to compare WT and KD neurons on the same coverslip. (A) MEDLR uses combinatorial lentiviral transgenesis with memGFP lentivirus and nlsGFP-linked amiRNA lentivirus to compare WT and KD cells. **(B)** Representative immunolabled GFP images at 20× or **(C)** 60× magnification of memGFP-labled amiRNA− and amiRNA+ neurons at 15 DIV in cultures transduced with sub-saturating amounts of Scrambled1-3 amiRNAs. **(D)** Representative 40× images of live GFP fluorescence in 15 DIV amiRNA− and amiRNA+ neurons. **(B–D)** Note the perisynaptic memGFP accumulation that could potentially be misinterpreted as nlsGFP in amiRNA− cells. **(B)** Scale, 50 μm; **(C,D)** Scale, 10 μm.

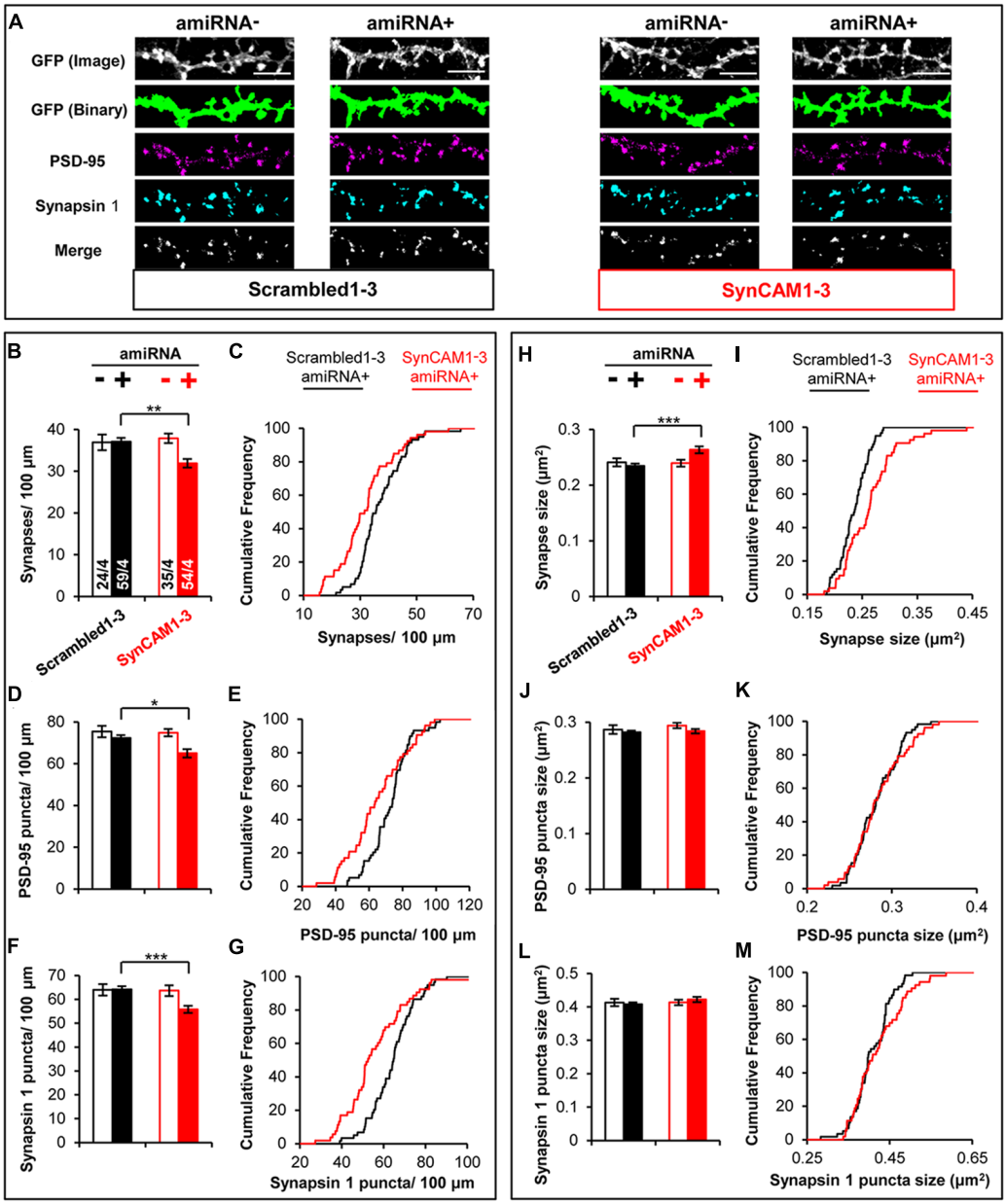

FIGURE 4 | MEDLR shows synaptic phenotypes are due to postsynaptic SynCAM1–3 depletion. (A) Representative images of memGFP-labled basal dendrites from amiRNA− and amiRNA+ neurons at 15 DIV in cultures transduced with sub-saturating amounts of Scrambled1–3 or SynCAM1–3 amiRNAs. Automated puncta detection for PSD-95 and Synapsin 1 immunostaining and synapses (merge) was performed after manual selection of GFP masks. Scale, 5 µm. **(B,D,F)** Average dendritic puncta density as indicated on graph of amiRNA− and amiRNA+ neurons and **(C,E,G)** corresponding cumulative puncta density distribution plot (%) of amiRNA+ neurons from cultures transduced with Scrambled1–3 or SynCAM1–3 amiRNAs. **(H,J,L)** Average puncta area as indicated on graph of amiRNA− and amiRNA+ neurons and **(I,K,M)** corresponding cumulative puncta area distribution plot (%) of amiRNA+ neurons from cultures transduced with Scrambled1–3 or SynCAM1–3 amiRNAs. *n* = number of cells/isolations as indicated on bars from 13 to 15 DIV cultures. $^{*}p < 0.05$, $^{**}p < 0.01$, $^{***}p < 0.001$, *t* test on cell average values. Cumulative distribution plots represent cell average values. Error bars, SEM.

Therefore if presynaptic SynCAM1–3 is necessary for proper synapse formation then WT cells would be expected to display a similar phenotype to SynCAM1–3 KD neurons. However, if postsynaptic SynCAM1–3 instructs synapse development, no phenotype would be expected in WT cells. We note that as used here, MEDLR cannot determine if postsynaptic SynCAM1–3 is necessary for synapse formation, because in amiRNA+ cells both pre- and postsynaptic SynCAM1–3 would be removed. Instead, MEDLR can determine if the presence of postsynaptic SynCAM1–3 is sufficient for synapse formation.

We used MEDLR to compare synaptic phenotypes between amiRNA− and amiRNA+ cells in cultures transduced with

sub-saturating amounts of Scrambled1–3 or SynCAM1–3 amiRNA lentivirus (**Figure 4A**). WT amiRNA− cells did not display reduced synaptic density compared to Scrambled1–3 amiRNA+ neurons (**Figures 4B,C**) suggesting that the reduction in SynCAM1–3 amiRNA+ neurons was due to depletion of postsynaptic SynCAM1–3. Further, analysis of PSD-95 (**Figures 4D,E**) and Synapsin 1 puncta density (**Figures 4F,G**) showed that both were reduced along dendrites of SynCAM1–3 amiRNA+ neurons but not on Scrambled1–3 amiRNA+ neurons or amiRNA− cells, positing that reduced synapse density is due to the inability to recruit both pre- and postsynaptic structures. MEDLR also revealed no difference in synapse area in amiRNA− cells compared to Scrambled1–3 amiRNA+ neurons (**Figures 4H,I**), again suggesting that the increased synapse size is because of postsynaptic SynCAM1–3 loss. In contrast to puncta density, there was no difference in mean PSD-95 (**Figure 4J**) or Synapsin 1 (**Figure 4L**) puncta size between Scrambled1–3 and SynCAM1–3 amiRNA− or amiRNA+ cells, although we note that distribution plots indicated a subset of amiRNA+ cells that had larger mean PSD-95 and Synapsin 1 puncta areas (**Figures 4K,M**). Given that roughly twice as many Synapsin 1 and PSD-95 structures are detected than synapses, we cannot rule out that subtle increases in the size of Synapsin 1 and PSD-95 puncta size in SynCAM1–3 KD cells may contribute to the observed, enlarged synapse size. Alternatively, the increased synapse area may be due to the increased overlap of a subset of pre- and postsynaptic markers, which would be indicative of an effect primarily at trans-synaptic complexes. Further, it should be noted that increased puncta overlap in SynCAM1–3 amiRNA+ cells is unlikely to be from a non-specific effect that generally brings puncta in closer apposition, because individual puncta density was also decreased in these cells (**Figures 4D–G**).

SynCAM1–3 Knockdown Affects Quantal Transmission Through a Postsynaptic Mechanism

The MEDLR approach enabled us to determine the extent to which quantal glutamatergic synaptic transmission was altered in SynCAM1–3 KD neurons. Using whole-cell patch clamp electrophysiology, we measured mEPSCs at 13–16 DIV onto amiRNA− and amiRNA+ neurons transduced with sub-saturating amounts of Scrambled1–3 or SynCAM1–3 amiRNAs (**Figure 5A**). Distributions of average mEPSC frequencies across cells were highly variable, logarithmically distributed, and spanned nearly two orders of magnitude (**Figure 5B**). Because of the spread of frequencies, we did not observe a systematic difference between any group suggesting that SynCAM1–3 do not significantly impact the net frequency of quantal release. This result highlights that quantal release frequency is a product of multiple factors, including intrinsic release probability (Branco and Staras, 2009), in addition to synapse density, and is not necessarily an accurate measure of synapse number.

We also compared mEPSC event traces between groups. On average, mEPSCs were larger in SynCAM1–3 KD neurons compared to Scrambled1–3 amiRNA+ cells (**Figure 5C**). Waveform fitting analysis showed that while peak amplitude was not different between Scrambled1–3 and SynCAM1–3 amiRNA+ cells (**Figure 5D**; $p = 0.36$, t test), peaks in SynCAM1–3 KD neurons tended to have a larger area (**Figure 5E**; $p = 0.14$, t test) and had significantly longer rise times and decay-time constants (**Figures 5F,G**); indicating that SynCAM1–3 KD causes broader mEPSCs. MEDLR showed no differences between amiRNA− cells and Scrambled1–3 amiRNA+ neurons, demonstrating that postsynaptic depletion of SynCAM1–3 enlarges mEPSCs (**Figures 5D–G**). Additionally, there was no difference in average cell capacitance between conditions (Scrambled amiRNA+ = 52.5 ± 3.2 pF, $n = 25$; Scrambled amiRNA− = 55.3 ± 3.5 pF, $n = 14$; SynCAM1–3 amiRNA+ = 55.8 ± 3.4 pF, $n = 32$; SynCAM1–3 amiRNA− = 54.0 ± 4.8 pF, $n = 20$), indicating that changes in mESPC kinetics was not due to a change in cell size. Collectively, these results are consistent with an increased synapse size caused by postsynaptic loss of SynCAM1–3, and lend further evidence that defining synapses as juxtaposed pre- and postsynaptic puncta accurately represents functional contacts.

DISCUSSION

This report describes the first investigation into the functional redundancy of SynCAM1–3 during excitatory synapse development. We present three main observations that enhance our understanding of SynCAM synaptogenic functions: (1) only triple KD of SynCAM1–3 reduced synapse number, implying functional compensation during synapse formation; (2) triple KD increased synapse and mEPSC size, suggesting that intact SynCAM1–3 signaling functions redundantly to limit the physical size of trans-synaptic complexes; and (3) use of MEDLR provides strong evidence that postsynaptic, not presynaptic, SynCAM1–3 regulate synapse density and size. Additionally, the development of MEDLR should prove useful for future investigations not only in neuronal cultures, but in other adaptations where comparisons of WT cells to treated cells in the same culture is beneficial.

The observation of SynCAM1–3 functional redundancy appears to conflict with previous reports suggesting SynCAM1 knockout (KO) alone reduces synapse density in excitatory neurons (Robbins et al., 2010; Cheadle and Biederer, 2012; Giza et al., 2013; Park et al., 2016). While we cannot rule out the possibility that residual SynCAM1, due to incomplete KD, is sufficient for correct synaptogenesis, this seems unlikely because of high SynCAM1 KD potency using our enhanced amiRNA. Further, this would not explain why the triple KD decreased synapse number.

One possibility for this discrepancy could be global KO vs. mosaic KD, however, this does not seem likely considering ∼80% of cells were transduced with amiRNAs in our experiments. Moreover, for the synaptogenic adhesion molecule neuroligin-1, global KO does not alter synapse density, whereas sparse KD does (Kwon et al., 2012); this is the opposite of what is observed for SynCAM1 where global KO reduced synapse

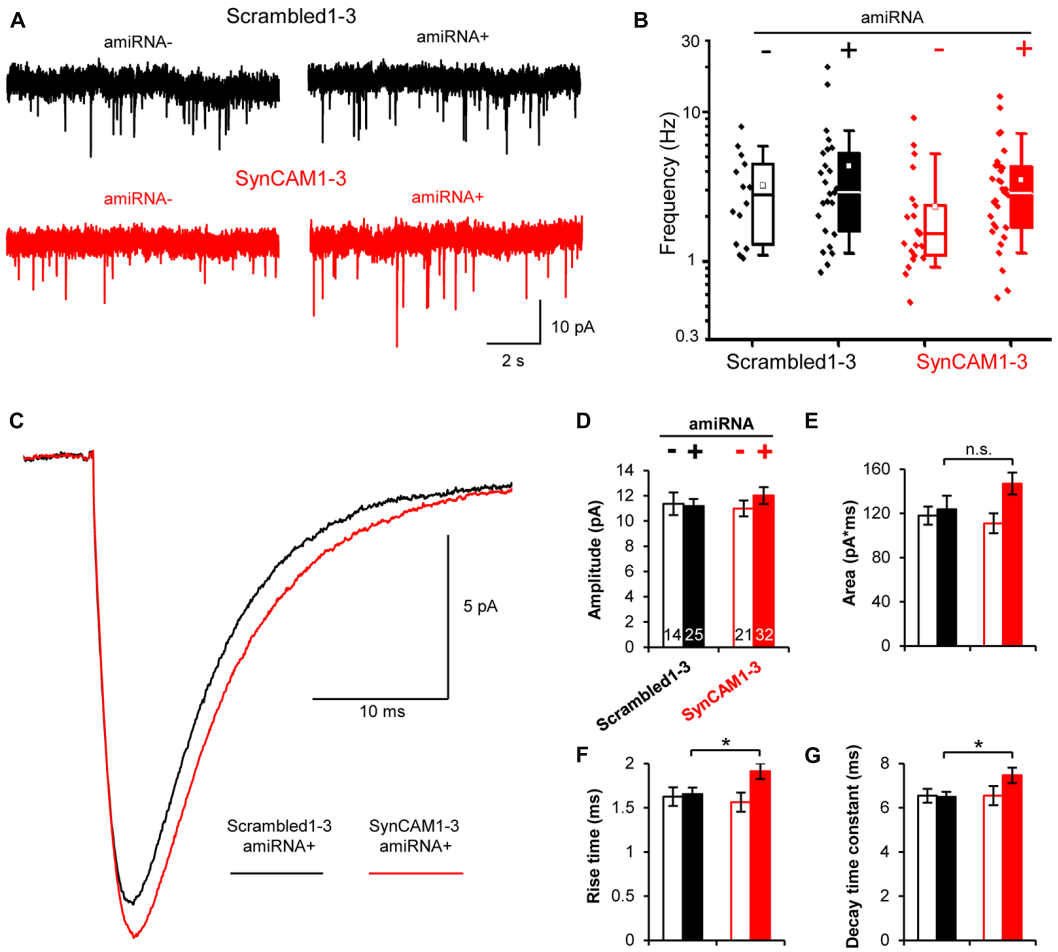

FIGURE 5 | Postsynaptic SynCAM1–3 loss does not alter miniature excitatory postsynaptic current (mEPSC) frequency but broadens mEPSC events. **(A)** Representative whole-cell patch clamp mEPSC traces of amiRNA− and amiRNA+ neurons from cultures treated with sub-saturating amounts of Scrambled1–3 or SynCAM1–3 amiRNAs. **(B)** Box and whisker plot of mEPSC frequencies with individual data points plotted to left of boxes. Box = 25–75%, whiskers = 10–90%, line = median, square = mean. **(C)** Average mEPSC event traces for amiRNA+ cells in cultures transduced with Scrambled1–3 or SynCAM1–3 amiRNAs. **(D–G)** Average mEPSC measurements as indicated on graph for amiRNA− and amiRNA+ cells in cultures transduced with Scrambled1–3 or SynCAM1–3 amiRNAs. **(B–G)** *n* = number of cells as indicated on bars in **(D)** from three isolations recorded at 13–16 DIV. $^*p < 0.05$, n.s., not significant, *t* test between Scrambled1–3 and SynCAM1–3 amiRNA+ conditions using cell average values. Error bars, SEM.

density (Robbins et al., 2010), whereas sparse KD using transfection of SynCAM1 shRNAs does not (Burton et al., 2012 and unpublished observations). Further, Kwon et al. (2012) demonstrated that at 1:1 mix of neuroligin-1 WT and KO neurons (50% of cells KO) in culture strongly reduced synapse formation on KO neurons, whereas our MEDLR experiments (80% of cells KD) do not show a phenotype from SynCAM1 KD alone. Together, this argues against global-vs.-local SynCAM1 depletion underlying differences in synapse formation. Unfortunately, due to a technical limitation of combinatorial viral transfection we were not able to investigate synapse development in cultures transduced sparsely with amiRNA virus because insufficient cells were co-transduced with both memGFP and amiRNAs.

Alternatively, differences in analysis methods may complicate direct comparisons. For instance, the discrepancy may stem from the different cell types assayed. SynCAM1 KO mice showed an overall reduction of hippocampal excitatory synapse number as measured by electron microscopy of whole tissue (Robbins et al., 2010). However, this technique does not differentiate between synapses onto interneurons or pyramidal cells. Indeed, a later study showed a specific reduction of excitatory inputs on hippocampal interneurons due to SynCAM1 KO (Park et al., 2016). Since the current study investigated pyramidal cells, it is possible that cell type differences account for the conflicting observations. Additionally, other reports have used dendritic spine density and mEPSC frequency as indirect measurements of synapse number (Robbins et al., 2010; Giza et al., 2013; Park et al., 2016), but these are by nature correlative measurements. Importantly, the only other SynCAM1 loss-of-function study to our knowledge that investigated synapse density used RNAi-mediated KD in hippocampal cultures also found no

change in synapse number as measured by Synapsin puncta along dendrites (Burton et al., 2012). Taken together with our studies, it is probable that a more stringent measurement of synapse density by immunolabeling is not altered by SynCAM1 depletion alone.

We also present imaging and electrophysiological data suggesting that triple KD of SynCAM1–3 increased synapse size. It is interesting to note that our imaging results showed enlarged synapses as measured by overlapping pre- and postsynaptic puncta area, yet the mean value of individual puncta was unchanged (**Figures 4H–M**). We believe this is indicative of changes primarily at trans-synaptic complexes for the following reasons: (1) synapses were smaller compared to individual puncta sizes so mean values for individual puncta would be less affected by similar changes in size; (2) the distribution data suggested a tendency towards increased individual puncta size in some cells; and (3) there were more individual puncta than synapses, with the possibility that the non-synaptically associated fraction is not enlarged. The combination of these factors could easily prevent a mean size shift for individual puncta size.

Moreover, results from previous studies support a model where intact SynCAM1–3 signaling limits synapse size at trans-synaptic structures. SynCAM1's ability to bind in *trans* is dependent on its ability to form oligomers in *cis* (Fogel et al., 2011). Intriguingly, postsynaptic disruption of SynCAM1 *trans* interactions by *cis*-binding to a dominant-negative SynCAM1 extracellular domain similarly increased immunolabeled synapse size (Fogel et al., 2011). SynCAM heteromers also form in *cis* to promote *trans* binding (Frei et al., 2014); therefore it is reasonable to infer that the dominant-negative SynCAM1 extracellular region disrupted trans-synaptic adhesion of all SynCAM1–3, leading to increased synapse size. Together with the recent report that postsynaptic SynCAM1 localizes to and shapes the synaptic periphery (Perez de Arce et al., 2015), it is tempting to speculate that postsynaptic SynCAM1–3 limit synapse size through a mechanism involving the development of the synaptic edge.

Further, the results using MEDLR to compare WT and KD neurons in the same cultures suggest that postsynaptic SynCAM1–3 instruct synapse formation. Because SynCAMs are assumed to function homo- or heterophilically in *trans* across the synapse, removal of SynCAMs from either the pre- or postsynaptic side would be expected to impair synapse development. Yet our observations show that postsynaptic expression of SynCAM1–3 in WT cells was sufficient for correct synapse development, even when the majority of presynaptic SynCAM1–3 was removed. These results imply that postsynaptic, and not presynaptic, SynCAM1–3 are the major determinant of SynCAM-mediated synapse formation, and posits a previously unrecognized postsynaptic function for SynCAM1–3. This was surprising due to the current assumption in the field that presynaptic SynCAMs dictate synapse formation since presentation of ectopic SynCAMs induces presynaptic, but not postsynaptic structures (Breillat et al., 2007; Czöndör et al., 2013). The overall reduction of Synapsin 1 and PSD-95 puncta upon SynCAM1–3 KD, however, indicates postsynaptic SynCAM1–3 are responsible for recruiting and/or stabilizing *both* pre- and postsynaptic structures. This notion is supported by the observation that postsynaptic SynCAM1 coordinates the assembly of both pre- and postsynaptic complexes through Farp1 (Cheadle and Biederer, 2012). However, Farp1 exclusively binds SynCAM1 and is unlikely to mediate the redundancy of SynCAM2 and 3.

Considered together, these results raise the question: how can postsynaptic SynCAM1–3 guide synapse assembly of both pre- and postsynapses when: (1) there is a severely reduced background of presynaptic SynCAM1–3; and (2) SynCAMs themselves lack the ability to induce postsynapse formation? We offer three possible explanations to reconcile these seemingly conflicting observations. First, it is possible that postsynaptic SynCAM1–3 bind to presynaptic SynCAM1–3 on WT axons, forming a much larger number of synapses on these processes to achieve an overall correct density. Second, it is possible that postsynaptic SynCAM1–3 binds residual SynCAM1–3 on KD axons, and this still allows synapse formation. This possibility would necessitate that a relatively tiny amount of presynaptic SynCAM1–3 is sufficient for correct synaptogenesis, whereas postsynaptic SynCAM1–3 removal is more apt to produce a phenotype. Both explanations would still require trans-synaptic SynCAM interactions to assemble a presynapse, which would recruit additional factors to in turn act across the cleft to induce postsynapse development. For example, the release of glutamate at nascent presynapses could trigger postsynapse assembly (Kwon and Sabatini, 2011), because clustering of presynaptic SynCAMs robustly induces functional presynaptic terminals (Biederer et al., 2002; Sara et al., 2005; Hoy et al., 2009; Czöndör et al., 2013).

A third possibility posits that presynaptic SynCAM1–3 are not actually necessary for synapse development. Instead, postsynaptic SynCAM1–3 could bind in *trans* to an unknown presynaptic adhesion molecule to induce presynaptic differentiation. This in turn could also induce postsynapse formation by recruiting additional postsynaptic factors, or may activate postsynaptic SynCAM1–3 to trigger development in a way that clustering in *trans* by SynCAMs does not. On the other hand, SynCAM1–3 could bind in *cis* to synaptogenic factors to both initiate postsynapse formation and signal retrogradely to instruct presynapse assembly. Because SynCAMs associate both in *cis* and *trans* with numerous adhesion molecules such as nectins (Mori et al., 2014), CRTAM (Arase et al., 2005; Boles et al., 2005; Galibert et al., 2005), and integrins (Mizutani et al., 2011; Sugiyama et al., 2013) and modulates receptor tyrosine kinase signaling in *cis* (Kawano et al., 2009; Kim et al., 2011; Sandau et al., 2011; Yamada et al., 2013), these may be worthwhile avenues for future investigations of how postsynaptic SynCAM1–3 guide synapse formation.

AUTHOR CONTRIBUTIONS

DKF, JHP and PW conceived and designed the experiments, DKF, JHP and CW performed the experiments and DKF and CW analyzed the data. All authors were involved in

drafting the manuscript and provided final approval for submission.

FUNDING

This work was supported by National Institutes of Health (NIH) grants from National Institute of Neurological Disorders and Stroke (award no. R01 NS065795) to PW, National Institute of Diabetes and Digestive and Kidney Diseases (award no. R01 DK092651) to JHP and Eunice Kennedy Shriver National Institute of Child Health and Human Development (award no. T32 HD07348) to DKF.

ACKNOWLEDGMENTS

We thank Kryn Stankunas and Scott Stewart for their contributions to and help with lentiviral design and production, and thank Megan Call and Jon Lindberg for technical assistance.

REFERENCES

Arase, N., Takeuchi, A., Unno, M., Hirano, S., Yokosuka, T., Arase, H., et al. (2005). Heterotypic interaction of CRTAM with Necl2 induces cell adhesion on activated NK cells and $CD8^+$ T cells. *Int. Immunol.* 17, 1227–1237. doi: 10.1093/intimm/dxh299

Biederer, T. (2006). Bioinformatic characterization of the SynCAM family of immunoglobulin-like domain-containing adhesion molecules. *Genomics* 87, 139–150. doi: 10.1016/j.ygeno.2005.08.017

Biederer, T., Sara, Y., Mozhayeva, M., Atasoy, D., Liu, X., Kavalali, E. T., et al. (2002). SynCAM, a synaptic adhesion molecule that drives synapse assembly. *Science* 297, 1525–1531. doi: 10.1126/science.1072356

Boles, K. S., Barchet, W., Diacovo, T., Cella, M., and Colonna, M. (2005). The tumor suppressor TSLC1/NECL-2 triggers NK-cell and $CD8^+$ T-cell responses through the cell-surface receptor CRTAM. *Blood* 106, 779–786. doi: 10.1182/blood-2005-02-0817

Breillat, C., Thoumine, O., and Choquet, D. (2007). Characterization of SynCAM surface trafficking using a SynCAM derived ligand with high homophilic binding affinity. *Biochem. Biophys. Res. Commun.* 359, 655–659. doi: 10.1016/j.bbrc.2007.05.152

Brewer, G. J., Torricelli, J. R., Evege, E. K., and Price, P. J. (1993). Optimized survival of hippocampal neurons in B27-supplemented neurobasal, a new serum-free medium combination. *J. Neurosci. Res.* 35, 567–576. doi: 10.1002/jnr.490350513

Branco, T., and Staras, K. (2009). The probability of neurotransmitter release: variability and feedback control at single synapses. *Nat. Rev. Neurosci.* 10, 373–383. doi: 10.1038/nrn2634

Burton, S. D., Johnson, J. W., Zeringue, H. C., and Meriney, S. D. (2012). Distinct roles of neuroligin-1 and SynCAM1 in synapse formation and function in primary hippocampal neuronal cultures. *Neuroscience* 215, 1–16. doi: 10.1016/j.neuroscience.2012.04.047

Casey, J. P., Magalhaes, T., Conroy, J. M., Regan, R., Shah, N., Anney, R., et al. (2012). A novel approach of homozygous haplotype sharing identifies candidate genes in autism spectrum disorder. *Hum. Genet.* 131, 565–579. doi: 10.1007/s00439-011-1094-6

Cheadle, L., and Biederer, T. (2012). The novel synaptogenic protein Farp1 links postsynaptic cytoskeletal dynamics and transsynaptic organization. *J. Cell Biol.* 199, 985–1001. doi: 10.1083/jcb.201205041

Chung, K. H., Hart, C. C., Al-Bassam, S., Avery, A., Taylor, J., Patel, P. D., et al. (2006). Polycistronic RNA polymerase II expression vectors for RNA interference based on BIC/miR-155. *Nucleic Acids Res.* 34:e53. doi: 10.1093/nar/gkl143

Czöndör, K., Garcia, M., Argento, A., Constals, A., Breillat, C., Tessier, B., et al. (2013). Micropatterned substrates coated with neuronal adhesion molecules for high-content study of synapse formation. *Nat. Commun.* 4:2252. doi: 10.1038/ncomms3252

Dull, T., Zufferey, R., Kelly, M., Mandel, R. J., Nguyen, M., Trono, D., et al. (1998). A third-generation lentivirus vector with a conditional packaging system. *J. Virol.* 72, 8463–8471.

Fogel, A. I., Akins, M. R., Krupp, A. J., Stagi, M., Stein, V., and Biederer, T. (2007). SynCAMs organize synapses through heterophilic adhesion. *J. Neurosci.* 27, 12516–12530. doi: 10.1523/JNEUROSCI.2739-07.2007

Fogel, A. I., Stagi, M., Perez de Arce, K., and Biederer, T. (2011). Lateral assembly of the immunoglobulin protein SynCAM 1 controls its adhesive function and instructs synapse formation. *EMBO J.* 30, 4728–4738. doi: 10.1038/emboj.2011.336

Fowler, D. K., Stewart, S., Seredick, S., Eisen, J. S., Stankunas, K., and Washbourne, P. (2016a). A multisite gateway toolkit for rapid cloning of vertebrate expression constructs with diverse research applications. *PLoS One* 11:e0159277. doi: 10.1371/journal.pone.0159277

Fowler, D. K., Williams, C., Gerritsen, A. T., and Washbourne, P. (2016b). Improved knockdown from artificial microRNAs in an enhanced miR-155 backbone: a designer's guide to potent multi-target RNAi. *Nucleic Acids Res.* 44:e48. doi: 10.1093/nar/gkv1246

Frei, J. A., Andermatt, I., Gesemann, M., and Stoeckli, E. T. (2014). The SynCAM synaptic cell adhesion molecules are involved in sensory axon pathfinding by regulating axon-axon contacts. *J. Cell Sci.* 127, 5288–5302. doi: 10.1242/jcs.157032

Galibert, L., Diemer, G. S., Liu, Z., Johnson, R. S., Smith, J. L., Walzer, T., et al. (2005). Nectin-like protein 2 defines a subset of T-cell zone dendritic cells and is a ligand for class-I-restricted T-cell-associated molecule. *J. Biol. Chem.* 280, 21955–21964. doi: 10.1074/jbc.m502095200

Giza, J. I., Jung, Y., Jeffrey, R. A., Neugebauer, N. M., Picciotto, M. R., and Biederer, T. (2013). The synaptic adhesion molecule SynCAM 1 contributes to cocaine effects on synapse structure and psychostimulant behavior. *Neuropsychopharmacology* 38, 628–638. doi: 10.1038/npp.2012.226

Gokce, O., and Südhof, T. C. (2013). Membrane-tethered monomeric neurexin LNS-domain triggers synapse formation. *J. Neurosci.* 33, 14617–14628. doi: 10.1523/JNEUROSCI.1232-13.2013

Hoy, J. L., Constable, J. R., Vicini, S., Fu, Z., and Washbourne, P. (2009). SynCAM1 recruits NMDA receptors via protein 4.1B. *Mol. Cell. Neurosci.* 42, 466–483. doi: 10.1016/j.mcn.2009.09.010

Kawano, S., Ikeda, W., Kishimoto, M., Ogita, H., and Takai, Y. (2009). Silencing of ErbB3/ErbB2 signaling by immunoglobulin-like Necl-2. *J. Biol. Chem.* 284, 23793–23805. doi: 10.1074/jbc.M109.025155

Kim, H. R., Jeon, B. H., Lee, H. S., Im, S. H., Araki, M., Araki, K., et al. (2011). IGSF4 is a novel TCR ζ-chain-interacting protein that enhances TCR-mediated signaling. *J. Exp. Med.* 208, 2545–2560. doi: 10.1084/jem.20110853

Kwan, K. M., Fujimoto, E., Grabher, C., Mangum, B. D., Hardy, M. E., Campbell, D. S., et al. (2007). The Tol2kit: a multisite gateway-based construction kit for Tol2 transposon transgenesis constructs. *Dev. Dyn.* 236, 3088–3099. doi: 10.1002/dvdy.21343

Kwon, H. B., Kozorovitskiy, Y., Oh, W. J., Peixoto, R. T., Akhtar, N., Saulnier, J. L., et al. (2012). Neuroligin-1-dependent competition regulates cortical synaptogenesis and synapse number. *Nat. Neurosci.* 15, 1667–1674. doi: 10.1038/nn.3256

Kwon, H. B., and Sabatini, B. L. (2011). Glutamate induces *de novo* growth of functional spines in developing cortex. *Nature* 474, 100–104. doi: 10.1038/nature09986

Loh, K. H., Stawski, P. S., Draycott, A. S., Udeshi, N. D., Lehrman, E. K., Wilton, D. K., et al. (2016). Proteomic analysis of unbounded cellular compartments: synaptic clefts. *Cell* 166, 1295.e21–1307.e21. doi: 10.1016/j.cell.2016.07.041

Mizutani, K., Kawano, S., Minami, A., Waseda, M., Ikeda, W., and Takai, Y. (2011). Interaction of nectin-like molecule 2 with integrin α6β4 and inhibition of disassembly of integrin α6β4 from hemidesmosomes. *J. Biol. Chem.* 286, 36667–36676. doi: 10.1074/jbc.M110.200535

Mori, M., Rikitake, Y., Mandai, K., and Takai, Y. (2014). Roles of nectins and nectin-like molecules in the nervous system. *Adv. Neurobiol.* 8, 91–116. doi: 10.1007/978-1-4614-8090-7_5

Park, K. A., Ribic, A., Laage Gaupp, F. M., Coman, D., Huang, Y., Dulla, C. G., et al. (2016). Excitatory synaptic drive and feedforward inhibition in the hippocampal CA3 circuit are regulated by SynCAM 1. *J. Neurosci.* 36, 7464–7475. doi: 10.1523/JNEUROSCI.0189-16.2016

Perez de Arce, K., Schrod, N., Metzbower, S. W., Allgeyer, E., Kong, G. K., Tang, A. H., et al. (2015). Topographic mapping of the synaptic cleft into adhesive nanodomains. *Neuron* 88, 1165–1172. doi: 10.1016/j.neuron.2015.11.011

Robbins, E. M., Krupp, A. J., Perez de Arce, K., Ghosh, A. K., Fogel, A. I., Boucard, A., et al. (2010). SynCAM 1 adhesion dynamically regulates synapse number and impacts plasticity and learning. *Neuron* 68, 894–906. doi: 10.1016/j.neuron.2010.11.003

Sandau, U. S., Mungenast, A. E., Alderman, Z., Sardi, S. P., Fogel, A. I., Taylor, B., et al. (2011). SynCAM1, a synaptic adhesion molecule, is expressed in astrocytes and contributes to erbB4 receptor-mediated control of female sexual development. *Endocrinology* 152, 2364–2376. doi: 10.1210/en.2010-1435

Sara, Y., Biederer, T., Atasoy, D., Chubykin, A., Mozhayeva, M. G., Sudhof, T. C., et al. (2005). Selective capability of SynCAM and neuroligin for functional synapse assembly. *J. Neurosci.* 25, 260–270. doi: 10.1523/JNEUROSCI.3165-04.2005

Shipman, S. L., Schnell, E., Hirai, T., Chen, B. S., Roche, K. W., and Nicoll, R. A. (2011). Functional dependence of neuroligin on a new non-PDZ intracellular domain. *Nat. Neurosci.* 14, 718–726. doi: 10.1038/nn.2825

Shu, X., Lev-Ram, V., Deerinck, T. J., Qi, Y., Ramko, E. B., Davidson, M. W., et al. (2011). A genetically encoded tag for correlated light and electron microscopy of intact cells, tissues and organisms. *PLoS Biol.* 9:e1001041. doi: 10.1371/journal.pbio.1001041

Stagi, M., Fogel, A. I., and Biederer, T. (2010). SynCAM 1 participates in axo-dendritic contact assembly and shapes neuronal growth cones. *Proc. Natl. Acad. Sci. U S A* 107, 7568–7573. doi: 10.1073/pnas.0911798107

Sugiyama, H., Mizutani, K., Kurita, S., Okimoto, N., Shimono, Y., and Takai, Y. (2013). Interaction of Necl-4/CADM4 with ErbB3 and integrin α6β4 and inhibition of ErbB2/ErbB3 signaling and hemidesmosome disassembly. *Genes Cells* 18, 519–528. doi: 10.1111/gtc.12056

Um, J. W., Pramanik, G., Ko, J. S., Song, M. Y., Lee, D., Kim, H., et al. (2014). Calsyntenins function as synaptogenic adhesion molecules in concert with neurexins. *Cell Rep.* 6, 1096–1109. doi: 10.1016/j.celrep.2014.02.010

Varoqueaux, F., Aramuni, G., Rawson, R. L., Mohrmann, R., Missler, M., Gottmann, K., et al. (2006). Neuroligins determine synapse maturation and function. *Neuron* 51, 741–754. doi: 10.1016/j.neuron.2006.09.003

Washbourne, P., Dityatev, A., Scheiffele, P., Biederer, T., Weiner, J. A., Christopherson, K. S., et al. (2004). Cell adhesion molecules in synapse formation. *J. Neurosci.* 24, 9244–9249. doi: 10.1523/JNEUROSCI.3339-04.2004

Yamada, A., Inoue, E., Deguchi-Tawarada, M., Matsui, C., Togawa, A., Nakatani, T., et al. (2013). Necl-2/CADM1 interacts with ErbB4 and regulates its activity in GABAergic neurons. *Mol. Cell. Neurosci.* 56, 234–243. doi: 10.1016/j.mcn.2013.06.003

Zhiling, Y., Fujita, E., Tanabe, Y., Yamagata, T., Momoi, T., and Momoi, M. Y. (2008). Mutations in the gene encoding CADM1 are associated with autism spectrum disorder. *Biochem. Biophys. Res. Commun.* 377, 926–929. doi: 10.1016/j.bbrc.2008.10.107

Conflict of Interest Statement: The authors declare that the research was conducted in the absence of any commercial or financial relationships that could be construed as a potential conflict of interest.

Advantages of publishing in Frontiers

OPEN ACCESS
Articles are free to read for greatest visibility and readership

FAST PUBLICATION
Around 90 days from submission to decision

HIGH QUALITY PEER-REVIEW
Rigorous, collaborative, and constructive peer-review

TRANSPARENT PEER-REVIEW
Editors and reviewers acknowledged by name on published articles

Frontiers
Avenue du Tribunal-Fédéral 34
1005 Lausanne | Switzerland

Visit us: www.frontiersin.org
Contact us: info@frontiersin.org | +41 21 510 17 00

REPRODUCIBILITY OF RESEARCH
Support open data and methods to enhance research reproducibility

DIGITAL PUBLISHING
Articles designed for optimal readership across devices

FOLLOW US
@frontiersin

IMPACT METRICS
Advanced article metrics track visibility across digital media

EXTENSIVE PROMOTION
Marketing and promotion of impactful research

LOOP RESEARCH NETWORK
Our network increases your article's readership